Die approbierte Originalversion dieser Dissertation ist in der Hauptbibliothek der Technischen Universität Wien aufgestellt und zugänglich.
http://www.ub.tuwien.ac.at

The approved original version of this thesis is available at the main library of the Vienna University of Technology.
http://www.ub.tuwien.ac.at/eng

TECHNISCHE UNIVERSITÄT WIEN
Vienna University of Technology

DISSERTATION

Development of Radiolabeled Bioorthogonal *In Vivo* Click Agents for Diagnostic Pretargeting

ausgeführt zum Zwecke der Erlangung des akademischen Grades eines Doktors der technischen Wissenschaften

unter der Leitung von

Univ.Prof. Dipl.-Ing. Dr. techn. Johannes **Fröhlich**
E 163
Institut für Angewandte Synthesechemie

eingereicht an der **Technischen Universität Wien**
Fakultät für Technische Chemie

von

Dipl.-Ing. Christoph Karl **Denk**, BSc
0525654
Seitenberggasse 78/34, A-1170 Wien

Wien, Juni 2016

When the going gets weird,
the weird turn pro.

Hunter S. Thompson

Contents

Danksagung (Acknowledgements) **1**

Abstract **3**

Kurzfassung **5**

Aims and Structure of this Thesis **7**

Collaborations **9**

1. Brief Introduction **11**

1.1 PET Imaging 13

1.2 Bioorthogonal Ligations 18

1.3 Bioorthogonal Ligations in PET Imaging 23

1.4 References 27

1.5 List of Abbreviations 34

2. Results and Discussion **35**

2.1 Overview of Contributions 37

2.2 Context of Contributions 39

2.3 Original Works 45

Manuscript #1 47
Manuscript #2 57
Manuscript #3 67
Manuscript #4 97
Manuscript #5 107

3. Conclusion **131**

4. Statement of Contribution **137**

5. Appendix **141**

Supporting Information – Manuscript #1 143
Supporting Information – Manuscript #2 173
Supporting Information – Manuscript #3 213
Supporting Information – Manuscript #5 265

6. Curriculum Vitae **289**

Danksagung

Größter Dank gilt meinen Eltern, Karin und Karl. Eure uneingeschränkte Unterstützung und Euer immerwährendes Vertrauen gaben mir stets großen Halt, und ermöglichten neben langen Studienjahren auch ein „Studium des Lebens“. Ohne dieses Vertrauen wäre vieles nicht möglich gewesen. – Vielen Dank!!

Auch möchte ich mich herzlich bei meinen Großeltern, und meinem Stiefvater Franz bedanken, Eure stetige Unterstützung war für meinen bisherigen Lebensweg äußerst wichtig! Meine lieben Geschwister Benedict, Melina, Melissa & Philip waren immer für mich da. Nie kam ein Vorwurf, dass der „große Bruder“ nur sehr wenig Zeit für Sie hatte. Ich hätte vermutlich weniger verständnisvoll reagiert. Ich möchte euch dafür von ganzem Herzen danken! (♥ !!)

Für die Möglichkeit der Durchführung meiner Dissertation, die ausgezeichnete Betreuung sowie die fortwährende Unterstützung gebührt meinem Doktorvater, Prof. Johannes Fröhlich, großer Dank! Meinem Supervisor, Hannes Mikula, möchte ich für das große Vertrauen danken, welches mir stets entgegengebracht wurde. Dieses Vertrauen, so wie die hervorragender Betreuung und Hilfe bei jeglicher Problemstellung ermöglichte eine Dissertation mit vielen Freiheitsgraden. Lieber Hannes, vielen Dank, dass du alle Ideen und Vorhaben stets unterstützt hast. Die Zusammenwirkung von ausgezeichneter Betreuung und Freiheit machten meine Zeit als Dissertant nicht nur zu hervorragenden „Lehrjahren“, sondern vor allem zu einer Zeit, an die ich mich stets gerne zurückerinnern werde!

Ohne die wertvollen Beiträge von Martin Wilkovitsch, Walter Kuba, Veronika Rosecker, Alwin Meledeth und Dominik Matscheko wäre diese Dissertation nicht möglich gewesen. Vielen Dank für Euren großen Einsatz! Meinen KollegInnen in der Forschungsgruppe möchte ich für die angenehme Arbeitsatmosphäre danken. Im speziellen sollen Julia Weber, Philipp Skrinjar, Barbara Sohr, Markus Schwarz, Dennis Svatunek, Christian Hametner, Ernst Horkel, Stefan Lexmüller, Johannes Bintinger, Stefan Kronister, Paul Kautny und Florian Glöcklhofer an dieser Stelle nicht unerwähnt bleiben. Danke für Eure (fachliche sowie persönliche) Unterstützung! Christian Hametner möchte ich besonders für die Durchführung unzähliger Hochfeld-NMR Experimente danken!

Dem Team der Seibersdorf Laboratories, im besonderen Roland Müller, Andreas Ipser und David Buchheit, möchte ich für die Unterstützung danken. Ohne die großzügige Bereitstellung von Laborinfrastruktur und Zyklotron-Waschwasser und das damit entgegengebrachte Vertrauen wäre diese Dissertation nicht möglich gewesen!

Großen Dank an das Team des AIT (Claudia Kuntner-Hannes, Thomas Wanek, Severin Mairinger, Johann Stanek, Thomas Filip, Michael Sauberer, Matthilde Löbsch) für die bereichernde Zusammenarbeit in ausgezeichneter Atmosphäre. Auch möchte ich mich herzlich bei Oliver Langer für die Begutachtung dieser Dissertation bedanken.

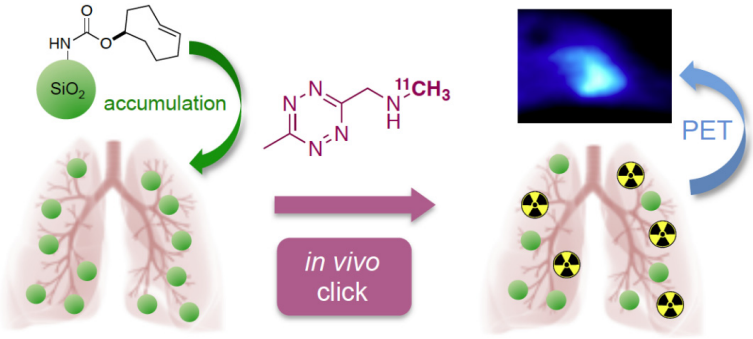
Kerstin, vielen Dank für Deine Liebe, Deine Nähe, Deine Hilfe, Deine Aufmerksamkeit und Unterstützung!

Abstract

Slow tracer accumulation of imaging probes can be circumvented by pretargeting using bioorthogonal ligations. These fast, highly selective and biocompatible “click” reactions are capable of forming a covalent linkage between a preadministered marker compound and a labeled Pull Down Reagent (PDR) *in vivo*. Several applications for the strain promoted azide alkyne cycloaddition (SPAAC) were reported, wherein the ring strain of the cyclooctyne eliminates the need for cytotoxic copper(I) catalysis, rendering this transformation bioorthogonal. Due to particular high ligation rates the bioorthogonal inverse electron demand Diels-Alder reaction (IEDDA) of strained dienophiles with 1,2,4,5-tetrazines (Tz) is especially suitable for applications in nuclear medicine, wherein low reagent concentrations require fast ligation rates. Until recently, only few radiolabeled tetrazines mainly based on radiometals and bulky chelating agents have been reported.

However, the beneficial use of short-lived PET isotopes (^{18}F, ^{11}C) employing favorable decay characteristics and high specific activity was limited due to stability and reactivity restrictions. Within this work the development of bioorthogonal probes (organic azides and 1,2,4,5-tetrazines) labeled with short-lived positron emitters carbon-11 and fluorine-18 is described.

Precursor substances for nucleophilic ^{18}F-fluorination or ^{11}C-methylation were designed, synthesized and characterized applying standard methods. Non-radioactive reference compounds were also prepared for identification of the radiolabeled species and for determination of specific activity. Radiolabeling procedures were optimized and synthesis sequences programmed to prepare labeled compounds in high activities using automated synthesis modules. Produced PDRs were investigated towards identity, purity, reactivity with *trans*-cyclooctene (TCO) or cyclooctyne derivatives and stability in human blood plasma.

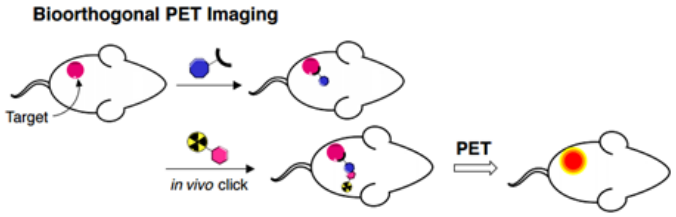


Simple in vivo model for testing a ^{11}C-labeled 1,2,4,5-tetrazine as Pull Down Reagent, using TCO-modified silica nanoparticles that accumulate in the lung

In addition to synthesis and radiolabeling, selected compounds were further evaluated in a murine *in vivo* model, wherein biodistribution, pharmacokinetics (using PET/MR scanning) and metabolism (as investigated by plasma and urine analysis using radio-TLC or radio-TLC) of the test substances was evaluated. PDRs that showed beneficial properties (homogenous biodistribution, fast renal excretion, high metabolic stability) were further tested towards their applicability for *in vivo* click chemistry using model substrates like TCO-tagged nanoparticles.

Kurzfassung

Bioorthogonale Reaktionen ermöglichen die nukleare Bildgebung (SPECT & PET) von langsam akkumulierenden molekularen Sonden mit kurzlebigen Radionukliden. Diese hochselektiven und biokompatiblen “Click”-Reaktionen erlauben die Knüpfung von kovalenten Bindungen im lebenden Organismus. Bei der bioorthogonalen Bildgebung wird im ersten Schritt ein mit einem bioorthogonalen Baustein modifizierter Marker (z.B. Antikörper) verabreicht, welcher sich im Zielgewebe anreichert. Nach erfolgter Akkumulation wird ein radioaktiv markiertes, niedermolekulares bioorthogonales “Pull-Down”-Reagenz (PDR) verabreicht, welches sich mit rascher Pharmakokinetik homogen im Organismus verteilt und an den Marker im Zielgewebe bindet. Durch diesen zweistufigen Prozess können im Vergleich zum direkt markierten Antikörper bessere Kontraste und geringere Strahlendosen erzielt werden.



Prinzip der bioorthogonalen Bildgebung

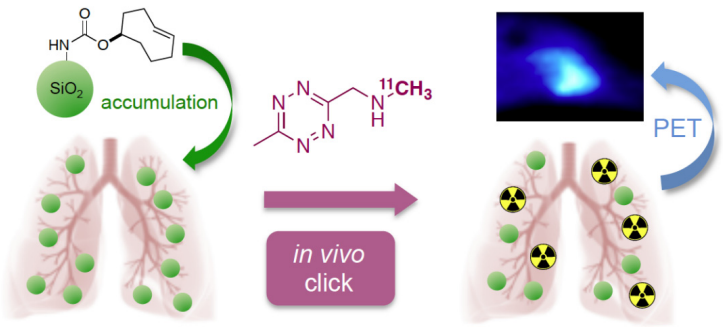
Häufig angewandt wird die kupferfreie Click-Chemie zwischen Cyclooctinen und Aziden, wobei durch die im Cyclooctin vorhandene Ringspannung auf das katalytische (aber zelltoxische) Kupfer(I) verzichtet werden kann. Besonders aber im Bereich der Nuklearmedizin, wo nur äußerst geringe Substanzkonzentrationen vorliegen, hat sich die Diels-Alder Reaktion mit inversem Elektronenbedarf (IEDDA) zwischen 1,2,4,5-Tetrazinen und gespannten Alkenen (*trans*-Cycloocten, TCO) durch besonders hohe Geschwindigkeitskonstanten bewährt. Radiomarkierte 1,2,4,5-Tetrazine sind daher universelle Werkzeuge, welche die Bildgebung von unterschiedlichen TCO-modifizierten (Makro)molekülen mit hohem Kontrast ermöglichen.

Zu Beginn der vorliegenden Dissertation (2013) waren nur wenige radiomarkierte Tetrazine bekannt. Diese Substanzen basierten zum überwiegenden Teil auf langlebigen Radiometallen, wobei durch den notwendigen Komplexbildner sehr polare und sperrige Moleküle entstanden. Der Einsatz von kovalent gebundenen, kurzlebigen Nukliden mit hoher spezifischer Aktivität (z.B.: Fluor-18) war jedoch durch Stabilitätsprobleme der 1,2,4,5-Tetrazine nicht möglich. In dieser Arbeit wird die Entwicklung von ^{11}C und ^{18}F markierten bioorthogonalen Sonden (Azide und 1,2,4,5-Tetrazine) für die zweistufige Positronen-Emissions-Tomographie beschrieben.

Die Auswahl der Zielstrukturen erfolgte durch computergestützte Abschätzung der Reaktivität. Precursorsubstanzen für die nukleophile ^{18}F-Fluorierung oder ^{11}C-Methylierung wurden entwickelt, synthetisiert und charakterisiert. Nicht-radioaktive Referenzsubstanzen wurden zur Identifizierung der radiomarkierten Spezies, sowie zur Bestimmung der spezifischen Aktivität dargestellt. Zusätzlich wurden die Reaktionskinetiken der Tetrazin-Derivate mit dem Dienophil TCO mittels “Stopped Flow” Messungen photometrisch

bestimmt. Die Radiomarkierungs-Reaktionen wurden hinsichtlich Ausbeute und Reaktionsführung optimiert, und auf automatisierte Syntheseeinheiten übertragen, um die bioorthogonalen Sonden (PDRs) in hohen Aktivitäten zu erhalten. Die Fluor-18 markierten PDRs wurden hinsichtlich Identität, radiochemischer Reinheit, Reaktivität gegenüber TCO, sowie Stabilität in Blutplasma untersucht.

Eine Auswahl der hergestellten radiomarkierten bioorthogonalen Sonden wurde im murinen Tiermodell untersucht. Hierbei wurde mittels Kleintier-PET/MR die Biodistribution und Pharmako-kinetik, so wie durch Analyse von Blut-, Organ- und Harnproben der Metabolismus der jeweiligen Substanzen untersucht. PDRs mit günstigen Eigenschaften wie einer homogenen Biodistribution und hoher metabolischer Stabilität wurden in einfachen Modellen hinsichtlich ihrer *in vivo* Reaktivität untersucht, wobei z.B.: TCO-modifizierte Siliziumoxid-Nanopartikel in der Lunge mittels bioorthogonaler Kohlenstoff-11 PET sichtbar gemacht werden konnten.



Einfaches in vivo Modell zur Evaluierung eines Kohlenstoff-11 markierten Tetrazins unter Verwendung von TCO-modifizierten Nanopartikeln, welche sich selektiv in der Lunge anreichern

Aims and Structure of this Thesis

The main objective of this doctoral research was to develop radiolabeled bioorthogonal reactants suitable for rapid radiolabeling and pretargeted imaging applications. The focus of this work was directed towards 1,2,4,5-tetrazines labeled with short-lived positron emitters fluorine-18 and carbon-11. This doctoral thesis led to development and publication of the first 1,2,4,5-tetrazine labeled with fluorine-18 that shows beneficial biodistribution pattern and high metabolic stability. In addition, the *in vivo* properties of low-molecular-weight ^{18}F-fluoroalkylazides that have previously been proposed as *in vivo* click agents, were reinvestigated.

This thesis is written as a cumulative work and consists of two parts:

(1) a brief introduction to the overall topic and

(2) the main part including the Results and Discussion section.

Original works (manuscripts #1 to #5, already published, submitted or in preparation) are included in the second part. Supporting information of these manuscripts can be found in the appendix of the thesis and contains most of the experimental details and data.

The applicant (C. Denk) is first author of four of these publications. These manuscripts were written and composed predominantly by C. Denk. Contributions of the applicant to the other manuscript were manifold and essential for successful completion of the respective research project.

Collaborations

The following collaborations were essential for a successful completion and the scientific outcome of this PhD thesis:

- PD Dr. Claudia Kuntner-Hannes, Dr. Thomas Wanek, Austrian Institute of Technology (AIT), Biomedical Systems, Forschungscenterstraße 1, 2444 Seibersdorf

- Prof. Dr. Michael Schäfers, Dr. Sven Hermann, European Institute for Molecular Imaging (EIMI), Westfälische Wilhelms-Universität Münster, Waldeyerstraße 15, D-48149 Münster

- Dr. Jan Matthew Welch, Atominstitut der Technischen Universität Wien, Stadionallee 2, A-1020 Wien

1. Brief Introduction

1.1 Positron Emission Tomography (PET)

Positron emission tomography (PET) is a highly sensitive imaging technique frequently employed in nuclear medicine and pharmacological research.[1,2] Several elements commonly encountered in biologically active molecules (Carbon, Nitrogen, Oxygen, Fluorine) have technical accessible short-lived radioisotopes (^{11}C, ^{13}N, ^{17}O, ^{18}F) that mainly exhibit ß$^+$ decay. The positron, emitted during this positive ß decay has, dependent on mean decay energy, a path length of about 1 mm in tissue.[1] After reducing its momentum due to elastic scatter events, the positron annihilates with a electron resulting in two gamma photons with 511 keV energy (representing the particles rest energy according to $E = mc^2$). The angle between the emitted photons is close to 180° due to conservation of momentum. The positron emission and subsequent annihilation process is depicted in figure 1.

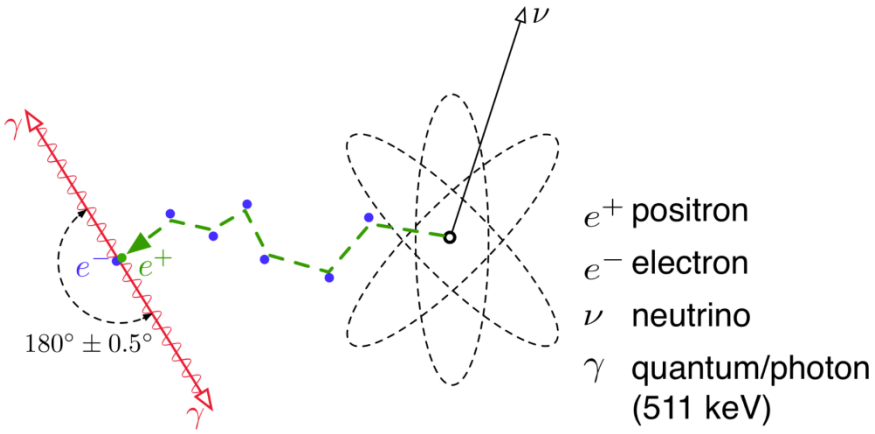


Figure 1: β$^+$ decay and subsequent annihilation[3]

The photons are detected using a ring of scintillation detectors placed around the volume of interest. LYSO (Lutetium Yttrium Silicon Oxide) is mainly used as detector material due to its high density (resulting in high probability of photon absorption) and low dead-time allowing for high count rates.[4] Out of many events registered by the detectors only coincident events measured within a time window of ~5 ns, so called "trues", are used for image reconstruction while data correction is used to discard non-coincidence events ("singles"), as well as scattered events.

Using the data of collected coincidence events a three-dimensional image of radionuclide distribution in the test volume can be reconstructed (Figure 2). Bioactive molecules labeled with positron emitters (*"PET-Tracers")* thus allow the dynamic imaging of metabolic and

other functional processes inside the body with high temporal and spatial resolution, making PET an essential tool in oncology, neurology and pharmacological research.

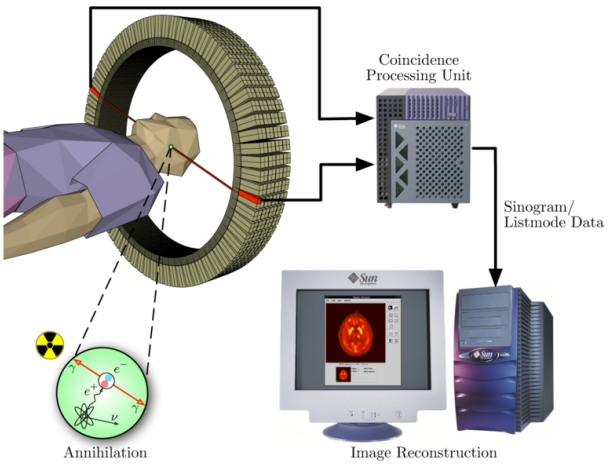


Figure 2: Schematics of a PET scanner[5]

A common PET-tracer in clinical practice is the ^{18}F-FDG (2-deoxy-2-(^{18}F)fluoro-D-glucose), wherein the 2-hydroxy group in glucose is replaced by the bioisosteric fluorine-18. The compound is actively transported into cells where it enters glycolysis and is phosphorylated at the 6-OH-position by the enzyme hexokinase. The resulting 2-[^{18}F]FDG-6-phosphate is no substrate for glucose-6-phosphate isomerase thus preventing further metabolism. For this reason ^{18}F-FDG is efficiently trapped in cells allowing PET imaging of metastases or functional neuro-imaging based on glucose metabolism.[6,7]

The most common PET radioisotopes exhibit half-lifes in the range of minutes to hours. Since the majority of positron emitters are nuclei with excess protons, neutron sources (such as nuclear reactors) are not suitable for their production. Instead accelerators (most commonly cyclotrons, Figure 3) are used to irradiate a suitable target with accelerated nuclei forming the desired PET radioisotope in a nuclear reaction.

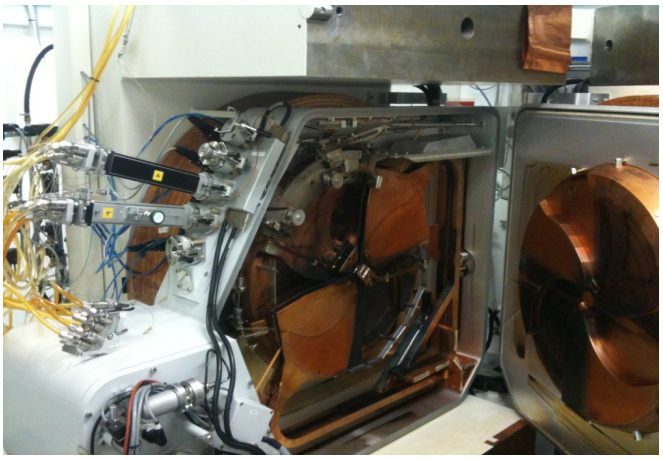
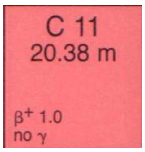
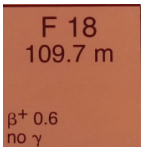


Figure 3: *GE PETtrace cyclotron*



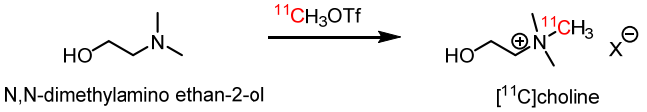
The main route for production of ^{11}C ($t_{1/2}$ = 20.38 min) is irradiation of gaseous nitrogen with 3-13 MeV protons using the $^{14}N(p,\alpha)^{11}C$ nuclear reaction. If oxygen is present in the irradiated nitrogen, $^{11}CO_2$ is produced, while a mixture of hydrogen and nitrogen yields $^{11}CH_4$, thus allowing different strategies for subsequent chemical modification.[8,9] Usually ^{11}C is introduced into molecules by N- or O-methylation using ^{11}C methyl iodide or ^{11}C methyl triflate as alkylating agents.



Fluorine-18 is the most commonly used PET radionuclide, due to low positron decay energy and a convenient half-life of 109.8 minutes, allowing for multi-step labeling reactions. The main route of production is the $^{18}O(p,n)^{18}F$ nuclear reaction. Nucleophilic ^{18}F-fluoride is produced by irradiation of ^{18}O-enriched water with protons, while electrophilic ^{18}F-F_2 is accessible by the irradiation of $^{18}O_2$ gas.[9,10]

Following radionuclide production time is a key factor in the synthesis of PET tracers due to the short half-lifes of employed isotopes. The overall process of synthesis, purification and formulation should not exceed two half-lifes to obtain a product of high specific activity.[9] For this reason fast and robust chemistry is required to label appropriate precursor materials with the radioisotope. If protection groups are necessary, deprotection must be rapid and quantitative. Since precursor material is used in huge excess compared to the radionuclide, and might compete with the radiotracer at binding sites, separation of unreacted precursor is often necessary and commonly achieved by HPLC. In addition, chemical and radiochemical byproducts need to be separated prior to administration to the patient. Due to diversity of published radiolabeling techniques only the most important are discussed at this point.

Carbon-11 radiotracers are usually synthesized from des-methyl precursors by alkylation of N- or O- nucleophiles, using $^{11}CH_3I$ or $^{11}CH_3OTf$ as alkylating agents.[11] $^{11}CH_3I$ is generated in a gas phase recirculation process from $^{11}CH_4$. Onward transformation to [^{11}C]methyl triflate is achieved by passage over heated silver trifluoromethanesulfonate. One



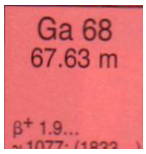
Scheme 1: Radiosynthesis of ^{11}C-choline

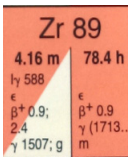
example is the synthesis of [^{11}C]choline (Scheme 1) which is used in imaging of prostate cancer.[12]

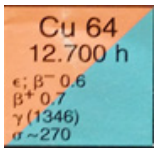
In addition to carbon-11 labeled methylation agents also labeled carbon monoxide, phosgene, cyanogen bromide, methanol, formic acid, etc. are accessible from $^{11}CO_2$ and $^{11}CH_4$ offering numerous synthetic strategies for preparation of compounds labeled with carbon-11.[11,13–15]

Fluorine-18 is introduced by nucleophilic or electrophilic fluorination reactions on according precursor materials.[9] Nucleophilic fluoride is accessible n.c.a (non carrier added), thus giving rise to probes with high specific activity. For this reason, nucleophilic fluorination is preferred whenever applicable. Use of protection groups to prohibit side reactions is often required, adding a cleavage step to the radiosynthesis sequence. In nucleophilic fluorinations n.c.a $^{18}F^-$ fluoride is used to displace leaving groups like tosylates, nosylates, mesylates or triflates. Due to poor nucleophility of the fluoride ion, reactivity is enhanced by cryptands or tetrabutyl ammonium salts, resulting in anhydrous fluoride species that are soluble in organic solvents such as acetonitrile or dimethyl sulfoxide.[2,9]

In addition to covalently bound PET-isotopes such as fluorine-18 and carbon-11 also radiometals such as gallium-68, copper-64 and zirconium-89 are used in PET imaging.[16–18]







Those radioisotopes are incorporated into tracer molecules by the aid of a chelating moiety such as DFO, DOTA or NOTA.[16,19] Short-lived ^{68}Ga is available from radionuclide generators employing the ^{68}Ge/^{68}Ga mother-daughter system.[20] For this reason ^{68}Ga is also available to PET centers and research facilities without access to cyclotron systems. Zirconium-89 ($t_{1/2}$ = 78.4 h) and copper-64 ($t_{1/2}$ = 12.7 h) are isotopes with considerably longer half-lifes.

Imaging quality in PET is highly dependent on pharmacokinetics and pharmacodynamics of the applied tracer molecule. Fast accumulation in target tissue in respect to the half-life of the applied radionuclide is essential. Furthermore, binding needs to be highly specific to tissues of interest, and non-bound tracer needs to be excreted in a fast manner to limit unspecific signals and gain signal to background ratio in acquired data. Of course high image

contrast (signal to background ratio) is required for high diagnostic value, while the patient dose should be kept as low as possible. For this reason, rapidly accumulating and clearing tracers are applied in standard imaging protocols that allow the use of short-lived radionuclides. As a consequence, slowly accumulating vectors (antibodies, nanomedicines, etc.) that show high target specificity are seldomly used as imaging agents since they would require labeling with long-lived isotopes (such as ^{89}Zr) resulting in undesirably high patient radiation doses.

1.2 Bioorthogonal Reactions

Bioorthogonal is a term introduced by Carolyn R. Bertozzy in 2004 and is describing a set of characteristics rendering a chemical transformation applicable to living systems:[21–24]

Inertness: Bioorthogonal reactants as well as products arising from a bioorthogonal transformation must be metabolically stable for a certain time span.

Selectivity: Bioorthogonal reactants must not react with any other functionalities present in living organisms.

Reactivity: Chemical transformation must be achieved, even in high dilution, prior to clearance (or metabolism) of the reactants.

Biocompatibility: The reaction needs to be compatible with characteristics encountered in biological systems (aqueous environment, body temperature) and employed reactants must not exhibit toxicity.

Mainly bioorthogonal ligations have been reported so far. In these transformations two bioorthogonal tags (low molecular weight compounds) are linked together *in vitro* or *in vivo* due to covalent bond formation (Figure 4).

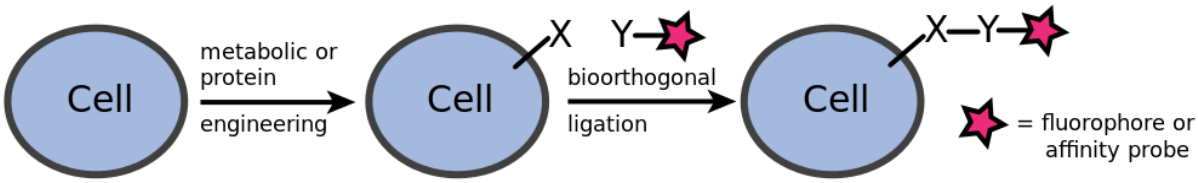


Figure 4: *Principle of bioorthogonal labeling*[25]

The strain promoted alkyne-azide cycloaddition (SPAAC), and inverse electron demand Diels Alder reactions (IEDDA) involving 1,2,4,5-tetrazines gathered most interest and will be briefly discussed in the following chapter. [10]

The Strain Promoted Alkyne-Azide Cycloaddition (SPAAC)

SPAAC, also referred to as copper free click chemistry (CFC) was developed by Carolyn R. Bertozzi in 2007.[26] The reaction is based on the copper(I)-catalyzed alkyne azide [3+2] dipolar cycloaddition.[27] Within SPAAC the ring strain of employed cyclooctynes is lowering activation energy of the transformation thus rendering (cytotoxic) Cu(I) catalysis unnecessary (Figure 5).[28] The strain-promoted alkyne-azide cycloaddition (SPAAC) was successfully employed in live-cells, zebrafish and mice.[29,30]

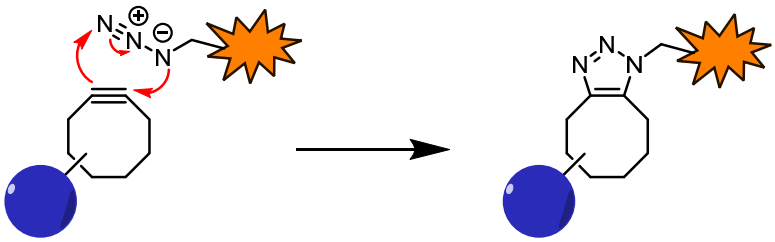
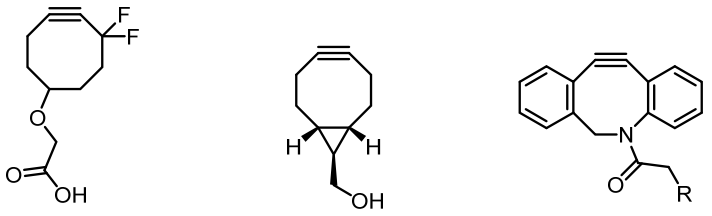


Figure 5: *Mechanism of the SPAAC reaction*

Due to its small size the azide tag is unlikely to influence functionality of host molecules. It is easily introduced into molecules by nucleophilic substitution or diazotransfer reactions, and exhibits high metabolic stability.[23] The second SPAAC reactant, cyclooctyne, is the smallest stable cyclic alkyne and its ring strain was calculated to be 19.9 kcal/mol.[28] Recent studies demonstrate that cyclooctynes undergo thiol-yne additions with cysteine thus limiting stability of this tag.[31] However, the reaction was successfully used *in vivo* demonstrating the applicability of this bioorthogonal ligation.[29]

SPAACs reaction kinetics are negligible influenced by the substitution pattern of aliphatic azides, if sterically non-demanding cyclooctynes such as BCN or DIFO (see Figure 6) are used. Cyclooctynes with high steric demand such as BARAC have very limited reactivity with tertiary azides, but undergo rapid ligation with primary or secondary azides.[32] Certain aryl azides exhibit drastically enhanced reactivity.[33] In general SPAAC ligation rates are highly dependent on the structure (and ring strain) of the applied cyclooctyne. Adding electron-withdrawing groups in α-position to the alkyne or increasing strain by annulations of benzene or cyclopropane rings enhances reaction rates (See Figure 6).[26,34]



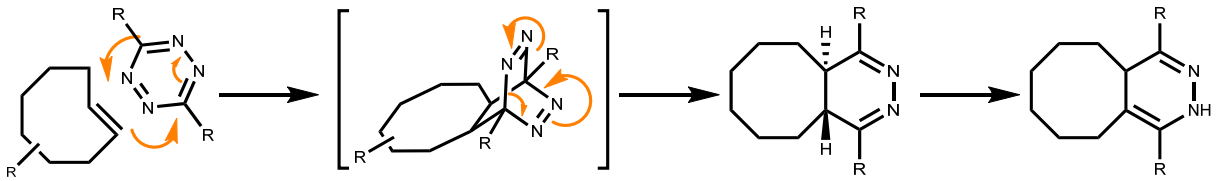
DIFO k = 0.076 M^{-1} s^{-1} | **BCN** k = 0.14 M^{-1} s^{-1} | **ADIBO** k = 0.96 M^{-1} s^{-1}

Figure 6: Several cyclooctynes with rate constants reported in literature[34–36]

In contrast to the low yielding multi-step synthesis of DIFO and BARAC, the cyclooctyne BCN is accessible from 1,5-cyclooctadiene in four steps and 46% overall yield.[34] Although several cyclooctyne derivatives have been reported, aiming for improved reactivity, rate constants are still < 5 $M^{-1}s^{-1}$, limiting SPAAC to applications where ligation speed is not critical or reactants are present in high concentrations.

The Inverse Electron Demand Diels Alder Reaction

Electron deficient 1,2,4,5-tetrazines and strained alkene dienophiles undergo inverse electron demand Diels Alder reactions.[37] Subsequent retro Diels Alder reaction driven by the elimination of N_2 gives rise to dihydropyridazine isomers (Scheme 2). This reaction has been reported as being bioorthogonal by Fox and Weissleder and their coworkers in 2008.[38,39]



Scheme 2: Mechanism of tetrazine ligations

Reported applications of the tetrazine ligation include *in vivo* pretargeting for nuclear imaging and therapy, the rapid construction of radiolabeled probes, drug delivery, nuclein acid amplification, fluorescence imaging, drug target identification and others.[39–47]

Extremely fast reaction rates of up to 3.3 x 10^6 $M^{-1}s^{-1}$ (MeOH, 25°C) were reported for this reaction making it about 10^5 times faster than SPAACs and therefore useable in high dilutions commonly encountered in living organisms.[48] IEDDA ligation rates are highly dependent on 3,6-substituents on the tetrazine moiety. In general, electron withdrawing groups are enhancing reactivity, while alkyl substituents result in diminished reactivity.[49] Hydrogen terminated tetrazines also exhibit very high reactivity, most likely due to favorable steric factors.[49]

The choice of dienophile has also great impact on ligation rates. Although norbornene and terminal alkene type reactants have been shown to be effective for live-cell imaging, reaction rates using this dienophiles are very limited.[50,51] *Trans*-cyclooctene derivatives (TCOs) are dienophiles with enhanced reactivity and are applied whenever rapid rates are essential.[48]

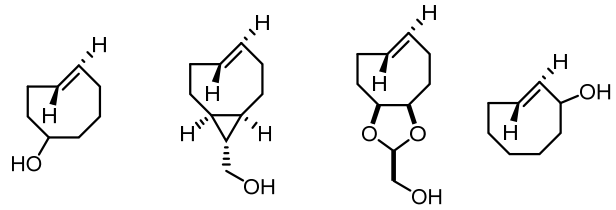


Figure 7: TCO based dienophiles for tetrazine ligations[45,48,52,53]

5-OH-TCO (available in axial and equatorial configuration of the hydroxyl group) is the most widely used TCO derivative. The hydroxyl function allows for straight forward modification and the compound has been shown to be stable in vivo for several days.[54] s-TCO developed by Fox and coworkers is about two orders of magnitude more reactive as compared to 5-OH-TCO but studies suggest, that the compound is rapidly deactivated *in vivo*.[52] It is mainly used in applications where ligation rate is more important than long-term stability of the reactants. d-TCO, a *trans*-cyclooctene with intermediate reactivity exhibits improved stability and increased water solubility due to the dioxolane functionality.[48] Although possessing lower cycloaddition reactivity, 3-OH-TCO is interesting due to its "click and release" behaviour: Molecules attached to the hydroxyl function via carbamate linkage are released from the scaffold once cycloaddition with a tetrazine took place allowing for the construction of activatable drugs.[45]

TCO derivatives are accessible by photoisomerization of the *cis* isomers using 254 nm radiation in a flow regime. The TCO species is actively removed from the equilibrium by the aid of a silver nitrate impregnated silica cartridge. This methodology allows for straight forward preparation of TCOs, if a flow photochemistry setup is available.[54,53,55]

1.3 Bioorthogonal Ligations in PET Imaging

Two main applications for bioorthogonal ligations exist in the field of nuclear imaging. In rapid radiolabeling, the selectivity and robustness of bioorthogonal ligations is used *ex vivo* for the rapid synthesis of radiolabeled probes (Figure 8, i). Consequently peptides and other sensitive molecules can be radiolabeled in aqueous media, furthermore omitting the use of protecting groups.[41,56–58] Bioorthogonal (or pretargeted) imaging, as depicted in Figure 8, II is taking full advantage of bioorthogonal ligation capabilities: First, a marker compound modified with a bioorthogonal tag is administered and allowed to accumulate. In a second step a radiolabeled bioorthogonal agent (pull down reagent) is administered and reacting *in vivo* with the pre-accumulated marker compound. Using this pretargeting methodology the pharmacokinetics of the marker is efficiently decoupled from the half-life of the radionuclide allowing imaging of long-circulating agents (e.g. antibodies) with short-lived radionuclides.[30,43,44,59]

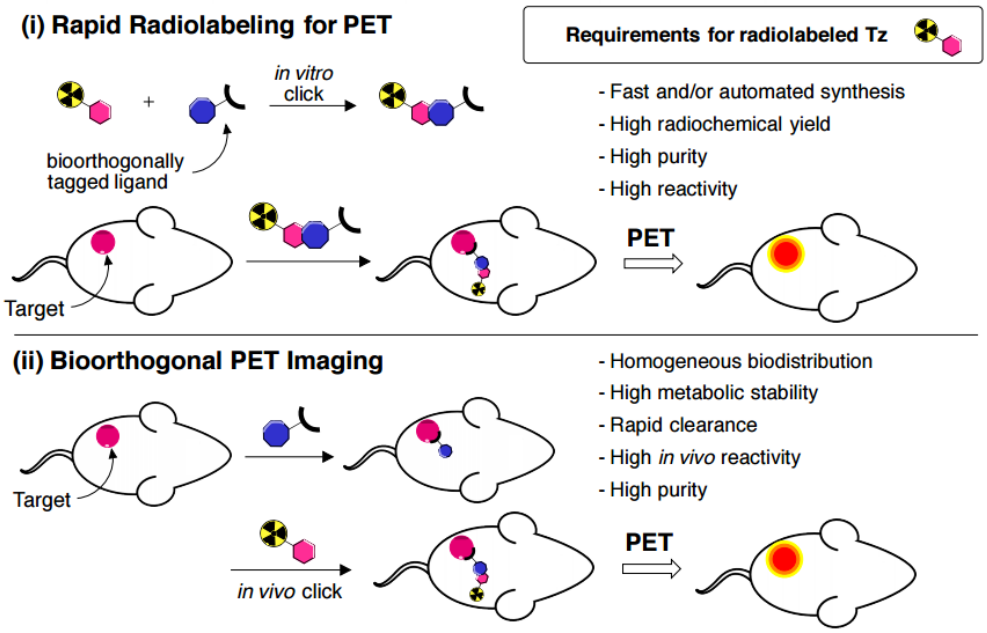


Figure 8: The main applications of bioorthogonal ligations in PET imaging

Rapid Radiolabeling

SPAAC has been used for rapid radiolabeling using ^{18}F-Azides such as [^{18}F]-2-fluoroethylazide (^{18}F-FEA) or ^{18}F-azides based on mini-PEGs.[60,61] For example RGD or bombesin based PET-

probes were synthesized using this approach.[62,63] In addition ^{18}F-cyclooctynes have been applied in the synthesis of ^{18}F-PET probes.[61] Due to slow ligation rates in SPAAC the precursor component (bearing the cyclooctyne or azide functionality) has to be used in excess to drive the reaction towards completion in a reasonable time-span. For this reason post-labeling purification is often required to achieve high specific activity of the radiolabeled probe. Subsequently, also copper-catalyzed azide-alkyne cycloadditions (CuAAC) are suitable for rapid radiolabeling, allowing the application of linear alkynes (e.g. propargyl) instead of cyclooctynes.[58,64–70] Linear alkynes are readily accessible and pose less steric impact on the tagged marker compound as compared to cyclooctynes. In addition, ligation with the azide species results in a single isomer, while ligation with unsymmetrical cyclooctynes results in a mixture of isomers that is often difficult to separate.[71] Especially ^{18}F-FEA is used in CuAAC rapid radiolabeling due to its high yielding synthesis and small size.[58,61] Furthermore, this method has been optimized by addition of Cu-ligands such as bathophenanthroline, to reduce the required amount of catalyst and facilitate reaction kinetics.[70] Reported rapid radiolabeling applications based on ^{18}F-FEA and CuAAC include the labeling of RGD-peptides and somatostatin receptor agonists, the construction of a library of hypoxia-sensitive probes, as well as the synthesis of multiple probes in one batch followed by HPLC purification.[61,65,66,72]

Also the Tz-ligation has found application in rapid radiolabeling: ^{18}F-labeled dienophiles such as ^{18}F-TCO or ^{18}F-s-TCO were prepared in good to excellent radiochemical yields and were further reacted with Tz-modified proteins.[41,56]

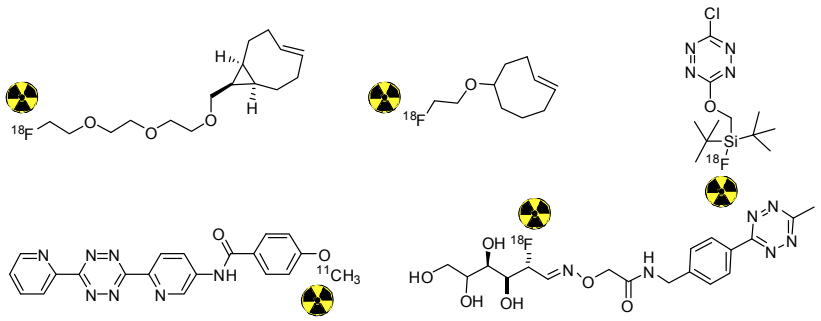


***Figure 9**: Radiolabeled agents reported for IEDDA based rapid radiolabeling* [56,73,74]

The high cycloaddition reactivity of s-TCO derivatives makes rapid radiolabeling with equimolar Tz possible in a reasonable time span, thus eliminating the need for further purification.[56] Also several labeled tetrazine derivatives (bearing ^{11}C, ^{18}F, ^{125}I and other

nuclides) were reported and successfully used in the synthesis of radiolabeled probes.[41,74–78] A selection of published derivatives for IEDDA based rapid radiolabeling is shown in Figure 9.

Pretargeted Imaging

The concept of pretargeting involves accumulation of a marker reagent at the tissue of interest, followed by administration of a secondary agent that binds to the preadministered marker *in vivo* (Figure 10).[79] First pretargeting systems in nuclear medicine utilized the avidin-biotin interaction, but size and allergic potential of the protein avidine poses serious limitations. In addition bispecific antibodies were successfully applied.[79–83] Bioorthogonal ligations offer the advantage that both involved reaction partners are non-peptidic small molecules. Having a tagged marker (e.g. a antibody or nanoparticle) on site allows for a multitude of possibilities: Drugs conjugated to the opposed bioorthogonal reactant may be used to selectively enrich this agent in the targeted tissue. Furthermore, pull down reagents labeled with therapeutic nuclides can be administered for pretargeted radioimmunotherapy thus boosting target-dose while limiting non-target dose as compared to a directly labeled antibody.[84] Pretargeted imaging is applicable as a stand-alone technique allowing low-dose imaging of antibodies and other long circulating agents with short-lived nuclides with high signal to background ratios, which is otherwise not possible. In addition, pretargeted imaging might serve as complementary technique in theranostic approaches, where the diagnostic PDR is used to evaluate marker accumulation prior to dosing of a therapeutic bioorthogonal agent.

Spivey and co-workers proposed SPAAC as tool for bioorthogonal PET imaging, and highlighted ^{18}F-FEA as potential pull down reagent.[85] In addition, Kim and co-workers were using the SPAAC reaction to link a mini-PEG based fluorine-18 azide to cyclooctyne derivatized nanoparticles *in vivo*.[30] However, despite the report from Kim et al, no successful application of the SPAAC reaction in nuclear pretargeting was reported.[44] Taking the limited rate constant of this particular bioorthogonal ligation and the diminutive concentration of radiotracers *in vivo* into consideration, applicability to SPAAC is questionable.

In contrast, the Tz ligation has been very successfully applied for pretargeted *in vivo* imaging.

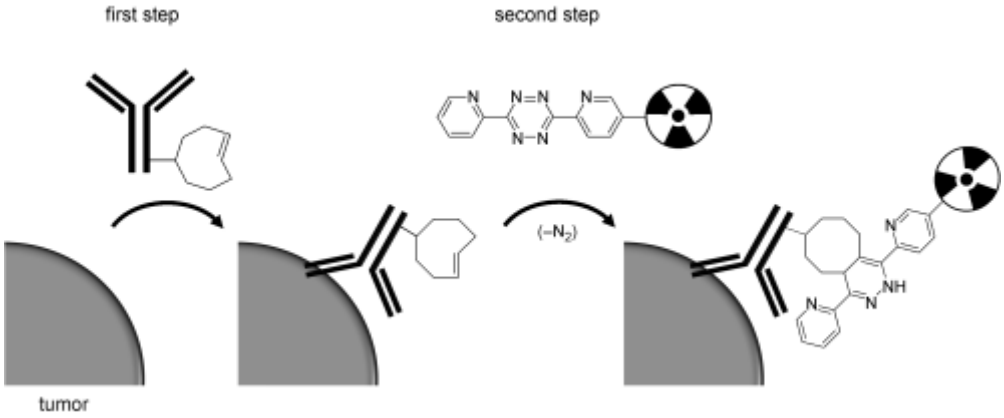


***Figure 10**: Concept of pretargeting based on the Tz-Ligation*[43]

In 2010 Robbiliard, Rossin and co-workers used a TCO-modified CC49-antibody for pretargeting of colocteral cancer xenografts in mice. Twenty-four hours post marker administration an indium-111 chelator based tetrazin PDR was injected followed by successful imaging of the xenograft using SPECT. Image contrast was still limited due to reaction of tetrazine-probe with free circulating TCO-antibody conjugate in blood.[43] A comparable pretargeting experiment, also based on a chelator bearing Tz species (labeled with copper-64), was successfully conducted in 2013 by Zeglis et. al. using A33 antibody TCO-conjugates.[59] Dosimetry in this study demonstrated a clear reduction in off-target dose compared to the directly labaled antibody.[59] IEDDA based pretargeted imaging was further improved to 250-fold tumor-to-blood ratios (see Figure 11) by Rossin, Robilliard and co-workers by dosing Tz-derived clearing agents prior to radiotetrazine administration.[84] Those macromolecular agents remove free circulating mAb-TCO conjugate from the blood stream by Tz-ligation followed by rapid excretion, thus boosting tumor-to-blood ratios.

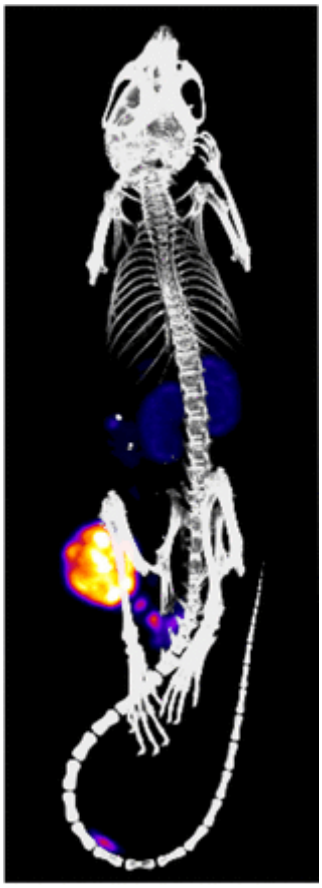


Figure 11: Pretargeted PET/CT fusion image [84]

Attempts using the inverse approach utilizing tetrazine-conjugated marker reagents and radiolabeled TCOs were so far unsuccessful due to reported metabolic instability of the TCO species, when applied in tracer amounts.[86]

1.4 References

(1) Phelps, M. E. (2006) PET : physics, instrumentation, and scanners. Springer.

(2) Bailey, D. L., Townsend, D. W., Maisey, M. N., and Valk, P. E. (2005) Positron emission tomography : basic sciences. Springer, Secaucus, NJ.

(3) https://upload.wikimedia.org/wikipedia/commons/b/b2/Annihilation.png.

(4) Pepin, C. M., Bérard, P., Perrot, A.-L., Pépin, C., Houde, D., Lecomte, R., Melcher, C. L., and Dautet, H. (2004) Properties of LYSO and Recent LSO Scintillators for Phoswich PET Detectors. *IEEE Trans. Nucl. Sci. 51*.

(5) https://commons.wikimedia.org/wiki/File:PET-schema.png.

(6) Ido, T., Wan, C.-N., Casella, V., Fowler, J. S., Wolf, A. P., Reivich, M., and Kuhl, D. E. (1978) Labeled 2-deoxy-D-glucose analogs. 18F-labeled 2-deoxy-2-fluoro-D-glucose, 2-deoxy-2-fluoro-D-mannose and 14C-2-deoxy-2-fluoro-D-glucose. *J. Label. Compd. Radiopharm. 14*, 175–183.

(7) Alavi, A., and Reivich, M. (2002) Guest editorial: The conception of FDG-PET imaging. *Semin. Nucl. Med. 32*, 2–5.

(8) (2008) Cyclotron Produced Radionuclides: Principles and Practice. *IAEA Tech. Rep. Ser. No. 465*.

(9) Schlyer, D. J. (2004) PET tracers and radiochemistry. *Ann. Acad. Med. Singapore 33*, 146–54.

(10) Denk, C. (2013) Master Thesis: Bioorthogonal Ligations in PET Imaging. Vienna University of Technology.

(11) Wuest, F., Berndt, M., and Kniess, T. Carbon-11 Labeling Chemistry Based upon [11C]Methyl Iodide, in *PET Chemistry*, pp 183–213. Springer Berlin Heidelberg.

(12) Rosen, M. A., Jones, R. M., Yano, Y., and Budinger, T. F. (1985) Carbon-11 choline: synthesis, purification, and brain uptake inhibition by 2-dimethylaminoethanol. *J. Nucl. Med. 26*, 1424–8.

(13) Nishijima, K., Kuge, Y., Seki, K., Ohkura, K., Motoki, N., Nagatsu, K., Tanaka, A., Tsukamoto, E., and Tamaki, N. (2002) A simplified and improved synthesis of [11C]phosgene with iron and iron (III) oxide. *Nucl. Med. Biol. 29*, 345–50.

(14) Westerberg, G., and Långström, B. (1997) On-line production of [11C]cyanogen bromide. *Appl. Radiat. Isot. 48*, 459–461.

(15) Långström, B., Itsenko, O., and Rahman, O. (2007) [11C]Carbon monoxide, a versatile and useful precursor in labelling chemistry for PET-ligand development. *J. Label. Compd. Radiopharm. 50*, 794–810.

(16) Anderson, C. J., and Ferdani, R. (2009) Copper-64 radiopharmaceuticals for PET imaging of cancer: advances in preclinical and clinical research. *Cancer Biother. Radiopharm. 24*, 379–93.

(17) Zhang, Y., Hong, H., and Cai, W. (2011) PET tracers based on Zirconium-89. *Curr. Radiopharm. 4*, 131–9.

(18) Banerjee, S. R., and Pomper, M. G. (2013) Clinical applications of Gallium-68. *Appl. Radiat. Isot. 76*, 2–13.

(19) Nedrow, J. R., White, A. G., Modi, J., Nguyen, K., Chang, A. J., and Anderson, C. J. (2014) Positron emission tomographic imaging of copper 64- and gallium 68-labeled chelator conjugates of the somatostatin agonist tyr3-octreotate. *Mol. Imaging 13*.

(20) Richard Lambrecht, B. M., Sajjad, M., Operations, C., and Faisal, K. (1988) Accelerator-Derived Radionuclide Generators t. *Radiochim. Acta 43*, 171–179.

(21) Sletten, E. M., and Bertozzi, C. R. (2009) Bioorthogonal chemistry: fishing for selectivity in a sea of functionality. *Angew. Chem. Int. Ed. Engl. 48*, 6974–98.

(22) Prescher, J. A., Dube, D. H., and Bertozzi, C. R. (2004) Chemical remodelling of cell surfaces in living animals. *Nature 430*, 873–7.

(23) Prescher, J. A., and Bertozzi, C. R. (2005) Chemistry in living systems. *Nat. Chem. Biol. 1*, 13–21.

(24) Sletten, E. M., and Bertozzi, C. R. (2011) From Mechanism to Mouse: A Tale of Two Bioorthogonal Reactions. *Acc. Chem. Res. 44*, 666–676.

(25) https://en.wikipedia.org/wiki/Bioorthogonal_chemistry#/media/File:Bioorthogonal_cell_labeling.svg.

(26) Baskin, J. M., Prescher, J. A., Laughlin, S. T., Agard, N. J., Chang, P. V, Miller, I. A., Lo, A., Codelli, J. A., and Bertozzi, C. R. (2007) Copper-free click chemistry for dynamic in vivo imaging. *Proc. Natl. Acad. Sci. U. S. A. 104*, 16793–7.

(27) Kolb, H. C., Finn, M. G., and Sharpless, K. B. (2001) Click Chemistry: Diverse Chemical Function from a Few Good Reactions. *Angew. Chem. Int. Ed. Engl. 40*, 2004–2021.

(28) Schoenebeck, F., Ess, D. H., Jones, G. O., and Houk, K. N. (2009) Reactivity and regioselectivity in 1,3-dipolar cycloadditions of azides to strained alkynes and alkenes: a computational study. *J. Am. Chem. Soc. 131*, 8121–33.

(29) Dehnert, K. W., Baskin, J. M., Laughlin, S. T., Beahm, B. J., Naidu, N. N., Amacher, S. L., and Bertozzi, C. R. (2012) Imaging the sialome during zebrafish development with copper-free click chemistry. *ChemBioChem 13*, 353–357.

(30) Lee, S. B., Kim, H. L., Jeong, H.-J., Lim, S. T., Sohn, M.-H., and Kim, D. W. (2013) Mesoporous Silica Nanoparticle Pretargeting for PET Imaging Based on a Rapid Bioorthogonal Reaction in a Living Body. *Angew. Chemie Int. Ed. 52*, 10549–10552.

(31) van Geel, R., Pruijn, G. J. M., van Delft, F. L., and Boelens, W. C. (2012) Preventing thiol-yne addition improves the specificity of strain-promoted azide-alkyne cycloaddition. *Bioconjug. Chem. 23*, 392–8.

(32) Svatunek, D., Houszka, N., and Denk, C. (2016) Reaktivität sekundärer und tertiärer Azide in der bioorthogonalen Click-Chemie. *Unpubl. Data*.

(33) Dommerholt, J., van Rooijen, O., Borrmann, A., Guerra, C. F., Bickelhaupt, F. M., and van Delft, F. L. (2014) Highly accelerated inverse electron-demand cycloaddition of electron-deficient azides with aliphatic cyclooctynes. *Nat. Commun. 5*, 5378.

(34) Dommerholt, J., Schmidt, S., Temming, R., Hendriks, L. J. A., Rutjes, F. P. J. T., Van Hest, J. C. M., Lefeber, D. J., Friedl, P., and Van Delft, F. L. (2010) Readily accessible bicyclononynes for bioorthogonal labeling and three-dimensional imaging of living cells. *Angew. Chemie - Int. Ed. 49*, 9422–9425.

(35) Codelli, J. A., Baskin, J. M., Agard, N. J., and Bertozzi, C. R. (2008) Second-generation difluorinated cyclooctynes for copper-free click chemistry. *J. Am. Chem. Soc. 130*, 11486–11493.

(36) Gordon, C. G., MacKey, J. L., Jewett, J. C., Sletten, E. M., Houk, K. N., and Bertozzi, C. R. (2012) Reactivity of biarylazacyclooctynones in copper-free click chemistry. *J. Am. Chem. Soc. 134*, 9199–9208.

(37) Boger, D. L., and Sakya, S. M. (1988) Inverse electron demand Diels-Alder reactions of 3,6-bis(methylthio)-1,2,4,5-tetrazine. 1,2-Diazine introduction and direct implementation of a divergent 1,2,4,5-tetrazine .fwdarw. 1,2-diazine .fwdarw. benzene (indoline/indole) Diels-Alder strategy. *J. Org. Chem. 53*, 1415–1423.

(38) Blackman, M. L., Royzen, M., and Fox, J. M. (2008) Tetrazine Ligation: Fast Bioconjugation Based on Inverse-Electron-Demand Diels−Alder Reactivity. *J. Am. Chem. Soc. 130*, 13518–13519.

(39) Devaraj, N. K., Weissleder, R., and Hilderbrand, S. a. (2008) Tetrazine-Based Cycloadditions : Application to Pretargeted Live Cell Imaging Tetrazine-Based Cycloadditions : Application to Pretargeted Live Cell Imaging. *Communications 19*, 2297–2299.

(40) Yang, J., Šečkute, J., Cole, C. M., and Devaraj, N. K. (2012) Live-cell imaging of cyclopropene tags with fluorogenic tetrazine cycloadditions. *Angew. Chemie - Int. Ed. 51*, 7476–7479.

(41) Li, Z., Cai, H., Hassink, M., Blackman, M. L., Brown, R. C. D., Conti, P. S., and Fox, J. M. (2010) Tetrazine-trans-cyclooctene ligation for the rapid construction of 18F labeled probes. *Chem. Commun. (Camb). 46*, 8043–5.

(42) Meyer, J. P., Houghton, J. L., Kozlowski, P., Abdel-Atti, D., Reiner, T., Pillarsetty, N. V. K., Scholz, W. W., Zeglis, B. M., and Lewis, J. S. (2016) 18F-Based Pretargeted PET Imaging Based on Bioorthogonal Diels-Alder Click Chemistry. *Bioconjug. Chem. 27*, 298–301.

(43) Rossin, R., Verkerk, P. R., Van Den Bosch, S. M., Vulders, R. C. M., Verel, I., Lub, J., and Robillard, M. S. (2010) In vivo chemistry for pretargeted tumor imaging in live mice. *Angew. Chemie - Int. Ed. 49*, 3375–3378.

(44) Rossin, R., and Robillard, M. S. (2014) Pretargeted imaging using bioorthogonal chemistry in mice. *Curr. Opin. Chem. Biol. 21*, 161–169.

(45) Versteegen, R. M., Rossin, R., ten Hoeve, W., Janssen, H. M., and Robillard, M. S. (2013) Click to Release: Instantaneous Doxorubicin Elimination upon Tetrazine Ligation. *Angew. Chemie Int. Ed. 52*, 14112–14116.

(46) Wu, H., Cisneros, B. T., Cole, C. M., and Devaraj, N. K. (2014) Bioorthogonal Tetrazine-Mediated Transfer Reactions Facilitate Reaction Turnover in Nucleic Acid-Templated Detection of MicroRNA. *J. Am. Chem. Soc. 136*, 17942–17945.

(47) Yang, K. S., Budin, G., Tassa, C., Kister, O., and Weissleder, R. (2013) Bioorthogonal approach to identify unsuspected drug targets in live cells. *Angew. Chem. Int. Ed. Engl. 52*, 10593–7.

(48) Darko, A., Wallace, S., Dmitrenko, O., Machovina, M. M., Mehl, R. A., Chin, J. W., and Fox, J. M. (2014) Conformationally Strained trans-Cyclooctene with Improved Stability and Excellent Reactivity in Tetrazine Ligation. *Chem. Sci. 5*, 3770–3776.

(49) Karver, M., Weissleder, R., and Hilderbrand, S. A. (2011) Synthesis and Evaluation of a Series of 1 , 2 , 4 , 5- Tetrazines for Bioorthogonal Conjugation Conjugation Center for Systems Biology.

(50) Lang, K., Davis, L., Torres-Kolbus, J., Chou, C., Deiters, A., and Chin, J. W. (2012) Genetically encoded norbornene directs site-specific cellular protein labelling via a rapid bioorthogonal reaction. *Nat. Chem. 4*, 298–304.

(51) Beckmann, H. S. G., Niederwieser, A., Wiessler, M., and Wittmann, V. (2012) Preparation of carbohydrate arrays by using Diels-Alder reactions with inverse electron demand. *Chem. - A Eur. J. 18*, 6548–6554.

(52) Taylor, M. T., Blackman, M. L., Dmitrenko, O., Fox, J. M., and Ligation, T. (2011) Design and Synthesis of Highly Reactive Dienophiles for the. *J. Am. Chem. Soc. 133*, 9646–9649.

(53) Royzen, M., Yap, G. P. A., and Fox, J. M. A Photochemical Approach to Functionalized trans -Cyclooctenes Driven by Metal Complexation 1–30.

(54) Royzen, M., Yap, G. P. A., and Fox, J. M. (2008) A photochemical synthesis of functionalized trans-cyclooctenes driven by metal complexation. *J. Am. Chem. Soc. 130*, 3760–3761.

(55) Svatunek, D., Denk, C., Rosecker, V., Sohr, B., Hametner, C., Allmaier, G., Fröhlich, J., and Mikula, H. (2016) Efficient low-cost preparation of trans-cyclooctenes using a simplified flow setup for photoisomerization. *Monatshefte für Chemie - Chem. Mon. 147*, 579–585.

(56) Wang, M., Svatunek, D., Rohlfing, K., Liu, Y., Wang, H., Giglio, B., Yuan, H., Wu, Z., Li, Z., and Fox, J. (2016) Conformationally Strained *trans*- Cyclooctene (sTCO) Enables the Rapid Construction of ^{18} F-PET Probes via Tetrazine Ligation. *Theranostics 6*, 887–895.

(57) Zeglis, B. M., Mohindra, P., Weissmann, G. I., Divilov, V., Hilderbrand, S. A., Weissleder, R., and Lewis, J. S. (2011) Modular strategy for the construction of radiometalated antibodies for positron emission tomography based on inverse electron demand diels-alder click chemistry. *Bioconjug. Chem. 22*, 2048–2059.

(58) Glaser, M., and Arstad, E. (2007) ``Click labeling{''} with 2-{[}F-18]fluoroethylazide for positron emission tomography. *Bioconjug. Chem. 18*, 989–993.

(59) Zeglis, B. M., Sevak, K. K., Reiner, T., Mohindra, P., Carlin, S. D., Zanzonico, P., Weissleder, R., and Lewis, J. S. (2013) A Pretargeted PET Imaging Strategy Based on Bioorthogonal Diels – Alder Click Chemistry. *J. Nucl. Med.* 1389–1396.

(60) Bouvet, V., Wuest, M., and Wuest, F. (2011) Copper-free click chemistry with the short-lived positron emitter fluorine-18. *Org. Biomol. Chem. 9*, 7393.

(61) Kettenbach, K., Schieferstein, H., Ross, T. L., Kettenbach, K., Schieferstein, H., and Ross, T. L. (2014) 18F-Labeling Using Click Cycloadditions. *Biomed Res. Int. 2014*, 1–16.

(62) Kim, H. L., Sachin, K., Jeong, H. J., Choi, W., Lee, H. S., and Kim, D. W. (2015) F-18 Labeled RGD Probes Based on Bioorthogonal Strain-Promoted Click Reaction for PET Imaging. *ACS Med. Chem. Lett. 6*, 402–7.

(63) Campbell-Verduyn, L. S., Mirfeizi, L., Schoonen, A. K., Dierckx, R. A., Elsinga, P. H., and Feringa, B. L. (2011) Strain-Promoted Copper-Free “Click” Chemistry for 18F Radiolabeling of Bombesin. *Angew. Chemie Int. Ed. 50*, 11117–11120.

(64) Glaser, M., Solbakken, M., Turton, D. R., Pettitt, R., Barnett, J., Arukwe, J., Karlsen, H., Cuthbertson, A., Luthra, S. K., and Årstad, E. (2009) Methods for 18F-labeling of RGD peptides: Comparison of aminooxy [18F]fluorobenzaldehyde condensation with “click labeling” using 2-[18F]fluoroethylazide, and S-alkylation with [18F] fluoropropanethiol. *Amino Acids 37*, 717–724.

(65) Iddon, L., Leyton, J., Indrevoll, B., Glaser, M., Robins, E. G., George, A. J. T., Cuthbertson, A., Luthra, S. K., and Aboagye, E. O. (2011) Synthesis and in vitro evaluation of [18F]fluoroethyl triazole labelled [Tyr3]octreotate analogues using click chemistry. *Bioorganic Med. Chem. Lett. 21*, 3122–3127.

(66) Jia, L., Cheng, Z., Shi, L., Li, J., Wang, C., Jiang, D., Zhou, W., Meng, H., Qi, Y., Cheng, D., and Zhang, L. (2013) Fluorine-18 labeling by click chemistry: Multiple probes in one pot. *Appl. Radiat. Isot. 75*, 64–70.

(67) Frullano, L., Catana, C., Benner, T., Sherry, A. D., and Caravan, P. (2010) Bimodal MR-PET agent for quantitative pH imaging. *Angew. Chemie 49*, 2382–2384.

(68) Smith, G., Glaser, M., Perumal, M., Nguyen, Q. De, Shan, B., ??rstad, E., and Aboagye, E. O. (2008) Design, synthesis, and biological characterization of a caspase 3/7 selective isatin labeled with 2-[18f]fluoroethylazide. *J. Med. Chem. 51*, 8057–8067.

(69) Pretze, M., Pietzsch, D., and Mamat, C. (2013) Recent trends in bioorthogonal click-radiolabeling reactions using fluorine-18. *Molecules 18*, 8618–8665.

(70) Zhou, D., Chu, W., Dence, C. S., Mach, R. H., and Welch, M. J. (2012) Highly efficient click labeling using 2-[18F]fluoroethyl azide and synthesis of an 18FN-hydroxysuccinimide ester as conjugation agent. *Nucl. Med. Biol. 39*, 1175–1181.

(71) Liang, L., and Astruc, D. (2011) The copper(I)-catalyzed alkyne-azide cycloaddition (CuAAC) "click" reaction and its applications. An overview. *Coord. Chem. Rev. 255*, 2933–2945.

(72) Bejot, R., Carroll, L., Bhakoo, K., Declerck, J., and Gouverneur, V. (2012) A fluorous and click approach for screening potential PET probes: Evaluation of potential hypoxia biomarkers. *Bioorganic Med. Chem. 20*, 324–329.

(73) Wyffels, L., Thomae, D., Waldron, A.-M., Fissers, J., Dedeurwaerdere, S., Van der Veken, P., Joossens, J., Stroobants, S., Augustyns, K., and Staelens, S. (2014) In vivo evaluation of (18)F-labeled TCO for pre-targeted PET imaging in the brain. *Nucl. Med. Biol. 41*, 513–23.

(74) Zhu, J., Li, S., Wängler, C., Wängler, B., Lennox, R. B., and Schirrmacher, R. (2015) Synthesis of 3-chloro-6-((4-(di-tert-butyl[(18)F]fluorosilyl)-benzyl)oxy)-1,2,4,5-tetrazine ([(18)F]SiFA-OTz) for rapid tetrazine-based (18)F-radiolabeling. *Chem. Commun. (Camb). 51*, 12415–8.

(75) Knight, J. C., Richter, S., Wuest, M., Way, J. D., and Wuest, F. (2013) Synthesis and evaluation of an 18F-labelled norbornene derivative for copper-free click chemistry reactions. *Org. Biomol. Chem. 11*, 3817–3825.

(76) Rashidian, M., Keliher, E. J., Dougan, M., Juras, P. K., Cavallari, M., Wojtkiewicz, G. R., Jacobsen, J. T., Edens, J. G., Tas, J. M. J., Victora, G., Weissleder, R., and Ploegh, H. L. (2015) Use of 18F-2-Fluorodeoxyglucose to Label Antibody Fragments for Immuno-Positron Emission Tomography of Pancreatic Cancer. *ACS Cent. Sci.* 150603073029009.

(77) Herth, M. M., Andersen, V. L., Lehel, S., Madsen, J., Knudsen, G. M., Kristensen, J. L., and Herth, M. M. (2013) Development of a (11)C-labeled tetrazine for rapid tetrazine-trans-cyclooctene ligation. *Chem. Commun. (Camb). 49*, 3805–7.

(78) Albu, S. A., Al-Karmi, S. A., Vito, A., Dzandzi, J. P. K., Zlitni, A., Beckford-Vera, D., Blacker, M., Janzen, N., Patel, R. M., Capretta, A., and Valliant, J. F. (2016) ^{125}I-Tetrazines and Inverse-Electron-Demand Diels–Alder Chemistry: A Convenient Radioiodination Strategy for Biomolecule Labeling, Screening, and Biodistribution Studies. *Bioconjug. Chem. 27*, 207–216.

(79) Chang, C.-H., Sharkey, R. M., Rossi, E. A., Karacay, H., McBride, W., Hansen, H. J., Chatal, J.-F., Barbet, J., and Goldenberg, D. M. (2002) Molecular advances in pretargeting radioimunotherapy with bispecific antibodies. *Mol. Cancer Ther. 1*, 553–63.

(80) Goldenberg, D. M., Chatal, J.-F., Barbet, J., Boerman, O., and Sharkey, R. M. (2007) Cancer imaging and therapy with bispecific antibody pretargeting. *Update Cancer Ther. 2*, 19–31.

(81) Goldenberg, D. M., Chang, C.-H., Sharkey, R. M., Rossi, E. A., Karacay, H., McBride, W., Hansen, H. J., Chatal, J.-F., and Barbet, J. (2003) Radioimmunotherapy: Is avidin-biotin pretargeting the preferred choice among pretargeting methods? *Eur. J. Nucl. Med. Mol. Imaging 30*, 777–780.

(82) Goldenberg, D. M. (2006) Antibody Pretargeting Advances Cancer Radioimmunodetection and Radioimmunotherapy. *J. Clin. Oncol. 24*, 823–834.

(83) Goldenberg, D. M., Chang, C.-H., Rossi, E. A., McBride, W. J., and Sharkey, R. M. (2012) Pretargeted Molecular Imaging and Radioimmunotherapy. *Theranostics 2*, 523–540.

(84) Rossin, R., Läppchen, T., Van Den Bosch, S. M., Laforest, R., and Robillard, M. S. (2013) Diels–Alder Reaction for Tumor Pretargeting: In Vivo Chemistry Can Boost Tumor Radiation Dose Compared with Directly Labeled Antibody. *J Nucl Med 54*, 1–7.

(85) Evans, H. L., Slade, R. L., Carroll, L., Smith, G., Nguyen, Q.-D., Iddon, L., Kamaly, N. N., Stöckmann, H., Leeper, F. J., Aboagye, E. O., Spivey, A. C., and Aboagye, O. (2012) Copper-free click--a promising tool for pre-targeted PET imaging. *Chem. Commun. (Camb). 48*, 991–3.

(86) Wyffels, L., Thomae, D., Waldron, A. M., Fissers, J., Dedeurwaerdere, S., Van der Veken, P., Joossens, J., Stroobants, S., Augustyns, K., and Staelens, S. (2014) In vivo evaluation of 18F-labeled TCO for pre-targeted PET imaging in the brain. *Nucl. Med. Biol. 41*, 513–523.

(87) Denk, C., Svatunek, D., Filip, T., Wanek, T., Lumpi, D., Fröhlich, J., Kuntner, C., and Mikula, H. (2014) Development of a (18) F-Labeled Tetrazine with Favorable Pharmacokinetics for Bioorthogonal PET Imaging. *Angew. Chem. Int. Ed. Engl.* 1–6.

1.5 List of Abbreviations

ADIBO	Dibenzocyclooctyne
BARAC	biarylazacyclooctynone
BCN	*(1R,8S,9s)*-Bicyclo[6.1.0]non-4-yn-9-ylmethanol
CFC	Copper Free Click
DFO	Desferrioxamine
DIFO	2-((6,6-difluorocyclooct-4-yn-1-yl)oxy)acetic acid
DMDO	Dimethyldioxirane
DOTA	1,4,7,10-tetraazacyclododecane-1,4,7,10-tetraacetic acid
FEA	1-azido-2-fluoroethane
GC/FID	Gas Chromatography with Flame Ionization Detector
HPLC	High Performance Liquid Chromatography
IEDDA	Inverse Electron Demand Diels Alder Reaction
MR	Magnetic Resonance
NOTA	2,2',2''-(1,4,7-triazonane-1,4,7-triyl)triacetic acid
PDR	Pull Down Reagent, (radio)labeled bioorthogonal reactant
PET	Positron Emission Tomography
RGD	Arg-Gly-Asp
SPAAC	Strain Promoted Alkyne Azide Cycloaddition
SPECT	Single Photon Emission Computed Tomography
SUV	Standardized Uptake Value
TCO	*trans*-Cyclooctene
TLC	Thin Layer Chromatography
Tz	1,2,4,5-Tetrazine

2. Results and Discussion

2.1 Overview of Contributions

Manuscript #1:

Denk, C.; Svatunek, D.; Filip, T.; Wanek, T.; Lumpi, D.; Fröhlich, J.; Kuntner-Hannes, C.; Mikula, H.: **Development of a ^{18}F-labeled Tetrazine with Favorable Pharmacokinetics for Bioorthogonal PET Imaging**, *Angewandte Chemie International Edition*, **2014**, 53, 9655-9659.

Manuscript #2:

Denk, C.; Svatunek, D.; Mairinger, S.; Stanek, J.; Filip, T.; Matscheko, D.; Kuntner-Hannes, C.; Wanek, T.; Mikula, H.: **Design, Synthesis and Evaluation of a Low-Molecular-Weight ^{11}C-Labeled Tetrazine for Pretargeted PET Imaging applying Bioorthogonal *In Vivo* Click Chemistry**, *Bioconjugate Chemistry*, **2016**, accepted manuscript

Manuscript #3:

Denk, C.; Svatunek, D.; Mairinger, S.; Kuntner-Hannes, C.; Filip, T.; Sauberer, M.; Fröhlich, J.; Wanek, T.; Mikula, H.: **A Tale of 3-[^{18}F]Fluoropropyl-1,2,4,5-tetrazines**, manuscript draft

Manuscript #4:

Svatunek, D.; **Denk, C**.; Rosecker, V.; Sohr, B.; Hametner, C.; Allmaier, G.; Fröhlich, J.; Mikula, H.: **Efficient low-cost preparation of *trans*-cyclooctenes using a simplified flow setup for photoisomerization**, *Monatshefte für Chemie – Chemical Monthly*, **2016**, 147, 579-585.

Manuscript #5:

Denk, C.; Wilkovitsch, M.; Skrinjar, P.; Svatunek, D.; Mairinger, S.; Kuntner-Hannes, C.; Filip, T.; Fröhlich, J.; Wanek, T.; Mikula, H.: **Investigation of Small [^{18}F]-Fluoroalkylazides for Rapid Radiolabeling and *In Vivo* Click Chemistry**, *Bioconjugate Chemistry*, **2016**, submitted manuscript

2.2 Context of Contributions

In this chapter the context of the subsequently introduced manuscripts or paper drafts will be outlined. The next paragraphs will briefly explain the focus of research in the single contributions, refer to theoretical fundamentals and reveal how these contribute to the main topic of this thesis. For detailed background information and respective references see Chapter 2.3.

Consultation of literature in 2013 revealed, that the preparation of ^{18}F-tetrazines by direct nucleophilic radiofluorination is not possible, due to chemical instability of these moieties under basic radiolabeling conditions. However, a ^{18}F-tetrazine with favorable pharmacokinetics was considered of high importance for the field of bioorthogonal PET imaging due to high specific activity and favorable decay properties of this nuclide. At this point only chelator based radio-tetrazines labeled with radiometals were used for pretargeted imaging with good signal-to-blood ratios. Nevertheless, the polar structure of the chelator is limiting membrane permeability thus limiting those agents to extracellular targets. Furthermore, the long half-life of employed radiometals is partially conflicting the benefits of the pretargeting approach.

To fill this gap we aimed to synthesize a radiofluorinated tetrazine, utilizing a 3,6-dialkyl substituted Tz moiety that is less reactive in IEDDA cycoadditions, but would be sufficiently stable for radiolabeling (*Manuscript #1*). The compound 3-(3-fluoropropyl)-6-methyl-1,2,4,5-tetrazine showed good reactivity with dienophiles TCO and s-TCO (as predicted using *in silico* methods and confirmed by stopped flow photometry), and excellent plasma stability.

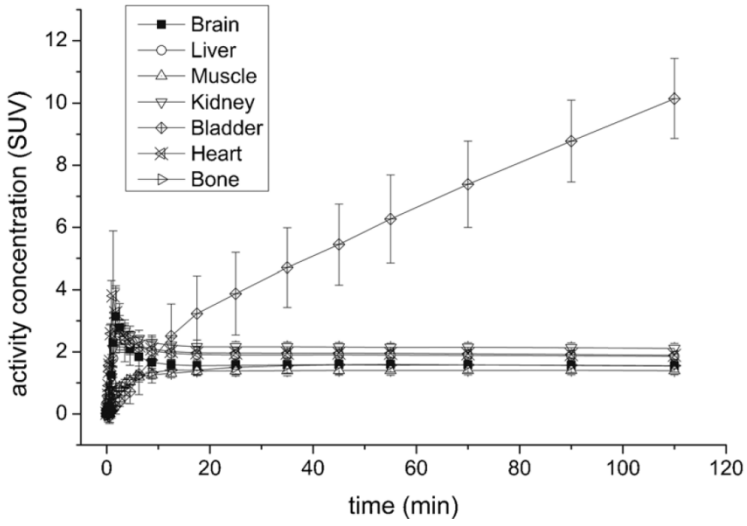


***Figure 12**: Time-activity-curves of the first ^{18}F-tetrazine in BALB/c mice showing homogenous biodistribution.*[87]

Reprint kindly granted by Wiley and Sons.

Radiolabeling was successful using straight forward ^{18}F-fluorination conditions in 5% decay-corrected yield. By applying optimized labeling conditions (using tetrabutyl ammonium hydrogen carbonate as base and mixtures of thexyl alcohol and MeCN as solvents) the isolated radiochemical yield of this compound could be improved to 35% (*Manuscript #3*). *In vivo* investigation by PET/MR (see Figure 12) and radiometabolite analysis revealed very uniform uptake, renal excretion and high metabolic stability, indeed relevant properties for a labeled compound to be used as secondary agent in bioorthogonal imaging. Furthermore, a simple experiment was designed to prove *in vivo* reactivity of this labeled tetrazine agent. For this reason dienophile s-TCO linked to a short oligoethylene glycol linker was administered to mice that were pre-treated with ^{18}F-tetrazine. Following five minutes of *in vivo* reaction time radio-TLC analysis of blood revealed near-quantitative reaction of the radiolabeled tetrazine (Figure 13). Indeed, this simple model experiment is able to evaluate *in vivo* reactivity within the blood-stream, but is unable to prove if the agent is also suitable for imaging. Dienophile-antibody conjugates in xenograft mouse models are complex testing platforms that are influenced by antibody pharmacokinetics, dienophile *in vivo* stability and disease state in each individual animal, and are therefore unsuitable to assess performance of the pull down reagent. Still, a solid imaging model applying *in vivo* click chemistry was highly desirable. Research conducted during a joint project involving a two-month stay at the European Institute for Molecular Imaging (Münster, Germany) aiming for tumor-targeting using functionalized silica-nanoparticles, revealed that the particles are almost exclusively and rapidly accumulated in the lung following intravenous administration. Consequently these results were used to set up a robust *in vivo* click imaging model that does not require disease models in mice, but instead can be used in naïve animals. In short, TCO-tagged nanoparticles were administered, and

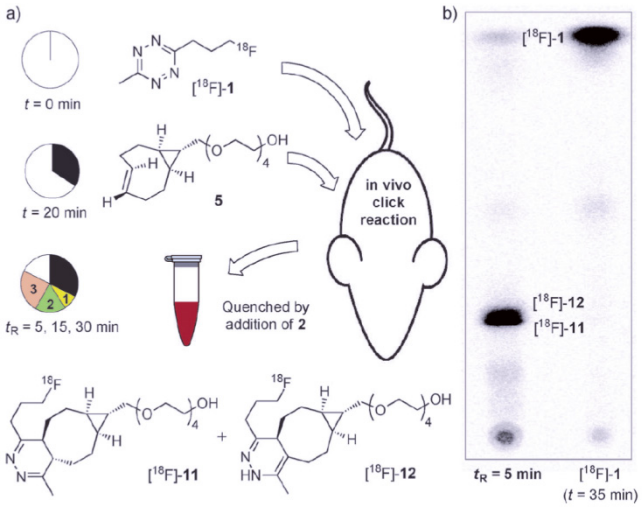


Figure 13: *Simple model proving bioorthogonal reactivity of the ^{18}F-tetrazine. IEDDA reaction in the blood stream with a s-TCO derivative, followed by quenching and radio-TLC analysis.*[87] *Reprint kindly granted by Wiley and Sons.*

after a short uptake time (5 min) the labeled tetrazine species was given followed by dynamic PET imaging (Figure 14, *Manuscript #2*).

Furthermore, we aimed to transfer the promising properties demonstrated for the 3,6-dialkyl substituted fluorine-18 tetrazine to a compound suitable for labeling with carbon-11. This isotope is advantageous due to a very short half-life thus minimizing patient dose. Aiming for a low-molecular-weight compound that is also based on a dialkyl scaffold, and could furthermore easily be labeled using ^{11}C-methylation we focused on N-methyl-1-(6-methyl-1,2,4,5-tetrazin-3-yl)methan amine. *In silico* prediction revealed good IEDDA reactivity, and the N-desmethyl precursor was labeled in good radiochemical yields (*Manuscript #2*). *In vivo* investigation using PET/MR and radio-TLC metabolite analysis revealed rapid renal excretion and homogenous biodistribution as well as high metabolic stability of this compound. The ability of this carbon-11 labeled tetrazine to act as secondary agent in pretargeted PET imaging was finally shown using lung-targeting TCO-modified Silica-nanoparticles (Figure 14).

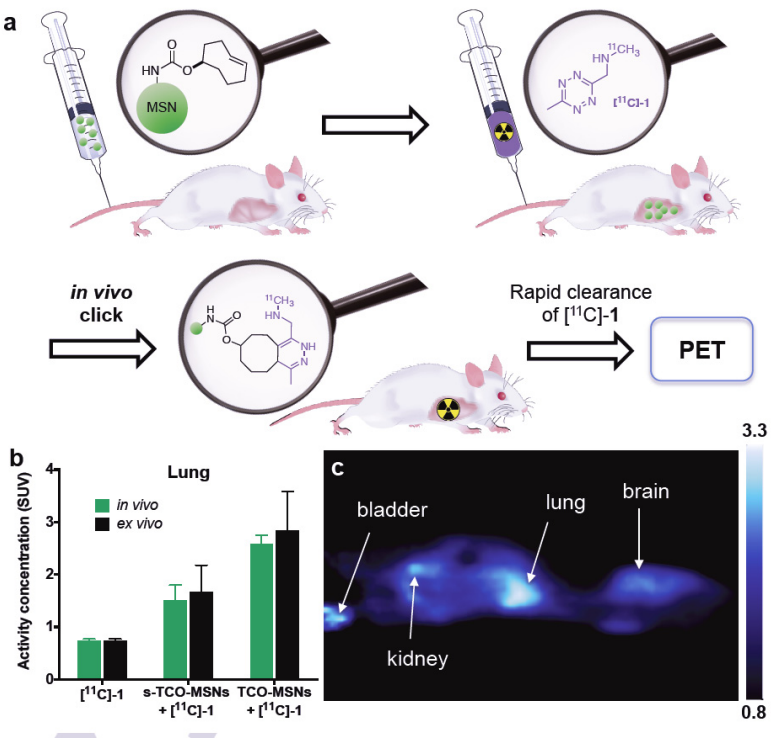


Figure 14: *Pretargeting model based on TCO-tagged SiO_2-nanoparticles for the in vivo evaluation of the [^{11}C]-tetrazine (for details see manuscript #2)*

Research in *Manuscript #3* focused on *in silico* and *in vivo* evaluation of a series of alkyl-aryl tetrazines that show elevated reactivity as compared to dialkyl derivatives. Although sufficiently reactive for pretargeting experiments in the mouse model, dialkyl tetrazines are unlikely to be suitable for imaging in larger animals. Building on results from *manuscript #1*, the 3-fluoropropyl moiety, that has shown to be suitable for radiolabeling, was left unchanged. The 6-methyl group was displaced by aryl functionalities varying in polarity and electronic properties (Figure 15). Cycloaddition reactivity for all derivatives was calculated using Gaussian, and measured using stopped-flow photometry with dienophile TCO. Direct

nucleophilic radiofluorination was successful for the four least reactive derivatives, while fluorination attempts of the more reactive compounds resulted in degradation or formation of by-products, thus shedding light on the reactivity threshold that still allows for direct labeling. Biodistribution and metabolism of tetrazines that were successfully radiofluorinated was investigated by PET/MR scanning and analysis of plasma and urine samples using radio-TLC. Methylsulfide bearing compound 3-(3-fluoropropyl)-6-(4-(methylthio)phenyl)-1,2,4,5-tetrazine was identified as promising agent that shows homogenous uptake in all analyzed organs including the brain. Moreover, this compound was shown by radio-TLC analysis to be rapidly oxidized *in vivo* to the according sulfoxide- and sulfone metabolites. Therefore this compound acts as pro-drug for tetrazines with enhanced bioorthogonal reactivity. The sulfone derivative, that we were not able to prepare by direct labeling, was successfully obtained by DMDO mediated oxidation of 3-(3-[^{18}F]fluoropropyl)-6-(4-(methylthio)phenyl)-1,2,4,5-tetrazine, thus bypassing the instability of this tetrazine using nucleophilic fluorinations. The sulfone derivative exhibited very uniform biodistribution and high metabolic stability, and is therefore also a promising agent for bioorthogonal imaging.

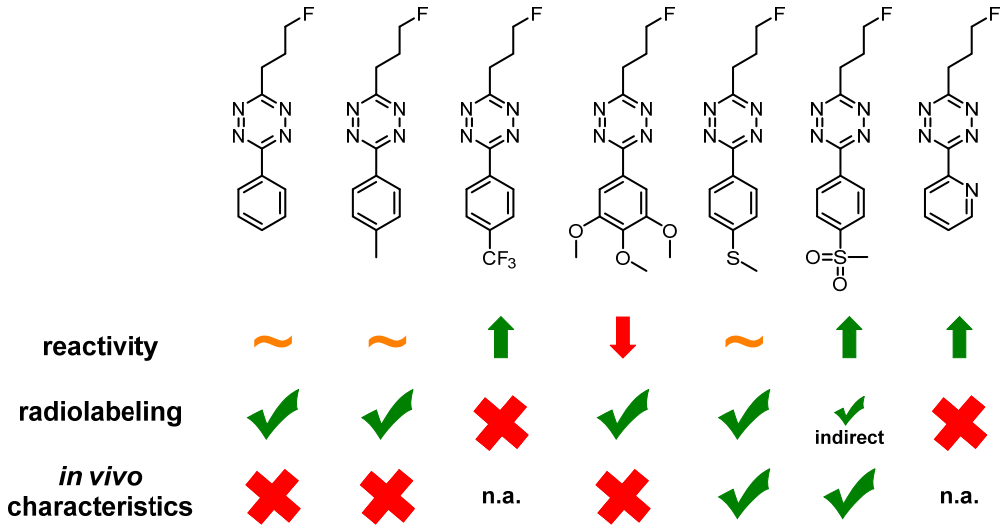


Figure 15: *Alkyl-aryl tetrazine derivatives investigated in manuscript #3*

Trans-cyclooctenes, fast dienophiles used in tetrazine ligations have very limited commercial availability. Synthesis of these compounds requires expensive photochemistry equipment such as UV-reactors and quartz glassware. In *manuscript #4* we develop a flow-photoreactor, assembled from readily available and low-cost parts, that allows for flexible large-scale preparation of TCOs. The system (Figure 16a) was tested in the synthesis of *trans*-cyclooctene as well as in the synthesis of functionalized TCO-derivatives TCO-5-OH, d-TCO,

s-TCO and TCO-3-OH (Figure 16b) resulting in yields compareable to previously published data (Figure 16). The kinetics of isomerization using the described photoisomerization system was determined using GC/FID.

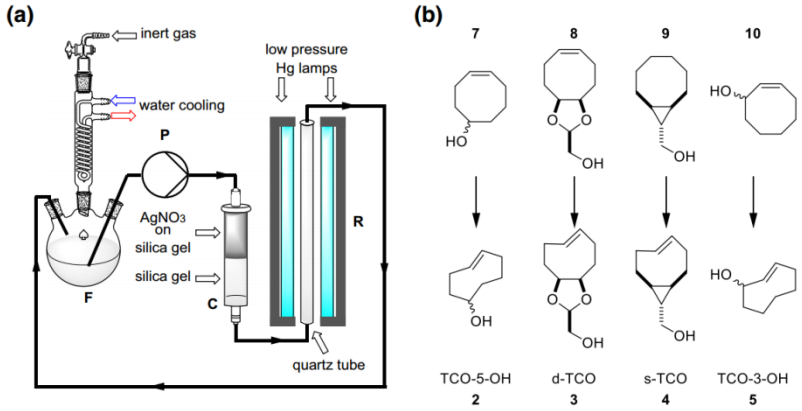


Figure 16: *Photoisomerization system (a) and isomerization reactions (b) as described in manuscript #4*[55]

In manuscript #5 we shed light on the metabolism of [^{18}F]-2-fluoroethylazide, a compound that has previously been proposed as pull down reagent for bioorthogonal PET imaging based on the SPAAC reaction. Within our contribution we show that ^{18}F-FEA, that was prepared using a novel crystalline precursor based on the p-nitrobenzenesulfonyl group, is rapidly degraded *in vivo* causing generation of free fluoride anions as visible by steady bone uptake in PET data and by plasma analysis using radio-HPLC. Closely related novel compounds [^{18}F] 1-azido-3-fluoropropane and [^{18}F] 2-azido-1-fluoropropane were prepared and investigated by PET/MR imaging and metabolite analysis, aiming for improved *in vivo* stability of those low-molecular-weight agents. Furthermore, the radiofluorinated azide species were successfully used for rapid radiolabeling of the endogenous μ-opioid-ligand endomorphin-1 using the copper(I) catalyzed azide alkyne cycloaddition (Figure 17)

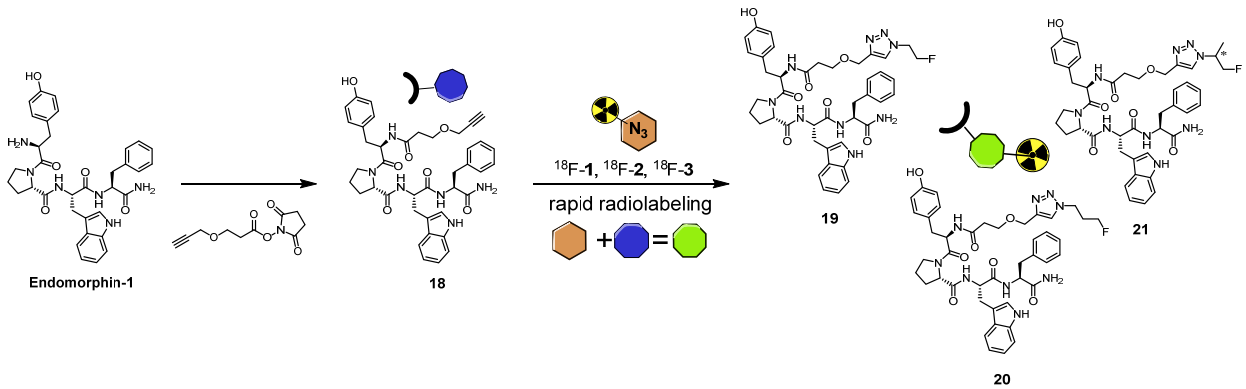


Figure 17: *Rapid radiolabeling of endomorphin-1, as described in manuscript #5*

2.3 Original Works

In the following section, all manuscripts (published, submitted, draft) are included. Permission for the reprint of manuscript #1 was kindly given by Wiley and Sons. Supporting information for manuscripts #1, #2, #3 and #5 containing most of experimental details and data is included in the appendix of this thesis.

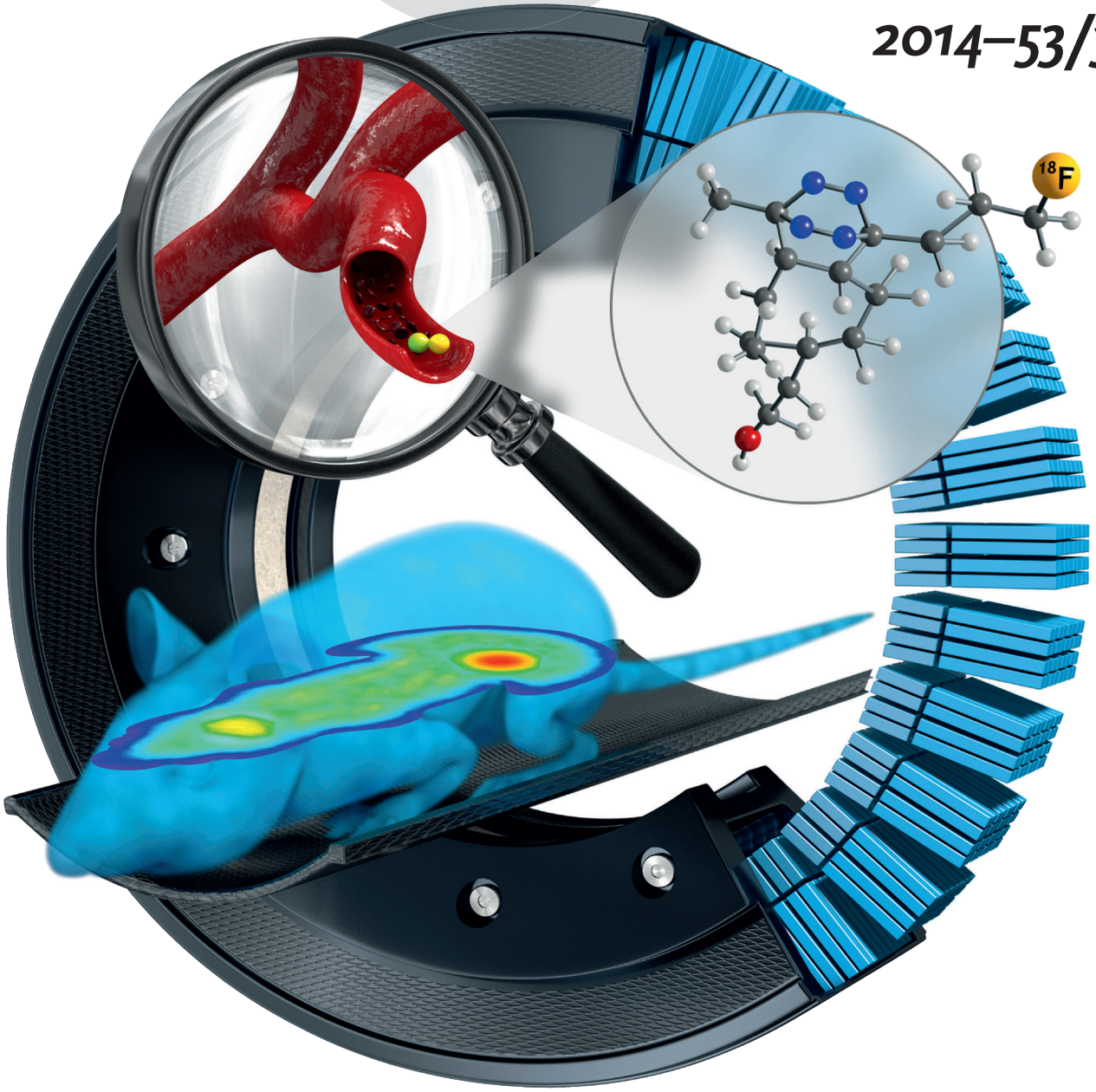
Manuscript #1

Reprinted from *Angewandte Chemie International Edition* (2014), 53, 9655-9659 with kind permission from Wiley and Sons.

Denk, C.; Svatunek, D.; Filip, T.; Wanek, T.; Lumpi, D.; Fröhlich, J.; Kuntner-Hannes, C.; Mikula, H.:

Development of a ^{18}F-labeled Tetrazine with Favorable Pharmacokinetics for Bioorthogonal PET Imaging

C. Denk (2016)
A Journal of the Gesellschaft Deutscher Chemiker
Angewandte Chemie
GDCh
International Edition
www.angewandte.org
2014–53/36



Bioorthogonal PET probes ...

... serve as highly valuable tools in the field of pretargeted molecular imaging. In their Communication on page 9655 ff., H. Mikula, C. Kuntner, and co-workers describe the development, synthesis, and characterization of a low-molecular-weight ^{18}F-labeled tetrazine derivative that can be used for bioorthogonal PET imaging of dienophile-tagged (bio)molecules through the application of in vivo chemistry.

WILEY-VCH

Angewandte International Edition Chemie

DOI: 10.1002/anie.201404277

Bioorthogonal Imaging

Development of a ^{18}F-Labeled Tetrazine with Favorable Pharmacokinetics for Bioorthogonal PET Imaging**

Christoph Denk, Dennis Svatunek, Thomas Filip, Thomas Wanek, Daniel Lumpi, Johannes Fröhlich, Claudia Kuntner, and Hannes Mikula**

Abstract: *A low-molecular-weight ^{18}F-labeled tetrazine derivative was developed as a highly versatile tool for bioorthogonal PET imaging. Prosthetic groups and undesired carrying of ^{18}F through additional steps were evaded by direct ^{18}F-fluorination of an appropriate tetrazine precursor. Reaction kinetics of the cycloaddition with trans-cyclooctenes were investigated by applying quantum chemical calculations and stopped-flow measurements in human plasma; the results indicated that the labeled tetrazine is suitable as a bioorthogonal probe for the imaging of dienophile-tagged (bio)molecules. In vitro and in vivo investigations revealed high stability and PET/MRI in mice showed fast homogeneous biodistribution of the ^{18}F-labeled tetrazine that also passes the blood–brain barrier. An in vivo click experiment confirmed the bioorthogonal behavior of this novel tetrazine probe. Due to favorable chemical and pharmacokinetic properties this bioorthogonal agent should find application in bioimaging and biomedical research.*

Bioorthogonal imaging applying in vivo chemistry has emerged as a highly versatile tool in chemical biology and biomedicine.[1] Since the development of copper-free click chemistry for bioimaging using the strain-promoted azide–alkyne cycloaddition (SPAAC),[2] this bioorthogonal ligation has been used for a wide variety of applications with the aim to examine the molecular details of biological processes.[3] Although reaction kinetics were successively improved during the last years,[4] rate constants of SPAAC ligations are still limited ($< 5\,M^{-1}s^{-1}$, acetonitrile, 20 °C) and therefore this chemistry is not fully suitable for bioconjugations in vivo. Nevertheless, in vivo SPAAC has recently been applied for the development of a pretargeted imaging approach using positron emission tomography (PET).[5] To circumvent problems in terms of (relatively) low reaction rates of SPAAC ligations, Fox et al. and Weissleder et al. have independently introduced the inverse-electron-demand Diels–Alder (IEDDA)-initiated conjugation between 1,2,4,5-tetrazines (Tz) and strained cycloalkenes as a highly efficient bioorthogonal ligation.[6] Since then, this reaction has attracted broad attention and has been extensively used in many biomedical applications including the development of bioorthogonal probes, live-cell imaging, protein labeling, and the synthesis of PET imaging agents.[7] Furthermore, IEDDA was successfully applied in combination with SPAAC for simultaneous multitarget imaging.[8] Recently, Carlson et al. reported the development of advanced bioorthogonal turn-on probes that apply through-bond energy transfer leading to fluorescence quenching within boron dipyrromethene (BODIPY)-tetrazine derivatives.[9] Reaction kinetics of IEDDA ligations were further improved by the development and application of the bicyclo[6.1.0]non-4-ene (s-TCO) moiety, an even more strained *trans*-cyclooctene derivative, as a highly reactive dienophile leading to tetrazine ligations with rate constants of up to approximately $20000\,M^{-1}s^{-1}$ (MeOH, 25 °C).[10] In addition to commonly used *trans*-cyclooctenes (TCO) and s-TCO,[11] cyclopropene (CP) tags have recently been reported as useful dienophiles with lower steric demand and have successfully been applied in live-cell imaging.[12]

Despite many applications of IEDDA ligations in the field of fluorescence imaging, the development of bioorthogonal PET approaches is still restricted due to a lack of efficient radiolabeled agents that distribute homogenously and show fast in vivo reaction kinetics, high stability, and adequate clearance. ^{18}F-Labeling of dienophiles such as TCO and norbornene was preferred in terms of pretargeting approaches applying IEDDA bioconjugations so far due to the previously observed and reported insufficient stability of tetrazines during direct fluorination.[13] Yet, this approach is still cumbersome due to the fact that instead of readily available cycloalkene tags the tetrazine moiety has to be attached to the pretargeting probe. Furthermore, a tetrazine-type radiolabeled agent would be capable of being applied for bioorthogonal imaging of various dienophiles and thus provide high versatility. A ^{11}C-labeled tetrazine was initially developed by Herth et al.[14] and metal radionuclides such as ^{64}Cu and ^{89}Zr were attached to tetrazines using chelating ligands resulting in relatively large and complex bioorthogonally imaging agents.[15] Furthermore, polymer-modified tetrazines were developed and used for pretargeted PET imaging.[16] However, the development of a readily accessible radiolabeled low-molecular-weight tetrazine taking advantage of the high specific radioactivity of ^{18}F (allowing admin-

[*] C. Denk, D. Svatunek, Dr. D. Lumpi, Prof. J. Fröhlich, Dr. H. Mikula
Institut für Angewandte Synthesechemie
Technische Universität Wien (TUW) (Austria)
E-mail: hannes.mikula@tuwien.ac.at
Dr. T. Filip, Dr. T. Wanek, Priv.-Doz. Dr. C. Kuntner
Health and Environment Department, Biomedical Systems
Austrian Institute of Technology (AIT)
Seibersdorf (Austria)
E-mail: claudia.kuntner@ait.ac.at

[**] Financial support from the Vienna Anniversary Foundation for Higher Education (H-2500/2012) is gratefully acknowledged. We thank Prof. Wolfgang Linert (VUT), Dr. Roland Müller (Seibersdorf Laboratories), Dominik Matscheko (VUT), and Walter Kuba (VUT) for their kind support during this work. PET = positron emission tomography.

Supporting information for this article is available on the WWW under http://dx.doi.org/10.1002/anie.201404277.

 © 2014 Wiley-VCH Verlag GmbH & Co. KGaA, Weinheim

istration of low-mass dosages and shorter radiation exposures) is still significant, which inspired us to focus on this particular problem in the field of bioorthogonal PET imaging.

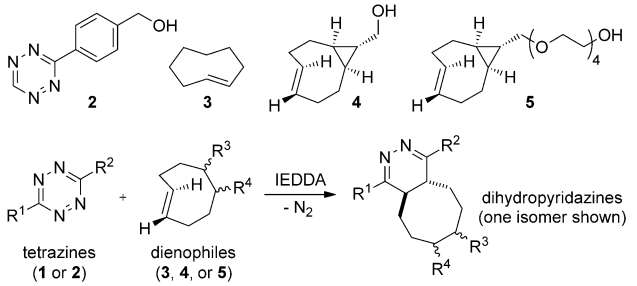
Herein we report our results on the synthesis and characterization of a low-molecular-weight ^{18}F-labeled tetrazine with favorable pharmacokinetics that is applicable as a versatile tool for pretargeted PET imaging using in vivo IEDDA chemistry.

During the development of improved procedures for the synthesis of 1,2,4,5-tetrazines, the characterization of a variety of these compounds revealed an inverse correlation between their stability in fetal bovine serum and the reaction rates of their cycloaddition with dienophiles.[17] Therefore, we hypothesized that stability problems during direct tetrazine fluorination can be avoided or minimized by using less reactive 3,6-dialkyltetrazines that still possess sufficiently high reaction rates for pretargeted in vivo applications. The availability of physiologically stable radiolabeled tetrazines is crucial for the development of reliable PET imaging approaches. In addition to this trade-off (reactivity vs. stability), we intended to develop water-soluble low-molecular-weight compounds with the aim to obtain imaging agents with favorable pharmacokinetic properties. These considerations led to the chemical structure of tetrazine **1**. The two alkyl substituents were chosen to be as small as reasonable. A derivative with a methyl group was preferred since it is more stable than an unsubstituted tetrazine, and a three-methylene spacer was considered between the fluorine and the tetrazine moiety to avoid the undesired high reactivity of benzyl-type precursors (Tz-CH_2-X) as well as possible elimination during nucleophilic fluorination (Tz-CH_2CH_2-X → Tz-CH=CH_2). Quantum chemical calculations on the basis of a recently reported computational approach (DFT, M06-2X/6-31G(d,p), Gaussian 09)[18] were applied to estimate the reaction kinetics (Table 1) of **1** in comparison to that of phenyl-substituted tetrazines (e.g. **2**),[19] which are commonly used in combination with TCO tags for various bioorthogonal ligation applications.[20] As expected, modeling of IEDDA reactions with *trans*-cyclooctene (**3**) showed an increased activation free energy for **1** (18.8 kcal mol^{-1}) relative to that for **2** (15.0 kcal mol^{-1}), but this difference is compensated when s-TCO **4** is used for cycloaddition with **1** (15.3 kcal mol^{-1}). Thus, applying the bioorthogonal reaction pair **1**/**4** should result in reasonable rate constants similar to those of the frequently applied ligation between **2** and **3**. This assumption was verified by stopped-flow measurements after preparation of **1** starting from 4-hydroxypropanenitrile (**6**) applying metal-catalyzed tetrazine synthesis[21] followed by DAST-mediated fluorination of the intermediate **7** (Scheme 1). Furthermore, a significantly increased reaction rate was observed for the cycloaddition of **1** with the water-soluble s-TCO derivative **5** in human plasma ($k_2 > 8000\ M^{-1}s^{-1}$, 37 °C), which is in agreement with previously reported studies on the effect of water on IEDDA reaction kinetics (Table 1).[22]

Regarding the preparation of compound **7**, we have studied the impact of different reaction parameters on tetrazine synthesis and have mainly focused on the reagent grade of hydrazine. Finally, we did not observe significantly decreased yields of **7** when the monohydrate (18%) was used instead of anhydrous hydrazine (21%) that was originally used for the metal-catalyzed preparation of 3,6-dialkyltetrazines.[21] This is of particular interest, since the availability of anhydrous hydrazine has been restricted in Europe since 2011 due to the REACH regulation of the European Chemicals Agency.[23] Although commercially available hydrazine cyanurate can be used as a reagent for the safe preparation of anhydrous hydrazine of high purity,[24] reliable synthetic methods using the monohydrate or other forms (e.g. hydrazine salts) should be preferred.

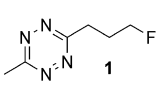
The in vitro stability of **1** in human plasma was assessed by spectrophotometric measurements and HPLC. Almost no degradation was observed after incubation at 37 °C for 12 h (99% recovery) further revealing the capability of **1** as a promising scaffold for the development of a radiolabeled agent for pretargeted PET imaging. Although the excellent stability of **4** (no degradation in human serum, 30 mM butylamine in MeOH or 5 mM ethanethiol in MeOH) was shown by Taylor et al.,[10] they also observed isomerization (58% after 3.5 h) to the unreactive *cis* isomer at a high concentration of ethanethiol (30 mM in MeOH). Furthermore, Rossin et al. have recently reported that *trans*-cyclooctenes are probably isomerized by interactions with copper-containing proteins; they also presented strategies to circumvent this problem by increasing the steric bulk of the tag.[25]

Table 1: Reaction kinetics of IEDDA cycloadditions obtained by computational methods (M06-2X/6-31G(d,p), Gaussian 09) and stopped-flow measurements.

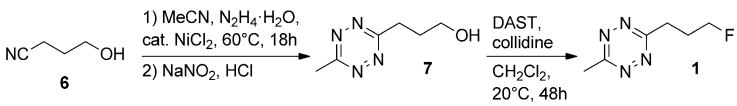


Tetrazine	DP[a]	Solvent	$\Delta G^{\ddagger}_{calcd}$[b]	$\Delta G^{\ddagger}$[c]	k_2 [$M^{-1}s^{-1}$][d]
1	**3**	1,4-dioxane	18.7	17.5	1.49 ± 0.01
1	**4**	1,4-dioxane	15.3	15.0	85.5 ± 2.3
1	**5**	human plasma	n.d.[e]	n.d.	8200 ± 300
2	**3**	1,4-dioxane	15.0	15.1	79.2 ± 1.3

[a] DP = dienophile. [b] Calculated activation free energies (kcal mol^{-1}; 25 °C). [c] Activation free energies determined by stopped-flow measurements (kcal mol^{-1}; 25 °C). [d] Second-order rate constants (measurements at 37 °C). [e] n.d. = not determined.



1



Scheme 1. Synthesis of tetrazine **1** (DAST = diethylaminosulfur trifluoride).

© 2014 Wiley-VCH Verlag GmbH & Co. KGaA, Weinheim

The stability of compound **5** was assessed by incubation in human plasma at 37 °C for 24 h leading to a recovery of > 80 %, a significantly higher value than those previously reported for reactive tetrazines.[17] Hence, the combination of radiolabeled tetrazines as pull-down reagents and (s-)TCO labeling should be advantageous for bioorthogonal in vivo imaging in contrast to inverse strategies involving tetrazine tags and radiolabeled dienophiles.

Radiosynthesis affording [^{18}F]-**1** was successfully carried out by direct fluorination of the tosylated intermediate **8** in a radiochemical yield of up to 18 % (Figure 1). Cycloaddition of [^{18}F]-**1** with s-TCO **4** occurred rapidly forming the conjugate [^{18}F]-**9** that slowly isomerized to [^{18}F]-**10** (both products as a mixture of regio- and stereoisomers).

In vivo studies were performed by administration of [^{18}F]-**1** to female BALB/c mice followed by dynamic PET ($n = 4$) and PET/MR ($n = 2$) imaging (MR = magnetic resonance tomography). A very homogenous biodistribution of [^{18}F]-**1** was observed in all regions in the body including the brain, which clearly indicates the ability of [^{18}F]-**1** to pass the blood–brain barrier (Figure 2). Furthermore, PET/MR revealed no significant extent of in vivo defluorination of [^{18}F]-**1**, since no enhanced radioactivity uptake in bone was observed.[26] Time–activity curves were similar for all analyzed organs

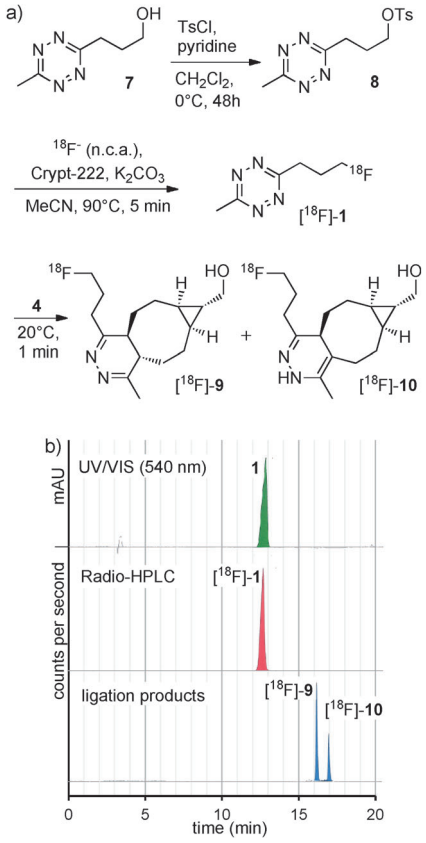


Figure 1. a) Radiosynthesis of [^{18}F]-**1** and IEDDA cycloaddition with s-TCO **4** (n.c.a. = no carrier added; only one isomer shown for [^{18}F]-**9** and [^{18}F]-**10**). b) HPLC of **1** (UV/Vis, 540 nm), radio-HPLC of purified [^{18}F]-**1** and ligation products after click reaction with s-TCO **4**. HPLC conditions: Zorbax SB-Aq reversed phase, H_2O/MeCN gradient elution.

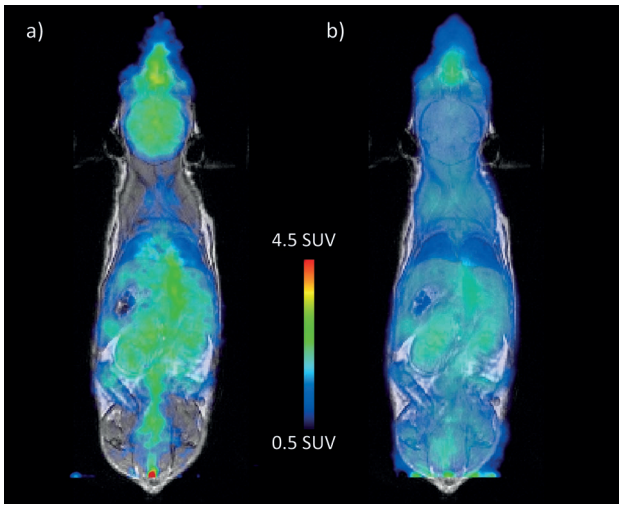


Figure 2. Combined PET/MRI summation images: 0–5 min (a) and 5–120 min (b) after injection of [^{18}F]-**1**.

(Figure 3a). After the initial perfusion directly after intravenous administration of [^{18}F]-**1** a very uniform uptake steadily decreasing from 2 to 1.5 SUV (standardized uptake value) was observed in all organs (except the urinary bladder) during the onset of the PET scan. Conversely, SUV in the urinary bladder increased from 2 to 10 SUV, suggesting

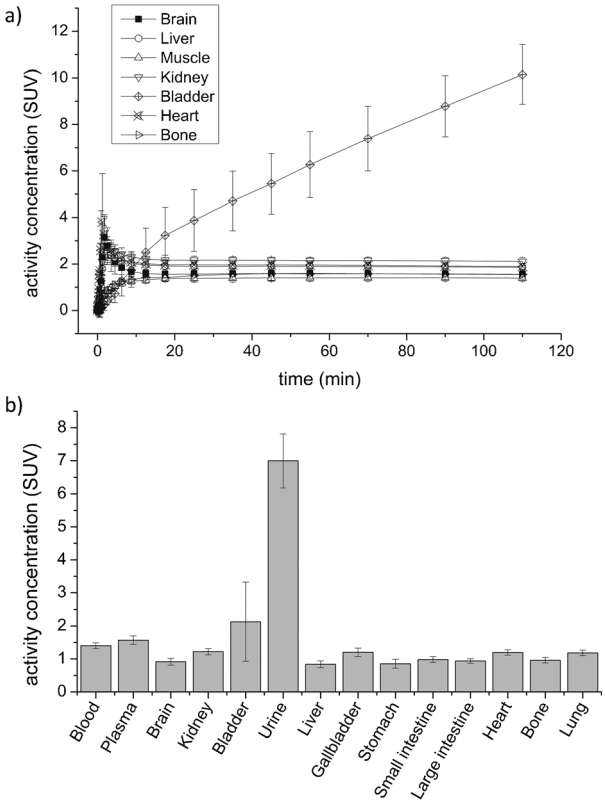


Figure 3. a) Mean organ time–activity curves obtained in BALB/c mice ($n = 6$; for bone $n = 2$). b) Ex vivo biodistribution of [^{18}F]-**1** in indicated organs 2 h after intravenous administration in mice ($n = 6$). Data are presented as mean SUV ± standard deviation. All organs (apart from the bladder) displayed similar radioactivity concentration values.

© 2014 Wiley-VCH Verlag GmbH & Co. KGaA, Weinheim

a rapid renal clearance of [^{18}F]-**1**. Evaluation of the ex vivo biodistribution determined 120 min after [^{18}F]-**1** injection gave values ranging from 1 SUV to 1.5 SUV with the exception of the urinary bladder (Figure 3b), which is in good agreement with the PET results. The in vivo stability of [^{18}F]-**1** was further examined by radio-TLC of mouse plasma obtained immediately after the imaging experiments (120 min after administration). We observed only a low degree of metabolic degradation (approximately 15%) as shown by the formation of more polar metabolites, which is assumed to occur via enzyme-catalyzed oxidation of the methyl group of [^{18}F]-**1** thus leading to xenobiotic metabolization similar to toluene and related compounds.[27]

Furthermore, the bioconjugation of [^{18}F]-**1** and the water-soluble dienophile **5** was performed in vivo to verify the bioorthogonal behavior of this novel tetrazine-type PET probe.[^{18}F]-**1** was administered to female BALB/c mice ($n = 4$) followed by **5** after an initial period of 20 min. In this experiment an inverse approach was used to allow for the homogenous biodistribution of the radiolabeled tetrazine prior to in vivo reaction. After 5, 15, and 30 min retroorbital blood was collected and the click reaction was quenched by addition of the more reactive tetrazine **2**. Murine plasma was obtained and analyzed using radio-TLC (Figure 4). Finally, we observed >90% conversion after 5 min and complete in vivo reaction 30 min after administration of **5** (see the Supporting Information, Figure S4). These results clearly indicate and confirm the capability of [^{18}F]-**1** as a highly valuable and versatile bioorthogonal probe for pretargeted PET imaging.

In summary, we have developed a fast and reliable procedure for the synthesis of a low-molecular-weight and water-soluble radiolabeled tetrazine; direct [^{18}F]-fluorination was applied to avoid additional steps and the need for prosthetic groups. Furthermore, [^{18}F]-**1** was prepared using readily accessible and/or commercially available reagents without the use of anhydrous hydrazine and [^{18}F]-**1** was shown to possess highly favorable pharmacokinetic properties. Although high stability of [^{18}F]-**1** was observed, its metabolic behavior has still to be verified in further studies. In vivo investigations clearly indicate the suitability of this radiolabeled tetrazine as a pull-down reagent for pretargeted PET imaging. Hence, we expect this highly versatile and readily accessible compound, which enables in vivo detection of dienophile-tagged (bio)molecules, to find many applications and lead to further investigations in the fields of bioorthogonal imaging and biomedical research.

Received: April 13, 2014
Revised: May 9, 2014
Published online: July 2, 2014

Keywords: bioorthogonal chemistry · click chemistry · imaging agents · kinetics · tetrazines

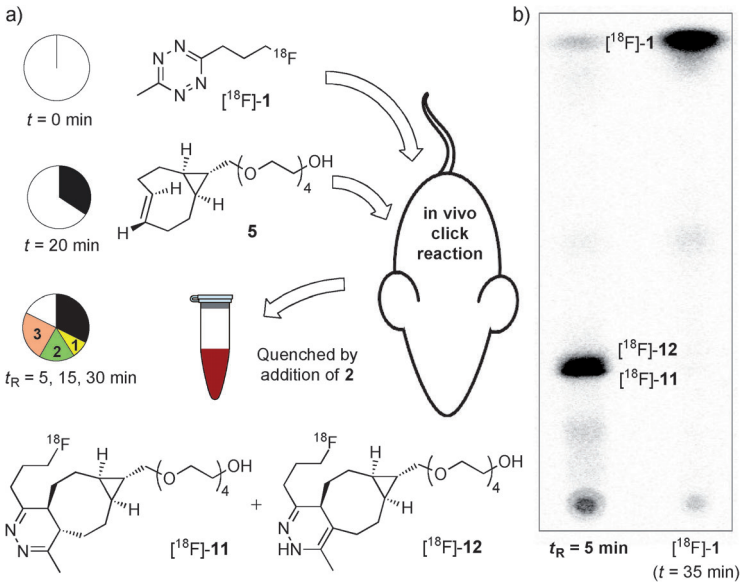


Figure 4. a) Bioorthogonal in vivo reaction of [^{18}F]-**1** and dienophile **5** leading to the formation of [^{18}F]-**11** and [^{18}F]-**12** (one isomer shown). b) Radio-TLC (SiO_2) of plasma obtained after 5 min of reaction time (left) and blank obtained 35 min after administration of [^{18}F]-**1** (right).

[1] a) L. Carroll, H. L. Evans, E. O. Aboagye, A. C. Spivey, *Org. Biomol. Chem.* **2013**, *11*, 5772–5781; b) N. K. Devaraj, R. Weissleder, *Acc. Chem. Res.* **2011**, *44*, 816–827; c) E. M. Sletten, C. R. Bertozzi, *Acc. Chem. Res.* **2011**, *44*, 666–676.

[2] J. M. Baskin, J. A. Prescher, S. T. Laughlin, N. J. Agard, P. V. Chang, I. A. Miller, A. Lo, J. A. Codelli, C. R. Bertozzi, *Proc. Natl. Acad. Sci. USA* **2007**, *104*, 16793–16797.

[3] a) S. T. Laughlin, J. M. Baskin, S. L. Amacher, C. R. Bertozzi, *Science* **2008**, *320*, 664–667; b) A. B. Neef, C. Schultz, *Angew. Chem.* **2009**, *121*, 1526–1529; *Angew. Chem. Int. Ed.* **2009**, *48*, 1498–1500; c) T. Plass, S. Milles, C. Koehler, C. Schultz, E. A. Lemke, *Angew. Chem.* **2011**, *123*, 3964–3967; *Angew. Chem. Int. Ed.* **2011**, *50*, 3878–3881; d) R. Xie, S. Hong, X. Chen, *Curr. Opin. Chem. Biol.* **2013**, *17*, 747–752; e) J. C. Jewett, C. R. Bertozzi, *Chem. Soc. Rev.* **2010**, *39*, 1272–1279; f) J. C. Jewett, E. M. Sletten, C. R. Bertozzi, *J. Am. Chem. Soc.* **2010**, *132*, 3688–3690.

[4] G. de Almeida, E. M. Sletten, H. Nakamura, K. K. Palaniappan, C. R. Bertozzi, *Angew. Chem.* **2012**, *124*, 2493–2497; *Angew. Chem. Int. Ed.* **2012**, *51*, 2443–2447.

[5] S. B. Lee, H. L. Kim, H.-J. Jeong, S. T. Lim, M.-H. Sohn, D. W. Kim, *Angew. Chem.* **2013**, *125*, 10743–10746; *Angew. Chem. Int. Ed.* **2013**, *52*, 10549–10552.

[6] a) M. L. Blackman, M. Royzen, J. M. Fox, *J. Am. Chem. Soc.* **2008**, *130*, 13518–13519; b) N. K. Devaraj, R. Weissleder, S. A. Hilderbrand, *Bioconjugate Chem.* **2008**, *19*, 2297–2299.

[7] a) G. Budin, K. S. Yang, T. Reiner, R. Weissleder, *Angew. Chem.* **2011**, *123*, 9550–9553; *Angew. Chem. Int. Ed.* **2011**, *50*, 9378–9381; b) K. Lang, L. Davis, J. Torres-Kolbus, C. Chou, A. Deiters, J. W. Chin, *Nat. Chem.* **2012**, *4*, 298–304; c) K. S. Yang, G. Budin, T. Reiner, C. Vinegoni, R. Weissleder, *Angew. Chem.* **2012**, *124*, 6702–6707; *Angew. Chem. Int. Ed.* **2012**, *51*, 6598–6603; d) D. S. Liu, A. Tangpeerachaikul, R. Selvaraj, M. T. Taylor, J. M. Fox, A. Y. Ting, *J. Am. Chem. Soc.* **2011**, *134*, 792–795; e) J. L. Seitchik, J. C. Peeler, M. T. Taylor, M. L. Blackman, T. W. Rhoads, R. B. Cooley, C. Refakis, J. M. Fox, R. A. Mehl, *J. Am. Chem. Soc.* **2012**, *134*, 2898–2901; f) E. Kim, K. S. Yang, R. Weissleder, *PLoS One* **2013**, *8*, e81275; g) T. Reiner, E. J.

© 2014 Wiley-VCH Verlag GmbH & Co. KGaA, Weinheim

Keliher, S. Earley, B. Marinelli, R. Weissleder, *Angew. Chem.* **2011**, *123*, 1963 – 1966; *Angew. Chem. Int. Ed.* **2011**, *50*, 1922 – 1925.

[8] M. R. Karver, R. Weissleder, S. A. Hilderbrand, *Angew. Chem.* **2012**, *124*, 944 – 946; *Angew. Chem. Int. Ed.* **2012**, *51*, 920 – 922.

[9] J. C. T. Carlson, L. G. Meimetis, S. A. Hilderbrand, R. Weissleder, *Angew. Chem.* **2013**, *125*, 7055 – 7058; *Angew. Chem. Int. Ed.* **2013**, *52*, 6917 – 6920.

[10] M. T. Taylor, M. L. Blackman, O. Dmitrenko, J. M. Fox, *J. Am. Chem. Soc.* **2011**, *133*, 9646 – 9649.

[11] R. Selvaraj, J. M. Fox, *Curr. Opin. Chem. Biol.* **2013**, *17*, 753 – 760.

[12] J. Yang, J. Šečkutė, C. M. Cole, N. K. Devaraj, *Angew. Chem.* **2012**, *124*, 7594 – 7597; *Angew. Chem. Int. Ed.* **2012**, *51*, 7476 – 7479.

[13] a) J. Šečkutė, N. K. Devaraj, *Curr. Opin. Chem. Biol.* **2013**, *17*, 761 – 767; b) Z. Li, H. Cai, M. Hassink, M. L. Blackman, R. C. D. Brown, P. S. Conti, J. M. Fox, *Chem. Commun.* **2010**, *46*, 8043 – 8045; c) J. C. Knight, S. Richter, M. Wuest, J. D. Way, F. Wuest, *Org. Biomol. Chem.* **2013**, *11*, 3817 – 3825.

[14] M. M. Herth, V. L. Andersen, S. Lehel, J. Madsen, G. M. Knudsen, J. L. Kristensen, *Chem. Commun.* **2013**, *49*, 3805 – 3807.

[15] a) R. Rossin, P. R. Verkerk, S. M. van den Bosch, R. C. M. Vulders, I. Verel, J. Lub, M. S. Robillard, *Angew. Chem.* **2010**, *122*, 3447 – 3450; *Angew. Chem. Int. Ed.* **2010**, *49*, 3375 – 3378; b) B. M. Zeglis, K. K. Sevak, T. Reiner, P. Mohindra, S. D. Carlin, P. Zanzonico, R. Weissleder, J. S. Lewis, *J. Nucl. Med.* **2013**, *54*, 1389 – 1396.

[16] N. K. Devaraj, G. M. Thurber, E. J. Keliher, B. Marinelli, R. Weissleder, *Proc. Natl. Acad. Sci. USA* **2012**, *109*, 4762 – 4767.

[17] M. R. Karver, R. Weissleder, S. A. Hilderbrand, *Bioconjugate Chem.* **2011**, *22*, 2263 – 2270.

[18] F. Liu, R. S. Paton, S. Kim, Y. Liang, K. N. Houk, *J. Am. Chem. Soc.* **2013**, *135*, 15642 – 15649.

[19] S. A. Lang, B. D. Johnson, E. Cohen, *J. Heterocycl. Chem.* **1975**, *12*, 1143 – 1153.

[20] a) E. J. Keliher, T. Reiner, G. M. Thurber, R. Upadhyay, R. Weissleder, *ChemistryOpen* **2012**, *1*, 177 – 183; b) E. J. Keliher, T. Reiner, A. Turetsky, S. A. Hilderbrand, R. Weissleder, *ChemMedChem* **2011**, *6*, 424 – 427; c) B. M. Zeglis, P. Mohindra, G. I. Weissmann, V. Divilov, S. A. Hilderbrand, R. Weissleder, J. S. Lewis, *Bioconjugate Chem.* **2011**, *22*, 2048 – 2059; d) H.-S. Han, N. K. Devaraj, J. Lee, S. A. Hilderbrand, R. Weissleder, M. G. Bawendi, *J. Am. Chem. Soc.* **2010**, *132*, 7838 – 7839; e) J. B. Haun, N. K. Devaraj, S. A. Hilderbrand, H. Lee, R. Weissleder, *Nat. Nanotechnol.* **2010**, *5*, 660 – 665.

[21] J. Yang, M. R. Karver, W. Li, S. Sahu, N. K. Devaraj, *Angew. Chem.* **2012**, *124*, 5312 – 5315; *Angew. Chem. Int. Ed.* **2012**, *51*, 5222 – 5225.

[22] J. W. Wijnen, S. Zavarise, J. B. F. N. Engberts, M. Charton, *J. Org. Chem.* **1996**, *61*, 2001 – 2005.

[23] Inclusion of Substances of Very High Concern in the Candidate List (2011). ED/31/2011 published in accordance with Article 59(10) of the Regulation No 1907/2006 of the European Parliament and of the Council of 18 December 2006 concerning the Registration, Evaluation, Authorisation and Restriction of Chemicals (REACH).

[24] E. Nachbaur, G. Leiseder, *Monatsh. Chem.* **1971**, *102*, 1718 – 1723.

[25] R. Rossin, S. M. van den Bosch, W. ten Hoeve, M. Carvelli, R. M. Versteegen, J. Lub, M. S. Robillard, *Bioconjugate Chem.* **2013**, *24*, 1210 – 1217.

[26] a) R. A. Hawkins, Y. Choi, S.-C. Huang, C. K. Hoh, M. Dahlbom, C. Schiepers, N. Satyamurthy, J. R. Barrio, M. E. Phelps, *J. Nucl. Med.* **1992**, *33*, 633 – 642; b) E. Even-Sapir, E. Mishani, G. Flusser, U. Metser, *Semin. Nucl. Med.* **2007**, *37*, 462 – 469.

[27] D. E. Chapman, T. J. Moore, S. R. Michener, G. Powis, *Drug Metab. Dispos.* **1990**, *18*, 929 – 936.

 © 2014 Wiley-VCH Verlag GmbH & Co. KGaA, Weinheim

Manuscript #2

Reprinted from *Bioconjugate Chemistry* (2016), accepted manuscript.

Denk, C.; Svatunek, D.; Mairinger, S.; Stanek, J.; Filip, T.; Matscheko, D.; Kuntner-Hannes, C.; Wanek, T.; Mikula, H.:

Design, Synthesis and Evaluation of a Low-Molecular-Weight ^{11}C-Labeled Tetrazine for Pretargeted PET Imaging applying Bioorthogonal *In Vivo* Click Chemistry

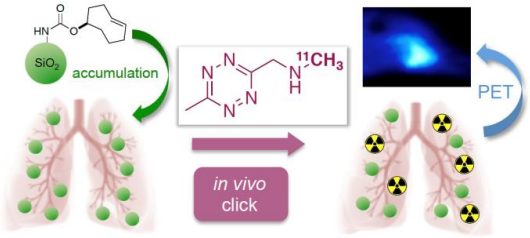
Design, Synthesis and Evaluation of a Low-Molecular-Weight ^{11}C-Labeled Tetrazine for Pretargeted PET Imaging applying Bioorthogonal *in Vivo* Click Chemistry

Christoph Denk,[†] Dennis Svatunek,[†] Severin Mairinger,[‡] Johann Stanek,[‡] Thomas Filip,[‡] Dominik Matscheko,[†] Claudia Kuntner,[‡] Thomas Wanek,[‡] and Hannes Mikula*[,†]

[†]Institute of Applied Synthetic Chemistry, Vienna University of Technology (TU Wien), Vienna, Austria

[‡]Health and Environment Department, Biomedical Systems, Austrian Institute of Technology (AIT), Seibersdorf, Austria

ABSTRACT: A low-molecular-weight tetrazine labeled with the short-lived positron emitter carbon-11 was developed as a bioorthogonal PET probe for pretargeted imaging. A method for efficient and fast synthesis of this imaging agent is presented using radiolabeling of a readily available precursor. High reactivity with *trans*-cyclooctenes was observed and *in vivo* investigations including PET/MR scanning showed homogenous biodistribution, good metabolic stability and rapid excretion in naive mice. These properties are key to the success of bioorthogonal ^{11}C-PET imaging, which has been shown in a simple pretargeting experiment using TCO-modified mesoporous silica nanoparticles. Overall, this ^{11}C-labeled tetrazine represents a highly versatile and advantageous chemical tool for bioorthogonal PET imaging and enables pretargeting approaches using carbon-11 for the first time.



INTRODUCTION

Bioorthogonal ligations have emerged in recent years as versatile and efficient chemical tools for forming covalent linkages within highly complex environments such as living organisms. In 2004, Bertozzi and co-workers were first to use the catalyst-free strain-promoted alkyne azide cycloaddition (SPAAC) for two-step glycome imaging in live developing zebrafish and introduced the concept of bioorthogonality.[1–3] In such pretargeting approaches, a chemical reporter bearing a bioorthogonal reactive group (tag) is administered, allowed to accumulate and (after clearance of unbound material) visualized using a labeled secondary agent that selectively reacts with the tag (*in vivo* chemistry).[4] This method has gained interest, especially in nuclear medicine wherein the short half-life of commonly used PET radioisotopes (^{18}F: 109.8 min, ^{11}C: 20.4 min) restricts their application for imaging of slow accumulation processes. Even though longer-lived PET isotopes (^{64}Cu: 12.7 h, ^{89}Zr: 78.4 h, ^{124}I: 100.2 h) can be used and applied for the development of slowly accumulating imaging agents (e.g. antibodies), their limited availability, high cost and, most importantly, the resulting prolonged radiation exposure pose serious limitations.[5]

The very low concentrations of radiolabeled agents *in vivo* require rapid bioorthogonal click reaction to achieve effective ligation within a short time period. Even though the SPAAC ligation has recently been successfully applied for pretargeted PET imaging, second order reaction rates of less than 5 $M^{-1}s^{-1}$ (MeCN, 20°C) are still a drawback, which limits further applications of this strategy.[6] Several other bioorthogonal reactions have been reported recently, of which the inverse electron demand Diels Alder reaction (IEDDA) of 1,2,4,5-tetrazines (Tz) and strained alkene dienophiles such as *trans*-cyclooctenes (TCO) has superior kinetics with rate constants of up to 3.3 x 10^6 $M^{-1}s^{-1}$ (water, 25°C).[7–12] Alongside applications in live cell imaging, protein labeling and rapid construction of PET probes, the tetrazine ligation has successfully been applied by Rossin, Robillard and co-workers in a SPECT pretargeting study using a ^{177}Lu labeled Tz and a TCO-CC49 antibody leading to images with outstanding tumor-to-background ratios.[7,13–15] Even though still synthetically challenging, the metal-catalyzed tetrazine synthesis reported by Yang *et al.* made unsymmetrical 1,2,4,5-tetrazines accessible, and the flow photoisomerization process reported by Fox and co-workers gave rise to a straightforward preparation of *trans*-cyclooctenes.[16,17] Several tetrazine and TCO derivatives were developed to fine-tune the reactivity and stability of the reactants, and different modes of attachment of IEDDA tags to biomolecules were investigated to optimize bioorthogonal reactivity.[4,11,18–21] The use of radiolabeled Tz is believed to be advantageous over the use of radiolabeled TCO derivatives since latter were shown to quickly metabolize when applied in tracer amounts.[5]

The first radiolabeled Tz were metal chelator bearing compounds labeled with long-lived radiometals such as ^{64}Cu, ^{89}Zr, ^{177}Lu and ^{111}In.[15,22,23] However, to take full advantage of the pretargeting approach, radiotetrazines with short-lived emitters are beneficial due to reduced radiation dose delivered to the patient. ^{18}F was first used for *in vivo* click reactions in combination with dextrans.[24] This approach has recently been extended to ^{68}Ga-PET imaging.[25]

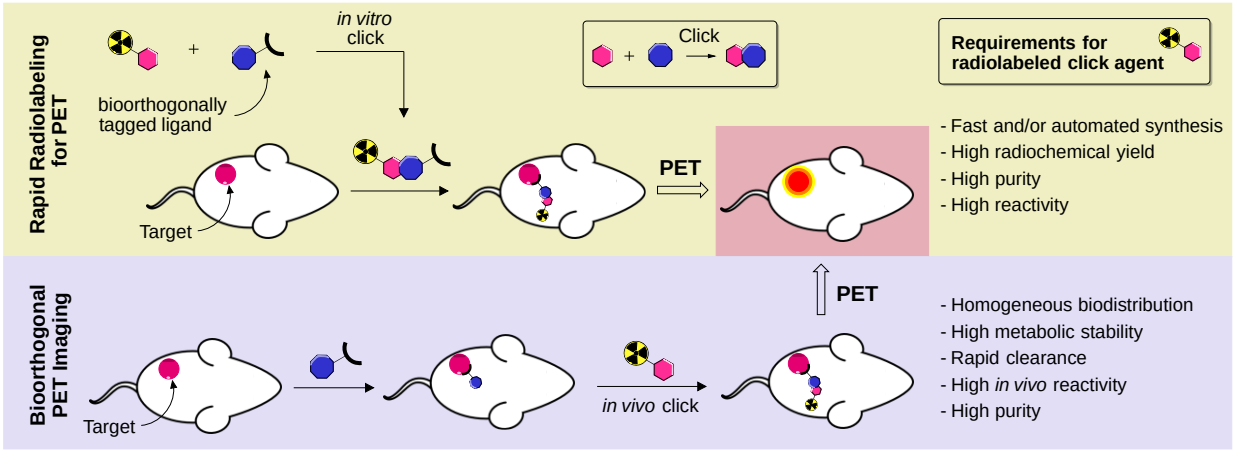


Figure 1. The two main applications of bioorthogonal ligations in the field of PET imaging: Rapid radiolabeling using *in vitro* click chemistry before administration (top), bioorthogonal PET imaging applying *in vivo* chemistry (bottom).

In 2014, we reported the development of the first fluorine-18 labeled low-molecular-weight Tz by bypassing the previously reported instability of tetrazines under fluorination conditions using a less reactive dialkyl-tetrazine scaffold that nonetheless possesses sufficient IEDDA reactivity for fast *in vivo* click chemistry.[26] This probe showed homogeneous biodistribution, rapid clearance and high stability, thus fulfilling the requirements for *in vivo* click applications. However, due to the low radiochemical yield, this ^{18}F-Tz is not suitable for *in vitro* radiolabeling applications prior to administration and subsequent imaging. Recently, Zhu *et al.* and Rashidian *et al.* reported optimized procedures for the synthesis of ^{18}F-tetrazines enabling rapid radiolabeling,[27,28] but did not include any *in vivo* or stability data. Carbon-11 labeled Tz offer additional benefits such as a short half-life of 20.4 min and a high specific activity that potentially allows for pretargeting experiments at multiple time points, since each dosing of ^{11}C-Tz is likely to consume only a small fraction of available dienophile-tags. In addition, carbon-11 is produced from ^{14}N (99.6% abundance), thus reducing production costs, although an on-site cyclotron is required (due to the short half-life), limiting the application of ^{11}C-labeled compounds in general. The first carbon-11 tetrazine was reported by Herth *et al.* in 2013, but no *in vivo*, biodistribution or stability data is available.[29] Moreover, the chemical structure of this ^{11}C-Tz, which consists of four aryl rings, is likely to limit water solubility and facilitate plasma protein binding and hepatic metabolization.

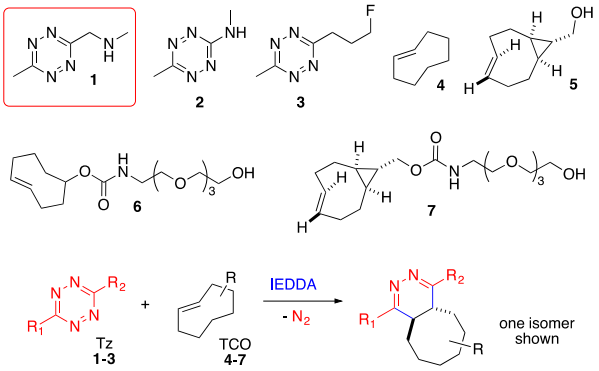
In addition to sufficient reaction rates, radiotetrazines intended to be used as *in vivo* imaging agents need to exhibit homogenous biodistribution, metabolic stability and fast excretion kinetics, which is exceptionally important for image contrast with short-lived isotopes such as ^{11}C. Overall, only a few radiolabeled tetrazines have been reported so far,[22,26–32] most are applicable to either *in vitro* or *in vivo* studies, whereas a multifunctional tool applicable to both principal uses of bioorthogonal ligations in the field of PET imaging (Figure 1) would be highly beneficial. Furthermore, to the best of our knowledge, not a single successful pretargeting approach has been reported so far using a small-molecule tetrazine that has been labeled with a covalently attached radionuclide (neither ^{18}F nor ^{11}C). Moreover, pretargeting has been impossible so far in the field of carbon-11 PET imaging in general due to the lack of a method that allows for fast *in vivo* labeling of a pre-administered and accumulated compound. Consequently, we focused on the development of a low-molecular-weight ^{11}C-tetrazine with emphasis on favorable pharmacokinetic properties (homogeneous biodistribution, high stability and fast clearance) for bioorthogonal PET imaging.

RESULTS AND DISCUSSION

Due to the *in vivo* properties of the previously described ^{18}F-dialkyltetrazine, we hypothesized that a ^{11}C-labeled compound with a similar structure is likely to be useful as a bioorthogonal PET probe. Hence, we aimed to keep the molecular weight of the compound to a minimum to facilitate fast pharmacokinetics. Furthermore, an NH_2 group was selected as nucleophilic labeling site for straightforward introduction of carbon-11 via ^{11}C-methylation. Thus, tetrazines **1** and **2** were considered (Table 1). Reactivity was estimated by computational methods (M06-2X/ 6-31G(d,p), 1,4-dioxane, Gaussian 09)[33] and compared to the ^{18}F-Tz **3** for which rapid *in vivo* ligation has already been demonstrated.[26] Free energies of activation ($\Delta G^{\ddagger}$) of the IEDDA-initiated reaction between the above mentioned tetrazines and the dienophiles TCO (**4**) and s-TCO (**5**) were calculated and differences ($\Delta\Delta G^{\ddagger}$) were used to estimate reaction rates relative to those of **3**+**4** and **3**+**5** (Table 1). **1** was predicted to exhibit reactivity comparable to **3** (relative rates of 1.32-1.36) whereas **2** was predicted to show only low reactivity (relative rates of 0.00009-0.0006). Based on these considerations Tz **1** was selected for further investigations.

Metal-catalyzed tetrazine synthesis starting from Boc-protected N-methylaminoacetonitrile (**8**) followed by deprotection afforded Tz **1** (Figure 2A).[17] Rate constants and free activation energies obtained by stopped-flow measurements were in good agreement with calculated values. The water-soluble TCO derivatives **6** and **7** have been used for measurements in PBS showing rates of 175.4 M^{-1} s^{-1} and more than 40 000 M^{-1} s^{-1}, respectively, in the IEDDA reaction with tetrazine **1** (Table 1). Furthermore, good plasma stability was observed by absorbance measurements and chromatography after incubation in human blood plasma at 37°C (see Supporting Information, Figure S6). Although stable for at least 2 months at -20°C, tetrazines **1** and desmethyl precursor **11**, which is accessible by deprotection of previously reported **10** (Figure 2B),[17] tend to slowly degrade and should be kept as Boc-protected compounds **9** and **10** if prolonged storage is intended. Alternatively, we have also prepared the trifluoroacetate salts of tetrazines **1** and **11** that show significantly improved stability.

Table 1. Reaction kinetics of IEDDA cycloadditions obtained by computational methods (M06-2X/6-31G(d,p), 1,4-dioxane (CPCM), Gaussian 09) and stopped-flow measurements.



Reaction	k_2 [M^{-1} s^{-1}]	Calculated relative rate	Relative rate
1 + **4**	1.04 ± 0.03[a]	1.32[c]	0.70[c]
2 + **4**	n.d.	0.00009[c]	n.d.
3 + **4**[26]	1.49 ± 0.01[a]	1.00[c]	1.00[c]
1 + **5**	89.5 ± 1.1[a]	1.36[d]	1.05[d]
2 + **5**	n.d.	0.0006[d]	n.d.
3 + **5**[26]	85.5 ± 2.3[a]	1.00 [d]	1.00[d]
1 + **6**	175.4 ± 1.2[b]	n.d.	118[c]
1 + **7**	42 500 ± 3100[b]	n.d.	497[d]

[a] Measured in 1,4-dioxane at 37°C. [b] Measured in PBS at 37°C. [c] Relative to the reaction between **3** and **4**. [d] Relative to the reaction between **3** and **5**. n.d. = not determined.

Radiolabeling of **11** was successfully carried out using the [^{11}C]-CH_3OTf route on a GE Tracerlab FXC Pro synthesis module to obtain [^{11}C]-**1** in radiochemical purities exceeding 95% and in a decay-corrected radiochemical yield of 52 ±6%, based on trapped [^{11}C]CH_3OTf (Figure 2C). The overall synthesis time was 30 min including purification by cation exchange chromatography. Hence, significant improvements in both radiochemical yield (52% vs. 33%) and synthesis time (30 min vs. 50-60 min) were obtained compared to the previously reported ^{11}C-labeled Tz.[29] The identity and radiochemical purity of [^{11}C]-**1** was verified by co-elution with reference substance **1** (SCX-HPLC, Figure 2D). [^{11}C]-**1** readily reacted with s-TCO (**5**) to give conjugate [^{11}C]-**12** that slowly isomerized to the thermodynamically favored tautomer [^{11}C]-**13** (both products as a mixture of regio- and stereoisomers) as shown by radio-TLC (Figure 2E).

In vivo biodistribution of [^{11}C]-**1** was investigated by intravenous administration into female BALB/c mice (n=3) and subsequent dynamic PET/MR scanning for 60 min (Figure 3A). Regions of interest were drawn for main organs in acquired PET/MR data to determine tissue specific time-radioactivity concentration curves (Figure 3B). After initial perfusion (0-5 min), [^{11}C]-**1** exhibited rapid renal clearance, as indicated by a steep increase of radioactivity concentration to 96 ± 17 SUV (standardized uptake value) in the urinary bladder at 60 min, which is highly beneficial or even essential considering the short half-life of ^{11}C (20.4 min). All other organs analyzed displayed a very uniform uptake of 2-4 SUV, which slowly decreased to 0.6-2 SUV in the course of the

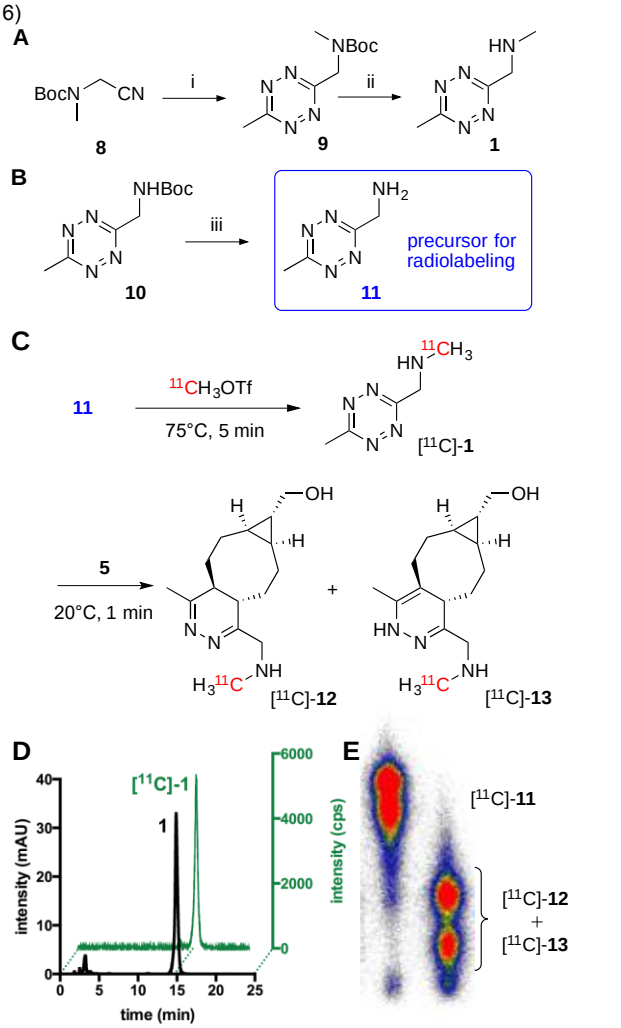


Figure 2. (A) Synthesis of tetrazine **1**: i) MeCN, $NiCl_2$, NH_2NH_2, 42°C, 18 h, then $NaNO_2$, aq. HCl, 20°C, 20 min ii) TFA in DCM, 0°C, 3 h. (B) Synthesis of precursor **11**: iii) TFA in DCM, 20°C, 26 h. (C) Radiosynthesis of [^{11}C]-**1** and further reaction with dienophile s-TCO (**5**); only one isomer shown for [^{11}C]-**12** and [11C]-**13**. (D) HPLC of **1** (UV/VIS, 530 nm) and radio-HPLC of purified [^{11}C]-**1** (cps = counts per second). (E) Radio-TLC (10% MeOH and 1% NEt_3 in CH_2Cl_2) of [^{11}C]-**1** (left lane) and ligation products with s-TCO (**5**) (right lane).

imaging experiment (Fig. 3A and Fig. 3B). It is noteworthy that the brain and medulla showed increased uptake, a good indicator for the ability of [^{11}C]-**1** to cross the blood brain barrier. *Ex vivo* biodistribution data (n=3) was obtained 60 min post administration of [^{11}C]-**1** using a gamma counter showing uptake of 0.5-1.5 SUV in all analyzed organs, which is in good agreement with the last time frame of PET measurements (Figure 3C). In addition, *in vivo* stability and metabolism were investigated by radio-TLC analysis of plasma and urine samples that were taken after the imaging experiments (see Supporting Information, Figure S7). Due to the homogenous biodistribution, high stability and low activity concentrations after 60 min (beside excretion organs), any signal arising from *in vivo* conjugated [^{11}C]-**1** is expected to show good contrast, making this radiotetrazine a promising tool for pretargeted PET imaging.

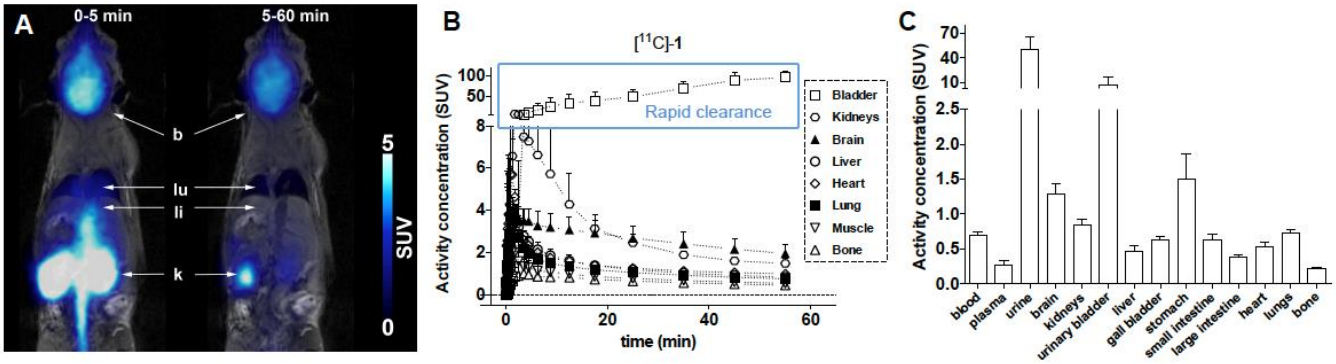


Figure 3. Biodistribution of [^{11}C]-**1**: (a) Combined coronal PET/MR images (b = brain, lu = lungs, li = liver, k = kidney); (b) Mean organ time vs. activity curves in female BALB/c mice (n=3) showing rapid clearance from the urinary bladder; (c) *Ex vivo* biodistribution data (obtained 60 min post administration of [^{11}C]-**1**).

Bioconjugation of [^{11}C]-**1** and the water-soluble dienophile **7** was performed *in vivo* to verify the bioorthogonal behavior of this novel click imaging agent. The s-TCO derivative **7** was administered to female BALB/c mice (n=2) followed by [^{11}C]-**1** after an initial period of 5 min. Retroorbital blood was collected after 5 min and the click reaction was quenched. Murine plasma was obtained and analyzed using radio-TLC showing one major click product and an overall conversion of >98 % after 5 min *in vivo* click reaction time (for details see Supporting Information, Figure S8).

To investigate the applicability of [^{11}C]-**1** for rapid radiolabeling and pretargeted PET imaging, mesoporous silica nanoparticles (MSNs) were prepared,[34] amino-functionalized[35] and modified with TCO and s-TCO, respectively. The reactive dienophile-loading was determined to be 115-120 µmol/g for both types of modified nanoparticles. s-TCO-MSNs were radiolabeled by fast click reaction with [^{11}C]-**1** (5 min reaction time) and administered to female BALB/c mice. In contrast to previously reported studies,[6,36] but also in accordance to recent findings[37] we observed rapid and almost exclusive accumulation in the lung (see Supporting Information, Figure S9). This behavior was further exploited to design a simple model for testing pretargeted carbon-11 PET imaging using [^{11}C]-**1**. MSNs labeled with TCO and s-TCO, respectively, were administered to female BALB/c mice in a first step. After sufficient time for accumulation of the MSNs in the lung (pretargeting step) [^{11}C]-**1** was injected and dynamic PET scanning was conducted. A significantly increased activity concentration in the lung was observed when using bioorthogonally labeled MSNs compared to biodistribution data of [^{11}C]-**1** as shown by PET imaging and *ex vivo* measurements (Figure 4). Notably, MSNs labeled with TCO performed better than such labeled with the more reactive s-TCO tag. Although both modified MSNs were shown to be stable prior to imaging experiments with an almost identical dienophile-loading, we hypothesize that there is less uptake of [^{11}C]-**1** when using s-TCO-MSNs due to the lower stability of s-TCO under *in vivo* conditions. Nevertheless, these experiments clearly indicate the applicability of [^{11}C]-**1** for pretargeted imaging using bioorthogonal *in vivo* click chemistry.

In summary, herein, we present the development of a carbon-11 labeled radiotetrazine as a secondary imaging agent for bioorthogonal PET applying *in vivo* click chemistry. The low-molecular-weight and water-soluble Tz **1** exihibits highly beneficial pharmacokinetic properties such as homogeneous biodistribution, rapid renal excretion and sufficient metabolic stability strengthening the hypothesis that 3,6-dialkyltetrazines are well suited for the development of bioorthogonal tools for *in*

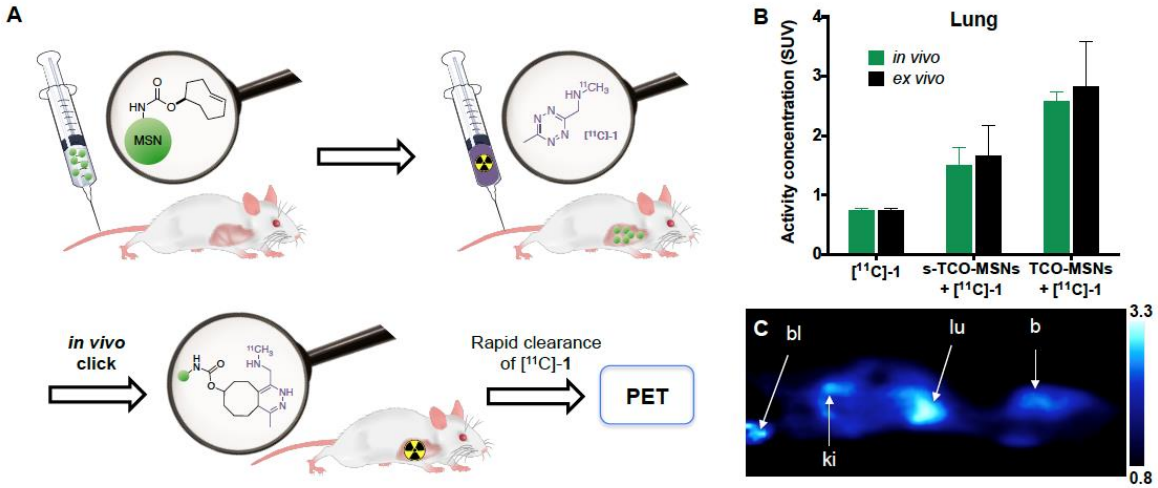


Figure 4. (A) *In vivo* click experiment using TCO- and s-TCO-modified silica nanoparticles (chemical structure shown for TCO). (B) Activity concentration measured *in vivo* by PET imaging (50-60 min) and *ex vivo* (after 60 min, gamma counter) showing increased lung uptake in female BALC/c mice when using s-TCO-MSNs (n=5) and TCO-MSNs (n=2). (C) Pretargeted PET image (sagittal view, 40-60 min): TCO-MSNs + [^{11}C]-**1** (scale bar unit: SUV; b = brain, bl = bladder, k = kidney, lu = lung).

vivo applications. Precursor **11** is readily accessible in two synthetic steps and can be efficiently labeled applying straightforward carbon-11 radiochemistry. The bioorthogonal behavior of [^{11}C]-**1** was demonstrated by selective *in vivo* click reaction with the water-soluble s-TCO derivative **7**. Furthermore, we were able to use [^{11}C]-**1** for rapid radiolabeling of silica nanoparticles that were shown by PET imaging to almost exclusively accumulate in the lung. Based on these results a pretargeting experiment was carried out showing that accumulated TCO-modified silica nanoparticles can be visualized by PET after *in vivo* click reaction with [^{11}C]-**1**. To the best of our knowledge, this represents the first reported example of pretargeted ^{11}C-PET imaging.

ASSOCIATED CONTENT

Supporting Information

The Supporting Information is available free of charge on the ACS Publications website.

Materials and methods; synthetic procedures and compound characterization data (incl. copies of NMR spectra); synthesis, modification and characterization of mesoporous silica nanoparticles; reaction kinetics; radiolabeling; quantum-chemical calculations (incl. Cartesian coordinates of all structures); *in vitro* plasma stability; *in vivo* investigations (PDF)

AUTHOR INFORMATION

Corresponding Author

*hannes.mikula@tuwien.ac.at

Notes

The authors declare no competing financial interest.

ACKNOWLEDGMENT

Financial support from the Vienna Anniversary Foundation for Higher Education (H-2500/2012) is gratefully acknowledged. We thank Dr. Roland Müller (Seibersdorf Laboratories), Prof. Wolfgang Linert, Prof. Christian Edtmaier and Elisabeth Eitenberger (all TU Wien) for their kind support of this work. Quantum-chemical calculations were performed using the Vienna Scientific Cluster (VSC).

REFERENCES

(1) Dehnert, K. W., Baskin, J. M., Laughlin, S. T., Beahm, B. J., Naidu, N. N., Amacher, S. L., and Bertozzi, C. R. (2012) Imaging the sialome during zebrafish development with copper-free click chemistry. *ChemBioChem 13*, 353–357.

(2) Agard, N. J., Prescher, J. A., and Bertozzi, C. R. (2004) A strain-promoted [3 + 2] azide-alkyne cycloaddition for covalent modification of biomolecules in living systems. *J. Am. Chem. Soc. 126*, 15046–15047.

(3) Prescher, J. A., Dube, D. H., and Bertozzi, C. R. (2004) Chemical remodelling of cell surfaces in living animals. *Nature 430*, 873–877.

(4) Rossin, R., van den Bosch, S. M., Ten Hoeve, W., Carvelli, M., Versteegen, R. M., Lub, J., and Robillard, M. S. (2013) Highly reactive trans-cyclooctene tags with improved stability for Diels-Alder chemistry in living systems. *Bioconjug. Chem. 24*, 1210–7.

(5) Wyffels, L., Thomae, D., Waldron, A.-M., Fissers, J., Dedeurwaerdere, S., Van der Veken, P., Joossens, J., Stroobants, S., Augustyns, K., and Staelens, S. (2014) In vivo evaluation of (18)F-labeled TCO for pre-targeted PET imaging in the brain. *Nucl. Med. Biol. 41*, 513–23.

(6) Lee, S. B., Kim, H. L., Jeong, H.-J., Lim, S. T., Sohn, M.-H., and Kim, D. W. (2013) Mesoporous silica nanoparticle pretargeting for PET imaging based on a rapid bioorthogonal reaction in a living body. *Angew. Chem. Int. Ed. Engl. 52*, 10549–52.

(7) Devaraj, N. K., Weissleder, R., and Hilderbrand, S. a. (2008) Tetrazine-based cycloadditions: application to pretargeted live cell imaging. *Bioconjug. Chem. 19*, 2297–9.

(8) Sletten, E. M., and Bertozzi, C. R. (2011) A bioorthogonal quadricyclane ligation. *J. Am. Chem. Soc. 133*, 17570–17573.

(9) Stöckmann, H., Neves, A. A., Stairs, S., Brindle, K. M., and Leeper, F. J. (2011) Exploring isonitrile-based click chemistry for ligation with biomolecules. *Org. Biomol. Chem. 9*, 7303–7305.

(10) Ning, X., Temming, R. P., Dommerholt, J., Guo, J., Ania, D. B., Debets, M. F., Wolfert, M. A., Boons, G. J., and Van Delft, F. L. (2010) Protein modification by strain-promoted alkyne-nitrone cycloaddition. *Angew. Chemie - Int. Ed. 49*, 3065–3068.

(11) Darko, A., Wallace, S., Dmitrenko, O., Machovina, M. M., Mehl, R. a., Chin, J. W., and Fox, J. M. (2014) Conformationally strained trans-cyclooctene with improved stability and excellent reactivity in tetrazine ligation. *Chem. Sci. 5*, 3770.

(12) Blackman, M. L., Royzen, M., and Fox, J. M. (2008) Tetrazine ligation: fast bioconjugation based on inverse-electron-demand Diels-Alder reactivity. *J. Am. Chem. Soc. 130*, 13518–9.

(13) Reiner, T., and Zeglis, B. M. (2014) The inverse electron demand Diels–Alder click reaction in radiochemistry. *J. Labelled Comp. Radiopharm. 57*, 285–290.

(14) Versteegen, R. M., Rossin, R., ten Hoeve, W., Janssen, H. M., and Robillard, M. S. (2013) Click to release: instantaneous doxorubicin elimination upon tetrazine ligation. *Angew. Chem. Int. Ed. Engl. 52*, 14112–6.

(15) Rossin, R., Läppchen, T., van den Bosch, S. M., Laforest, R., and Robillard, M. S. (2013) Diels–Alder Reaction for Tumor Pretargeting: In Vivo Chemistry Can Boost Tumor Radiation Dose Compared with Directly Labeled Antibody. *J. Nucl. Med. 54* , 1989–1995.

(16) Royzen, M., Yap, G. P. a, and Fox, J. M. (2008) A

photochemical synthesis of functionalized trans-cyclooctenes driven by metal complexation. *J. Am. Chem. Soc. 130*, 3760–1.

(17) Yang, J., Karver, M. R., Li, W., Sahu, S., and Devaraj, N. K. (2012) Metal-Catalyzed One-Pot Synthesis of Tetrazines Directly from Aliphatic Nitriles and Hydrazine. *Angew. Chemie 124*, 5312–5315.

(18) Taylor, M. T., Blackman, M. L., Dmitrenko, O., and Fox, J. M. (2011) Design and synthesis of highly reactive dienophiles for the tetrazine-trans-cyclooctene ligation. *J. Am. Chem. Soc. 133*, 9646–9.

(19) Karver, M. R., Weissleder, R., and Hilderbrand, S. A. (2011) Synthesis and Evaluation of a Series of 1,2,4,5-Tetrazines for Bioorthogonal Conjugation. *Bioconjug. Chem. 22*, 2263–2270.

(20) Rossin, R., van Duijnhoven, S. M. J., Läppchen, T., van den Bosch, S. M., and Robillard, M. S. (2014) Trans-cyclooctene tag with improved properties for tumor pretargeting with the diels-alder reaction. *Mol. Pharm. 11*, 3090–6.

(21) Rahim, M. K., Kota, R., and Haun, J. B. (2015) Enhancing Reactivity for Bioorthogonal Pretargeting by Unmasking Antibody-Conjugated trans -Cyclooctenes. *Bioconjug. Chem. 26*, 352–360.

(22) Zeglis, B. M., Sevak, K. K., Reiner, T., Mohindra, P., Carlin, S. D., Zanzonico, P., Weissleder, R., and Lewis, J. S. (2013) A Pretargeted PET Imaging Strategy Based on Bioorthogonal Diels-Alder Click Chemistry. *J. Nucl. Med. 54*, 1389–1396.

(23) Rossin, R., van den Bosch, S., Läppchen, T., Vulders, R., Lub, J., and Robillard, M. (2011) In vivo chemistry for pretargeted RIT of cancer. *J. Nucl. Med. 52* , 480.

(24) Devaraj, N. K., Thurber, G. M., Keliher, E. J., Marinelli, B., and Weissleder, R. (2012) Reactive polymer enables efficient in vivo bioorthogonal chemistry. *Proc. Natl. Acad. Sci. U. S. A. 109*, 4762–4767.

(25) Nichols, B., Qin, Z., Yang, J., Vera, D. R., and Devaraj, N. K. (2014) 68Ga chelating bioorthogonal tetrazine polymers for the multistep labeling of cancer biomarkers. *Chem. Commun. (Camb). 50*, 5215–7.

(26) Denk, C., Svatunek, D., Filip, T., Wanek, T., Lumpi, D., Fröhlich, J., Kuntner, C., and Mikula, H. (2014) Development of a 18 F-Labeled Tetrazine with Favorable Pharmacokinetics for Bioorthogonal PET Imaging. *Angew. Chemie Int. Ed. 53*, 9655–9659.

(27) Zhu, J., Li, S., Wängler, C., Wängler, B., Lennox, R. B., and Schirrmacher, R. (2015) Synthesis of 3-chloro-6-((4-(di-tert-butyl[18F]fluorosilyl)-benzyl)oxy)-1,2,4,5-tetrazine ([18F]SiFA-OTz) for Rapid Tetrazine-Based 18F-Radiolabeling. *Chem. Commun.*

(28) Rashidian, M., Keliher, E. J., Dougan, M., Juras, P. K., Cavallari, M., Wojtkiewicz, G. R., Jacobsen, J. T., Edens, J. G., Tas, J. M. J., Victora, G., Weissleder, R., and Ploegh, H. (2015) Use of ^{18} F-2-Fluorodeoxyglucose to Label Antibody Fragments for Immuno-Positron Emission Tomography of Pancreatic Cancer. *ACS Cent. Sci.* 150603073029009.

(29) Herth, M. M., Andersen, V. L., Lehel, S., Madsen, J., Knudsen, G. M., and Kristensen, J. L. (2013) Development of a (11)C-labeled tetrazine for rapid tetrazine-trans-cyclooctene ligation. *Chem. Commun. (Camb). 49*, 3805–7.

(30) Meyer, J. P., Houghton, J. L., Kozlowski, P., Abdel-Atti, D., Reiner, T., Pillarsetty, N. V. K., Scholz, W. W., Zeglis, B. M., and Lewis, J. S. (2016) 18F-Based Pretargeted PET Imaging Based on Bioorthogonal Diels-Alder Click Chemistry. *Bioconjug. Chem. 27*, 298–301.

(31) Rossin, R., Renart Verkerk, P., van den Bosch, S. M., Vulders, R. C. M., Verel, I., Lub, J., and Robillard, M. S. (2010) In Vivo Chemistry for Pretargeted Tumor Imaging in Live Mice. *Angew. Chemie Int. Ed. 49*, 3375–3378.

(32) Keinänen, O., Li, X. G., Chenna, N. K., Lumen, D., Ott, J., Molthoff, C. F. M., Sarparanta, M., Helariutta, K., Vuorinen, T., Windhorst, A. D., and Airaksinen, A. J. (2016) A New Highly Reactive and Low Lipophilicity Fluorine-18 Labeled Tetrazine Derivative for Pretargeted PET Imaging. *ACS Med. Chem. Lett. 7*, 62–66.

(33) Liu, F., Liang, Y., and Houk, K. N. (2014) Theoretical elucidation of the origins of substituent and strain effects on the rates of Diels-Alder reactions of 1,2,4,5-tetrazines. *J. Am. Chem. Soc. 136*, 11483–93.

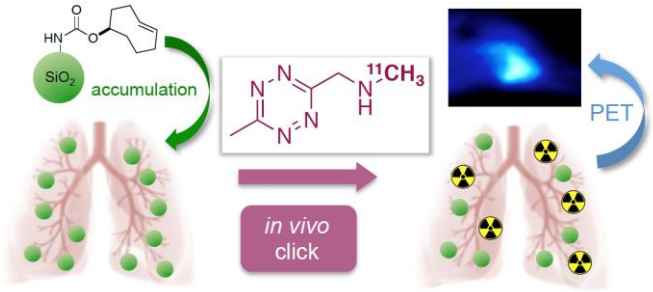
(34) Ostafin, A., Nooney, R. I., Thirunavukkarasu, D., Chen, Y., Josephs, R., and Ostafin, A. E. (2015) Synthesis of Nanoscale Mesoporous Silica Spheres with Controlled Particle Size Synthesis of Nanoscale Mesoporous Silica Spheres with Controlled Particle Size 4721–4728.

(35) Yokoi, T., Yoshitake, H., and Tatsumi, T. (2004) Synthesis of amino-functionalized MCM-41 via direct co-condensation and post-synthesis grafting methods using mono-, di- and tri-amino-organoalkoxysilanesElectronic supplementary information (ESI) available: XRD patterns of (A) x-dNN-MCM-41 and (B) x-dNNN. *J. Mater. Chem. 14*, 951.

(36) Lu, J., Liong, M., Li, Z., Zink, J. I., and Tamanoi, F. (2010) Biocompatibility, biodistribution, and drug-delivery efficiency of mesoporous silica nanoparticles for cancer therapy in animals. *Small 6*, 1794–1805.

(37) Keinänen, O., Li, X.-G., Chenna, N. K., Lumen, D., Sarparanta, M., Helariutta, K., Vuorinen, T., and Airaksinen, A. J. (2015) Synthesis and biological evaluation of a novel 18F-labelled tetrazine for bioorthogonal chemistry, in *Proceedings of the World Molecular Imaging Congress 2015, Honolulu, Hawaii, September 2-5, 2015: Scientific Session 25: Chemistry and Imaging Probes - Nuclear Imaging*.

TOC graphic



Manuscript #3

manuscript draft

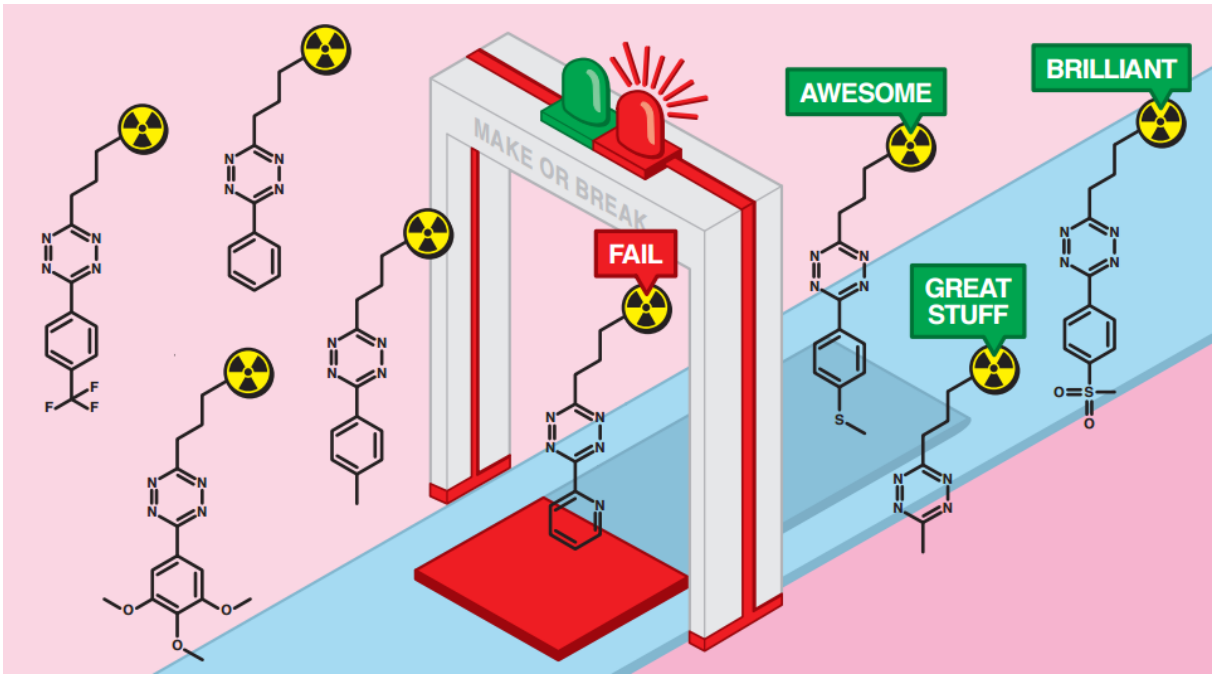
Denk, C.; Svatunek, D.; Mairinger, S.; Kuntner-Hannes, C.; Filip, T.; Sauberer, M.; Fröhlich, J.; Wanek, T.; Mikula, H.:

A Tale of 3-[^{18}F]Fluoropropyl-1,2,4,5-tetrazines

A Tale of 3-[^{18}F]Fluoropropyl-1,2,4,5-Tetrazines

Christoph Denk[a], Dennis Svatunek[a], Severin Mairinger[b], Claudia Kuntner[b], Thomas Filip[b], Michael Sauberer[b,] Johannes Fröhlich[a], Thomas Wanek[b] and Hannes Mikula[a*]

a) Institute of Applied Synthetic Chemistry, Vienna University of Technology (TUW), (Austria) E-mail: hannes.mikula@tuwien.ac.at b) Health and Environment Department, Biomedical Systems, Austrian Institute of Technology (AIT) Seibersdorf (Austria)



Radiolabeled 1,2,4,5-tetrazines are promising agents for bioorthogonal PET imaging. Derivatives based on the 3-fluoropropyl moiety are accessible by direct nucleophilic ^{18}F-fluorination. Building on previous results[1] a series of eight novel 3-fluoropropyl-tetrazines was designed, aiming for improved reactivity while retaining beneficial pharmacological properties. Reactivity was investigated *in silico* and by stopped flow measurements with dienophile *trans*-cyclooctene. Radiolabeling was optimized and the biodistribution, metabolic stability and pharmacokinetics of labeled compounds were investigated by PET/MR scanning in a murine model. One promising compound for pretargeted PET imaging was identified, and its cycloaddition reactivity was furthermore enhanced post-labeling by DMDO mediated oxidation of the fluorine-18 species.

Introduction

Bioorthogonal ligations have emerged as valuable tool for a variety of applications.[2,3] Pretargeting strategies decouple accumulation kinetics from the physical half-life of radionuclides: A tagged marker compound is administered and given sufficient time to accumulate in the desired target tissues. Following accumulation and subsequent excretion of non-bound marker, a radiolabeled agent is administered that rapidly binds to the preadministered compound via a bioorthogonal reaction.[2,4–7] In particular for nuclear medicine applications rapid ligation rates are crucial due to diminutive concentrations used commonly and radioactive decay of involved agents. Although a variety of bioorthogonal reactions has been reported, the ligation between 1,2,4,5-tetrazines (Tz)

and strained dienophiles proved especially suitable for radiolabeled agents due to particular high ligation rates of up to 10^7 $M^{-1}s^{-1}$.[6,8] In these inverse electron demand Diels Alder (IEDDA) cycloaaditions that were reported by Fox, Weissleder and co-workers in 2008, electron deficient 1,2,4,5-tetrazines react with electron rich dienophiles under liberation of nitrogen forming dihydropyridazines.[9,10] Cyclooctynes, cyclopropenes and trans-cyclooctenes (TCOs) offer adequate stability and reactivity to be used as bioorthogonal tags, but straight forward synthetic accessibility and highest rates made TCO the most frequently employed dienophile.[11–13] Fox and co-workers furthermore reported TCO-derivatives with enhanced reaction rates and increased polarity and stability.[8,13] Tetrazine derivatives are accessible by metal catalyzed tetrazine synthesis and other methods.[14,15] IEDDAs potential as pretargeting tool in SPECT and PET imaging was recognized as early as 2010 by Rossin, Robilliard and coworkers.[7] Studies investigating ^{18}F-labeled TCO as bioorthogonal PET probe revealed a very inhomogenous biodistribution profile as well as rapid metabolism of this highly lipophilic probe.[16] For this reason research was focused on the development of radiolabeled tetrazine agents to be used in combination with TCO-tagged marker compounds. Fluorine-18 was considered the “gold standard” isotope for imaging due to favourable decay characteristics, high specific activity, straight forward radiochemistry and broad availability in and around facilities with in-house cyclotron. Early radiofluorination attempts conducted by Fox and co-workers resulted in degradation and led to the conclusion that 1,2,4,5-tetrazines are unstable under typical ^{18}F labeling conditions.[17] Therefore research focused on chelator modified tetrazines labelled with radiometals like lutetium-177, copper-64 and indium-111.[5,7,18] Pretargeted immunoimaging with high signal-to-background ratios using these derivatives was demonstrated by Zeglis et al. and Robilliard, Rossin and co-workers thus proofing the abilities of pretargeted (bioorthogonal) imaging.[5,6] Nevertheless, the use of chelators results in highly polar compounds that are restricted to extracellular targets. In 2013 Herth and co-workers reported the development of a carbon-11 labeled Tz probe, but no *in vivo* data of this compound was collected.[19] In 2014 the first radiofluorinated Tz was developed in our lab by utilization of a dialkyl-scaffold that renders the Tz moiety less reactive in IEDDA reactions, but on the other hand improves stability to allow for direct fluorine-18 labeling. The compound 3-(3-[^{18}F]fluoropropyl)-6-methyl-1,2,4,5-tetrazine (**1**) was prepared by nucleophilic displacement of a tosylate group by non-carrier-added fluoride in moderate radiochemical yield. The derivative exhibited very uniform biodistribution as well as good metabolic stability, both key factors for successful application as secondary agent in imaging.[1] However, the dialkyl-scaffolld, although shown to be sufficiently fast for pretargeting in mice, is limiting reactivity and therefore the *in vivo* applicability of this probe. Although ^{18}F-tetrazine probes prepared by a two-step radiochemical procedure based on labeled carbohydrates were reported, direct labelling is still advantageous due to shorter overall synthesis time and easier purification.[20,21] We hypothesized that replacing the 6-methyl group in **1** with aryl groups would lead to derivatives with increased reactivity that are still suitable for direct labelling with fluorine-18. Furthermore we aimed to explore the chemical space between reactivity and stability of the probes.

Synthesis of Reference Compounds

Based on structure **1,** we aimed to exchange the 6-methyl group by an aryl group (compounds **2-8**, Figure 1) to enhance reactivity. For this reason phenyl-derivative **2** was considered. For compound **1** very favourable *in vivo* properties (homogenous biodistribution, good metabolic stability) were noted.[1] Renal excretion took place in form of several polar metabolites, which we hypothesized arise from oxidation and conjugation at the 6-methyl position. To explore the influence of such a metabolic handle, derivatives with oxidizable groups (compounds **3** and **6**) were included in this study. In addition compound **4** seemed interesting due to a blockage of the oxidative metabolism at the methyl-group combined with increased reactivity caused by the electron withdrawing properties of the trifluoromethyl group. Furthermore the 3,4,5-trimethoxy **5** and methylsulfone **7** derived compounds were selected due to higher polarity as compared to compounds **2** – **4** that is likely to facilitate renal rather than hepatobiliary excretion. Hepatobiliary excretion would contribute to a high background signal in liver, gall bladder and intestines thus limiting the diagnostic utility of the probe. To address the top end of the IEDDA reactivity scale of alkyl-aryl-tetrazines electron deficient pyridyl-tetrazine **8** was included in our study**.**

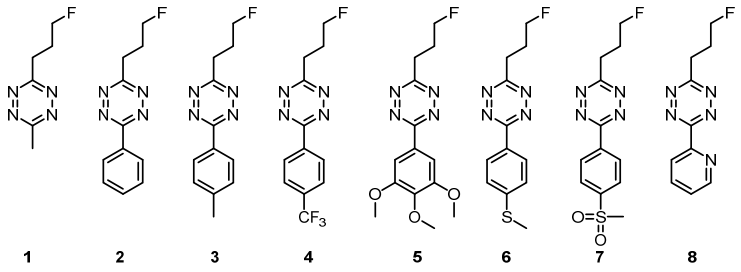
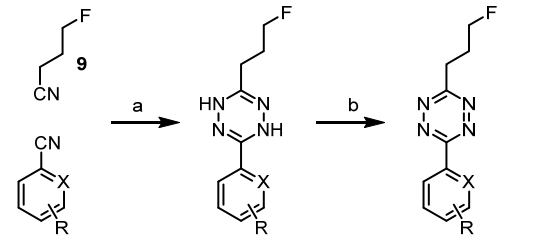


Figure 1: *3-(3-Fluoropropyl)tetrazines considered in this work*

Instead of applying the published procedure using deoxofluorination reagents (such as DAST) on hydroxypropyl-tetrazine derivatives,[1] we directly employed 4-fluorobutyronitrile (**9**) in the metal catalyzed tetrazine synthesis yielding reference compounds **1**-**6** and **8** directly (Scheme 1). 4-Fluorobutyronitrile was synthesized by reacting 3-bromo-1-fluoropropane with sodium cyanide in tetraethylene glycol followed by distillation in 63% yield.[22] Although 3-bromo-1-fluoropropane is commercially available its preparation from low priced 1,3-dibromopropane is highly recommended).[23] Employing the fluoroalkylnitrile **9** and acetonitrile in a metal catalyzed tetrazine synthesis with $NiCl_2$ and anhydrous hydrazine, **1** could be prepared in significantly improved 37% yield compared to previously published procedures.[1] We noticed that the use of anhydrous hydrazine is advantageous for dialkyl derivatives, but aryl-alkyl substituted 1,2,4,5-tetrazines are also accessible using hydrazine monohydrate thus eliminating the need for preparation and handling of anhydrous hydrazine. Yields of the metal catalyzed Tz synthesis varied from substrate to substrate ranging from 1.3 to 16.5%. An optimization towards reaction stochiometry, reaction time and temperature for each individual substrate would be necessary to achieve optimum yield. Within this work we focused on "target



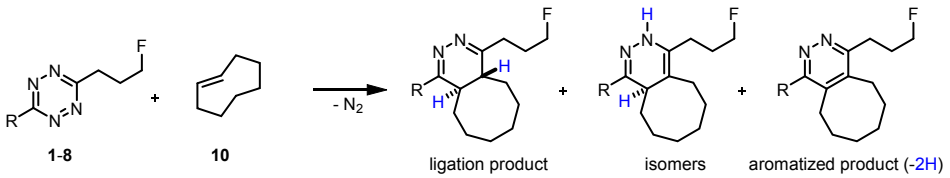
Scheme 1: *Synthesis of 3-fluoropropyl tetrazines a) N_2H_2 x H_2O, $NiCl_2$ b) $NaNO_2$ / HCl*

oriented synthesis" and did not optimize reaction parameters beyond the point where sufficient material for the study could be obtained. **2** was synthesized from 4-fluorobutyronitrile and benzonitrile using nickel(II)chloride and hydrazine monohydrate followed by oxidation of the dihydrotetrazine by the $NaNO_2$/HCl system in 16.5% overall yield. The *p*-tolyl derivative **3** was obtained from *p*-methylbenzonitrile and 4-fluorobutyronitrile using comparable conditions in 6.4% yield. Tetrazine **4** (4.7%), trimethoxy derivative **5** (12.5%), thiomethyl-tetrazine **6** (1.3%) and pyridyl-Tz **8** (10.8%) were prepared using similar synthetic procedures on substituted benzonitriles and 4-fluorobutyronitrile. Oxygen must be excluded from syntheses of sulfide **6**, since the compound readily oxidizes in air to the methylsulfoxide-derivative **26**, that we could isolate as by-product in 16% yield. Methylsulfone Tz derivative **7** was synthesized from **6** by dimethyldioxirane (DMDO) mediated oxidation.[24] All substances appeared as deep purple to red crystalline solids that did not show signs of decomposition, even after prolonged storage (-20°C, > 1 yr).

Kinetic investigations

Relative reactivity values (RRVs) of tetrazines **2** through **8** were predicted using a previously described computational method.[1] Therefore ΔG of activation of the IEDDA reaction with *trans*-cyclooctene **10** was determined by DFT calculations using the Minnesota density functional M06-2X in combination with the 6-311G+(d,p) basis set in the gas phase. $\Delta G^{\ddagger}$ was then used to calculate relative reaction rates. RRVs were predicted to be in the range of 1.8 to 9.8 in comparison to **1** for tetrazine **2-7**, while pyridyl derivative **8** was predicted to show a 70-fold enhanced reactivity as compared to **1** (detailed data see supporting information, Section 6).

Reactivity of tetrazines **1-8** towards *trans*-cyclooctene (**10**) in 1,4-dioxane was then investigated using stopped-flow photometry. Measured rates, relative reactivity values as well as ΔG of activation are shown in Table 1. A comparison of experimental second order rate constants is furthermore shown in Figure 2. As expected for IEDDA reactions, electron donating substituents, like methoxy- or methyl-groups on the aryl substituent lower the reactivity towards dienophiles such as TCO in comparison with electron withdrawing groups, like the trifluoromethyl-group. Interestingly, the trimethoxy substituted derivative **5** showed a lower reactivity (0.9 RRV) as compared to the dialkyl substituted Tz **1**. While tetrazines **2** to **4** show elevated reactivities, ranging from 1.2 – 3.6 RRV, the methyl sulfone compound **7** and pyridyl substituted Tz **8** showed a considerably higher value of 4.5 and 13.6 RRVs respectively.



Reactant Pair	Second order rate constants [$M^{-1}s^{-1}$] 25°C	37°C	50°C	$\Delta G^{\ddagger}$ [kcal/mol]	RRV
1 + 10	1.11	1.57	2.20	17.39	1.00
2 + 10	1.58	2.30	3.18	17.18	1.44
3 + 10	1.26	1.90	2.91	17.32	1.22
4 + 10	3.87	5.72	8.05	16.65	3.60
5 + 10	1.00	1.44	1.96	17.45	0.90
6 + 10	1.30	1.97	2.53	17.28	1.19
7 + 10	5.10	7.51	8.84	16.47	4.47
8 + 10	14.63	20.90	31.08	15.87	13.55

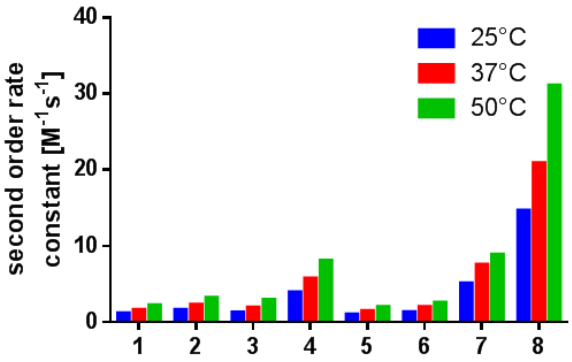
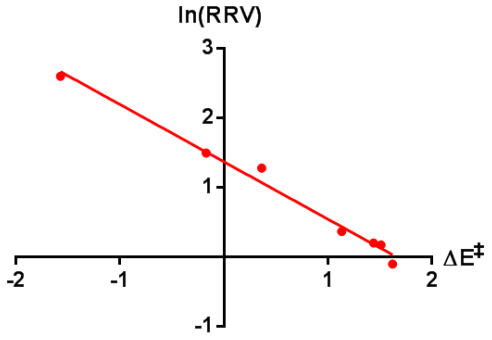


Table 2 and Figure 2: *Measured rates (stopped flow) of tetrazines **1-8** with dienophile TCO (**10**) (RRV =mean relative reactivity value compared to **1** + **10**)*

These experimental results are in agreement with the prediction that tetrazines **2**-**7** will show a comparable rate to **1** while **8** displays enhanced IEDDA reactivity. However, this computational method was not able to predict the correct increase of reactivity for **8** and furthermore failed to predict the order of reactivities for tetrazines **2-7**.



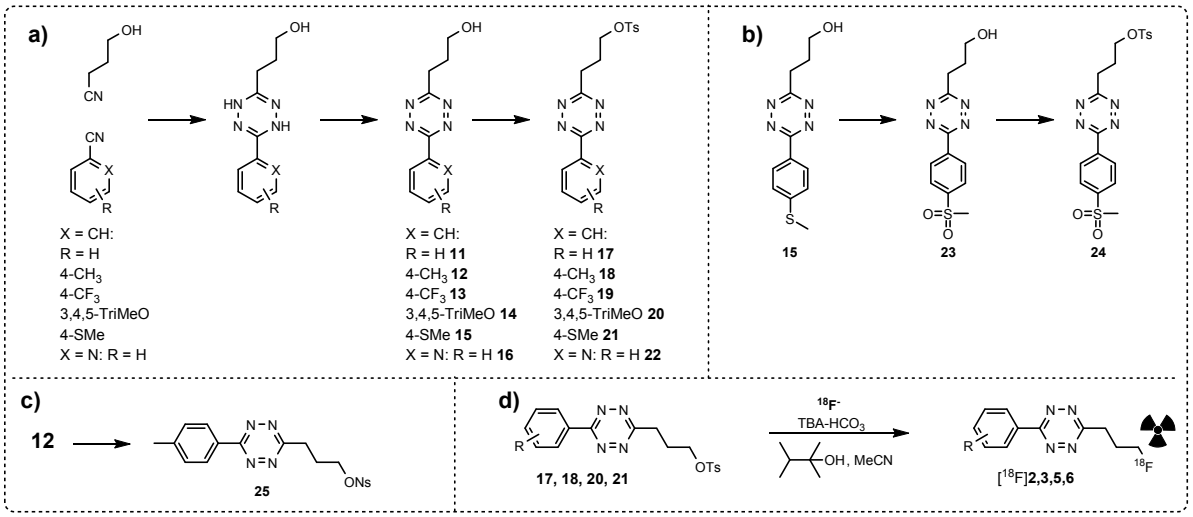
$$k_{calcd} = e^{(-0.8273 \times \Delta E_{act} + 1.3728)} \times 1.108$$

Figure 3 *and* ***Formula 1:*** *Correlation between relative rates and $\Delta E^{\ddagger}$ found for alkyl-aryl substituted tetrazines*

However, using $\Delta E^{\ddagger}$, calculated using the M06-2X density functional in combination with the 6-311+G(d,p) basis set, was found to show an excellent correlation with the logarithm of the relative reactivities (Figure 3). $\Delta E^{\ddagger}$ can therefore be used to predict reactivities of alkyl-aryl substituted tetrazines in the IEDDA reaction with *trans*-cyclooctene. Formula 1 describes the found relation between calculated $\Delta E^{\ddagger}$ and second order rate constants at 25°C in dry 1,4-dioxane.

Precursor Synthesis & Radiolabeling

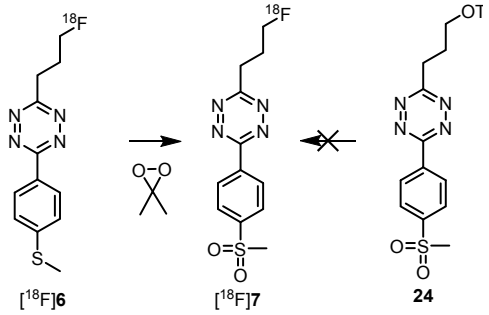
To obtain precursor substances suitable for fluorine-18 radiolabeling, the according alcohols (**11**-**16**, **23**) were synthesized followed by installation of a suitable leaving group. 3-Hydroxypropyl tetrazine derivatives (**11**-**16**) were obtained by nickel catalyzed Tz synthesis with hydrazine monohydrate from according benzonitriles and 4-hydroxybutanenitrile followed by oxidation (Scheme 2a). In the case of phenyl-Tz **11** a yield of 42% was achieved, while p-tolyl-derivative **12** was isolated in 31% yield. Furthermore using the same methodology *p*-trifluoromethylphenyl-Tz **13** (27.2%), 3,4,5-trimethoxyphenyl-Tz **14** (12.5%), 4-thiomethylphenyl-Tz **15** (5.4%) and pyridyl Tz **16** (6.2%) were obtained as pink to red crystalline materials.



Scheme 2: *a) Synthesis of radiolabeling precursors **17**-**22*** b-c) synthesis of radiolabeling precursors **24** and **25** and d) radiolabeling using thexyl alcohol and TBA-HCO_3

In general we noticed higher yields for tetrazine synthesis involving hydroxybutyronitrile compared to synthesis applying the fluorinated alkyl nitrile **9**. Sulfon derivative **23** was synthesized from thiomethyl tetrazine **15** by oxidation using dimethyl dioxirane (Scheme 2b). All alcohols were subjected to tosylation using *p*-tosyl chloride and pyridine in anhydrous dichloromethane giving tosylates **17**-**22** and **24** in good yields (see Scheme 2a+b). In case of the p-tolyl-tetrazine **12** also the nosylate **25** was prepared due to better reactivity in nucleophilic substitutions (Scheme 2c). However, poor solubility as well as stability problems prompted us to focus on tosylated species. The p-tolyl tosylate **18** was used for optimization of the radiofluorination reaction. When the standard [2.2.2]cryptand/K_2CO_3 method, that proved most suitable in the preparation of [^{18}F]**1**, was applied, around 11.2% incorporation yield into [^{18}F]**3** (determined by radio-HPLC) was observed. DMSO as solvent, nosylate **25** as precursor or the use of $KHCO_3$ instead of potassium carbonate resulted in reduced incorporation yields to values below 6%. When tetrabutylammonium hydrogencarbonate in anhydrous acetonitrile was used for labeling a significantly improved radiochemical yield of [^{18}F]**3** (22.9%) was noted. Further optimization of the reaction solvent revealed a very good incorporation yield of 56% when a 1:1 (v/v) mixture of acetonitrile and 2,3-dimethyl-2-butanol (thexyl alcohol) was used as labeling solvent, which is in agreement with previous reports documenting the positive influence of tertiary alcohols on fluorine-18 radiolabeling.[25,26] This method was transferred onto an automated synthesis module (TRACERlab FX_{FDG} synthesis module (GE Healthcare) housed in a shielded hot cell, where in a non-optimized sequence 10 GBq of [^{18}F]**3** could be obtained from 181 GBq cyclotron produced fluorine-18 (9.5% decay corrected radiochemical yield). In automated synthesis, purification of the compounds was achieved by preparative RP-HPLC using 10 mM PO_4-puffer (pH 6) and acetonitrile as eluents. The HPLC eluate was monitored in series for radioactivity and UV absorption, the product fraction was collected, diluted with water and passed over a preactivated C18 Sep-Pak Plus cartridge (Waters, Milford, MA, USA). The cartridge was then eluted with 2.5 ml ethanol to obtain the [^{18}F]tetrazine. The ethanolic solution was diluted with saline to < 10% ethanol content at an approximate activity concentration of 370MBq/mL for intravenous (iv) administration into mice. Applying the optimized radiolabeling conditions to phenyl-Tz-Precursor **17**, 40% of radioactivity was incorporated into the precursor as investigated by radio-TLC and radio-HPLC. 8.9 GBq of [^{18}F]**2** with a specific activity of 99 GBq/µmol ready for i.v. administration were obtained using the automated synthesizer (6.3% isolated radiochemical yield). All attempts of

nucleophilic fluorination using 3-(6-(4-(trifluoromethyl)phenyl)-1,2,4,5-tetrazin-3-yl)propyl 4-methylbenzenesulfonate **(19)** as precursor failed to produce > 1% incorporation yield of [^{18}F]**4**. A variety of reaction conditions and two individual batches of **19** were tested, but mainly unreacted [^{18}F]-fluoride was present in the reaction mixture as investigated by radio-HPLC. No signs of base promoted decomposition was noted, so the inaccessibility of [^{18}F]**4** by nucleophilic fluorination remains an enigma. [^{18}F]**5** could be isolated in 15.8% decay corrected radiochemical yield from **20** (18% incorporation yield as investigated by HPLC) using the TBA/thexyl alcohol/acetonitrile system. Attempts to further optimize conditions for this particular derivative (solvent, stochiometry, temperature and duration) all resulted in diminished incorporation yields. Using the automated synthesizer, 7.0 GBq of formulated [^{18}F]**5** could be obtained, corresponding to 4.9% decay corrected radiochemical yield. For the thiomethyl derivative [^{18}F]**6** up to 47.5% incorporation yield were measured by radio-HPLC. For animal experiments, 11.5 GBq [^{18}F]**6** (8.6% decay corrected radiochemical yield) in excellent (230 GBq/µmol) specific activity were obtained using the automated TRACERlab FX$_{FDG}$ synthesis module. Attempts of preparing sulfone [^{18}F]**7** by direct radiofluorination of tosylate **24** failed to give practical yields. Decomposition was noted using HPLC analysis of the reaction mixture. We assume that the high reactivity of this particular tetrazine derivative renders direct ^{18}F-labeling impossible.



Scheme 3: *Radiosynthesis of [^{18}F]**7** by DMDO mediated oxidation of [^{18}F]**6***

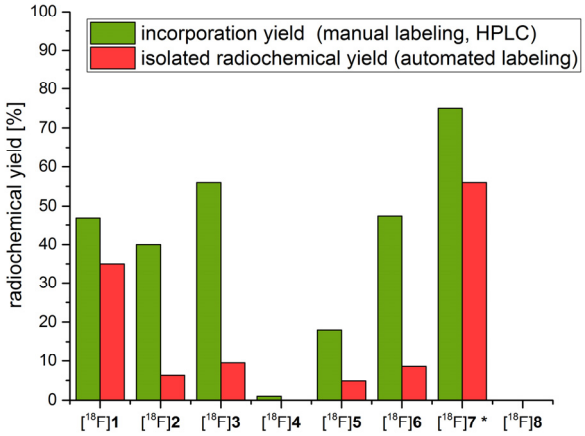


Figure 4: *Overview of incorporation yields (evaluated by radio-HPLC) and isolated radiochemical yields for tetrazines 1-8. *) two-step labelling, yield based on [^{18}F]**6***

Instead a two step radiochemical synthesis sequence was chosen to access [^{18}F]**7** by DMDO mediated oxidation of sulfide [^{18}F]**6**. For this reason [^{18}F]**6** in ethanol, as obtained by automated radiosynthesis, was concentrated to dryness and redissolved in 1 ml acetone c ontaining dimethyldioxirane (~ 40 mM). After short reaction time (60-80 seconds) volatiles were removed on the rotary evaporator and the residue was purified using RP-HPLC to obtain [^{18}F]**7** in 56% radiochemical yield and good specific activity of 56 GBq/µmol thus bypassing the inaccessibility by direct radiolabeling (Scheme 3). Despite optimization attempts, we were not able to prepare pyridyl tetrazine derivative [^{18}F]**8** by nucleophilic fluorination of precursor **22**. In all cases radiofluoride incorporation into [^{18}F]**8** was below 1%, while the major product was a highly apolar compound, whose identity could not be clarified. In addition to successful preparation of novel radiotetrazines [^{18}F]**2**, [^{18}F]**3** and [^{18}F]**5**-**7**, the radiosynthesis of already described dialkyltetrazine [^{18}F]**1** could also be significantly improved to 35% decay corrected isolated radiochemical yield (vs. previously reported 5%)[1] using the TBA, thexyl alcohol and acetonitrile labeling system. A overview of incorporation and isolated radiochemical yields is shown in Figure 4.

In vivo evaluation

Compounds [^{18}F]**2**, [^{18}F]**3** and [^{18}F]**5**-**7** were administered to female BALB/c mice via a tail vein catheter. Anatomic MR imaging (n= 1 for [^{18}F]**2**, [^{18}F]**3**, [^{18}F]**5** and [^{18}F]**6**) followed by a 120 min dynamic PET (n=3 for [^{18}F]**2**, [^{18}F]**3**, [^{18}F]**5** and [^{18}F]**6**, n=2 for [^{18}F]**7**) scan was performed. At the end of PET a terminal blood sample was withdrawn under isoflurane anesthesia from the retroorbital sinus vein and animals were sacrificed by cervical dislocation. Urine samples were collected and organs were harvested. Aliquots of blood and plasma and all organ samples were measured for radioactivity in a y counter (Wizard 1470; Perkin-Elmer). Plasma and urine proteins were precipitated by addition of acetonitrile and consequently removed by centrifugation. Each supernatant and diluted radiotracer solution as reference was spotted on thin-layer chromatography (TLC) plates (silica gel 60F 254 nm, 10 x 20 cm; Merck, Darmstadt, Germany) and plates were developed in a appropriate solvent system. Detection was performed by placing the TLC plates on multisensitive phosphor screens (Perkin-Elmer Life Sciences, Waltham, MA). The screens were scanned at 300 dpi resolution using a PerkinElmer Cyclone® Plus Phosphor Imager (Perkin-Elmer Life Sciences) to obtain metabolism data.

Organ time activity curves (TACs) for phenyl tetrazine [^{18}F]**2**, p-tolyl tetrazine[^{18}F]**3** and 3,4,5-trimethoxy phenyl tetrazine derivative [^{18}F]**5** (shown in supporting information) show rapid renal clearance as indicated by a steep rise of activity concentration within the urinary bladder. The liver shows high initial uptake of these three substances, but activity is cleared rapidly from most organs despite bone, where a steady increase of activity concentration throughout the experiment is observed. These findings are a good indicator for metabolic instability and liberation of free fluoride from the test substances. Bone uptake of these derivatives is also visible in PET/MR summation images (see ESI), that is especially pronounced in the well perfused nasal bone. Metabolite analysis of [^{18}F]**2,** [^{18}F]**3** and [^{18}F]**5** using radio-TLC (see ESI) indicate the presence of free fluoride (Rf = 0) and polar metabolites, while the amount of unchanged tetrazine in plasma and urine are below the limit of detection, furthermore confirming rapid degradation of this probes *in vivo*.

In contrast to above mentioned compounds, data obtained from thiomethyl-tetrazine derivative [^{18}F]**6** does not indicate *in vivo* defluorination. PET/MR images show homogenous biodistribution with slightly elevated uptake in the liver (see Figure 5a-b). After initial perfusion [^{18}F]**6** exhibits very uniform uptake in all analyzed organs but the urinary bladder, wherein a steady increase of activity concentration indicates rapid renal clearance (see Figure 5c, for TACs without urinary bladder signal see ESI). PET data also clearly demonstrates the ability of [^{18}F]**6** to pass the blood brain barrier.

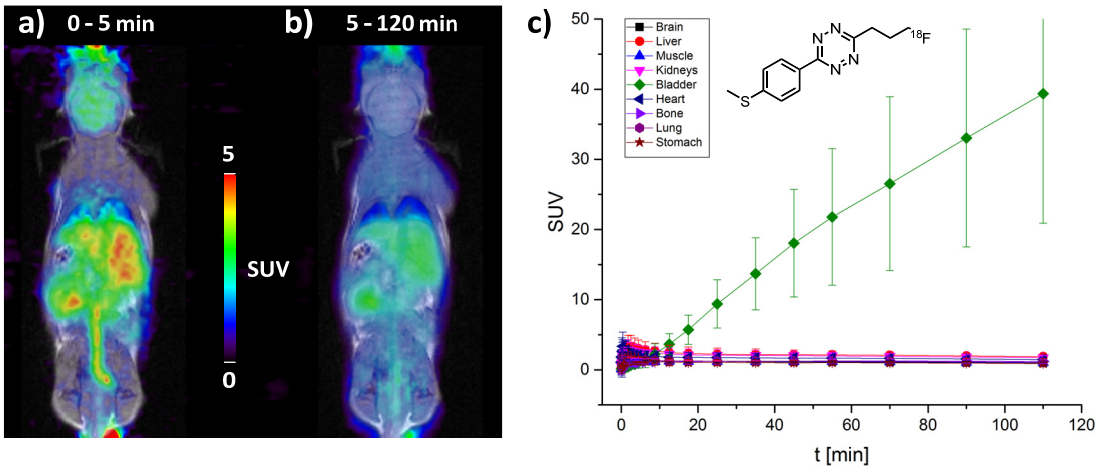


Figure 5: *Coronal PET/MR slices showing time frames 0-5 min (a) and 5-120 min (b) post administration of [^{18}F]**6**. c) Dynamic PET data obtained for [^{18}F]**6** showing homogenous biodistribution and renal excretion*

TLC metabolite analysis revealed oxidative metabolism of [^{18}F]**6** (see Figure 6). As seen in Figure 6b the radiofluorinated reference compound (left lane) already contains 5% impurity in form of the sulfoxide-derivative **26**, most likely due to air oxidation during work-up and formulation of the radiotracer. Identity of the sulfoxide was determined by TLC-Rf comparison with authentic standard (Figure 6c). Two hours post administration < 1% of [^{18}F]**6** is detected in plasma, while 13.9 (±3.2)% of plasma radioactivity is attributed to the sulfone [^{18}F]**7**, and 61.8 (±4.9)% to the sulfoxide-species [^{18}F]**26**, both active "clickable" metabolites of [^{18}F]**6** that exhibit accelerated bioorthogonal cycloaddition reactivity as compared to the parent compound (calculated rate relative to reaction of **1** + **10** is 2.51 for **26** and 4.47 for **7**, see ESI for details). The compound is excreted renally mainly as sulfoxide metabolite (up to 45% in urine), accompanied by more polar metabolites.

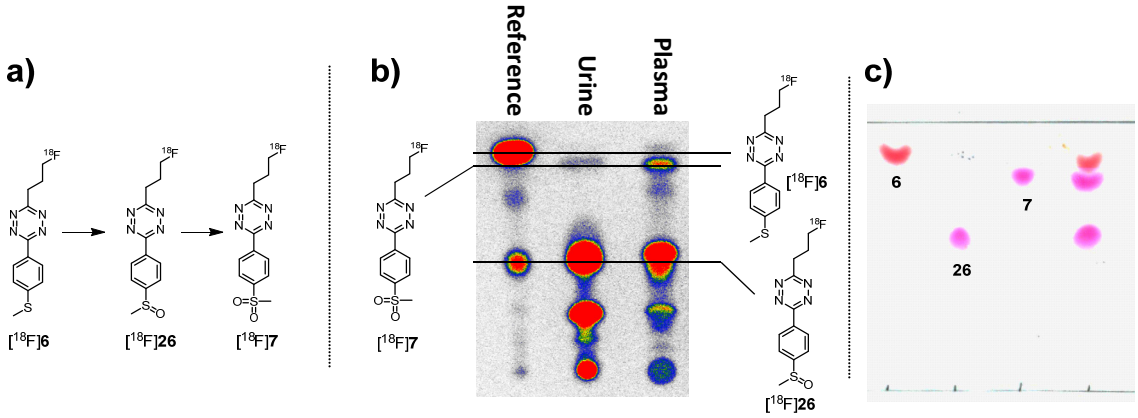


Figure 6: *a) Oxidative metabolism of [^{18}F]**6**, b)Radio-TLC (SiO_2, 5% MeOH in DCM) showing reference compound [^{18}F]**6** (left lane), urine (middle lane) and plasma samples 120 min post [^{18}F]**6** administration to native BALB/c mice c) TLC showing retention behaviour of compounds **6**, **7** and **26** (SiO_2, 5% MeOH in DCM)*

To further shed light on the metabolism of [^{18}F]**6,** the compound was administered to BALB/c mice (n=3), and the animals were sacrificed 60 minutes post radiotracer administration. Organs and blood were harvested for gamma counter analysis to obtain biodistribution data. In addition, plasma, urine, bile, as well as liver and brain extracts were analyzed using radio-TLC (see ESI for TLC lanes). At the 60 min time point [^{18}F]**6** is already absent in plasma (< 1%) while the active metabolite composition resembles the 120 min time point. Within the central nervous system 18.8 (±4.6)% of native [^{18}F]**6** is

still intact, 49.3 (±9.0)% of activity is attributed to the sulfoxide and 11.5 (±1.6)% to the sulfone metabolite, clearly showing that this bioorthogonal imaging agent is also suitable for neuro-targets inside the brain. Within the liver the main fraction of activity (39.9 ±0.3%) is attributed to unchanged [^{18}F]**6**, while 14.5 (±4.2)% and 11.3 (±0.5)% are the fractions of sulfoxide and sulfone metabolites respectively. The urine composition one hour post tracer administration resembles the urine composition after two hours of uptake time. Beside highly polar radiometabolites, the sulfoxide is the main active species (17.3 ±2.0%) in bile. The metabolism of [^{18}F]**6** is in good agreement with previously reported data describing the metabolism of organic sulfides.[27]

PET scanning of the sulfone tetrazine derivative [^{18}F]**7** revealed renal excretion as well as homogenous biodistribution, that is clearly visible in PET images and organ time activity curves shown in Figure 7b-c.The main mode of excretion for [^{18}F]**7** is renal (as visible in the time activity curve of the urinary bladder), but also to a certain extent hepatobiliar, as indicated by uptake in the intestines (Figure 7). TACs without the urinary bladder signal can be found in the supporting information of this manuscript. Similar to the thioether [^{18}F]**6**, also the sulfone [^{18}F]**7** penetrates the blood-brain-barrier, and is thus applicable for pretargeting tasks within the central nervous system.

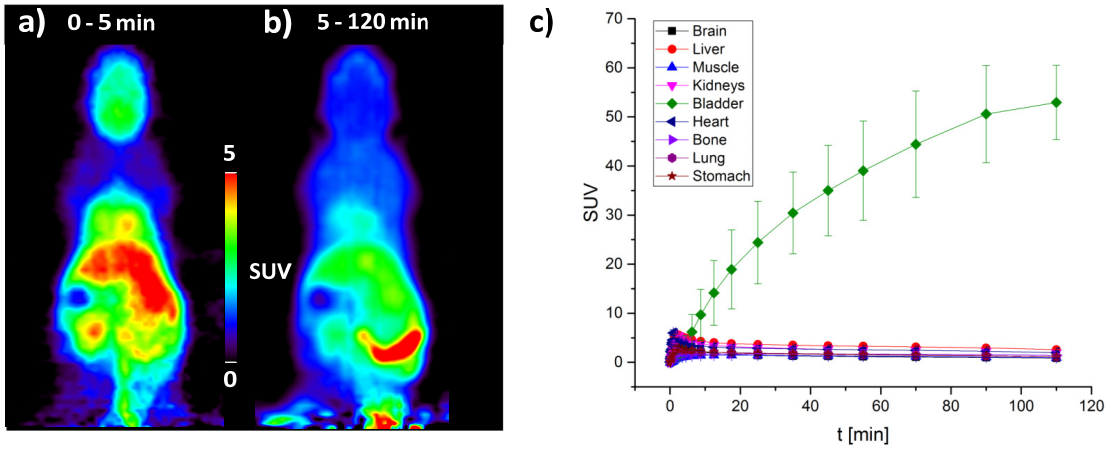


Figure 7: *Coronal PET slices showing time frames 0-5 min (a) and 5-120 min (b) post administration of [^{18}F]**7**. c) Dynamic PET data obtained for [^{18}F]**7** showing homogenous biodistribution and mainly renal excretion*

Plasma metabolite analysis 2 hours post tracer administration revealed a high fraction (65%) of unchanged tetrazine probe, rendering [^{18}F]**7** nearly as metabolically stable as previously published [^{18}F]**1**. Although not common, literature reports also reductive metabolism of sulfur[28] compounds in higher animals.[29] 18.2-19.9% of radioactivity in plasma is, according to radio-TLC, attributed to the reduced sulfoxide tetrazine species. Analysis of urine radioactivity revealed that 10.4-13.7% [^{18}F]**7** is excreted unmetabolized, while the majority of radioactivity in the urine arises from polar metabolites, whose identity has not been further investigated.

Data from the *ex vivo* biodistributions is summarized in Figure 8. In general *ex vivo* biodistribution data for all analyzed compounds is in good agreement with data obtained from the PET experiments.

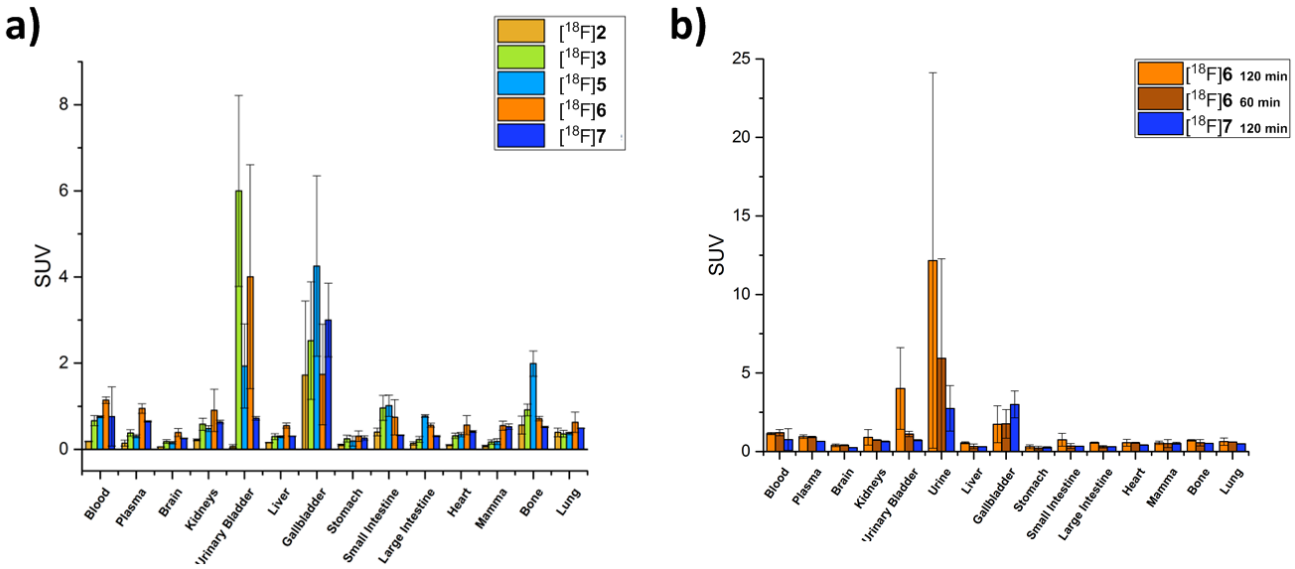


Figure 8: *Ex vivo biodistribution data for compounds a) [^{18}F]**2**, **3**, **5-7** 120 min post administration and b) [^{18}F]**6** (120 & 60 min post injection) and [^{18}F]**7** 120 min post administration*

The biodistribution of [^{18}F]**6** at the 60 min and 120 min terminal time points is compared in Figure 8b. Beside excretion organs only minor changes in the biodistribution pattern of [^{18}F]**6** are visible between those time points, indicating that 60 – 120 min post tracer administration would be a beneficial time window for image acquisition in actual bioorthogonal PET pretargeting experiments.

Conclusion

A series of 3-fluoropropyl-aryl-tetrazines was designed based on the structure of **1**. The compounds were successfully synthesized and their reactivity towards the dienophile *trans*-cyclooctene was investigated using stopped flow photometry. Furthermore a simple computational method was established, that allows reactivity prediction for aryl-alkyl-tetrazines.

Direct nucleophilic radiofluorination, using an optimized protocol, enabled the synthesis of four novel ^{18}F-fluoropropyl tetrazines ([^{18}F]**2**, [^{18}F]**3**, [^{18}F]**5**, [^{18}F]**6**). In addition, using this modified procedure, the isolated yield of [^{18}F]**1** was increased 7-fold. Still, the most reactive derivatives ([^{18}F]**4,** [^{18}F]**7,** [^{18}F]**8**) could not be prepared using this methodology. However, we were able to prepare [^{18}F]**7** by fast post-labeling oxidation of [^{18}F]**6** in high yield using dimethyl dioxirane (DMDO), thus boosting bioorthogonal reactivity of this compound.

In vivo evaluation using PET and MR imaging as well as radiometabolite analysis revealed highly promising properties for compounds [^{18}F]**6** and [^{18}F]**7** to be used as secondary probe in bioorthogonal PET imaging. Both agents exhibit homogenous biodistribution in the mouse model and are renally excreted. In addition, both tetrazines are capable of penetrating the blood-brain-barrier, and should thus allow pretargeted imaging within the central nervous system.

[^{18}F]**6**, that is accessible by direct radiofluorination, acts as a pro-drug, which is metabolically activated to more reactive sulfoxide and sulfone species [^{18}F]**7**. Administration of [^{18}F]**7** revealed high metabolic stability of this oxidized probe.

Within this contribution we further explored the chemical space of ^{18}F-tetrazines and present two derivatives that show improved kinetics and beneficial pharmacokinetic properties as compared to previously published dialkyltetrazine [^{18}F]**1**.

Experimental

Materials and Methods

Unless otherwise noted, all reagents were purchased from commercial suppliers and used without further purification. DCM and 1,4-dioxane were dried using PURESOLV-columns (Innovative Technology Inc.). Dry acetonitrile (Sigma Aldrich) was commercially obtained and stored under argon. Dienophile TCO (**10**) and DMDO were prepared following known procedures.[30,31] Anhydrous hydrazine was prepared by the vacuum thermolysis of hydrazine cyanurate.[32] All other solvents were distilled prior to use. Drying of organic solvents after extraction was performed using anhydrous Na_2SO_4 or $MgSO_4$ (Sigma Aldrich) and subsequent filtration. Reactions were carried out under an atmosphere of argon in air-dried glassware with magnetic stirring. Sensitive liquids were transferred via syringe. Thin layer chromatography was performed using TLC alumina plates (Merck, silica gel 60, fluorescence indicator F254, or Merck, aluminium oxide neutral, fluorescence indicator F254). Detection in radio-TLC was performed by placing the TLC plates on multisensitive phosphor screens (Perkin-Elmer Life Sciences, Waltham, MA). The screens were scanned at 300 dpi resolution using a PerkinElmer Cyclone® Plus Phosphor Imager (Perkin-Elmer Life Sciences). Preparative column chromatography was performed using a Büchi Sepacore Flash System (2 x Büchi Pump Module C-605, Büchi Pump Manager C-615, Büchi UV Photometer C-635, Büchi Fraction Collector C-660) using silica gel 60 (40-63 µm) as obtained from Merck and distilled or redistilled solvents. ^{1}H, ^{13}C and ^{19}F NMR spectra were recorded on a Bruker Avance IIIHD 600 MHz spectrometer equipped with a Prodigy BBO cryo probe or on a Bruker Avance UltraShield 400 spectrometer at 20 °C. Chemical shifts are reported in ppm (δ) relative to tetramethylsilane and calibrated using solvent residual peaks. Data are shown as follows: Chemical shift, multiplicity (s = singlet, d = doublet, t = triplet, q = quartet, quin = quintet, m = multiplet, br = broad signal) and integration. A temperature-controlled Applied Photophysics SX20 (535 nm LED light source) stopped flow photometer systems (Applied Photophysics, Surrey, UK) was used for stopped flow measurements. HR-MS analysis was carried out from methanol solutions (concentration: 10 ppm) by using an HTC PAL system autosampler (CTC Analytics AG, Zwingen, Switzerland), an Agilent 1100/1200 HPLC with binary pumps, degasser and column thermostat (Agilent Technologies, Waldbronn, Germany) and Agilent 6230 AJS ESI–TOF mass spectrometer (Agilent Technologies, Palo Alto, United States). [^{18}F]Fluoride was produced *via* the $^{18}O(p,n)^{18}F$ nuclear reaction by irradiating oxygen-18 enriched water (IASON, Austria) using a PETtrace cyclotron equipped with high yield liquid target system (GE Healthcare, Uppsala, Sweden). HPLC analysis was performed on a 1200 series system (Agilent Technologies) using a reversed phase columns and acetonitrile / water or acetonitrile / phosphate buffer gradients. Analytical conditions: (A): Agilent Extend-C18 3.5 µm, 3 x 100 mm, gradient 10mM PO4-puffer pH=6/ acetonitrile , 1.3 ml/min, 0-1 min 15% acetonitrile, 1→8 min 15%→85% acetonitrile, 8-9 min 85% acetonitrile. (B): Agilent ZORBAX SB-Aq 5 µm, 4.6 x 250 mm, water / acetonitrile , 1.2 ml/min, 0-2 min 5% acetonitrile, 2→10 min 5%→20% acetonitrile, 10-16 min 20%→90%, 16-20 min 90% acetonitrile. For radio-HPLC a GABI star radioactivity detector (raytest Isotopenmessgeraete GmbH, Straubenhardt, Germany) was used. Preparative HPLC separations were done on the built in HPLC system on a synthesis module (TRACERlab™ FX_{FDG}, General Electric Healthcare, Uppsala, Sweden) using a Macherey-Nagel EP 250/16 100-7 C-18 (10 µm, 16 x 250 mm) column and phosphate puffer (10mM, pH = 6) / acetonitrile-gradient (flow rate: 5 mL/min, 0-6 min 10% acetonitrile, 6.01 min 30% acetonitrile, 6.01→40 min 30%→80% acetonitrile) in combination with a K-2001 UV detector (Knauer) and radioactivity detector.

Chemical Synthesis

3-(3-fluoropropyl)-6-methyl-1,2,4,5-tetrazine (1)

4-fluorobutanenitrile (**9**, 1 eq., 100 mg, 1.15 mmol) and zinc triflate (0.46 eq., 192 mg, 0.528 mmol) in anhydrous acetonitrile (7 eq., 330 mg, 8 mmol) were treated dropwise with anhydrous hydrazine (36 eq., 1.3 g, 41.1 mmol) at 0°C (Caution: gas evolution, exothermic!). The reaction mixture was heated to 42°C for 24 hours. The reaction mixture was cooled to room temperature and diluted with a 10% aqueous solution of sodium nitrite (7 eq., 0.55 g, 8 mmol). 5% HCl was added slowly until gas evolution ceased. The red solution was extracted five times with diethyl ether. Pooled extracts were dried over $MgSO_4$ and the solvent was removed on the rotary evaporator. Column chromatography over 40 g SiO_2 (5-12% diethyl ether in petroleum ether) afforded **1** (67.3 mg, 37.5% of theory) as red oil. Spectroscopic data matched previously reported values.

3-(3-fluoropropyl)-6-phenyl-1,2,4,5-tetrazine (2)

A mixture of benzonitrile (1 eq., 237 mg, 2.3 mmol), 4-fluorobutanenitrile (2 eq., 400 mg, 4.6 mmol) and anhydrous $NiCl_2$ (0.15 eq., 45 mg, 0.345 mmol) was treated dropwise with hydrazine monohydrate (9 eq., 1.1 g, 21 mmol) (Caution: gas evolution, exothermic!). The purple reaction mixture was kept at 52°C for 16 hours. After returning to room temperature the reaction mixture was diluted with a solution of sodium nitrite (8 eq., 2.54 g, 37 mmol) in 25 ml water and cooled with an ice bath. 1N HCl was added slowly until gas evolution ceased, and the intense red mixture was extracted three times with ethyl acetate. Pooled extracts were washed with brine, dried over $MgSO_4$ and concentrated on the rotary evaporator. Purification by column chromatography over 40 g SiO_2 (3-12% EE in PE) yielded **2** as purple solid (83 mg, 16.5% of theory). TLC-Rf (DCM) = 0.77, ^{1}H NMR (400 MHz, $CDCl_3$) δ = 2.36 - 2.50 (m, 2 H) 3.53 (t, *J*=7.80 Hz, 2 H) 4.65 (dt, *J*=47.22, 5.90 Hz, 2 H) 7.57 - 7.66 (m, 3 H) 8.57 - 8.63 (m, 2 H) ppm ^{13}C NMR (100.61 MHz, $CDCl_3$) δ = 28.5 (d, *J*=20.49Hz), 30.9 (d, *J*=4.94Hz), 82.8 (d, *J*=166.72Hz), 127.9, 129.2, 131.7, 132.6, 164.3, 169.2 ppm ^{19}F NMR (376.5 MHz, $CDCl_3$) δ = -219.9 ppm HR-ESI-MS: calcd. for $[M+H]^+$ $C_{11}H_{12}FN_4^+$: 219.1041, found: 219.1048.

3-(3-fluoropropyl)-6-(p-tolyl)-1,2,4,5-tetrazine (3)

A mixture of 4-methylbenzonitrile (1 eq., 404 mg, 3.44 mmol), 4-fluorobutanenitrile (1.87 eq., 560 mg, 6.43 mmol) and anhydrous $NiCl_2$ (0.15 eq., 68 mg, 0.52 mmol) was treated dropwise with hydrazine monohydrate (9 eq., 1.55 g, 31 mmol) (Caution: gas evolution, exothermic!) and heated to 65°C for 20 hours. After returning to room temperature the reaction mixture was diluted with a solution of sodium nitrite (12 eq., 2.85 g, 41.3 mmol). 2N HCl was added slowly until gas evolution ceased, and the deep red mixture was extracted three times with ethyl acetate. Pooled extracts were washed with brine, dried over Na_2SO_4 and concentrated on the rotary evaporator. Column chromatography over 40 g SiO_2 afforded **3** (51 mg, 6.4% of theory) as red crystalline solid. TLC-Rf (DCM) = 0.73, ^{1}H NMR (400 MHz, $CDCl_3$) δ = 2.33 - 2.50 (m, 5 H) 3.51 (t, *J*=7.60 Hz, 2 H) 4.64 (dt, *J*=47.06, 5.60 Hz, 2 H) 7.39 (d, *J*=8.18 Hz, 2 H) 8.48 (d, *J*=8.18 Hz, 2 H) ppm ^{13}C NMR (100.61 MHz, $CDCl_3$) δ = 21.6, 28.5 (d, *J*=20.70 Hz), 30.8 (d, *J*=5.37 Hz), 82.9 (d, *J*=166.39 Hz), 127.9, 128.9, 130.0, 143.3, 164.3, 168.9 ppm ^{19}F NMR (376.5 MHz, $CDCl_3$) δ = -219.9 ppm HR-ESI-MS: calcd. for $[M+H]^+$ $C_{12}H_{14}FN_4^+$: 233.11970, found: 233.11922.

3-(3-fluoropropyl)-6-(4-(trifluoromethyl)phenyl)-1,2,4,5-tetrazine (4)

A mixture of 4-trifluoromethylbenzonitrile (1 eq., 500 mg, 2.92 mmol), 4-fluorobutanenitrile (2 eq., 509 mg, 5.84 mmol) and anhydrous $NiCl_2$ (0.15 eq., 56.8 mg, 0.44 mmol) was treated dropwise with hydrazine monohydrate (9 eq., 1.32 g, 26.2 mmol) (Caution: gas evolution, exothermic!) and heated to 65°C for 24 hours. After returning to room temperature the reaction mixture was diluted with a solution of sodium nitrite (6 eq., 1.2 g, 17.5 mmol) in 15 ml water. 2N HCl was added slowly until gas evolution ceased. The purple solution was extracted three times with ethyl acetate. Pooled extracts were washed with water, dried over $MgSO_4$ and the solvent was removed on the rotary evaporator. Column chromatography over 90 g SiO_2 (3-10% ethyl acetate in petroleum ether) afforded **4** (39 mg, 4.7% of theory) as purple crystalline solid. TLC-Rf (PE:EE =3:1) = 0.79 ^{1}H NMR (400 MHz, $CDCl_3$) δ = 2.38 - 2.53 (m, 2 H) 3.58 (t, *J*=7.80 Hz, 2 H) 4.67 (dt, *J*=46.83, 5.50 Hz, 2 H) 7.87 (d, *J*=8.20 Hz, 2 H) 8.75 (d, *J*=8.20 Hz, 2 H) ppm ^{13}C NMR (100.61 MHz, $CDCl_3$) δ = 28.5 (d, *J*=19.80 Hz), 31.1 (d, *J*=4.94 Hz), 82.8 (d, *J*=166.01 Hz), 123.7 (q, *J*=272.68 Hz), 126.2 (q, *J*=3.53 Hz), 128.3, 134.2 (q, *J*=33.20 Hz), 163.5, 169.9 ppm, ^{19}F NMR (376.5 MHz, $CDCl_3$) δ = -219,9 (1 F), -63.1 (3 F) ppm, HR-ESI-MS: calcd. for $[M+H]^+$ $C_{12}H_{11}F_4N_4^+$: 287.09144, found: 287.09058.

3-(3-fluoropropyl)-6-(3,4,5-trimethoxyphenyl)-1,2,4,5-tetrazine (5)

A mixture of 3,4,5-trimethoxybenzonitrile (1 eq., 444 mg, 2.3 mmol), 4-fluorobutanenitrile (2 eq., 400 mg, 4.6 mmol) and anhydrous $NiCl_2$ (0.15 eq., 45 mg, 0.345 mmol) was treated dropwise with hydrazine monohydrate (9 eq., 1.1 g, 21 mmol) (Caution: gas evolution, exothermic!). The purple reaction mixture was kept at 52°C for 16 hours. After returning to room temperature the reaction mixture was diluted with a solution of sodium nitrite (8 eq., 2.54 g, 37 mmol) in 25 ml water and cooled with an ice bath. 1N HCl was added slowly until gas evolution ceased, and the intense red was extracted three times with ethyl acetate. Pooled extracts were washed with brine, dried over $MgSO_4$ and concentrated on the rotary evaporator. Purification by column chromatography over 40 g SiO_2 (10-50% EE in PE) yielded **5** as red solid (13 mg, 1.8% of theory). TLC-Rf (DCM) = 0.12 ^{1}H NMR (400 MHz, $CDCl_3$) δ = 2.35 - 2.51 (m, 2 H) 3.53 (t, *J*=7.80 Hz, 2 H) 3.98 (s, 3 H) 4.00 (s, 6 H) 4.66 (dt, *J*=46.83, 5.90 Hz, 2 H) 7.90 (s, 2 H) ppm ^{13}C NMR (100.61 MHz, $CDCl_3$) δ = 28.4 (d, *J*=20.49 Hz), 30.8 (d, *J*=4.94 Hz), 56.3, 61.0, 82.9 (d, *J*=166.01 Hz), 105.1, 126.6, 142.1, 153.9, 163.8, 168.9 ppm ^{19}F NMR (376.5 MHz, $CDCl_3$) δ = -219.9 ppm HR-ESI-MS: calcd. for $[M+H]^+$ $C_{14}H_{18}FN_4O_3^+$: 309.1357, found: 309.1359

3-(3-fluoropropyl)-6-(4-(methylthio)phenyl)-1,2,4,5-tetrazine (6) & 3-(3-fluoropropyl)-6-(4-(methylsulfinyl)phenyl)-1,2,4,5-tetrazine (26)

A mixture of 4-thiomethylbenzonitrile (1 eq., 343 mg, 2.3 mmol), 4-fluorobutanenitrile (2 eq., 400 mg, 4.6 mmol) and anhydrous $NiCl_2$ (0.15 eq., 45 mg, 0.345 mmol) was treated dropwise with hydrazine monohydrate (9 eq., 1.1 g, 21 mmol) (Caution: gas evolution, exothermic!). The purple reaction mixture was kept at 42°C for 18 hours. After returning to room temperature the reaction mixture was diluted with a solution of sodium nitrite (8 eq., 2.54 g, 37 mmol) in 25 ml water and cooled with an ice bath. 1N HCl was added slowly until gas evolution ceased, and the intense red was extracted three times with ethyl acetate. Pooled extracts were washed with brine, dried over $MgSO_4$ and concentrated on the rotary evaporator. Purification by column chromatography over 40 g SiO_2 (20-50% DCM in PE) yielded **6** as red solid (8 mg, 1.3% of theory). TLC-Rf (DCM:PE = 1:1) = 0.15, ^{1}H NMR (400 MHz, $CDCl_3$) δ = 2.35 - 2.51 (m, 2 H) 2.58 (s, 3 H) 3.52 (t, *J*=7.80 Hz, 2 H) 4.66 (dt, *J*=47.22, 5.50 Hz, 2 H) 7.42 (dt, *J*=8.59, 2.00 Hz, 2 H) 8.52 (dt, *J*=8.98, 2.00 Hz, 2 H) ppm ^{13}C NMR (100.61 MHz, $CDCl_3$) δ = 14.9, 28.5 (d, *J*=20.49Hz), 30.6 (d, *J*=5.65Hz), 82.9 (d, *J*=166.72Hz), 125.9, 127.8, 128.1,

145.4, 164.1, 168.9 ppm ^{19}F NMR (376.5 MHz, $CDCl_3$) δ = -219.9 ppm HR-ESI-MS: calcd. for $[M+H]^+$ $C_{12}H_{14}FN_4S^+$: 265.0918, found: 265.0923. Eluting from the same column with 2% MeOH in DCM 105 mg (16.3% of theory) of sulfoxide 3-(3-fluoropropyl)-6-(4-(methylsulfinyl)phenyl)-1,2,4,5-tetrazine (**26**) was obtained as oxidated byproduct. ^{1}H NMR (600 MHz, $CDCl_3$) δ = 2.40 - 2.50 (m, 2 H) 2.83 (s, 3 H) 3.58 (t, *J*=7.60 Hz, 2 H) 4.67 (dt, *J*=46.95, 5.60 Hz, 2 H) 7.89 (dt, *J*=8.80, 1.80 Hz, 2 H) 8.79 (dt, *J*=8.80, 1.80 Hz, 2 H) ppm ^{13}C NMR (150.91 MHz, $CDCl_3$) δ = 28.4 (d, *J*=19.62 Hz), 31.0 (d, *J*=5.45 Hz), 43.9, 82.9 (d, *J*=166.76 Hz), 124.4, 128.8, 134.3, 150.6, 163.6, 169.8 ppm ^{19}F NMR (376.5 MHz, $CDCl_3$) δ = -219.9 ppm

3-(3-fluoropropyl)-6-(4-(methylsulfonyl)phenyl)-1,2,4,5-tetrazine (7)

3-(3-fluoropropyl)-6-(4-(methylsulfinyl)phenyl)-1,2,4,5-tetrazine (**6**, 1 eq., 20 mg, 0.07 mmol) was treated with a ice cold solution of dimethyl dioxirane (DMDO) in 10 ml acetone (~40 mM). The pink reaction mixture was allowed to reach room temperature and stirred for additional 40 minutes. Volatiles were removed on the rotary evaporator and the residue was purified by column chromatography over 8 g SiO_2 (10-50% EE in PE). **7** was obtained as pink solid in (13 mg, 63 % of theory). TLC-Rf (5% MeOH in DCM) = 0.77, ^{1}H NMR (400 MHz, $CDCl_3$) δ = 2.39 - 2.54 (m, 2 H) 3.14 - 3.17 (m, 3 H) 3.60 (t, *J*=7.80 Hz, 2 H) 4.67 (dt, *J*=46.83, 5.50 Hz, 2 H) 8.20 (dt, *J*=8.50, 2.00 Hz, 2 H) 8.84 (dt, *J*=8.59, 2.00 Hz, 2 H) ppm ^{13}C NMR (100.61 MHz, $CDCl_3$) δ = 28.5 (d, *J*=20.49Hz), 31.2 (d, *J*=5.65Hz), 44.4, 82.8 (d, *J*=166.72Hz), 128.3, 128.8, 136.7, 144.1, 163.25, 170.1 ppm ^{19}F NMR (376.5 MHz, $CDCl_3$) δ = -219.8 ppm, HR-ESI-MS: calcd. for $[M+H]^+$ $C_{12}H_{14}FN_4O_2S^+$: 297.0816, found: 297.0816

3-(3-fluoropropyl)-6-(pyridin-2-yl)-1,2,4,5-tetrazine (8)

A mixture of 2-pyridinecarbonitrile (1 eq., 561 mg, 5.4 mmol), 4-fluorobutanenitrile (1 eq., 470 mg, 5.4 mmol) and anhydrous $NiCl_2$ (0.1 eq., 70 mg, 0.54 mmol) was treated dropwise with hydrazine monohydrate (6 eq., 1.62 g, 32.4 mmol) at 0°C (Caution: gas evolution, exothermic!). The inhomogenous reaction mixture was heated to 60°C for 24 hours. The reaction mixture was cooled and diluted with a 10% aqueous solution of sodium nitrite (4 eq., 1.52 g, 22 mmol). 2N HCl was added slowly until gas evolution ceased. The red solution was extracted three times with ethyl acetate. Pooled extracts were washed with brine, dried over Na_2SO_4 and the solvent was removed on the rotary evaporator. Column chromatography over 40 g SiO_2 (20-70% ethyl acetate in petroleum ether) afforded **8** (128 mg, 10.8% of theory) as red oil. TLC-Rf (EE) = 0.78, ^{1}H NMR (400 MHz, $CDCl_3$) δ = 2.29 - 2.44 (m, 2 H) 3.52 (t, *J*=7.70 Hz, 2 H) 4.58 (dt, *J*=47.20, 5.90 Hz, 2 H) 7.46 - 7.52 (m, 1 H) 7.92 (td, *J*=7.87, 1.83 Hz, 1 H) 8.56 (d, *J*=7.68 Hz, 1 H) 8.87 (d, *J*=4.03 Hz, 1 H) ppm ^{13}C NMR (100.61 MHz, $CDCl_3$) δ = 28.3 (d, *J*=20.70Hz), 30.9 (d, *J*=4.60 Hz), 82.7 (d, *J*=166.39 Hz), 123.8, 126.2, 137.3, 150.0, 150.7, 163.6, 169.9 ppm, ^{19}F NMR (376.5 MHz, $CDCl_3$) δ = -219.9 ppm, HR-ESI-MS: calcd. for $[M+H]^+$ $C_{10}H_{11}FN_5^+$: 220.09930, found: 220.09865.

4-Fluorobutanenitrile (9)

Warning: Alkylfluorides are potentially highly toxic! NaCN is highly toxic! A mixture of 1-bromo-3-fluoropropane (1 eq., 14.1 g, 100 mmol), powdered NaCN (1.25 eq., 6.12 g, 125 mmol) and triethylene glycol was slowly heated to 130°C. Care must be taken due to a exothermic reaction setting in at ~40°C. The mixture was kept between 120°C and 140°C for 120 minutes. After cooling to room temperature the mixture was distilled at 125 mbar to obtain 3.8 g **9** as colorless liquid. Another fraction (1.7 g) of product was obtained at 60°C/25 mbar. Combined yield: 5.5 g (63% of theory) ^{1}H NMR (200 MHz, $CDCl_3$) δ = 1.86 - 2.14 (m, 2 H) 2.47 (t, *J*=7.00 Hz, 2 H) 4.51 (dt, *J*=46.95, 5.50 Hz, 2 H)

ppm, ^{13}C NMR (50.32 MHz, $CDCl_3$) δ = 13.2 (d, *J*=5.06 Hz), 26.2 (d, *J*=20.68 Hz), 81.2 (d, *J*=166.84 Hz), 118.7 ppm

3-(6-phenyl-1,2,4,5-tetrazin-3-yl)propan-1-ol (11)

A mixture of benzonitrile (1 eq., 4 g, 38.8 mmol), 4-hydroxybutanenitrile (2 eq., 6.6 g, 77.6 mmol) and anhydrous $NiCl_2$ (0.15 eq., 753 mg, 5.8 mmol) was treated dropwise with hydrazine monohydrate (9 eq., 17.5 g, 350 mmol) (Caution: gas evolution, exothermic!). The purple reaction mixture was heated to 42°C for 72 hours. After returning to room temperature the reaction mixture was diluted with a solution of sodium nitrite (6 eq., 16 g, 233 mmol) in 150 ml water and cooled with an ice bath. 2N HCl was added slowly until gas evolution ceased, and the intense red mixture was extracted three times with ethyl acetate. Pooled extracts were washed with brine, dried over Na_2SO_4 and concentrated on the rotary evaporator. Raw material (7 g) was purified by column chromatography over 90 g SiO_2 (30-75% EE in PE). **11** was obtained as purple solid (3.55 g, 42.3% of theory). TLC-Rf (PE:EE =1:1) = 0.42 ^{1}H NMR (400 MHz, $CDCl_3$) δ = 1.73 (br. s., 1 H) 2.24 - 2.33 (m, 2 H) 3.52 (t, *J*=7.41 Hz, 2 H) 3.85 (t, *J*=6.05 Hz, 2 H) 7.57 - 7.67 (m, 3 H) 8.58 - 8.63 (m, 2 H) ppm ^{13}C NMR (100.61 MHz, $CDCl_3$) δ = 30.6, 31.5, 61.8, 127.9, 129.2, 131.8, 132.6, 164.2, 169.9 ppm HR-ESI-MS: calcd. for $[M+H]^+$ $C_{11}H_{13}N_4O^+$: 217.1084, found: 217.1089.

3-(6-(p-tolyl)-1,2,4,5-tetrazin-3-yl)propan-1-ol (12)

A mixture of 4-methylbenzonitrile (1 eq., 1 g, 8.54 mmol), 4-hydroxybutanenitrile (2 eq., 1.45 g, 17.1 mmol) and anhydrous $NiCl_2$ (0.15 eq., 166 mg, 1.28 mmol) was treated dropwise with hydrazine monohydrate (9 eq., 3.85 g, 77 mmol) (Caution: gas evolution, exothermic!). The purple solution was heated to 65°C for 23 hours. After returning to room temperature the reaction mixture was diluted with a solution of sodium nitrite (6 eq., 3.5 g, 51 mmol) in 30 ml water and cooled with a ice bath. 2N HCl was added slowly until gas evolution ceased, and the intense red mixture was extracted three times with ethyl acetate. Pooled extracts were washed with brine, dried over Na_2SO_4 and concentrated on the rotary evaporator. Column chromatography over 90 g SiO_2 (15-50% EE in PE) afforded **12** (620 mg, 31.5% of theory) as purple crystalline solid. TLC-Rf (PE:EE =1:1) = 0.42 ^{1}H NMR (400 MHz, $CDCl_3$) δ = 2.25 (quin, *J*=7.30 Hz, 2 H) 2.41 (br. s., 1 H) 2.44 (s, 3 H) 3.46 (t, *J*=7.45 Hz, 2 H) 3.82 (t, *J*=6.14 Hz, 2 H) 7.36 (d, *J*=8.18 Hz, 2 H) 8.43 (d, *J*=8.18 Hz, 2 H) ppm ^{13}C NMR (100.61 MHz, $CDCl_3$) δ = 21.6, 30.6, 31.4, 61.6, 127.8, 128.9, 129.9, 143.2, 164.2, 169.5 ppm HR-ESI-MS: calcd. for $[M+H]^+$ $C_{12}H_{15}N_4O^+$: 231.12404, found: 231.12349.

3-(6-(4-(trifluoromethyl)phenyl)-1,2,4,5-tetrazin-3-yl)propan-1-ol (13)

A mixture of 4-trifluoromethylbenzonitrile (1 eq., 500 mg, 2.92 mmol), 4-hydroxybutanenitrile (2 eq., 497 mg, 5.84 mmol) and anhydrous $NiCl_2$ (0.15 eq., 56.8 mg, 0.44 mmol) was treated dropwise with hydrazine monohydrate (9 eq., 1.31 g, 26.2 mmol) (Caution: gas evolution, exothermic!). The purple solution was heated to 60°C for 24 hours. After returning to room temperature the reaction mixture was diluted with a solution of sodium nitrite (6 eq., 1.20 g, 17.5 mmol) and cooled with a ice bath. 2N HCl was added slowly until gas evolution ceased, and the intense purple mixture was extracted twice with ethyl acetate. Pooled extracts were washed with brine, dried over $MgSO_4$ and concentrated on the rotary evaporator. Column chromatography over 40 g SiO_2 (35% EE in PE) afforded **13** (226 mg, 27.2% of theory) as purple crystalline solid. TLC-Rf (PE:EE =3:1) = 0.09 ^{1}H NMR (400 MHz, $CDCl_3$) δ = 1.74 (br. s., 1 H) 2.30 (quin, *J*=6.72 Hz, 2 H) 3.55 (t, *J*=7.45 Hz, 2 H) 3.86 (t, *J*=5.99 Hz, 2 H) 7.86 (d, *J*=8.18 Hz, 2 H) 8.73 (d, *J*=8.18 Hz, 2 H) ppm ^{13}C NMR (100.61 MHz, $CDCl_3$) δ = 30.6, 31.7, 61.7, 123.7

(q, *J*=272.20 Hz), 126.2 (q, *J*=3.83 Hz), 128.2, 134.1 (q, *J*=32.97 Hz), 135.1, 163.3, 170.5 ppm, ^{19}F NMR (376.5 MHz, $CDCl_3$) δ = -63.1 ppm, HR-ESI-MS: calcd. for $[M-H]^-$ $C_{12}H_{10}F_3N_4O^-$: 283.08122, found: 283.08203.

3-(6-(3,4,5-trimethoxyphenyl)-1,2,4,5-tetrazin-3-yl)propan-1-ol (14)

A mixture of 3,4,5-trimethoxybenzonitrile (1 eq., 1 g, 5.18 mmol), 4-hydroxybutanenitrile (2 eq., 881 mg, 10.35 mmol) and anhydrous $NiCl_2$ (0.15 eq., 100 mg, 0.77 mmol) was treated dropwise with hydrazine monohydrate (12.2 eq., 3.15 g, 63 mmol) (Caution: gas evolution, exothermic!). The inhomogenous reaction mixture was heated to 50°C for 72 hours. After returning to room temperature the reaction mixture was diluted with a solution of sodium nitrite (6 eq., 2.15 g, 31 mmol) in 20 ml water and cooled with an ice bath. 2N HCl was added slowly until gas evolution ceased, and the intense red mixture was extracted four times with ethyl acetate. Pooled extracts were washed with brine, dried over $MgSO_4$ and concentrated on the rotary evaporator. Column chromatography over 90 g SiO_2 (30-75% EE in PE) afforded **14** (198 mg, 12.5% of theory) as pink crystalline solid. ^{1}H NMR (400 MHz, $CDCl_3$) δ = 2.22 - 2.32 (m, 2 H) 3.50 (t, *J*=7.41 Hz, 2 H) 3.85 (t, *J*=6.05 Hz, 2 H) 3.97 (s, 3 H) 4.00 (s, 6 H) 7.89 (s, 2 H) ppm ^{13}C NMR (100.61 MHz, $CDCl_3$) δ = 30.6, 31.4, 56.3, 61.0, 61.8, 105.0, 126.7, 142.0, 153.9, 163.7, 169.6 ppm HR-ESI-MS: calcd. for $[M+H]^+$ $C_{14}H_{19}F_3N_4O_4^+$: 307.1401, found: 307.1406.

3-(6-(4-(methylthio)phenyl)-1,2,4,5-tetrazin-3-yl)propan-1-ol (15)

A mixture of 4-thiomethylbenzonitrile (1 eq., 1 g, 6.7 mmol), 4-hydroxybutanenitrile (2 eq., 1.14 g, 13.4 mmol) and anhydrous $NiCl_2$ (0.15 eq., 129 mg, 1 mmol) was treated dropwise with hydrazine monohydrate (9 eq., 3 g, 60.3 mmol) (Caution: gas evolution, exothermic!). The purple solution was heated to 52°C for 18 hours. After returning to room temperature the reaction mixture was diluted with a solution of sodium nitrite (8 eq., 4 g, 54 mmol) and cooled with a ice bath. 1N HCl was added slowly until gas evolution ceased, and the intense red mixture was extracted with ethyl acetate. A insoluble white solid was removed by filtration. Pooled extracts were washed with brine, dried over $MgSO_4$ and concentrated on the rotary evaporator. Column chromatography over 40 g SiO_2 (10-25% EE in PE) afforded **15** (95.6 mg, 5.4% of theory) as red solid. TLC-Rf (PE:EE =1:1) = 0.37 ^{1}H NMR (400 MHz, $CDCl_3$) δ = 2.26 (tt, *J*=7.41, 6.24 Hz, 2 H) 2.57 (s, 3 H) 3.48 (t, *J*=7.41 Hz, 2 H) 3.83 (t, *J*=6.05 Hz, 2 H) 7.40 (dt, *J*=8.59, 2.30 Hz, 13 H) 8.48 (dt, *J*=8.59, 2.30 Hz, 13 H) ppm ^{13}C NMR (100.61 MHz, $CDCl_3$) δ = 14.8, 30.6, 31.4, 61.7, 125.9, 128.0, 145.2, 163.9, 169.5 ppm HR-ESI-MS: calcd. for $[M+H]^+$ $C_{12}H_{15}N_4OS^+$: 263.0961, found: 263.0970

3-(6-(pyridin-2-yl)-1,2,4,5-tetrazin-3-yl)propan-1-ol (16)

A mixture of 2-pyridinecarbonitrile (1 eq., 1 g, 9.6 mmol), 4-hydroxybutanenitrile (2 eq., 1.63 g, 19.21 mmol) and anhydrous $NiCl_2$ (0.15 eq., 188 mg, 1.44 mmol) was treated dropwise with hydrazine monohydrate (9 eq., 4.3 g, 86.4 mmol) (Caution: gas evolution, exothermic!). The purple solution was heated to 45°C for 16 hours. After returning to room temperature the reaction mixture was diluted with a solution of sodium nitrite (6.25 eq., 4.14 g, 60 mmol) in 40 ml water and cooled with a ice bath. 1N HCl was added slowly until gas evolution ceased, and the red solution was extracted three times with ethyl acetate. Pooled extracts were washed with brine, dried over Na_2SO_4 and concentrated on the rotary evaporator. Column chromatography over 60 g SiO_2 (75-100% EE in PE) afforded **16** (129.5 mg, 6.2% of theory) as red crystalline solid. TLC-Rf (EE) = 0.22 ^{1}H NMR (400 MHz, $CDCl_3$) δ = 2.23 - 2.32 (m, 2 H) 3.55 (t, *J*=7.41 Hz, 2 H) 3.83 (t, *J*=6.05 Hz, 2 H) 7.55 (ddd, *J*=7.71, 4.78,

1.17 Hz, 1 H) 7.97 (td, *J*=7.80, 1.95 Hz, 1 H) 8.61 - 8.65 (m, 1 H) 8.90 - 8.96 (m, 1 H) ppm,^{13}C NMR (100.61 MHz, $CDCl_3$) δ = 30.7, 31.7, 61.6, 123.9, 126.4, 137.5, 150.2, 150.8, 163.5, 170.8 ppm HR-ESI-MS: calcd. for $[M+H]^+$ $C_{10}H_{12}N_5O^+$: 218.10364, found: 218.10316.

3-(6-phenyl-1,2,4,5-tetrazin-3-yl)propyl 4-methylbenzenesulfonate (17)

A mixture of 3-(6-phenyl-1,2,4,5-tetrazin-3-yl)propan-1-ol (**11**, 1 eq., 200 mg, 0.925 mmol) and tosyl chloride (2 eq., 353 mg 1.85 mmol) in 5 ml dry dichloromethane was cooled to 0°C and treated dropwise with anhydrous pyridine (2 eq., 146 mg, 1.85 mmol). The mixture was stirred for 24h at room temperature and diluted with 30 ml DCM. The organic layer was separated and washed with cold 1N HCl followed by cold half concentrated $NaHCO_3$ solution. Drying over Na_2SO_4, removal of solvent and column chromatography over 40 g SiO_2 eluting with 3-20% ethyl acetate in petrol ether afforded 250.4 mg **17** as purple crystalline solid (73% of theory). TLC-Rf (PE:EE =1:1) = 0.91, ^{1}H NMR (400 MHz, $CDCl_3$) δ = 2.36 - 2.44 (m, 5 H) 3.44 (t, *J*=7.41 Hz, 2 H) 4.25 (t, *J*=6.05 Hz, 2 H) 7.30 (d, *J*=8.20 Hz, 2 H) 7.57 - 7.68 (m, 3 H) 7.74 - 7.80 (m, 2 H) 8.56 - 8.60 (m, 2 H) ppm ^{13}C NMR (100.61 MHz, $CDCl_3$) δ = 21.6, 26.6, 30.7, 68.9, 127.9, 128.0, 129.3, 129.8, 131.6, 132.7, 132.8, 144.9, 164.3, 168.6 ppm

3-(6-(p-tolyl)-1,2,4,5-tetrazin-3-yl)propyl 4-methylbenzenesulfonate (18)

A mixture of 3-(6-(p-tolyl)-1,2,4,5-tetrazin-3-yl)propan-1-ol (**12**, 1 eq., 330 mg, 1.43 mmol) and tosyl chloride (2.5 eq., 681 mg 3.6 mmol) in 8 ml dry dichloromethane was cooled to 0°C and treated dropwise with anhydrous pyridine (3 eq., 350 µl, 4.3mmol). The mixture was stirred overnight at room temperature until TLC indicated consumption of starting material. The reaction mixture was diluted with 50 ml DCM, washed once with ice cold 1N HCl followed by half concentrated cold $NaHCO_3$ solution and brine. Drying over $MgSO_4$, removal of solvent and column chromatography over 40g SiO_2 eluting with 0-30% ethyl acetate in petrol ether afforded 430 mg **18** as red crystalline solid (78% of theory). TLC-Rf (PE:EE =3:1) = 0.62 ^{1}H NMR (400 MHz, $CDCl_3$) δ = 2.35 - 2.43 (m, 5 H) 2.48 (s, 3 H) 3.41 (t, *J*=7.45 Hz, 2 H) 4.24 (t, *J*=6.14 Hz, 2 H) 7.30 (d, *J*=8.18 Hz, 2 H) 7.40 (d, *J*=8.18 Hz, 2 H) 7.77 (d, *J*=8.18 Hz, 2 H) 8.46 (d, *J*=8.18 Hz, 2 H) ppm^{13}C NMR (100.61 MHz, $CDCl_3$) δ = 21.6, 21.7, 26.6, 30.7, 69.0, 127.8, 127.9, 128.8, 129.8, 130.0, 143.4, 144.9, 164.3, 168.3 ppm HR-ESI-MS: calcd. for $[M+H]^+$ $C_{19}H_{21}N_4O_3S^+$: 385.13289, found: 385.13181.

3-(6-(4-(trifluoromethyl)phenyl)-1,2,4,5-tetrazin-3-yl)propyl 4-methylbenzenesulfonate (19)

A mixture of 3-(6-(4-(trifluoromethyl)phenyl)-1,2,4,5-tetrazin-3-yl)propan-1-ol (**13**, 1 eq., 100 mg, 0.352 mmol) and tosyl chloride (2 eq., 134.2 mg 0.71 mmol) in 5 ml dry dichloromethane was cooled to 3°C and treated dropwise with anhydrous pyridine (2 eq., 55.6 mg, 0.71 mmol). The mixture was stirred for 168h at 3°C and poured onto a mixture of 0.5N HCl and ice. The organic layer was separated and washed with half concentrated cold $NaHCO_3$ solution and brine. Drying over $MgSO_4$, removal of solvent and column chromatography over SiO_2 eluting with 0-20% ethyl acetate in petrol ether afforded 124.8 mg **19** as purple crystalline solid (81% of theory). TLC-Rf (PE:EE =3:1) = 0.55, ^{1}H NMR (400 MHz, $CDCl_3$) δ = 2.37 - 2.47 (m, 5 H) 3.49 (t, *J*=7.45 Hz, 2 H) 4.26 (t, *J*=5.99 Hz, 2 H) 7.31 (d, *J*=7.89 Hz, 2 H) 7.77 (d, *J*=8.18 Hz, 2 H) 7.87 (d, *J*=8.18 Hz, 2 H) 8.71 (d, *J*=8.18 Hz, 2 H) ppm ^{13}C NMR (100.61 MHz, $CDCl_3$) δ = 21.6, 26.6, 31.0, 68.9, 123.7 (q, *J*=272.2Hz), 126.2 (q, *J*=3.1Hz), 127.9, 128.3, 129.9, 132.7, 134.2 (q, *J*=32.97Hz), 135.0, 144.9, 163.4, 169.3 ppm

3-(6-(3,4,5-trimethoxyphenyl)-1,2,4,5-tetrazin-3-yl)propyl 4-methylbenzenesulfonate (20)

A mixture of 3-(6-(3,4,5-trimethoxyphenyl)-1,2,4,5-tetrazin-3-yl)propan-1-ol (**14**, 1 eq., 100 mg, 0.326 mmol) and tosyl chloride (2 eq., 124 mg 0.653 mmol) in 2 ml dry dichloromethane was cooled to 0°C and treated dropwise with anhydrous pyridine (2 eq., 51 mg, 0.653 mmol). The mixture was stirred for 24h at room temperature and diluted with 20 ml DCM. The organic layer was separated and washed with cold 1N HCl followed by cold half-concentrated $NaHCO_3$ solution. Drying over Na_2SO_4, removal of solvent and column chromatography over 40 g SiO_2 eluting with 10-50% ethyl acetate in petrol ether afforded 142.2 mg **20** as red crystalline solid (95% of theory). TLC-Rf (PE:EE =1:1) = 0.65, ^{1}H NMR (400 MHz, $CDCl_3$) δ = 2.36 - 2.44 (m, 5 H) 3.43 (t, *J*=7.41 Hz, 2 H) 3.98 (s, 3 H) 3.99 - 4.03 (m, 6 H) 4.26 (t, *J*=6.05 Hz, 2 H) 7.32 (d, *J*=7.80 Hz, 2 H) 7.75 - 7.80 (m, 2 H) 7.87 (s, 2 H) ppm ^{13}C NMR (100.61 MHz, $CDCl_3$) δ = 21.6, 26.6, 30.7, 56.4, 61.0, 69.0, 105.1, 126.5, 127.9, 129.9, 132.8, 142.2, 144.9, 153.9, 163.8, 168.3 ppm HR-ESI-MS: calcd. for $[M+H]^+$ $C_{21}H_{25}N_4O_6S^+$: 461.1489, found: 461.1504

3-(6-(4-(methylthio)phenyl)-1,2,4,5-tetrazin-3-yl)propyl 4-methylbenzenesulfonate (21)

A mixture of 3-(6-(4-(methylthio)phenyl)-1,2,4,5-tetrazin-3-yl)propan-1-ol (**15**, 1 eq., 54 mg, 0.205 mmol) and tosyl chloride (4 eq., 156 mg 0.82 mmol) in 3 ml dry dichloromethane was cooled to 0°C and treated dropwise with anhydrous pyridine (4 eq., 65 mg, 0.82 mmol). The mixture was stirred overnight at 0°C and for 3 hours at room temperature. The reaction mixture was diluted with 20 ml DCM, washed once with ice cold 1N HCl followed by half concentrated cold $NaHCO_3$ solution and brine. Drying over $MgSO_4$, removal of solvent and column chromatography over SiO_2 eluting with 0-50% ethyl acetate in petrol ether afforded 57 mg **21** as red crystalline solid (66.7% of theory). TLC-Rf (PE:EE =1:1) = 0.75, ^{1}H NMR (400 MHz, $CDCl_3$) δ = 2.35 - 2.43 (m, 5 H) 2.58 (s, 3 H) 3.41 (t, *J*=7.41 Hz, 2 H) 4.25 (t, *J*=6.05 Hz, 2 H) 7.31 (d, *J*=7.81 Hz, 2 H) 7.42 (dt, *J*=8.59, 2.30 Hz, 2 H) 7.78 (dt, *J*=8.20, 2.00 Hz, 2 H) 8.49 (dt, *J*=8.98, 2.00 Hz, 2 H) ppm ^{13}C NMR (100.61 MHz, $CDCl_3$) δ = 14.9, 21.6, 26.6, 30.7, 69.0, 125.9, 127.7, 127.9, 128.1, 129.9, 132.8, 144.9, 145.5, 164.1, 168.3 ppm

3-(6-(pyridin-2-yl)-1,2,4,5-tetrazin-3-yl)propyl 4-methylbenzenesulfonate (22)

To a cooled (0°C) solution of 3-(6-(pyridin-2-yl)-1,2,4,5-tetrazin-3-yl)propan-1-ol (**16**, 1 eq., 64 mg, 0.29 mmol) and anhydrous pyridine (2 eq., 47 mg, 0.6 mmol) in 3 ml dry dichloromethane was added tosyl chloride (2 eq., 115 mg 0.60 mmol) in one portion. The reaction was stirred at 0°C until TLC indicated consumption of starting materials (3 days). The solution was poured onto a 40 ml ice cold 1% HCl. The organic layer was separated and the aqueous layer was extracted three times with DCM. Pooled extracts were washed with half concentrated cold $NaHCO_3$ solution and dried over Na_2SO_4. Removal of solvent and column chromatography over SiO_2 (8 g) eluting with 50-70% ethyl acetate in petrol ether afforded 72 mg **22** as pink crystalline solid (66.8% of theory). TLC-Rf (EE) = 0.75, ^{1}H NMR (400 MHz, $CDCl_3$) δ = 2.35 - 2.45 (m, 5 H) 3.48 (t, *J*=7.32 Hz, 2 H) 4.23 (t, *J*=6.04 Hz, 2 H) 7.30 (d, *J*=8.05 Hz, 2 H) 7.56 (dd, *J*=7.50, 4.94 Hz, 1 H) 7.76 (d, *J*=8.05 Hz, 2 H) 7.98 (t, *J*=7.50 Hz, 1 H) 8.61 (d, *J*=8.05 Hz, 1 H) 8.94 (d, *J*=4.76 Hz, 1 H) ppm ^{13}C NMR (100.61 MHz, $CDCl_3$) δ = 21.5, 26.6, 30.9, 68.9, 123.9, 126.4, 127.8, 129.8, 132.7, 137.4, 144.9, 150.1, 150.8, 163.7, 169.5 ppm, HR-ESI-MS: calcd. for $[M+H]^+$ $C_{17}H_{18}N_5O_3S^+$: 372.11249, found: 372.11156.

3-(6-(4-(methylsulfonyl)phenyl)-1,2,4,5-tetrazin-3-yl)propan-1-ol (23)

3-(6-(4-(methylthio)phenyl)-1,2,4,5-tetrazin-3-yl)propan-1-ol (**15**, 1 eq., 40 mg, 0.15 mmol) was treated with a ice cold solution of dimethyl dioxirane (DMDO) in 25 ml acetone (~40 mM). The pink reaction mixture was allowed to reach room temperature and stirred for additional 30 minutes. Volatiles were removed on the rotary evaporator and **25** was obtained in 75% yield following purification by column chromatography over 8 g SiO_2 (0-15% MeOH in DCM).^{1}H NMR (600 MHz, DMSO-d_6) δ = 2.06 - 2.13 (m, 2 H) 3.39 (t, *J*=7.60 Hz, 2 H) 3.55 - 3.60 (m, 2 H) 4.63 (t, *J*=5.14 Hz, 1 H) 8.22 (dt, *J*=8.51, 1.80 Hz, 2 H) 8.72 (dt, *J*=8.80, 2.10 Hz, 2 H) ppm ^{13}C NMR (150.91 MHz, DMSO-d_6) δ = 30.6, 31.3, 43.3, 60.0, 128.0, 128.4, 136.6, 143.8, 162.6, 170.3 ppm, HR-ESI-MS: calcd. for $[M+H]^+$ $C_{12}H_{15}N_4O_3S^+$: 295.0859, found: 295.0873

3-(6-(4-(methylsulfonyl)phenyl)-1,2,4,5-tetrazin-3-yl)propyl 4-methylbenzenesulfonate (24)

A mixture of 3-(6-(4-(methylsulfonyl)phenyl)-1,2,4,5-tetrazin-3-yl)propan-1-ol (**23**, 1 eq., 26.6 mg, 90 µmol) and tosyl chloride (4 eq., 69 mg, 0.36 mmol) in 4 ml dry dichloromethane was cooled to 0°C and treated with anhydrous pyridine (5 eq., 50 µl, 0.45 mmol). The mixture was stirred at 4°C until TLC indicated consumption of starting material. The reaction mixture was diluted with 20 ml DCM. The organic layer was separated and washed with cold 1N HCl followed by cold half-concentrated $NaHCO_3$ solution. Drying over Na_2SO_4, removal of solvent and column chromatography over 40 g SiO_2 eluting with 0-3% MeOH in DCM afforded 32 mg **24** as pink crystalline solid (79% of theory). ^{1}H NMR (600 MHz, $CDCl_3$) δ = 2.39 - 2.46 (m, 5 H) 3.15 (s, 3 H) 3.51 (t, *J*=7.48 Hz, 2 H) 4.26 (t, *J*=5.90 Hz, 2 H) 7.33 (d, *J*=7.92 Hz, 2 H) 7.77 (dt, *J*=8.51, 2.10 Hz, 2 H) 8.19 (dt, *J*=8.51, 1.80 Hz, 2 H) 8.81 (dt, *J*=8.80, 1.80 Hz, 2 H) ppm ^{13}C NMR (150.91 MHz, $CDCl_3$) δ = 21.6, 26.7, 31.1, 44.4, 68.9, 127.9, 128.3, 128.8, 129.9, 132.7, 136.6, 144.0, 145.0, 163.2, 169.5

3-(6-(p-tolyl)-1,2,4,5-tetrazin-3-yl)propyl 4-nitrobenzenesulfonate (25)

A mixture of 3-(6-(p-tolyl)-1,2,4,5-tetrazin-3-yl)propan-1-ol (**12**, 1 eq., 70 mg, 0.30 mmol) and nosyl chloride (2.07 eq., 140 mg 0.63 mmol) in 4 ml dry dichloromethane was cooled to 0°C and treated dropwise with anhydrous pyridine (2.07 eq., 50 mg, 0.63 mmol). The mixture was stirred for 48 hours at 0°C (conducting the reaction at room temperature causes elimination and sharply reduced yield). The reaction mixture was diluted with 100 ml DCM, washed once with ice cold 1N HCl followed by half concentrated cold $NaHCO_3$ solution and brine. Drying over $MgSO_4$, removal of solvent and column chromatography over 40g SiO_2 eluting with 0-20% ethyl acetate in petrol ether afforded 90.9 mg **25** as red crystalline solid (72% of theory). TLC-Rf (PE:EE =1:1) = 0.95 ^{1}H NMR (400 MHz, $CDCl_3$) δ = 2.40 - 2.51 (m, 5 H) 3.45 (t, *J*=7.16 Hz, 2 H) 4.36 (t, *J*=5.99 Hz, 2 H) 7.40 (d, *J*=7.89 Hz, 2 H) 8.10 (d, *J*=8.77 Hz, 2 H) 8.38 (d, *J*=8.77 Hz, 2 H) 8.44 (d, *J*=8.19 Hz, 2 H) ppm ^{13}C NMR (100.61 MHz, $CDCl_3$) δ = 21.7, 26.8, 30.7, 70.0, 124.5, 127.9, 129.2, 130.1, 141.5, 143.7, 150.8, 164.4, 168.2 ppm HR-ESI-MS: calcd. for $[M+H]^+$ $C_{18}H_{18}N_5O_5S^+$: 416.1023, found: 416.1040.

Radiolabeling

General procedure for manual radiolabeling

A QMA light cartridge (Waters) was preconditioned with 0.5M K_2CO_3 solution (7 ml) followed by 15 ml water. Cyclotron produced ^{18}F-fluoride in water (0.5-2.5 ml) was passed over the cartridge, and the cartridge was eluted with a solution 0.075M tetrabutylammonium hydrogen carbonate solution, followed by 1 ml of acetonitrile. Volatiles were removed in a stream of argon at 105°C and residual water was removed by addition and subsequent evaporation of 700 µl anhydrous acetonitrile. The azeotropic drying step was repeated two more times. Precursor was added in the labelling solvent, and the reaction mixture was heated to the indicated temperature for the indicated time span. After cooling of the reaction contents incorporation yield was investigated by radio-HPLC and/or radio-TLC. In several cases the fluorine-18 tetrazine derivatives were additionally isolated using preparative HPLC.

[^{18}F]1: 328 MBq ^{18}F fluoride, 430 µl TBA-HCO_3-Lsg (32.25 µmol), 10 mg (32.4 µmol) 3-(6-methyl-1,2,4,5-tetrazin-3-yl)propyl 4-methylbenzenesulfonate in 400 µl thexyl alcohol/anhydrous acetonitrile v/v = 1:1, 4.5 min; 95°C: incorporation yield (HPLC) = 46.5%, incorporation yield (TLC) = 48.3%, isolated yield (decay corrected) = 33.4%

[^{18}F]2: 356 MBq ^{18}F fluoride, 250 µl TBA-HCO_3-Lsg (18.75 µmol), 6.7 mg (18.1 µmol) **17** in 400 µl thexyl alcohol/anhydrous acetonitrile v/v = 1:1, 5 min; 95°C: incorporation yield (HPLC) = 40%, incorporation yield (TLC) = 40.5%

[^{18}F]3: 363 MBq ^{18}F fluoride, 500 µl TBA-HCO_3-Lsg (37.5 µmol), 12.7 mg (33.0 µmol) **18** in 500 µl thexyl alcohol/anhydrous acetonitrile v/v = 1:1, 5 min, 107°C: incorporation yield (HPLC) = 56.2%, isolated yield (decay corrected) = 41.7%

[^{18}F]5: 355 MBq ^{18}F fluoride, 250 µl TBA-HCO_3-Lsg (18.75 µmol), 9.0 mg (19.5 µmol) **20** in 400 µl thexyl alcohol/anhydrous acetonitrile v/v = 1:1, 5 min; 95°C: incorporation yield (HPLC) = 13.7%, incorporation yield (TLC) = 18%

[^{18}F]6: 481.7 MBq ^{18}F fluoride, 166 µl TBA-HCO_3-Lsg (12.5 µmol), 5.2 mg (12.5 µmol) **21** in 400 µl thexyl alcohol/anhydrous acetonitrile v/v = 1:1, 8 min; 97°C: incorporation yield (HPLC) = 47.7%

^{18}F-species prepared by manual labeling matched HPLC retention times with authentic standards (see supporting information)

General procedure for automated radiolabeling

A remote controlled synthesis module (TRACERlab™ FXFDG, General Electric Healthcare, Uppsala, Sweden) with 3 mL glass reactor housed in a hot cell was used for automated labeling experiments. In general cyclotron produced no carrier added [^{18}F] fluoride was trapped on a preconditioned (5 ml 0.5 M K_2CO_3 followed by 15 ml water) Waters QMA light cartridge. The radioactivity was eluted with 500 µl 0.075M TBA-HCO_3 solution followed by 1 ml acetonitrile. Volatiles were removed in vacuo at a

temperature of 60-120 °C. After cooling to 50 °C a solution of precursor in a mixture of dry acetonitrile and thexyl alcohol was added. The reaction mixture was heated to 93°C for 8 minutes followed by cooling to 45°C and consequent transfer into a vial. The reactor was rinsed with 2 ml DMSO:water = 1:1 (v/v). Combined solutions were injected into a preparative HPLC column (Macherey-Nagel EP 250/16 100-7 C-18, 10 µm, 16 x 250 mm) and eluted using a gradient of phosphate puffer (10 mM pH = 6) and acetonitrile at a flow rate of 5 ml/min (0-6 min 10% acetonitrile, 6.01 min 30% acetonitrile, 6.01→40 min 30%→80% acetonitrile) The product fraction was diluted with 50 ml water, prior to passage over a preconditioned (5 ml acetonitrile followed by 15 ml H_2O) tc18 plus SepPak cartridge (Waters). The cartridge was eluted with 1.5 ml ethanol, and the ethanolic solution was diluted with saline to < 10% EtOH for in vivo experiments. The products were further diluted with physiological saline to a activity concentration of ~370 MBq/ml for iv administration. pH was between 5 and 7 for all formulations and osmolarity was within physiological range (300-500 mmol/kg). ^{18}F-species prepared by automated labeling matched HPLC retention times with authentic standards.

[^{18}F]**2:** 246.4 GBq ^{18}F fluoride, 12.2 mg (33 µmol) **17** in a mixture of 200 µl thexyl alcohol and 300 µl anhydrous acetonitrile yielded 8.88 GBq [^{18}F]**2** (6.3% decay corrected), retention time on preparative HPLC: 29.0 min, radiochemical purity (analytical HPLC) = 95%. Specific activity (HPLC) = 99 GBq/µmol (see ESI for determination of SA).

[^{18}F]**3:** 181.3 GBq ^{18}F fluoride, 12.0 mg (31.2 µmol) **18** in a mixture of 300 µl thexyl alcohol and 300 µl anhydrous acetonitrile yielded 9.99 GBq [^{18}F]**3** (9.5% decay corrected), radiochemical purity (analytical HPLC) = 98.3%

[^{18}F]**5:** 233.2 GBq ^{18}F fluoride, 11.7 mg (25.4 µmol) **20** in a mixture of 200 µl thexyl alcohol and 300 µl anhydrous acetonitrile yielded 6.98 GBq [^{18}F]**5** (4.9% decay corrected), retention time on preparative HPLC: 28.1 min, radiochemical purity (analytical HPLC) = 94.4%

[^{18}F]**6:** 218.3 GBq ^{18}F fluoride, 11.0 mg (26.4 µmol) **21** in a mixture of 200 µl thexyl alcohol and 300 µl anhydrous acetonitrile yielded 11.5 GBq [^{18}F]**6** (8.6% decay corrected), retention time on preparative HPLC: 32.6 min, radiochemical purity (analytical HPLC) = 95.4% Specific activity (HPLC) = 229.5 GBq/µmol (see ESI for determination of SA).

Preparation of [^{18}F]7

5.3 GBq [^{18}F]**6** in 1.5 ml EtOH as obtained by automated labelling was evaporated to dryness on the rotary evaporator (40°C, 20 mbar) in a 8 ml vial. The residue was treated with 0.5 ml of an ice cold solution of dimethyldioxirane (DMDO) in acetone (~40 mM). After 60 seconds reaction time volatiles were removed on the rotary evaporator. The residue was re-dissolved in 2.5 ml DMSO:water = 1:1 (v/v) and injected into the preparative HPLC system described at the section automated labelling. 2.36 GBq [^{18}F]**7** (56% decay corrected yield) eluted with a retention time of 23.1 min. The product containing fraction was evaporated to dryness on the rotary evaporator and formulated in 0.9% saline to obtain a product ready for iv administration. Radiochemical purity (analytical HPLC) =

93.0%, specific activity (HPLC) = 56.2 GBq/µmol (see ESI for determination of SA). HPLC retention time of [^{18}F]**7** matched with the retention time of authentic standard.

PET/MR Imaging – Biodistribution study

Mice underwent PET scanning on a dual animal bed in a dedicated small-animal PET scanner (n=2 for [^{18}F]**2**, [^{18}F]**3**, [^{18}F]**5,** [^{18}F]**6** and [^{18}F]**7** and one mouse per test substance (except [^{18}F]**7)** underwent sequential PET/MRI on two stand-alone scanners. Prior imaging, mice were pre-anesthetized in an induction chamber using isoflurane (2.5% in oxygen), placed in prone position on a heated animal bed (38°C) and the lateral tail vein was cannulated using a custom made tail vein catheter. Animal respiratory rate and body temperature were constantly monitored (SA Instruments Inc, Stony Brook, NY, USA) and the isoflurane level was adjusted (1.5-2.5% on oxygen) to achieve a constant depth of anesthesia. Anesthesia was maintained for the whole imaging period. A humidifier was used to moisten the gas mixture before supplying it to the animal(s). For anatomical magnetic resonance imaging (MRI) a single mouse body bed mounted with a mouse whole body RF coil was used. The whole body coil covers an axial field of view (FOV) of about 8 cm that is very similar to the axial FOV of the PET scanner (7.6 cm). Images were acquired on a 1 Tesla benchtop MRI (ICON, Bruker Biospin GmbH, Ettlingen, Germany) using a modified 3D T_1-weighted gradient echo sequence (T1-FLASH) with the following imaging parameters: echo time (TE) = 4.7 ms; repetition time (TR) = 25 ms; flip angle (FA) = 25 °; field of view (FOV) = 7.6 x 2.6 x 2.4 cm; matrix = 253 x 93; 32 slices; slice thickness = 750 µm; 5 repetitions; total imaging time = 6 min 15 sec. After MRI, the animal bed was transferred into the gantry of a microPET scanner (Focus 220, Siemens Medical Solutions, Knoxville, TN, USA). Total anesthesia time prior start of PET scanning for mice that underwent PET scanning only was similar to that of the PET/MRI examined animals. Direct after positioning of the animal bed in the gantry of the PET scanner a 10 min transmission scan using a rotating ^{57}Co point source was recorded. Simultaneously with intravenous injection of 6.8 ± 3.4 MBq [^{18}F]-**2**, 4.2 ± 1.9 MBq [^{18}F]-**3**, 10.8 ± 0.3 MBq [^{18}F]-**5,** 13.1 ± 8.6 MBq [^{18}F]-**6** or 34.2 ± 7.0 MBq [^{18}F]-**7** dynamic PET imaging was initiated for 120 min using an energy window of 250-750 keV and a timing window of 6 ns. After completion of the imaging procedure, a terminal blood sample was withdrawn under isoflurane anesthesia from the retro-orbital sinus vein and the animals were sacrificed by cervical dislocation. Blood was centrifuged (17000 *g*, 4°C, 4 min) to obtain plasma, and organ samples as well as urine were collected. Aliquots of blood, plasma and urine as well as organ samples were transferred into pre-weighted tubes and measured for radioactivity in a gamma counter (Wizard 1470, Perkin-Elmer, Wellesley, MA, USA). The measured radioactivity data were corrected for radioactive decay and expressed as standardized uptake value ((radioactivity per g/injected radioactivity) x body weight). The 60 min dynamic emission PET data were sorted into 26 frames, which incrementally increased in time length from 5 seconds to 10 min. Images were reconstructed using Fourier rebinning of the 3D sinograms followed by two-dimensional filtered back projection with a ramp filter, resulting in an image voxel size of 0.4 x 0.4 x 0.796 mm^3. A standard data correction protocol (normalization, attenuation and decay correction) was applied to the PET data. The PET units were converted into units of radioactivity concentration by applying a calibration factor derived from imaging of a cylindrical phantom with a known ^{18}F-radioactivity concentration. Corresponding PET/MRI images were aligned using a pre-calculated, fixed transformation matrix. Using the image analysis software Amide, different volumes of interest (brain, liver, kidneys, urinary bladder, heart, bone (left humerus), muscle (right forearm muscle)), lung, stomach were manually outlined on multiple planes

and time-radioactivity concentration curves (TACs), expressed in standardized uptake values, were derived.

Analysis of murine metabolites

Blood and urine samples harvested directly after imaging experiments (120 min post administration) were used for metabolity studies. Murine plasma was obtained by centrifugation(17000 *g*, 4°C, 4 min), and plasma proteins were precipitated by addition of a equal volume acetonitrile and centrifuged (17000 *g*, 4°C, 1 min). Urine was also diluted with acetonitrile (1:10 v/v) and briefly centrifuged. Supernatant solutions were spotted on silica TLC plates, and eluted using an appropriate solvent mixture (0-5% MeOH in DCM). For Details of used mobile phase and developed TLC plates see section 1 of the supporting information. The diluted test substances were spotted as reference materials. Three mice dosed with [^{18}F]**7** were sacrificed 60 min post tracer administration. Aliquots of blood, plasma and urine as well as organ samples were transferred into pre-weighted tubes and measured for radioactivity in a gamma counter (Wizard 1470, Perkin-Elmer, Wellesley, MA, USA). The measured radioactivity data were corrected for radioactive decay and expressed as standardized uptake value ((radioactivity per g/injected radioactivity) x body weight). Plasma and urine was prepared for TLC analysis as described above. The brain was homogenized with 300 µL acetonitrile using a IKA T10 basic Ultra-turrax (IKA Laboratory Equipment, Staufen, Germany). The same procedure was applied to the liver using 1500 µL acetonitrile. Bile was diluted 1: 10 (v/v) with acetonitrile. All samples were briefly centrifuged and the supernatants were spotted on silica TLC plates that were eluted with 5% MeOH in DCM. Radioactivity distribution on TLC plates was visualized using the procedure described in the materials and methods section.

References

(1) Denk, C., Svatunek, D., Filip, T., Wanek, T., Lumpi, D., Fröhlich, J., Kuntner, C., and Mikula, H. (2014) Development of a (18) F-Labeled Tetrazine with Favorable Pharmacokinetics for Bioorthogonal PET Imaging. *Angew. Chem. Int. Ed. Engl.* 1–6.

(2) Knight, J. C., and Cornelissen, B. (2014) Bioorthogonal chemistry: implications for pretargeted nuclear (PET/SPECT) imaging and therapy. *Am. J. Nucl. Med. Mol. Imaging 4*, 96–113.

(3) Patterson, D. M., Nazarova, L. A., and Prescher, J. A. (2014) Finding the right (bioorthogonal) chemistry. *ACS Chem. Biol. 9*, 592–605.

(4) Meyer, J. P., Houghton, J. L., Kozlowski, P., Abdel-Atti, D., Reiner, T., Pillarsetty, N. V. K., Scholz, W. W., Zeglis, B. M., and Lewis, J. S. (2016) 18F-Based Pretargeted PET Imaging Based on Bioorthogonal Diels-Alder Click Chemistry. *Bioconjug. Chem. 27*, 298–301.

(5) Zeglis, B. M., Sevak, K. K., Reiner, T., Mohindra, P., Carlin, S. D., Zanzonico, P., Weissleder, R., and Lewis, J. S. (2013) A Pretargeted PET Imaging Strategy Based on Bioorthogonal Diels – Alder Click Chemistry. *J. Nucl. Med.* 1389–1396.

(6) Rossin, R., and Robillard, M. S. (2014) Pretargeted imaging using bioorthogonal chemistry in mice. *Curr. Opin. Chem. Biol. 21*, 161–169.

(7) Rossin, R., Verkerk, P. R., Van Den Bosch, S. M., Vulders, R. C. M., Verel, I., Lub, J., and Robillard, M. S. (2010) In vivo chemistry for pretargeted tumor imaging in live mice. *Angew. Chemie - Int. Ed. 49*, 3375–3378.

(8) Darko, A., Wallace, S., Dmitrenko, O., Machovina, M. M., Mehl, R. A., Chin, J. W., and Fox, J. M. (2014) Conformationally Strained trans-Cyclooctene with Improved Stability and Excellent Reactivity in Tetrazine Ligation. *Chem. Sci. 5*, 3770–3776.

(9) Blackman, M. L., Royzen, M., and Fox, J. M. (2008) Tetrazine Ligation: Fast Bioconjugation Based on Inverse-Electron-Demand Diels−Alder Reactivity. *J. Am. Chem. Soc. 130*, 13518–13519.

(10) Devaraj, N. K., Weissleder, R., and Hilderbrand, S. a. (2008) Tetrazine-Based Cycloadditions : Application to Pretargeted Live Cell Imaging Tetrazine-Based Cycloadditions : Application to Pretargeted Live Cell Imaging. *Communications 19*, 2297–2299.

(11) Yang, J., Šečkute, J., Cole, C. M., and Devaraj, N. K. (2012) Live-cell imaging of cyclopropene tags with fluorogenic tetrazine cycloadditions. *Angew. Chemie - Int. Ed.*

(12) Royzen, M., Yap, G. P. A., and Fox, J. M. A Photochemical Approach to Functionalized trans - Cyclooctenes Driven by Metal Complexation 1–30.

(13) Taylor, M. T., Blackman, M. L., Dmitrenko, O., Fox, J. M., and Ligation, T. (2011) Design and Synthesis of Highly Reactive Dienophiles for the. *J. Am. Chem. Soc. 133*, 9646–9649.

(14) Yang, J., Karver, M. R., Li, W., Sahu, S., and Devaraj, N. K. (2012) Metal-catalyzed one-pot synthesis of tetrazines directly from aliphatic nitriles and hydrazine. *Angew. Chemie - Int. Ed. 51*, 5222–5225.

(15) Hu, W.-X., and Xu, F. (2008) Synthesis, structures of some unsymmetrical 3,6-disubstituted-1,2,4,5-tetrazines. *J. Heterocycl. Chem. 45*, 1745–1750.

(16) Wyffels, L., Thomae, D., Waldron, A. M., Fissers, J., Dedeurwaerdere, S., Van der Veken, P., Joossens, J., Stroobants, S., Augustyns, K., and Staelens, S. (2014) In vivo evaluation of 18F-labeled

TCO for pre-targeted PET imaging in the brain. *Nucl. Med. Biol. 41*, 513–523.

(17) Li, Z., Cai, H., Hassink, M., Blackman, M. L., Brown, R. C. D., Conti, P. S., and Fox, J. M. (2010) Tetrazine-trans-cyclooctene ligation for the rapid construction of 18F labeled probes. *Chem. Commun. (Camb). 46*, 8043–5.

(18) Kumar, A., Hao, G., Liu, L., Ramezani, S., Hsieh, J. T., Öz, O. K., and Sun, X. (2015) Click-chemistry strategy for labeling antibodies with copper-64 via a cross-bridged tetraazamacrocyclic chelator scaffold. *Bioconjug. Chem. 26*, 782–789.

(19) Herth, M. M., Andersen, V. L., Lehel, S., Madsen, J., Knudsen, G. M., Kristensen, J. L., and Herth, M. M. (2013) Development of a (11)C-labeled tetrazine for rapid tetrazine-trans-cyclooctene ligation. *Chem. Commun. (Camb). 49*, 3805–7.

(20) Keinänen, O., Li, X. G., Chenna, N. K., Lumen, D., Ott, J., Molthoff, C. F. M., Sarparanta, M., Helariutta, K., Vuorinen, T., Windhorst, A. D., and Airaksinen, A. J. (2016) A New Highly Reactive and Low Lipophilicity Fluorine-18 Labeled Tetrazine Derivative for Pretargeted PET Imaging. *ACS Med. Chem. Lett. 7*, 62–66.

(21) Rashidian, M., Keliher, E. J., Dougan, M., Juras, P. K., Cavallari, M., Wojtkiewicz, G. R., Jacobsen, J. T., Edens, J. G., Tas, J. M. J., Victora, G., Weissleder, R., and Ploegh, H. L. (2015) Use of 18F-2-Fluorodeoxyglucose to Label Antibody Fragments for Immuno-Positron Emission Tomography of Pancreatic Cancer. *ACS Cent. Sci.* 150603073029009.

(22) Cott, W. J., Howell, C., and White, W. (1948) Toxic Fluorine Compounds. V. w-Fluoronitriles and w-Fluoro-w ’-nitroalkanes *3604*, 3484–3487.

(23) HOFFMANN, F. W. (1949) ALIPHATIC FLUORIDES. I. ι,ι’-DIFLUOROALKANES. *J. Org. Chem. 14*, 105–110.

(24) Hanson, P., Hendrickx, R. a a J., and Lindsay Smith, J. R. (2008) Kinetic studies on the oxidation of aryl methyl sulfides and sulfoxides by dimethyldioxirane; absolute rate constants and activation parameters for 4-nitrophenyl methyl sulfide and sulfoxide. *Org. Biomol. Chem. 6*, 762–71.

(25) Lee, S. J., Oh, S. J., Chi, D. Y., Lee, B. S., Ryu, J. S., and Moon, D. H. (2008) Comparison of synthesis yields of 3’-deoxy-3’-[18F]fluorothymidine by nucleophilic fluorination in various alcohol solvents. *J. Label. Compd. Radiopharm. 51*, 80–82.

(26) Kim, D. W., Jeong, H. J., Lim, S. T., and Sohn, M. H. (2010) Recent trends in the nucleophilic [18F]-radiolabeling method with no-carrier-added [18F]fluoride. *Nucl. Med. Mol. Imaging (2010). 44*, 25–32.

(27) Williams, K. I. H., Burstein, S. H., and Layne, D. S. (1966) Metabolism of dimethyl sulfide, dimethyl sulfoxide, and dimethyl sulfone in the rabbit. *Arch. Biochem. Biophys. 117*, 84–87.

(28) (2009) So long sulphur. *Nat. Chem. 1*, 333–333.

(29) Angus, P. W., Mihaly, G. W., Morgan, D. J., and Smallwood, R. A. (1989) Oxygen dependence of omeprazole clearance and sulfone and sulfide metabolite formation in the isolated perfused rat liver. *J. Pharmacol. Exp. Ther. 250*, 1043–7.

(30) Mikula, H., Svatunek, D., Lumpi, D., Glöcklhofer, F., Hametner, C., and Fröhlich, J. (2013) Practical and Efficient Large-Scale Preparation of Dimethyldioxirane. *Org. Process Res. Dev. 17*, 313–316.

(31) Royzen, M., Yap, G. P. A., and Fox, J. M. (2008) A photochemical synthesis of functionalized trans-cyclooctenes driven by metal complexation. *J. Am. Chem. Soc. 130*, 3760–3761.

(32) Nachbaur, E., and Leiseder, G. (1971) Ueber eine einfache und gefahrlose Methode zur Darstellung von wasserfreiem Hydrazin. *Monatshefte fuer Chemie 102*, 1718–1723.

Manuscript #4

Reprinted from *Monatshefte für Chemie – Chemical Monthly* (2016), 147, 579-585

(open access)

Svatunek, D.; **Denk, C**.; Rosecker, V.; Sohr, B.; Hametner, C.; Allmaier, G.; Fröhlich, J.; Mikula, H.:

Efficient low-cost preparation of trans-cyclooctenes using a simplified flow setup for photoisomerization

Monatsh Chem (2016) 147:579–585
DOI 10.1007/s00706-016-1668-z

ORIGINAL PAPER

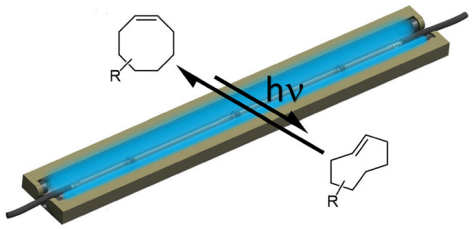
Efficient low-cost preparation of *trans*-cyclooctenes using a simplified flow setup for photoisomerization

Dennis Svatunek[1,2] · Christoph Denk[1] · Veronika Rosecker[1] · Barbara Sohr[1] · Christian Hametner[1] · Günter Allmaier[2] · Johannes Fröhlich[1] · Hannes Mikula[1]

Received: 15 November 2015 / Accepted: 24 December 2015 / Published online: 22 February 2016
© The Author(s) 2016. This article is published with open access at Springerlink.com

Abstract Bioorthogonal ligations have emerged as highly versatile chemical tools for biomedical research. The exceptionally fast reaction between 1,2,4,5-tetrazines and *trans*-cyclooctenes (TCOs), also known as tetrazine ligation, is frequently used in this regard. Growing numbers of applications for the tetrazine ligation led to an increased demand for TCO compounds, whose commercial availability is still very limited. Reported photochemical procedures for the preparation of TCOs using flow chemistry are straightforward and high yielding but require expensive equipment. Within this contribution, we present the construction and characterization of a low-cost flow photoreactor assembled from readily accessible components. Syntheses of all commonly used *trans*-cyclooctene derivatives were successfully carried out using the described system. We are convinced that the presented system for photoisomerization will promote access to bioorthogonally reactive TCO derivatives.

Graphical abstract



Keywords Photochemistry · Cycloadditions · Click chemistry · Alkenes · Isomerization · Bioorthogonal chemistry

Introduction

From a chemists perspective biological systems are extraordinarily complex. Each individual cell combines a broad range of functional groups, macromolecules, enzymes, and organelles with different pH values as well as sub-compartments with oxidizing or reducing conditions. Stepping up from the single cell level to a higher organism adds another magnitude of complexity to the "in vivo chemical space", which are far off simple mixtures usually present in a typical synthetic experiment.

Bioorthogonal chemistry, a term first introduced by Carolyn R. Bertozzi [1], is a tool that allows covalent bond formation within highly complex environments, using small molecule reaction partners. Those reactions (also referred to as "in vivo click chemistry") meanwhile found numerous applications in fluorescent imaging, drug delivery, PET and SPECT imaging, radionuclide therapy,

Electronic supplementary material The online version of this article (doi:10.1007/s00706-016-1668-z) contains supplementary material, which is available to authorized users.

✉ Hannes Mikula
hannes.mikula@tuwien.ac.at

[1] Institute of Applied Synthetic Chemistry, TU Wien, Vienna, Austria

[2] Institute of Chemical Technologies and Analytics, TU Wien, Vienna, Austria

radiochemistry or drug target identification among several others [2–6]. High selectivity and fast ligation rates of the involved bioorthogonal groups are as important as the metabolic stability of reaction partners and ligation products, as well as their biocompatibility (also in regards of toxicity). A prominent example is the reaction of organic azides with cyclooctynes to form 1,2,3-triazoles, wherein the strained conformation of the cyclooctyne eliminates the need for (cytotoxic) copper(I)-catalysis thus also referred to as the copper-free click (CFC) or strain-promoted alkyne azide cycloaddition (SPAAC) [7]. SPAAC ligation rates are highly dependent on substitution motifs on the cyclooctyne moiety, whose synthesis is often cumbersome and low-yielding. Several improved and more easily accessible cyclooctyne derivatives have been reported, but reaction rates of SPAAC ligations are still limited to $\sim 5\ M^{-1}\ s^{-1}$. Nevertheless, besides many in vitro applications SPAAC has been successfully used for in vivo fluorescent imaging in developing zebrafish [8] as well as for pretargeting in positron emission tomography (PET) [9].

A significant improvement was achieved by the groups of Joseph Fox [10] and Ralph Weissleder [11] in 2008, when they independently introduced the inverse electron demand Diels–Alder reaction (IEDDA) between 1,2,4,5-tetrazines (Tz) and strained dienophiles as highly efficient bioorthogonal reaction (Fig. 1a). When *trans*-cyclooctene (TCO) derivatives react with electron deficient Tz compounds second order rate constants of up to $3.3 \times 10^6\ M^{-1}\ s^{-1}$ (25 °C, H_2O) [12] were observed, making the IEDDA reaction several orders of magnitude faster than SPAAC and the fastest bioorthogonal ligation discovered so far. Hence, rapid ligation can be achieved even at very high dilutions frequently encountered within living systems. IEDDA has successfully been applied in pretargeted PET imaging [13, 14]. The recent development of tetrazines labeled with short-lived fluorine-18 [15–17] also allows imaging of long-circulating nanomedicines with short-lived isotopes as well as rapid radiolabeling of dienophile-tagged (bio)molecules [18–22], avoiding further purification steps. In pharmaceutical and biomedical research dienophile-tagged small molecules were used in vitro in combination with fluorogenic tetrazines [23–26] to visualize sites of drug accumulation at sub-cellular resolution. Tz ligations were also applied for target identification studies [27] and the synthesis of biocompatible polymers and hydrogels [28, 29].

Ligation rates of IEDDA conjugations are strongly dependent on steric and electronic influences on the tetrazine and the dienophile employed [30–32]. Norbornene and terminal alkenes were used as dienophiles, but low rates even with highly reactive Tz derivatives limit their use [33–35]. Cyclopropenes were introduced as dienophiles with less steric demand and higher reactivity compared to norbornene [36–38]. However, the most reactive dienophiles are *trans*-cyclooctenes (TCOs) (Fig. 1b). The parent compound *trans*-cyclooctene (TCO, **1**) is useful as reagent for ligation rate measurements using spectrophotometric techniques, but lacks a site for further derivatization thus making it unusable for bioconjugation. Consequently TCO derivatives including a functional group for further modification have been developed, out of which *trans*-cycloocten-5-ol (TCO-5-OH, **2**), which exists in two diastereomers, is the most frequently used. The diastereomer with axially configured hydroxyl group is formed in smaller amounts using photoisomerization and is thus often referred to as the "minor" TCO-5-OH (**2a**). **2a** shows moderately elevated reactivity compared to "major" (equatorial configuration) TCO-5-OH (**2e**). Nevertheless, steric hindrance makes further modifications of **2a** difficult, which is why **2e** is the most commonly used TCO in literature so far. TCO-5-OH has been proven to be reactive in vivo for prolonged times ranging to several days, but the mode of attachment and the microenvironment of the functionality is reported to influence the half-life inside the living system [39]. Annihilation of a cyclopropane ring to the cyclooctene core structure led to the development of (rel-1*R*,8*S*,9*R*,4*E*)-bicyclo[6.1.0]non-4-en-9-ylmethanol (s-TCO, **4**), which is one order of magnitude more reactive than TCO-5-OH. This dienophile was reported in 2011 by the Fox group [40], and is by far the fastest reacting TCO derivative known so far. Unfortunately high reactivity

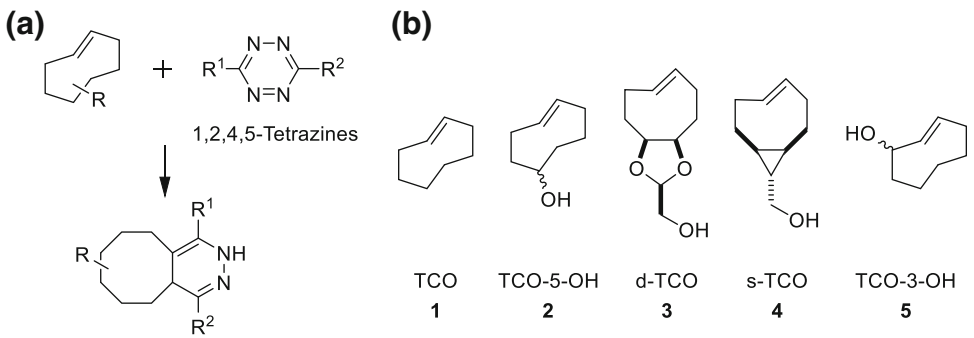


Fig. 1 **a** Inverse electron demand Diels–Alder (IEDDA) reaction between *trans*-cyclooctenes and 1,2,4,5-tetrazines; **b** selected known *trans*-cyclooctene derivatives

comes for the price of reduced stability, making s-TCO the choice whenever rapid reaction is more relevant than prolonged stability. Another highly reactive dienophile ((2*S*,3a*R*,9a*S*,*E*)-3a,4,5,8,9,9a-hexahydrocyclooct[*d*] [1, 3] dioxol-2-yl)methanol (d-TCO, **3**) [12], contains a dioxolane as structural motif enhancing its polarity and water solubility, which is a clear benefit when working in biological media. It exhibits IEDDA reactivity in between the rates for TCO-5-OH and s-TCO and is reported to display high stability. Another compound, *trans*-cycloocten-3-ol (TCO-3-OH, **5**), which also exists in an equatorial (**5e**) and axial configured (**5a**) isomer, deserves special attention due to its "click-to-release" behavior. The cytotoxic drug doxorubicin was conjugated to **5a** using a carbamate linkage on its 3-OH functionality leading to a pro-drug that can be activated by bioorthogonal click reaction with tetrazines [41]. This methodology gives rise to new therapeutic strategies, and the full potential of release chemistry is expected to unfold in years to come. The choice of which dienophile is suited best has to be made for every particular bioconjugation task depending on the necessities for ligation rate, stability, steric impact, and availability. Currently only the two isomers of TCO-5-OH, **2e** and **2a** are commercially available (**2e** also in activated form for conjugation reactions) and quite cost intensive when larger quantities are required.

State of the art TCO synthesis was introduced by Fox and coworkers in 2008 and made these useful small molecules more accessible [42]. When *cis*-cyclooctenes are irradiated with UV-C (254 nm) in the presence of a singlet sensitizer an equilibrium between *cis*- and *trans*-isomers is reached (photoisomerization) [43, 44]. The *trans*-isomers, in contrast to the *cis*-compounds, form stable complexes with silver cations. Hence, passing the reaction mixture through a cartridge filled with $AgNO_3$ on silica ($AgNO_3$/SiO_2) actively removes the TCO species from the equilibrium, allowing excellent reaction yields of TCOs from the respective *cis*-isomers in multigram quantities (Fig. 2a). Despite being broadly applicable for TCO synthesis the described setup uses a commercial UV reactor in which a quartz flask containing the reaction mixture has to be immersed (Fig. 2b). Both UV source and special glassware are cost intensive, and differently sized quartz flasks are necessary to maintain high flexibility regarding the scale of the reaction. Systems including flow photoreactors would eliminate this problem. Such reactors are commercially available (e.g. UV-150 photochemical reactor, Vapourtec Ltd.; Advanced-Flow™ G1 Photo Reactor, Corning®), but cost intensive and often require even more expensive flow chemistry equipment. We, therefore, aimed to develop and characterize an effective, versatile, and low-cost flow photoreactor using readily available components for the preparation of various TCO derivatives.

Results and discussion

The most promising design featured a quartz glass tube (Ø 16 mm, length 790 mm) connected to tubes at both ends and a total volume of 165 cm^3 as a flow cell. Two 55 W low-pressure mercury lamps (OSRAM, HNS 55 W OFR, T8, 90 cm) with a dominant wavelength of 254 nm were used for irradiation and placed alongside the quartz glass tube (Fig. 3). For a picture of the used setup see Electronic Supplementary Material (Fig. S1). This setup was mounted onto a back plate, covered with aluminum foil to prevent harmful radiation from exiting the system and aligned in vertical orientation. Solutions were pumped through the reactor upwards to allow for better filling of the reactor (see Electronic Supplementary Material). The total cost of this

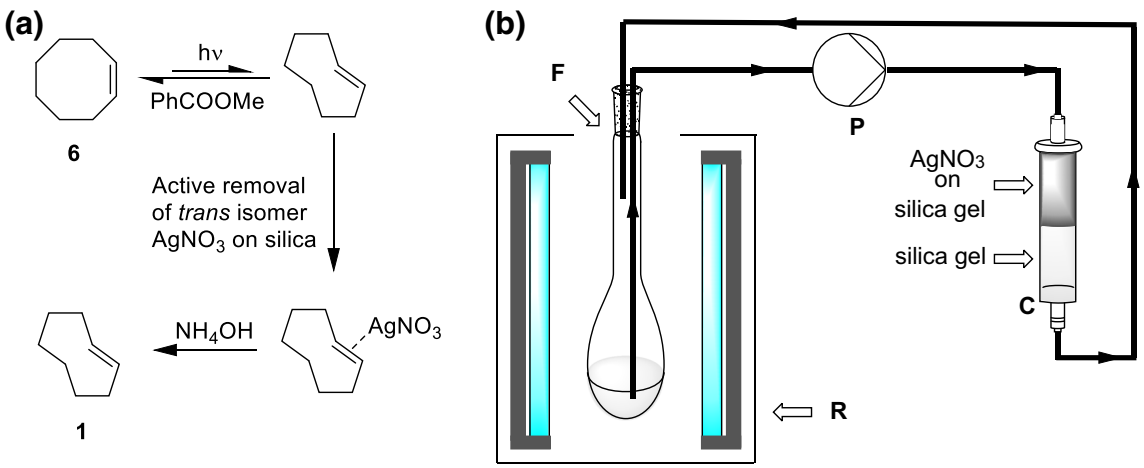


Fig. 2 **a** Photochemical isomerization of *cis*-cyclooctene with active removal of *trans* compound; **b** Reaction setup used by Fox et al.: ***C*** column, ***P*** metering pump, ***F*** quartz glass flask filled with reaction solution, ***R*** Rayonet photochemical reactor

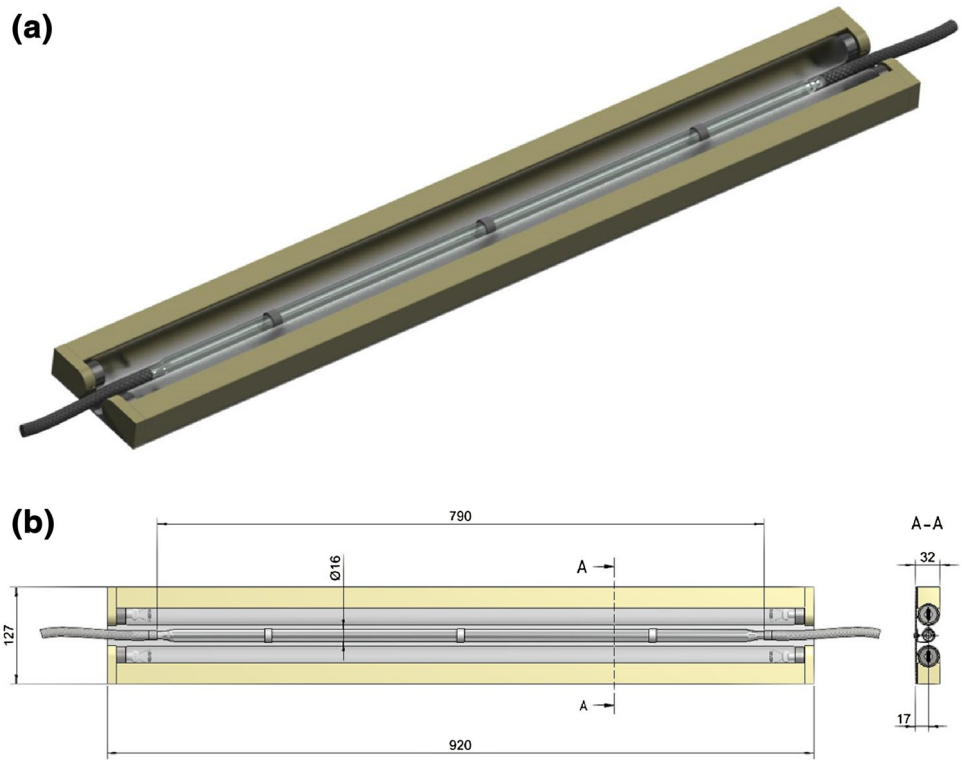


Fig. 3 **a** 3D view of the flow photoreactor; **b** dimensions in mm

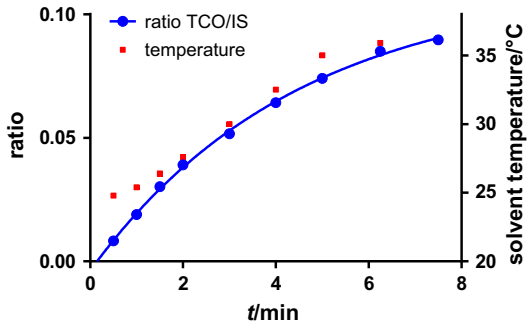


Fig. 4 Development of TCO/IS ratio and temperature during isomerization

device was below 300€ while the costs for commercially available systems (photoreactor including lamps and quartz glass flasks) are significantly higher (2000–5000€ or even more).

To determine the required time for reaching the equilibrium during photoisomerization a solution of *cis*-cyclooctene (**6**), methyl benzoate as singlet sensitizer and undecane as internal standard (IS, used for GC-FID measurements) in diethyl ether/hexanes (1/1) was irradiated without flow. Samples were taken after different irradiation times and analyzed by GC-FID. The temperature in the system reached 36 °C after about 6.5 min, which resulted in boiling of the solvent. The TCO/IS ratio was calculated over time and the data was fitted to a one phase association equation resulting in a predicted half-time of around 3.1 min (Fig. 4). The exact irradiation time for reaching the equilibrium could not be determined due to the rising temperature.

A flow rate of 100 cm^3/min was chosen for photoisomerization, which results in a rather short dwell time of 99 s. This is beneficial since the rate of isomerization is highest within the first minutes and the increase of temperature is only moderate.

For flow photoisomerization, the setup shown in Fig. 5a was used, for a picture see Electronic Supplementary Material (Fig. S2). An HPLC pump (**P**) was used to pass the reaction mixture from a reservoir flask (**F**) through a column (**C**) filled with silica and topped with $AgNO_3$-impregnated silica ($AgNO_3/SiO_2$) and covered with aluminum foil, then through the vertically aligned flow reactor (**R**) back to the reservoir. The column was placed right after the pump and prior to the photoreactor to prevent damage due to backpressure. The use of the reservoir flask enables simple scaling of the reaction without the use of expensive quartz glass flasks in different dimensions, since containers of any size and shape can be used for **F**. Implementation of cooling/heating of the solution as well as reactions under inert gas atmosphere can easily be realized in this setup. In this case a 3-neck round bottom flask equipped with a condenser was used, which was cooled and put under inert gas atmosphere.

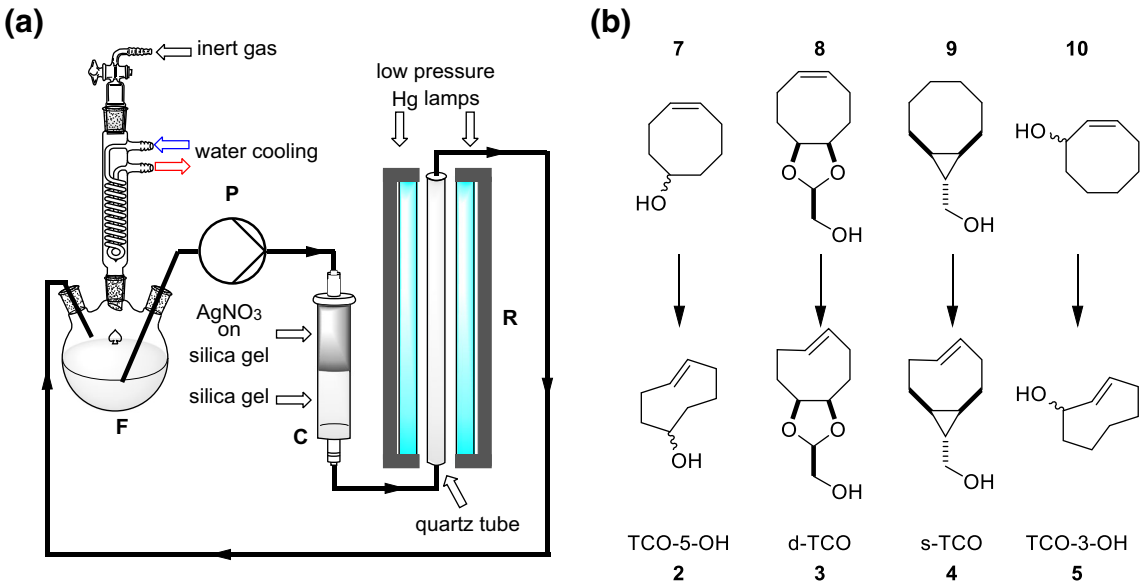


Fig. 5 **a** Flow photoisomerization setup; **b** isomerization of compounds **2**, **3**, **4**, and **5**

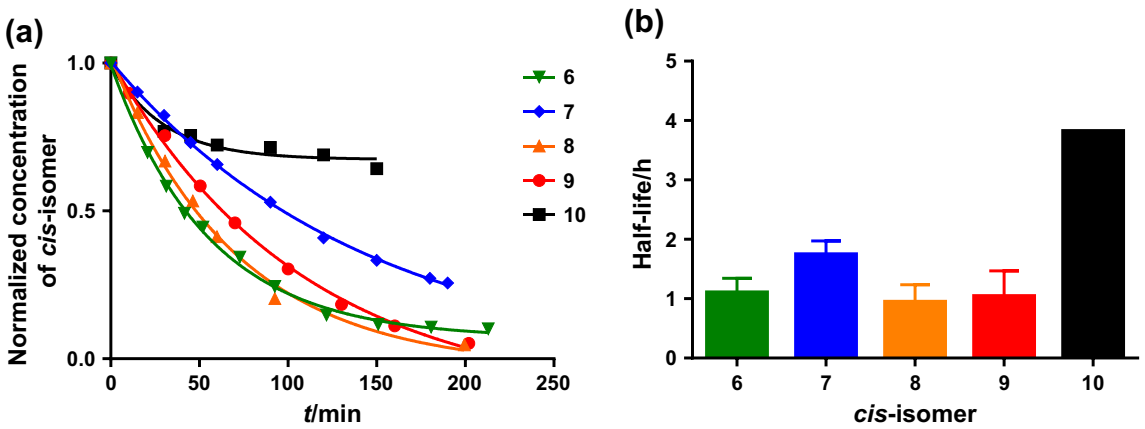


Fig. 6 **a** Decline of CCO derivatives during photoisomerization; **b** half-lifes of CCO compounds during photoisomerization

This setup was used for the synthesis of *trans*-cyclooctene (**1**) as a test substance followed by isomerization of *cis*-cycloocten-5-ol (**7**), ((2*S*,3a*R*,9a*S*,*Z*)-3a,4,5,8,9,9a-hexahydrocycloocta[*d*] [1, 3] dioxol-2-yl)methanol (**8**) and (1*R*,8*S*,9*R*,4*Z*)-bicyclo[6.1.0]non-4-en-9-ylmethanol (**9**) as well as *cis*-cycloocten-3-ol (**10**) to their corresponding *trans*-isomers (Fig. 5b). Reactions were monitored by measuring the remaining *cis*-configured starting material by GC (Fig. 6a). Isomerizations of **6**, **7**, **8**, and **9** were performed at least in duplicates and revealed similar isomerization times and a mean half-life of 72 ± 24 min for all 9 reactions (Fig. 6b). The isomerization of **10** to TCO-3-OH (mixture of **5a/5e**) was significantly slower with a half-life of 3.8 h, which is in good agreement with the reported reaction time of 32 h [41] for this derivative in comparison to 6-26 h reported for other TCOs [12, 40, 42]. Furthermore, isolated yields were compared with previously reported results (Table 1).

Conclusion

We were able to develop a low-cost and easy-to-build flow photoreactor that can be used for efficient synthesis of *trans*-cyclooctenes starting from respective *cis*-derivatives by photoisomerization. The setup was tested and characterized using different substituted and frequently used TCO derivatives. Isomerization was possible in relatively short time for all used substances with an average half-life of about 70 min with exception of **10** that showed a half-life of 3.8 h.

This simple design of a flow photoisomerization apparatus, which can easily be set up in any lab, enables the

Table 1 Comparison of yields for photoisomerization of **2**, **3**, **4**, and **5** reported in literature and those reached in this work

TCO	**2** (**2e**/**2a**)	**3**	**4**	**5** (**5e**/**5a**)
Literature	71 % [42] (47/24)	59 % [12]	74 % [40]	43 % [41] (25/18)
This work	47 % (32/15)	58 %	79 %	75 % (36/39)

efficient and cheap production of TCO derivatives up to multigram scale.

Experimental

Unless otherwise noted, all reagents were purchased from commercial suppliers and used without further purification. *Cis*-isomers **7** [42], **8** [12], **9** [40], and **10** [45] as well as $AgNO_3$-impregnated silica gel ($AgNO_3/SiO_2$) [42] were prepared following known procedures. GC-FID measurements were performed on a Trace^{TM} 1310 GC chromatograph from Thermo Scientific equipped with TR-5MS columns (length 15 m, I.D. 0.25 mm, film 1.0 µm). ^1H and ^{13}C NMR spectra were recorded on a Bruker AC 200 or Bruker Avance UltraShield 400 spectrometer at 20 °C.

Kinetics of photoisomerization

The flow photoreactor as illustrated in Fig. 3 was closed at the bottom and filled with a 10 mM solution of 187 mg *cis*-cyclooctene (1.7 mmol), 231 mg methylbenzoate (1.7 mmol), and 265 mg *n*-undecane (1.7 mmol) in 170 cm^3 hexanes/Et_2O (1:1). A resistance thermometer was placed inside the tube to follow the temperature of the solvent. The lamps were turned on and samples were taken at different time points and analyzed by GC-FID.

Photoisomerization and synthesis of TCO compounds: general procedure

The setup shown in Fig. 5a was used. The column was filled with silica gel, topped with $AgNO_3/SiO_2$ (10 %) and flushed with solvent. Then the reservoir was filled with solvent and put under argon atmosphere. The pump was turned on and set to a flow rate of 100 cm^3/min. After the solvent had filled the whole system *cis*-cyclooctene (final concentration between 5 and 20 mM), methyl benzoate and, if applicable, *n*-undecane was slowly added to the reservoir over the course of several minutes to ensure homogeneous distribution of all reactants. Afterwards the solution was pumped through the system for another 20 min. The lamps were turned on and the reaction progress was monitored by GC-FID following the decline of the starting material in the reservoir flask using either methyl benzoate or *n*-undecane as internal standard. The reservoir flask was cooled with ice-water during isomerization. After the reaction was completed, as indicated by consumption of the starting material, the lamps were turned off. The column was flushed with generous amounts of the solvent as used during isomerization (>60 cm^3/mmol of *cis*-configured starting material) and then dried with compressed air. Silica and $AgNO_3/SiO_2$ were taken out of the column, stirred in a mixture of concentrated NH_4OH (37 %) and dichloromethane (each 10 cm^3/g $AgNO_3/SiO_2$) and filtrated. The filter cake was washed twice with concentrated NH_4OH (5 cm^3/g $AgNO_3/SiO_2$) and dichloromethane (5 cm^3/g $AgNO_3/SiO_2$). The organic layer was separated, washed twice with water, dried over Na_2SO_4, and concentrated. Column chromatography was used for further purification if needed.

trans-Cyclooctene (**1**)
Following the general procedure using 9.50 g **6** (86 mmol), 12.30 g methyl benzoate (91 mmol), 130 g $AgNO_3/SiO_2$ (10 %), 100 g SiO_2, and 3500 cm^3 Et_2O/hexanes (1:99); 5.50 g (50 mmol, 58 %) of pure **1** were obtained without further purification. Spectroscopic data matched those reported in the literature [42].

TCO-5-OH, rel-(1R,4E,pR)-cyclooct-4-enol (**2e**) and *rel-(1R,4E,pS)-cyclooct-4-enol* (**2a**)
Following the general procedure using 2.03 g **7** (11.9 mmol), 2.00 g methyl benzoate (14.7 mmol), 27 g $AgNO_3/SiO_2$ (10 %), 18 g SiO_2, 700 cm^3 Et_2O/hexanes (9:1), 1.00 g *n*-undecane (6.4 mmol); the crude product was purified by column chromatography (90 g silica, hexanes/ethyl acetate, 4:1) to yield 658 mg (32 %, 5.2 mmol) of equatorial product (**2e**) and 313 mg (15 %, 2.5 mmol) of axial product (**2a**). Spectroscopic data matched that reported in the literature [42].

d-TCO, ((2 s,3aR,9aS,E)-3a,4,5,8,9,9a-hexahydrocyclooct a[d][1, 3]dioxol-2-yl)methanol (**3**)
Following the general procedure using 1.50 g **8** (8.2 mmol), 2.00 g methyl benzoate (14.7 mmol), 19 g $AgNO_3/SiO_2$ (10 %), 20 g SiO_2, 500 cm^3 Et_2O/hexanes (1:1), 1.00 g *n*-undecane (6.4 mmol); column chromatography (Et_2O/hexanes, 2:1) was performed to yield 875 mg (58 %, 4.8 mmol) of desired product **3**. Spectroscopic data matched that reported in the literature [12].

s-TCO, (rel-1R,8S,9R,4E)-bicyclo[6.1.0]non-4-en-9-ylmethanol (**4**)

Following the general procedure using 1.50 g **9** (9.9 mmol), 1.30 g methyl benzoate (9.5 mmol), 33 g $AgNO_3/SiO_2$ (10 %), 50 g SiO_2, 1000 cm^3 Et_2O/hexanes (1:1), 1.00 g *n*-undecane (6.4 mmol); 1.19 g (79 %, 7.8 mmol) of pure **4** were obtained without chromatographic purification. Spectroscopic data matched that reported in the literature [40].

TCO-3-OH, (1RS,2RS)-trans-cyclooct-2-enol (**5e**) and *(1SR,2RS)-trans-cyclooct-2-enol* (**5a**)

Following the general procedure using 2.00 g **10** (15.8 mmol), 2.15 g methyl benzoate (15.8 mmol), 35 g $AgNO_3/SiO_2$ (10 %), 40 g SiO_2, 800 cm^3 Et_2O/hexanes (1:1), 2.50 g *n*-undecane (15.8 mmol); the crude product was purified by column chromatography (90 g silica gel, 10-50 % ethyl acetate in hexanes) to yield 694 mg (35 %, 5.5 mmol) of axial isomer **5a**, 669 mg (33 %, 5.3 mmol) of equatorial isomer **5e** and 146 mg of a mixture (**5a**/**5e** = 1.3:1, 7 %, 1.2 mmol). NMR spectra matched those reported in the literature [41].

Acknowledgments We thank Rudolf Svatunek for the design drawings and the doctoral program 'Molecular and Elemental Imaging in Biosciences (MEIBio)' of TU Wien for funding.

Open Access This article is distributed under the terms of the Creative Commons Attribution 4.0 International License (http://creativecommons.org/licenses/by/4.0/), which permits unrestricted use, distribution, and reproduction in any medium, provided you give appropriate credit to the original author(s) and the source, provide a link to the Creative Commons license, and indicate if changes were made.

References

1. Sletten EM, Bertozzi CR (2009) Angew Chem Int Ed 48:6974
2. Devaraj NK, Weissleder R (2011) Acc Chem Res 44:816
3. Knall A-C, Slugovc C (2013) Chem Soc Rev 42:5131
4. Lang K, Chin JW (2014) ACS Chem Biol 9:16
5. Willems LI, van der Linden WA, Li N, Li K, Liu N, Hoogendoorn S, van der Marel GA, Florea BI, Overkleeft HS (2011) Acc Chem Res 44:718
6. Knight JC, Cornelissen B (2014) Am J Nucl Med Mol Imaging 4:96
7. Jewett JC, Bertozzi CR (2010) Chem Soc Rev 39:1272
8. Laughlin ST, Baskin JM, Amacher SL, Bertozzi CR (2008) Science 320:664
9. Lee SB, Kim HL, Jeong H-J, Lim ST, Sohn M-H, Kim DW (2013) Angew Chem Int Ed 52:10549
10. Blackman ML, Royzen M, Fox JM (2008) J Am Chem Soc 130:13518
11. Devaraj NK, Weissleder R, Hilderbrand SA (2008) Bioconjugate Chem 19:2297
12. Darko A, Wallace S, Dmitrenko O, Machovina MM, Mehl RA, Chin JW, Fox JM (2014) Chem Sci 5:3770
13. Rossin R, van Duijnhoven SMJ, Läppchen T, van den Bosch SM, Robillard MS (2014) Mol Pharm 11:3090
14. Nichols B, Qin Z, Yang J, Vera DR, Devaraj NK (2014) Chem Commun 50:5215
15. Denk C, Svatunek D, Filip T, Wanek T, Lumpi D, Fröhlich J, Kuntner C, Mikula H (2014) Angew Chemie Int Ed 53:9655
16. Zhu J, Li S, Wängler C, Wängler B, Lennox RB, Schirrmacher R (2015) Chem Commun 51:12415
17. Rashidian M, Keliher EJ, Dougan M, Juras PK, Cavallari M, Wojtkiewicz GR, Jacobsen JT, Edens JG, Tas JMJ, Victora G, Weissleder R, Ploegh H (2015) ACS Cent Sci 1:142
18. Wu Z, Liu S, Hassink M, Nair I, Park R, Li L, Todorov I, Fox JM, Li Z, Shively JE, Conti PS, Kandeel F (2013) J Nucl Med 54:244
19. Selvaraj R, Liu S, Hassink M, Huang C-W, Yap L-P, Park R, Fox JM, Li Z, Conti PS (2011) Bioorg Med Chem Lett 21:5011
20. Liu S, Hassink M, Selvaraj R, Yap L, Park R, Wang H, Chen X, Fox JM, Li Z, Conti PS (2013) Mol Imaging 12:121
21. Selvaraj R, Giglio BC, Liu S, Wang H, Wang M, Yuan H, Chintala SR, Yap L, Conti PS, Fox JM, Li Z (2015) Bioconjugate Chem 26:435
22. Li Z, Cai H, Hassink M, Blackman ML, Brown RCD, Conti PS, Fox JM (2010) Chem Commun 46:8043
23. Meimetis LG, Carlson JCT, Giedt RJ, Kohler RH, Weissleder R (2014) Angew Chem Int Ed 29:7531
24. Yang J, Šečkutė J, Cole CM, Devaraj NK (2012) Angew Chem Int Ed 51:7476
25. Devaraj NK, Hilderbrand S, Upadhyay R, Mazitschek R, Weissleder R (2010) Angew Chem Int Ed 49:2869
26. Carlson JCT, Meimetis LG, Hilderbrand SA, Weissleder R (2013) Angew Chem Int Ed 52:6917
27. Yang KS, Budin G, Tassa C, Kister O, Weissleder R (2013) Angew Chem Int Ed 52:10593
28. Zhang H, Dicker KT, Xu X, Jia X, Fox JM (2014) ACS Macro Lett 3:727
29. Liu S, Zhang H, Remy RA, Deng F, Mackay ME, Fox JM, Jia X (2015) Adv Mater 27:2783
30. Liu F, Liang Y, Houk KN (2014) J Am Chem Soc 136:11483
31. Liu F, Paton RS, Kim S, Liang Y, Houk KN (2013) J Am Chem Soc 135:15642
32. Karver M, Weissleder R, Hilderbrand SA (2011) Bioconjugate Chem 22:2263
33. Lang K, Davis L, Torres-Kolbus J, Chou C, Deiters A, Chin JW (2012) Nat Chem 4:298
34. Knall A-C, Hollauf M, Slugovc C (2014) Tetrahedron Lett 55:4763
35. Beckmann HSG, Niederwieser A, Wiessler M, Wittmann V (2012) Chem Eur J 18:6548
36. Patterson DM, Nazarova LA, Xie B, Kamber DN, Prescher JA (2012) J Am Chem Soc 134:18638
37. Devaraj N (2012) Synlett 23:2147
38. Yang J, Liang Y, Šečkutė J, Houk KN, Devaraj NK (2014) Chemistry 20:3365
39. Rossin R, van den Bosch SM, Ten Hoeve W, Carvelli M, Versteegen RM, Lub J, Robillard MS (2013) Bioconjugate Chem 24:1210
40. Taylor MT, Blackman ML, Dmitrenko O, Fox JM (2011) J Am Chem Soc 133:9646
41. Versteegen RM, Rossin R, ten Hoeve W, Janssen HM, Robillard MS (2013) Angew Chem Int Ed 52:14112
42. Royzen M, Yap GPA, Fox JM (2008) J Am Chem Soc 130:3760
43. Inoue Y, Kunitomi Y, Takamuku S, Sakurai H (1978) J Chem Soc Chem Commun 1024
44. Inoue Y, Takamuku S, Kunitomi Y, Sakurai H (1980) J Chem Soc Perkin Trans 2:1672
45. Zhang J, Matta ME, Martinez H, Hillmyer MA (2013) Macromolecules 46:2535

Manuscript #5

submitted manuscript

Denk, C.; Wilkovitsch, M.; Skrinjar, P.; Svatunek, D.; Mairinger, S.; Kuntner-Hannes, C.; Filip, T.; Fröhlich, J.; Wanek, T.; Mikula, H.:

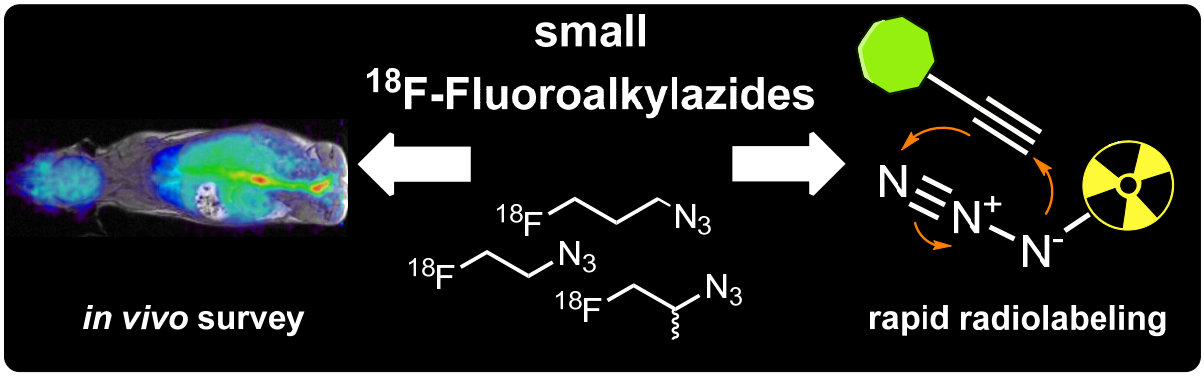
Investigation of Small [^{18}F]-Fluoroalkylazides for Rapid Radiolabeling and *In Vivo* Click Chemistry

Investigation of Small [^{18}F]-Fluoroalkylazides for Rapid Radiolabeling and *In Vivo* Click Chemistry

Christoph Denk[a], Martin Wilkovitsch[a], Philipp Skrinjar[a], Dennis Svatunek[a], Severin Mairinger[b], Claudia Kuntner[b], Thomas Filip[b], Johannes Fröhlich[a], Thomas Wanek[b] and Hannes Mikula[a*]

a) Institut für Angewandte Synthesechemie, Technische Universität Wien (TUW) (Austria) E-mail: hannes.mikula@tuwien.ac.at b) Health and Environment Department, Biomedical Systems, Austrian Institute of Technology (AIT) Seibersdorf (Austria)

Graphical Abstract



Abstract

Radiofluorinated alkylazides have been reported for *click* radiolabeling and pretargeted PET imaging. However, little data is available about their biodistribution and metabolism *in vivo*. Therefore, the synthesis of known 1-azido-2-[^{18}F]-fluoroethane was improved and it´s *in vivo* behavior investigated in detail. A panel of novel low-molecular-weight fluoroalkylazides that should exhibit beneficial properties were developed and radiolabeled. Biodistribution, pharmacokinetic and *in vivo* stability data in mice were collected by PET/MR studies in mice. Reactivity in copper catalyzed cycloadditions was confirmed by labeling propargyl tagged peptide endomorphin-1 in high yields and short reaction times.

Introduction

Positron Emission Tomography (PET) allows non invasive molecular imaging and quantification of metabolic processes. High sensitivity, spatial and temporal resolution makes PET an indispensable diagnostic tool in clinic and biomedical research. The versatility of this imaging modality is highly dependent on the availability of specific radiolabeled probes. Short lived nuclides are generally preferred, due to low patient radiation dose and potentially high specific activity. However, sufficient time is still necessary for production, quality control, delivery and application of the probe. Fluorine-18 (t1/2 = 109.8 min) is thus considered the “ideal” PET radioisotope that enables the radiochemist to conduct multi-step synthesis and purifications using chromatographic methods.

[^{18}F]Fluoroethylazide ([^{18}F]FEA) is reported to be a highly versatile tool for PET imaging and radiochemistry. [^{18}F]FEA has frequently been used as prosthetic group for labeling applications, and has also been proposed as secondary agent in pretargeted (bioorthogonal) PET imaging.[1–3]

For its use as prosthetic group a precursor compound is modified to carry a terminal alkyne, and subsequently reacted with [^{18}F]FEA in a copper(I) catalyzed cycloaddition (CuAAC) (Figure 1a).[2–6] This methodology is highly selective and in contrast to direct ^{18}F-labeling no protecting groups are required.[7] Furthermore, this technique is fast, high-yielding and applicable to sensitive molecules like peptides and other biomolecules.[7,8]

[^{18}F]FEA was moreover reported as secondary agent for bioorthogonal PET imaging.[1] This two-step pre-targeting process allows imaging of long circulating nanomedicines with short half-life nuclides like fluorine-18. In a first step the probe modified with a reactive tag (chemical reporter) is administered and allowed to accumulate. In a second step a fast clearing radiolabeled agent (pull down reagent, PDR) is given that ligates to the pre-administered compound *in vivo* (Figure 1b). The strain promoted alkyne-azide cycloaddition (SPAAC) using organic azides and cyclooctynes as reactants has been frequently applied *in vitro* and *in vivo*.[9–13]

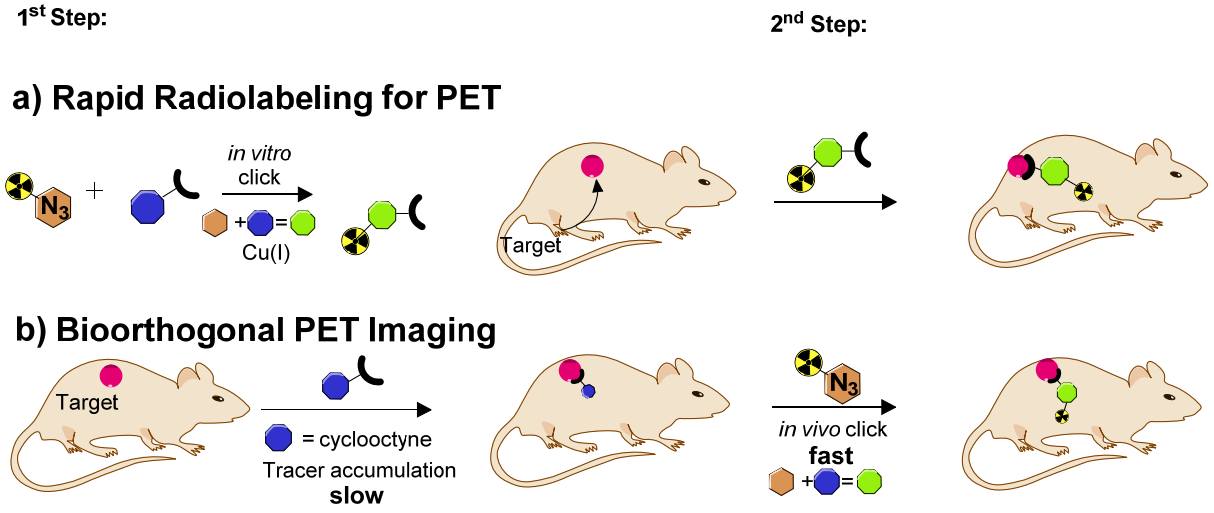


Figure 1: *Use of* [^{18}F]*fluorinated azides as prosthetic group for „click" radiolabeling (a) and as secondary agent in bioorthogonal PET imaging (b)*

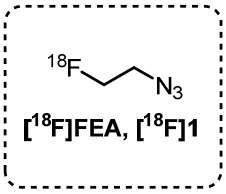
Moreover good results using pre-targeting in positron emission tomography (PET) with pre-administered cyclooctyne-labeled nanoparticles and an azide-functionalized fluorine-18 probe based on ethylene glycol were reported.[9] Due to its polarity this mini-PEG (polyethylene glycol) derived compound is unlikely to cross cell membranes and thus not suitable for internalizing chemical reporters. A metabolically stable probe with low molecular weight (fast pharmacokinetics) and medium polarity (crossing of biological membranes) is proposed to be of high versatility for SPAAC mediated pre-targeted PET imaging, but up to now no data on metabolic stability of ^{18}F-FEA was available.[1]

Despite the usefulness of [^{18}F]FEA several problems are associated with this low-molecular weight agent. [^{18}F]FEA is highly volatile and usually purified from the labeling reaction mixture by co-distillation with acetonitrile.[2] However this purification is time consuming, since care must be taken not to exceed 90°C distillation temperature. Otherwise, precursor is carried over, causing impurities

and interferences in subsequent cycloaddition reactions.[14] Moreover, the tosylated precursor is highly viscous making it difficult to handle in small quantities. Stable 2-fluoroethylazide, required for synthesis of cold reference materials, is potentially explosive, gaseous and difficult to handle in substance.[2]

Within this paper we aim to shed light on the applicability of [^{18}F]FEA and related compounds as PDR by studying the biodistribution and metabolism of this low molecular weight compounds. Furthermore we present new tools that circumvent problems associated with [^{18}F]FEA. A novel crystalline precursor for [^{18}F]FEA that allows higher yields and also eliminates distillation carry-over is introduced. In addition two novel low-molecular-weight ^{18}F-fluoroalkylazides (1-azido-3-[^{18}F]fluoropropane and 2-Azido-1-[^{18}F]fluoropropane) are presented as prosthetic groups with beneficial properties, and further investigated towards their usability as pull down reagents for pretargeted PET imaging and rapid radiolabeling.

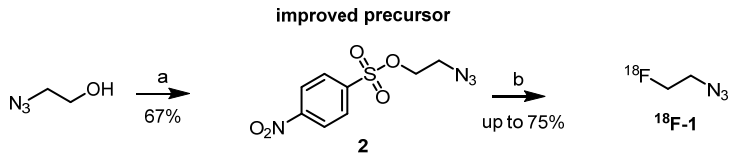
Results and discussion



When our group started to work on PET radiochemistry we required a multifunctional tool that allows for rapid radiolabeling and bioorthogonal imaging based on the azide-alkyne click cycloaddition (SPAAC). Moreover small molecular weight (to achieve fast pharmacokinetics and migration between compartments) as well as medium polarity (to allow for membrane diffusion) were key attributes of the sought for radiolabeled agent. In addition to numerous reported successful examples in rapid radiolabeling, a promising biodistribution study reported for 1-Azido-2-[^{18}F]fluoroethane ([^{18}F]FEA, [^{18}F]**1**) prompted us to pursue further evaluation of this compound.[1]

Radiosynthesis of [^{18}F]**1** is based on the K_2CO_3/K222 system for nucleophilic substitution on tosylated precursor 2-azidoethyl 4-methylbenzenesulfonate.[2,7,15] After short reaction time at elevated temperature (80-110°C) the product is isolated by co-distillation with acetonitrile. However different measures including time consuming distillation at low temperature, reduced pressure and the use of low precursor mass are required to minimize carry-over of the volatile tosylate. Codistilled precursor causes chemical impurities and furthermore competes with [^{18}F]**1** for alkyne groups.

To circumvent this problem 2-azidoethyl 4-nitrobenzenesulfonate (**2**) was synthesized as novel precursor material from 2-azidoethanol and nosyl chloride in 67% yield (Scheme I). The nosylate was obtained as crystalline solid, thus making handling of small quantities easier as compared to the highly viscous 2-azidoethyl 4-methylbenzenesulfonate. [^{18}F]**1** for click radiolabeling applications was obtained by reacting **2** with azeotropically dried ^{18}F-fluoride and K_2CO_3/K222 in acetonitrile for 5 min at 105°C. Time efficient distillation at 105-110°C in a stream of argon afforded [^{18}F]**1** in 75% decay corrected yield and >99% radiochemical purity. Most noteworthy, no precursor was detectable in the distilled product by HPLC due to reduced volatility of **2** in comparison with 2-azidoethyl 4-methylbenzenesulfonate.

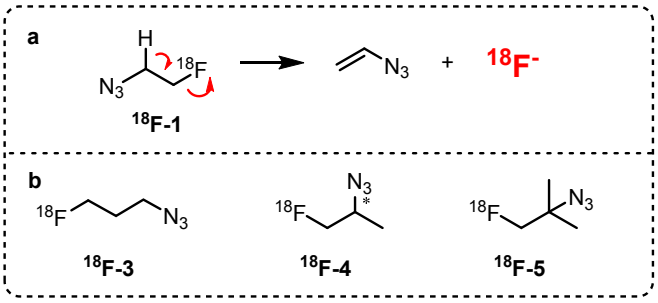


Scheme I: *Synthesis of precursor materials* ***2*** *and subsequent radiolabeling, a) NsCl, N(Et)$_3$ b) ^{18}F-HF, K_2CO_3, Kryptofix-222*

For biodistribution and metabolic studies another method of purification had to be chosen due to toxicity associated with acetonitrile. [^{18}F]FEA for animal experiments was synthesized from **2** using a

automated GE TRACERlab FX_{FDG} module with integrated HPLC purification system. A water/ethanol gradient in combination with a reversed phase column was used for isolation to yield the product in biocompatible media. [^{18}F]FEA was obtained in 48% decay corrected radiochemical yield (non-optimized) and in radiochemical purity exceeding 99.6%. Identity of [^{18}F]**1** was confirmed by comparison of HPLC retention times with authentic standard, and stability of the formulation was assessed by radio HPLC six hours post tracer synthesis that still revealed > 97% purity

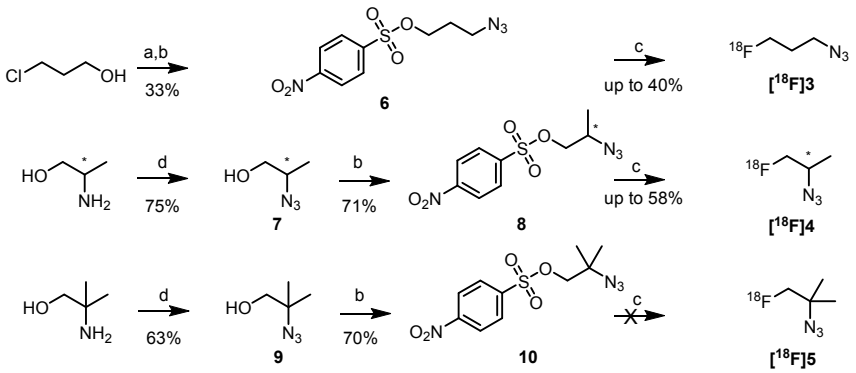
However, our findings from the murine metabolic study of [^{18}F]**1** revealed high bone uptake indicating metabolic instability and liberation of free ^{18}F-anions (details see *in vivo* section). Noteworthy, probes synthesized by rapid radiolabeling using [^{18}F]**1** are not generally known to exhibit metabolic instability *in vivo*. We reasoned that a possible pathway for this degradation is the abstraction of hydrogen alpha to the azide resulting in elimination of fluoride (Scheme IIa). To minimize this effect we designed a series of close analogs, with the aim to improve *in vivo* stability while retaining high versatility of the probe (Scheme IIb).



Scheme II: a) *Possible degradation pathway of [^{18}F]**1***
b) *Derivatives considered to increase metabolic stability*

We assumed that 1-azido-3-[^{18}F]fluoropropane ([^{18}F]**3**) might show reduced tendency to liberate fluorine ions due to diminished electronic interactions between the azide functionality and hydrogens in beta position to fluorine. Still, essential properties such as low molecular weight and medium polarity are retained in this molecule. In 2-azido-1-[^{18}F]fluoropropane ([^{18}F]**4**) the approach of branching, thus introducing steric bulk was followed. Introduction of a methyl group in alpha position to the azide functionality limits H-acidity (inductive effects) and accessibility (steric effects) of the adjacent hydrogen. Finally, replacing all alpha-hydrogens by methyl groups gives 2-azido-2-methy-1-[^{18}F]fluoropropane ([^{18}F]**5**). If the liberation of fluorine ions *in vivo* follows an elimination mechanism as depicted in Scheme IIa, this form of degradation should no longer be possible in [^{18}F]**5**.

To access these compounds the nosylate approach already successfully applied in the synthesis of [^{18}F]**1** was followed. Precursor substance for [^{18}F]**2**, 3-azidopropyl 4-nitrobenzenesulfonate **(6)** was synthesized in two steps from 3-chloropropan-1-ol which was reacted at 50°C with sodium azide in DMF. The crude product was further treated with p-nitrobenzenesulfonyl chloride and triethylamine in anhydrous dichloromethane. Subsequent purification by column chromatography afforded **6** as crystalline solid in 33% overall yield (Scheme III). Radiolabeling using conditions described above for the radiolabeling of [^{18}F]**1** afforded [^{18}F]**3** after co-distillation with acetonitrile in



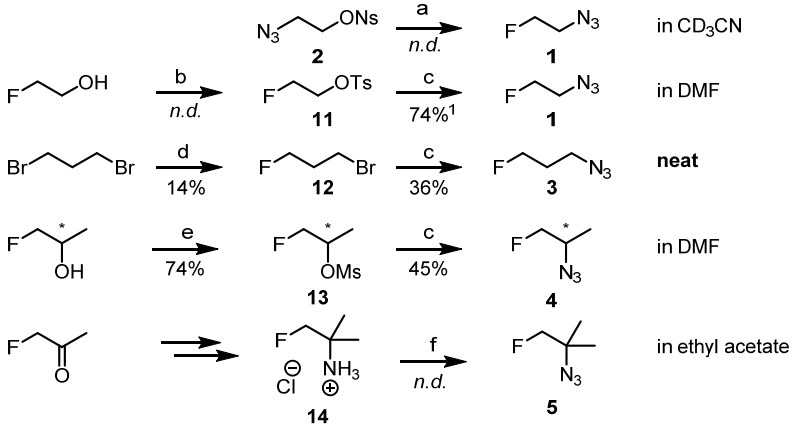
Scheme III: *Synthesis of precursor materials **6, 8, 10** and subsequent radiolabeling: a) NaN_3 b) NsCl, $N(Et)_3$ c) ^{18}F-HF, K_2CO_3, Kryptofix-222 d) 1H-Imidazole-1-sulfonyl azide, K_2CO_3, $CuSO_4$*

39.3% decay corrected radiochemical yield and in > 98% radiochemical purity. Preparative HPLC (using water/ethanol as eluent system) was used to obtain a product free of acetonitrile for murine biodistribution experiments. The experiment was conducted using a GE Tracerlab FX_{FDG} module with integrated HPLC purification system. [^{18}F]**3** was obtained in 23.5% decay corrected radiochemical yield (non-optimized) and radiochemical purity exceeding 94%. Identity of [^{18}F]**3** was confirmed by comparison of HPLC retention times with authentic standard, and stability of the formulation was assessed by radio HPLC three hours post tracer synthesis that still revealed > 89% radiochemical purity.

[^{18}F]**4** was synthesized from crystalline precursor **8**. Commercially available racemic alaninol was subjected to copper catalyzed diazotransfer conditions using 1*H*-imidazole-1-sulfonyl azide to obtain 2-azidopropan-1-ol (**7**) in 75% yield.[16,17] Nosylation using conditions described for **2**, followed by column chromatography gave rise to racemic **8** in 71% yield (Scheme III). Noteworthy, alaninol is also available as *R* or *S* isomer, making enantiopure [^{18}F]**4** accessible whenever required. However, in this study we decided to investigate racemic [^{18}F]**4** for ethnic reasons thus limiting the number of required animals. When **8** was reacted with azeotropically dried ^{18}F-K222 complex in anhydrous acetonitrile for 7 min at 100°C followed by distillation in a stream of argon [^{18}F]**4** was yielded as solution in anhydrous acetonitrile in 58% decay-corrected yield and 99.7% radiochemical purity. For biodistribution studies acetonitrile-free [^{18}F]**4** was synthesized on an automated GE Tracerlab FX module followed by preparative HPLC purification in 27% decay-corrected radiochemical yield and >96% radiochemical purity.

Applying a similar synthetic strategy for [^{18}F]**5,** 2-amino-2-methylpropan-1-ol was subjected to copper catalyzed diazotransfer conditions to obtain 2-azido-2-methylpropanol (**9**) in 63% isolated yield. The nosylated compound **10** was obtained in 70% yield by reaction of alcohol **9** with nosyl chloride and triethylamine in anhydrous DCM (Scheme III). Unfortunately radiolabeling attempts using the K_2CO_3/K222 method resulted in formation of a unknown radiolabeled species of unexpected lipophilicity in 70% radiochemical yield. HPLC retention times did not match retention times of authentic standard. Although the identity of the formed compound could not be clarified, modeling the labeling reaction in deuterated acetonitrile using “cold” potassium fluoride followed by ^{19}F-NMR spectroscopy indicated the absence of a primary alkylfluoride (shift -220 ppm). Instead signals at -105 ppm indicated formation of re-arrangement or elimination products.

Access to non-radioactive (“cold”) reference compounds is essential for identification of the radiolabeled agent by comparison of HPLC retention times. Furthermore when *click* radiolabeling is intended the stable (fluorine-19) azides are required as building blocks for synthesis of cold click-cycloaddition reference compounds. 1-Azido-2-fluoroethane (**1**) is highly volatile and potentially explosive and

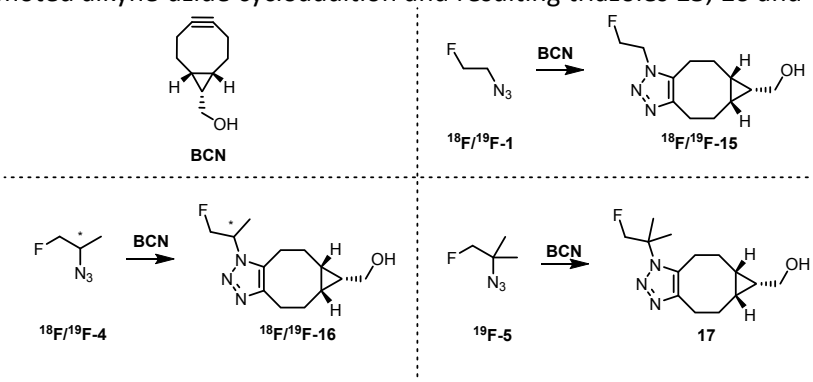


Scheme IV: *Synthesis of reference compounds **1, 3, 4** and **5**. a) KF, Kryptofix-222, b) TsCl, pyridine, c) NaN_3, d) KF e) DMAP, MsCl, $N(Et)_3$, f) 1H-Imidazole-1-sulfonyl azide, K_2CO_3, $CuSO_4$*
n.d.= not determined; [1])overall yield over steps b+c

should thus not be isolated *in substance*.[2] The already reported[18] tosylation of 2-fluoroethan-1-ol followed by reaction with sodium azide and subsequent filtration yielded a 1.36 M solution of **1** in DMF that was successfully used in cycloaddition reactions. In addition **1**, free of DMF, was obtained by reacting **2** with anhydrous potassium fluoride and Kryptofix-222 in CD_3CN followed by evaporation at low pressure and trapping of volatiles in a liquid nitrogen trap (Scheme IV).

1-Azido-3-fluoropropane (**3**) was synthesized starting from 1,3-dibromopropane to form 1-bromo-3-fluoropropane (**12**). Although **12** was isolated in only 14% yield its synthesis from cheap starting materials is still economically favorable.[19] Nucleophilic substitution with sodium azide in DMF afforded **3** in 36% yield. Due to a higher boiling point compared to **1** we were able to isolate neat **3** as colorless liquid by careful distillation; a clear benefit when onward use for chemical modification is intended. Although we did not encounter any problems, safety precautions like blast shields as well as performing reactions in small scale are highly recommended. In addition all reactions involving azide as nucleophile must be free of alkylhalogenides including dichloromethane. We observed the formation of potentially dangerous (explosive) diazidomethane when traces of dichloromethane were present in the reaction mixture. 2-azido-1-fluoropropane (**4**) was also obtained as solution in DMF (1.05 M) by mesylation of commercially available 1-fluoropropan-2-ol followed by reaction with sodium azide in anhydrous DMF and subsequent filtration.[20] No attempts were made to isolate neat **4**. Tertiary azide **5** was obtained as a solution in ethyl acetate applying diazotransfer conditions on 2-amino-2-methyl-1-fluoropropane hydrochloride (**14**).[17] Amine **14** was prepared following a published sequence starting from fluoroacetone.[21]

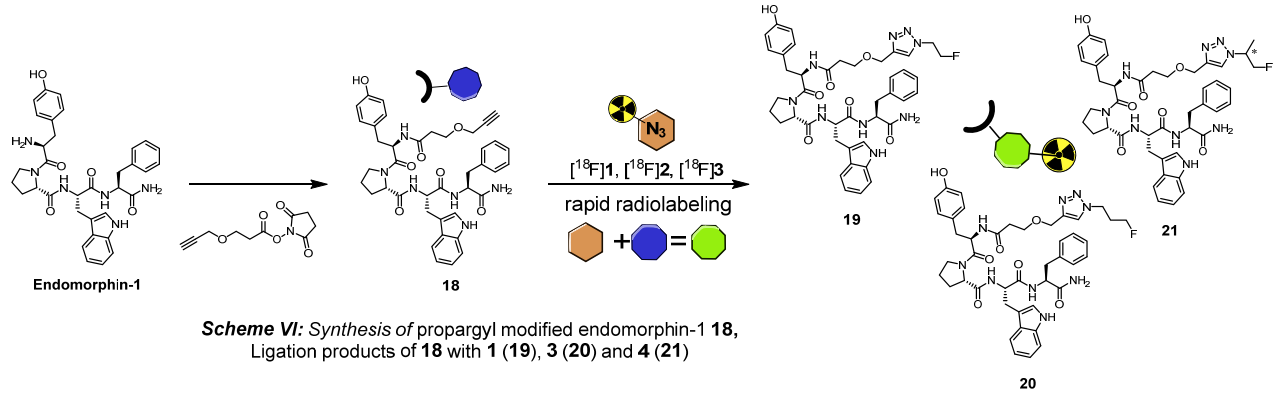
HPLC retention times of radiolabeled species (as distillate in acetonitrile for rapid radiolabeling or in aqueous medium for *in vivo* use) were compared with retention times of cold compounds to proof identity of the radiolabeled agent (see ESI for chromatographic data). Compounds that were not isolated in substance (**1, 4** and **5**) were ligated with cyclooctyne (1*R*,8*S*,9s)-Bicyclo[6.1.0]non-4-yn-9-ylmethanol (BCN)[22] in a strain promoted alkyne-azide cycloaddition and resulting triazoles **15**, **16** and **17** were isolated and fully characterized by NMR and MS. [^{18}F]**1** and [^{18}F]**4** were also treated with BCN resulting in rapid ligation. HPLC retention times of resulting ^{18}F-triazoles ([^{18}F]**15** and [^{18}F]**16**) were compared with their non-radioactive counterparts to further ensure identity of investigated compounds (Scheme V). When the labeling product arising from tertiary azide precursor **10,** was reacted with BCN, HPLC retention times with **17** did not match, confirming formation of an undesired re-arrangement or elimination product during the labeling reaction.



Scheme V: *Synthesis of* BCN ligation products **15, 16** and **17**

Application of [^{18}F]**1** as prosthetic group for rapid "click" radiolabeling is well documented.[2–8,23] Several modifications of the original procedure from Arstad and Glaser were reported to shorten reaction times and eliminate the need for heating. Especially noteworthy, addition of the water soluble copper-ligand bathophenanthroline sodium sulfonate reduces the required amount of copper and sodium ascorbate while maintaining, or even enhancing ligation rates at room temperature.[3]

To test and compare [^{18}F]**3** and [^{18}F]**4** as prosthetic group against already established [^{18}F]**1** we chose the tetrapeptide endomorphin-1 (EM-1) as substrate. EM-1 is a endogenous substance and powerful μ-opioid receptor agonist (K_i = 360 pM), that is of potential interest for imaging purposes.[24] In addition EM-1 is commercially available and possesses only one nucleophilic amine to allow for site specific modification. EM-1 was treated with commercially available 2,5-dioxopyrrolidin-1-yl-3-(prop-2-yn-1-yloxy)propanoate and triethylamine in anhydrous DMF to introduce an alkyne functional group (Scheme VI). Propargyl modified endomorphin-1 **18** was obtained in 42% yield following HPLC purification. Ligation products **19, 20** and **21** formed by reaction of propargylated EM-1 **18** with **1, 3** and **4** were prepared using the copper(II)sulfate/sodium ascorbate/bathophenantroline system in DMF, and isolated by RP-HPLC. [^{18}F]**19, [**^{18}F]**20** were formed in good radiochemical yields within 10



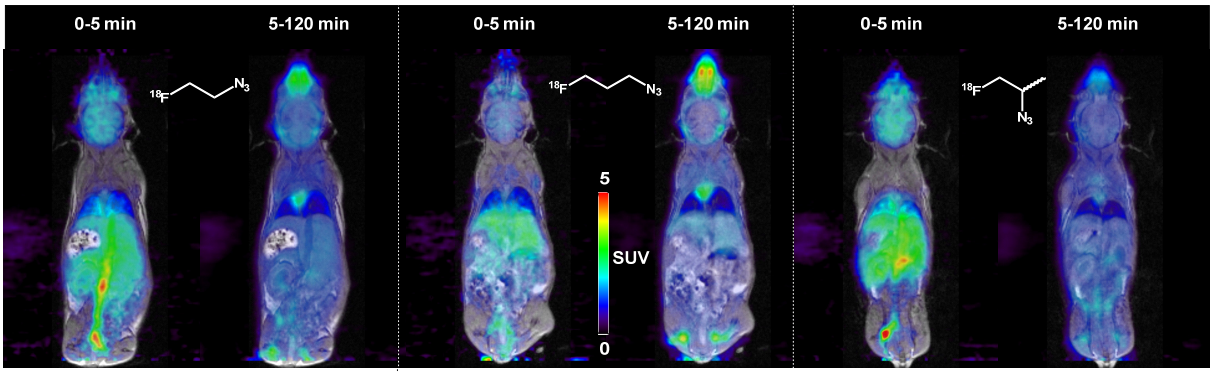
Scheme VI: *Synthesis of* propargyl modified endomorphin-1 **18,** Ligation products of **18** with **1** (**19**), **3** (**20**) and **4** (**21**)

minutes by reacting 1 mg of **18** with the according ^{18}F-fluoroalkylazide ([^{18}F]**1** and [^{18}F]**3**) using the copper(II)sulfate/sodium ascorbate/bathophenanthroline system in a mixture of acetonitrile and DMF (Scheme VI).

Subjecting [^{18}F]**4** to similar experimental conditions yielded [^{18}F]**21** in excellent radiochemical yield of 98%. Retention times of ligation products were compared by radio-HPLC with authentic standards **19**-**21**. In addition plasma stability of ligation products was assayed by incubation in human blood plasma for 120 minutes followed by radio-TLC analysis. Similar stabilities (~80-86%) were observed for all ligation products further indicating the applicability of [^{18}F]**3** and [^{18}F]**4** as prosthetic group equal or better compared to frequently used [^{18}F]**1**.

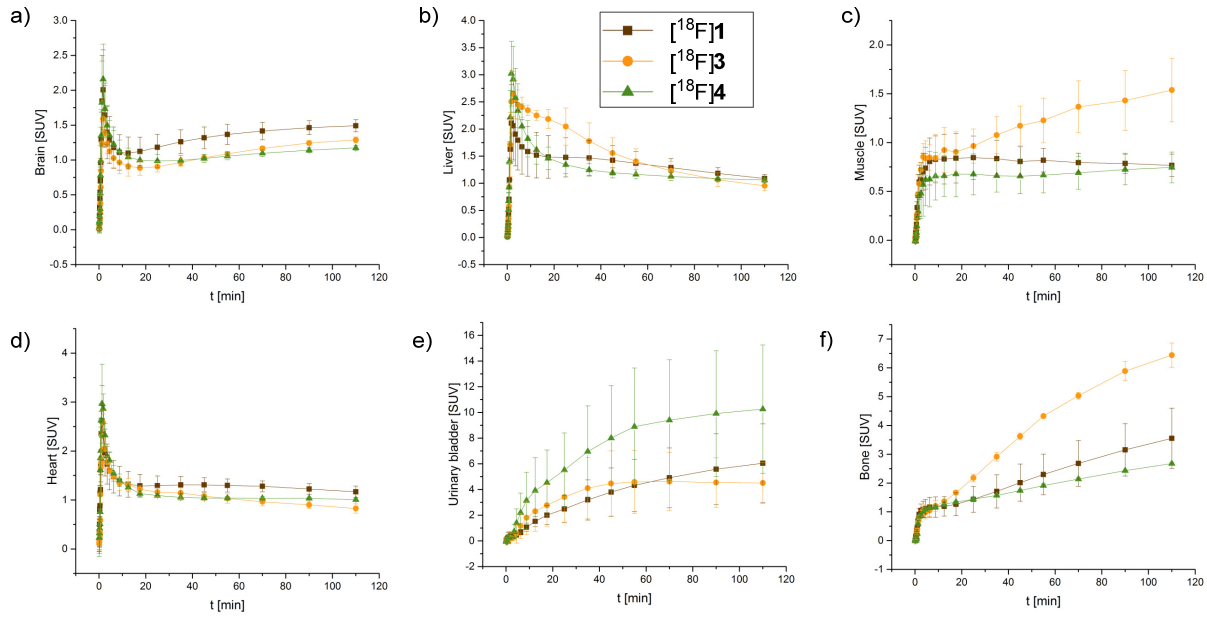
In vivo **investigation**

The test substances ([^{18}F]**1**, [^{18}F]**3**, [^{18}F]**4**) were injected into female BALB/c mice and dynamic PET (n=4 for [^{18}F]**1**, n = 2 for [^{18}F]**3** and [^{18}F]**4**) or PET/MR (n=1 for all test substances) scanning was performed for 120 minutes. Coronal PET/MR images are shown in Graph I. Analysis of organ time activity curves (Graph II) reveals a uniform uptake of all agents in most analyzed organs that slowly decreases from ~1.5 to ~1 SUV (standardized uptake value) during the course of the experiment. High uptake in the urinary bladder suggests renal elimination as main excretion route for all investigated substances. Secondary azide **4** exhibits the fastest clearance, a clear benefit when use as PDR in bioorthogonal PET imaging is intended (Graph IIe). Interestingly brain uptake shows a slight but steady increase for all analyzed tracers (Graph IIa).



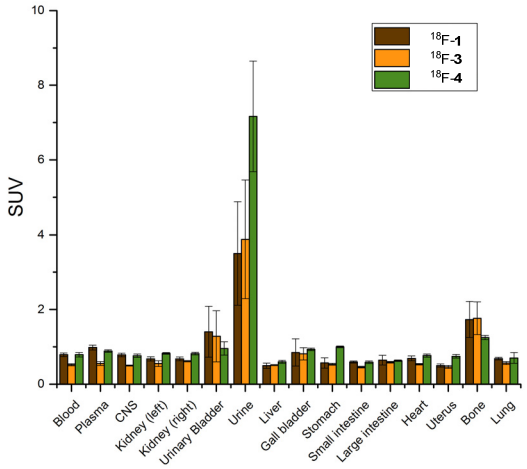
Graph I**: Coronal PET/MR slices of test substances [^{18}F]**1**, [^{18}F]**3** and [^{18}F]**4

[^{18}F]**3** exhibits a higher muscular uptake compared to [^{18}F]**1** and [^{18}F]**4** that increased throughout the experiment (Graph IIc). Most noteworthy, an increase of radioactivity concentration in bone was observed – a good indicator for metabolic instability and *in vivo* defluorination of the tracer molecules. Activity concentration in bone peaked at 3.6 SUV for [^{18}F]**1** and 6.5 SUV for [^{18}F]**3**, thus showing that *in vivo* stability could not be improved by insertion of one extra methylene group. [^{18}F]**4** showed lowest bone uptake (peak SUV = 2.7), compared to [^{18}F]**1** and [^{18}F]**3**, indicating improved *in vivo* stability over [^{18}F]**1** and [^{18}F]**3** (Graph IIf). In addition, coronal PET/MR images (Graph I) show skull uptake in the 5-120 min summation images, that is least pronounced in [^{18}F]**4** while [^{18}F]**3** exhibits the most pronounced uptake. Placing a "total box" ROI over the entire animal indicated revealed constant activity over the entire imaging period, showing that [^{18}F]**1,** [^{18}F]**3** and [^{18}F]**4** are not lost by respiration.



***Graph II**: Time activity curves of analyzed tracers in a) brain, b) liver, c) muscle, d) heart, e) urinary bladder, f) bone in female BALB/c mice.*

Following imaging, blood and urine samples were collected and the mice were sacrificed. Organ samples were collected and measured for radioactivity in a gamma counter. Data obtained by gamma counting at 120 min post injection of the tracers reflect data obtained in the PET experiment (Graph III). Radio-HPLC was chosen for analysis of metabolites due to the volatile nature of the test



Graph III: *Biodistribution of [^{18}F]**1**, [^{18}F]**3** and [^{18}F]**4** obtained by γ-counting of organ samples 120 min post tracer administration*

substances that renders radio-TLC uncertain. Murine plasma was obtained by centrifugation of whole blood in heparin tubes, and plasma proteins were precipitated by addition of an equal volume of acetonitrile. Following centrifugation the supernatant was injected into the HPLC system for analysis of plasma metabolites. Urine samples were injected after dilution with water. Data obtained from HPLC injections show diminutive (<4% of total radioactivity) amounts of intact compounds while the main fraction of radioactivity (> 90%) was detected as highly polar compound, most likely free ^{18}F-fluoride ions, confirming the metabolic instability of [^{18}F]**1**, [^{18}F]**3** and [^{18}F]**4**. Taking the rate of bone uptake into consideration (Graph IIf) [^{18}F]**4** shows increased stability compared to [^{18}F]**1** and especially [^{18}F]**3** that exhibits the least *in vivo* stability. This data is also reflected in plasma metabolite HPLC analysis, wherein [^{18}F]**4** displayed the highest percentage (up to 4%) of intact tracer 120 min post administration. Despite nuances in metabolic stability, degradation seems to happen on a time scale that is not compatible with reaction kinetics of the SPAAC ligation. In addition high bone uptake will contribute to background signal hindering image interpretation.

In summary we present an improved synthesis of [^{18}F]-fluoroethylazide based on novel precursor substance **2**, that is crystalline, easier to handle, and less volatile thus preventing the problem of distillative carry-over. In addition two novel [^{18}F]-fluoroalkylazide agents ([^{18}F]**3,** [^{18}F]**4)** were developed, expanding the library of prosthetic groups for ^{18}F-labeling. Rapid radiolabeling was demonstrated on endogenous μ-opioid agonistic peptide endomorphin-1, and biodistribution and metabolism data on all compounds was collected. Our findings demonstrate that [^{18}F]**3** and [^{18}F]**4** are valuable tools for click radiolabeling coequal to [^{18}F]**1**. Application of [^{18}F]**1,** [^{18}F]**3** and [^{18}F]**4** as PDRs for *in vivo* click chemistry is not promising due to metabolic instability of all analyzed probes.

Experimental

General

Unless otherwise noted, all reagents were purchased from commercial suppliers and used without further purification. DCM was dried using PURESOLV-columns (Innovative Technology Inc.). Dry acetonitrile (Merck) and *N,N*-Dimethylformamide (Acros) was commercially obtained and stored under argon. All other solvents were distilled prior to use. BCN was synthesized following published procedures.[22] Imidazol-1-sulfonyl azide hydrochloride was prepared following known procedures.[17] Drying of organic solvents after extraction was performed using anhydrous Na_2SO_4 or $MgSO_4$ (Sigma Aldrich) and subsequent filtration. Reactions were carried out under an atmosphere of argon in air-dried glassware with magnetic stirring. Sensitive liquids were transferred via syringe. Thin layer chromatography was performed using TLC alumina plates (Merck, silica gel 60, fluorescence indicator F254, or Merck RP18 fluorescence indicator F254). Detection in radio-TLC was performed by placing the TLC plates on multisensitive phosphor screens (Perkin-Elmer Life Sciences, Waltham, MA). The screens were scanned at 300 dpi resolution using a PerkinElmer Cyclone® Plus Phosphor Imager (Perkin-Elmer Life Sciences). Preparative column chromatography was performed using a Büchi Sepacore Flash System (2 x Büchi Pump Module C-605, Büchi Pump Manager C-615, Büchi UV Photometer C-635, Büchi Fraction Collector C-660) or a Reveleris Grace system using silica gel 60 (40-63 µm) as obtained from Merck and distilled or redistilled solvents. Preparative HPLC was done on a Reveleris Grace system. ^{1}H, ^{13}C and ^{19}F NMR spectra were recorded on a Bruker Avance IIIHD 600 MHz spectrometer equipped with a Prodigy BBO cryo probe, on a Bruker Avance UltraShield 400 spectrometer or on a Bruker AC200 spectrometer at 20 °C. Chemical shifts are reported in ppm (δ) relative to tetramethylsilane and calibrated using solvent residual peaks. Data are shown as follows: Chemical shift, multiplicity (s = singlet, d = doublet, t = triplet, q = quartet, quin = quintet, m = multiplet, br = broad signal) and integration. [^{18}F]Fluoride was produced *via* the $^{18}O(p, n)^{18}F$ nuclear reaction by irradiating oxygen-18 enriched water (IASON, Austria) using a PETtrace cyclotron equipped with high yield liquid target system (GE Healthcare, Uppsala, Sweden). HPLC analysis was performed on a 1200 series system (Agilent Technologies) using a reversed phase columns and acetonitrile/water or phosphate buffer gradients. Analytical HPLC Conditions A: Agilent ZORBAX SB-Aq 5 µm, 4.6 x 250 mm, water / acetonitrile , 1.2 ml/min, 0-2 min 5% acetonitrile, 2→10 min 5%→20% acetonitrile, 10-16 min 20%→90%, 16-20 min 90% acetonitrile, B: Agilent Extend-C18 3.5 µm, 3 x 100 mm, gradient water/acetonitrile (+0.1 vol% TFA), 1.3 ml/min, 0-1 min 10%, 1→8 min 10%→60%, 8-9 min 60%. For radio-HPLC a GABI* radioactivity detector (raytest Isotopenmessgeraete GmbH, Straubenhardt, Germany) was used. Preparative HPLC separations were done on the built in HPLC system on the synthesis module (TRACERlab™ FX_{FDG}, General Electric Healthcare, Uppsala, Sweden) using a Macherey-Nagel EP 250/16 100-7 C-18 (10 µm, 16 x 250 mm) column and ethanol/water-gradients (flow rate: 4 mL/min) in combination with a K-2001 UV detector (Knauer) and radioactivity detector. LC-MS measurements were carried out on a HPLC system of Agilent Technologies with the following components: Agilent 1200 Series G1367B HiP ALS Autosampler, Agilent 1100 Series G1311A Quat Pump, Agilent 1100 Series G1379A Degasser, Agilent 1200 Series G1316B TCCSL, Agilent 1260 Infinity G1315D DAD as well as an Esquire HCT Ion Trap MS of Bruker as detectors. A Phenomenex Luna 10 µm, C18, 250 x 4.6 mm column eluted with a gradient of 10-90% acetonitrile in water was used at a flowrate of 1ml/min.

1-azido-2-fluoroethane (1)

2-Fluorethanol (1 eq., 1.0 g, 15.6 mmol) in 5 ml dry pyridine was cooled to 0°C and treated dropwise with a solution of TsCl (2 eq., 5.95 g, 31.2 mmol) in 8 ml of pyridine. The reaction mixture was stirred at 0°C for 3 hours and poured onto ice which caused the product to precipitate. Extraction with ethyl acetate, washing of the organic phase with 2N HCl, half-saturated Na_2CO_3 solution and brine, followed by drying over Na_2SO_4 and removal of the solvent yielded crude 2-fluoroethyl 4-methylbenzenesulfonate as colorless liquid. The tosylate was further stirred in 10 ml of anhydrous DMF with sodium azide (1.08 eq., 1.1 g, 16.9 mmol) for 48 hours at room temperature. Filtration of solids yielded a pale yellow solution containing 1.43 mmol/g (8.1 g, 74% of theory) **1** as investigated by ^{1}H NMR. **1** free of DMF was obtained by heating a mixture of 2-Azidoethyl 4-nitrobenzenesulfonate(**4**) (1 eq., 136 mg, 0.5 mmol) , Kryptofix-222 (0.95 eq., 136 mg, 0.47 mmol) and anhydrous potassium fluoride (1 eq., 30 mg, 0.5 mmol) in 1.5ml CD_3CN to 80°C for 10 minutes using a laboratory microwave. After cooling to room temperature vacuum (10 mbar) was applied and volatiles were collected in a trap cooled with liquid nitrogen resulting in a solution of **1** in deuterated acetonitrile. ^{1}H NMR (400 MHz, MeCN-d_3) δ = 3.53 (dt, *J*=28.9, 4.7 Hz, 2 H) 4.57 (dt, *J*=47.6, 4.7 Hz, 2 H) ppm ^{13}C NMR (50.32 MHz, MeCN-d_3) δ = 51.9 (d, *J*=19.3 Hz) 83.8 (d, *J*=166.8 Hz) ppm ^{19}F NMR (376.5 MHz, MeCN-d_3) δ = -223.2 ppm

2-Azidoethyl 4-nitrobenzenesulfonate (2)

2-azidoethanol (1 eq., 2.0 g, 23 mmol) and triethylamine (2.04 eq., 4.78 g, 47 mmol) in 20 ml absolute methylene chloride were cooled to 0°C and p-nitrobenzenesulfonyl chloride (2.04 eq., 10.4 g, 47 mmol) in 30 ml abs. methylene chloride was added during 20 minutes. After finished addition the mixture was gradually warmed to room temperature and stirred for additional 2 h. The reaction mixture was diluted with 100 ml DCM, washed twice with 2N HCl, followed by brine. Drying over Na_2SO_4, filtration and evaporation gave 10 g crude product which was subjected to column chromatography (10-20% ethyl acetate in hexanes). Stripping of solvents yielded nosylate **2** (4.2 g, 67% of theory) as yellow crystals. Recrystallization from toluene yielded **2** (3.93 g, 63% of theory) as slightly yellow crystals. ^{1}H NMR (200 MHz, $CDCl_3$): δ = 3.55 (t, *J*=4.9 Hz, 2 H) 4.27 (t, *J*=5.3 Hz, 2 H) 8.14 (dt, *J*=8.8, 2.3 Hz, 2 H) 8.42 (dt, *J*=8.8, 2.0 Hz, 2 H) ppm ^{13}C NMR (50 MHz, $CDCl_3$): δ = 49.4, 69.2, 124.5, 129.2, 141.2, 150.8 ppm

1-azido-3-fluoropropane (3)

1-bromo-3-fluoropropane (**12**, 1 eq., 2.5 g, 17.7 mmol) and sodium azide (3 eq., 3.45 g, 53.1 mmol) were stirred in 10 ml anhydrous DMF at 50°C for 4 days. The reaction mixture was diluted with 150 ml H_2O and extracted three times with diethyl ether. Pooled extracts were washed twice with sat. NH_4Cl and once with brine, dried over $MgSO_4$ and the solvent removed on the rotary evaporator. The raw product was distilled at 46-48°C/100 mbar to yield 650 mg **3** (35.5% of theory) as colorless liquid**.** ^{1}H NMR (400 MHz, CD_3CN): δ = 1.63 - 1.78 (m, 2 H) 3.20 (t, *J*=6.83 Hz, 2 H) 4.29 (dt, *J*=47.22, 5.90 Hz, 2 H) ppm ^{13}C NMR (101 MHz, CD_3CN): δ = 30.1 (d, *J*=19.78 Hz) 48.0 (d, *J*=5.65 Hz) 81.9 (d, *J*=162.48 Hz) ppm ^{19}F NMR (376.5 MHz, CD_3CN): δ = 222.9 ppm IR v= 2092 cm^{-1} among others

3-azidopropyl 4-nitrobenzenesulfonate (6)

3-Chloropropan-1-ol (1 eq., 3.0 g, 31.7 mmol) and sodium azide (3 eq., 6.17 g, 95 mmol) were stirred in 25 ml anhydrous DMF at 50°C for 4 days. The reaction mixture was diluted with 200 ml H_2O and

extracted three times with diethyl ether. Pooled extracts were washed with brine, dried over $MgSO_4$ and the solvent distillied off. The crude residue was taken up in 40 ml anhydrous DCM, treated with triethylamine (1.25 eq., 4.0 g, 39.6 mmol) and cooled to 0°C. A solution of nosyl chloride (1.25 eq., 8.8 g, 39.6 mmol) in 100 ml absolute DCM was added dropwise and the reaction stirred at room temperature for 16 hours. The reaction mixture was extracted twice with ice cold 2N HCl followed by sat. $NaHCO_3$. After drying over $MgSO_4$ and removal of solvent the crude product was purified over 90g SiO_2 eluting with 5 – 15% ethyl acetate in petrol ether yielding 2.95 g (33 % of theory) yellowish oil that crystallized in the freezer. ^{1}H NMR (400 MHz, $CDCl_3$): δ = 1.93 (quin, *J*=6.24 Hz, 2 H) 3.40 (t, *J*=6.24 Hz, 2 H) 4.21 (t, *J*=6.05 Hz, 2 H) 8.11 (dt, *J*=8.98, 2.00 Hz, 2 H) 8.40 (dt, *J*=9.37, 2.30 Hz, 2 H) ppm ^{13}C NMR (101 MHz, $CDCl_3$): δ = 28.3, 47.0, 68.2, 124.5, 129.2, 141.4, 150.8 ppm IR ν= 2099 cm^{-1} among others

2-azidopropan-1-ol (7)

Potassium carbonate (1.21 eq., 4.52 g, 32.7 mmol) and copper sulfate pentahydrate (0.01 eq., 0.07 g, 0.27 mmol) were added to a stirring solution of 2-aminopropanol (1 eq., 2 g, 26.63 mmol) in 135 mL anhydrous methanol under argon atmosphere. Imidazole-1-sulfonyl azide hydrochloride (1.2 eq., 6.7 g, 57.25 mmol) was added and the mixture stirred for 3.5 h at room temperature. Afterwards methanol was removed *in vacuo*, the residue diluted with water (400 mL), acidified with conc. HCl until pH 5, extracted with ethyl acetate (3x200 mL), dried over $MgSO_4$, filtered and concentrated. The crude product was filtered over a pad of silica (hexanes:diethyl ether, 2:1) to obtain **7** (2.03 g, 75% of theory) as a yellowish oil. Rf (PE:Et_2O = 2:1) = 0.16; NMR data matched previously reported values.[19]

2-azidopropyl -4-nitrobenzenesulfonate (8)

7 (1 eq., 1 g, 9.89 mmol) and triethylamine (1.2 eq., 1.2 g, 11.87 mmol) were dissolved in 25 mL anhydrous DCM. After cooling to 0°C 4-nitrobenzenesulfonyl chloride (1.2 eq., 2.63 g, 11.87 mmol) was added and the mixture stirred for 100 min during which contents gradually warmed to room temperature. The reaction mixture was diluted with 120 mL DCM, extracted with 2 N HCl (2x100 mL), the combined organic layers were washed with brine, dried over $MgSO_4$, filtered and the solvent stripped. The product was purified by column chromatography over 90 g silica-gel (3-25% EE in hexanes) to afford **8** (2 g, 71% of theory) as a yellow powder. Rf (PE:EE = 4:1) = 0.23; ^{1}H NMR (400 MHz, $CDCl_3$): δ = 1.27 (d, *J*=6.63 Hz, 3 H) 3.80 (quind, *J*=6.78, 6.78, 6.78, 6.78, 4.10 Hz, 1 H) 4.03 (dd, *J*=10.15, 7.02 Hz, 1 H) 4.15 (dd, *J*=10.34, 4.10 Hz, 1 H) 8.15 (dt, *J*=8.98, 2.00 Hz, 2 H) 8.43 (dt, *J*=8.98, 2.00 Hz, 2 H) ppm ^{13}C NMR (101 MHz, $CDCl_3$): δ = 15.6, 55.5, 72.9, 124.5, 129.3, 141.4, 150.9 ppm

2-azido-2-methylpropan-1-ol (9)

To a stirred mixture of 2-amino-2-methyl-propan-1-ol (1 eq., 4.25 g, 47.7 mmol), potassium carbonate (1.2 eq., 8.0 g, 58 mmol) and $CuSO_4$ x 5 H_2O (0.01 eq., 119 mg, 0.48 mmol) in 200 ml methanol was added imidazol-1-sulfonyl azide hydrochloride (1.2 eq., 10 g, 57.25 mmol) in portions. The mixture was stirred overnight at room temperatureand the majority of MeOH was carefully removed on the rotary evaporator. The residue was taken up in 500 ml water, acidified (pH 4) with HCl, and the solution was extracted three times with ethyl acetate. Combined extracts were dried over $MgSO_4$ and the solvent was removed on the rotary evaporator (50 mbar). The residue was purified by filtration over a plug of SiO2 using PE:Et_2O = 2:1 as eluent. Stripping of solvent afforded 3.47 g tertiary azide **9** as colorless liquid (63% of theory). TLC-Rf (PE:Et_2O = 2:1) = 0.4, ^{1}H NMR (200

MHz, $CDCl_3$) δ = 1.27 (s, 6 H) 2.54 (br. s, 1 H) 3.42 (s, 2 H) ppm, ^{13}C NMR (50.32 MHz, $CDCl_3$): δ = 22.5, 62.4, 70.0 ppm

2-azido-2-methylpropyl 4-nitrobenzenesulfonate (10)

9 (1 eq., 1 g, 8.69 mmol) and triethylamine (1.2 eq., 1.05 g, 10.42 mmol) were dissolved in 10 mL anhydrous DCM. After cooling to 0°C 4-nitrobenzenesulfonyl chloride (1.2 eq., 2.31 g, 10.42 mmol) was added dropwise as a solution in 15 ml anhydrous DCM. The mixture was stirred for 100 min during which contents gradually warmed to room temperature. The reaction mixture was diluted with 100 mL DCM and washed twice with 2 N HCl and once with brine. Drying over $MgSO_4$ and stripping of the solvent afforded the crude product which was purified over 90g SiO_2 eluting with 3-28% EE in PE. **10** was obtained as off-white crystalline solid in 70.5% yield. Rf (PE:EE = 2:1) = 0.75; ^1H NMR (400 MHz, $CDCl_3$): δ = 1.29 - 1.33 (m, 6 H) 3.96 (s, 2 H) 8.15 (dt, *J*=8.98, 2.30 Hz, 2 H) 8.44 (dt, *J*=8.98, 2.30 Hz, 2 H) ppm ^{13}C NMR (101 MHz, $CDCl_3$): δ = 22.9, 59.5, 76.2, 124.5, 129.3, 141.1, 150.9 ppm

1-fluoropropan-2-yl methanesulfonate (13)

1-fluorpropan-2-ol (1 eq., 300 mg, 3.84 mmol) triethylamine (1.1 eq., 426 mg, 4.2 mmol) and N,N-dimethylaminopyridine (0.1 eq., 47 mg, 0.384 mmol) in 7 ml anhydrous DCM were cooled to 0°C. Mesyl chloride (1.1 eq., 324 µl, 4.2 mmol) was added dropwise and the mixture was allowed to reach room temperature and stirred for 1 additional our. The reaction mixture was partitioned between 100 ml DCM and saturated NH_4Cl solution, the organic phase was dried over sodium sulphate and the solvent removed to obtain **13** as yellow oil that crystallized in the freezer into slightly yellow needles (440 mg, 74% of theory). The product was sufficiently pure for carrying it into the next synthetic step. ^1H NMR (400 MHz, $CDCl_3$) δ = 1.41 (dd, *J*=6.63, 1.56 Hz, 3 H) 3.05 (s, 3 H) 4.33 - 4.56 (m, 2 H) 4.90 - 5.03 (m, 1 H) ppm ^{13}C NMR (100.61 MHz, $CDCl_3$) δ = 16.3 (d, *J*=7.1 Hz) 48.4 (d, *J*=2.8 Hz) 77.1 (d, *J*=21.2 Hz) 84.3 (d, *J*=175.2 Hz) ppm ^{19}F NMR (376.5 MHz, $CDCl_3$) δ = -223.7 ppm

2-azido-1-fluoropropane (4)

1-fluoropropan-2-yl methanesulfonate (**13**, 1 eq., 211 mg, 1.35 mmol) and sodium azide (1.05 eq., 92 mg, 1.42 mmol) was stirred in anhydrous DMF at 50°C overnight. Additional NaN_3 (0.11 eq., 10 mg, 0.15 mmol) was added and the heating continued for further 24 hours after which ^1H-NMR indicated full conversion. The reaction mixture was centrifuged (13.4 krpm, 5 min) to remove insolubles. A solution of **4** in DMF was obtained (550 mg, 1.1 mmol/g as determined by ^1H-NMR, corresponding to 45% of theory). ^1H NMR (400 MHz, $CDCl_3$) δ = 1.16 (dd, *J*=6.80, 1.56 Hz, 3 H) 3.56 - 3.81 (m, 1 H) 4.18 (dd, *J*=9.76, 6.63 Hz, 0.5 H) 4.25 - 4.34 (m, 1 H) 4.40 (dd, *J*=9.56, 3.71 Hz, 0.5 H) ppm ^{13}C NMR (100.61 MHz, $CDCl_3$) δ = 14.4 (d, *J*=6.4 Hz) 56.4 (d, *J*=19.1 Hz) 85.6 (d, *J*=174.5Hz) ppm ^{19}F NMR (376.5 MHz, $CDCl_3$) δ = -223.5 ppm

((5aR,6S,6aS)-1-(2-fluoroethyl)-1,4,5,5a,6,6a,7,8-octahydrocyclopropa[5,6]cycloocta[1,2-d][1,2,3]triazol-6-yl)methanol, BCN-1-Conjugate (15)

BCN (1.7 eq., 23.2 mg, 0.155 mmol) and 1-Azido-2-fluoroethane (**1**, 1 eq., 8 mg, 0.09 mmol) were stirred in 2.2 ml acetonitrile for 4 hours. The solvent was removed and volatiles removed on the rotary evaporator. The residue was dissolved in 1ml DCM and loaded onto 8 g of silica that were eluted with 20-100% ethyl acetate in light petroleum. The product (Rf = 0.15 in EE) was obtained in

85% yield. ^{1}H NMR (400 MHz, $CDCl_3$) δ = 0.97 - 1.12 (m, 2 H) 1.16 - 1.28 (m, 1 H) 1.50 - 1.65 (m, 2 H) 1.76 (br. s, 1 H) 2.20 - 2.34 (m, 2 H) 2.66 - 2.78 (m, 1 H) 2.85 - 3.02 (m, 2 H) 3.08 - 3.20 (m, 1 H) 3.73 (qd, *J*=11.40, 7.87 Hz, 2 H) 4.55 (dt, *J*=25.61, 4.80 Hz, 2 H) 4.78 (dt, *J*=46.84, 4.80 Hz, 2 H) ppm ^{13}C NMR (100.61 MHz, $CDCl_3$) δ = 19.4, 19.9, 21.3, 22.2, 22.6, 23.0, 23.03, 25.9, 48.1 (d, *J*=20.7 Hz), 59.8, 82.3 (d, *J*=173.3 Hz), 134.5, 144.6 ppm. LC/MS data see SI. ESI-MS: $[M+H]^+$ calcd. for $C_{12}H_{19}FN_3O^+$: 240.2 found: 240.5

((5aR,6S,6aS)-1-(2-fluoropropyl)-1,4,5,5a,6,6a,7,8-octahydrocyclopropa[5,6]cycloocta[1,2-d][1,2,3]triazol-6-yl)methanol, BCN-4-Conjugate (16)

BCN (1 eq., 25 mg, 0.160 mmol) and 1-Azido-1-fluoropropane (**4**, 1.04 eq., 17.1 mg, 0.166 mmol) were stirred in 150 µl DMF overnight. The reaction mixture was diluted with 1 ml water and 1 ml DMSO and loaded onto 30 g C18-SiO_2, which was eluted with 5-85% acetonitrile in water. The product containing fractions were combined and lyophilized to obtain 35 mg (83% of theory) of inseperable diastereomers as a colorless oil. ^{1}H NMR (600 MHz, $CDCl_3$) δ = 0.95 - 1.10 (m, 2 H) 1.16 - 1.24 (m, 1 H) 1.54 - 1.65 (m, 5 H) 2.21 - 2.31 (m, 2 H) 2.64 - 2.77 (m, 1 H) 2.87 - 3.00 (m, 2 H) 3.12 (dddd, *J*=15.74, 11.77, 7.85, 3.96 Hz, 1 H) 3.67 - 3.79 (m, 2 H) 4.61 - 4.83 (m, 3 H) ppm ^{13}C NMR (150.91 MHz, $CDCl_3$) δ = 16.06 (d, *J*=6.54 Hz), 16.1 (d, *J*=6.54 Hz), 16.2 (d, *J*=6.54 Hz),19.1, 19.2, 19.4, 19.9, 21.0, 21.2, 22.0, 22.2, 22.4, 22.7, 22.75, 23.1, 53.5, 53.6, 59.7, 59.8, 85.3 (d, *J*=175.48 Hz), 85.34 (d, *J*=175.48 Hz), 133.7, 133.9, 144.3, 144.4 ppm ^{19}F NMR (376.5 MHz, $CDCl_3$) δ = -218.9, -219.0 ppm. LC/MS data see SI. ESI-MS: $[M+H]^+$ calcd. for $C_{13}H_{21}FN_3O^+$: 254.2 found: 254.2

((5aR,6S,6aS)-1-(2-fluoro-2-methylpropyl)-1,4,5,5a,6,6a,7,8-octahydrocyclopropa[5,6]cycloocta[1,2-d][1,2,3]triazol-6-yl)methanol, BCN-5-Conjugate (17)

A mixture of 1-fluoro-2-methylpropan-2-amine hydrochloride (**14**, 1 eq., 340 mg, 2.66 mmol), potassium carbonate (2.2 eq., 808 mg, 5.8 mmol) and copper(II)sulphate pentahydrate (0.01 eq., 7 mg, 30 µmol) in 5 ml MeOH was treated with imidazol-1-sulfonyl azide hydrochloride (1.2 eq., 670 mg, 3.2 mmol) in one portion. The reaction mixture was stirred at room temperature overnight, diluted with 30 ml brine and extracted two times with ethyl acetate. Pooled extracts were washed with 2N HCl and brine and dried over $MgSO_4$. Following filtration an aliquot of the EE solution containing **5** was treated with BCN (30 mg, 200 µmol) and stirred for three hours at room temperature. Evaporation to dryness followed by column chromatography (60-100% EE in PE) afforded 35.8 mg **17** as white solid (68% of theory based on BCN). TLC-Rf (EE) = 0.17, ^{1}H NMR (400 MHz, $CDCl_3$) δ = 0.84 - 0.99 (m, 2 H) 1.07 - 1.18 (m, 1 H) 1.40 - 1.55 (m, 2 H) 1.67 (d, *J*=1.95 Hz, 6 H) 2.14 - 2.28 (m, 2 H) 2.75 - 2.88 (m, 2 H) 2.91 - 3.00 (m, 1 H) 3.05 - 3.14 (m, 1 H) 3.57 - 3.64 (m, 1 H) 3.65 - 3.71 (m, 1 H) 4.67 (d, *J*=47.61 Hz, 2 H) ppm ^{13}C NMR (100.61 MHz, $CDCl_3$) δ = 19.0, 19.7, 21.5, 23.6 (d, J = 2.83 Hz), 24.4 (d, J = 3.53 Hz), 25.3, 59.7, 62.1 (d, J = 19.78 Hz), 88.0 (d, J = 178.73 Hz), 134.0, 146.8 ppm, ^{19}F NMR (376.5 MHz, $CDCl_3$) δ = -221.46 ppm LC/MS data see SI. ESI-MS: $[M+H]^+$ calcd. for $C_{14}H_{23}FN_3O^+$: 268.2 found: 268.0

(S)-N-((S)-1-(((S)-1-amino-1-oxo-3-phenylpropan-2-yl)amino)-3-(1H-indol-3-yl)-1-oxopropan-2-yl)-1-((3-(prop-2-yn-1-yloxy)propanoyl)-D-tyrosyl)pyrrolidine-2-carboxamide, Propargyl-EM-1 (18)

25 mg endomorphin-1 (1 eq., 25 mg, 41 µmol) was dissolved in 1.2 ml DMSO:DMF = 1:1 (v/v) and triethylamine (5 eq., 28 µl, 205 µmol) was added. 2,5-Dioxopyrrolidin-1-yl 3-(prop-2-ynyloxy)propanoate (1.5 eq., 13.8 mg, 61 µmol) in 280 µl DMF was added in one portion, and the reaction mixture was stirred at 4°C overnight. LC/MS indicated quantitative transformation. The reaction mixture was diluted with 2 ml 0.1% TFA in water, loaded onto a preparative HPLC column (Phenomenex Luna C18, 21.2x250 mm, 10 µm) and eluted using a gradient of 10-90% acetonitrile + 0.1% TFA (v/v) in water. The product containing fraction was lyophilized to obtain **18** as yellow oil (42% of theory, 12.4 mg). ^{1}H NMR (600 MHz) and ^{13}C-NMR (150.91MHz) data see ESI. LC/MS data see ESI. ESI-MS: $[M-H]^-$ m/z calcd. for $C_{40}H_{43}N_6O_7^-$: 719.3 found: 719.8

(S)-N-((S)-1-(((S)-1-amino-1-oxo-3-phenylpropan-2-yl)amino)-3-(1H-indol-3-yl)-1-oxopropan-2-yl)-1-((3-((1-(2-fluoroethyl)-1H-1,2,3-triazol-4-yl)methoxy)propanoyl)-D-tyrosyl)pyrrolidine-2-carboxamide, EM-1-1 Conjugate (19)

Copper(II)sulfate pentahydrate (0.92 eq., 560 µg, 2.24 µmol) was mixed with sodium ascorbate (3.1 eq., 1500 µg, 7.6 µmol) in 10 µl water. After the mixture turned from black to yellow bathophenanthrolinedisulfonic acid disodium salt (0.76 eq., 1 mg, 1.86 µmol) in 20 µl water was added causing dark green coloration. The catalyst mixture was added to a solution of propargyl-endomoprphin-1 **18** (1 eq., 2 mg, 2.44 µmol) and **1** (10 eq., 2.17 mg, 24.4 µmol) in 220 µl DMF. The mixture was stirred for 2 hours at room temperature and kept at 4°C overnight. The reaction was quenched by addition of 500 µl 1% TFA in water, and loaded onto a preparative HPLC column (Phenomenex Luna C18(2), 10x250 mm, 10 µm). The column was eluted with a gradient of 10% to 90% acetonitrile in H_2O (+ 0.1% v/v TFA). The product containing fraction was lyophilized to obtain **19** as a white solid. A meaningful yield could not be determined due to the scale of the reaction. ^{19}F NMR (376.5 MHz, DMSO-*d6*) δ = -73.6 (residual TFA), -222.1 ppm**.** LC/MS data see ESI. ESI-MS: $[M-H]^-$ m/z calcd. for $C_{42}H_{47}FN_9O_7^-$: 808.4 found: 808.8

(S)-N-((S)-1-(((S)-1-amino-1-oxo-3-phenylpropan-2-yl)amino)-3-(1H-indol-3-yl)-1-oxopropan-2-yl)-1-((3-((1-(3-fluoropropyl)-1H-1,2,3-triazol-4-yl)methoxy)propanoyl)-D-tyrosyl)pyrrolidine-2-carboxamide, EM-1-2 Conjugate (20)

$CuSO_4$ pentahydrate (0.92 eq., 560 µg, 2.24 µmol) was mixed with sodium ascorbate (3.1 eq., 1500 µg, 7.6 µmol) in 10 µl water. After the mixture turned from black to yellow bathophenanthrolinedisulfonic acid disodium salt (0.76 eq., 1 mg, 1.86 µmol) in 20 µl water was added causing dark green coloration. The catalyst mixture was added to a solution of propargyl-endomoprphin-1 **18** (1 eq., 2 mg, 2.44 µmol) and **3** (10 eq., 2.5 mg, 24.4 µmol) in 200 µl DMF. The mixture was stirred for 2 hours at room temperature and kept at 4°C overnight. The reaction was quenched by addition of 500 µl 1% TFA in water, and loaded onto a preparative HPLC column (Phenomenex Luna C18(2), 10x250 mm, 10 µm). The column was eluted with a gradient of 10% to 90% acetonitrile in H_2O (+ 0.1% v/v TFA). The product containing fraction was lyophilized to obtain **20** as a white solid. A meaningful yield could not be determined due to the scale of the reaction. ^{19}F NMR (376.5 MHz, DMSO-*d6*) δ = -73.8 (residual TFA), -220.4 ppm LC/MS data see ESI. ESI-MS: $[M-H]^-$ m/z calcd. for $C_{43}H_{49}FN_9O_7^-$: 822.4 found: 822.8

(2S)-N-((S)-1-(((S)-1-amino-1-oxo-3-phenylpropan-2-yl)amino)-3-(1H-indol-3-yl)-1-oxopropan-2-yl)-1-((3-((1-(1-fluoropropan-2-yl)-1H-1,2,3-triazol-4-yl)methoxy)propanoyl)-D-tyrosyl)pyrrolidine-2-carboxamide, EM-1-3 Conjugate (21)

$CuSO_4$ pentahydrate (0.92 eq., 560 µg, 2.24 µmol) was mixed with sodium ascorbate (3.1 eq., 1500 µg, 7.6 µmol) in 10 µl water. After the mixture turned from black to yellow bathophenanthrolinedisulfonic acid disodium salt (0.76 eq., 1 mg, 1.86 µmol) in 20 µl water was added causing dark green coloration. The catalyst mixture was added to a solution of propargyl-endomoprphin-1 **18** (1 eq., 2 mg, 2.44 µmol) and **4** (10 eq., 22 µl C= 1.1 mmol/g in DMF, 24.4 µmol) in 200 µl DMF. The mixture was stirred for 4 hours at room temperature and kept at 4°C overnight. The reaction was quenched by addition of 500 µl 1% TFA in water, and loaded onto a preparative HPLC column (Phenomenex Luna C18(2), 10x250 mm, 10 µm). The column was eluted with a gradient of 10% to 90% acetonitrile in H_2O (+ 0.1% v/v TFA). The product containing fraction was lyophilized to obtain **16** as a white solid. A meaningful yield could not be determined due to the scale of the reaction. C/MS data see ESI. ESI-MS: $[M-H]^-$ m/z calcd. for $C_{43}H_{49}FN_9O_7^-$: 822.4 found: 822.8

Radiosynthesis of [^{18}F]**1**

A Sep-Pak Accell Plus QMA Plus Light Cartridge (Waters) was preconditioned with 0.5M K_2CO_3 solution (7 ml) followed by 15 ml water. Cyclotron produced ^{18}F-fluoride (836 MBq) in 2.5 ml water was passed over the cartridge, and the cartridge was eluted with a solution of 3.5 mg K_2CO_3 (25.3 µmol) and 14.1 mg [2.2.2]cryptand (37.5 µmol) in 1000 µl acetonitrile:H_2O = 9:1 (v/v). Volatiles were removed in a stream of argon at 105°C and residual water was removed by addition and subsequent evaporation of 700 µl anhydrous acetonitrile. The azeotropic drying step was repeated two times. 14.5 mg (53.2 µmol) of nosylate **2** in 500 µl dry acetonitrile was added, and the reaction mixture heated to 105°C for 5 min. Volatiles were distilled into 1 ml cooled (-20°C) acetonitrile in a slow stream of argon using a short polyethylene tubing with two attached needles. Two Sep-Pak AC2 Plus activated carbon cartridges (Waters) were connected in series to the outlet of the receiving vial as a safety measure. [^{18}F]**1** was obtained in 75.4% decay corrected yield. HPLC (Conditions A): [^{18}F]**1** has a retention time of 5.26 min. Radiochemical purity as determined by radio-HPLC exceeded 99%.

Conjugation of [^{18}F]**1** with BCN

300 µl of acetonitrile solution containing [^{18}F]**1** (126 MBq) was treated with cyclooctyne BCN (2 mg, 13.3 µmol), and the reaction mixture was stirred at room temperature. 108 minutes post cyclooctyne addition the reaction mixture was investigated by radio-HPLC (HPLC conditions A, 230 nm) to reveal 98.5% conversion to the ligation product [^{18}F]**15.** The retention time of [^{18}F]**15** (14.6 min) matched the retention time of **15**.

Radiosynthesis of [^{18}F]**3**

Cyclotron produced ^{18}F-fluoride (947 MBq) in 0.4 ml water was trapped on a PS-HCO_3^- (Cromafix) cartridge and was eluted with a solution of 1.75 mg K_2CO_3 (12.7 µmol) and 8.5 mg [2.2.2]cryptand (22.6 µmol) in 1000 µl acetonitrile:H_2O = 9:1 (v/v). Volatiles were removed in a stream of argon at 110°C and residual water was removed by addition and subsequent evaporation of 700 µl anhydrous acetonitrile. The azeotropic drying step was repeated twice. 7 mg (24.5 µmol) of nosylate **6** in 250 µl

dry acetonitrile was added, and the reaction mixture heated to 90°C for 8 min. Volatiles were distilled into 200 µl cooled (-20°C) acetonitrile in a slow stream of argon using a short polyethylene tubing with two attached needles. Two Sep-Pak AC2 Plus activated carbon cartridges were connected in series to the outlet of the receiving vial as a safety measure. [^{18}F]**3** was obtained in 39.3% decay corrected yield. HPLC conditions A (216 nm) were used, where [^{18}F]**3** has a retention time of 12.1 min that matched the retention time of reference compound **3**. Radiochemical purity exceeded 98%.

Radiosynthesis of [^{18}F]4

Cyclotron produced ^{18}F-fluoride (1.65 GBq) in 1.5 ml water was trapped on a PS-HCO_3^- (Cromafix) cartridge and was eluted with a solution of 3.5 mg K_2CO_3 (25.3 µmol) and 14.1 mg [2.2.2]cryptand (37.5 µmol) in 1000 µl acetonitrile:H_2O = 9:1 (v/v). Volatiles were removed in a stream of argon at 110°C and residual water was removed by addition and subsequent evaporation of 700 µl anhydrous acetonitrile. The azeotropic drying step was repeated twice. 14 mg (48.9 µmol) of nosylate **8** in 300 µl dry acetonitrile was added, and the reaction mixture heated to 100°C for 7 min. Volatiles were distilled into 200 µl cooled (-20°C) acetonitrile in a slow stream of argon using a short polyethylene tubing with two attached needles. Two Sep-Pak AC2 Plus activated carbon cartridges were connected in series to the outlet of the receiving vial as a safety measure. [^{18}F]**4** was obtained in 58.1% decay corrected yield. HPLC conditions A were used, where [^{18}F]**4** has a retention time of 11.8 min that matched the retention time of reference compound **4**. Radiochemical purity exceeded 99%.

Conjugation of [^{18}F]4 with cyclooctyne BCN

500 µl of acetonitrile solution containing [^{18}F]**4** (80 MBq) was treated with cyclooctyne BCN (0.5 mg, 3.3 µmol), and the reaction mixture was stirred at room temperature. The reaction was analyzed by radio-HPLC (HPLC Conditions A, 230 nm) 47 min and 134 min post cyclooctyne addition revealing 72% and 87% conversion to triazole [^{18}F]**16**. The retention time of [^{18}F]**16** (8.53 min) matched the retention time of reference compound **16**.

Synthesis of [^{18}F]19: Rapid radiolabeling of endomorphin-1 using [^{18}F]1

In a 1.5 ml tube $CuSO_4$ pentahydrate (1.2 mg, 4.48 µmol) was mixed with sodium ascorbate (3 mg, 15.2 µmol) in 20 µl water. After the mixture turned from black to yellow bathophenanthrolinedisulfonic acid disodium salt (2 mg, 3.72 µmol) in 40 µl water:DMF (4:1 v/v) was added causing dark green coloration. Propargylated endomorphin-1 **18** (1 mg, 2.22 µmol) in 100 µl DMF followed by [^{18}F]**1** (73 MBq) was added to the catalyst. Following homogenization the mixture was allowed to react for 10 min at room temperature followed by quenching with 500 µl 0.1% TFA in acetonitrile:H_2O = 1:1 (v/v). Radio-HPLC analysis (conditions B, 280 nm) revealed 65% yield of [^{18}F]-**19**. Using the same conditions with reduced catalyst amount (50%) afforded 63% incorporation yield. The retention time of [^{18}F]**19** (5.95 min) matched that of reference material **14**. (Chromatograms see ESI) A aliquot of purified [^{18}F]**19** (2.2 MBq) was collected from the analytical HPLC for stability testing in human blood plasma.

Synthesis of [^{18}F]20: Rapid radiolabeling of endomorphin-1 using [^{18}F]3

In a 1.5 ml tube $CuSO_4$ pentahydrate (1.2 mg, 4.48 µmol) was mixed with sodium ascorbate (3 mg, 15.2 µmol) in 20 µl water. After the mixture turned from black to yellow

bathophenanthrolinedisulfonic acid disodium salt (2 mg, 3.72 µmol) in 40 µl water:DMF (4:1 v/v) was added causing dark green coloration. Propargylated endomorphin-1 **18** (1 mg, 2.22 µmol) in 100 µl DMF followed by [^{18}F]**3** (37 MBq) was added to the catalyst. Following homogenization the mixture was allowed to react for 10 min at room temperature followed by quenching with 500 µl 0.1% TFA in acetonitrile:H_2O = 1:1 (v/v). Radio-HPLC analysis (conditions B, 280 nm) revealed 64% yield of [^{18}F]**20**. The retention time of [^{18}F]**20** (6.12 min) matched that of reference material **20.** (Chromatograms see ESI) A aliquot of purified [^{18}F]**20** (1.4 MBq) was collected from the analytical HPLC for stability testing in human blood plasma.

Synthesis of [^{18}F]21: Rapid radiolabeling of endomorphin-1 using [^{18}F]4

In a 1.5 ml tube $CuSO_4$ pentahydrate (1.2 mg, 4.48 µmol) was mixed with sodium ascorbate (3 mg, 15.2 µmol) in 20 µl water. After the mixture turned from black to yellow bathophenanthrolinedisulfonic acid disodium salt (2 mg, 3.72 µmol) in 40 µl water:DMF (4:1 v/v) was added causing dark green coloration. Propargylated endomorphin-1 **18** (1 mg, 2.22 µmol) in 100 µl DMF followed by [^{18}F]**4** (70.7 MBq) in 50 µl acetonitrile was added to the catalyst. Following homogenization the mixture was allowed to react for 10 min at room temperature followed by quenching with 500 µl 0.1% TFA in acetonitrile:H_2O = 1:1 (v/v). Radio-HPLC analysis (conditions B, 280 nm) revealed 98% yield of [^{18}F]**21**. The retention time of [^{18}F]**21** (6.08 min) matched that of reference material **16.** (Chromatograms see ESI) A aliquot of purified [^{18}F]**21** (1.8 MBq) was collected from the analytical HPLC for stability testing in human blood plasma.

Plasma stability of [^{18}F] endomorphin-1 conjugates [^{18}F]19, [^{18}F]20 and [^{18}F]21

100-150 kBq of [^{18}F]**19**, [^{18}F]**20** or [^{18}F]**21** were incubated in 500 µl human blood plasma at 37°C for 120 minutes. To assess plasma stability the solutions were spotted on reversed phase TLC plates. [^{18}F]**14**, [^{18}F]**15** and [^{18}F]**16** were spotted as reference. The plates were developed using acetonitrile:H_2O = 1:1 (v/v + 0.1vol% TFA) as mobile phase. Radioactivity was quantified using a Hewlett Packard Cyclone Phosphor Imager autoradiography system (see ESI). Analysis revealed 81% intact [^{18}F]**19,** 82% intact [^{18}F]**20** and 86% intact [^{18}F]**21.**

Synthesis of [^{18}F]1, [^{18}F]3 and [^{18}F]4 using a automated synthesis module (for *in vivo* study)

A remote controlled synthesis module (TRACERlab™ FXFDG, General Electric Healthcare, Uppsala, Sweden) with 3 mL glass reactor housed in a hot cell was used for automated labeling experiments. In general cyclotron produced no carrier added [^{18}F] fluoride was trapped on a preconditioned (5 ml 0.5 M K_2CO_3 followed by 15 ml water) Waters QMA light cartridge. The radioactivity was eluted with a solution of [2.2.2]cryptand (15 mg, 40 µmol) in acetonitrile (900 µl) to which a 3.5% aq. K_2CO_3 (100 µL, 25 µmol) solution had been added. After addition of dry acetonitrile (500 µL) volatiles were removed in vacuo at a temperature of 60-120 °C. After cooling to 60 °C a solution of precursor (12.5 mg, 46 µmol **2** for [^{18}F]**1**, 13.1 mg, 46 µmol **6** for [^{18}F]**3** and 13.7 mg, 48 µmol **8** for [^{18}F]**4**) in dry acetonitrile (650-700 µl) was added. The reaction mixture was heated to 100-105°C for 5 minutes followed by cooling to 35°C to prevent activity loss when venting the reactor. The reactor contents were loaded onto a preparative HPLC column (Macherey-Nagel EP 250/16 100-7 C-18, 10 µm, 16 x 250 mm) and eluted using a gradient of ethanol/water at a flow rate of 4 ml/min (0-10m 2% EtOH, 10m→50m 2%→30% EtOH for [^{18}F]**1**, 0-6m 3% EtOH, 6m→40m 3%→40% for [^{18}F]**3** and 0-10m 5%

EtOH, 10m→50m 5%→50% EtOH for [^{18}F]**4**. 9.9 GBq [^{18}F]**1** was obtained from 36.2 GBq starting activity (48% decay corrected radiochemical yield), 16.7 GBq [^{18}F]**3** was obtained from 117 GBq starting activity (23.5% decay corrected radiochemical yield) and 18.6 GBq [^{18}F]**4** was obtained from 122 GBq starting activity (27% decay corrected radiochemical yield). The products were diluted with physiological saline to a activity concentration of ~370 MBq/ml for iv administration. pH was between 5 and 7 for all formulations and osmolarity was within physiological range (300-500 mmol/kg). ^{18}F-species prepared by automated labeling matched HPLC retention times of authentic standards.

PET/MR Imaging – Biodistribution study

Mice underwent PET scanning on a dual animal bed in a dedicated small-animal PET scanner (n=4 for [^{18}F]**1**, n= 2 for [^{18}F]**3** and [^{18}F]**4**) and one mouse per test substance underwent sequential PET/MRI on two stand-alone scanners. Prior imaging, mice were pre-anesthetized in an induction chamber using isoflurane (2.5% in oxygen), placed in prone position on a heated animal bed (38°C) and the lateral tail vein was cannulated using a custom made tail vein catheter. Animal respiratory rate and body temperature were constantly monitored (SA Instruments Inc, Stony Brook, NY, USA) and the isoflurane level was adjusted (1.5-2.5% on oxygen) to achieve a constant depth of anesthesia. Anesthesia was maintained for the whole imaging period. A humidifier was used to moisten the gas mixture before supplying it to the animal(s). For anatomical magnetic resonance imaging (MRI) a single mouse body bed mounted with a mouse whole body RF coil was used. The whole body coil covers an axial field of view (FOV) of about 8 cm that is very similar to the axial FOV of the PET scanner (7.6 cm). Images were acquired on a 1 Tesla benchtop MRI (ICON, Bruker Biospin GmbH, Ettlingen, Germany) using a modified 3D T_1-weighted gradient echo sequence (T1-FLASH) with the following imaging parameters: echo time (TE) = 4.7 ms; repetition time (TR) = 25 ms; flip angle (FA) = 25 °; field of view (FOV) = 7.6 x 2.6 x 2.4 cm; matrix = 253 x 93; 32 slices; slice thickness = 750 µm; 5 repetitions; total imaging time = 6 min 15 sec. After MRI, the animal bed was transferred into the gantry of a microPET scanner (Focus 220, Siemens Medical Solutions, Knoxville, TN, USA). Total anesthesia time prior start of PET scanning for mice that underwent PET scanning only was similar to that of the PET/MRI examined animal. Direct after positioning of the animal bed in the gantry of the PET scanner a 10 min transmission scan using a rotating ^{57}Co point source was recorded. Simultaneously with intravenous injection of 6.1 ± 0.9 MBq [^{18}F]-**1**, 4.7 ± 0.2 MBq [^{18}F]-**3** or 6.5 ± 0.6 MBq [^{18}F]-**4** dynamic PET imaging was initiated for 120 min using an energy window of 250-750 keV and a timing window of 6 ns. After completion of the imaging procedure, a terminal blood sample was withdrawn under isoflurane anesthesia from the retro-orbital sinus vein and the animals were sacrificed by cervical dislocation. Blood was centrifuged (17000 *g*, 4°C, 4 min) to obtain plasma, and organ samples as well as urine were collected. Aliquots of blood, plasma and urine as well as organ samples were transferred into pre-weighted tubes and measured for radioactivity in a gamma counter (Wizard 1470, Perkin-Elmer, Wellesley, MA, USA). The measured radioactivity data were corrected for radioactive decay and expressed as standardized uptake value ((radioactivity per g/injected radioactivity) x body weight). The 60 min dynamic emission PET data were sorted into 26 frames, which incrementally increased in time length from 5 seconds to 20 min. Images were reconstructed using Fourier rebinning of the 3D sonograms followed by two-dimensional filtered back projection with a ramp filter, resulting in an image voxel size of 0.4 x 0.4 x 0.796 mm^3. A standard data correction protocol (normalization, attenuation and decay correction) was applied to the PET data. The PET units were converted into units of radioactivity concentration by applying a

calibration factor derived from imaging of a cylindrical phantom with a known ^{18}F-radioactivity concentration. Corresponding PET/MRI images were aligned using a pre-calculated, fixed transformation matrix. Using the image analysis software Amide,[25] different volumes of interest (brain, liver, kidneys, urinary bladder, heart, bone (left humerus), muscle (right lower arm muscle)) were manually outlined on multiple planes and time-radioactivity concentration curves (TACs), expressed in standardized uptake values, were derived.

Analysis of murine metabolites – *in vivo* stability of small [^{18}F]-fluoroalkylazides

Blood and urine samples harvested directly after imaging experiments (120 min post administration) were used for metabolite studies. Murine plasma was obtained by centrifugation(17000 *g*, 4°C, 4 min), and plasma proteins were precipitated by addition of a equal volume acetonitrile and removed by centrifugation (17000 *g*, 4°C, 1 min). Supernatant solution was diluted with water and injected into a HPLC system using a lead shielded Berthold LB 507B radioactivity detector. [^{18}F]**1**, [^{18}F]**3** and [^{18}F]**4** were injected as reference materials. Urine was directly injected after dilution with water (1:10 v/v). Analysis revealed < 2% intact [^{18}F]**1**, < 3% intact [^{18}F]**3** and < 4% intact [^{18}F]**4** in plasma while the fraction of unchanged tracers was < 1% in urine for all test substances. The majority of activity (>90%) was detected as highly polar metabolites proofing the metabolic instability of the test substances.

References

(1) Evans, H. L., Slade, R. L., Carroll, L., Smith, G., Nguyen, Q.-D., Iddon, L., Kamaly, N. N., Stöckmann, H., Leeper, F. J., Aboagye, E. O., Spivey, A. C., and Aboagye, O. (2012) Copper-free click--a promising tool for pre-targeted PET imaging. *Chem. Commun. (Camb). 48*, 991–3.

(2) Glaser, M., and Arstad, E. (2007) "Click labeling" with 2-[F-18]fluoroethylazide for positron emission tomography. *Bioconjug. Chem. 18*, 989–993.

(3) Zhou, D., Chu, W., Dence, C. S., Mach, R. H., and Welch, M. J. (2012) Highly efficient click labeling using 2-[18F]fluoroethyl azide and synthesis of an 18FN-hydroxysuccinimide ester as conjugation agent. *Nucl. Med. Biol. 39*, 1175–1181.

(4) Bejot, R., Carroll, L., Bhakoo, K., Declerck, J., and Gouverneur, V. (2012) A fluorous and click approach for screening potential PET probes: Evaluation of potential hypoxia biomarkers. *Bioorganic Med. Chem. 20*, 324–329.

(5) Glaser, M., Solbakken, M., Turton, D. R., Pettitt, R., Barnett, J., Arukwe, J., Karlsen, H., Cuthbertson, A., Luthra, S. K., and Årstad, E. (2009) Methods for 18F-labeling of RGD peptides: Comparison of aminooxy [18F]fluorobenzaldehyde condensation with "click labeling" using 2-[18F]fluoroethylazide, and S-alkylation with [18F] fluoropropanethiol. *Amino Acids 37*, 717–724.

(6) Jia, L., Cheng, Z., Shi, L., Li, J., Wang, C., Jiang, D., Zhou, W., Meng, H., Qi, Y., Cheng, D., and Zhang, L. (2013) Fluorine-18 labeling by click chemistry: Multiple probes in one pot. *Appl. Radiat. Isot. 75*, 64–70.

(7) Iddon, L., Leyton, J., Indrevoll, B., Glaser, M., Robins, E. G., George, A. J. T., Cuthbertson, A., Luthra, S. K., and Aboagye, E. O. (2011) Synthesis and in vitro evaluation of [18F]fluoroethyl triazole labelled [Tyr3]octreotate analogues using click chemistry. *Bioorganic Med. Chem. Lett. 21*, 3122–3127.

(8) Kettenbach, K., Schieferstein, H., Ross, T. L., Kettenbach, K., Schieferstein, H., and Ross, T. L. (2014) 18F-Labeling Using Click Cycloadditions. *Biomed Res. Int. 2014*, 1–16.

(9) Lee, S. B., Kim, H. L., Jeong, H.-J., Lim, S. T., Sohn, M.-H., and Kim, D. W. (2013) Mesoporous Silica Nanoparticle Pretargeting for PET Imaging Based on a Rapid Bioorthogonal Reaction in a Living Body. *Angew. Chemie Int. Ed. 52*, 10549–10552.

(10) Prescher, J. A., and Bertozzi, C. R. (2005) Chemistry in living systems. *Nat. Chem. Biol. 1*, 13–21.

(11) Sletten, E. M., and Bertozzi, C. R. (2009) Bioorthogonal chemistry: fishing for selectivity in a sea of functionality. *Angew. Chem. Int. Ed. Engl. 48*, 6974–98.

(12) Baskin, J. M., Prescher, J. A., Laughlin, S. T., Agard, N. J., Chang, P. V, Miller, I. A., Lo, A., Codelli, J. A., and Bertozzi, C. R. (2007) Copper-free click chemistry for dynamic in vivo imaging. *Proc. Natl. Acad. Sci. U. S. A. 104*, 16793–7.

(13) Plass, T., Milles, S., Koehler, C., Schultz, C., and Lemke, E. A. (2011) Genetically Encoded Copper-Free Click Chemistry. *Angew. Chemie Int. Ed. 50*, 3878–3881.

(14) Pretze, M., Pietzsch, D., and Mamat, C. (2013) Recent trends in bioorthogonal click-radiolabeling reactions using fluorine-18. *Molecules 18*, 8618–8665.

(15) Kobus, D., Giesen, Y., Ullrich, R., Backes, H., and Neumaier, B. (2009) A fully automated two-step synthesis of an 18F-labelled tyrosine kinase inhibitor for EGFR kinase activity imaging in tumors. *Appl. Radiat. Isot. 67*, 1977–1984.

(16) Goddard-Borger, E. D., and Stick, R. V. (2007) An Efficient, Inexpensive, and Shelf-Stable Diazotransfer Reagent: Imidazole-1-sulfonyl Azide Hydrochloride. *Org. Lett. 9*, 3797–3800.

(17) Goddard-Borger, E. D., and Stick, R. V. (2011) An Efficient, Inexpensive, and Shelf-Stable Diazotransfer Reagent: Imidazole-1-sulfonyl Azide Hydrochloride. *Org. Lett. 13*, 2514–2514.

(18) Li, J., Shi, L., Jia, L., Jiang, D., Zhou, W., Hu, W., Qi, Y., and Zhang, L. (2012) Radiolabeling of RGD peptide and preliminary biological evaluation in mice bearing U87MG tumors. *Bioorg. Med. Chem. 20*, 3850–3855.

(19) HOFFMANN, F. W. (1949) ALIPHATIC FLUORIDES. I. w,w´-DIFLUOROALKANES. *J. Org. Chem. 14*, 105–110.

(20) Jean-Damien, C., Haley, M., and Binch, D. (2011) Compounds useful as inhibitors of atr kinase.

(21) Ok, D., Fisher, M. H., Wyvratt, M. J., and Meinke, P. T. (1999) Improved syntheses of fluorinated tertiary butylamines. *Tetrahedron Lett. 40*, 3831–3834.

(22) Dommerholt, J., Schmidt, S., Temming, R., Hendriks, L. J. A., Rutjes, F. P. J. T., Van Hest, J. C. M., Lefeber, D. J., Friedl, P., and Van Delft, F. L. (2010) Readily accessible bicyclononynes for bioorthogonal labeling and three-dimensional imaging of living cells. *Angew. Chemie - Int. Ed. 49*, 9422–9425.

(23) Gaeta, A., Woodcraft, J., Plant, S., Goggi, J., Jones, P., Battle, M., Trigg, W., Luthra, S. K., and Glaser, M. (2010) Use of 2-[(18)F]fluoroethylazide for the Staudinger ligation - Preparation and characterisation of GABA(A) receptor binding 4-quinolones. *Bioorg. Med. Chem. Lett. 20*, 4649–52.

(24) Horvath, G. (2000) Endomorphin-1 and endomorphin-2: pharmacology of the selective endogenous mu-opioid receptor agonists. *Pharmacol. Ther. 88*, 437–63.

(25) Loening, A. M., and Gambhir, S. S. (2003) AMIDE: A Free Software Tool for Multimodality Medical Image Analysis. *Mol. Imaging 2*, 131–137.

3. Conclusion

In summary, manifold contributions to the field of bioorthogonal PET imaging were delivered within this thesis, thus extending the toolbox of available radiolabeled agents for rapid radiolabeling and pretargeting applications (Figure C1).

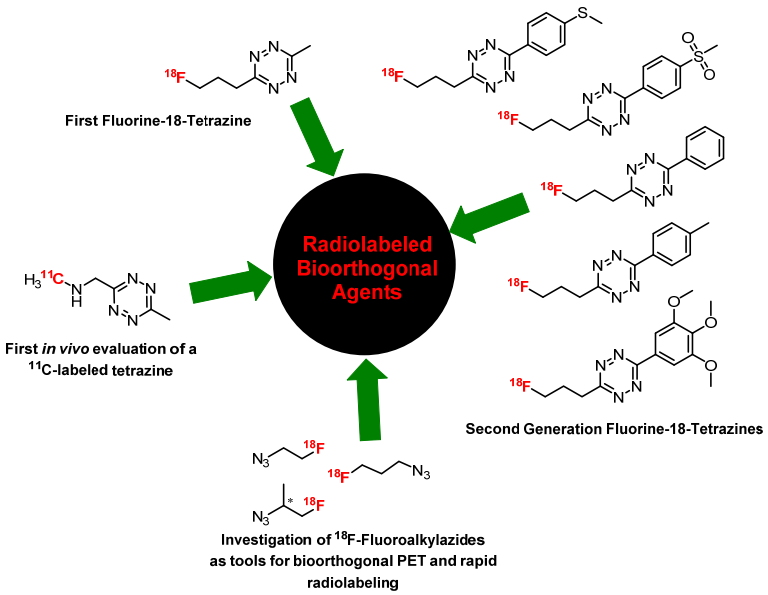


Figure C1: *Radiolabeled bioorthogonal agents developed and evaluated within this thesis*

The first tetrazine labeled with the short-lived positron emitter fluorine-18 (3-(3-[^{18}F]fluoropropyl)-6-methyl-1,2,4,5-tetrazine) was prepared in good (up to 35%) isolated radiochemical yields. The substance was evaluated *in vivo* using PET/MR scanning in naïve mice, revealing excellent biodistribution pattern (Figure C2), and high metabolic stability. Furthermore, bioorthogonality was demonstrated by fast and quantitative reaction with the dienophile s-TCO within the bloodstream of live mice. In summary, this agent that is based on a low-molecular-weight dialkyltetrazine scaffold exhibits decreased cycloaddition reactivity but possesses high stability, making this compound accessible by direct labeling. This radiofluorinated tetrazine shows highly promising properties to be used as secondary agent in bioorthogonal PET imaging.

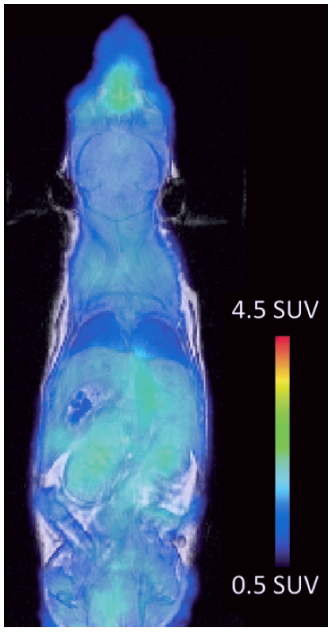


Figure C2: *Biodistribution of the first Fluorine-18-labeled 1,2,4,5-Tetrazine (5-120 min, coronal PET/MR summation image)*

Furthermore, these findings were fetched into the development of a tetrazine agent labeled with carbon-11. The compound *N*-[^{11}C]methyl-1-(6-methyl-1,2,4,5-tetrazin-3-yl)methanamine was prepared in good radiochemical yields (52% decay corrected). In addition to promising pharmacokinetic properties observed in the *in vivo* study (PET/MR and metabolite analysis), the compound was successfully applied in the first pretargeted imaging experiment utilizing a carbon-11 labeled bioorthogonal agent.

Additionally, a series of eight aryl-alkyl tetrazines, based on the 3-(3-fluoropropyl) moiety was designed, aiming for improved cycloaddition reactivity, while retaining beneficial pharmacological properties. In short, four novel radiofluorinated alkyl-aryl tetrazines were prepared by nucleophilic ^{18}F-fluorination in good (up to 56%) radiochemical yields. The methylsulfide bearing compound 3-(3-[^{18}F]fluoropropyl)-6-(4-(methylthio)phenyl)-1,2,4,5-tetrazine was shown by PET/MR to show homogenous biodistribution (Figure C3r). Metabolite studies further revealed that the compound is rapidly oxidized to its sulfoxide and sulfone metabolites *in vivo*, thus acting as a pro-drug for ^{18}F-tetrazines with elevated IEDDA reactivity, as compared to the parent compound (Figure C3l).

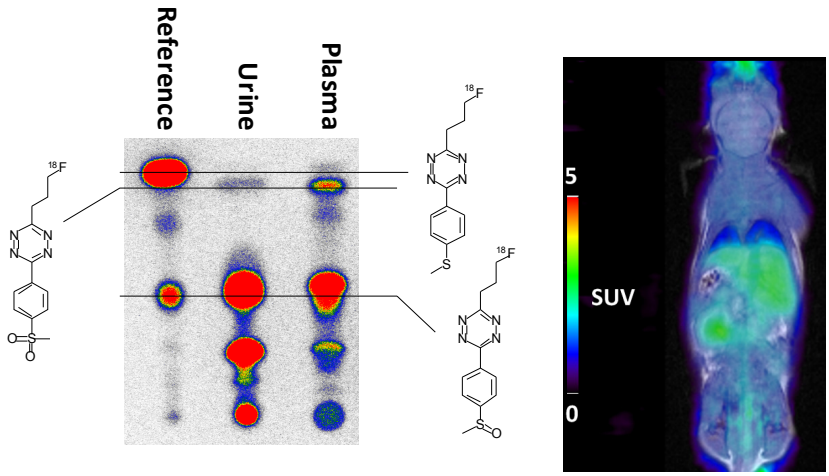


Figure C3: *left: Radio-TLC showing radio-metabolites* right: coronal PET/MR summation images (5-120 min) of 3-(3-[^{18}F]fluoropropyl)-6- (4-(methylthio)phenyl)-1,2,4,5-tetrazine,

Furthermore, methylsulfone tetrazine 3-(3-[^{18}F]fluoropropyl)-6-(4-(methylsulfonyl)phenyl)-1,2,4,5-tetrazine was prepared by DMDO mediated post-labeling oxidation of the appropriate methylsulfide. In addition to homogenous biodistribution this compound also exhibits excellent metabolic stability.

Although focus of this work was directed towards reactants for the IEDDA reaction, a series of low-molecular-weight ^{18}F-fluoroalkylazides was also investigated. The compounds, that were prepared in high yields exhibited excellent properties as prosthetic group for rapid radiolabeling, but did not possess sufficient metabolic stability to be applicable as pull down reagent in pretargeted imaging.

4. Statement of Contribution

Manuscript #1

The lead structure of manuscript #1 was proposed by the applicant (C. Denk). The main part of the synthetic work within this manuscript was conducted by the applicant. During this PhD thesis (radio)synthetic procedures were improved, and the radiosynthesis was transferred onto a automated synthesizer module for production of high activities. The applicant participated in planning and execution of all *in vivo* experiments. Computational predictions were carried out and interpreted by Dennis Svatunek. PET data was evaluated by Claudia Kuntner and Thomas Wanek. The data was assembled and the manuscript was written by Hannes Mikula and the applicant. All authors contributed to the manuscript discussion and correction.

Manuscript #2

The lead structure of manuscript #2 was proposed by the applicant (C. Denk). The major part of synthetic work within this manuscript was conducted by the applicant. All radiolabeling procedured in the manuscript were planned and conducted by the applicant with aid from Severin Mairinger and Johann Stanek. The applicant participated in planning and execution of all *in vivo* experiments. Computational predictions as well as stopped flow measurements were carried out and interpreted by Dennis Svatunek. PET data was evaluated by Claudia Kuntner and Thomas Wanek. The data was assembled and the manuscript was written by the applicant. All authors contributed to the manuscript discussion and correction.

Manuscript #3

The lead structures of manuscript #3 were proposed by the applicant (C. Denk). The main part of the synthetic work within this manuscript was conducted by the applicant. All radiolabeling procedured in the manuscript were planned and conducted by the applicant. Furthermore, the applicant participated in planning and execution of all *in vivo* experiments. Computational predictions as well as stopped flow kinetic measurements were carried out and interpreted by Dennis Svatunek. PET data was evaluated by Claudia Kuntner, Michael Sauberer and Thomas Wanek. The data was assembled and the manuscript was written by the applicant. All authors contributed to the manuscript discussion and correction.

Manuscript #4

The photoreactor described in manuscript #4 was designed by the applicant (C. Denk) and was built with support from Veronika Rosecker (during her optional organic chemistry lab course, supervised by C.Denk). Dennis Svatunek, Barbara Sohr and the applicant contributed synthetic work to this project. The introduction of manuscript #4 was written by the applicant. Data was assembled and the manuscript was written by Dennis Svatunek. All authors contributed to the manuscript discussion and correction.

Manuscript #5

All radiochemical procedures in manuscript #5 were planned and conducted by the applicant (C. Denk). Synthetic work within this project was mainly conducted by the applicant. Substances **7**-**10** were synthesized by Martin Wilkovitsch (during his bachelor thesis, co-supervised by the applicant). The structure of **4** was proposed by Dennis Svatunek, the structure of **5** was proposed by Philipp Skrinjar. Furthermore, the applicant participated in planning and execution of all *in vivo* experiments. PET data was evaluated by Claudia Kuntner, Michael Sauberer and Thomas Wanek. The data was assembled and the manuscript was written by the applicant. All authors contributed to the manuscript discussion and correction.

5. Appendix

Manuscript #1 – Supporting Information

Reprinted from *Angewandte Chemie International Edition* (2014), 53, 9655-9659 with kind permission from Wiley and Sons.

Denk, C.; Svatunek, D.; Filip, T.; Wanek, T.; Lumpi, D.; Fröhlich, J.; Kuntner-Hannes, C.; Mikula, H.:

Development of a ^{18}F-labeled Tetrazine with Favorable Pharmacokinetics for Bioorthogonal PET Imaging

Angewandte Chemie
Eine Zeitschrift der Gesellschaft Deutscher Chemiker

Supporting Information

© Wiley-VCH 2014

69451 Weinheim, Germany

Development of a ^{18}F-Labeled Tetrazine with Favorable Pharmacokinetics for Bioorthogonal PET Imaging**

Christoph Denk, Dennis Svatunek, Thomas Filip, Thomas Wanek, Daniel Lumpi, Johannes Fröhlich, Claudia Kuntner, and Hannes Mikula**

anie_201404277_sm_miscellaneous_information.pdf

Supporting Information

Table of Contents

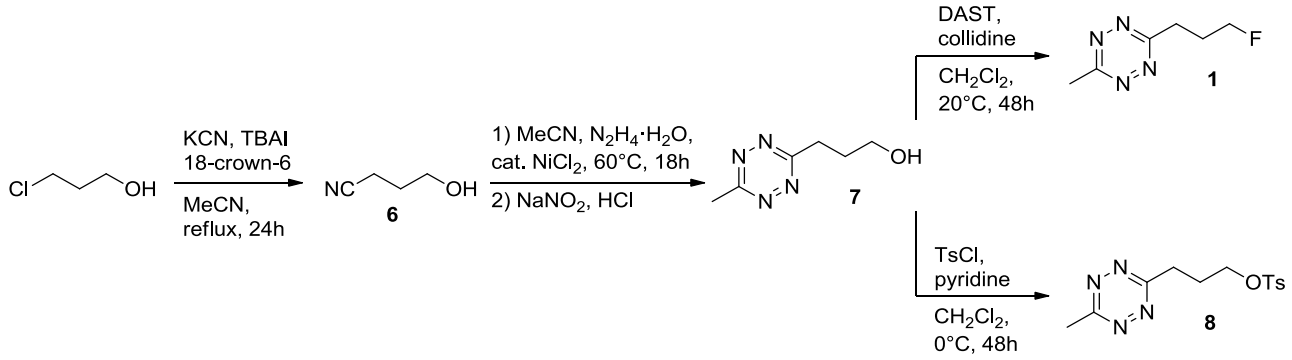
1.	Materials and Methods	S1
2.	Chemical Synthesis and Radiochemistry	S2
3.	Reaction kinetics	S6
4.	In vitro and in vivo investigations	S8
5.	NMR Spectra	S10
6.	Quantum Chemical Calculations	S12
7.	References	S27

1. Materials and Methods

Unless otherwise noted, all reagents were purchased from commercial suppliers and used without further purification. DCM and 1,4-dioxane were dried using PURESOLV-columns (Innovative Technology Inc.). Dry acetonitrile (Sigma Aldrich) and dry DMF (Acros) were commercially obtained and stored under argon. Tetrazine **2**[1], trans-cyclooctene (**3**)[2] and s-TCO **4**[3] were prepared following known procedures. Anhydrous hydrazine was prepared by the vacuum thermolysis of hydrazine cyanurate.[4] All other solvents were distilled prior to use. Drying of organic solvents after extraction was performed using anhydrous Na_2SO_4 or $MgSO_4$ (Sigma Aldrich) and subsequent filtration. Human Plasma for research purposes was purchased from the Austrian Red Cross blood donation service. Reactions were carried out under an atmosphere of argon in air-dried glassware with magnetic stirring. Sensitive liquids were transferred via syringe. Thin layer chromatography was performed using TLC alumina plates (Merck, silica gel 60, fluorescence indicator F254, or Merck, aluminium oxide neutral, fluorescence indicator F254). Preparative column chromatography was performed using a Büchi Sepacore Flash System (2 x Büchi Pump Module C-605, Büchi Pump Manager C-615, Büchi UV Photometer C-635, Büchi Fraction Collector C-660) using silica gel 60 (40-63 µm) as obtained from Merck and distilled or redistilled solvents. ^1H, ^{13}C and ^{19}F NMR spectra were recorded on a Bruker AC 200 or Bruker Avance UltraShield 400 spectrometer at 20 °C. Chemical shifts are reported in ppm (δ) relative to tetramethylsilane and calibrated using solvent residual peaks. Data are shown as follows: Chemical shift, multiplicity (s = singlet, d = doublet, t = triplet, q = quartet, quin = quintet, m = multiplet, br = broad signal), coupling constant (J, Hz) and integration. UV/VIS spectrophotometry was done on a UV-1800 Spectrophotometer (Shimadzu) and a temperature-controlled Applied Photophysics 05-19 system was used for stopped flow measurements. A Thermo Scientific LTQ Orbitrap XL hybrid FTMS (Fourier Transform Mass Spectrometer) equipped with Thermo Scientific MALDI Interface or Thermo Fischer Exactive Plus Orbitrap (LC-ESI+) and a Shimadzu IT-TOF Mass Spectrometer were used for high resolution mass spectrometry. α-Cyano-4-hydroxycinnamic acid was used as matrix for MALDI measurements. Aqueous [^{18}F]-fluoride (n.c.a.) was produced in a General Electrics PETtrace cyclotron (General Electric Healthcare, Uppsala, Sweden) via the $^{18}O(p,n)^{18}F$ nuclear reaction by irradiation of a 2.5 mL water target containing 95.9% enriched [^{18}O]H_2O (IASON, Graz, Austria) with a 16.5 MeV proton beam. Typical irradiation times were 65 min with a beam current of 45 µA, which yielded a [^{18}F]-fluoride amount of about 110 GBq at end of bombardment. A remote controlled GE Tracerlab FX module with 2.5 mL glass reactor housed in a lead castle was used for automated radiolabeling experiments. HPLC analysis was performed on a 1200 series system (Agilent Technologies) using a Zorbax SB-AQ (5 µm, 4.6 x 250 mm) column and H_2O/MeCN gradient elution (flow rate: 1.2 mL/min, 0-2 min: 5% MeCN, 2-10 min: 5 to 20% MeCN linear gradient, 10-16 min: 20 to 90% MeCN linear gradient). For radio-HPLC a GABI* radioactivity detector (Raytest) was used. Retention times were 17.2 min for precursor **8**, 12.4 min for [^{18}F]-**1** and 16.0 min/16.7 min for the ligation products [^{18}F]-**9** and [^{18}F]-**10**, respectively (see Manuscript, Figure 1). Preparative HPLC separation was done on an 1100 Series preparative HPLC system (Agilent Technologies) using a VP250/8 Nucleosil 100-5 C18 HD column (Macherey Nagel) and H_2O/EtOH gradient elution (flow rate 2.5 mL/min, 0-12 min: 8% EtOH, 12-32 min: 8 to 50% EtOH linear gradient) in combination with a K-2001 UV detector (Knauer) and a radioactivity detector from the Tracerlab Fx synthesis module.

2. Chemical Synthesis and Radiochemistry

2.1. Synthesis of tetrazine **1** and the precursor **8**

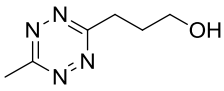


4-Hydroxybutanenitrile (6)



A mixture of 3-chloropropanole (1 eq., 25.7 ml, 307 mmol), potassium cyanide (1 eq., 20.0 g, 307 mmol), 18-crown-6 (0.003 eq., 244 mg, 0.92 mmol) and tetrabutylammonium iodide (0.003 eq., 340 mg, 0.92 mmol) in 50 mL MeCN was refluxed for 24 h. The reaction mixture was diluted with diethyl ether (100 mL), filtered and the solid residue was rinsed with additional Et_2O. Pooled filtrates were washed with water and brine, dried over Na_2SO_4 and concentrated. The residue was purified by distillation to yield **6** as colorless liquid (12.6 g, 48%); bp 128 °C / 25 mbar; ^{1}H NMR (200 MHz, $CDCl_3$) δ 3.61 (t, *J*=5.9 Hz, 2 H), 3.17 (brs, 1 H), 2.41 (t, *J*=7.0 Hz, 2 H), 1.86-1.71 (m, 2 H); ^{13}C NMR (50 MHz, $CDCl_3$) δ 119.6, 59.7, 27.7,13.4.

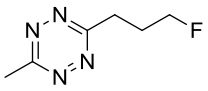
3-(6-Methyl-1,2,4,5-tetrazin-3-yl)propan-1-ol (7)



Procedure A (anhydrous hydrazine): A mixture of compound **6** (1 eq., 0.4 g, 4.7 mmol), MeCN (7 eq., 1.34 g, 32.6 mol) and $Zn(OTf)_2$ (0.85 g, 2.34 mmol) was treated dropwise with anhydrous hydrazine (36 eq., 5.4 g, 168.7 mmol). After stirring for 4 hours at 65°C a solution of sodium nitrite (8 eq., 2.58 g, 38 mmol) in 25 ml water was added followed by slow addition of 2 N HCl until gas evolution ceased. The pH was adjusted to 7 with $NaHCO_3$ and the mixture extracted with EtOAc (6 x 25 mL). Drying over Na_2SO_4 and removal of the solvent yielded the crude product, which was purified by column chromatography (25 g SiO_2, 15-50% EtOAc in hexanes) to yield **7** as a red liquid (160 mg, 21% of theory); R_f (hexanes/EtOAc, 3/1) 0.08; ^{1}H NMR (400 MHz, $CDCl_3$) δ 3.80 (q, *J*=5.8 Hz, 2 H), 3.43 (t, *J*=7.5 Hz, 2 H), 3.04 (s, 3 H), 2.22 (quin, *J*=6.7 Hz, 2 H), 1.61 (t, *J*=5.3 Hz, 1 H); ^{13}C NMR (101 MHz, $CDCl_3$) δ 169.8, 167.4, 61.8, 31.4, 30.6, 21.1; HR-ESI-TOF-MS $[M+H]^+$ *m/z* calcd. 155.0927 for $C_6H_{11}N_4O^+$, found 155.0924.

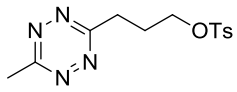
Procedure B (hydrazine monohydrate): A stirred mixture of compound **6** (1 eq., 5 g, 58.8 mmol), MeCN (7 eq., 16.9 g, 0.411 mol) and anhydrous $NiCl_2$ (5 mol%, 3.05 g, 23.5 mmol) was treated dropwise with hydrazine monohydrate (25 eq., 73.5 g, 1.47 mol). The purple reaction mixture was stirred at 60°C for 18 hours. Afterwards a solution of $NaNO_2$ (14.5 eq., 58.8 g, 0.85 mol) in 400 ml H_2O was carefully added. 2N HCl was added until the evolution of nitrous oxides ceased. The dark red solution was extracted with ethyl acetate for three hours using a continuous extractor. The extract was dried over Na_2SO_4 and concentrated. The residue was purified by column chromatography (100 g SiO_2, 30-45% EtOAc in hexanes) to give **7** as a red liquid (1.62 g, 18%); for characterization data see Procedure A.

3-(3-Fluoropropyl)-6-methyl-1,2,4,5-tetrazine (1)



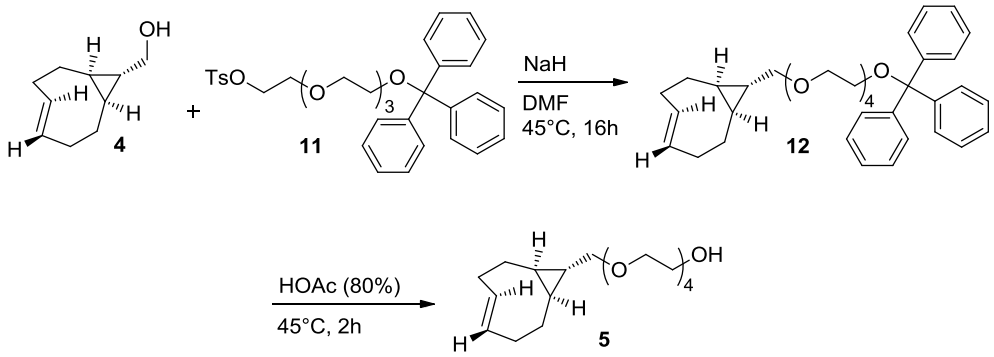
To a stirred solution of 3-(6-methyl-1,2,4,5-tetrazin-3-yl)propan-1-ol (**7**) (1 eq., 70 mg, 0.454 mmol) and 2,4,6-collidine (2.7 eq., 150 mg, 1.23 mmol) in dry DCM (2 mL) cooled to -10°C a solution of DAST (1.5 eq., 110 mg, 0.68 mmol) in dry DCM (1 mL) was dropwise added. After stirring for 48 h at room temperature, the reaction was quenched by addition of MeOH (200 µL) and concentrated. Column chromatography (8 g SiO_2, Et_2O/hexanes gradient elution) afforded **1** as a purple liquid (16 mg, 23%); Rf (hexanes/EtOAc, 3/1) 0.62; ^{1}H NMR (400 MHz, $CDCl_3$) δ 4.61 (dt, *J*=47.1, 5.60 Hz, 2 H), 3.46 (t, *J*=7.6 Hz, 2 H), 3.05 (s, 3 H), 2.45-2.28 (m, 2 H); ^{13}C NMR (101 MHz, $CDCl_3$) δ 169.2, 167.6, 82.9 (d, $^1J_{13C\text{-}19F}$ =167.2 Hz), 30.8 (d, $^3J_{13C\text{-}19F}$ =5.4 Hz), 28.5 (d, $^2J_{13C\text{-}19F}$ =20.7 Hz), 21.1; ^{19}F NMR (376.5 MHz, $CDCl_3$) δ -220.0; HR-ESI-FTMS $[M+H]^+$ *m/z* calcd. 157.0884 for $C_6H_{10}FN_4^+$, found 157.0883.

3-(6-Methyl-1,2,4,5-tetrazin-3-yl)propyl p-tolylsulfonate (8)

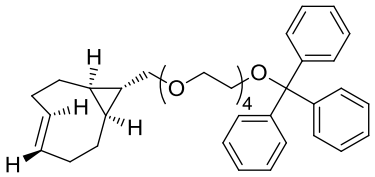


A stirred solution of 3-(6-methyl-1,2,4,5-tetrazin-3-yl)propan-1-ol (**7**) (1 eq., 18 mg, 0.117 mmol) and tosyl chloride (4 eq., 89 mg, 0.47 mmol) in dry DCM (2 mL) was treated with pyridine (4 eq., 37 mg, 0.47 mmol) at 0°C. The mixture was stirred at 0 °C for 48 hours, diluted with DCM (30 mL) and washed with cold 1N HCl followed by cold aq. 2% $NaHCO_3$ and water. The organic layer was dried over $MgSO_4$ and concentrated. Column chromatography (8 g SiO_2, 10-50% EtOAc in hexanes) afforded **8** as a red solid (29.8 mg, 83%); Rf (hexanes/EtOAc, 3/1) 0.28; ^{1}H NMR (400 MHz, CD_2Cl_2) δ 7.76 (d, *J*=8.2 Hz, 2 H), 7.36 (d, *J*=8.2 Hz, 2 H), 4.17 (t, *J*=6.1 Hz, 2 H), 3.33 (t, *J*=7.5 Hz, 2 H), 3.00 (s, 3 H), 2.45 (s, 3 H), 2.31 (quin, *J*=6.7 Hz, 2 H); ^{13}C NMR (101 MHz, CD_2Cl_2) δ 169.3, 168.2, 145.7, 133.3, 130.5, 128.4, 69.9, 31.3, 27.3, 21.9, 21.5; HR-ESI-TOF-MS $[M+H]^+$ *m/z* calcd. 309.1016 for $C_{13}H_{17}N_4O_3S^+$, found 309.1011.

2.2. Synthesis of s-TCO derivative **5**

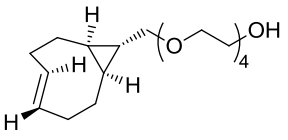


15-(*(1R*,8S*,9R*,E)*-Bicyclo[6.1.0]non-3-en-9-yl)-1,1,1-triphenyl-2,5,8,11,14-pentaoxapentadecane (12)



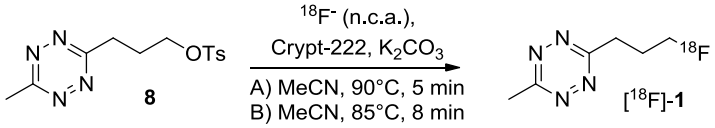
To a dispersion of sodium hydride (6 eq., 410 mg, 10.25 mmol) in dry DMF (0.6 mL) was dropwise added a solution of s-TCO **4**[3] (1 eq., 260 mg, 1.71 mmol) in dry DMF (1.8 mL). After stirring for 30 minutes at room temperature tosylate **11**[5] (1.1 eq., 1.1 g, 1.86 mmol) dissolved dry DMF (1.5 mL) was added dropwise. The resulting brownish reaction mixture was stirred at 45°C for 16 hours, then poured into ice/NH_4Cl and extracted with DCM. The combined organic layer was washed with brine, dried over $MgSO_4$ and concentrated. The residue was purified by column chromatography (90g SiO_2, 5-40% EtOAc in hexanes) to yield **12** as a yellowish oil (318 mg, 33%); Rf (hexanes/EtOAc, 1/1) 0.68; ^{1}H NMR (200 MHz, $CDCl_3$) δ 7.46-7.32 (m, 6 H) 7.29-7.06 (m, 9 H) 5.92-5.66 (m, 1 H) 5.14-4.95 (m, 1 H) 3.68-3.43 (m, 16 H) 3.16 (t, *J*=5.3 Hz, 3 H) , 2.41-2.02 (m, 5 H) 1.92-1.67 (m, 2 H) 0.63-0.90 (m, 2 H); ^{13}C NMR (50 MHz, $CDCl_3$) δ 144.1, 138.4, 131.2, 128.7, 127.7, 126.7, 75.6, 70.8, 70.7, 70.6, 69.4, 63.3, 38.7, 33.9, 32.6, 27.8, 25.2, 21.8, 20.8.

1-(*(1R*,8S*,9R*,E)*-Bicyclo[6.1.0]non-3-en-9-yl)-2,5,8,11-tetraoxatridecan-13-ol (5)



A solution of **12** (1 eq., 250 mg, 0.438 mmol) in 80% HOAc (4 mL) was stirred at 45°C for 2 h leading to precipitation of triphenylmethanol. The reaction mixture was poured into ice-water (10 mL) and filtrated. The removed solid was thoroughly washed with water and the combined filtrate was lyophilized to yield **5** as a yellowish oil (110 mg, 77%); Rf (hexanes/EtOAc, 1/1) 0.16; ^{1}H NMR (200 MHz, D_2O) δ 5.99-5.58 (m, 1 H), 5.23-4.93 (m, 1 H), 3.82-3.45 (m, 16 H), 3.37 (d, *J*=5.7 Hz, 2 H), 2.62-1.33 (m, 6 H), 0.98-0.24 (m, 4 H); ^{13}C NMR (50 MHz, D_2O) δ 138.3, 131.3, 75.4, 71.9, 69.8, 69.6, 69.0, 60.4, 38.5, 33.8, 32.4, 27.6, 24.8, 21.8, 20.7; HR-MALDI-FTMS $[M+Na]^+$ calcd. 351.2142 for $C_{18}H_{32}NaO_5^+$, found 351.2151.

2.3. Radiosynthesis of [^{18}F]-**1**



Procedure A (manual radiolabeling)[1]: 319 MBq (8.62 mCi) [^{18}F]-HF in water (500 µL) was added to a HCO_3^- anion exchange cartridge (^{18}F separation cartridge) previously conditioned with H_2O (5 mL). The radioactivity was eluted with a solution of [2.2.2]cryptand (14.4 mg) in MeCN (900 µL) to which a 3.5% aq. K_2CO_3 solution (100 µL) had been added. The eluate was collected in a 2.5 mL vial with stir bar and septum. Volatiles were removed at 90°C under a stream of argon, and the residue was azeotropically dried twice by addition and subsequent evaporation of dry MeCN (2 x 900 µL) at 90°C heating block temperature. Precursor **8** (10 mg, 32.4 µmol) dissolved in dry MeCN (700 µL) was added and after stirring for 5 min at 90 °C a sample was analyzed by radio-HPLC to determine the radiochemical yield of [^{18}F]-**1** (16 ± 2% decay corrected).

Procedure B (automated labeling – non-optimized): A remote controlled GE Tracerlab FX module (Figure S1) with 2.5 mL glass reactor housed in a lead castle was used for automated labeling experiments. In a typical labeling experiment [^{18}F]-fluoride (109 GBq) was produced in the cyclotron target by bombardment of ^{18}O-enriched water with a 16.5 MeV proton beam. The activity was transferred into the synthesis module and trapped on a preconditioned Waters QMA light cartridge. The radioactivity was eluted with a solution of [2.2.2]cryptand (14.8 mg) in MeCN (900 µl) to which a 3.5% aq. K_2CO_3 (100 µL) solution had been added. After addition of dry MeCN (500 µL) volatiles were removed in vacuo at a temperature of 60-120 °C. After cooling to 60 °C the precursor **8** (9.8 mg, 31.8 µmol) in dry MeCN (800 µL) was added, and the reaction mixture was heated to 85°C for 8 minutes. The reaction product was separated by preparative HPLC cutting the peak at retention time 15 min. Last traces of [^{18}F]-fluoride were removed by passing over a SepPAK Alumina-N cartridge, yielding 3.9 GBq [^{18}F]-**1** (5.2% decay corrected). The product was brought to physiological osmolality (320 mmol/kg) by addition of 10% aq. NaCl solution. Starting from 370.8 MBq/mL almost no radiolysis of [^{18}F]-**1** (< 1%) was observed after 4 h as determined by radio-HPLC.

[1] Procedures using other solvents (e.g. DMSO) or fluorination reagents (e.g. TBAF) afforded [^{18}F]-**1** in radiochemical yields below 11%.

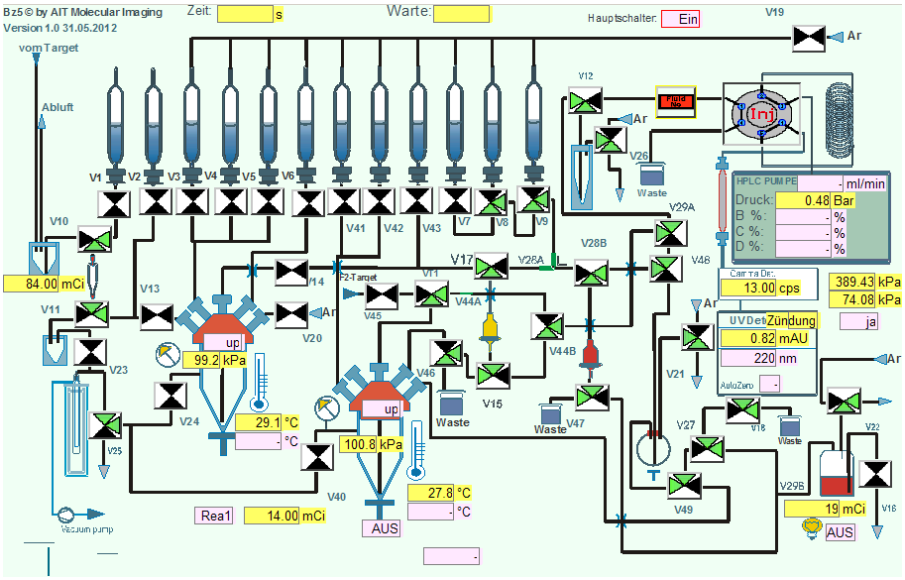
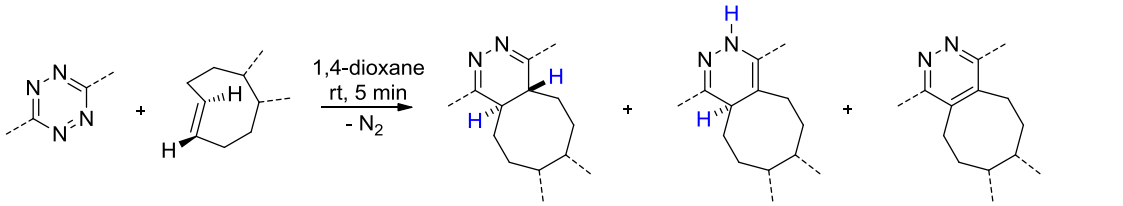


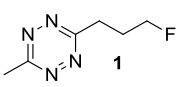
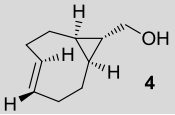
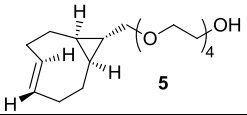
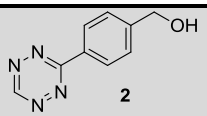
Figure S1. Schematic flow chart of automated labeling.

2.4. IEDDA-initiated conjugations



General procedure: To a 3 mM solution of tetrazine **1** or **2** in dry 1,4-dioxane (1 mL) was added a 3 mM solution of dienophile **3**, **4**, or **5** (1 eq.) in dry 1,4-dioxane (1 mL) and the resulting mixture was stirred for 1-5 min at room temperature. Due to the fast isomerization and aromatization known for tetrazine/TCO-ligation products, these samples were directly subjected to LC/HR-ESI-FTMS analysis for characterization (Table S1).

Table S1. Results of IEDDA-initiated conjugations of tetrazines (**1** and **2**) and dienophiles (**3**, **4**, and **5**).

Tetrazine	Dienophile	Products	Product formula	Product Calcd. mass	Found mass (HR-ESI-FTMS)
 **1**	 **3**	-	$C_{14}H_{23}FN_2$	$[M+H]^+$ 239.1918	$[M+H]^+$ 239.1917
	 **4**	**9** + **10**	$C_{16}H_{25}FN_2O$	$[M+H]^+$ 281.2024	$[M+H]^+$ 281.2025
	 **5**	**11** + **12**	$C_{24}H_{41}FN_2O_5$	$[M+H]^+$ 457.3072	$[M+H]^+$ 457.3069
 **2**	 **3**	-	$C_{17}H_{22}N_2O$	$[M+H]^+$ 271.1805	$[M+H]^+$ 271.1810

3. Reaction kinetics

The tetrazine (**1** or **2**) was weighted into a volumetric flask and filled with solvent (absolute 1,4-dioxane or human plasma) to generate a 3 mM solution. The dienophile was weighted into a volumetric flask and filled with solvent (absolute 1,4-dioxane or human plasma) to generate a 30 mM solution. The reactant solutions were transferred into the driver syringes of the stopped flow apparatus (Applied Photophysics, Surrey, UK). Upon temperature constancy (± 0.1°C of aimed value) triggering of driver syringe pneumatics caused mixing of equal reactant volumes. Depending on reaction rate time intervals between 0.1 to 1000 s were chosen to collect 4000 data points at 540 nm. All measurements were made in duplicate or triplicate. Reactions in 1,4-dioxane were monitored at 20°C, 37 °C and 60°C, reactions in human plasma were conducted at 37°C only. The pseudo first order rate constant (k_{obs}) was determined by linearization of the decay curve followed by linear fitting. The second order rate constant (k) was calculated from the pseudo-first order rate constant. Linearization and direct fitting to the Eyring equation (Equation 1) was used to calculate the enthalpy of activation ($\Delta H^{\ddagger}$) and the entropy of activation ($\Delta S^{\ddagger}$). Equation 2 gave rise to free energy of activation at 298.15 K ($\Delta G^{\ddagger}$). Results are summarized in Table S2 (rate constants) and Table S3 (thermodynamic data). Selected plots of kinetic measurements and Eyring linearization are shown in Figure S2.

$$\ln\left(\frac{k}{T}\right) = -\left(\frac{\Delta H^{\ddagger}}{R}\right) * \left(\frac{1}{T}\right) + \ln\left(\frac{K_b}{h}\right) + \left(\frac{\Delta S^{\ddagger}}{R}\right) \quad (1)$$

$$\Delta G^{\ddagger} = \Delta H^{\ddagger} - \mathrm{T}\Delta S^{\ddagger} \quad (2)$$

Table S2. Results of kinetic measurements (rate constants).

Reaction	Solvent	T (°C)	k_{obs} (s^{-1})	k ($M^{-1}s^{-1}$)
1 + **3**	1,4-dioxane	20	$(13.0 \pm 0.1) \cdot 10^{-3}$	0.81 ± 0.01
		37	$(23.9 \pm 0.2) \cdot 10^{-3}$	1.49 ± 0.01
		60	$(46.3 \pm 0.4) \cdot 10^{-3}$	2.89 ± 0.03
1 + **4**	1,4-dioxane	20	0.90 ± 0.02	60.1 ± 0.9
		37	1.28 ± 0.04	85.5 ± 2.3
		60	1.86 ± 0.03	124.2 ± 1.5
1 + **5**	Human plasma	37	123.0 ± 4.5	8200 ± 300
2 + **3**	1,4-dioxane	20	0.74 ± 0.01	49.0 ± 0.7
		37	1.19 ± 0.02	79.2 ± 1.3
		60	1.98 ± 0.01	131.8 ± 0.7

Table S3. Results of kinetic measurements (thermodynamic data).

Reaction	Solvent	$\Delta H^{\ddagger}$ (kcal/mol)	$\Delta S^{\ddagger}$ (kcal/mol)	$\Delta G^{\ddagger}$ (kcal/mol)
1 + **3**	1,4-dioxane	5.54	-0.040	17.5
1 + **4**	1,4-dioxane	2.89	-0.040	15.0
2 + **3**	1,4-dioxane	4.17	-0.036	15.1

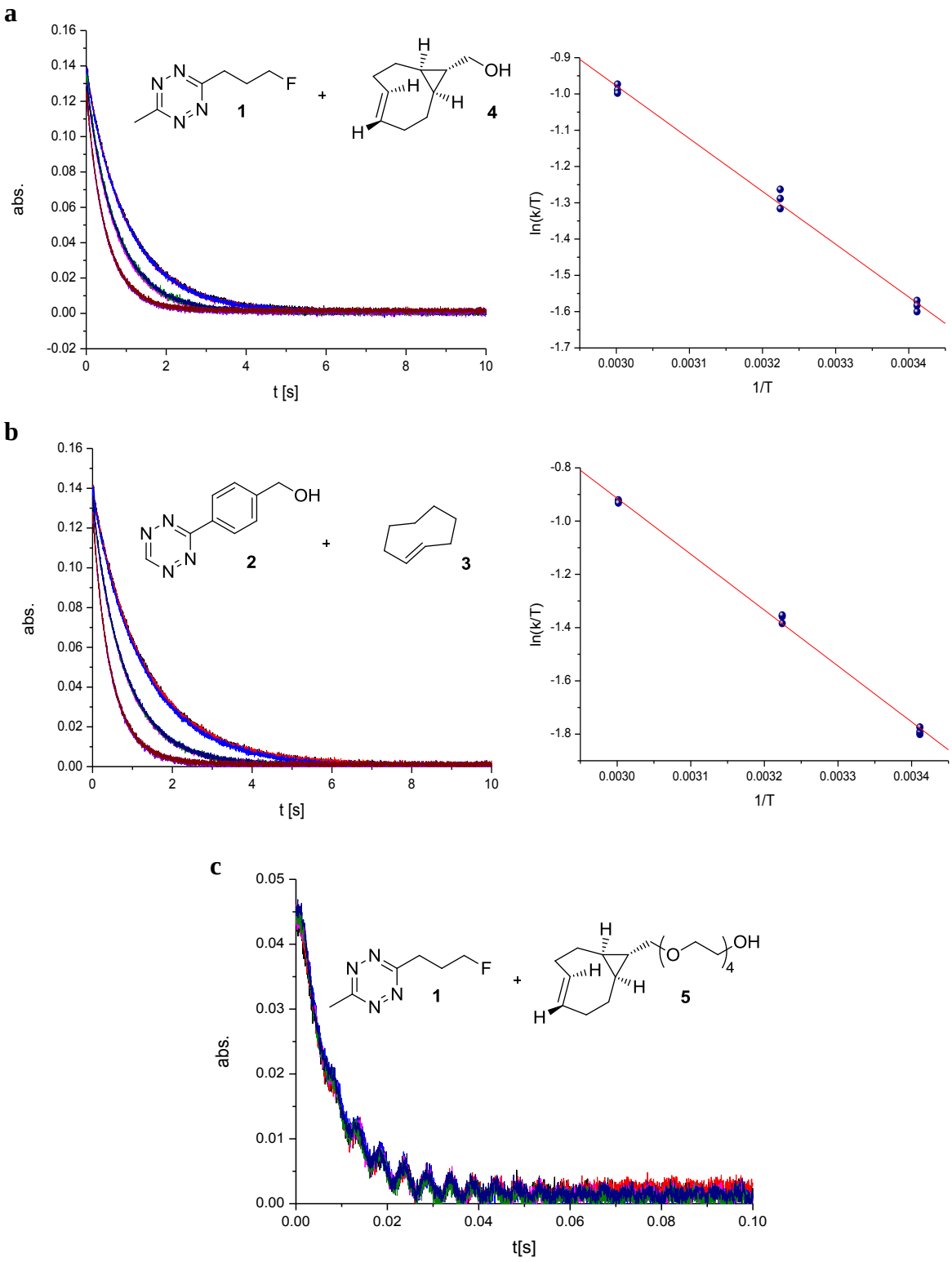


Figure S2. Selected data and plots of kinetic investigations: a) **1**+**4** in 1,4-dioxane at 20, 37 and 60 °C. b) **2**+**3** in 1,4-dixoane at 20, 37 and 60 °C. c) **1**+**5** in human plasma at 37 °C (abs. = absorbance).

4. In vitro and in vivo investigations

4.1. In vitro stability of tetrazine **1** and s-TCO derivative **5** in human plasma

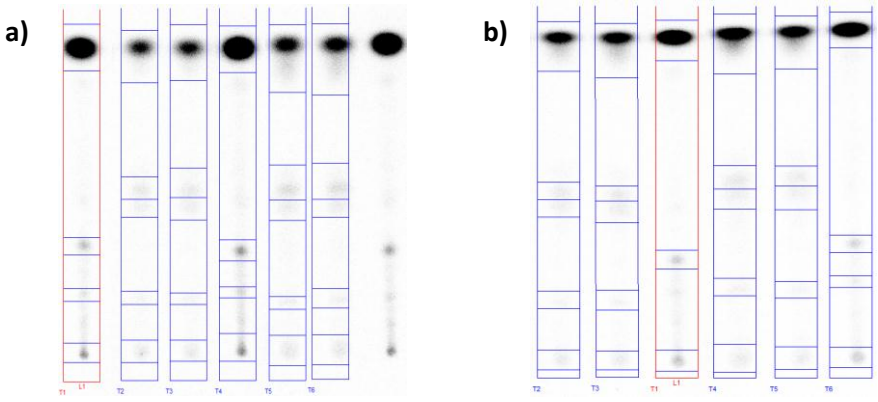
Freshly prepared solutions of **1** and **5** in human plasma (3 mM) were incubated at 37 °C for 12 h and 24 h, respectively. The amount of degradation was determined by UV/VIS spectrophotometry and HPLC (both used for **1**) and titration with a tetrazine standard solution followed by UV/VIS (used for **5**). Recoveries: 99% **1**, 85 ± 5% **5** (n = 2).

4.2. In vivo experiments

Animals. Female BALB/c mice were scanned at a weight of 19.4±1.6 g and housed in groups of up to five individuals under controlled environmental conditions (22±1°C, 40-70% humidity) with a 12 h light-dark cycle (lights on at 6:00) and ad libitum access to food and water. Before PET scanning, an adaptation period of at least one week was accorded to each animal. The study was authorized by the institutional animal care and use committees, and all study procedures were performed in accordance with the European Communities Council Directive of November 24, 1986 (86/609/EEC). Every effort was made to minimize both the suffering and the number of animals used in this study. Anesthesia (2.0% isoflurane mixed in oxygen) was induced and the animals were warmed at 38°C to prevent hypothermia. Anesthesia and warming was maintained during the whole experimental procedure. Body temperature and respiratory rate were constantly monitored during the whole experiment using an MR compatible small animal monitoring and gating system (SA Instruments Inc., Stony Brook, NY). A humidifier was used to moisten the gas mixture before supplying it to the animal, thus preventing impairment of air passages.

PET/MR imaging. For imaging experiments animals were divided into two groups. In the first group (n=4), mice were scanned in prone position on a dual animal bed. In the second group (n=2) mice underwent a sequential PET/MRI scan on two stand-alone scanners. MRI was performed using a Bruker ICON 1T system (Bruker BioSpin, Ettlingen, Germany) and the animal holder mounted with the mouse body bed and mouse whole body RF coil. The whole body coil covers an axial field of view (FOV) of around 8 cm which is very similar to the PET axial FOV (7.6 cm). Images were acquired using a T1-weighted gradient echo sequence (FLASH-nav-3D) with the following parameters: field of view 76x28x24 mm, matrix 253x93x32, resolution 0.3x0.3x0.75 mm, repetition time 25 ms, echo time 4.7 ms, flip angle 25 deg., 5 repetitions, total scan time 6 min 15 sec. For the PET scan, a catheter, placed into a lateral tail vein, was used for i.v. administration of [^{18}F]-**1**. At the beginning of tracer administration (4.9±1.4 MB in 100 µL), dynamic PET imaging was initiated for 120 min using a µPET Focus220 scanner (Siemens Medical Solutions, Knoxville, TN, USA). Prior to the PET scan, a transmission scan using a ^{57}Co point source was recorded over 10 min. At the end of the scan the animals were sacrificed, organ samples and blood were extracted, weighted and counted for activity in a 1-detector Wallac gamma counter (Perkin Elmer Instruments, Wellesley, USA), which had been cross-calibrated with the PET camera. Organ activity data and blood were corrected for radioactive decay and normalized to injected dose per gram body weight and expressed as standardized uptake value (SUV = (radioactivity per mL/injected radioactivity) x body weight). PET data from the 120-min dynamic scans were sorted into three-dimensional sinograms according to the following frame sequence: 8×5 s, 2×10 s, 2×30 s, 3×60 s, 2×150 s, 2×300 s, 4×600 s and 3x1200 s. PET images were reconstructed by Fourier rebinning followed by 2-dimensional filtered back projection with a ramp filter resulting in a voxel size of 0.4x0.4x0.8 mm^3. The standard data correction protocol (normalization, attenuation and decay correction) was applied to the data. For the PET/MRI group, images were aligned using a fixed transformation matrix. Different volumes of interest (brain, liver, muscle, kidneys, urinary bladder, and heart) were manually outlined on multiple planes using the image analysis software Amide[6] and time-activity curves (TACs), expressed as SUV, were calculated.

Analysis of murine plasma metabolites – In vivo stability of [^{18}F]-1. Direct after imaging experiments (120 min) murine plasma was obtained by centrifugation and proteins were precipitated with acetonitrile and removed by centrifugation. Supernatant solution was spotted on SiO_2 TLC plates and developed using DCM as mobile phase. [^{18}F]-**1** was spotted as reference. After development radioactivity was quantified using a Hewlett Packard Cyclone Phosphor Imager autoradiography system (Figure S3).



c)

In vivo stability of [^{18}F]-**1**	**#41**	**#42**	**#43**	**#44**
Unchanged [^{18}F]-**1** in plasma [%]	82.0	82.2	88.7	89.8

Figure S3. In vivo stability of [^{18}F]-**1** as determined by TLC radiochromatography of murine plasma after imaging experiments**:** a) Lane 1: Reference [^{18}F]-**1**; Lane 2 & Lane 3: Plasma metabolites mouse #41; Lane 4: Reference [^{18}F]-**1**; Lane 5 & Lane 6: Plasma metabolites mouse #42; Lane 7: Reference [^{18}F]-**1**. b) Lane 1 & Lane 2: Plasma metabolites mouse #43; Lane 3: Reference [^{18}F]-**1**; Lane 4 & Lane 5: Plasma metabolites mouse #44; Lane 6: Reference [^{18}F]-**1**. c) Results after quantification.

In vivo click reaction. For in vivo click experiments a third group of female BALB/c mice (n=4) was used. A lateral tail vein was used for i.v. administration of [^{18}F]-**1** (2.5 ± 0.5 MBq, 100 µl). After 20 min uptake time three mice received water-soluble s-TCO derivative **5** i.v. (10.5 mg/kg, 2.1 mg/mL in 0.9% NaCl). A control mouse received 0.9% NaCl instead. Retroorbital blood was collected 5, 15 (+ control) and 30 min after administration of **5**. 200 µl of blood were quenched immediately after blood retrieval with 107 µg of tetrazine **2** in 214 µl water (saturated solution). Murine plasma was obtained by centrifugation and proteins were precipitated with acetonitrile and removed by centrifugation. Supernatant solution was spotted on SiO_2 TLC plates and developed using 5% MeOH and 1% triethylamine in DCM as mobile phase (Figure S4).

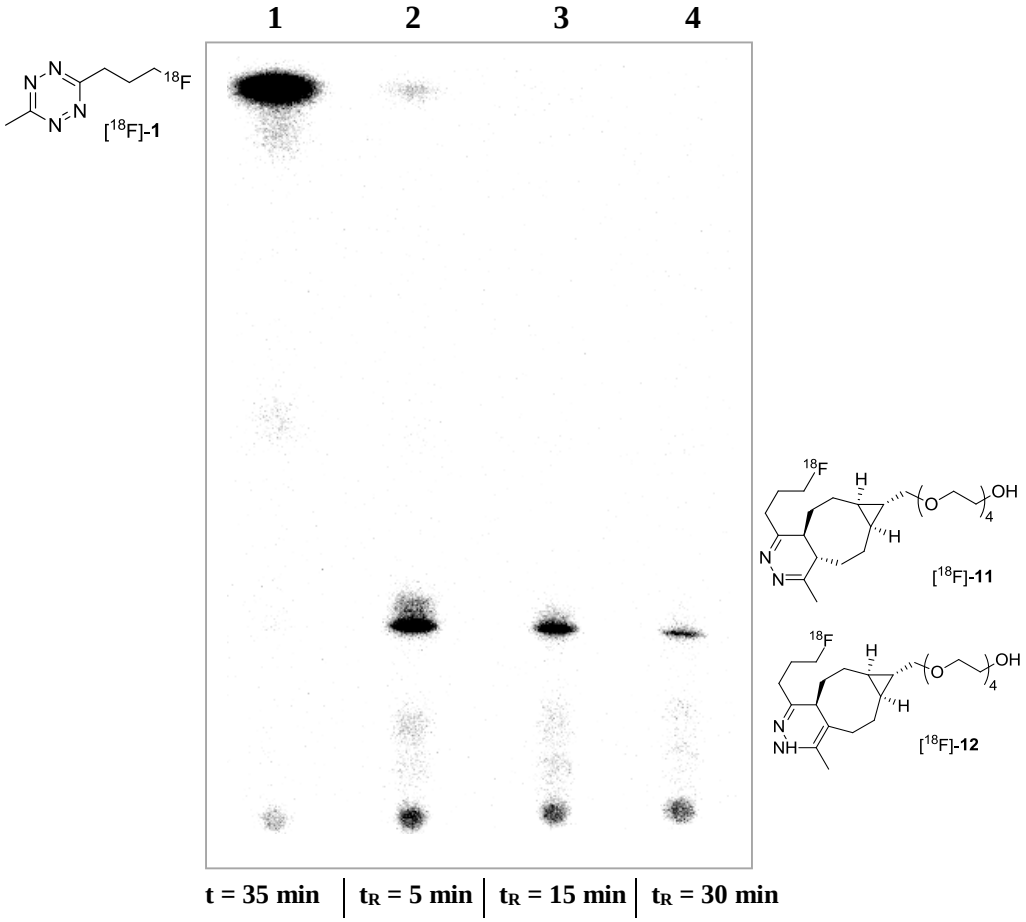
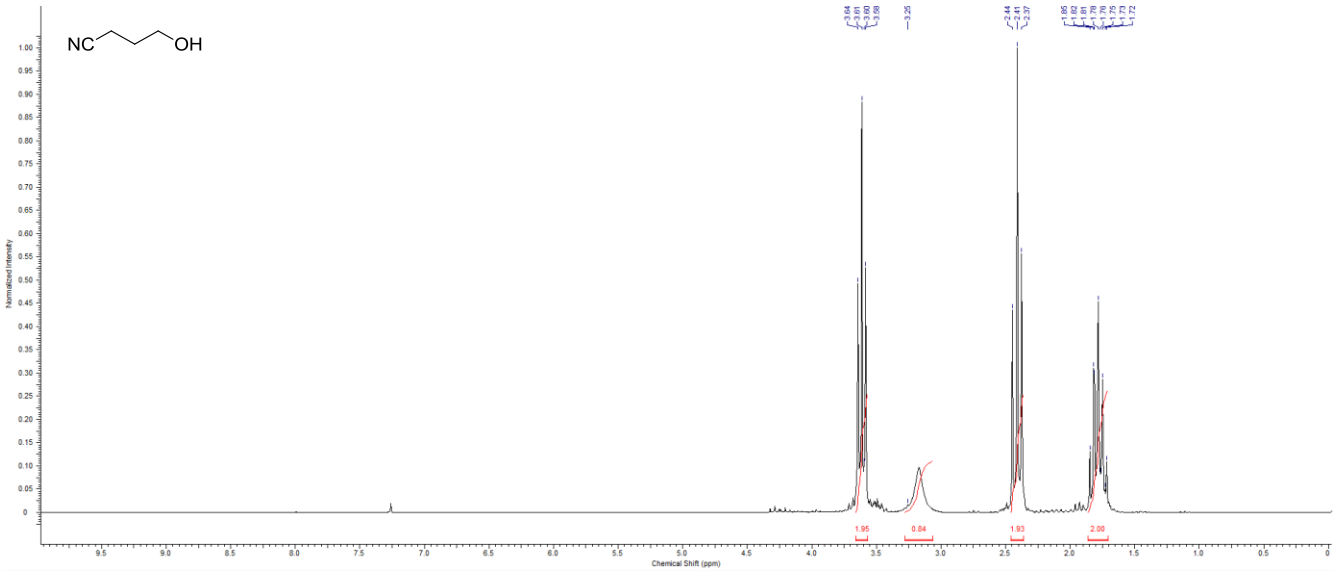


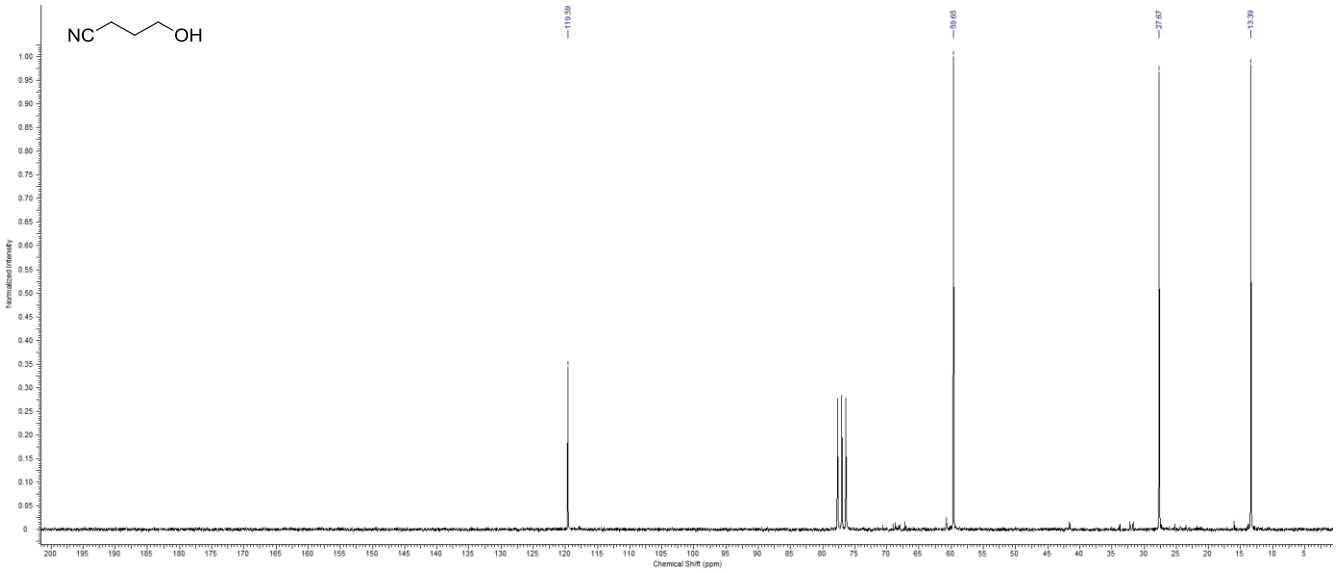
Figure S4. Radio-TLC after in vivo reaction of [^{18}F]-**1** and **5**. Lane 1: control, 35 min biodistribution of [^{18}F]-**1**. Lane 2: 5 min reaction time. Lane 3: 15 min reaction time. Lane 4: 30 min reaction time. For lanes 2-4, [^{18}F]-**1** was administered 20 min prior to **5** ($t = t_R + 20$ min).

5. NMR Spectra

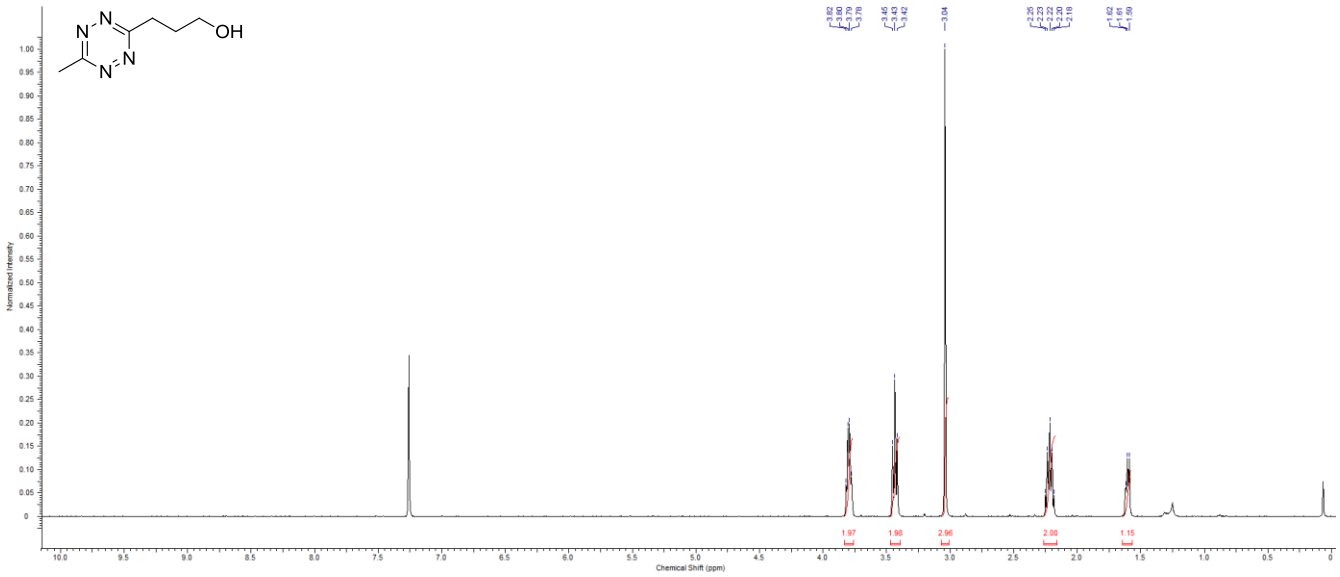
^{1}H spectrum of compound **6**



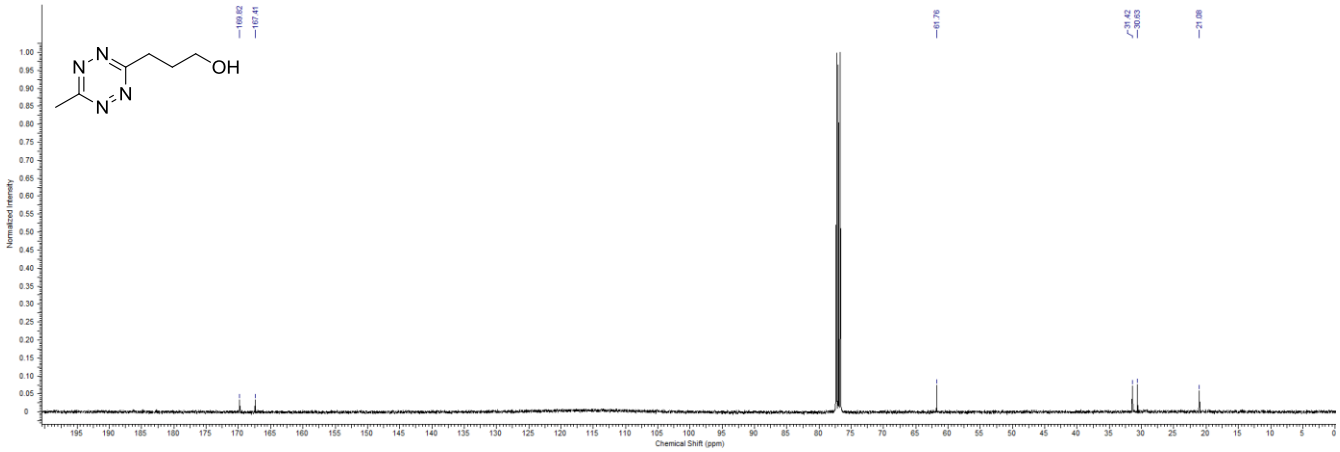
^{13}C spectrum of compound **6**



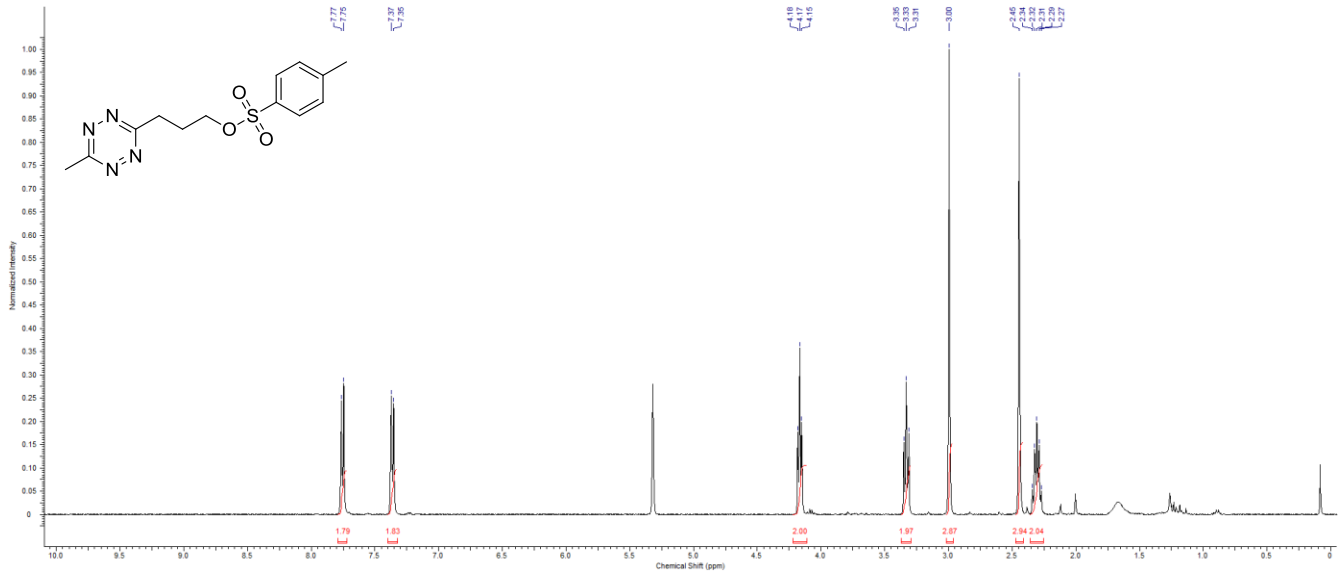
^{1}H spectrum of compound **7**



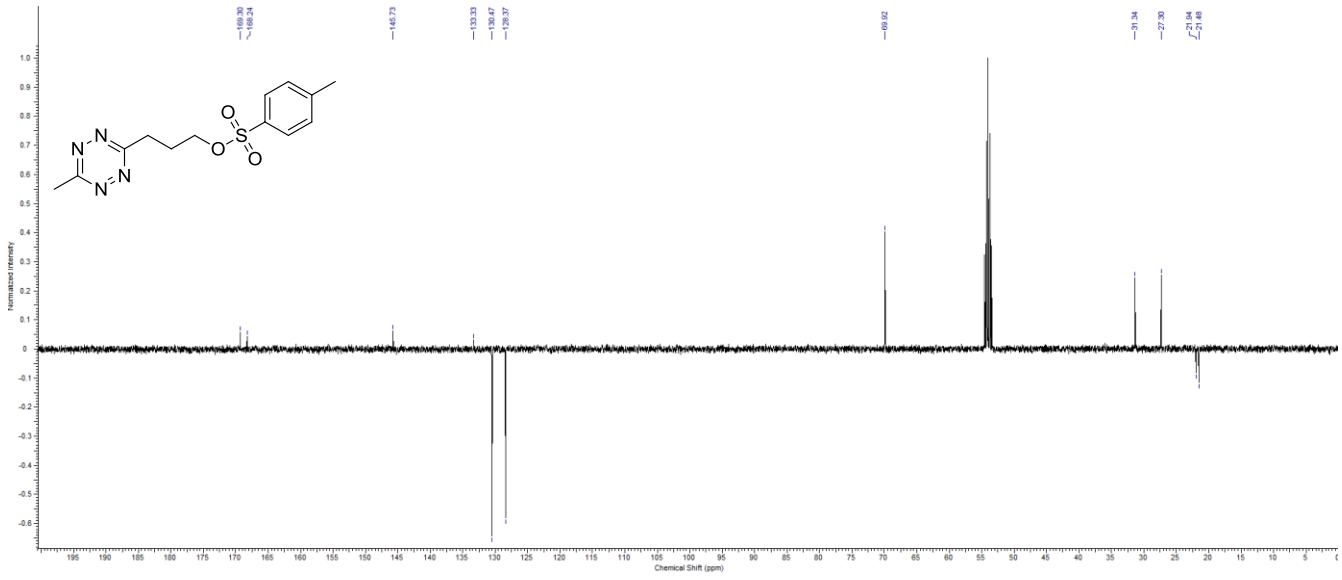
^{13}C spectrum of compound **7**



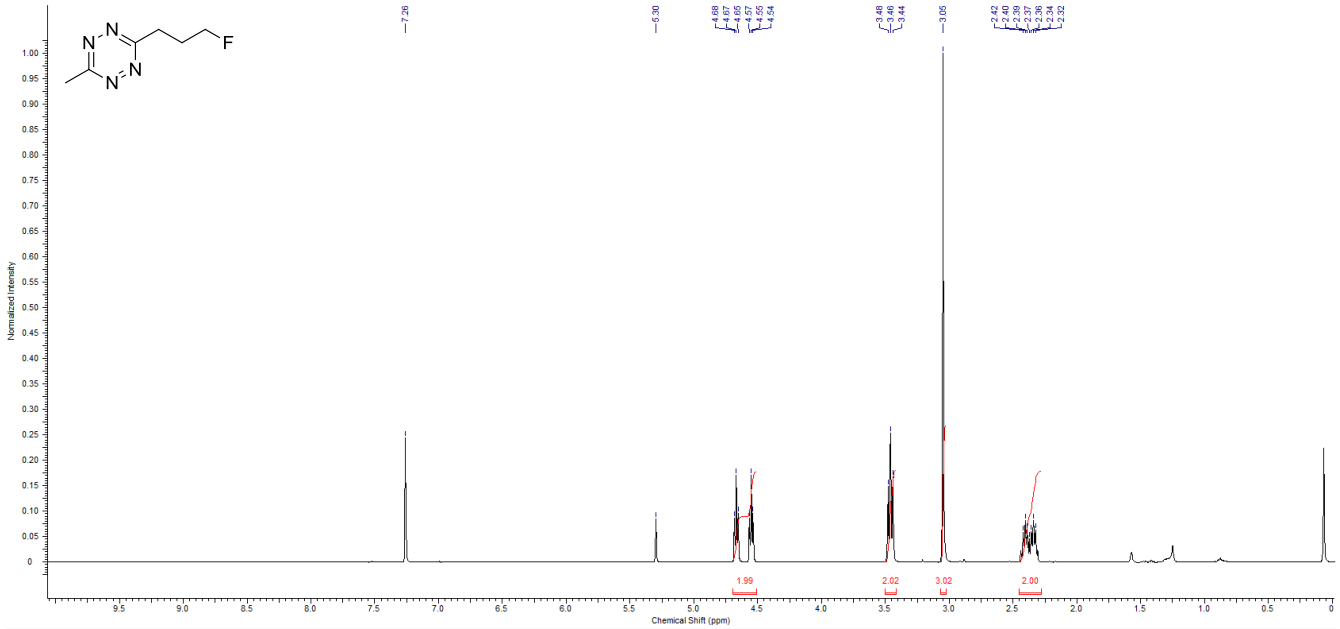
^{1}H spectum of compound **8**



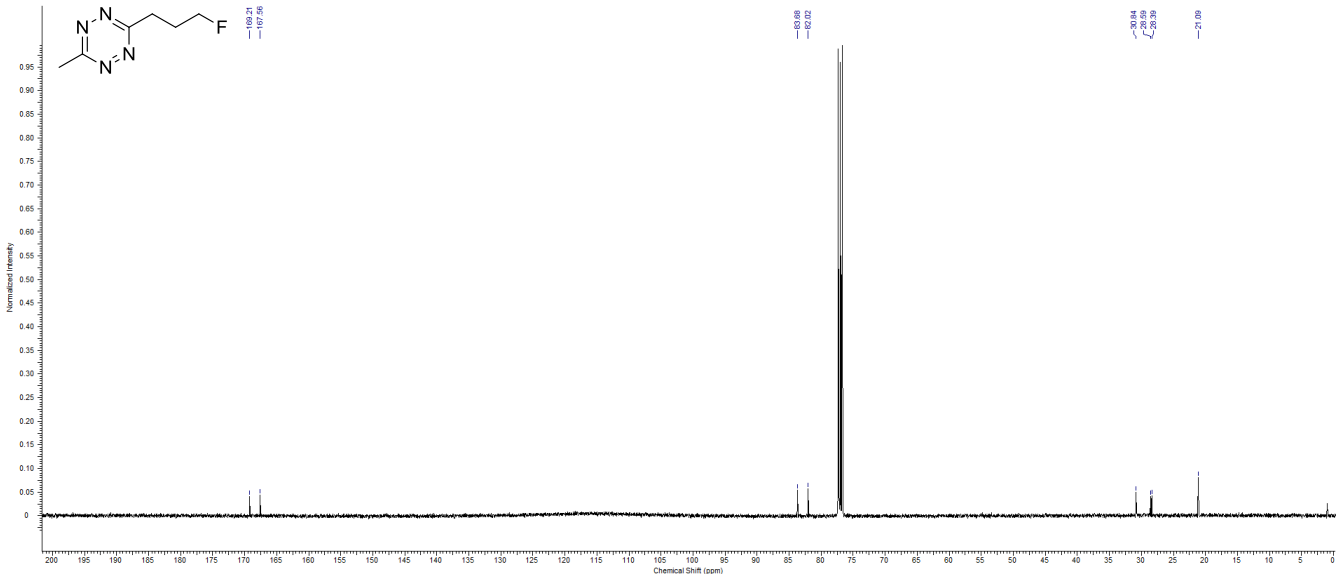
^{13}C spectum of compound **8**



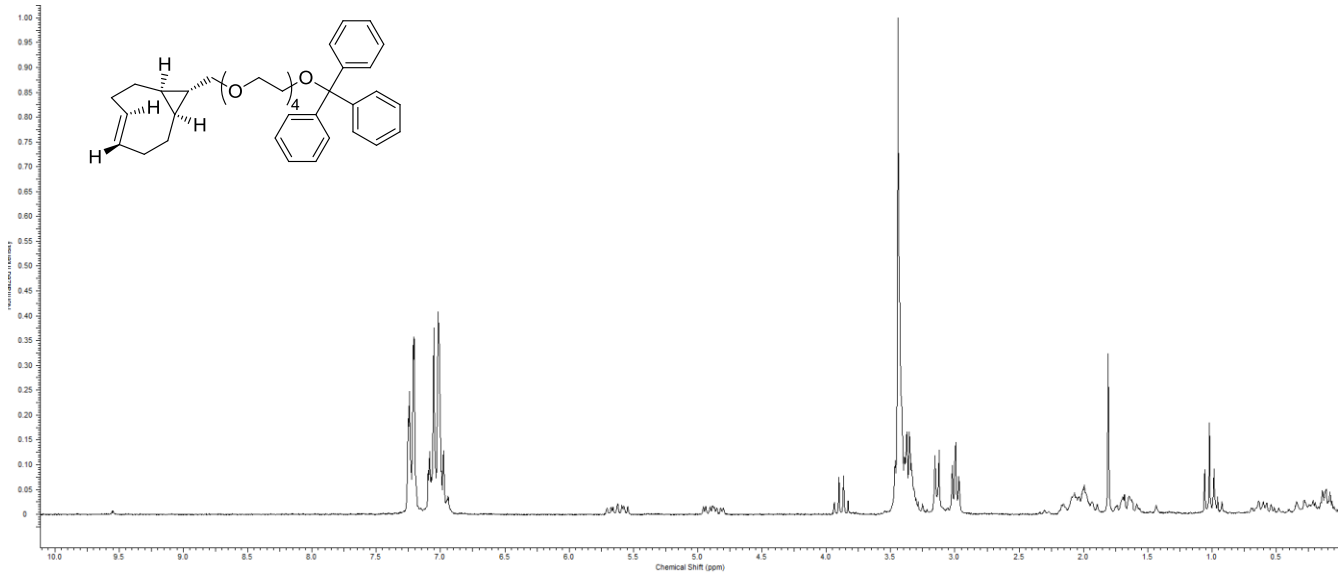
^{1}H spectrum of compound **1**



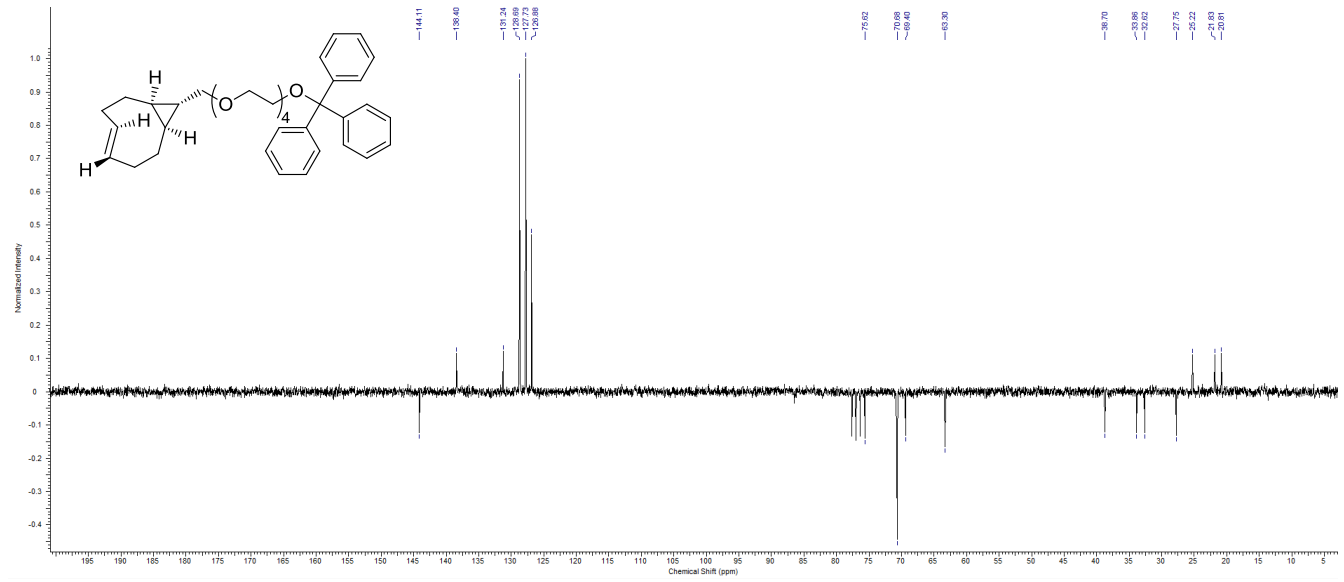
^{13}C spectrum of compound **1**



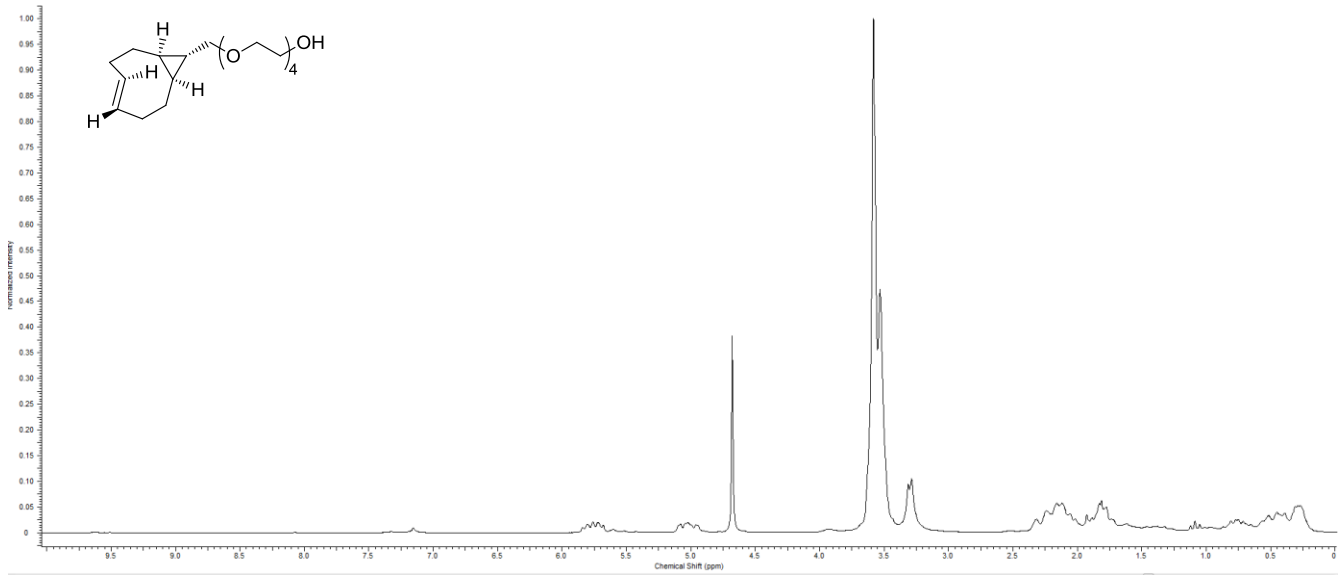
^{1}H spectrum of compound **12**



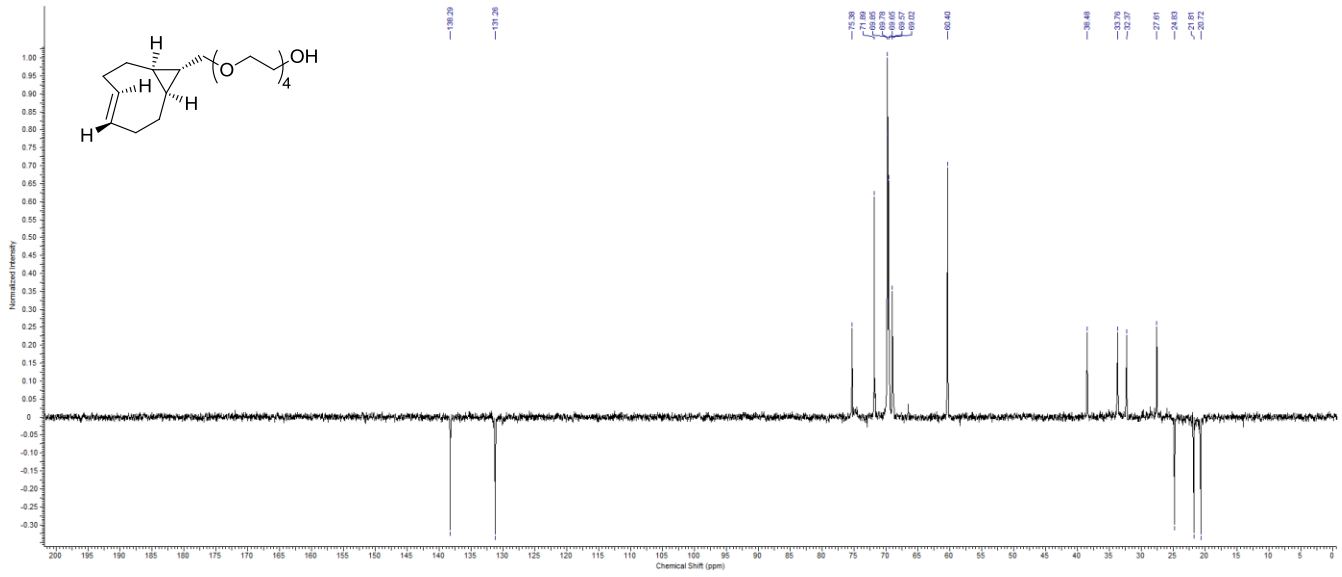
^{13}C spectrum of compound **12**



^{1}H spectrum of compound **5**



^{13}C spectrum of compound **5**



6. Quantum Chemical Calculations

All DFT calculations were performed using the Gaussian 09 (Rev. A.1) program package.[7] Geometry optimizations to energy minima or transition states as well as subsequent frequency analyses at 298.15 K of all considered compounds and intermediates were achieved with 6-31G(d,p)[8] basis set using the M06-2X density functional[9] as implemented in Gaussian 09, which has been found to give relatively accurate energy profiles for cycloadditions.[10] For calculations in water and 1,4-dioxane the polarizable continuum model (PCM)[11] using the CPCM polarizable conductor calculation model[12] with UFFI radii was applied. Imaginary frequencies corresponding to the desired reaction coordinates were obtained only in the case of transition state calculations. Data analysis was done using GaussView 5 (Gaussian, Inc.).

Full energy profiles for reactions of tetrazine **1** and **2** with TCO **3** are shown in Figure S5. $\Delta G^{\ddagger}$ for the first step (inverse electron demand Diels Alder) are 18.73 and 15.26 kcal/mol, respectively, whereas $\Delta G^{\ddagger}$ values for the second step (retro Diels Alder) are 10.57 and 12.97 kcal/mol, showing that the first step is rate determining. Therefore, $\Delta G^{\ddagger}$ values of the first step were considered to determine reaction activation barriers (see Manuscript) at 298.15 K. Optimized geometries of all starting materials and the transition states of the IEDDA cycloaddition are shown in Figure S6 and original data is summarized in Table S4 followed by listing of Cartesian coordinates of all relevant structures.

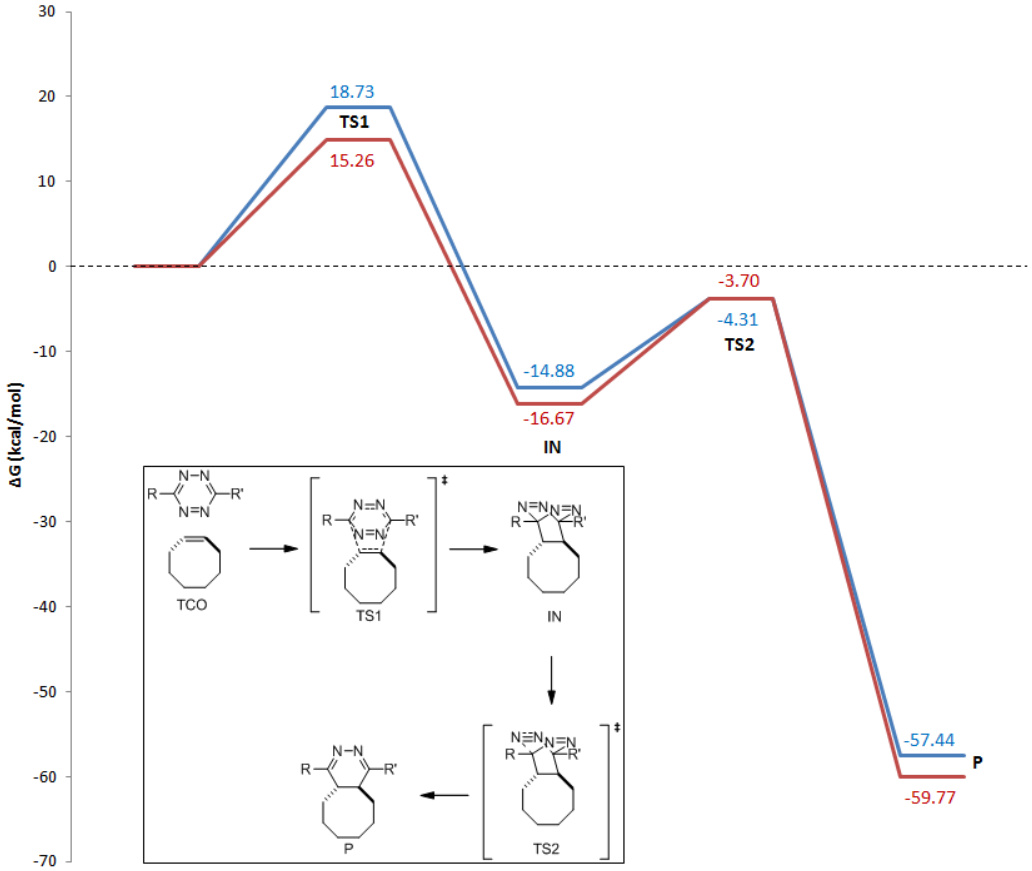


Figure S5. M06-2X/6-31G(d,p) calculated Gibbs free energies of IEDDA initiated ligations of tetrazine **1** (blue) and tetrazine **2** (red) with TCO **3** in gas phase relative to the Gibbs free energies of the starting materials.

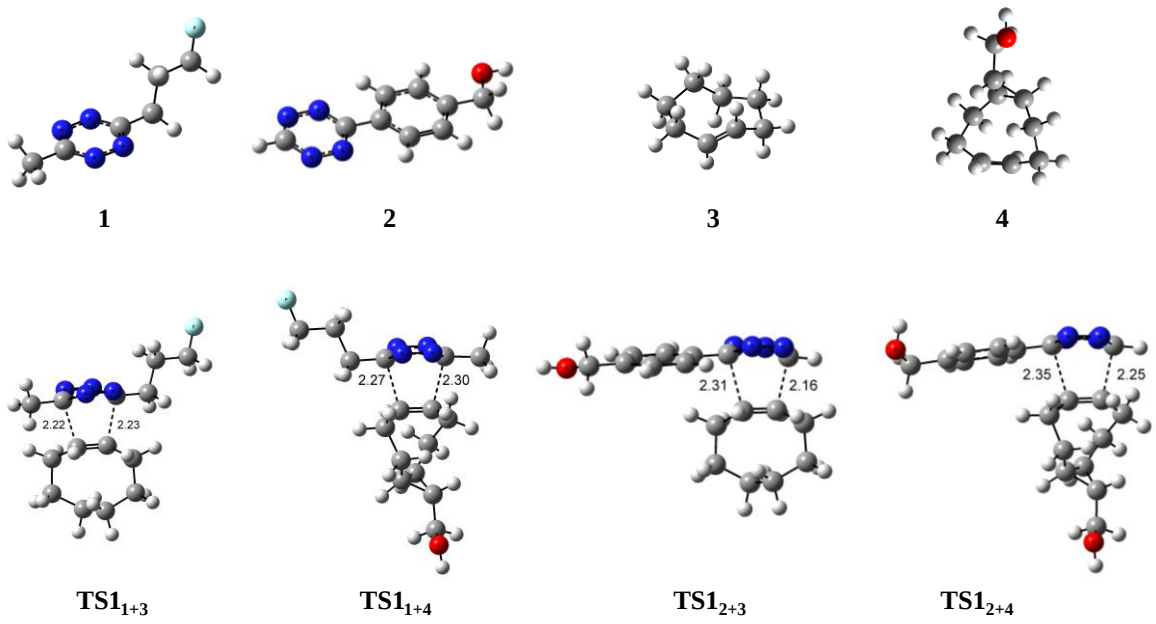


Figure S6. Optimized geometries (M06-2X/6-31G(d,p), gas phase) of tetrazines (**1** and **2)**, dienophiles (**3** and **4**) and corresponding transition states of IEDDA cycloaddition.

Table S4. Selected original data from Gaussian calculations (E: total electronic energy, ZPE: zero point energy).

Compound	Calculated in	E (hartree)	H (hartree)[a]	G (hartree)[a]	S (J/(mol*K))[a]	ZPE (hartree)[a]
1	gas phase	-552.60350	-552.43287	-552.48402	107.653	-552.44466
	1,4-dioxane	-552.60855	-552.43803	-552.48962	108.567	-552.44987
	water	-552.61306	-552.44261	-552.49426	108.701	-552.45444
2	gas phase	-641.66272	-641.48295	-641.53351	106.395	-641.49515
	1,4-dioxane	-641.66881	-641.48914	-641.53993	106.903	-641.50137
3	gas phase	-313.10240	-312.88840	-312.92808	83.507	-313.06245
	1,4-dioxane	-313.10306	-312.88924	-312.92893	83.531	-312.89773
4	gas phase	-465.62872	-465.37225	-465.42029	101.107	-465.38401
	water	-465.63523	-465.37910	-465.42711	101.038	-465.39087
	1,4-dioxane	-465.63215	-465.37586	-465.42388	101.059	-465.38762
TS1$_{1+3}$	gas phase	-865.70338	-865.31706	-865.38225	137.190	-865.33618
	1,4-dioxane	-865.70950	-865.32337	-865.38860	137.297	-865.34251
TS1$_{1+4}$	gas phase	-1018.23454	-1017.80590	-1017.88035	156.698	-1017.82842
	water	-1018.25100	-1017.82280	-1017.89724	156.667	-1017.84538
	1,4-dioxane	-1018.24310	-1017.81469	-1017.88909	156.598	-1017.83722
TS1$_{2+3}$	gas phase	-954.76435	-954.36931	-954.43726	143.019	-954.38933
	1,4-dioxane	-954.77176	-954.37691	-954.44502	143.347	-954.39697
TS1$_{2+4}$	gas phase	-1107.29658	-1106.85907	-1106.93554	160.953	-1106.88228
	1,4-dioxane	-1107.30608	-1106.86886	-1106.94542	161.134	-1106.89221

[a] calculated for T = 298.15 K

Cartesian coordinates

TCO **3**, gas phase

C	-0.5319740	-1.3578980	-0.4009380
C	0.5319750	-1.3579000	0.4009390
C	1.8698840	-0.9014570	-0.0815100
C	-1.8698850	-0.9014570	0.0815090
C	1.8818250	0.6352820	0.1353760
C	-1.8818250	0.6352830	-0.1353780
C	-0.6505410	1.3762610	0.4300970
C	0.6505410	1.3762620	-0.4300940
H	-0.3725530	-1.3346870	-1.4809250
H	0.3725550	-1.3346940	1.4809260
H	2.7154270	-1.3581900	0.4428170
H	1.9792520	-1.1137950	-1.1515330
H	-2.7154260	-1.3581900	-0.4428210
H	-1.9792550	-1.1137960	1.1515320
H	2.7903930	1.0481690	-0.3184690
H	1.9561630	0.8413180	1.2111750
H	-2.7903940	1.0481700	0.3184640
H	-1.9561580	0.8413170	-1.2111770
H	-0.9508090	2.4184330	0.5838000
H	-0.4299190	0.9856240	1.4317690
H	0.9508100	2.4184350	-0.5837940
H	0.4299180	0.9856290	-1.4317680

1,4-dioxane

C	0.5323020	-1.3580770	0.4009860
H	0.3731520	-1.3329450	1.4810650
C	-0.5323020	-1.3580780	-0.4009850
H	-0.3731520	-1.3329490	-1.4810640
C	-1.8700870	-0.9014460	0.0821540
H	-2.7157920	-1.3572480	-0.4428260
H	-1.9796150	-1.1124530	1.1524500
C	1.8700870	-0.9014460	-0.0821530
H	2.7157920	-1.3572480	0.4428280
H	1.9796150	-1.1124540	-1.1524480
C	-1.8814500	0.6353650	-0.1357310
H	-2.7902340	1.0477190	0.3181550
H	-1.9549930	0.8401980	-1.2117080
C	1.8814500	0.6353650	0.1357300
H	2.7902340	1.0477180	-0.3181560
H	1.9549930	0.8401990	1.2117080
C	0.6504440	1.3761190	-0.4302620
H	0.9507390	2.4183430	-0.5839040
H	0.4298420	0.9846280	-1.4315770
C	-0.6504440	1.3761190	0.4302600
H	-0.9507380	2.4183440	0.5839000
H	-0.4298420	0.9846310	1.4315760

sTCO **4**, gas phase			
C	1.2755100	-0.3310120	-0.1709970
C	0.2659260	-0.8284380	0.8168240
C	0.4891150	0.6835330	0.6218020
H	0.9721390	-0.3839270	-1.2169120
H	0.7416980	-1.1163880	1.7558430
H	1.0385810	1.0798220	1.4747650
C	-0.8650550	-1.8337730	0.5538230
H	-0.3999340	-2.8281040	0.5391790
H	-1.5106670	-1.8316780	1.4399200
C	-0.2857170	1.7901490	-0.1133580
H	0.2553440	2.7283780	0.0570810
H	-0.2249230	1.5928800	-1.1876220
C	-1.7936530	1.9551820	0.2110670
H	-2.2549200	2.5855490	-0.5568590
H	-1.9508760	2.4394620	1.1787310
C	-1.7502900	-1.6841250	-0.6965960
H	-2.5827830	-2.3958410	-0.6322980
H	-1.1800230	-1.9680350	-1.5881460
C	-2.1725750	-0.2449530	-0.8521330
H	-2.0534880	0.2100540	-1.8359750
C	-2.3006220	0.5438130	0.2128880
H	-2.3733300	0.0810150	1.1948480
C	2.7472580	-0.5225660	0.0520950
H	3.0674580	-1.4993510	-0.3423980
H	2.9417800	-0.5252020	1.1372570
O	3.4343200	0.5363470	-0.5896650
H	4.3800140	0.3737200	-0.5125840

water			
C	1.2770130	-0.3265590	-0.1720290
C	0.2680210	-0.8247750	0.8160720
C	0.4864140	0.6874680	0.6195330
H	0.9722290	-0.3837460	-1.2176030
H	0.7447390	-1.1101530	1.7552390
H	1.0328670	1.0865230	1.4732960
C	-0.8601740	-1.8335720	0.5541170
H	-0.3917860	-2.8262590	0.5393730
H	-1.5048600	-1.8330520	1.4407810
C	-0.2932010	1.7898180	-0.1172500
H	0.2439700	2.7310870	0.0501380
H	-0.2364350	1.5894420	-1.1912880
C	-1.8006710	1.9520890	0.2109920
H	-2.2638580	2.5816850	-0.5564210
H	-1.9559990	2.4358120	1.1791860
C	-1.7466680	-1.6875490	-0.6957810
H	-2.5758050	-2.4030560	-0.6303840
H	-1.1765290	-1.9681460	-1.5883120
C	-2.1744370	-0.2496800	-0.8509040
H	-2.0549100	0.2059810	-1.8345130
C	-2.3045460	0.5392050	0.2143880
H	-2.3752270	0.0765400	1.1966890
C	2.7484190	-0.5193130	0.0540280
H	3.0693380	-1.4956820	-0.3387980
H	2.9425990	-0.5195260	1.1384900
O	3.4426510	0.5377180	-0.5885190
H	4.3874320	0.3680210	-0.5067180

1,4-dioxane			
C	1.2770130	-0.3265590	-0.1720290
C	0.2680210	-0.8247750	0.8160720
C	0.4864140	0.6874680	0.6195330
H	0.9722290	-0.3837460	-1.2176030
H	0.7447390	-1.1101530	1.7552390
H	1.0328670	1.0865230	1.4732960
C	-0.8601740	-1.8335720	0.5541170
H	-0.3917860	-2.8262590	0.5393730
H	-1.5048600	-1.8330520	1.4407810
C	-0.2932010	1.7898180	-0.1172500
H	0.2439700	2.7310870	0.0501380
H	-0.2364350	1.5894420	-1.1912880
C	-1.8006710	1.9520890	0.2109920
H	-2.2638580	2.5816850	-0.5564210
H	-1.9559990	2.4358120	1.1791860
C	-1.7466680	-1.6875490	-0.6957810
H	-2.5758050	-2.4030560	-0.6303840
H	-1.1765290	-1.9681460	-1.5883120
C	-2.1744370	-0.2496800	-0.8509040
H	-2.0549100	0.2059810	-1.8345130
C	-2.3045460	0.5392050	0.2143880
H	-2.3752270	0.0765400	1.1966890
C	2.7484190	-0.5193130	0.0540280
H	3.0693380	-1.4956820	-0.3387980
H	2.9425990	-0.5195260	1.1384900
O	3.4426510	0.5377180	-0.5885190
H	4.3874320	0.3680210	-0.5067180

Tetrazine **1**, gas phase			
C	-0.2218010	0.2202470	0.5196200
C	-2.6616510	-0.0851050	-0.1948560
N	-2.1241970	1.1334720	-0.3132390
N	-0.8718500	1.2893830	0.0527440
N	-2.0039090	-1.1607990	0.2689710
N	-0.7583680	-1.0051090	0.6323500
C	-4.0886550	-0.2712960	-0.6004390
C	1.2176940	0.3798450	0.8992620
H	1.3975720	1.4338550	1.1285890
H	1.4090020	-0.2149460	1.7980990
H	-4.1636400	-1.0525930	-1.3599240
H	-4.4843590	0.6648190	-0.9920550
H	-4.6827140	-0.5890150	0.2598080
C	2.1339320	-0.0849100	-0.2390180
H	1.9261720	-1.1338640	-0.4744280
H	1.9351460	0.5036500	-1.1410250
C	3.5946640	0.0616980	0.1358880
H	3.8339790	-0.5405850	1.0206790
H	3.8404980	1.1087920	0.3507380
F	4.3835020	-0.3668470	-0.9110030

water			
C	-0.2175960	0.2050270	0.5324700
C	-2.6654050	-0.0777140	-0.2007890
N	-2.1157620	1.1374130	-0.2970420
N	-0.8645540	1.2810680	0.0770220
N	-2.0111860	-1.1599430	0.2536850
N	-0.7670920	-1.0165020	0.6253160
C	-4.0898660	-0.2519410	-0.6154680
C	1.2213480	0.3504740	0.9166490
H	1.4068260	1.3950770	1.1799150
H	1.4140930	-0.2708270	1.7962880
H	-4.1649780	-1.0262780	-1.3818150
H	-4.4804150	0.6873760	-1.0041140
H	-4.6906110	-0.5683360	0.2405020
C	2.1336080	-0.0789300	-0.2396530
H	1.9254090	-1.1202190	-0.5071290
H	1.9319500	0.5386240	-1.1212900
C	3.5935370	0.0563490	0.1392360
H	3.8395050	-0.5769850	0.9982800
H	3.8439140	1.0945220	0.3822510
F	4.3811890	-0.3407550	-0.9322690

1,4-dioxane			
C	-0.2196930	0.2021440	0.5314190
C	-2.6630720	-0.0767910	-0.2001400
N	-2.1158670	1.1396240	-0.2928810
N	-0.8643610	1.2816100	0.0810250
N	-2.0111710	-1.1624920	0.2489620
N	-0.7666270	-1.0206660	0.6204010
C	-4.0885450	-0.2485560	-0.6149810
C	1.2196030	0.3462860	0.9162920
H	1.4031890	1.3905540	1.1833780
H	1.4113740	-0.2798420	1.7930620
H	-4.1648030	-1.0205860	-1.3836180
H	-4.4772710	0.6934550	-0.9992500
H	-4.6893110	-0.5692840	0.2394400
C	2.1334480	-0.0781030	-0.2402790
H	1.9257910	-1.1183190	-0.5119450
H	1.9323830	0.5424250	-1.1199500
C	3.5938370	0.0559830	0.1382650
H	3.8379110	-0.5791590	0.9974300
H	3.8423070	1.0940860	0.3866480
F	4.3812390	-0.3361830	-0.9301340

Tetrazine **2**, gas phase

C	-1.6804960	-0.0052510	-0.0000110
C	-4.2252090	-0.1713360	0.0000320
N	-3.5389400	-1.3156700	0.0001970
N	-2.2335910	-1.2309670	0.0002000
N	-2.3886010	1.1378490	-0.0001710
N	-3.6943830	1.0521940	-0.0001210
C	-0.2084140	0.0906470	-0.0000540
C	0.4140580	1.3448350	0.0000980
C	1.7970370	1.4276820	0.0001050
H	-0.1956860	2.2408890	0.0002170
C	1.9610940	-0.9755680	-0.0002090
C	2.5824660	0.2713230	-0.0000390
H	2.2763410	2.4038880	0.0002520
H	2.5735990	-1.8691520	-0.0003090
C	0.5739590	-1.0670900	-0.0002080
H	0.0858270	-2.0352430	-0.0003180
H	-5.3067180	-0.2424760	0.0000400
C	4.0853900	0.3990940	0.0000210
H	4.3885880	0.9790720	-0.8853450
H	4.3885140	0.9790920	0.8853990
O	4.6691380	-0.8828650	0.0000410
H	5.6257440	-0.7830050	0.0005940

1,4-dioxane

C	1.6809430	-0.0049220	0.0000100
C	4.2300680	-0.1711840	-0.0000070
N	3.5411520	-1.3139630	0.0000430
N	2.2359220	-1.2295540	0.0000590
N	2.3905590	1.1370760	-0.0000610
N	3.6961240	1.0511270	-0.0000580
C	0.2088690	0.0905410	0.0000060
C	-0.4155820	1.3443200	0.0000410
C	-1.7987760	1.4273650	0.0000400
H	0.1908600	2.2425070	0.0000820
C	-1.9612390	-0.9757820	-0.0000250
C	-2.5847570	0.2705770	0.0000040
H	-2.2780460	2.4032630	0.0000740
H	-2.5706790	-1.8714730	-0.0000390
C	-0.5738240	-1.0672900	-0.0000350
H	-0.0887040	-2.0368520	-0.0000620
H	5.3112830	-0.2420940	0.0000140
C	-4.0875620	0.3989530	0.0000050
H	-4.3908210	0.9789870	0.8844610
H	-4.3908180	0.9790300	-0.8844230
O	-4.6734890	-0.8830590	-0.0000260
H	-5.6303010	-0.7771630	-0.0000110

TS1$_{1+3}$, gas phase

C	-0.4486110	2.2438020	0.3462180
C	1.2012590	0.3792600	0.1204820
C	-0.7906720	-0.6208040	0.0062830
H	-0.5339730	-0.9855930	-0.9897300
C	-1.6899860	0.4210090	0.0737250
H	-2.1459040	0.6085340	1.0474660
N	1.0438120	0.9004130	1.3768170
N	0.1933220	1.8535800	1.4927200
N	1.0474740	1.1928510	-0.9701140
N	0.2036680	2.1520380	-0.8552220
C	-2.5376290	0.7498180	-1.1226810
H	-2.8559680	1.7963260	-1.1438780
H	-1.9616260	0.5621900	-2.0361420
C	-0.7626670	-1.6419700	1.1084750
H	0.2068930	-2.1390040	1.2039470
H	-0.9744310	-1.1477760	2.0638510
C	-3.7891100	-0.1543820	-1.0948690
H	-4.3443810	0.0113120	-2.0247720
H	-4.4479870	0.1764770	-0.2815260
C	-1.8404840	-2.7087190	0.8152590
H	-1.8872110	-3.3839160	1.6769300
H	-1.5121110	-3.3206780	-0.0348470
C	-3.2502830	-2.1673900	0.5176480
H	-3.9548480	-2.9790560	0.7246530
H	-3.4964290	-1.3790980	1.2407840
C	-3.5140100	-1.6597390	-0.9284750
H	-4.3877230	-2.1907810	-1.3193390
H	-2.6815500	-1.9498940	-1.5827950
C	2.1901090	-0.7416960	-0.0257410
C	-1.4659080	3.3366560	0.4924190
H	-2.3395120	2.9923210	1.0508960
H	-1.7733650	3.6920290	-0.4910570
H	-1.0215060	4.1673800	1.0458490
H	1.9083900	-1.3612810	-0.8847930
H	2.1508390	-1.3600370	0.8755560
C	3.6088000	-0.1940870	-0.2137860
H	3.6404800	0.4442870	-1.1016120
H	3.8792330	0.4222900	0.6497660
C	4.6177830	-1.3143890	-0.3608770
H	4.3892940	-1.9345550	-1.2366200
H	4.6243460	-1.9575520	0.5279170
F	5.8810640	-0.7822570	-0.5215990

1,4-dioxane

C	-0.4510940	2.2505260	0.3467880
C	1.2053250	0.3852740	0.1166960
C	-0.7941350	-0.6229390	0.0086110
H	-0.5329750	-0.9916990	-0.9847230
C	-1.6946030	0.4173980	0.0706000
H	-2.1527260	0.6097810	1.0422750
N	1.0487040	0.9083380	1.3718400
N	0.1960410	1.8602400	1.4898060
N	1.0480880	1.2018360	-0.9705940
N	0.2024830	2.1600920	-0.8534360
C	-2.5380340	0.7432880	-1.1291860
H	-2.8586800	1.7889210	-1.1535770
H	-1.9614480	0.5501850	-2.0411900
C	-0.7641110	-1.6375400	1.1164430
H	0.2060150	-2.1322950	1.2162940
H	-0.9836920	-1.1405330	2.0686410
C	-3.7885160	-0.1630090	-1.0990440
H	-4.3418730	-0.0008180	-2.0305990
H	-4.4477020	0.1704980	-0.2873040
C	-1.8386870	-2.7079550	0.8226300
H	-1.8853270	-3.3800470	1.6866000
H	-1.5055860	-3.3203640	-0.0250740
C	-3.2489480	-2.1702520	0.5206020
H	-3.9517020	-2.9833810	0.7278980
H	-3.4985270	-1.3805860	1.2411190
C	-3.5108400	-1.6673520	-0.9276710
H	-4.3835300	-2.2005030	-1.3178900
H	-2.6769560	-1.9583340	-1.5798480
C	2.1903140	-0.7383280	-0.0326900
C	-1.4747310	3.3365780	0.4950880
H	-2.3412870	2.9877810	1.0612130
H	-1.7945960	3.6845910	-0.4869350
H	-1.0327770	4.1749160	1.0391630
H	1.9083180	-1.3527490	-0.8947210
H	2.1471620	-1.3624370	0.8641150
C	3.6120600	-0.1955070	-0.2139990
H	3.6509990	0.4441260	-1.1008100
H	3.8828770	0.4174010	0.6520190
C	4.6155480	-1.3203480	-0.3605120
H	4.3902200	-1.9365340	-1.2387380
H	4.6205890	-1.9638670	0.5269130
F	5.8843020	-0.7885110	-0.5171440

TS1$_{1+4}$, gas phase			
C	-3.9612780	-0.5611950	0.1339090
C	-2.9416510	-0.6319390	1.2284710
C	-2.7740960	-1.4728400	-0.0440470
H	-3.9182150	0.3311260	-0.4910680
H	-3.2654720	-1.2920370	2.0342350
H	-2.9944940	-2.5166980	0.1746180
C	-2.2026950	0.5456000	1.8670180
H	-2.9101260	1.0247690	2.5553510
H	-1.4157930	0.1295140	2.5068180
C	-1.8774950	-1.3323870	-1.2762460
H	-2.0977830	-2.1818400	-1.9321240
H	-2.1758810	-0.4412670	-1.8356170
C	-0.3561300	-1.2363710	-1.0331920
H	0.1456630	-0.9754700	-1.9727370
H	0.0485450	-2.1936090	-0.6910100
C	-1.5740930	1.6416760	0.9902250
H	-0.9643310	2.2787030	1.6424280
H	-2.3530400	2.2808730	0.5612010
C	-0.7673650	1.0422070	-0.1420710
H	-1.0794460	1.3070330	-1.1513910
C	-0.1566100	-0.1724850	0.0189110
H	-0.0328830	-0.5347540	1.0374260
C	0.9763150	2.5195700	-0.3820840
C	2.0666250	0.2835080	-0.1052900
C	2.6798370	-1.0757830	0.0652430
C	0.2491870	3.8180500	-0.5512250
N	1.5432170	2.2670150	0.8338090
N	2.0589540	0.8021720	-1.3668360
N	2.0992570	1.1150500	0.9757750
N	1.4895130	1.9474030	-1.5088720
H	0.9734980	4.6253260	-0.6907760
H	-0.3922650	3.7779190	-1.4329750
H	-0.3450730	4.0437140	0.3347850
H	2.2866120	-1.5288660	0.9821350
H	2.3819200	-1.6986780	-0.7841170
C	-5.3450710	-1.1140140	0.3161870
H	-5.9999010	-0.3536540	0.7687820
H	-5.2963720	-1.9657180	1.0142800
O	-5.8277270	-1.5141610	-0.9523650
H	-6.7413180	-1.8012690	-0.8539520
C	4.2071700	-0.9807580	0.1364490
H	4.4957310	-0.3401300	0.9756140
H	4.5877040	-0.5206830	-0.7812370
C	4.8381500	-2.3474320	0.3071020
H	4.4988090	-2.8228160	1.2359270
H	4.5828540	-3.0047960	-0.5333240
F	6.2112760	-2.2208130	0.3591500

water			
C	-3.9674610	-0.5703200	0.1230310
C	-2.9459680	-0.6316440	1.2165250
C	-2.7708160	-1.4737360	-0.0536630
H	-3.9295590	0.3247960	-0.4990480
H	-3.2649650	-1.2926020	2.0229830
H	-2.9782030	-2.5195150	0.1689760
C	-2.2169910	0.5527860	1.8546010
H	-2.9320220	1.0317560	2.5346030
H	-1.4339920	0.1414950	2.5020160
C	-1.8725320	-1.3256430	-1.2841430
H	-2.0843960	-2.1747220	-1.9437400
H	-2.1683820	-0.4309730	-1.8395870
C	-0.3512610	-1.2291970	-1.0360980
H	0.1493140	-0.9657120	-1.9754920
H	0.0537540	-2.1856500	-0.6942230
C	-1.5880400	1.6489210	0.9778550
H	-0.9896530	2.2937410	1.6328470
H	-2.3646960	2.2823810	0.5377390
C	-0.7724760	1.0468270	-0.1461380
H	-1.0721790	1.3168200	-1.1579540
C	-0.1637980	-0.1667290	0.0189960
H	-0.0399050	-0.5304970	1.0370980
C	0.9905960	2.5407860	-0.3773270
C	2.0862540	0.2954870	-0.0961150
C	2.6814710	-1.0707770	0.0762400
C	0.2500130	3.8305340	-0.5470130
N	1.5574130	2.2840380	0.8366570
N	2.0840080	0.8208530	-1.3538660
N	2.1142870	1.1309570	0.9805200
N	1.5139330	1.9671930	-1.4976800
H	0.9630860	4.6450500	-0.7029100
H	-0.4069010	3.7767100	-1.4163840
H	-0.3368790	4.0556870	0.3438060
H	2.2839910	-1.5178790	0.9932490
H	2.3727710	-1.6930170	-0.7690540
C	-5.3472350	-1.1285700	0.3213400
H	-6.0005150	-0.3725680	0.7800900
H	-5.2900900	-1.9816410	1.0147560
O	-5.8545180	-1.5320150	-0.9424090
H	-6.7654470	-1.8218100	-0.8173960
C	4.2109670	-0.9993320	0.1420450
H	4.5150130	-0.3678090	0.9829920
H	4.5972600	-0.5441200	-0.7759490
C	4.8166680	-2.3775860	0.3057730
H	4.4817030	-2.8493030	1.2359500
H	4.5521690	-3.0277360	-0.5351700
F	6.2001150	-2.2676540	0.3493560

1,4-dioxane			
C	-3.9643560	-0.5659780	0.1282810
C	-2.9439070	-0.6310430	1.2225080
C	-2.7722020	-1.4733550	-0.0482830
H	-3.9239630	0.3273090	-0.4958750
H	-3.2653090	-1.2910640	2.0290620
H	-2.9859500	-2.5181240	0.1729140
C	-2.2101800	0.5506020	1.8599150
H	-2.9215320	1.0301770	2.5436530
H	-1.4251680	0.1377050	2.5039710
C	-1.8745020	-1.3294970	-1.2794800
H	-2.0903920	-2.1790400	-1.9369260
H	-2.1714420	-0.4367980	-1.8372830
C	-0.3532460	-1.2331850	-1.0336760
H	0.1480050	-0.9716890	-1.9732770
H	0.0514820	-2.1898530	-0.6909930
C	-1.5815810	1.6461040	0.9823120
H	-0.9783230	2.2880150	1.6356810
H	-2.3595310	2.2815170	0.5466170
C	-0.7693970	1.0448030	-0.1448970
H	-1.0749420	1.3112720	-1.1558250
C	-0.1596460	-0.1692900	0.0192440
H	-0.0363670	-0.5316300	1.0378590
C	0.9828190	2.5297600	-0.3798350
C	2.0758630	0.2892470	-0.0999630
C	2.6807860	-1.0732200	0.0718630
C	0.2497300	3.8242500	-0.5499170
N	1.5492670	2.2753670	0.8354140
N	2.0713430	0.8110250	-1.3597760
N	2.1057320	1.1229930	0.9787710
N	1.5016480	1.9566600	-1.5031370
H	0.9690960	4.6344220	-0.6986060
H	-0.3999160	3.7770780	-1.4252120
H	-0.3402400	4.0506810	0.3386470
H	2.2859200	-1.5229580	0.9892010
H	2.3773650	-1.6962750	-0.7750990
C	-5.3460760	-1.1217810	0.3186790
H	-6.0004540	-0.3635360	0.7737680
H	-5.2930010	-1.9737800	1.0148980
O	-5.8407940	-1.5244050	-0.9473070
H	-6.7531520	-1.8129130	-0.8357680
C	4.2092870	-0.9894770	0.1396120
H	4.5059610	-0.3534880	0.9796130
H	4.5921040	-0.5315750	-0.7783120
C	4.8276830	-2.3620300	0.3061720
H	4.4910890	-2.8357650	1.2357570
H	4.5674460	-3.0155130	-0.5345990
F	6.2061320	-2.2440780	0.3533860

TS1$_{2+3}$, gas phase

C	0.0506210	-1.5579120	-0.0906270
C	-1.3252380	0.3024670	-0.0537890
H	-0.9746730	0.4823500	0.9639350
C	-2.5901160	-0.2207180	-0.2056490
H	-3.0157720	-0.1748610	-1.2097230
N	-0.3045150	-1.9633200	-1.3489440
N	-1.5088370	-2.3803930	-1.4984900
N	-0.5266100	-2.1583630	0.9980350
N	-1.7295530	-2.5799590	0.8527980
C	-3.5796700	-0.1248280	0.9234160
H	-4.3386470	-0.9138720	0.8852300
H	-3.0506420	-0.2273470	1.8777360
C	-0.7474000	1.1857000	-1.1169150
H	0.3466750	1.1683350	-1.1277430
H	-1.1010330	0.8499380	-2.0993550
C	-4.2692560	1.2542400	0.8481550
H	-4.9036520	1.3638810	1.7348350
H	-4.9460250	1.2676640	-0.0158750
C	-1.2312100	2.6305120	-0.8527080
H	-0.9045730	3.2532050	-1.6928750
H	-0.7166190	3.0191820	0.0354050
C	-2.7498840	2.7924290	-0.6595600
H	-2.9938460	3.8355880	-0.8847250
H	-3.2751280	2.2012340	-1.4211250
C	-3.3164160	2.4602940	0.7508580
H	-3.8670280	3.3357290	1.1096940
H	-2.4905470	2.3248550	1.4611110
C	1.3807720	-0.9419720	0.0952130
C	1.8055320	-0.5752000	1.3766180
C	2.2103170	-0.6918890	-0.9999720
C	3.0399040	0.0328680	1.5501860
H	1.1631080	-0.7807130	2.2267900
C	3.4498960	-0.0859950	-0.8182760
H	1.8754640	-0.9824000	-1.9901100
C	3.8736410	0.2812100	0.4570480
H	3.3621200	0.3193410	2.5486530
H	4.0980550	0.1113490	-1.6640740
C	-2.2841640	-2.3512020	-0.3743710
H	-3.3201230	-2.6472000	-0.4979360
C	5.2230700	0.9178740	0.6807500
H	5.1016440	1.7865550	1.3461540
H	5.8691060	0.1971330	1.2061450
O	5.7809200	1.2919960	-0.5588680
H	6.6789810	1.6010750	-0.4072670

1,4-dioxane

C	0.0552290	-1.5668440	-0.0860160
C	-1.3299540	0.3070440	-0.0571430
H	-0.9739890	0.4903430	0.9581420
C	-2.5947560	-0.2149750	-0.2020190
H	-3.0244060	-0.1792320	-1.2047290
N	-0.3029220	-1.9769380	-1.3409140
N	-1.5088660	-2.3929520	-1.4879250
N	-0.5223370	-2.1652280	1.0024080
N	-1.7270150	-2.5857060	0.8591790
C	-3.5795870	-0.1167170	0.9303080
H	-4.3388750	-0.9053360	0.8971030
H	-3.0473550	-0.2097640	1.8838970
C	-0.7524910	1.1797690	-1.1284490
H	0.3416060	1.1596060	-1.1433540
H	-1.1126070	0.8415370	-2.1075930
C	-4.2686160	1.2628650	0.8470580
H	-4.9005330	1.3777650	1.7346880
H	-4.9463070	1.2701810	-0.0160630
C	-1.2326030	2.6272150	-0.8686340
H	-0.9072770	3.2446420	-1.7130570
H	-0.7148990	3.0178520	0.0166630
C	-2.7507100	2.7914630	-0.6725730
H	-2.9932630	3.8339430	-0.9020530
H	-3.2783000	2.1971490	-1.4300580
C	-3.3144640	2.4672980	0.7410300
H	-3.8639770	3.3450550	1.0956490
H	-2.4873610	2.3351800	1.4505270
C	1.3823280	-0.9446460	0.0977480
C	1.7965100	-0.5517190	1.3754940
C	2.2206280	-0.7131810	-0.9949400
C	3.0289090	0.0608550	1.5485420
H	1.1463920	-0.7346180	2.2250350
C	3.4584260	-0.1028730	-0.8137650
H	1.8962840	-1.0184840	-1.9839650
C	3.8725490	0.2892190	0.4577990
H	3.3413580	0.3681750	2.5435750
H	4.1115690	0.0776500	-1.6594900
C	-2.2855740	-2.3595790	-0.3656770
H	-3.3233420	-2.6487510	-0.4872730
C	5.2176210	0.9352570	0.6816130
H	5.0857210	1.8204320	1.3217710
H	5.8588610	0.2319690	1.2342510
O	5.7914800	1.2789530	-0.5605780
H	6.6861660	1.5961380	-0.4005200

TS1$_{2+4}$, gas phase

C	-4.0224090	-1.3331360	0.0456020
C	-3.0924930	-0.8456140	1.1156580
C	-2.5533970	-1.6440830	-0.0783520
H	-4.3661790	-0.5779670	-0.6613840
H	-3.1099970	-1.5002550	1.9879590
H	-2.2925510	-2.6540320	0.2350700
C	-2.9555880	0.5943700	1.6186620
H	-3.8393800	0.7977780	2.2361640
H	-2.1064510	0.6241180	2.3116670
C	-1.7876660	-1.2227740	-1.3335510
H	-1.6551040	-2.1202870	-1.9479790
H	-2.4130150	-0.5431270	-1.9205810
C	-0.4285930	-0.5200480	-1.1099290
H	-0.0666280	-0.1104150	-2.0611080
H	0.3293600	-1.2112650	-0.7310630
C	-2.7984950	1.7507090	0.6226610
H	-2.6457050	2.6729530	1.1957210
H	-3.7272390	1.8860610	0.0567990
C	-1.6910150	1.4849360	-0.3810140
H	-1.9550130	1.6152840	-1.4305780
C	-0.7149940	0.5648730	-0.1097630
H	-0.5452450	0.2955820	0.9302620
C	-0.5752400	3.4383480	-0.3902150
C	1.2782320	1.8067530	-0.0885440
N	-0.0465630	3.3697280	0.8612540
N	1.1425900	2.3523170	-1.3322450
N	0.9094180	2.5221230	1.0152540
N	0.1873100	3.1994440	-1.4900580
C	-5.0231070	-2.4192530	0.3146230
H	-5.9581660	-1.9861940	0.7013090
H	-4.6204300	-3.0861870	1.0946260
O	-5.2447140	-3.1189860	-0.8953160
H	-5.9547430	-3.7536780	-0.7543150
C	2.2478000	0.7052460	0.0853050
C	2.4886550	0.1791410	1.3579880
C	2.8995970	0.1559470	-1.0220600
C	3.3744350	-0.8785140	1.5154190
H	1.9906780	0.6200700	2.2153340
C	3.7798960	-0.9064950	-0.8559030
H	2.7118140	0.5732960	-2.0054950
C	4.0248300	-1.4348550	0.4123120
H	3.5686990	-1.2743740	2.5093190
H	4.2906390	-1.3377370	-1.7110600
C	4.9706460	-2.6037030	0.5821460
H	4.4118500	-3.5440360	0.5219510
H	5.4234830	-2.5639670	1.5841130
O	5.9496800	-2.6800290	-0.4299770
H	6.4472160	-1.8538490	-0.4176000
H	-1.4334700	4.0879800	-0.5225010

1,4-dioxane

C	-3.9941490	-1.3660690	0.0292240
C	-3.0723580	-0.8300650	1.0836390
C	-2.5157630	-1.6315930	-0.0997890
H	-4.3695120	-0.6338070	-0.6858760
H	-3.0654930	-1.4691740	1.9673330
H	-2.2176340	-2.6267530	0.2279190
C	-2.9766820	0.6232370	1.5594330
H	-3.8750480	0.8181080	2.1579910
H	-2.1399940	0.6860780	2.2654670
C	-1.7675940	-1.2002880	-1.3617920
H	-1.6276820	-2.0945920	-1.9796500
H	-2.4020300	-0.5217540	-1.9408040
C	-0.4139250	-0.4836530	-1.1417570
H	-0.0585190	-0.0689400	-2.0929590
H	0.3504170	-1.1676250	-0.7623580
C	-2.8321270	1.7612690	0.5419910
H	-2.7405180	2.7042940	1.0937450
H	-3.7460100	1.8435030	-0.0573670
C	-1.6899480	1.5159330	-0.4272620
H	-1.9170860	1.6715860	-1.4822100
C	-0.7235400	0.5927380	-0.1409780
H	-0.5805400	0.3116130	0.8998580
C	-0.5562460	3.4830740	-0.3510660
C	1.2930470	1.8368020	-0.0534620
N	-0.0524740	3.3773610	0.9066650
N	1.1811710	2.4155640	-1.2831850
N	0.9012510	2.5246780	1.0585670
N	0.2301800	3.2696250	-1.4380950
C	-4.9566870	-2.4769920	0.3353240
H	-5.8987680	-2.0664230	0.7275800
H	-4.5218750	-3.1161730	1.1200190
O	-5.1794460	-3.2113340	-0.8566510
H	-5.8395970	-3.8885480	-0.6725690
C	2.2457350	0.7201890	0.1099720
C	2.4340750	0.1392060	1.3685340
C	2.9292840	0.2051440	-0.9944760
C	3.2997260	-0.9363290	1.5145950
H	1.9068650	0.5452700	2.2257030
C	3.7903790	-0.8753650	-0.8403130
H	2.7800520	0.6574280	-1.9688440
C	3.9826830	-1.4575040	0.4130610
H	3.4498170	-1.3762330	2.4973500
H	4.3236850	-1.2784290	-1.6951190
C	4.8982570	-2.6517040	0.5747700
H	4.3076870	-3.5732980	0.5317900
H	5.3678550	-2.6189140	1.5682950
O	5.8598390	-2.7647700	-0.4517880
H	6.4192600	-1.9791300	-0.4186910
H	-1.4143590	4.1319710	-0.4846440

7. References

[1] S. A. Lang, B. D. Johnson, E. Cohen, *J. Heterocyclic Chem.* **1975**, *12*, 1143-1153.

[2] M. Royzen, G. P. A. Yap, J. M. Fox, *J. Am. Chem. Soc.* **2008**, *130*, 3760-3761.

[3] M. T. Taylor, M. L. Blackman, O. Dmitrenko, J. M. Fox, *J. Am. Chem. Soc.* **2011**, *133*, 9646-9649.

[4] E. Nachbaur, G. Leiseder, *Monatsh. Chem.* **1971**, *102*, 1718-1723.

[5] D. Lumpi, C. Braunshier, C. Hametner, E. Horkel, B. Zachhuber, B. Lendl, J. Fröhlich, *Tetrahedron Lett.* **2009**, *50*, 6469-6471.

[6] A. M. Loening, S. S. Gambhir, *Mol. Imaging* **2003**, *2*, 131-137.

[7] M. J. T. Frisch, G. W.; Schlegel, H. B.; Scuseria, G. E.; Robb, M. A.; Cheeseman, J. R.; Scalmani, G.; Barone, V.; Mennucci, B.; Petersson, G. A.; Nakatsuji, H.; Caricato, M.; Li, X.; Hratchian, H. P.; Izmaylov, A. F.; Bloino, J.; Zheng, G.; Sonnenberg, J. L.; Hada, M.; Ehara, M.; Toyota, K.; Fukuda, R.; Hasegawa, J.; Ishida, M.; Nakajima, T.; Honda, Y.; Kitao, O.; Nakai, H.; Vreven, T.; Montgomery, Jr., J. A.; Peralta, J. E.; Ogliaro, F.; Bearpark, M.; Heyd, J. J.; Brothers, E.; Kudin, K. N.; Staroverov, V. N.; Kobayashi, R.; Normand, J.; Raghavachari, K.; Rendell, A.; Burant, J. C.; Iyengar, S. S.; Tomasi, J.; Cossi, M.; Rega, N.; Millam, J. M.; Klene, M.; Knox, J. E.; Cross, J. B.; Bakken, V.; Adamo, C.; Jaramillo, J.; Gomperts, R.; Stratmann, R. E.; Yazyev, O.; Austin, A. J.; Cammi, R.; Pomelli, C.; Ochterski, J. W.; Martin, R. L.; Morokuma, K.; Zakrzewski, V. G.; Voth, G. A.; Salvador, P.; Dannenberg, J. J.; Dapprich, S.; Daniels, A. D.; Farkas, Ö.; Foresman, J. B.; Ortiz, J. V.; Cioslowski, J.; Fox, D. J, *Gaussian 09, Revision A.1*, Gaussian Inc, Wallingford CT, **2009**.

[8] R. Ditchfield, W. J. Hehre, J. A. Pople, *J. Chem. Phys.* **1971**, *54*, 724-728.

[9] Y. Zhao, D. Truhlar, *Theor. Chem. Acc.* **2008**, *120*, 215-241.

[10] a) Y. Lan, L. Zou, Y. Cao, K. N. Houk, *J. Phys. Chem. A* **2011**, *115*, 13906-13920; b) R. S. Paton, J. L. Mackey, W. H. Kim, J. H. Lee, S. J. Danishefsky, K. N. Houk, *J. Am. Chem. Soc.* **2010**, *132*, 9335-9340.

[11] J. Tomasi, B. Mennucci, R. Cammi, *Chem. Rev.* **2005**, *105*, 2999-3094.

[12] a) V. Barone, M. Cossi, *J. Phys. Chem. A* **1998**, *102*, 1995-2001; b) M. Cossi, N. Rega, G. Scalmani, V. Barone, *J. Comput. Chem.* **2003**, *24*, 669-681.

Manuscript #2 – Supporting Information

Reprinted from *Bioconjugate Chemistry* (2016), accepted manuscript.

Denk, C.; Svatunek, D.; Mairinger, S.; Stanek, J.; Filip, T.; Matscheko, D.; Kuntner-Hannes, C.; Wanek, T.; Mikula, H.:

Design, Synthesis and Evaluation of a Low-Molecular-Weight ^{11}C-Labeled Tetrazine for Pretargeted PET Imaging applying Bioorthogonal *In Vivo* Click Chemistry

Supplementary Material

Design, Synthesis and Evaluation of a Low-Molecular-Weight ^{11}C-Labeled Tetrazine for Pretargeted PET Imaging applying Bioorthogonal *in Vivo* Click Chemistry

Christoph Denk,[†] Dennis Svatunek,[†] Severin Mairinger,[‡] Johann Stanek,[‡] Thomas Filip,[‡] Dominik Matscheko,[†] Claudia Kuntner,[‡] Thomas Wanek,[‡] and Hannes Mikula*[,†]

[†]Institute of Applied Synthetic Chemistry, Vienna University of Technology (TU Wien), Vienna, Austria

[‡]Health and Environment Department, Biomedical Systems, Austrian Institute of Technology (AIT), Seibersdorf, Austria

Corresponding Author

*hannes.mikula@tuwien.ac.at

Table of Contents

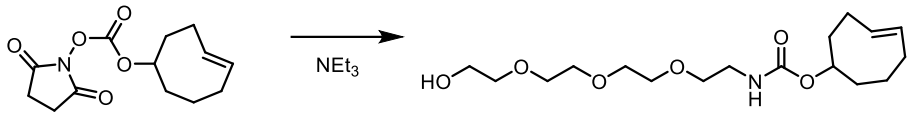
1. Materials and Methods S2
2. Chemical Synthesis and Radiolabeling S3
3. Reaction Kinetics S15
4. *In vitro* and *in vivo* Investigations S17
5. NMR Spectra S21
6. Quantum Chemical Calculations S27
7. References S35

1. Materials and Methods

Unless otherwise noted, all reagents were purchased from commercial suppliers and used without further purification. DCM and 1,4-dioxane were dried using PURESOLV-columns (Innovative Technology Inc.). Dry acetonitrile (Sigma Aldrich) was commercially obtained and stored under argon. Boc protected aminoacetonitrile and dienophiles *s*-TCO **4** and s-TCO-OPNP were prepared following known procedures.[1,2] Anhydrous hydrazine was prepared by the vacuum thermolysis of hydrazine cyanurate.[3] All other solvents were distilled prior to use. Drying of organic solvents after extraction was performed using anhydrous Na_2SO_4 or $MgSO_4$ (Sigma Aldrich) and subsequent filtration. Human Plasma for research purposes was purchased from the Austrian Red Cross blood donation service. Reactions were carried out under an atmosphere of argon in air-dried glassware with magnetic stirring. Sensitive liquids were transferred via syringe. Thin layer chromatography was performed using TLC alumina plates (Merck, silica gel 60, fluorescence indicator F254, or Merck, aluminium oxide neutral, fluorescence indicator F254). Detection in radio-TLC was performed by placing the TLC plates on multisensitive phosphor screens (Perkin-Elmer Life Sciences, Waltham, MA). The screens were scanned at 300 dpi resolution using a PerkinElmer Cyclone® Plus Phosphor Imager (Perkin-Elmer Life Sciences). Preparative column chromatography was performed using a Büchi Sepacore Flash System (2 x Büchi Pump Module C-605, Büchi Pump Manager C-615, Büchi UV Photometer C-635, Büchi Fraction Collector C-660) using silica gel 60 (40-63 µm) as obtained from Merck and distilled or redistilled solvents. ^{1}H, ^{13}C and ^{19}F NMR spectra were recorded on a Bruker Avance IIIHD 600 MHz spectrometer equipped with a Prodigy BBO cryo probe or on a Bruker Avance UltraShield 400 spectrometer at 20 °C. Chemical shifts are reported in ppm (δ) relative to tetramethylsilane and calibrated using solvent residual peaks. Data are shown as follows: Chemical shift, multiplicity (s = singlet, d = doublet, t = triplet, q = quartet, quin = quintet, m = multiplet, br = broad signal) and integration. UV/VIS spectrophotometry was done on a UV-1800 Spectrophotometer (Shimadzu) and temperature-controlled Applied Photophysics 05-19 and SX20 (535 nm LED light source) stopped flow spectrophotometer systems (Applied Photophysics, Surrey, UK) were used for stopped flow measurements. Fluorescence measurements were done on an Edinburgh FLS920 system (Livingston, UK) using Suprasil glass cuvettes. ESI-MS was performed on an HCT ion trap mass spectrometer (Bruker, Germany). A Thermo Fischer Exactive Plus Orbitrap (LC-ESI+) Mass Spectrometer was used for high-resolution mass spectrometry. [^{11}C]Methane was produced *via* the $^{14}N(p, \alpha)^{11}C$ nuclear reaction by irradiating nitrogen gas containing 10% hydrogen using a PETtrace cyclotron equipped with a methane target system (GE Healthcare, Uppsala, Sweden). [^{11}C]Methyl iodide was prepared *via* the gas-phase method in a TracerLab FXC Pro synthesis module (GE Healthcare) and converted into [^{11}C]methyl triflate by passage through a column containing silver-triflate impregnated graphitized carbon.[4,5] HPLC analysis was performed on a 1200 series system (Agilent Technologies) using a Phenomenex Luna SCX (5 µm, 4.6 x 250 mm) column and 9:1 50 mM phosphate buffer pH=2.4:EtOH (flow rate: 1.5 mL/min). For radio-HPLC a GABI* radioactivity detector (Raytest) was used. Retention times were 12.3 min for precursor **8** and 16 min for [^{11}C]-**1**. Preparative HPLC separation was done on the built in HPLC system on the TracerLab FXC pro synthesis module using a Phenomenex Luna SCX (5 µm, 4.6 x 250 mm) column and 9:1 50 mM phosphate buffer pH=2.4:EtOH (flow rate: 1.5 mL/min) in combination with a K-2001 UV detector (Knauer) and radioactivity detector.

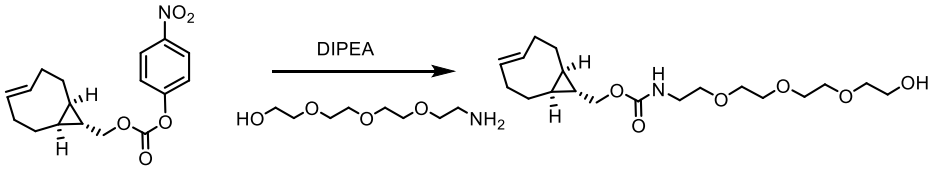
2. Chemical Synthesis and Radiolabeling

(E)-cyclooct-4-en-1-yl (2-(2-(2-(2-hydroxyethoxy)ethoxy)ethoxy)ethyl)carbamate (6)



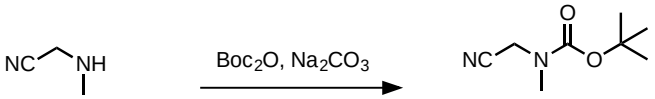
2-(2-(2-(2-aminoethoxy)ethoxy)ethoxy)ethan-1-ol (27 mg, 0.14 mmol, 1.5 eq.) in 200 µl anhydrous DMF was treated with triethyl amine (39 µl, 0.28 mmol, 3 eq.), followed by TCO-O(CO)NHS [6] (25 mg, 0.093 mmol, 1 eq.) in 800 µl anhydrous DMF. The mixture was stirred at room temperature for 22 hours, diluted with 1.25 mL DMSO and 1.25 mL water and loaded onto 30 g C18-silica. The column was eluted with a gradient of acetonitril in water (5-80%). Freeze drying of the product containing fraction yielded 28 mg of title compound as colorless oil (87% of theory). ^{1}H NMR (400 MHz, D_2O) ^{1}H NMR (400 MHz, D_2O) d = 1.54 - 1.71 (m, 3 H) 1.84 - 2.07 (m, 4 H) 2.22 - 2.37 (m, 3 H) 3.25 (t, *J*=5.27 Hz, 2 H) 3.55 (t, *J*=5.27 Hz, 2 H) 3.58 - 3.62 (m, 2 H) 3.63 - 3.72 (m, 10 H) 4.25 (d, *J*=8.20 Hz, 1 H) 5.45 - 5.58 (m, 1 H) 5.59 - 5.74 (m, 1 H) ppm; ^{13}C NMR (100 MHz, D_2O) ? = 30.6, 32.1, 33.7, 37.9, 40.4, 60.4, 69.4, 69.5, 69.6, 69.7, 71.7, 81.9, 133.4, 135.7, 158.3 ppm; ESI-MS $[M+H]^+$ calcd. 346.2 for $C_{17}H_{32}NO_6^+$, found 346.3.

((1R,8S,9r,E)-bicyclo[6.1.0]non-4-en-9-yl)methyl (2-(2-(2-(2-hydroxyethoxy)ethoxy)ethoxy)ethyl) carbamate (7)



2-(2-(2-(2-aminoethoxy)ethoxy)ethoxy)ethan-1-ol (50 mg, 0.259 mmol, 1.1 eq.) in anhydrous DMF was treated with s-TCO-OC(O)PNP[1] (75 mg, 0.235 mmol, 1 eq.) in one portion followed by diisopropyl ethyl amine (76 mg, 0.59 mmol, 2.5 eq.) causing intense yellow coloration. The mixture was stirred at room temperature for 2 hours, diluted with 1.25 mL DMSO and 1.25 mL water and loaded onto a preparative HPLC column (Phenomenex Luna C18, 21.2x250 mm, 10 µm). Elution with a gradient from 10 to 90% MeCN in water followed by freeze drying of the product fraction yielded 55 mg of title compound as colorless oil (63% of theory). ^{1}H NMR (400 MHz, D_2O) δ = 0.38 - 0.49 (m, 2 H) 0.49 - 0.63 (m, 2 H) 0.77 - 0.90 (m, 1 H) 1.82 - 1.96 (m, 2 H) 2.11 - 2.27 (m, 3 H) 2.32 (d, *J*=12.10 Hz, 1 H) 3.28 (t, *J*=5.27 Hz, 2 H) 3.55 (t, *J*=5.46 Hz, 2 H) 3.58 - 3.71 (m, 13 H) 3.91 (d, *J*=5.07 Hz, 2 H) 5.08 - 5.18 (m, 1 H) 5.81 - 5.93 (m, 1 H); ^{13}C NMR (100 MHz, D_2O) δ = 20.8, 21.9, 24.4, 27.5, 32.3, 33.6, 38.4, 40.12, 60.5, 69.5, 69.6, 69.7, 69.8, 71.9, 131.6, 138.7, 158.1 ppm; ESI-MS $[M+Na]^+$ calcd. 394.2 for $C_{19}H_{33}NNaO_6^+$, found 394.2.

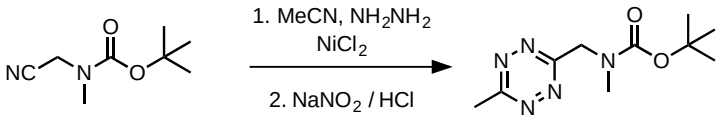
tert-butyl N-cyanomethyl-N-methylcarbamate (8)



8

N-Methylaminoacetonitrile hydrochloride (1 eq., 1.44 g, 13.51 mmol) was dissolved in a mixture of MeOH (12 mL) and water (4 mL). The solution was treated with sodium carbonate (1.15 eq., 1.64 g, 15.5 mmol). Afterwards Boc_2O (1.5 eq., 4.42 g, 20.2 mmol) was added in one portion. The reaction mixture was stirred for 3 h at room temperature and concentrated. The residue was dissolved in dichloromethane and washed with water. The aqueous phase was re-extracted twice with DCM. The combined organic layer was dried over sodium sulfate and concentrated. Purification by column chromatography (40 g SiO_2, 25% ethyl acetate in hexanes + 0.1% Et_3N) yielded the title compound (2.3 g, 13.5 mmol, 99%) as a white solid. ^{1}H NMR data matched that previously reported.[7]

tert-butyl N-methyl-N-((6-methyl-1,2,4,5-tetrazin-3-yl)methyl)carbamate (9)



8 **9**

To a stirred mixture of Boc-protected N-methylaminoacetonitrile **8** (1 eq., 0.6 g, 3.5 mmol), dry acetonitrile (7 eq., 0.98 g, 24 mmol) and nickel chloride (0.4 eq., 0.18 g, 1.4 mmol) was carefully added anhydrous hydrazine (36 eq., 4 g, 125 mmol) while cooling using an ice/salt bath. After finished addition the mixture was heated to 42°C for 18 hours. Afterwards the mixture was cooled to 0°C and a ~10% solution of sodium nitrite (2 eq., 0.5 g, 7 mmol) in water was added. While cooling 1N HCl was added slowly until gas evolution ceased. The mixture was extracted ten times with diethyl ether, combined extracts dried over Na_2SO_4, and concentrated. Column chromatography (90 g SiO_2, 50% Et_2O in hexanes + 1% Et_3N) afforded **9** (238 mg, 28%) as a pink oil that crystallized in the freezer.^{1}H NMR (600 MHz, C_6D_6) δ 4.74 (s, 1.2 H), 4.53 (s, 0.8 H), 2.91 (s, 1.3 H), 2.81 (s, 1.7 H), 2.47 (s, 1.3 H), 2.39 (s, 1.7 H), 1.42 (s, 5 H), 1.30 (s, 4 H); ^{13}C NMR (151 MHz, C_6D_6) δ 168.9, 168.7, 167.6, 167.4, 156.4, 155.4, 80.2, 80.1, 52.2, 52.0, 36.1, 36.0, 28.7, 28.6, 21.0 ppm (NMR spectra show a mixture of rotamers); Attempted HR-ESI-FTMS resulted in fragmentation and detection of deprotected substance **1** as $[M+H]^+$ ion (for MS data of **1** see below).

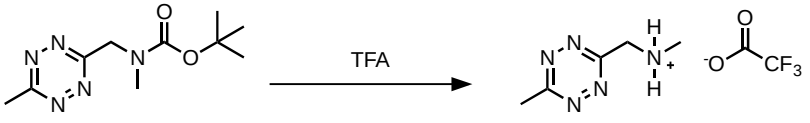
N-methyl-1-(6-methyl-1,2,4,5-tetrazin-3-yl)methanamine (1)



9 **1**

To a stirred solution of **9** (1 eq., 137 mg, 0.573 mmol) in dry DCM (5 mL) was added trifluoroacetic acid (11.4 eq., 0.5 mL, 6.5 mmol) at 0°C. The mixture was stirred at 0°C until TLC indicated complete consumption of starting material (3h). The reaction mixture was partitioned between water and DCM. The organic layer was extracted twice with water and the combined aqueous phases were made alkaline by addition of NaOH. The mixture was extracted several times with DCM and the combined organic layer was washed with water and dried over sodium sulfate. Removal of solvent afforded **1** (40 mg, 51%) as a pink solid. ^{1}H NMR (600 MHz, CD_2Cl_2) δ 4.32 (s, 2 H), 3.03 (s, 3 H), 2.49 (s, 3 H), 1.93 (br. s, 1 H); ^{13}C NMR (151 MHz, CD_2Cl_2) δ 168.8, 168.4, 54.3, 36.2, 21.6 ppm; HR-ESI-FTMS $[M+H]^+$ calcd. 140.0931 for $C_5H_{10}N_5^+$, found 140.0926.

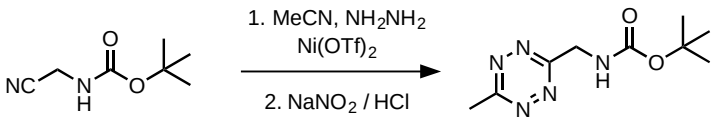
N-methyl-1-(6-methyl-1,2,4,5-tetrazin-3-yl)methanamine trifluoroacetate (1·TFA)



9 **1·TFA**

To a stirred solution of **9** (1 eq., 36 mg, 0.15 mmol) in dry DCM (1 mL) was added trifluoroacetic acid (8.7 eq., 0.1 mL, 1.3 mmol) at 0°C. The mixture was stirred at 0°C until TLC indicated complete consumption of starting material. The reaction mixture was evaporated to dryness on the rotary evaporator. The dark red residue was dissolved in 5 mL water, frozen and lyophilized to obtain **1·TFA** as red oil in quantitative yield. No signs of degradation were noted even after prolonged storage at room temperature. ^{1}H NMR (400 MHz, D_2O) δ 4.90 (s, 2 H), 3.02 (s, 3 H), 2.90 (s, 3 H); ^{13}C NMR (101 MHz, D_2O) δ 169.3, 162.9 (q, J = 35.3 Hz), 162.1, 116.3 (q, J = 292 Hz), 49.6, 33.2, 20.4; ^{19}F NMR (376.5 MHz, D_2O) δ -75.6 ppm.

***tert*-butyl N-((6-methyl-1,2,4,5-tetrazin-3-yl)methyl)carbamate** (**10**)



10

To a stirred mixture of tert-butyl (cyanomethyl)carbamate (1 eq., 0.62 g, 4 mmol), dry acetonitrile (7 eq., 1.46 mL, 28 mmol) and nickel trifluoromethanesulfonate (0.52 eq., 0.74 g, 2.08 mmol) was carefully added anhydrous hydrazine (36 eq., 4.5 mL, 144 mmol) while cooling using an ice/salt bath. After finished addition the mixture was heated to 65°C for 20 hours. Afterwards the mixture was cooled to 0°C and a ~10% solution of sodium nitrite (2 eq., 0.55 g, 8 mmol) in water was added. While cooling 1N HCl was added slowly until gas evolution ceased (pH 3). The mixture was extracted three

times with diethyl ether, combined extracts dried over Na_2SO_4, and the solvent removed. Column chromatography (90 g SiO_2, 50% Et_2O in hexanes) afforded **10** (260 mg, 29%) as a pink oil. ^1H and ^{13}C NMR data matched that previously reported.[8]

(6-methyl-1,2,4,5-tetrazin-3-yl)methanamine (11)



10 **11**

To a stirred solution of **10** (1 eq., 315 mg, 1.4 mmol) in dry DCM (8 mL) was added trifluoroacetic acid (4.6 eq., 0.5 mL, 6.5 mmol) at 0°C. The mixture was stirred at room temperature for 26 h. The reaction mixture was diluted with DCM (40 mL) and 25% NH_4OH (30 mL). Brine (~40 mL) was added, the organic phase was separated and the aqueous phase extracted five times with DCM. The combined organic layer was dried over sodium sulfate and concentrated to yield 156 mg **11** (89%) as a pink-red solid. Even though purity of the raw product was high according to ^1H-NMR the product was further purified (column chromatography over SiO_2 using 5% MeOH in DCM) prior to ^{11}C labeling and NMR measurements. ^1H NMR (600 MHz, $CDCl_3$) δ 4.51 (s, 2 H), 3.08 (s, 3 H), 1.85 (br. s, 2 H); ^{13}C NMR (151 MHz, $CDCl_3$) δ 169.3, 168.1, 45.3, 21.2 ppm; HR-ESI-FTMS $[M+H]^+$ calcd. 126.0774 for $C_4H_8N_5^+$, found 126.0772.

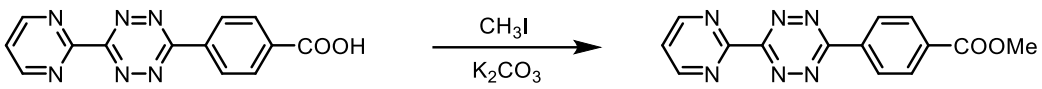
(6-methyl-1,2,4,5-tetrazin-3-yl)methanamine trifluoroacetate (11·TFA)



10 **11·TFA**

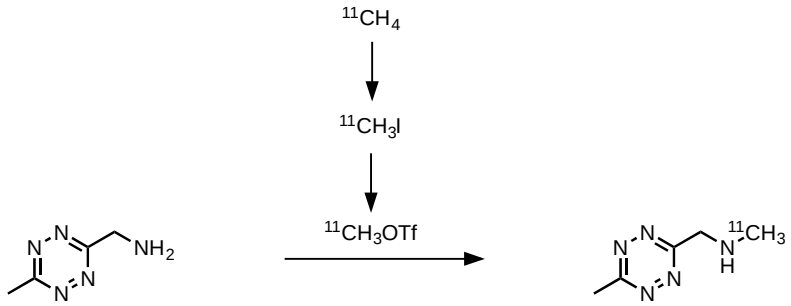
To a stirred solution of **10** (1 eq., 20.1 mg, 0.089 mmol) in dry DCM (1 mL) was added trifluoroacetic acid (14.6 eq., 0.1 mL, 1.3 mmol) at 0°C. The mixture was stirred at 0°C until TLC indicated complete consumption of starting material. The reaction mixture was evaporated to dryness on the rotary evaporator. The dark red residue was redissolved in 5 mL water, frozen and lyophilized to obtain **11·TFA** as a pink solid. No signs of degradation were noted even after prolonged storage at room temperature. ^1H NMR (400 MHz, D_2O) δ 4.91 (s, 2 H), 3.08 (s, 3 H); ^{13}C NMR (101 MHz, D_2O) δ 169.2, 163.0 (q, J = 35.3 Hz), 162.8, 116.3 (q, J = 292 Hz), 41.0, 20.4; ^{19}F NMR (376.5 MHz, D_2O) δ -75.6 ppm

methyl 4-(6-(pyrimidin-2-yl)-1,2,4,5-tetrazin-3-yl)benzoate



4-(6-(pyrimidin-2-yl)-1,2,4,5-tetrazin-3-yl)benzoic acid [9] (1 eq., 0.56 g, 2 mmol) and potassium carbonate (2 eq., 0.55 g, 4 mmol) were stirred in 37 mL anhydrous DMF under an argon atmosphere. Methyl iodide (1.1 eq., 0.311 g, 2.20 mmol) was added in one portion, and the reaction was stirred at room temperature for 16 h after which TLC showed full conversion. The reaction mixture was diluted with 300 mL EtOAc, washed twice with H_2O and brine, dried over $MgSO_4$, and the solvent was removed on the rotary evaporator. Flash chromatography with 5% MeOH in DCM over a pad of silica yielded the title compound (520 mg, 88.3% of theory) as a deep purple solid. Rf (5% MeOH in DCM) = 0.76, ^{1}H NMR (600 MHz, DMSO-d_6) d = 3.94 (s, 3 H) 7.85 (t, *J*=4.84 Hz, 1 H) 8.26 - 8.29 (m, 2 H) 8.72 - 8.74 (m, 2 H) 9.21 (d, *J*=4.69 Hz, 2 H) ppm; ^{13}C NMR (150 MHz, DMSO-d_6) d = 52.6, 123.1, 128.5, 130.2, 133.2, 135.8, 158.6, 159.0, 162.9, 163.1, 165.7 ppm; FT-MS [M+H$^+$] calcd. 295.0938, found 295.0946

Radiosynthesis of N-[^{11}C]methyl-1-(6-methyl-1,2,4,5-tetrazin-3-yl)methanamine ([^{11}C]-1)



11 [^{11}C]-**1**

[^{11}C]methyl triflate was bubbeled through a solution of compound **11** (0.5 mg, 4 µmol) dissolved in anhydrous MeCN (400 µL) using a TracerLab FXC Pro synthesis module. The reaction mixture was heated for 5 min to 75°C, followed by cooling to 25°C and dilution with HPLC eluent (500 µL, 50 mM phosphate buffer pH = 2.4/ EtOH, 9/1, v/v) and injected into a built-in HPLC system. A Phenomenex Luna SCX 250 x 4.6 mm was eluted with 50 mM phosphate buffer pH=2.4 (solvent A) and EtOH (solvent B), A:B= 9:1 (v/v) at a flow rate of 1.5 mL/min. The HPLC eluate was monitored in series for radioactivity and ultraviolet (UV) absorption at a wavelength of 280 nm. On this system, radiolabeling precursor **11** and product [^{11}C]-**1** eluted with retention times of 11.5—13.5 min and 16-18 min, respectively.

The product fraction from HPLC was collected and evaporated to dryness on a rotary evaporator, followed by reformulation in 0.1 M Na_2HPO_4 at an approximate concentration of 37 MBq/mL for intravenous (IV) injection into animals. The formulated product had a pH of 6 and an osmolarity of 485 mmol/kg.

[^{11}C]-**1** ready for IV injection was obtained in a decay-corrected radiochemical yield based on $^{11}CH_3OTf$ of 52 ± 6% (*n* = 3) in a total synthesis time of 30 min. Radiochemical purity of [^{11}C]-**1** was

determined by analytical radio-HPLC using a Phenomenex Luna SCX column (5 µm, 4.6 x 250 mm) and elution with 50 mM phosphate buffer pH=2.4 (solvent A) and EtOH (solvent B), A:B= 9:1 (v/v) at a flow rate of 1.5 mL/min. UV detection was performed at a wave-length of 530 nm. The retention time of [^{11}C]-**1** was 16 min on this HPLC system. The identity of [^{11}C]-**1** was confirmed by HPLC-comparison injecting unlabeled **1**. Radiochemical purity of [^{11}C]-1 was > 95%. The specific activity of [^{11}C]-**1** was determined by measuring radioactivity of a 1 mL aliquot (using a Capintec Dose calibrator) and by HPLC quantification of **1** (conditions described above ; dilution series**:** 0.01 mM, 0.1 mM, 0.5 mM). The Specific activity was determined to be 10 ± 5.4 GBq/µmol (n=4).

Radiosynthesis of N-[^{11}C]methyl-1-(6-methyl-1,2,4,5-tetrazin-3-yl)methanamine ([^{11}C]-1) using 8·TFA as precursor

The general labeling procedure was followed using 1.2 mg **11·TFA** (5.3 µmol) in 400 µl anhydrous MeCN. Prior to labeling 1 µl diisopropylethyl amine (5.75 µmol, 1.08 eq) was added to the reaction mixture. [^{11}C]-**1** was obtained in 34.6% (n = 1) decay corrected radiochemical yield and in >98% radiochemical purity.

Synthesis of mesoporous silica nanoparticles (MSNs) [10]

1 g (2.74 mmol) cetyltrimethylammonium bromide (CTAB) was suspended in 490 mL 15 mM NaOH. The mixture was stirred using a mechanical stirrer at 300 rpm and heated to 80°C which resulted in a homogenous solution. Tetraethylorthosilicate (TEOS, 6.7 ml, 30.23 mmol) was added within 10 seconds and the turbid mixture was stirred at 80°C for additional 2 hours. The mixture was allowed to reach room temperature, the stirring was turned off and the precipitate was allowed to settle. The supernatant was decanted off and the precipitate was collected by centrifugation (10 m, 3000 x g). The pellet was resuspended in 50 mL distilled water, vortexed for 60 seconds followed by centrifugation (10 m, 3000 x g). This washing cycle was repeated twice with water and once with methanol. Drying in vacuo yielded 1.5 g MSNs as white powder (83% of theory). The surfactant was removed by heating in air using the following temperature program: 20°C → 300°C (2°C/min), 300°C (2 h), 300°C → 550°C (2°C/min), 550°C (16 h). The size of the particles was in the range of 120-145 nm (determined by SEM, Fig. S1).

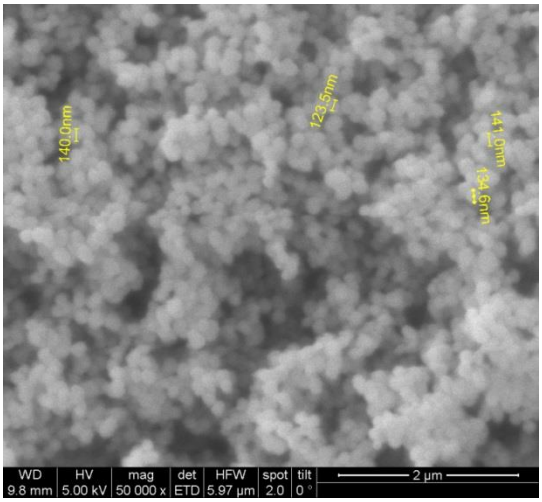


Figure S1: *Electron microscopy of mesoporous silica nanoparticles*

Amino-functionalization of MSNs[11]

357 mg of MSNs were suspended in 20 mL anhydrous toluene and heated on a dean stark trap for 2 h to remove traces of moisture. The dean stark trap was removed and 3-aminopropyltrimethoxysilane (APTMS, 80 µl, 0.458 mmol) was added. The mixture was refluxed for additional 3 h and allowed to cool and settle. The majority of toluene was decanted off and the solids were collected by centrifugation (5 min, 3000 x g). The pellet was resuspended in MeOH, and the solids again collected by centrifugation. Drying in vacuo at 60°C afforded 223 mg amino-grafted MSNs as white powder. The modification did not influence particle size as determined by SEM (Fig. S2).

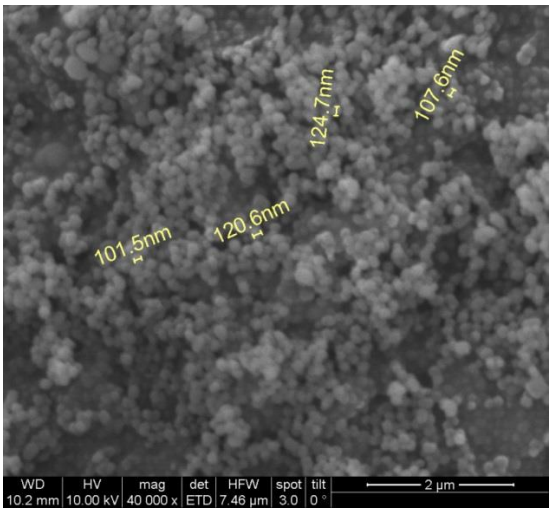


Figure S2: *Electron microscopy of amino-functionalized MSNs*

Determination of amine surface modification

The Fluram (4'-phenylspiro[2-benzofuran-3,2'-furan]-1,3'-dione) assay was chosen for analysis of the degree of surface functionalization with amines.[12] Fluram forms highly fluorescent adducts with primary amines. A stock solution was made by dissolving 14.98 mg native MSNs in 30 g 0.02 N NaOH

followed by the addition of 6.07 mg APTMS (2.26 mmol amine/g MSNs). This stock solution was diluted 1:1, 1:9, 1:99 with a matrix solution (containing 0.5 mg/g native MSNs in 0.02N NaOH) giving solutions corresponding to 1.13 mmol/g, 0.226 mmol/g and 0.0226 mmol/g amine surface modification). The analyte (amino modified MSNs) was also dissolved in dilute NaOH (0.495 mg/g 0.02N NaOH; total 11.22 mg). The blank contained only matrix solution. 100 µl of standard, blank or sample solution were treated with 2 mL 200 mM phosphate buffer pH 8 in a quartz cuvette followed by 1 mL 1 mM fluram solution in acetone. The samples were measured 5 min after fluram addition at 22°C in an Edinburgh FLS920 fluorometer (excitation: 366 nm, emission: 480 nm). Results are summarized in Table S1.

Table S1: *Dilution series concentrations and measured fluorescence intensities*

mmol NH_2/g	cts
blank	1.21E+05
0.022586	1.24E+05
0.22586	1.81E+05
1.1293	3.82E+05
2.2586	6.04E+05

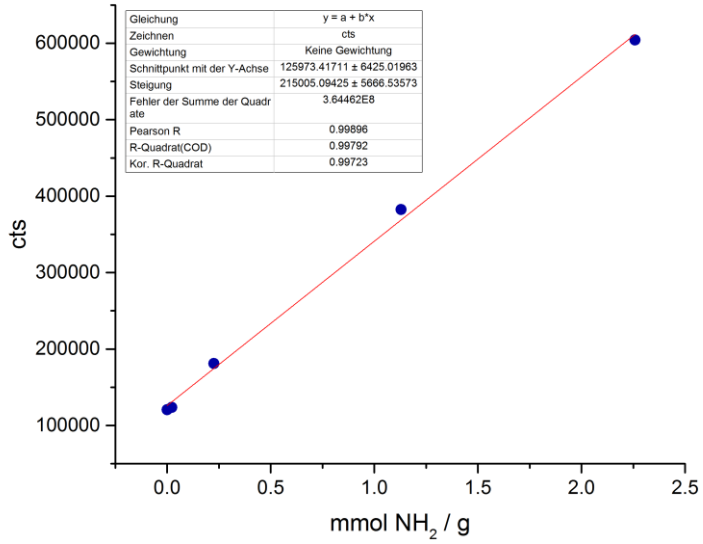
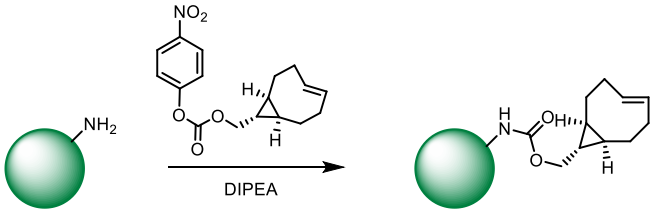


Figure S3: *Linear regression of dilution series data points*

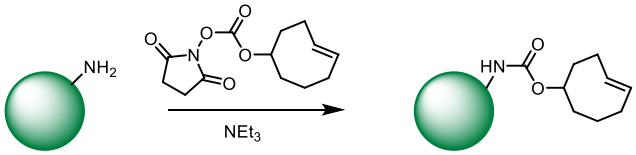
Results of standard and blank measurements were fitted by a linear regression. The sample was found to have **a functionalization degree of 0.92 mmol NH_2/g MSNs**. (3.24E+05 cts; calculated from linear regression shown in Fig. S3).

s-TCO modification of amino-MSNs



600 µl anhydrous DMF and 30 µl diisopropyl ethyl amine (0.172 mmol) were added to 8 mg of amino-MSNs (7.36 µmol amine). 5 mg of s-TCO-OC(O)PNP[1] (15.75 µmol, 2.14 eq) were added in one portion resulting in intense yellow coloration. The reaction mixture was shaken for 16 hours at room temperature and the particles harvested by centrifugation (13.4krpm, 3 min). The supernatant was discarded and the pellet resuspended in 1.5 mL DMF by vortexing. The solvent was again removed following centrifugation. These washing cycles were repeated three times with DMF and once with EtOH. The particles were dried in high vacuum at ambient temperature using a speedvac system.

TCO-modification of amino-MSNs



100 µl anhydrous DMF and 15 µl triethyl amine (0.108 mmol) were added to 5.8 mg of amino-MSNs (5.3 µmol amine). 1 mg of TCO-O(CO)NHS[6] (3.74 µmol, 0.81 eq) in 200 µl anhydrous DMF was added in one portion. The reaction mixture was shaken for 16 hours at room temperature and the particles harvested by centrifugation (13.4 krpm, 3 min). The supernatant was discarded and the pellet resuspended in 1.5 mL DMF by vortexing. The solvent was again removed following centrifugation. These washing cycles were repeated three times with DMF and twice with water. The pellet was resuspended in 1.2 mL 0.9% saline.

Analysis of reactive dienophile loading on s-TCO-MSNs and TCO-MSNs

Highly reactive tetrazine methyl 4-(6-(pyrimidin-2-yl)-1,2,4,5-tetrazin-3-yl)benzoate (15.43 mg, 52.43 µmol) was dissolved in MeOH (100 mL) to obtain a 0.524 mM solution. The stock solution and a dilution series (1:1, 1:3, 1:9: 1:19, stock solution diluted with MeOH) were analyzed by HPLC (isocratic, 30% MeCN in 10 mM phosphate buffer pH 6, Agilent Extend-C18 column 3.0 x 100 mm, 3.5 µm, 1.3 ml/min), monitoring the absorption at 530 nm. The tetrazine eluted at 1.6-1.7 min. A linear regression was calculated based on HPLC results (Fig. S4). A defined mass (1-1.45 mg) of nanoparticles (s-TCO-MSNs, TCO-MSNs, Amino-MSNs) was weighted into 1.5 mL tubes and treated with tetrazine stock solution (400-500 µl, corresponding to 210 – 262 nmol). The vials were vortexed for 60 s and shaken for additional 10 min at 37°C to allow for quantitative IEDDA reaction. Following

centrifugation (13.3 krpm, 5 min) excess tetrazine in the supernatant was analyzed by HPLC using the method described above. The calibration factor was obtained by linear regression of HPLC data arising from the dilution series (Table S2, Fig. S4).

Table S2: *Dilution series concentrations and detector response*

Dilution	c [µmol/ml]	Mean area [mAu*s]
Stock	0.524	185.34
1:1	0.262	91.69
1:3	0.131	48.25
1:9	0.052	18.47
1:19	0.026	9.63

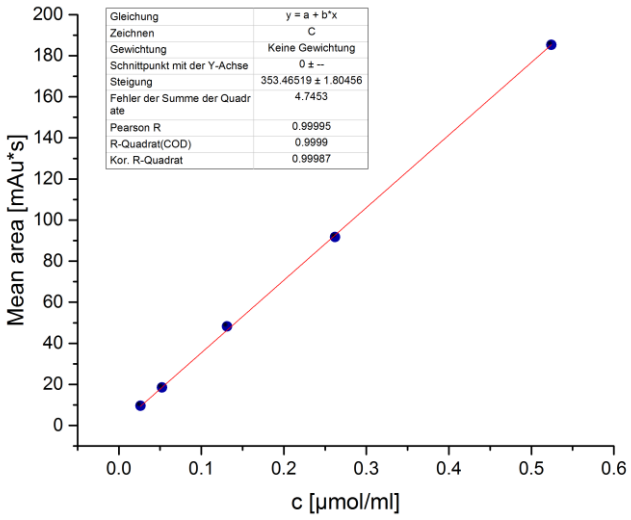


Figure S4: *Linear regression of dilution series data points used for dienophile loading assay*

The dienophile-loading in µmol/g was calculated using the following formula. Results are summarized in Table S3.

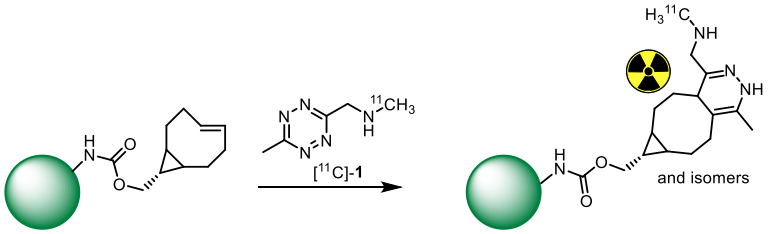
$$TCO\ loading\ \left[\frac{\mu mol}{g}\right] = \frac{1000 * V_{stock}\ [ml]}{m\ NP\ [mg]} * \left(0.52435 - \frac{area\ [mAu * s]}{calibration\ factor}\right)$$

Table S3: *Results of dienophile loading assay*

Particle	mass [mg]	V_{stock} [ml]	Mean area [mAu*s]	Dienophile [µmol/g]

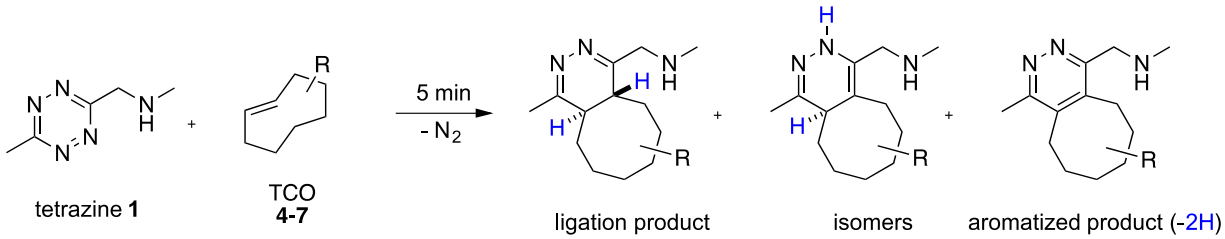
Amino-MSNs	1.450	0.50	184.26	**1**
s-TCO-MSNs	1.160	0.40	63.41	**119**
TCO-MSNs	0.500	0.50	144.21	**116**

Synthesis of ^{11}C-labeled MSNs



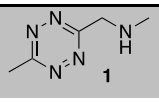
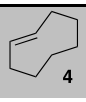
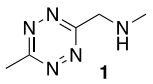
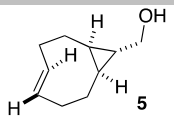
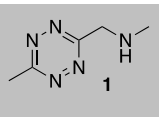
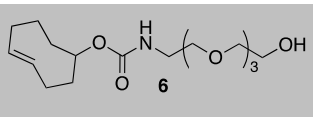
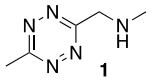
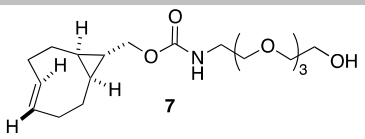
[^{11}C]-**1** (70.3 MBq in 1.5 mL phosphate buffer pH 5.9) was added to 1.48 mg s-TCO-MSNs (176 nmol s-TCO) and vortexed briefly. After 5 min standing at room temperature the suspension was centrifuged (13.3 krpm, 2 min). The supernatant was discarded and the pellet consisting of [^{11}C]MSNs (44.4 MBq, 80% decay-corrected yield) was resuspended in 300 µl 0.9% saline to obtain a suspension ready for i.v. administration.

IEDDA-initiated conjugations

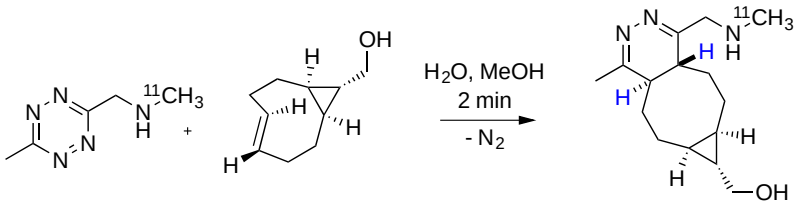


To a 3 mM solution of tetrazine **1** in dry 1,4-dioxane (for **1**+**4** and **1**+**5**) (1 mL) or PBS (for **1**+**6** and **1**+**7**) was added a 3 mM solution of TCO-derivative (1 eq.) in dry 1,4-dioxane (**4** and **5**) or water (**6** and **7**) (1 mL) and the resulting mixture was stirred for 5 min at room temperature. Due to the fast isomerization and aromatization known for the tetrazine/TCO-ligation products, the sample was directly subjected to LCMS analysis for characterization (Table S4).

Table S4. IEDDA-initiated conjugation of tetrazine (**1)** and TCO-derivatives **4**-**7**

Tetrazine	Dienophile	Product formula	Product Calcd. mass	Found mass
 **1**	 **4**	$[M+H]^+$ $C_{13}H_{24}N_3^+$	$[M+H]^+$ 222.2	$[M+H]^+$ 222.0
 **1**	 **5**	$[M+H]^+$ $C_{15}H_{26}N_3O^+$	$[M+H]^+$ 264.2	$[M+H]^+$ 264.2
 **1**	 **6**	$[M+H]^+$ $C_{22}H_{39}N_4O_6^+$ (aromatized)	$[M+H]^+$ 455.3	$[M+H]^+$ 455.3
 **1**	 **7**	$[M+H]^+$ $C_{24}H_{41}N_4O_6^+$ (aromatized)	$[M+H]^+$ 481.3	$[M+H]^+$ 481.5

IEDDA initiated conjugation of [^{11}C]-1 with dienophile 5



tetrazine [^{11}C]-**1**

s-TCO (**5**)

ligation products + isomers [^{11}C]-**12** + [^{11}C]-**13**

To prove IEDDA reactivity of tetrazine [^{11}C]-**1**, a solution of s-TCO (**5**) (0.5 mg, 3.3 µmol) in MeOH (5 µL) was added to 37 MBq of tetrazine [^{11}C]-**1** dissolved in a mixture of 50 mM phosphate buffer pH=2.4 (solvent A) and EtOH (solvent B), A:B= 9:1 (v/v), 200 µL. The reaction was stirred for 2 min and ~0.5 µL were spotted on SiO_2 plates (together with [^{11}C]-**1** as reference) and TLCs were developed with 10% MeOH + 1% triethylamine in DCM. Analysis of radioactivity distribution on the TLC plates using a Cyclone Phospho Imager indicated complete consumption of [^{11}C]-**1** and the formation of more hydrophilic ligation products [^{11}C]-**12** and [^{11}C]-**13** (Manuscript Fig. 2c).

3. Reaction kinetics

Tetrazine **1** was weighted into a volumetric flask and filled with dry 1,4-dioxane to generate a 3 mM solution. Dienophiles TCO **(4)** and s-TCO (**5**) were weighted into a volumetric flask and filled with dry 1,4-dioxane to generate a 30 mM solution. The reactant solutions were transferred into the driver syringes of the stopped-flow apparatus (Applied Photophysics, Surrey, UK). Upon temperature constancy (± 0.1°C of aimed value) triggering of driver syringe pneumatics caused mixing of equal reactant volumes. Depending on reaction rate time intervals between 10 to 200 s were chosen to collect 4000 data points at 530 nm. All measurements were made in duplicate or triplicate. Reactions in 1,4-dioxane were monitored at 20°C, 37 °C and 60°C. The pseudo first order rate constant (k_{obs}) was determined by linearization of the decay curve followed by linear fitting. The second order rate constant (k) was calculated from the pseudo-first order rate constant. Linearization and direct fitting to the Eyring equation (Equation 1) was used to calculate the enthalpy of activation ($\Delta H^{\ddagger}$) and the entropy of activation ($\Delta S^{\ddagger}$). Equation 2 gave rise to free energy of activation at 298.15 K ($\Delta G^{\ddagger}$). Results are summarized in Table S5 (rate constants) and Table S6 (thermodynamic data). Selected plots of kinetic measurements and Eyring linearization are shown in Fig. S5.

$$\ln\left(\frac{k}{T}\right) = -\left(\frac{\Delta H^{\ddagger}}{R}\right) * \left(\frac{1}{T}\right) + \ln\left(\frac{K_b}{h}\right) + \left(\frac{\Delta S^{\ddagger}}{R}\right) \qquad (1)$$

$$\Delta G^{\ddagger} = \Delta H^{\ddagger} - \mathrm{T}\Delta S^{\ddagger} \qquad (2)$$

Table S5. Results of kinetic measurements (rate constants).

Reaction	Solvent	T (°C)	k_{obs} (s^{-1})	k ($M^{-1}s^{-1}$)
1 + **4**	1,4-dioxane	20	$(8.6 \pm 0.1) \cdot 10^{-3}$	0.57 ± 0.01
		37	$(15.6 \pm 0.5) \cdot 10^{-3}$	1.04 ± 0.03
		60	$(29.9 \pm 0.4) \cdot 10^{-3}$	1.99 ± 0.03
1 + **5**	1,4-dioxane	20	0.99 ± 0.03	65.9 ± 2
		37	1.34 ± 0.02	89.5 ± 1.3
		60	2.026 ± 0.03	135.1 ± 2

Table S6. Results of kinetic measurements (thermodynamic data).

Reaction	Solvent	$\Delta H^{\ddagger}$ (kcal/mol)	$\Delta S^{\ddagger}$ (kcal/mol)	$\Delta G^{\ddagger}$ (kcal/mol)
1 + **4**	1,4-dioxane	5.44	-0.041	17.67
1 + **5**	1,4-dioxane	2.65	-0.041	14.92

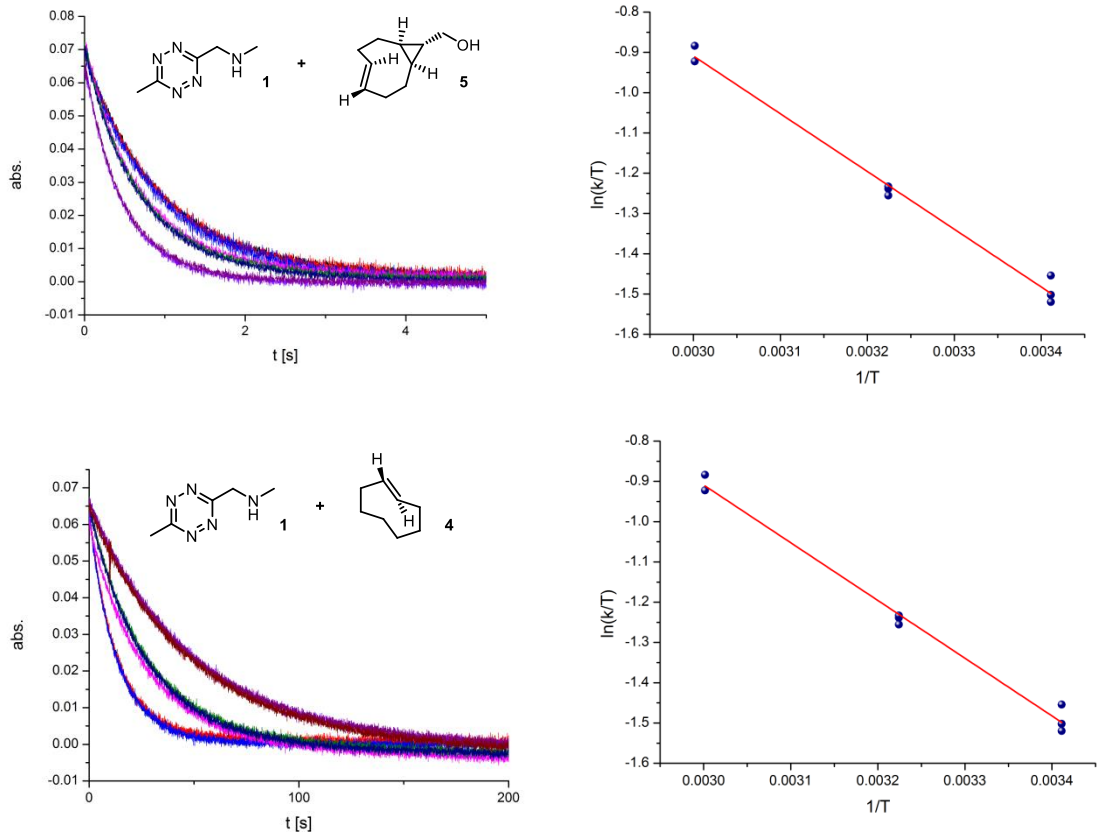


Figure S5. Stopped flow measurements of **1** + **5** and **1** + **4** at 20°C, 37°C and 60°C (left) and Eyring linearization (right)

Reaction rates of **1** with water-soluble dienophiles **6** and **7** were determined in PBS (Fluka, pH 7.4) using a SX20 stopped flow spectrophotometer system (Applied Photophysics, Surrey, UK) equipped with a 535 nm LED light source and a cell temperature of 37.00 ± 0.05 °C. Measurements were done under pseudo-first order conditions with a starting concentration of 1 mM for **1** (as trifluoroacetate), 10.0 mM for **6** and 16.6 mM for **7**. Equal volumes of Tz and TCO solutions were mixed, resulting in concentrations of 0.5 mM for **1**, 5.0 mM for **6** and 8.3 for **7**. Measurements were performed in quintuplicates. The pseudo first order rate constants (k_{obs}) were determined by linearization of the decay curve followed by linear fitting. The second order rate constant (k) was calculated from the pseudo-first order rate constant. Results are summarized in Table S7.

Table S7. Results of kinetic measurements (rate constants).

Reaction	Solvent	T (°C)	k_{obs} (s^{-1})	k ($M^{-1}s^{-1}$)
1 + **6**	PBS	37.00 ± 0.05	0.88 ± 0.01	175.4 ± 1.2
1 + **7**			352.7 ± 25.8	42500 ± 3100

4. *In vitro* and *in vivo* investigations

4.1 Plasma stability of 1

Plasma stability was determined by absorbance measurement. A 5.3 mM solution of **1** in human blood plasma was incubated at 37°C and absorbance at 530 nm was followed over a period of 120 min revealing > 90% recovery (Fig. S6). Identity of remaining **1** was verified by TLC.

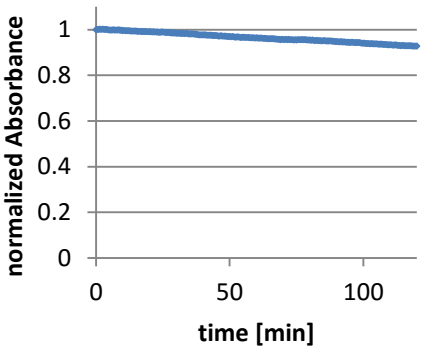


Figure S6. Absorbance of **1** in human blood plasma at 37°C over the course of 120 min

4.2 Animals

For the biodistribution experiments, female BALB/c mice weighting 21.6 ± 5.4 g were purchased from the Division of Laboratory Animal Science and Genetics, Medical University of Vienna, Himberg, Austria. All animals were housed in groups under individual ventilated cage (IVC) conditions in polysulfon type III cages. Environmental conditions were temperature: 22 ±3 °C, humidity: 40% to 70% and a 12-hour light/dark cycle (lights on at 6:00) with free access to standard laboratory diet (ssniff R/m-H, ssniff Spezialdiäten GmbH, Soest, Germany) and tap water. An acclimatization period of at least 1 week was allowed before the animals were used in the experiments. All studies involving laboratory animals were approved by national authorities (*Amt der Niederösterreichischen Landesregierung*) and all study procedures were performed in full accordance to the European Council Directive of September 22, 2010 (2010/63/EU). All efforts were made to comply with the 3R principle.

4.3 PET/MR Imaging – Biodistribution study

Two mice underwent PET scanning on a dual animal bed in a dedicated small-animal PET scanner and one mouse underwent sequential PET/MRI on two stand-alone scanners. Prior imaging, mice were pre-anesthetized in an induction chamber using isoflurane (2.5% in oxygen), placed in prone position on a heated animal bed (38°C) and the lateral tail vein was cannulated using a custom made tail vein catheter. Animal respiratory rate and body temperature were constantly monitored (SA Instruments Inc, Stony Brook, NY, USA) and the isoflurane level was adjusted (1.5-2.5% on oxygen) to achieve a constant depth of anesthesia. Anesthesia was maintained for the whole imaging period. A humidifier was used to moisten the gas mixture before supplying it to the animal(s). For anatomical magnetic resonance imaging (MRI) a single mouse body bed mounted with a mouse whole body RF coil was

used. The whole body coil covers an axial field of view (FOV) of about 8 cm that is very similar to the axial FOV of the PET scanner (7.6 cm). Images were acquired on a 1 Tesla benchtop MRI (ICON, Bruker Biospin GmbH, Ettlingen, Germany) using a modified 3D T_1-weighted gradient echo sequence (T1-FLASH) with the following imaging parameters: echo time (TE) = 5 ms; repetition time (TR) = 25 ms; flip angle (FA) = 25 °; field of view (FOV) = 7.6 x 2.6 x 2.4 cm; matrix = 253 x 93; 32 slices; slice thickness = 750 µm; 5 repetitions; total imaging time = 6 min 15 sec. After MRI, the animal bed was transferred into the gantry of a microPET scanner (Focus 220, Siemens Medical Solutions, Knoxville, TN, USA). Total anesthesia time prior start of PET scanning for mice that underwent PET scanning only was similar to that of the PET/MRI examined animal. Direct after positioning of the animal bed in the gantry of the PET scanner a 10 min transmission scan using a rotating ^{57}Co point source was recorded. Simultaneously with intravenous injection of 16.2 ± 5.9 Mbq [^{11}C]-**1**, dynamic PET imaging was initiated for 60 min using an energy window of 250-750 keV and a timing window of 6 ns. After completion of the imaging procedure, a terminal blood sample was withdrawn under isoflurane anesthesia from the retrobulbar venous plexus and the animals were sacrificed by cervical dislocation. Blood was centrifuged (17000 *g*, 4°C, 4 min) to obtain plasma, and organ samples as well as urine were collected. Aliquots of blood, plasma and urine as well as organ samples were transferred into pre-weighted tubes and measured for radioactivity in a gamma counter (Wizard 1470, Perkin-Elmer, Wellesley, MA, USA). The measured radioactivity data were corrected for radioactive decay and expressed as standardized uptake value ((radioactivity per g/injected radioactivity) x body weight). The 60 min dynamic emission PET data were sorted into 23 frames, which incrementally increased in time length from 5 seconds to 10 min. Images were reconstructed using Fourier rebinning of the 3D sonograms followed by two-dimensional filtered back projection with a ramp filter, resulting in an image voxel size of 0.4 x 0.4 x 0.796 mm^3. A standard data correction protocol (normalization, attenuation and decay correction) was applied to the PET data. The PET units were converted into units of radioactivity concentration by applying a calibration factor derived from imaging of a cylindrical phantom with a known ^{11}C-radioactivity concentration. Corresponding PET/MRI images were aligned using a pre-calculated, fixed transformation matrix. Using the image analysis software Amide,[13] different volumes of interest (brain, liver, kidneys, urinary bladder, heart, lung, bone (left humerus), muscle (right forearm muscle)) were manually outlined on multiple planes and time-radioactivity concentration curves (TACs), expressed in standardized uptake values, were derived.

4.4 Analysis of murine metabolites – *In vivo* stability of [^{11}C]-1

Urine and blood samples were harvested directly after imaging experiments (60 min post administration). Murine plasma was obtained by centrifugation. Proteins were precipitated with acetonitrile and removed by centrifugation. Supernatant solution was spotted on SiO_2 plates and TLCs were developed using 10% MeOH and 1% Et_3N in DCM as mobile phase. [^{11}C]-**1** was spotted as reference. Radioactivity was quantified using a Hewlett Packard Cyclone Phosphor Imager autoradiography system (Figure S7). Analysis showed 50% [^{11}C]-**1** in urine and 38% in plasma together with one main metabolite that is considered to be formed by oxidation of the methyl group at position 6 of the Tz scaffold (similar to the previously reported ^{18}F-labeled Tz[15]).

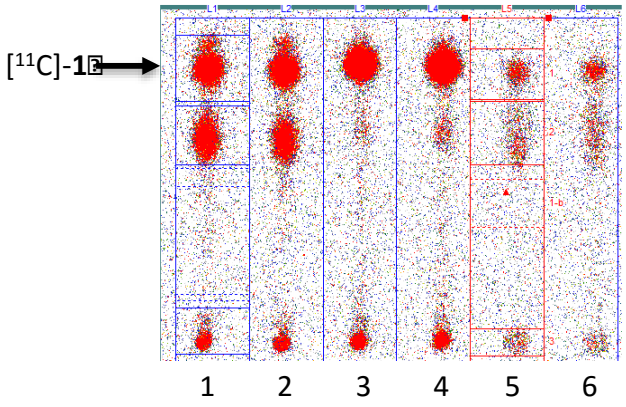


Figure S7. *In vivo* stability of [^{11}C]-**1** as determined by TLC radiochromatography of murine plasma and urine after imaging experiments**:** Lane 1 & 2: Urine metabolites ; Lane 3 & 4: Reference [^{11}C]-**1**; Lane 5 & Lane 6: Plasma metabolites.

4.5 *In vivo* click

For *in vivo* click experiments a group of female BALB/c mice (n=4) was used. A lateral tail vein was used for i.v. administration of water soluble s-TCO derivative **7** (11.8 mg/kg in 0.9% saline, n=2) or 0.9% saline (control group, n=2). After 5 min uptake time the mice were injected with of ^{11}C-[**1**] (mean 8.15 MBq). Retroorbital blood was collected 5 min after administration of ^{11}C-[**1**]. 200 µl of blood was quenched immediately after blood retrieval with 107 µg of tetrazine (4-(1,2,4,5-tetrazin-3-yl)phenyl)methanol in 214 µl water (saturated solution). Murine plasma was obtained by centrifugation and proteins were precipitated with acetonitrile and removed by centrifugation. Supernatant solution was spotted on SiO_2 TLC plates and developed using 20% MeOH in DCM as mobile phase (Fig. S8)

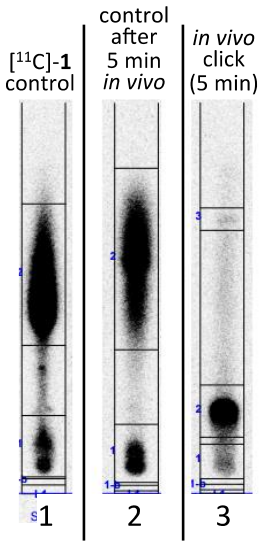


*Figure **S8**. Radio-TLC after in vivo reaction of [^{11}C]-**1** and **7**. Lane 1: [^{11}C]-**1**, Lane 2: control, 5 min biodistribution of [^{11}C]-**1**. Lane 3: after 5 min in vivo reaction .*

Results from this experiment indicate high *in vivo* reactivity between water-soluble s-TCO derivative **7** and [^{11}C]-**1**. After 5 min of *in vivo* reaction time only 1.5 % of total radioactivity originated from [^{11}C]-**1** while >90% of activity was encountered as a single ligation product (Fig. S8, lane 3). Most likely the dihydropyridazine isomers are rapidly oxidized to the appropriate pyridazine resulting in only one detectable aromatized ligation product when the reaction is carried out *in vivo*.

4.6 Biodistribution of [^{11}C]MSNs

The general method for PET data acquisition and reconstruction described under point 4.3 was followed. The nanoparticle suspension was sonicated prior to administration to minimize agglomeration of particles. Female BALB/c mice (n=2) were injected with ^{11}C-labeled MSNs (0.5 mg, 12.9 ± 1.8 MBq) via tail vein catheder and dynamic PET imaging performed for 60 min. PET data revealed rapid and high (18-25 SUV) uptake in the lungs (already after 5 min), while other organs showed much lower activity concentration (Fig. S9). These findings were also confirmed by gamma counter measurements (*ex vivo*).

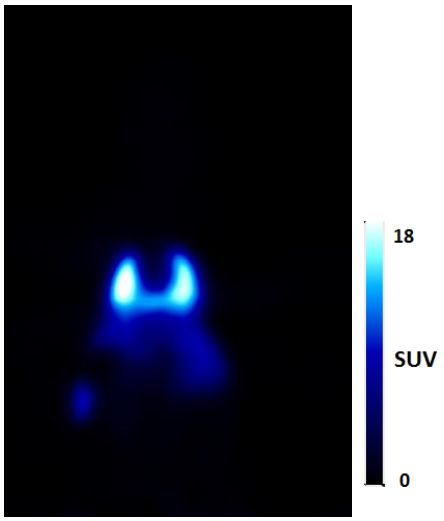


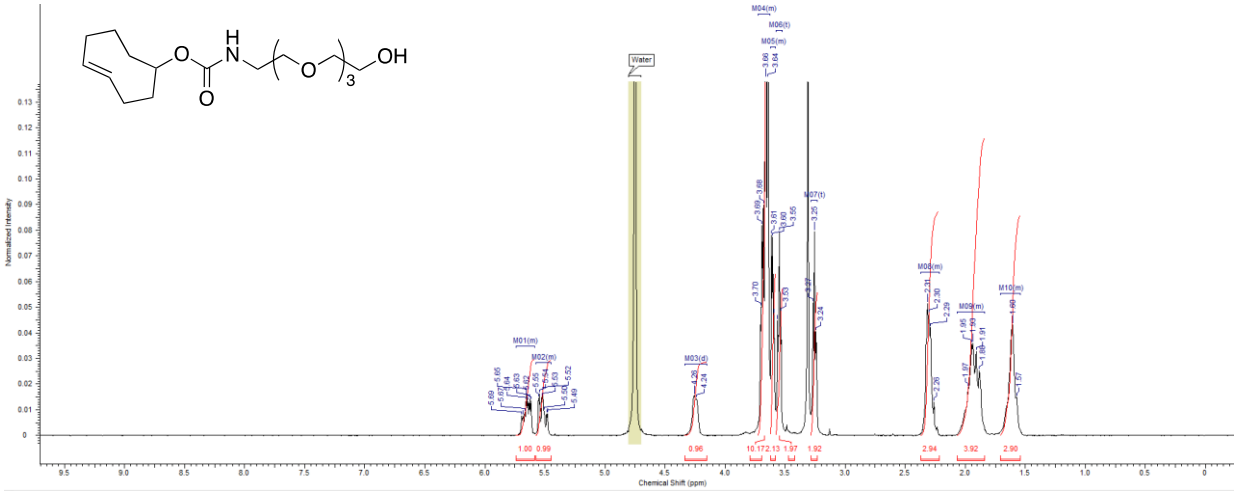
Figure S9. Coronal PET slice (0-60 min) showing high accumulation of [^{11}C]-MSNs in the lung.

4.7 Pretargeted imaging using TCO/s-TCO-MSNs

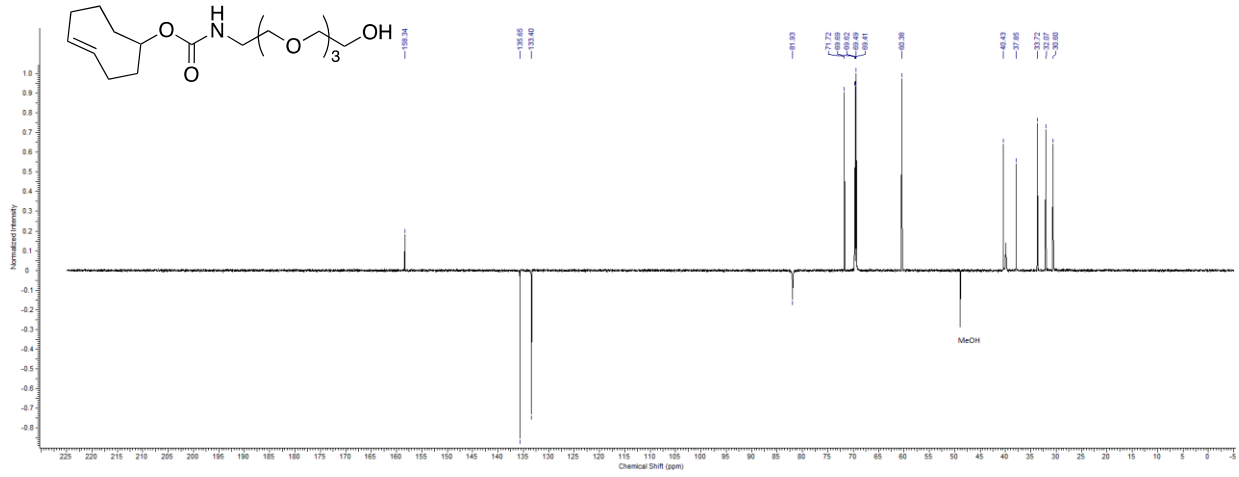
The general method for PET data acquisition and reconstruction described under point 4.3 was followed. Prior to PET imaging functionalized nanoparticles were administered using a tail vein catheter. The nanoparticle suspensions in 0.9% saline were vortexed and sonicated for 60 seconds prior to administration to minimize agglomeration of particles. Animals were divided into two study groups receiving s-TCO-MSNs (n=5, 0.5 mg, 59 nmol s-TCO) or TCO-MSNs (n=2, 0.5 mg, 58 nmol TCO) as suspension in 100 µL physiological saline. 5 min post nanoparticle administration PET data acquisition was started and the animals were dosed with [^{11}C]-**1** (15.4 ± 6.0 MBq, i.v., 100 µl). Dynamic PET scanning was conducted for 60 min. *Ex vivo* measurements were done using a gamma counter.

5. NMR Spectra

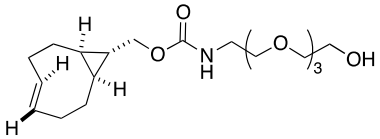
^{1}H spectrum of compound **6**

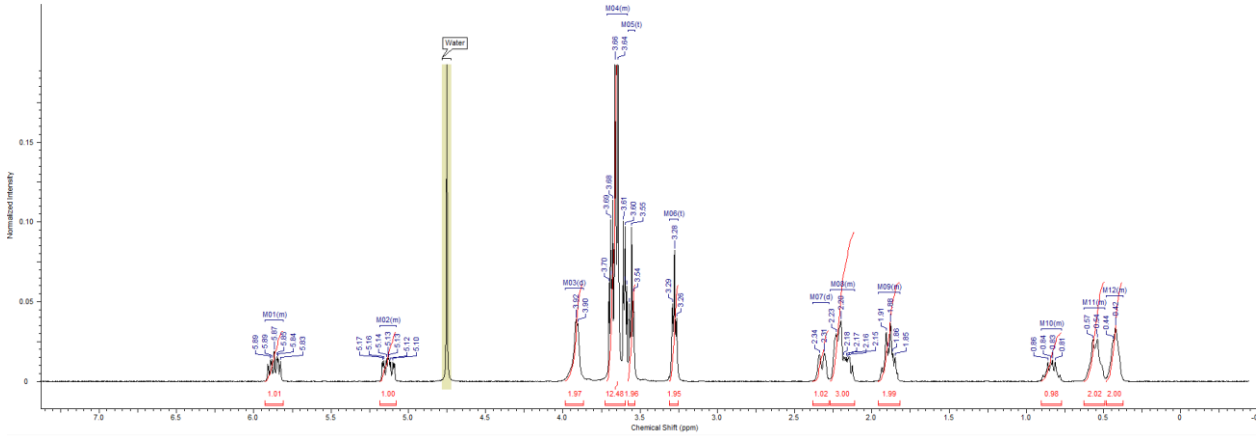


^{13}C spectrum of compound **6**

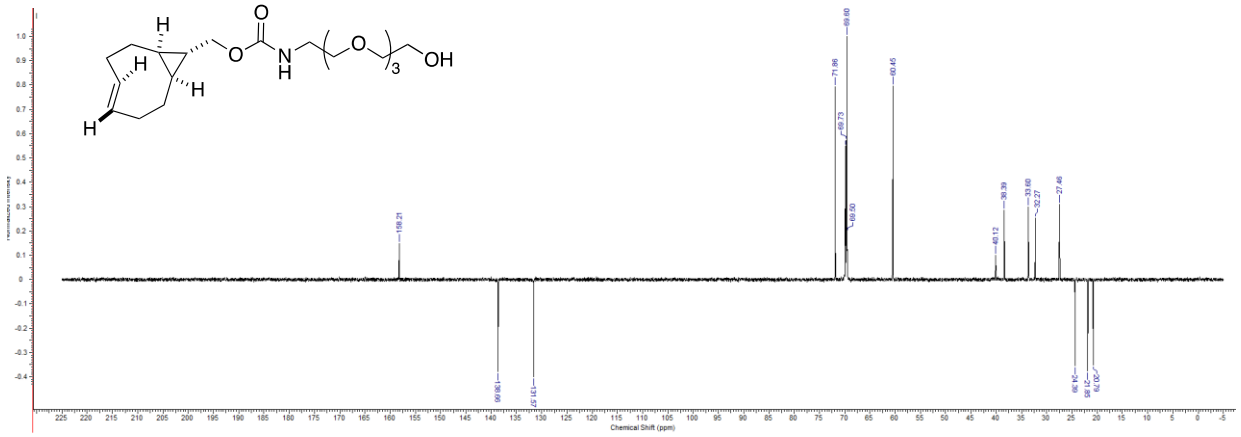


^{1}H spectrum of compound **7**

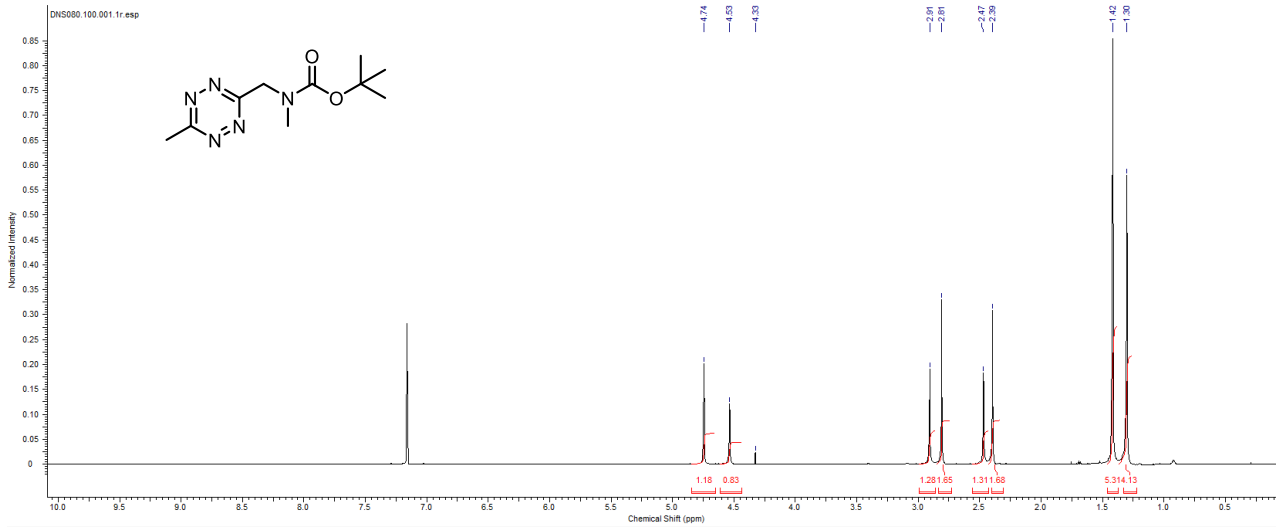




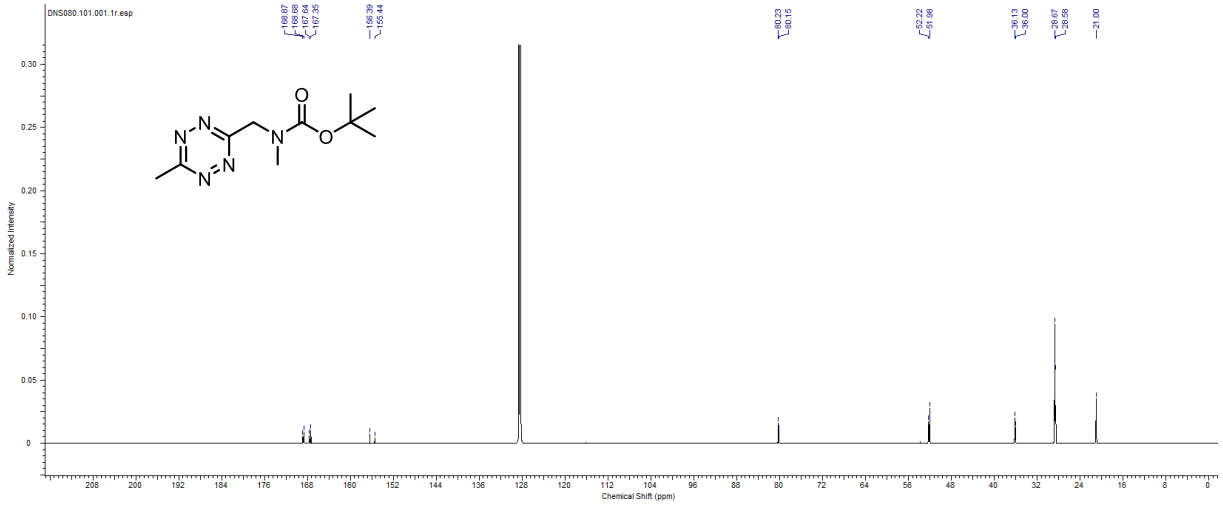
^{13}C spectrum of compound **7**



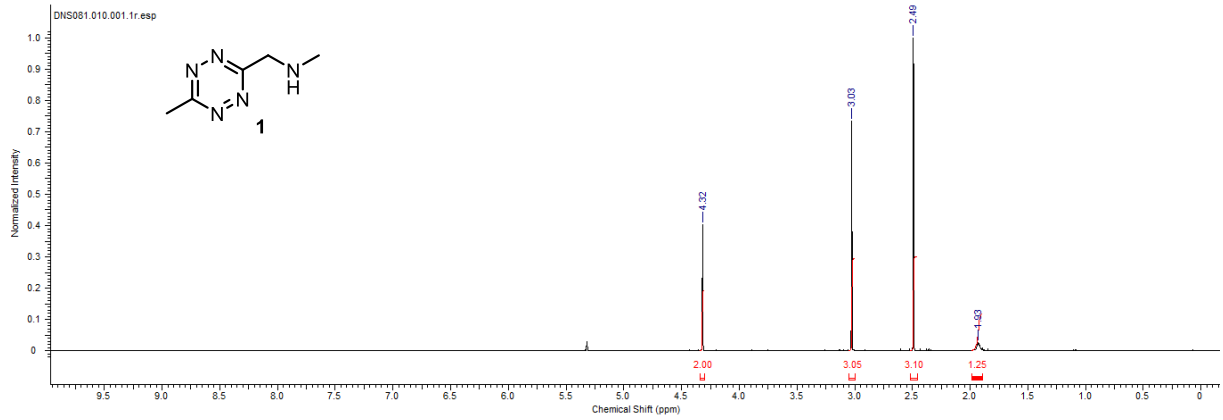
^{1}H spectrum of compound **9**



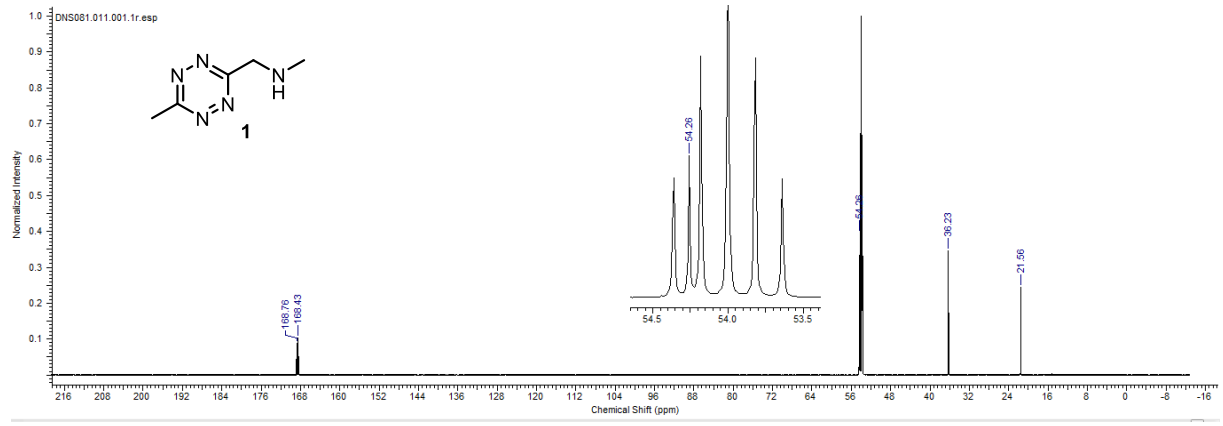
^{13}C spectrum of compound **9**



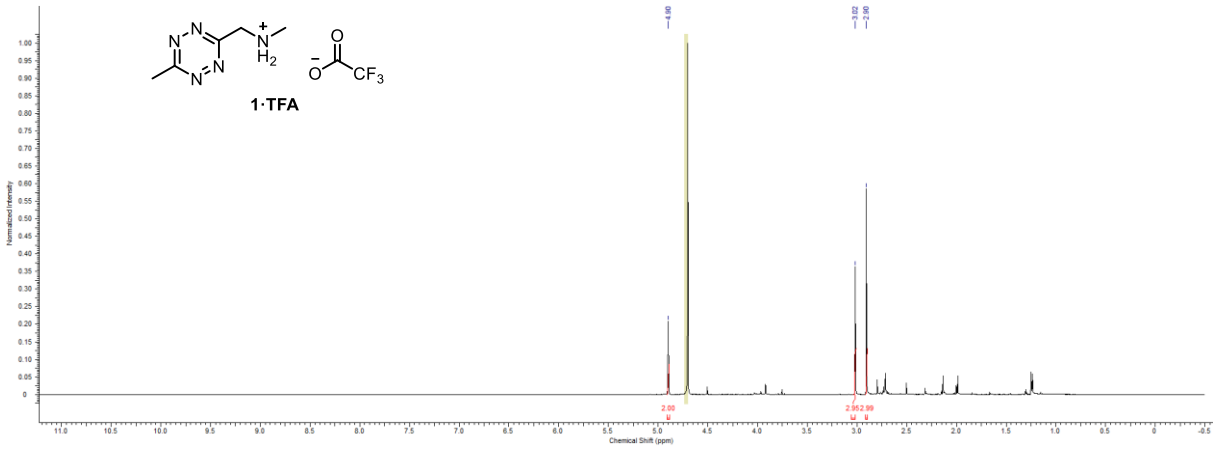
^{1}H spectrum of compound **1**



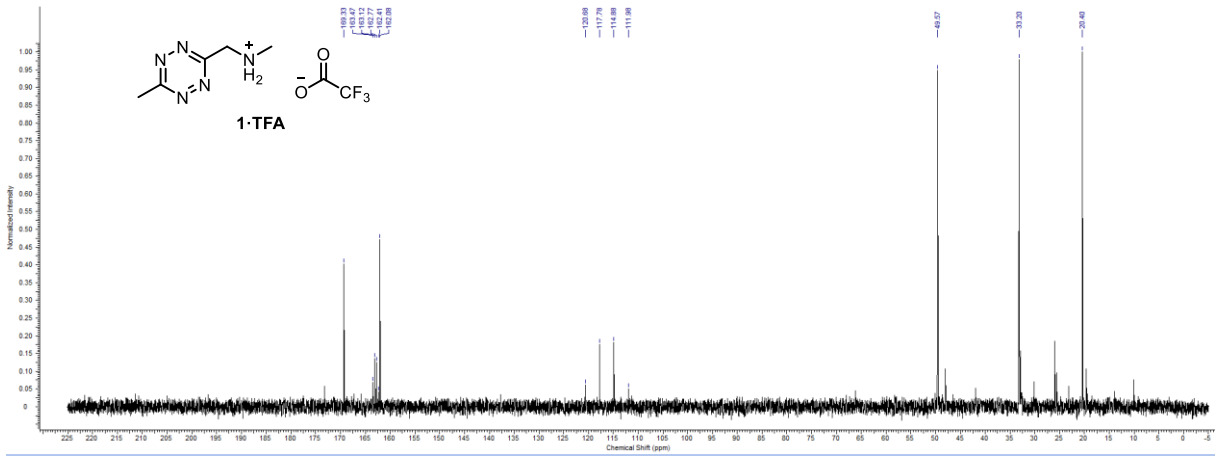
^{13}C spectrum of compound **1**



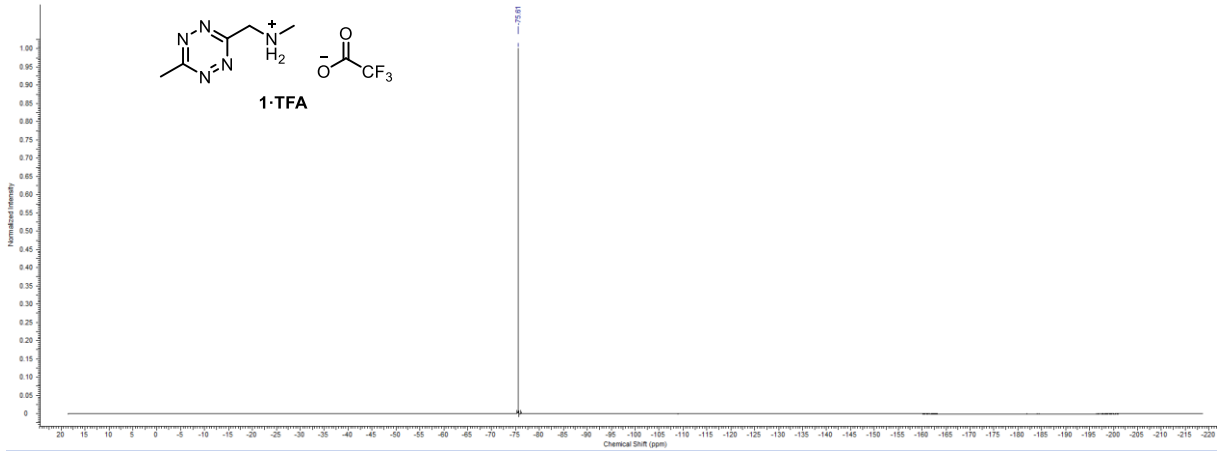
^{1}H spectrum of compound **1·TFA**



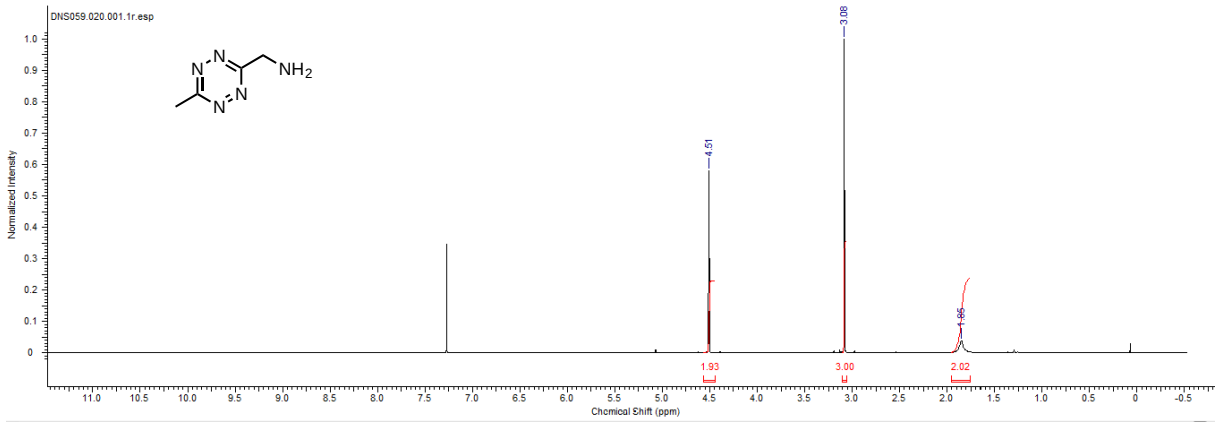
^{13}C spectrum of compound **1·TFA**



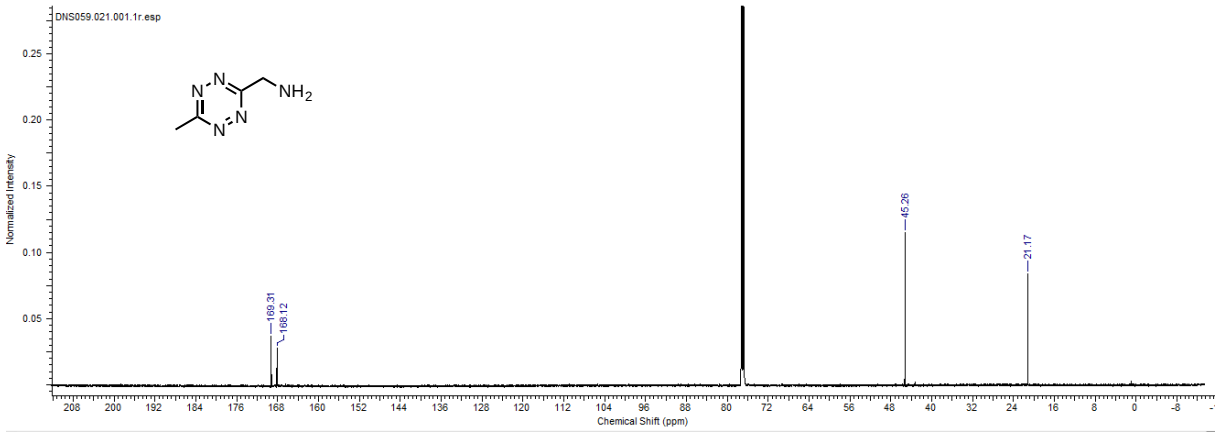
^{19}F spectrum of compound **1·TFA**



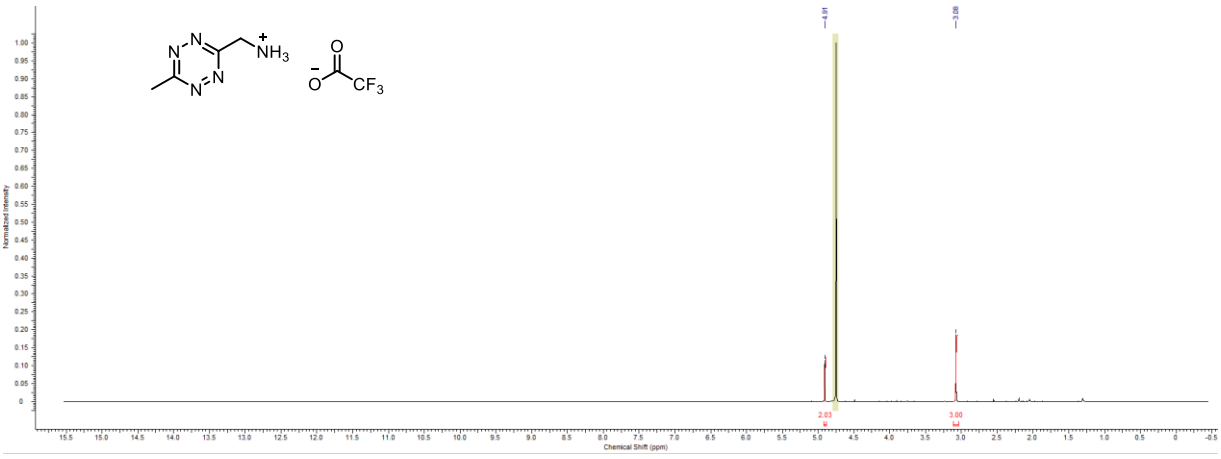
^{1}H spectrum of compound **11**



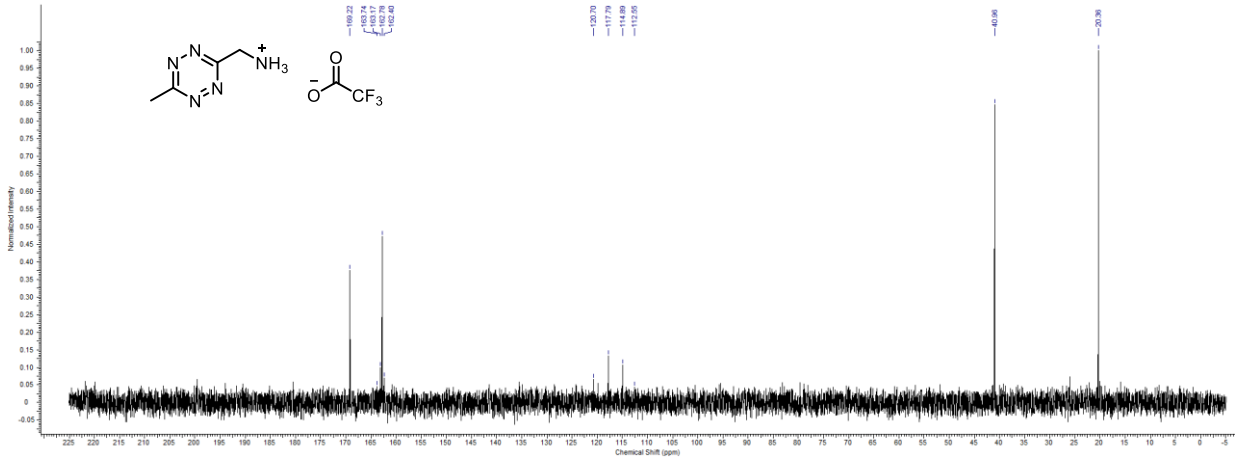
^{13}C spectrum of compound **11**



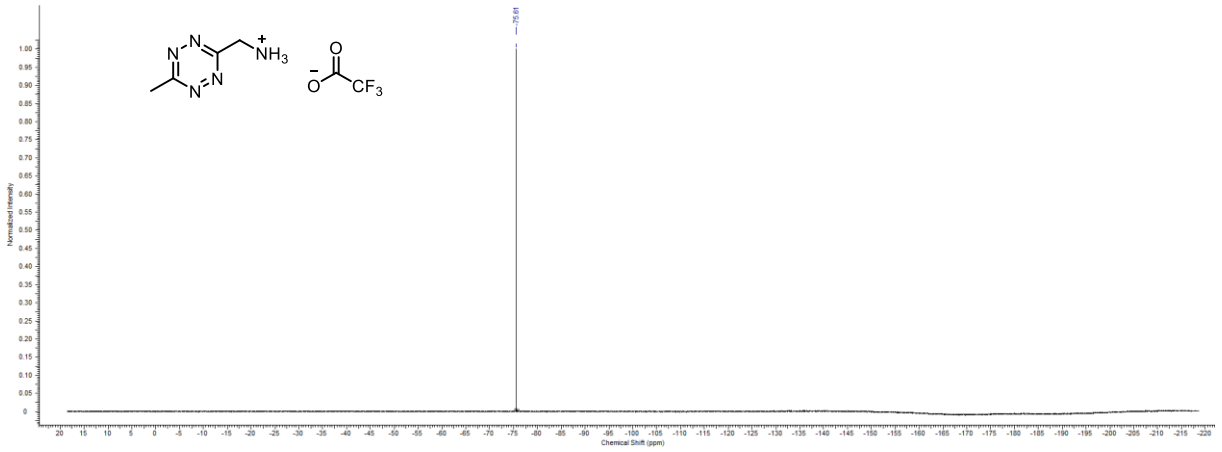
^{1}H spectrum of compound **11·TFA**



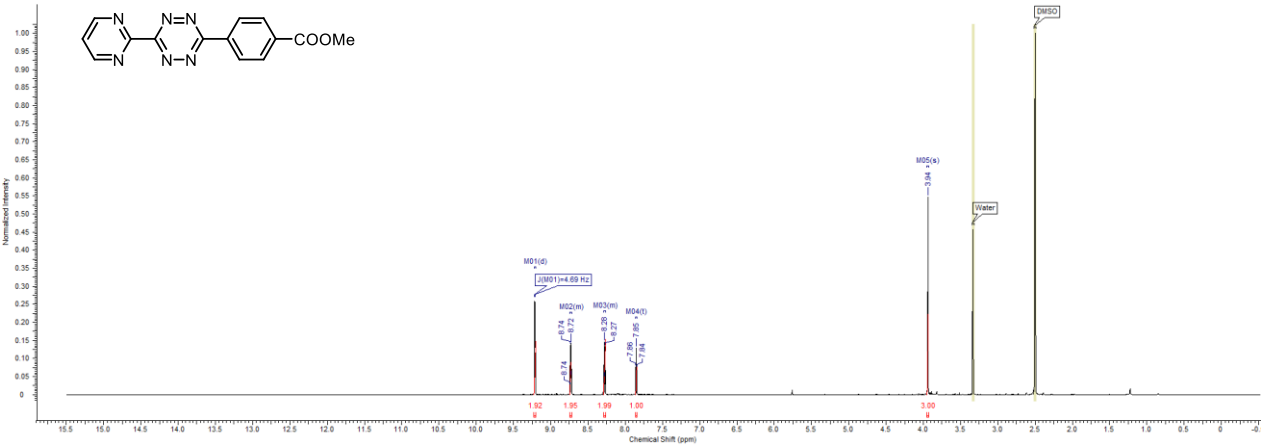
^{13}C spectrum of compound **11·TFA**



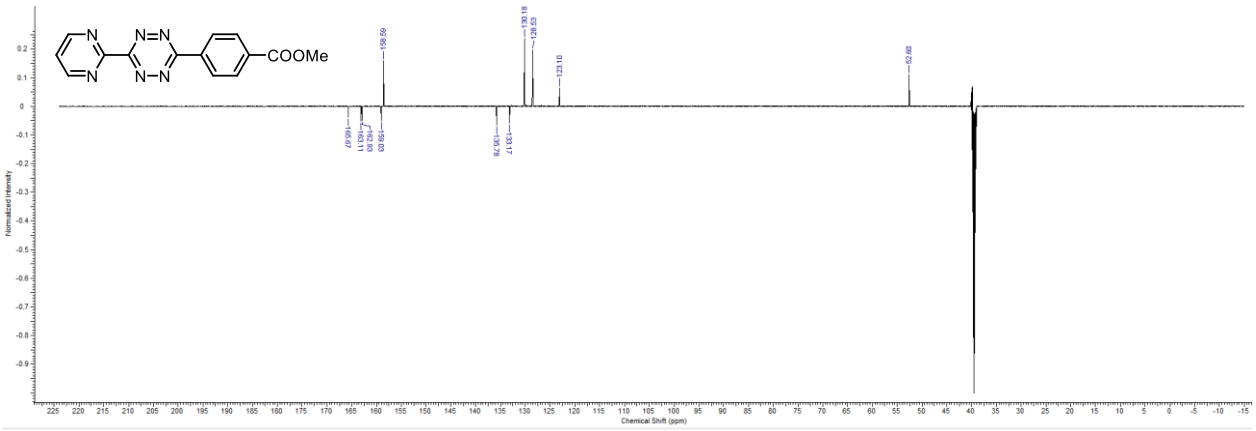
^{19}F spectrum of compound **11·TFA**



^{1}H spectrum of **methyl 4-(6-(pyrimidin-2-yl)-1,2,4,5-tetrazin-3-yl)benzoate**



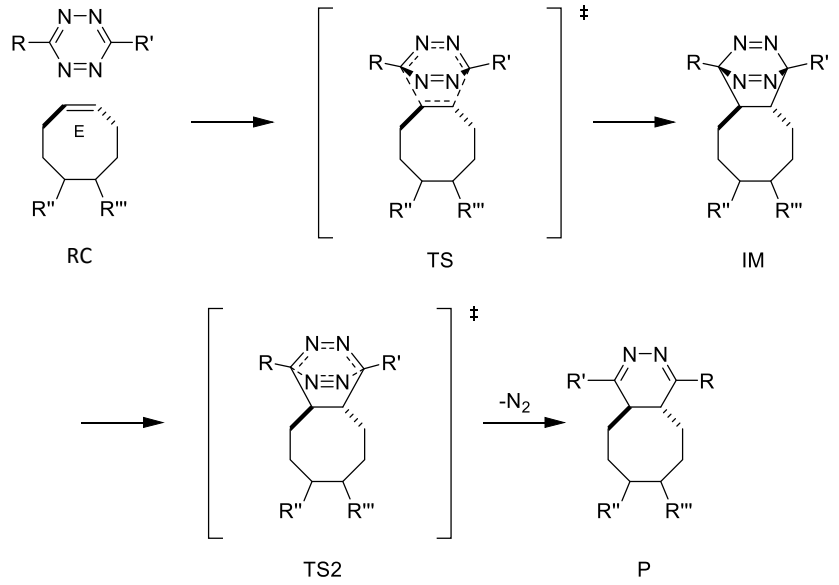
^{13}C spectrum of **methyl 4-(6-(pyrimidin-2-yl)-1,2,4,5-tetrazin-3-yl)benzoate**


COOMe
158.59
130.18
126.53
123.10
52.60
Normalized Intensity
Chemical Shift (ppm)

6. Quantum chemical calculations

All DFT calculations were performed on the Vienna Scientific Cluster 3 using the Gaussian 09 (Rev. D.01) program package.[14] Geometry optimizations to energy minima or transition states as well as subsequent frequency analyses at 298.15 K of all considered compounds and intermediates were achieved using the M06-2X density functional[15] in combination with the 6-31G(d,p)[16] basis set as implemented in Gaussian 09, which has been found to give relatively accurate energy profiles for cycloadditions.[17,18] All calculations were performed in 1,4-dioxane applying the polarizable conductor calculation model (CPCM) as provided in Gaussian 09. Imaginary frequencies corresponding to the desired reaction coordinates were obtained only in the case of transition state calculations. Data analysis was done using GaussView 5 (Gaussian, Inc.).

The reaction of tetrazines with strained dienophiles proceeds in two steps, the first being an inverse electron demand Diels-Alder (IEDDA)-initiated reaction leading to an intermediate that subsequently undergoes retro-Diels-Alder reaction with the loss of N_2 (Scheme S1).



Scheme S1: General mechanism of the tetrazine ligation (RC = reactant complex, TS = transition state, IM = intermediate, P = product).

The first step of this reaction (RC → TS), the inverse electron demand Diels-Alder reaction, is the rate-determining step.[19,20] Therefore, $\Delta G^{\ddagger}$ values of this cycloaddition were considered to determine reaction activation barriers at 298.15 K. Original data is summarized in Table S8 followed by listing of Cartesian coordinates of all relevant structures.

Table S8: Selected original data from Gaussian calculations (E: total electronic energy, ZPE: zero point energy).

Structure	E (hartree)	H (hartree)[a]	G (hartree)[a]	S (Cal/(mol*K))[a]	ZPE (hartree)[a]
TS_{1+4}	-782.533302622	-782.152443	-782.215082	131.835	-782.170739
RC_{1+4}	-782.545771650	-782.164423	-782.234466	147.418	-782.184624
TS_{2+4}	-743.252237286	-742.901448	-742.959890	123.001	-742.918240
RC_{2+4}	-743.272434428	-742.921403	-742.989495	143.313	-742.940619
TS_{3+4}	-865.709502963	-865.323370	-865.388604	137.296	-865.342514
RC_{3+4}	-865.722926843	-865.336327	-865.408282	151.443	-865.357273
TS_{1+5}	-935.088736580	-934.665951	-934.735503	146.384	-934.687298
RC_{1+5}	-935.096619506	-934.673420	-934.749388	159.886	-934.696541
TS_{2+5}	-895.805512643	-895.412924	-895.478989	139.045	-895.432909
RC_{2+5}	-895.820924491	-895.427532	-895.501096	154.829	-895.449600
TS_{3+5}	-1018.26259416	-1017.834645	-1017.908032	154.455	-1017.857081
RC_{3+5}	-1018.27136121	-1017.842855	-1017.922242	167.085	-1017.866880

[a] calculated for T = 298.15

Cartesian Coordinates

TS_{1+4}

C	-0.8947280	2.2034350	-0.1678950
C	-1.8477810	-0.1115990	-0.3334160
C	0.3780830	-0.4376670	-0.2154100
H	0.2098390	-1.0263830	0.6854980
C	0.9026640	0.8240760	-0.0736050
H	1.2853020	1.3073030	-0.9745580
N	-1.8241150	0.6246260	-1.4875910
N	-1.3385720	1.8096960	-1.4014940
N	-2.0102210	0.5343410	0.8588830
N	-1.5150950	1.7180110	0.9481110
C	1.5710320	1.2068610	1.2153040
H	1.5585910	2.2854810	1.3989790
H	1.0536330	0.7190320	2.0498070
C	0.6699980	-1.2370890	-1.4509380
H	-0.1090160	-1.9725360	-1.6667040
H	0.7609670	-0.5667510	-2.3138350
C	3.0381230	0.7226840	1.1567650
H	3.4914380	0.9013430	2.1382270
H	3.5903110	1.3494700	0.4446060
C	2.0034310	-1.9807250	-1.2157500
H	2.2807110	-2.4845420	-2.1485160
H	1.8335500	-2.7725250	-0.4748440
C	3.1743460	-1.0980510	-0.7460670
H	4.0988140	-1.6231450	-1.0068990
H	3.1873730	-0.1734610	-1.3379230
C	3.2282430	-0.7553970	0.7710460
H	4.2071550	-1.0633440	1.1523110
H	2.4974070	-1.3662910	1.3163880
C	-2.4186190	-1.5080600	-0.4525410
C	-0.2702080	3.5631660	-0.0791380
H	0.6468570	3.6121930	-0.6700730
H	-0.0516920	3.8065980	0.9604360
H	-0.9667070	4.3063080	-0.4756250
H	-2.3273870	-1.7968120	-1.5020940
H	-3.4968850	-1.4247340	-0.2272420
N	-1.7572550	-2.5042050	0.3790700
H	-1.9737860	-3.4179540	-0.0051650
C	-2.1746670	-2.4729850	1.7784920
H	-3.2688590	-2.4980280	1.9059700
H	-1.7411870	-3.3303130	2.2982620
H	-1.8091210	-1.5600890	2.2530520

RC_{1+4}

C	-1.6153570	2.0906250	-0.2399240
C	-2.3769350	-0.3532520	-0.2083010
C	0.7691130	-0.3635000	-0.0911220
H	0.6675230	-1.0964170	0.7109460
C	1.1558760	0.8779620	0.2094500
H	1.3067410	1.5872480	-0.6091210
N	-2.0726510	0.1907830	-1.3920760
N	-1.6876250	1.4428200	-1.4100440
N	-2.4208770	0.3316750	0.9434590
N	-2.0260350	1.5778070	0.9295530
C	1.8529210	1.1843950	1.4943950
H	1.7115520	2.2107780	1.8505400
H	1.5088450	0.5022240	2.2808910
C	0.9282680	-0.9162850	-1.4678680
H	0.1925180	-1.6915820	-1.7012500
H	0.8390550	-0.1148030	-2.2116950
C	3.3579570	0.9257630	1.2142460
H	3.9091760	0.9995980	2.1589350
H	3.7406500	1.7279540	0.5700120
C	2.3651940	-1.5016470	-1.5045290
H	2.5978050	-1.7996350	-2.5336270
H	2.3862220	-2.4213180	-0.9053080
C	3.4682520	-0.5486600	-0.9923900
H	4.4131790	-0.8952820	-1.4248950
H	3.3001900	0.4491410	-1.4170940
C	3.6643590	-0.4351030	0.5512020
H	4.7116570	-0.6663140	0.7740530
H	3.0788760	-1.2148360	1.0548380
C	-2.7481470	-1.8116790	-0.1783430
C	-1.0926790	3.4903670	-0.2338490
H	-0.2426850	3.5601590	0.4497290
H	-1.8630220	4.1802050	0.1187980
H	-0.7797400	3.7726810	-1.2384240
H	-3.0276620	-2.0947620	-1.1951140
H	-3.6252590	-1.9281920	0.4793880
N	-1.6131540	-2.6267000	0.2430990
H	-1.7638730	-3.5749420	-0.0847920
C	-1.4308220	-2.6395830	1.6896650
H	-2.3316780	-2.9540090	2.2405910
H	-0.6084920	-3.3127470	1.9429770
H	-1.1671730	-1.6362580	2.0358970

TS_{2+4}

C	-1.1426650	1.7907920	-0.3240800
C	-1.8486690	-0.5978000	-0.0624200
C	0.3379150	-0.5716970	-0.0165180
H	0.3110750	-0.9808160	0.9951420
C	0.6937780	0.7608270	-0.1425640
H	1.0031140	1.0845100	-1.1383150
N	-1.9820530	-0.0580570	-1.3288630
N	-1.6199140	1.1566440	-1.4564530
N	-2.0472570	0.2205230	1.0261490
N	-1.6879390	1.4420110	0.8889290
C	1.4000400	1.4402400	1.0004320
H	1.2619890	2.5254290	0.9946360
H	1.0003240	1.0601330	1.9477840
C	0.6973940	-1.5510590	-1.0926260
H	-0.0071320	-2.3891920	-1.1186290
H	0.6733730	-1.0499290	-2.0678640
C	2.9092180	1.1313580	0.9074000
H	3.3913410	1.5577210	1.7942480
H	3.3275130	1.6660830	0.0447150
C	2.1197850	-2.0830560	-0.8206760
H	2.4079590	-2.7232600	-1.6620640
H	2.0954370	-2.7311440	0.0649080
C	3.1953390	-1.0011420	-0.6165460
H	4.1634760	-1.4626090	-0.8362300
H	3.0669350	-0.2183450	-1.3757190
C	3.2820730	-0.3577370	0.7965560
H	4.3147800	-0.4541640	1.1469460
H	2.6795860	-0.9367250	1.5085750
C	-0.7664060	3.2349790	-0.5046040
H	0.1340060	3.3351550	-1.1155000
H	-0.5987430	3.6993020	0.4673730
H	-1.5782670	3.7624870	-1.0107300
N	-2.1520650	-1.9310730	0.0621450
H	-2.5863140	-2.3087600	-0.7691140
C	-2.6199100	-2.4437910	1.3373120
H	-2.7506730	-3.5223150	1.2462930
H	-1.8706590	-2.2490510	2.1081740
H	-3.5618890	-1.9863170	1.6620290

RC_{2+4}

C	-1.8949710	1.7655720	-0.2336070
C	-2.2085400	-0.7702360	-0.1082070
C	0.7709130	-0.5718850	0.1742720
H	0.7635830	-0.8293680	1.2360780
C	0.9398460	0.7071280	-0.1681490
H	0.9899770	0.9636690	-1.2292030
N	-2.1458880	-0.2056080	-1.3408500
N	-1.9785780	1.0776200	-1.3909920
N	-2.2525910	-0.0807000	1.0452850
N	-2.0880090	1.2174800	0.9661880
C	1.5265810	1.6919650	0.7890210
H	1.2044530	2.7254790	0.6211740
H	1.2651050	1.4185400	1.8180070
C	1.0757840	-1.6789010	-0.7808860
H	0.5041760	-2.5955420	-0.5944230
H	0.8749490	-1.3553980	-1.8094030
C	3.0637110	1.5825770	0.6001400
H	3.5563190	2.1772730	1.3780810
H	3.3357940	2.0427410	-0.3585450
C	2.5931740	-1.9632530	-0.6130300
H	2.9075060	-2.6675440	-1.3920390
H	2.7518670	-2.4726600	0.3461750
C	3.4953710	-0.7110650	-0.6648160
H	4.4990780	-1.0551150	-0.9367560
H	3.1699820	-0.0719380	-1.4952750
C	3.6179890	0.1414240	0.6359530
H	4.6811670	0.2173980	0.8882440
H	3.1560200	-0.3957570	1.4739710
C	-1.6286880	3.2354250	-0.3213170
H	-0.7185970	3.4185100	-0.8984960
H	-1.5097700	3.6461860	0.6812420
H	-2.4521520	3.7482970	-0.8248600
N	-2.2939610	-2.1135440	-0.0602290
H	-2.1639530	-2.5898970	-0.9396200
C	-2.1869570	-2.8427230	1.1868270
H	-1.2334620	-2.6393240	1.6884200
H	-2.9955020	-2.5608280	1.8645730
H	-2.2586240	-3.9076200	0.9696320

TS_{3+4}

C	-0.4510910	2.2505400	0.3467970
C	1.2053330	0.3852900	0.1166910
C	-0.7941460	-0.6229410	0.0086290
H	-0.5329680	-0.9917220	-0.9846920
C	-1.6946110	0.4173940	0.0705840
H	-2.1527470	0.6098010	1.0422490
N	1.0487120	0.9083460	1.3718360
N	0.1960450	1.8602480	1.4898090
N	1.0480830	1.2018490	-0.9705960
N	0.2024760	2.1601050	-0.8534310
C	-2.5380150	0.7432730	-1.1292200
H	-2.8586500	1.7889100	-1.1536310
H	-1.9614140	0.5501560	-2.0412110
C	-0.7641340	-1.6375120	1.1164880
H	0.2059990	-2.1322460	1.2163860
H	-0.9837570	-1.1404860	2.0686660
C	-3.7884950	-0.1630250	-1.0990800
H	-4.3418410	-0.0008530	-2.0306450
H	-4.4476940	0.1704940	-0.2873550
C	-1.8386890	-2.7079450	0.8226660
H	-1.8853400	-3.3800260	1.6866430
H	-1.5055650	-3.3203600	-0.0250240
C	-3.2489510	-2.1702600	0.5206020
H	-3.9516970	-2.9834010	0.7278840
H	-3.4985620	-1.3805980	1.2411130
C	-3.5108230	-1.6673680	-0.9276800
H	-4.3835090	-2.2005210	-1.3179030
H	-2.6769310	-1.9583610	-1.5798420
C	2.1903100	-0.7383220	-0.0327060
C	-1.4747460	3.3365760	0.4950990
H	-2.3413340	2.9877450	1.0611570
H	-1.7945630	3.6846300	-0.4869250
H	-1.0328300	4.1748900	1.0392390
H	1.9083120	-1.3527180	-0.8947530
H	2.1471380	-1.3624450	0.8640870
C	3.6120650	-0.1955140	-0.2139940
H	3.6510160	0.4441350	-1.1007920
H	3.8828830	0.4173730	0.6520390
C	4.6155420	-1.3203620	-0.3605230
H	4.3902160	-1.9365310	-1.2387620
H	4.6205770	-1.9638960	0.5268910
F	5.8843050	-0.7885280	-0.5171400

RC_{3+4}

C	0.0134640	2.5858340	0.2722770
C	1.5415420	0.5365480	0.2078290
C	-1.1564470	-0.7594440	0.0138320
H	-0.8498360	-1.0395950	-0.9971760
C	-1.9447830	0.3075330	0.1652900
H	-2.2890350	0.5649100	1.1700130
N	1.2172750	1.0338060	1.4090100
N	0.4359820	2.0814320	1.4411400
N	1.2373790	1.1255860	-0.9556320
N	0.4544540	2.1729830	-0.9248860
C	-2.7401550	0.8466150	-0.9788480
H	-2.9660710	1.9159690	-0.9034310
H	-2.2047050	0.6791710	-1.9208420
C	-1.0850460	-1.8291850	1.0538610
H	-0.1331140	-2.3712730	1.0725580
H	-1.2512310	-1.3999570	2.0488120
C	-4.0605750	0.0300390	-0.9824430
H	-4.6290310	0.2880730	-1.8832720
H	-4.6741410	0.3464380	-0.1291330
C	-2.2403720	-2.8092660	0.7135090
H	-2.3303890	-3.5399160	1.5256080
H	-1.9674170	-3.3788920	-0.1840790
C	-3.6115250	-2.1385420	0.4794150
H	-4.3720150	-2.9090990	0.6445460
H	-3.7797800	-1.3887860	1.2627980
C	-3.8734690	-1.5012330	-0.9200390
H	-4.7880280	-1.9474300	-1.3251730
H	-3.0746260	-1.7911100	-1.6145300
C	2.3765800	-0.7054310	0.1592460
C	-0.9576700	3.7207790	0.3187200
H	-1.8541810	3.4180090	0.8657590
H	-1.2285930	4.0174670	-0.6940380
H	-0.5176040	4.5716020	0.8444690
H	1.9363030	-1.3898380	-0.5747020
H	2.3342680	-1.1815810	1.1430300
C	3.8248400	-0.3869610	-0.2292240
H	3.8416330	0.1083590	-1.2053670
H	4.2636270	0.3016220	0.5004220
C	4.6669380	-1.6443180	-0.2930860
H	4.2678500	-2.3482750	-1.0324490
H	4.7060390	-2.1436840	0.6817630
F	5.9582810	-1.3107380	-0.6627820

TS_{1+5}

C	-2.5956420	0.4068510	-0.5141960
C	-0.1805810	1.2820370	-0.8509890
C	-0.5201260	-1.7053070	1.2891840
C	0.3846330	0.2920350	0.1267220
C	0.0160180	-1.0222260	0.0559330
C	-1.6291040	1.5699780	-0.3828990
C	-1.8325270	-0.9712180	1.6593670
H	-0.1835370	0.8711470	-1.8679240
H	0.1935450	-1.6403440	2.1183470
H	0.6197690	0.7048770	1.1088520
H	-0.3776910	-1.3739470	-0.8983340
H	0.3829040	2.2189400	-0.8482480
H	-0.7253870	-2.7635220	1.1003820
H	-2.0326950	2.4091840	-0.9616210
H	-1.5751080	0.0008470	2.0957900
H	-1.5918760	1.9109370	0.6593140
H	-2.3768030	-1.5313550	2.4288670
N	2.6815160	-1.6652730	0.7634490
N	2.5325070	-0.4047970	-1.6115620
C	2.0040300	-2.1702830	-0.3050870
C	2.6447930	0.2524150	-0.4243280
N	2.2066130	-1.6480890	-1.5501260
N	3.0112150	-0.4204460	0.6988600
C	-2.7226910	-0.7615480	0.4488690
C	-3.7839340	0.2989780	0.4039760
H	-3.7897230	1.0007720	1.2371340
H	-2.9950520	-1.6951500	-0.0450500
H	-2.8028830	0.1393320	-1.5503490
C	1.5506970	-3.5954330	-0.2291430
C	2.9897860	1.7147480	-0.4800160
C	-5.1395240	-0.0056960	-0.1650490
H	-5.8050610	-0.3852020	0.6240590
H	-5.0378580	-0.7990650	-0.9221100
O	-5.6574960	1.1831260	-0.7382200
H	-6.5532390	1.0032550	-1.0439030
H	2.4724070	2.1619350	-1.3350420
H	4.0721630	1.7920360	-0.6930280
H	2.3337630	-4.2489870	-0.6233120
H	1.3556830	-3.8705610	0.8074580
H	0.6507840	-3.7450060	-0.8288800
N	2.6031760	2.3938960	0.7421820
H	3.0245230	1.8967900	1.5233930
C	3.0382900	3.7830170	0.7477250
H	2.5096300	4.3287410	-0.0404640
H	2.7824430	4.2427520	1.7044230
H	4.1193740	3.9094560	0.5759670

RC_{1+5}

C	-2.7867280	0.4070500	-0.5005950
C	-0.3806880	1.3735680	-0.6227120
C	-0.6891780	-1.9607790	0.9866150
C	0.1059330	0.2486620	0.2351940
C	-0.1871000	-1.0169520	-0.0714450
C	-1.8570320	1.5670840	-0.1748690
C	-2.0562400	-1.3602760	1.4215460
H	-0.3432770	1.1098740	-1.6868870
H	-0.0170440	-2.0093650	1.8515020
H	0.3253340	0.5062770	1.2741630
H	-0.4549560	-1.2478100	-1.1036810
H	0.1803690	2.2999400	-0.4642570
H	-0.8180820	-2.9779690	0.6021010
H	-2.2721380	2.4688660	-0.6411720
H	-1.8492400	-0.4904630	2.0561690
H	-1.8633410	1.7525770	0.9069010
H	-2.6233200	-2.0749850	2.0309510
N	2.9313680	-1.4955290	0.8647600
N	2.8099230	-0.3052590	-1.5605470
C	2.5695480	-2.1411720	-0.2506700
C	2.9714040	0.3723700	-0.4157020
N	2.6042570	-1.5908910	-1.4762720
N	3.1387050	-0.2054610	0.7769220
C	-2.9034990	-0.9206220	0.2366750
C	-3.9857910	0.1126180	0.3619050
H	-4.0134140	0.6531630	1.3075140
H	-3.1506490	-1.7464450	-0.4321000
H	-2.9744530	0.3085180	-1.5701560
C	2.2028870	-3.5862830	-0.1466340
C	3.0843890	1.8679090	-0.4982360
C	-5.3311050	-0.1077390	-0.2671330
H	-5.9900530	-0.6485110	0.4282610
H	-5.2072080	-0.7378360	-1.1621400
O	-5.8782450	1.1562310	-0.6047910
H	-6.7742350	1.0171740	-0.9303190
H	2.4668580	2.2019100	-1.3398070
H	4.1302290	2.1219510	-0.7551430
H	3.0493550	-4.2121450	-0.4432400
H	1.9300680	-3.8256700	0.8812660
H	1.3686080	-3.8050790	-0.8153280
N	2.6222600	2.4952140	0.7235690
H	3.1150830	2.0807450	1.5094060
C	2.8243350	3.9355500	0.6995730
H	2.1961200	4.3749990	-0.0823550
H	2.5167060	4.3627260	1.6560260
H	3.8662400	4.2352520	0.5005690

TS_{2+5}

C	2.5028470	-0.4292780	-0.4649670
C	0.1706670	-1.5102170	-0.7037850
C	0.2512310	1.6630290	1.1613240
C	-0.4862630	-0.5081130	0.1982350
C	-0.2546340	0.8339720	0.0040430
C	1.6345440	-1.6513800	-0.2227870
C	1.6184950	1.0706750	1.5758470
H	0.1516530	-1.1591240	-1.7427200
H	-0.4469070	1.6231660	2.0049570
H	-0.6345220	-0.8425950	1.2280560
H	0.1289850	1.1150430	-0.9774690
H	-0.3350730	-2.4794810	-0.6559660
H	0.3705590	2.7119220	0.8717930
H	2.1035140	-2.5020350	-0.7311320
H	1.4460180	0.1208280	2.0948590
H	1.6301430	-1.9010070	0.8459920
H	2.1157810	1.7373540	2.2902800
N	-2.8617620	1.2518810	0.6903460
N	-2.6504110	-0.2922800	-1.5078480
C	-2.2040900	1.6551570	-0.4405210
C	-2.6689840	-0.8014740	-0.2256040
N	-2.4143280	0.9584050	-1.6102370
N	-3.1013020	-0.0047890	0.8046820
C	2.5236460	0.8310860	0.3828290
C	3.6738590	-0.1325130	0.4329320
H	3.7370680	-0.7490400	1.3289240
H	2.7156830	1.7355540	-0.1957690
H	2.6890040	-0.2426950	-1.5226140
C	4.9998680	0.2357360	-0.1667570
H	5.6226680	0.7508620	0.5793050
H	4.8315080	0.9377470	-0.9986090
O	5.6272930	-0.9521540	-0.6194100
H	6.5066120	-0.7240490	-0.9401600
C	-1.9450390	3.1270110	-0.5871920
H	-2.7986750	3.6072640	-1.0724910
H	-1.8028070	3.5784930	0.3950590
H	-1.0605330	3.3046930	-1.2027760
N	-2.8174730	-2.1571230	-0.1097520
C	-3.3921710	-2.7253000	1.0950270
H	-2.7997840	-2.4242000	1.9620570
H	-4.4261990	-2.4034860	1.2667840
H	-3.3581730	-3.8117380	1.0125120
H	-3.0317790	-2.6092430	-0.9876890

RC_{2+5}

C	-2.6823310	0.4312540	-0.4290070
C	-0.3801880	1.6234710	-0.3375130
C	-0.4258190	-1.8680210	0.9268730
C	0.1808070	0.4720970	0.4378490
C	0.0183060	-0.7756580	-0.0042480
C	-1.8863570	1.6365860	0.0508050
C	-1.8641420	-1.4499010	1.3467470
H	-0.2719070	1.4603990	-1.4168530
H	0.2132230	-1.9403830	1.8142160
H	0.3223970	0.6349890	1.5097310
H	-0.1846980	-0.9231500	-1.0660000
H	0.0756980	2.5881630	-0.0885410
H	-0.4342450	-2.8473520	0.4373470
H	-2.3676790	2.5364250	-0.3511210
H	-1.7753030	-0.6371870	2.0771870
H	-1.9554280	1.7137370	1.1434600
H	-2.3818900	-2.2766740	1.8485140
N	3.2026280	-1.0578600	0.7924960
N	2.8660710	0.3248550	-1.5142310
C	2.8830460	-1.6377430	-0.3647860
C	3.0312800	0.9140630	-0.3035010
N	2.7822130	-0.9678890	-1.5308160
N	3.2853280	0.2491080	0.8380100
C	-2.7000170	-0.9697240	0.1692540
C	-3.8812870	-0.0588620	0.3394070
H	-3.9993690	0.3775850	1.3307220
H	-2.8365840	-1.7409570	-0.5900910
H	-2.8168090	0.4242430	-1.5110030
C	-5.1725230	-0.3357670	-0.3748210
H	-5.8070790	-0.9953650	0.2349550
H	-4.9537560	-0.8644800	-1.3160310
O	-5.8192310	0.9017800	-0.6233690
H	-6.6854320	0.7155700	-1.0017040
C	2.6962520	-3.1222490	-0.3994690
H	1.7927820	-3.3718290	-0.9604060
H	3.5423070	-3.6088730	-0.8925160
H	2.6112120	-3.5050720	0.6177140
N	3.0056310	2.2607590	-0.2727380
H	2.7073370	2.7088660	-1.1257630
C	2.9856280	2.9928330	0.9772290
H	2.9294870	4.0569790	0.7518510
H	2.1255370	2.7071090	1.5945830
H	3.8950210	2.7959400	1.5487320

TS_{3+5}

C	-3.0883090	-0.2794450	-0.5369970
C	-1.5781320	1.8121450	-0.7542370
C	-0.3155960	-0.8436990	1.4703580
C	-0.6282250	1.3275460	0.3048240
C	-0.1749170	0.0384140	0.2548150
C	-2.9659080	1.2269100	-0.3906040
C	-1.8352750	-0.9920400	1.7283360
H	-1.2626900	1.4554410	-1.7418720
H	0.1740700	-0.3958690	2.3425820
H	-0.7577160	1.7722780	1.2946010
H	-0.2355820	-0.4621910	-0.7118770
H	-1.6481460	2.9028890	-0.7914160
H	0.1303790	-1.8283830	1.2995050
H	-3.7284460	1.6891320	-1.0282030
H	-2.2115920	-0.0509120	2.1458050
H	-3.2093630	1.5231950	0.6375900
H	-2.0171100	-1.7688580	2.4801540
N	2.3221780	0.9933550	1.1417190
N	1.6201420	2.0717350	-1.2218680
C	2.1036160	0.2497310	0.0200250
C	1.2701560	2.6181340	-0.0221350
N	2.0501620	0.8583200	-1.1987240
N	1.8919770	2.2065040	1.1204850
C	-2.5961670	-1.3184210	0.4567710
C	-4.0652880	-1.0492450	0.3111490
H	-4.5254830	-0.4799520	1.1179220
H	-2.2547570	-2.2381670	-0.0198080
H	-3.0331590	-0.6120230	-1.5735010
C	2.5620390	-1.1787930	0.0458980
C	0.7042020	4.0046620	-0.0280090
C	-4.9679500	-2.0660700	-0.3257370
H	-5.3442240	-2.7661220	0.4343000
H	-4.3872900	-2.6514950	-1.0560680
O	-6.0347670	-1.3770430	-0.9551540
H	-6.6576510	-2.0308460	-1.2910560
H	0.2501950	4.2176110	-0.9958050
H	-0.0374070	4.1252000	0.7642550
H	1.5070000	4.7253080	0.1491710
H	2.3876330	-1.5812640	1.0480680
H	1.9637200	-1.7577070	-0.6663860
C	4.5183380	-2.7210640	-0.3008740
H	4.3690260	-3.1805910	0.6830040
H	3.9792900	-3.3133990	-1.0495680
C	4.0495620	-1.2809100	-0.3071190
H	4.6375860	-0.7077780	0.4173590
H	4.2236650	-0.8463870	-1.2963890
F	5.8691220	-2.7688100	-0.6001330

RC_{3+5}

C	-3.3779760	-0.2115390	-0.5392920
C	-1.7920550	1.8351970	-0.6793960
C	-0.5006070	-1.0659880	1.2494900
C	-0.8774010	1.1868430	0.3132390
C	-0.4641600	-0.0680620	0.1253420
C	-3.1956040	1.2806270	-0.3039780
C	-2.0135770	-1.2242280	1.5747180
H	-1.5347340	1.5413340	-1.7037020
H	0.0349060	-0.7113890	2.1376620
H	-0.9209290	1.5771050	1.3342520
H	-0.4887870	-0.4690160	-0.8892330
H	-1.8004330	2.9288460	-0.6280680
H	-0.0661030	-2.0274260	0.9557870
H	-3.9687480	1.8059910	-0.8773770
H	-2.3298150	-0.3336370	2.1305260
H	-3.3853950	1.5150280	0.7513470
H	-2.1850440	-2.0879730	2.2288640
N	2.4232140	0.9595480	1.2096830
N	1.8884980	2.1308170	-1.1697400
C	2.4817810	0.3074990	0.0397390
C	1.6613570	2.7271340	0.0090520
N	2.3105520	0.8926790	-1.1524520
N	2.0034910	2.1967760	1.1934900
C	-2.8672240	-1.3587640	0.3233280
C	-4.3290270	-1.0164590	0.3067700
H	-4.7008770	-0.5016820	1.1920750
H	-2.6070210	-2.2375490	-0.2684660
H	-3.4038350	-0.4664860	-1.5990820
C	2.8749070	-1.1368210	0.0544680
C	1.0623050	4.0960940	0.0090770
C	-5.3265530	-1.9284620	-0.3466650
H	-5.6926140	-2.6712920	0.3770890
H	-4.8279080	-2.4770580	-1.1610320
O	-6.3919460	-1.1351100	-0.8426490
H	-7.0703590	-1.7244680	-1.1900550
H	0.7814140	4.3759190	-1.0058050
H	0.1798300	4.1117250	0.6533140
H	1.7774070	4.8221650	0.4035160
H	2.6486980	-1.5444330	1.0441950
H	2.2665450	-1.6665300	-0.6866280
C	4.7588540	-2.7670290	-0.2975170
H	4.5763560	-3.2425440	0.6728890
H	4.1989710	-3.3114050	-1.0666260
C	4.3635670	-1.3051640	-0.2708620
H	4.9681810	-0.7831410	0.4781490
H	4.5783650	-0.8549080	-1.2454840
F	6.1084100	-2.8722560	-0.58543

7. References

(1) Taylor, M. T., Blackman, M. L., Dmitrenko, O., and Fox, J. M. (2011) Design and synthesis of highly reactive dienophiles for the tetrazine-trans-cyclooctene ligation. *J. Am. Chem. Soc. 133*, 9646–9.

(2) Matt, T., and Seebach, D. (1998) C-Alkylation of Peptides Containing Aminomalonate and (Amino)(cyano)acetate Residues. *Helv. Chim. Acta 81*, 1845–1895.

(3) Nachbaur, E., and Leiseder, G. (1971) Über eine einfache und gefahrlose Methode zur Darstellung von wasserfreiem Hydrazin. *Monatshefte für Chemie 102*, 1718–1723.

(4) Larsen, P., Ulin, J., Dahlstrøm, K., and Jensen, M. (1997) Synthesis of [11C]iodomethane by iodination of [11C]methane. *Appl. Radiat. Isot. 48*, 153–157.

(5) Jewett, D. M. (1992) A simple synthesis of [11C]methyl triflate. *Int. J. Radiat. Appl. Instrumentation. Part A. Appl. Radiat. Isot. 43*, 1383–1385.

(6) Devaraj, N. K., Upadhyay, R., Haun, J. B., Hilderbrand, S. A., and Weissleder, R. (2009) Fast and sensitive pretargeted labeling of cancer cells through a tetrazine/trans-cyclooctene cycloaddition. *Angew. Chemie - Int. Ed. 48*, 7013–7016.

(7) Eisenbrand, G., Lauck-Birkel, S., and Tang, W. C. (1996) An Approach Towards More Selective Anticancer Agents. *Synthesis (Stuttg). 1996*, 1246–1258.

(8) Yang, J., Karver, M. R., Li, W., Sahu, S., and Devaraj, N. K. (2012) Metal-Catalyzed One-Pot Synthesis of Tetrazines Directly from Aliphatic Nitriles and Hydrazine. *Angew. Chemie 124*, 5312–5315.

(9) Beckmann, H. S. G., Niederwieser, A., Wiessler, M., and Wittmann, V. (2012) Preparation of Carbohydrate Arrays by Using Diels-Alder Reactions with Inverse Electron Demand. *Chem. - A Eur. J. 18*, 6548–6554.

(10) Ostafin, A., Nooney, R. I., Thirunavukkarasu, D., Chen, Y., Josephs, R., and Ostafin, A. E. (2015) Synthesis of Nanoscale Mesoporous Silica Spheres with Controlled Particle Size Synthesis of Nanoscale Mesoporous Silica Spheres with Controlled Particle Size 4721–4728.

(11) Yokoi, T., Yoshitake, H., and Tatsumi, T. (2004) Synthesis of amino-functionalized MCM-41 via direct co-condensation and post-synthesis grafting methods using mono-{,} di- and tri-amino-organoalkoxysilanes. *J. Mater. Chem. 14*, 951–957.

(12) Ritter, H., Nieminen, M., Karppinen, M., and Br??hwiler, D. (2009) A comparative study of the functionalization of mesoporous silica MCM-41 by deposition of 3-aminopropyltrimethoxysilane from toluene and from the vapor phase. *Microporous Mesoporous Mater. 121*, 79–83.

(13) Loening, A. M., and Gambhir, S. S. (2003) AMIDE: A Free Software Tool for Multimodality Medical Image Analysis. *Mol. Imaging 2*, 131–137.

(14) Frisch, M. J. G., Trucks, W., Schlegel, H. B., Scuseria, G. E., Robb, M. A., Cheeseman, J. R., Scalmani, G., Barone, V., Mennucci, B., Petersson, G. A., *et al.* (2009) Gaussian 09, Revision D.01. *Inc. Wallingford, CT*.

(15) Zhao, Y., and Truhlar, D. G. (2008) The M06 suite of density functionals for main group thermochemistry, thermochemical kinetics, noncovalent interactions, excited states, and transition elements: Two new functionals and systematic testing of four M06-class functionals and 12 other functionals. *Theor. Chem. Acc. 120*, 215–241.

(16) Ditchfield, R., Hehre, W. J., and Pople, J. A. (1971) Self-Consistent Molecular-Orbital Methods. IX. An Extended Gaussian-Type Basis for Molecular-Orbital Studies of Organic Molecules. *J. Chem. Phys. 54*, 724.

(17) Lan, Y., Zou, L., Cao, Y., and Houk, K. N. (2011) Computational methods to calculate accurate activation and reaction energies of 1,3-dipolar cycloadditions of 24 1,3-dipoles. *J. Phys. Chem. A 115*, 13906–13920.

(18) Liu, F., Paton, R. S., Kim, S., Liang, Y., and Houk, K. N. (2013) Diels-Alder reactivities of strained and unstrained cycloalkenes with normal and inverse-electron-demand dienes: activation barriers and distortion/interaction analysis. *J. Am. Chem. Soc. 135*, 15642–9.

(19) Talbot, A., Devarajan, D., Gustafson, S. J., Fernández, I., Bickelhaupt, F. M., and Ess, D. H. (2014) Activation-Strain Analysis Reveals Unexpected Origin of Fast Reactivity in Heteroaromatic Azadiene Inverse-Electron-Demand Diels–Alder Cycloadditions. *J. Org. Chem.* 141204145525004.

(20) Denk, C., Svatunek, D., Filip, T., Wanek, T., Lumpi, D., Fröhlich, J., Kuntner, C., and Mikula, H. (2014) Development of a 18 F-Labeled Tetrazine with Favorable Pharmacokinetics for Bioorthogonal PET Imaging. *Angew. Chemie Int. Ed. 53*, 9655–9659.

Manuscript #3 – Supporting Information

manuscript draft

Denk, C.; Svatunek, D.; Mairinger, S.; Kuntner-Hannes, C.; Filip, T.; Sauberer, M.; Fröhlich, J.; Wanek, T.; Mikula, H.:

A Tale of 3-[^{18}F]Fluoropropyl-1,2,4,5-tetrazines

A Tale of 3-[^{18}F]Fluoropropyl-1,2,4,5-Tetrazines

Christoph Denk[a], Dennis Svatunek[a], Severin Mairinger[b], Claudia Kuntner[b], Thomas Filip[b], Michael Sauberer[b,] Johannes Fröhlich[a], Thomas Wanek[b] and Hannes Mikula[a*]

a) Institut für Angewandte Synthesechemie, Technische Universität Wien (TUW) (Austria) E-mail: hannes.mikula@tuwien.ac.at b) Health and Environment Department, Biomedical Systems, Austrian Institute of Technology (AIT) Seibersdorf (Austria)

Supporting Information

Contents

1. *In vivo* Data 2

2. NMR Spectra 7

3. HPLC Data 26

4. Determination of Specific Activity 29

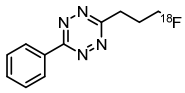
5. Kinetic Measurements 31

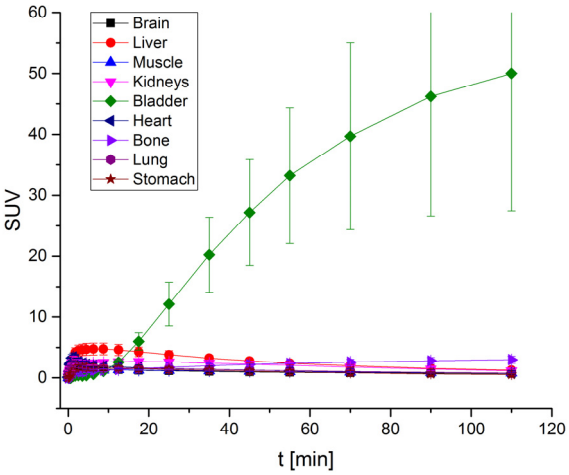
6. Quantum Chemical Calculations 42

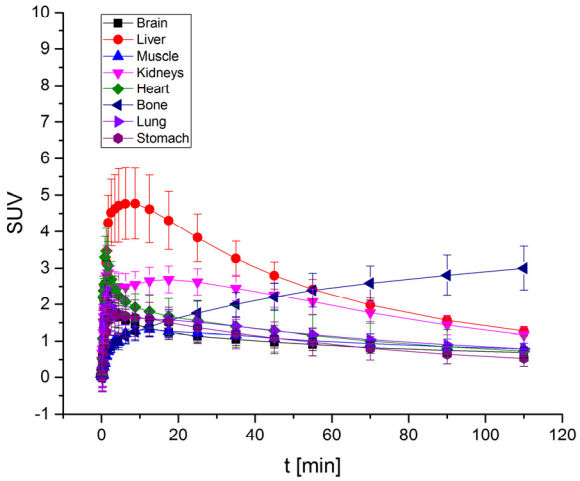
7. References 50

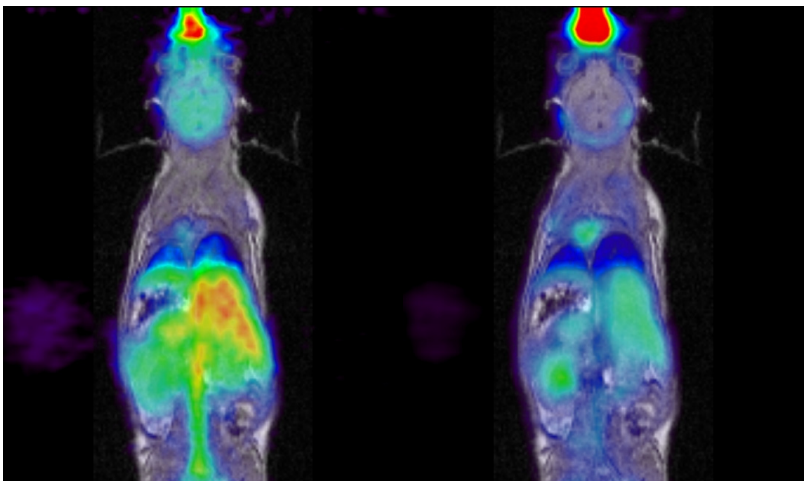
1. *In vivo* Data

[^{18}F]**2**

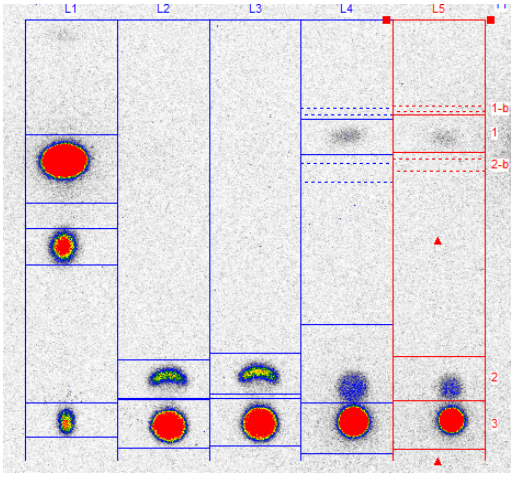








0-5 min **5-120 min**

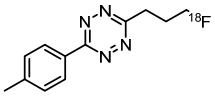


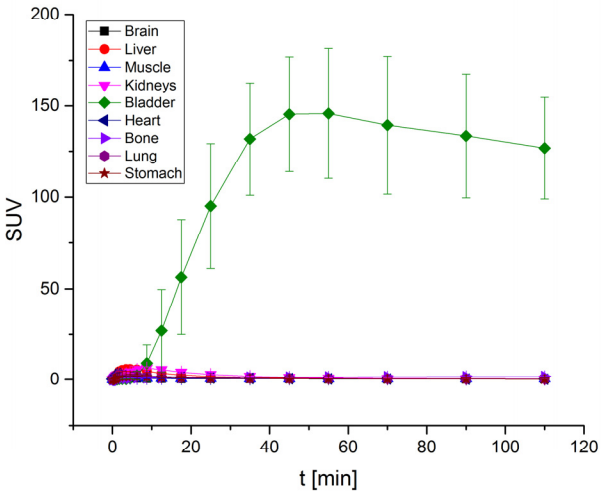
Radio-TLC metabolite analysis:

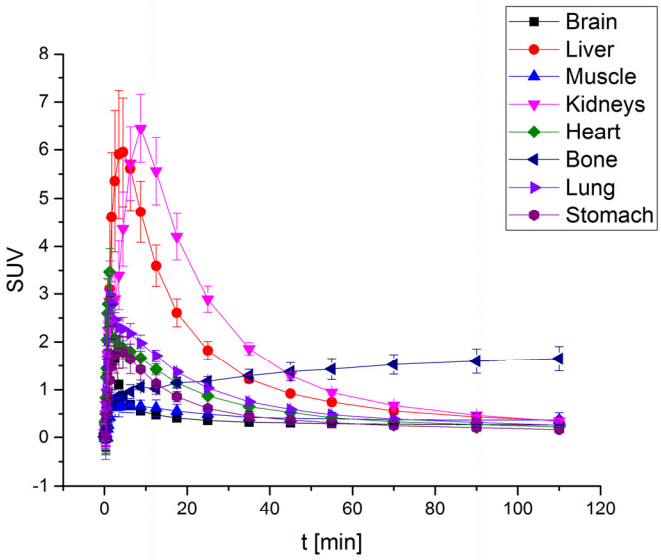
Eluent: DCM

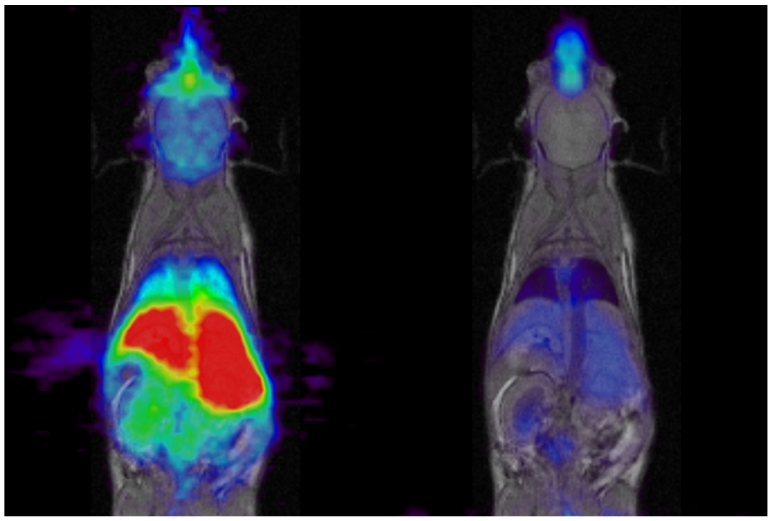
Lane 1: Reference [^{18}F]**2**
Lane 2: Plasma
Lane 3: Plasma
Lane 4: Urine
Lane 5: Urine

$[^{18}F]$**3**

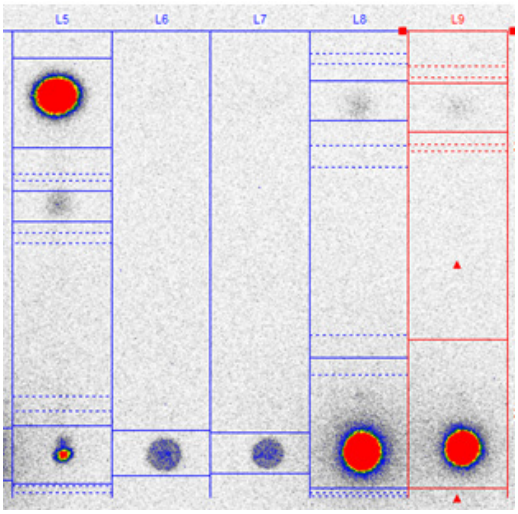








0-5 min **5-120 min**

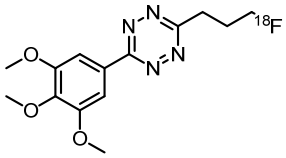


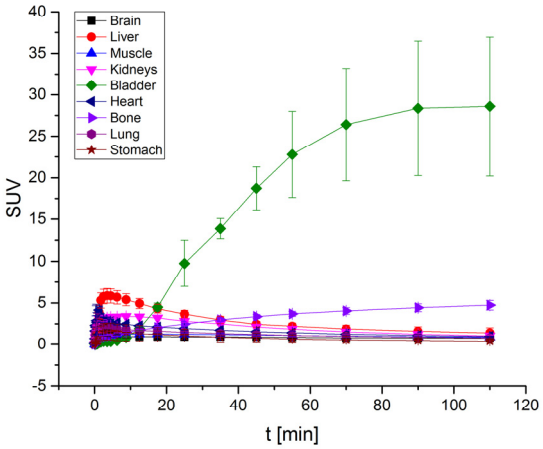
Radio-TLC metabolite analysis:

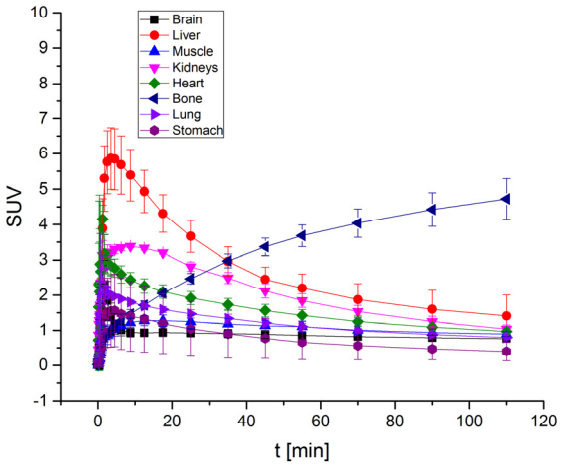
Eluent: DCM

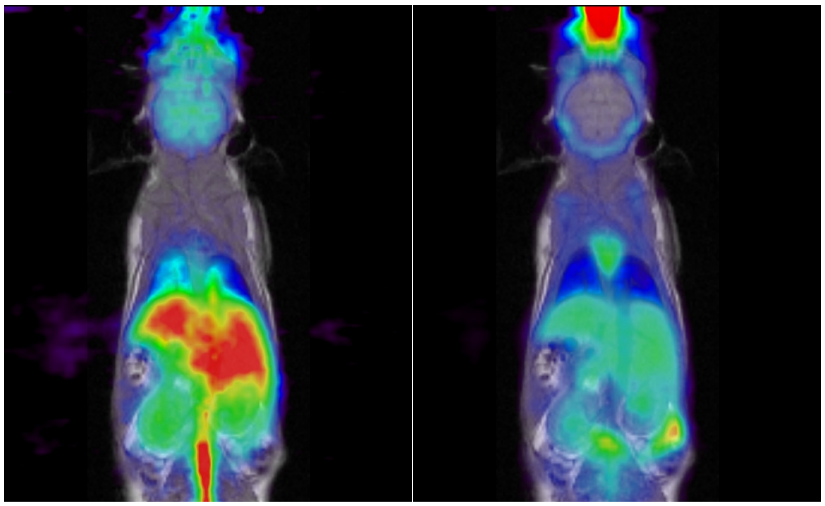
Lane 1: Reference $[^{18}F]$**3**
Lane 2: Plasma
Lane 3: Plasma
Lane 4: Urine
Lane 5: Urine

[^{18}F]**5**

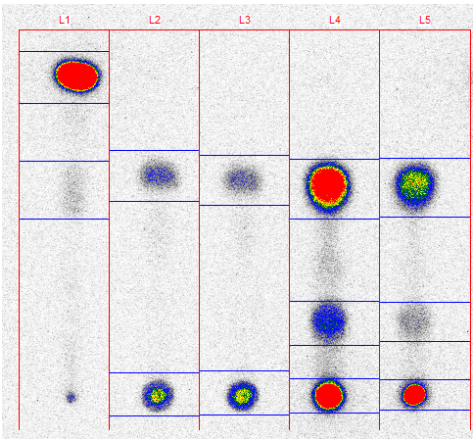








0-5 min **5-120 min**

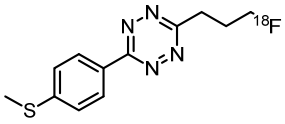


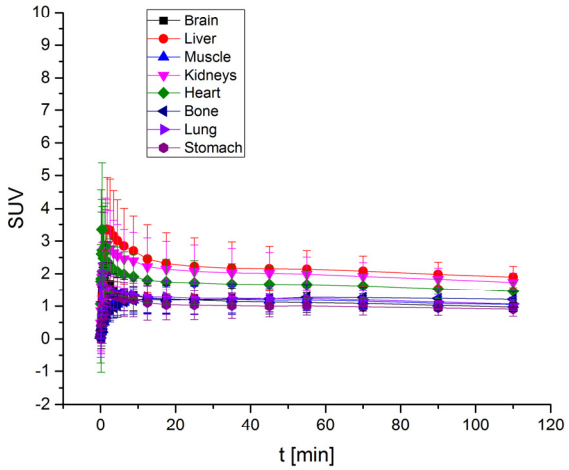
Radio-TLC metabolite analysis:

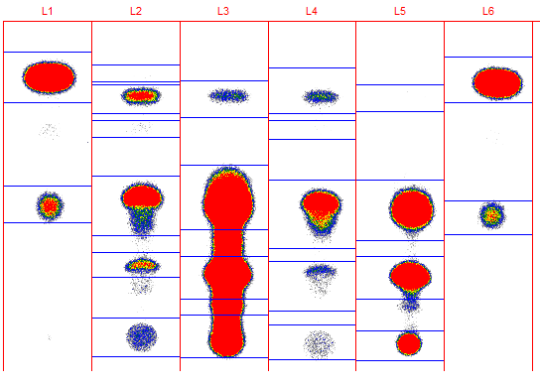
Eluent: 3% MeOH in DCM

Lane 1: Reference [^{18}F]**5**
Lane 2: Plasma
Lane 3: Plasma
Lane 4: Urine
Lane 5: Urine

[^{18}F]**6**



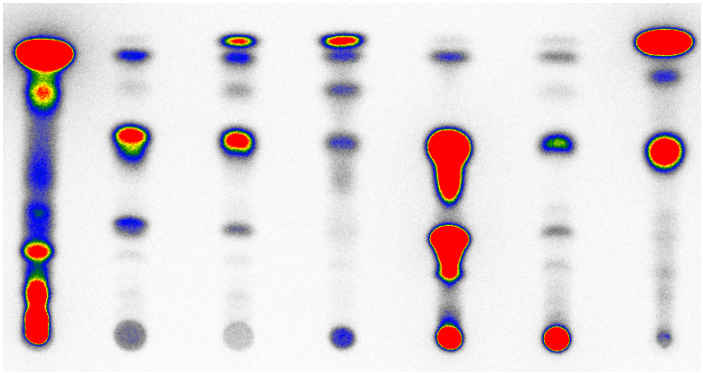




Radio-TLC metabolite analysis 120 min post administration:

Eluent: 5% MeOH in DCM

Lane 1: Reference [^{18}F]**6**
Lane 2: Plasma
Lane 3: Urine
Lane 4: Plasma
Lane 5: Urine
Lane 6: Reference [^{18}F]**6**

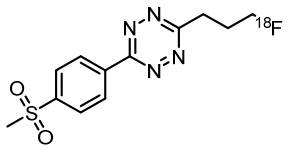


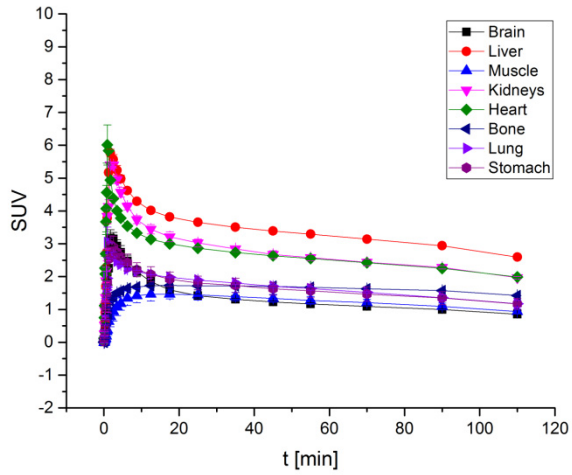
Radio-TLC metabolite analysis 60 min post administration:

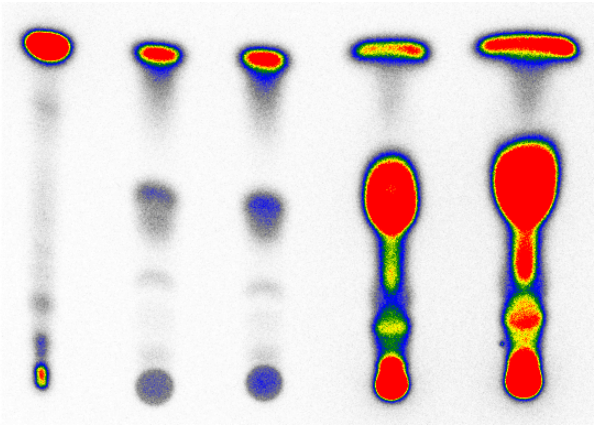
Eluent: 5% MeOH in DCM

Lane 1: Reference [^{18}F]**7** (Sulfone derivative)
Lane 2: Plasma
Lane 3: CNS extract
Lane 4: Liver extract
Lane 5: Urine
Lane 6: Bile
Lane 7: Reference [^{18}F]**6**

[^{18}F]**7**







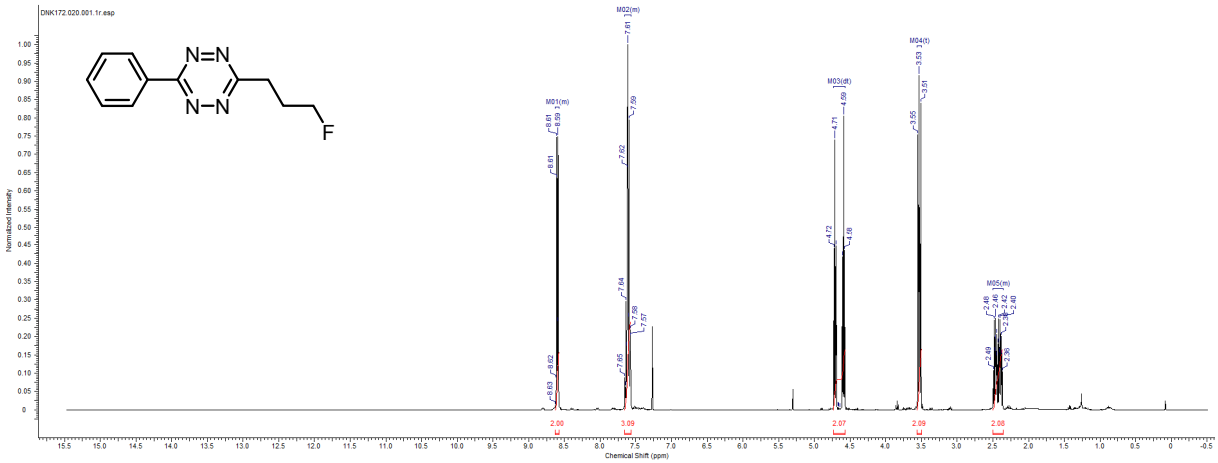
Radio-TLC metabolite analysis 120 min post administration:

Eluent: 5% MeOH in DCM

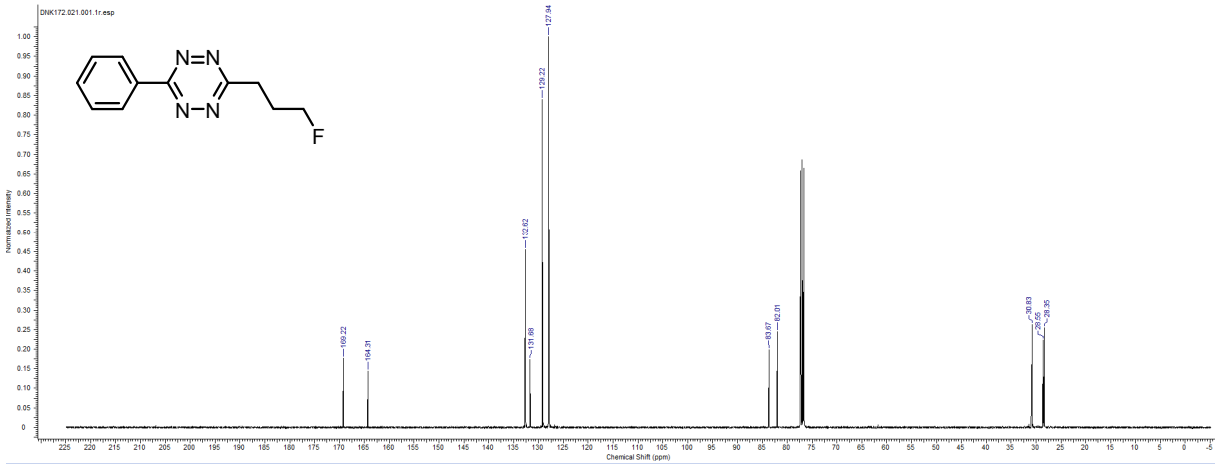
Lane 1: Reference [^{18}F]**7**
Lane 2: Plasma
Lane 3: Plasma
Lane 4: Urine
Lane 5: Urine
Lane 6: Reference [^{18}F]**6**

2. NMR Spectra

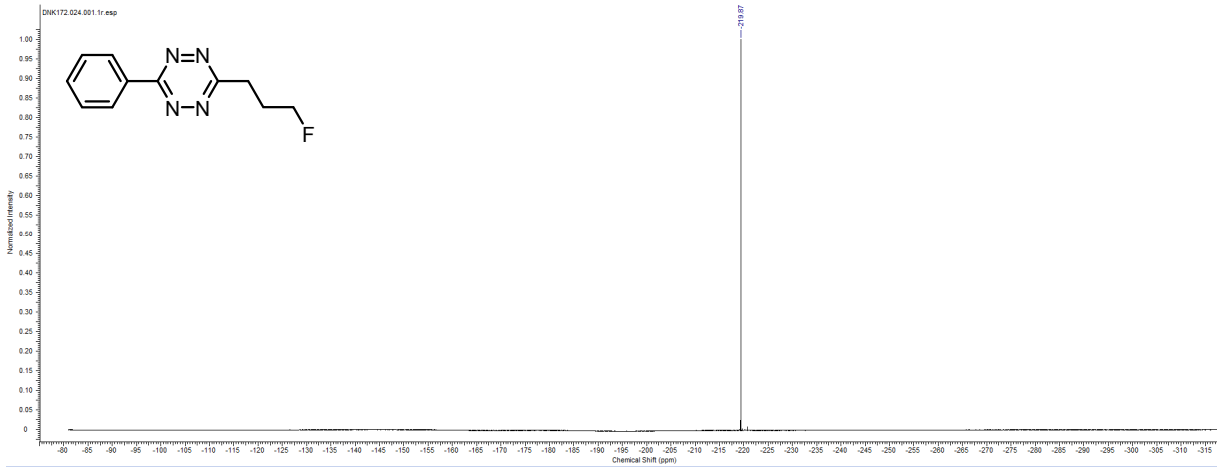
^{1}H Spectrum of compound **2**



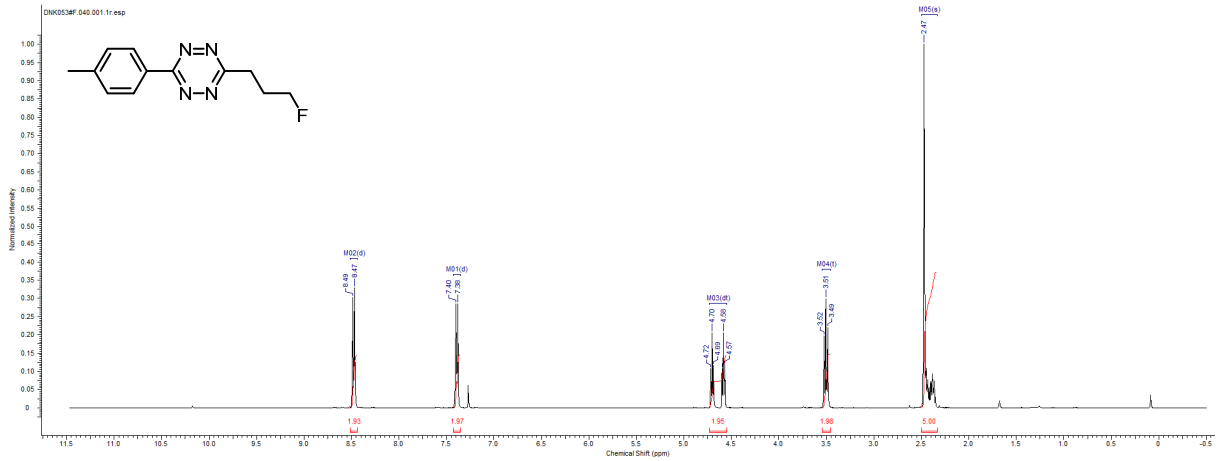
^{13}C Spectrum of compound **2**



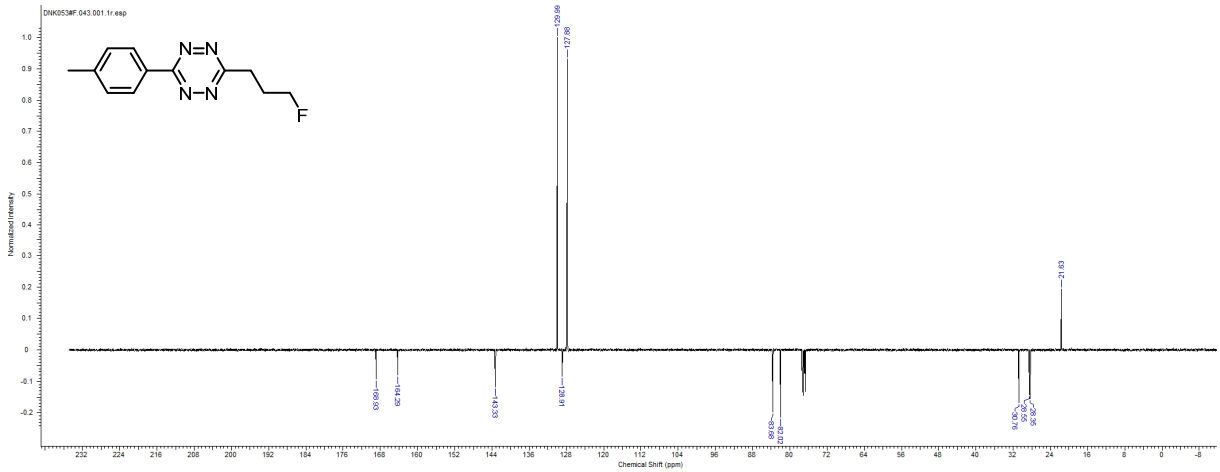
^{19}F Spectrum of compound **2**



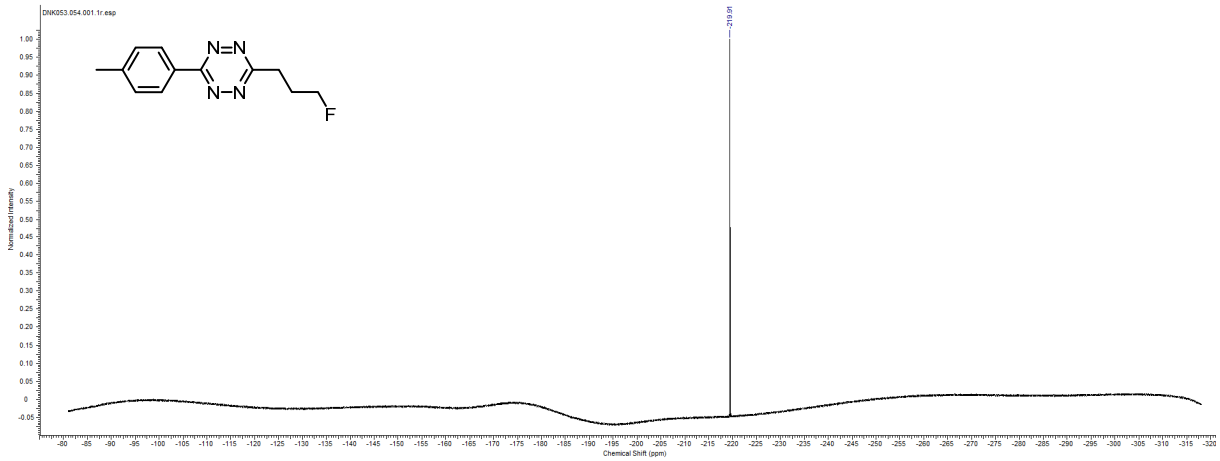
^{1}H Spectrum of compound **3**



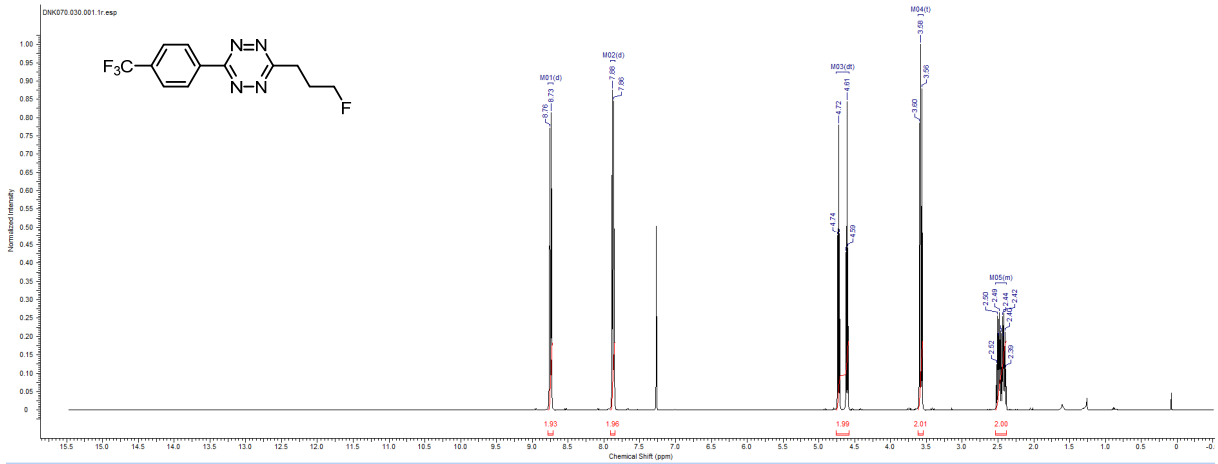
^{13}C Spectrum of compound **3**



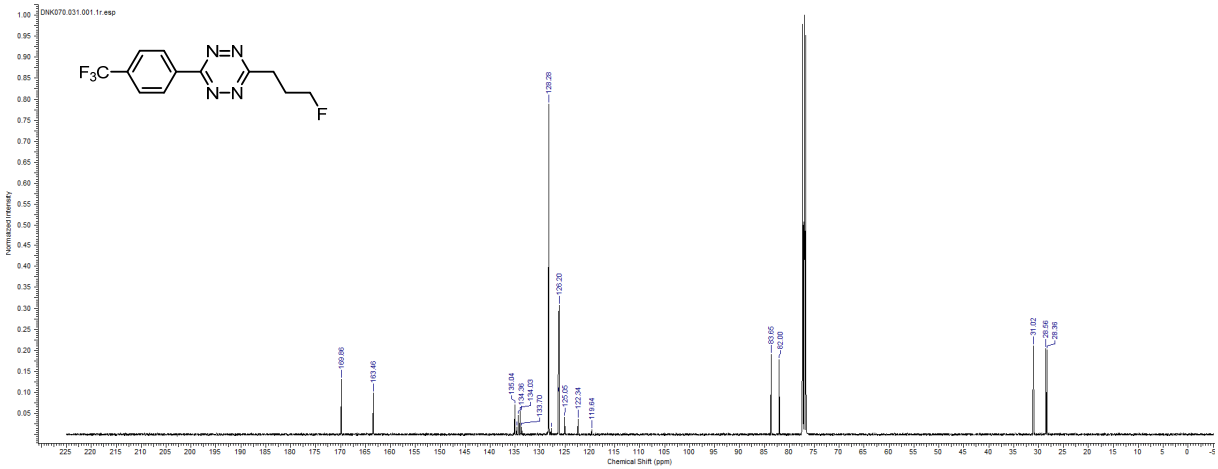
^{19}F Spectrum of compound **3**



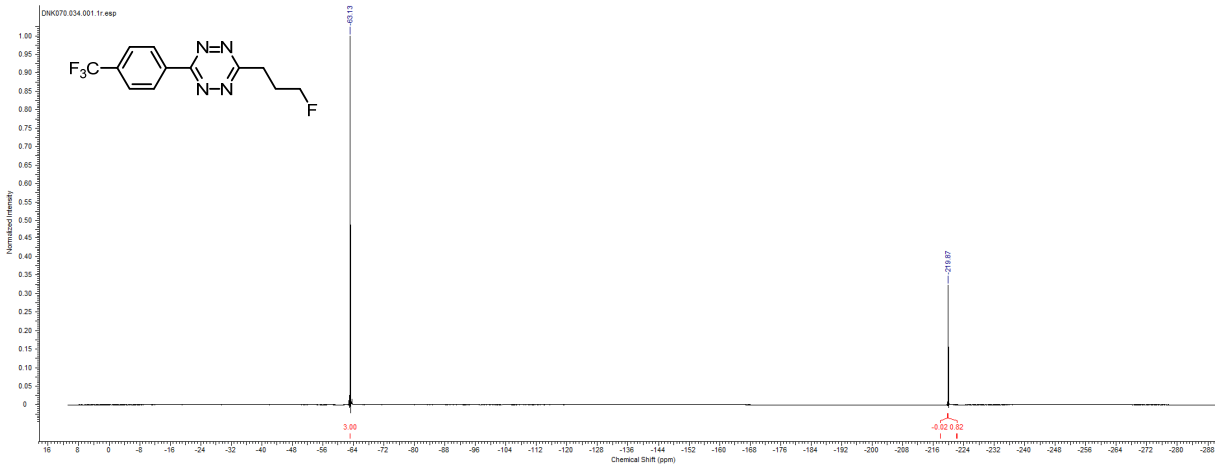
^{1}H Spectrum of compound **4**



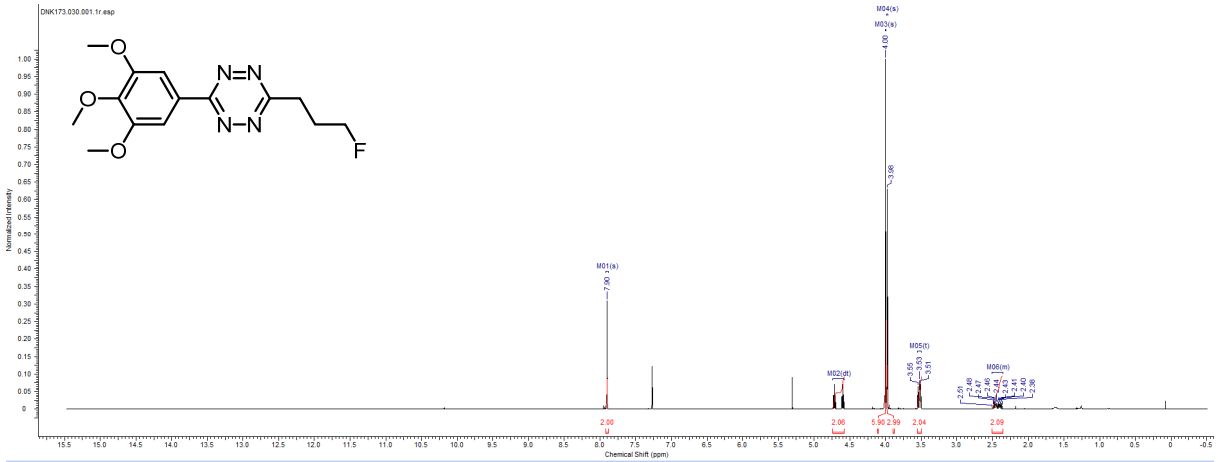
^{13}C Spectrum of compound **4**



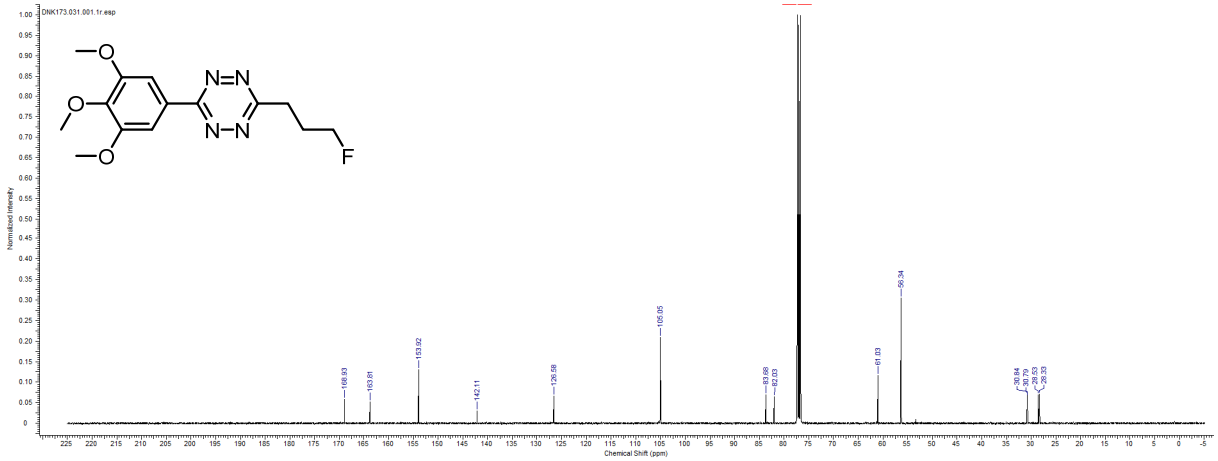
^{19}F Spectrum of compound **4**



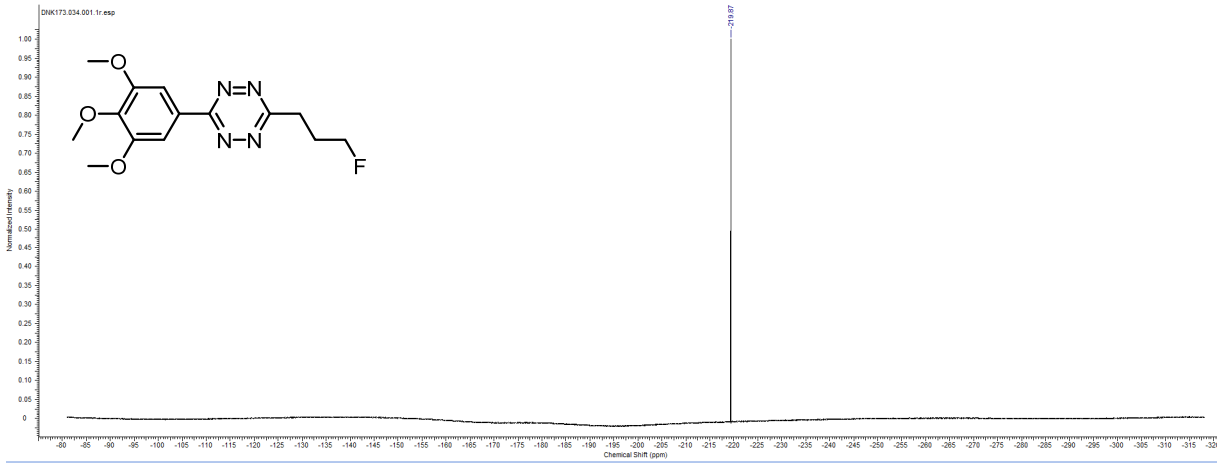
^{1}H Spectrum of compound **5**



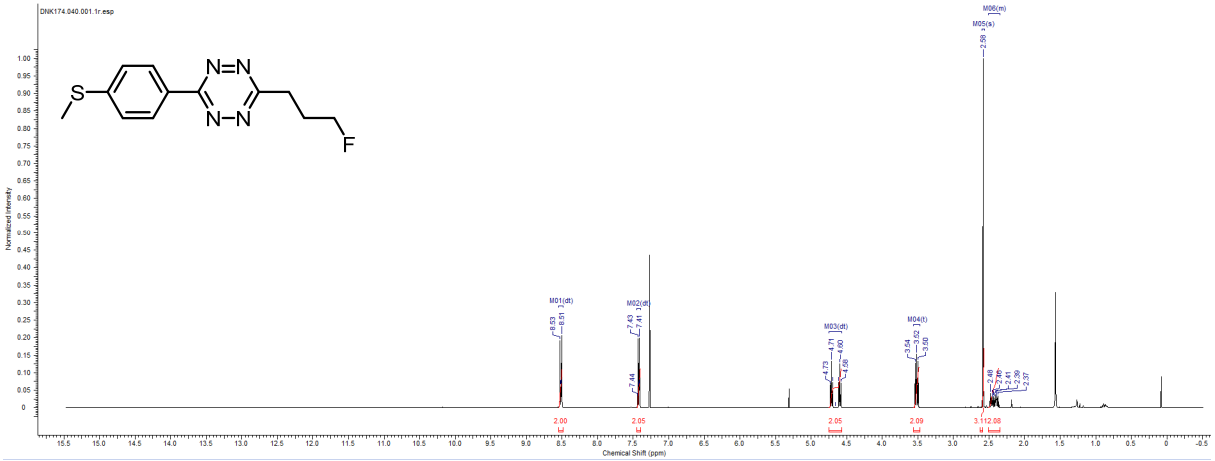
^{13}C Spectrum of compound **5**



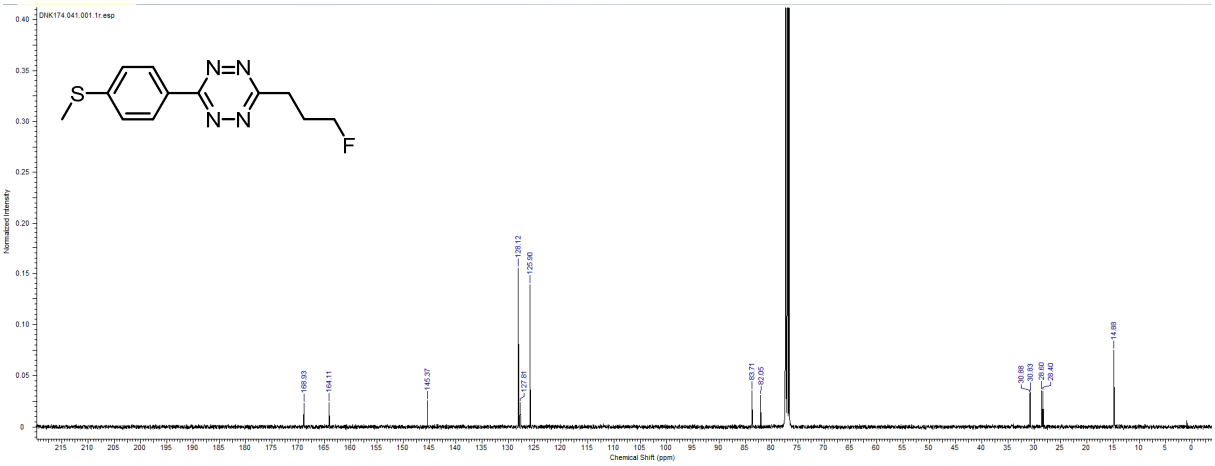
^{19}F Spectrum of compound **5**



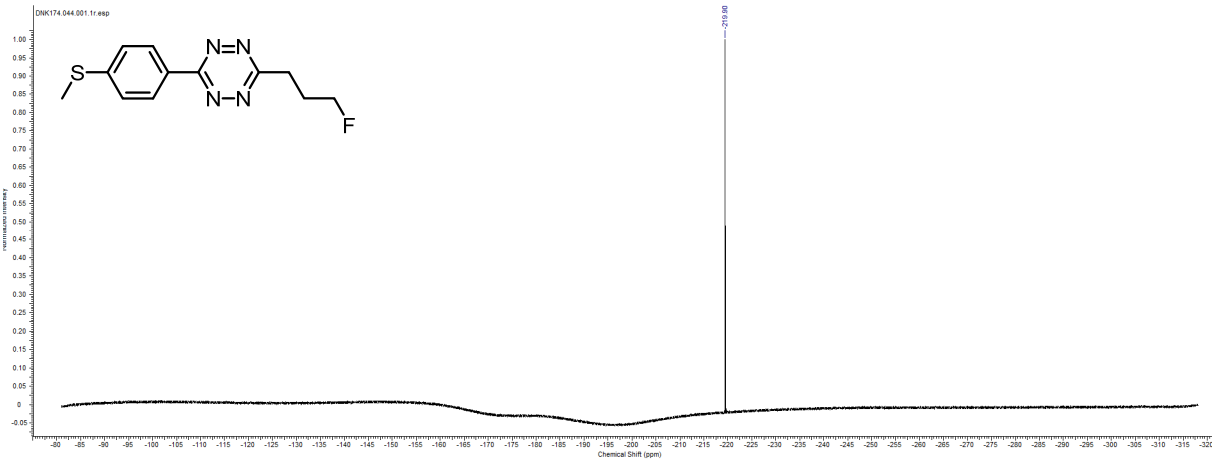
^{1}H Spectrum of compound **6**



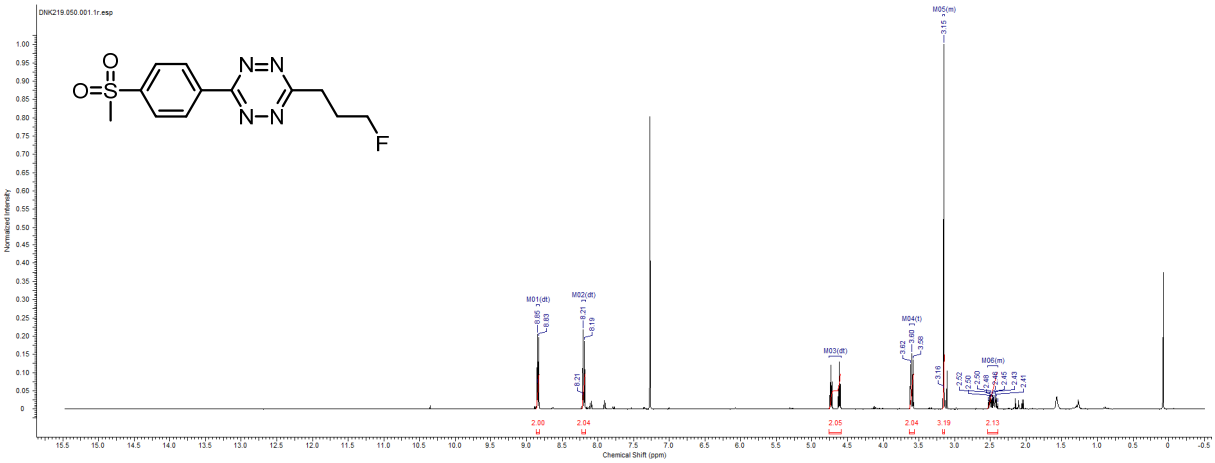
^{13}C Spectrum of compound **6**



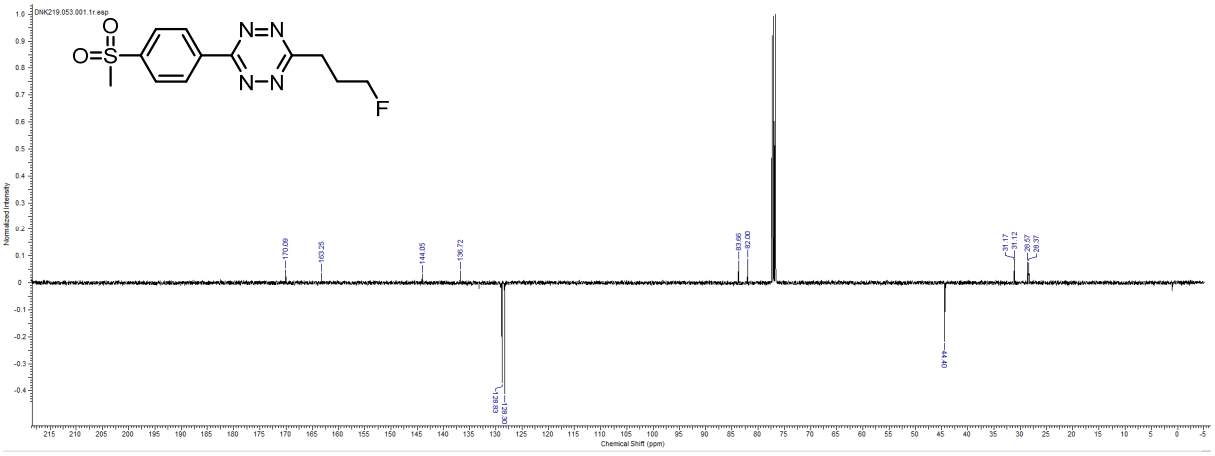
^{19}F Spectrum of compound **6**



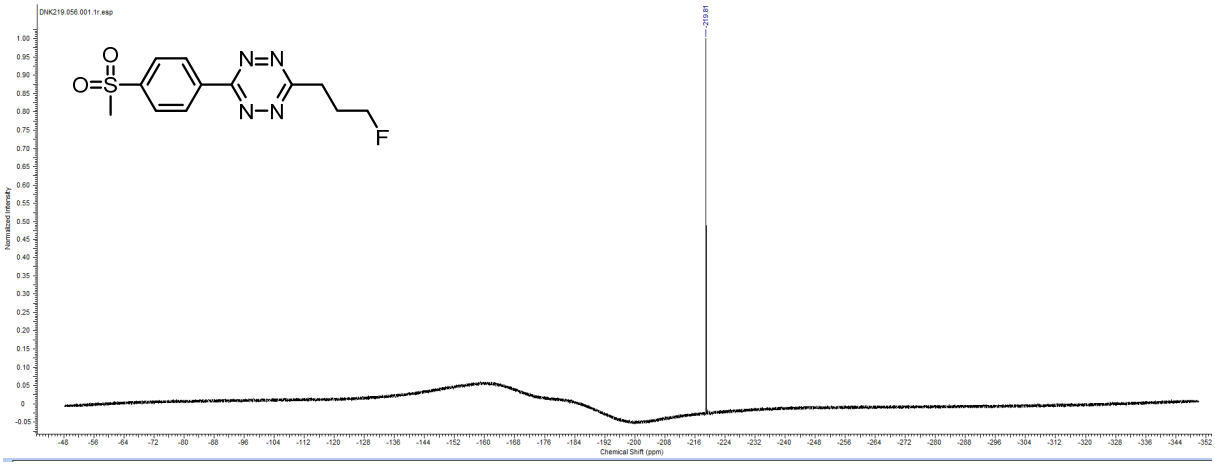
^{1}H Spectrum of compound **7**



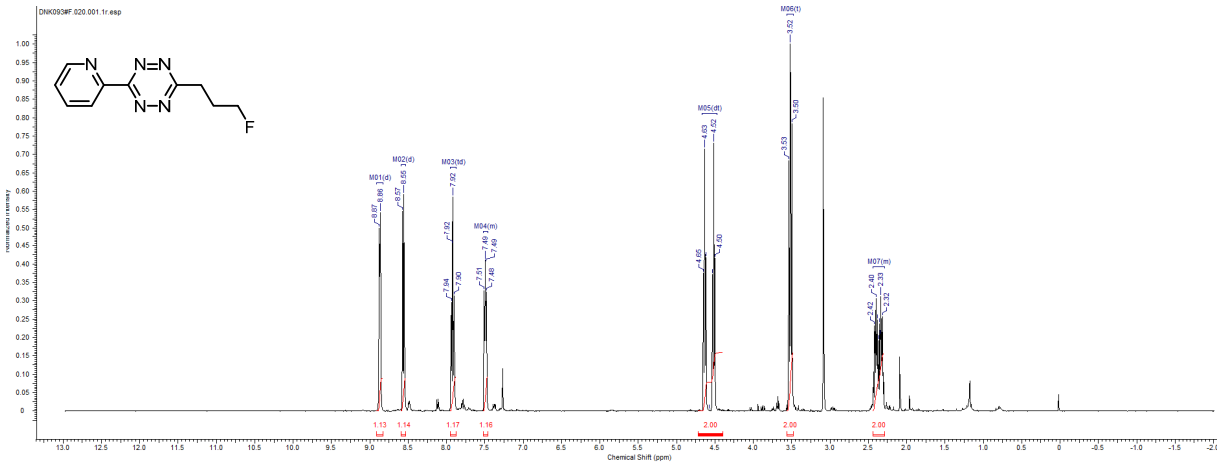
^{13}C Spectrum of compound **7**



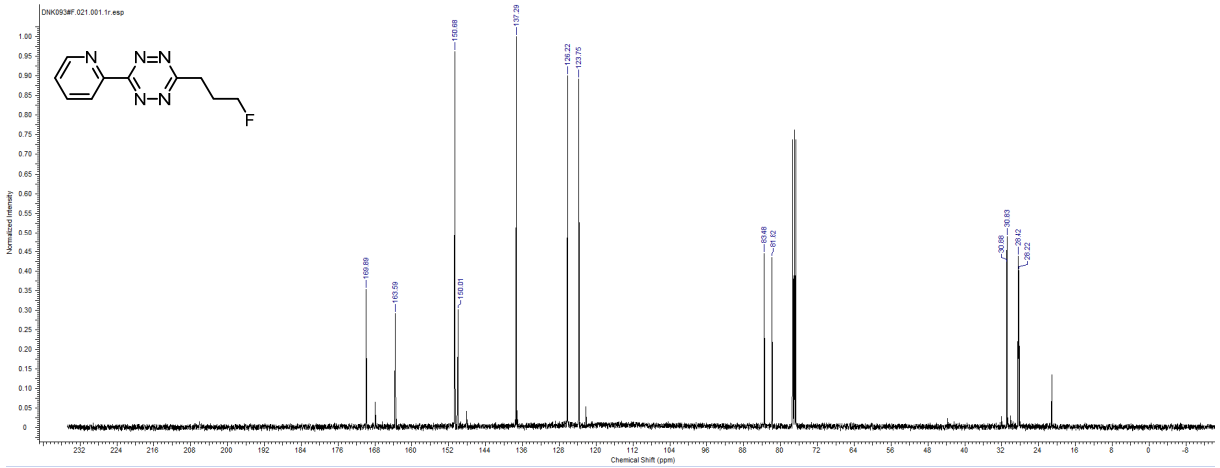
^{19}F Spectrum of compound **7**



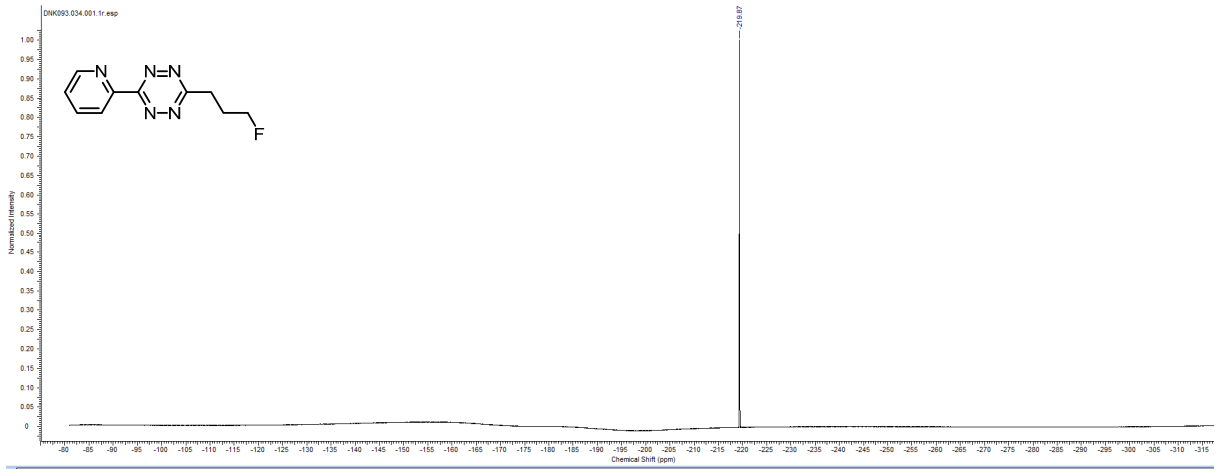
^{1}H Spectrum of compound **8**



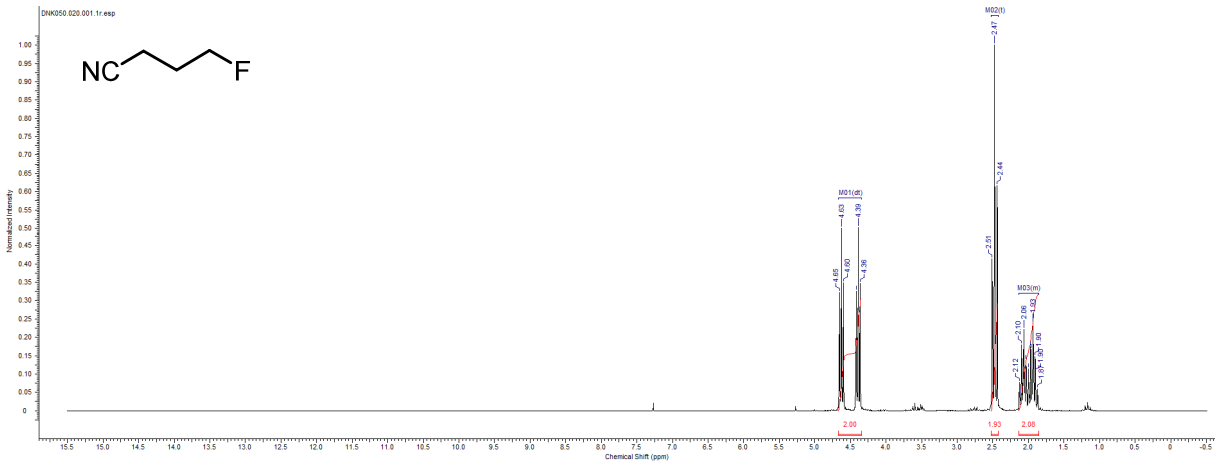
^{13}C Spectrum of compound **8**



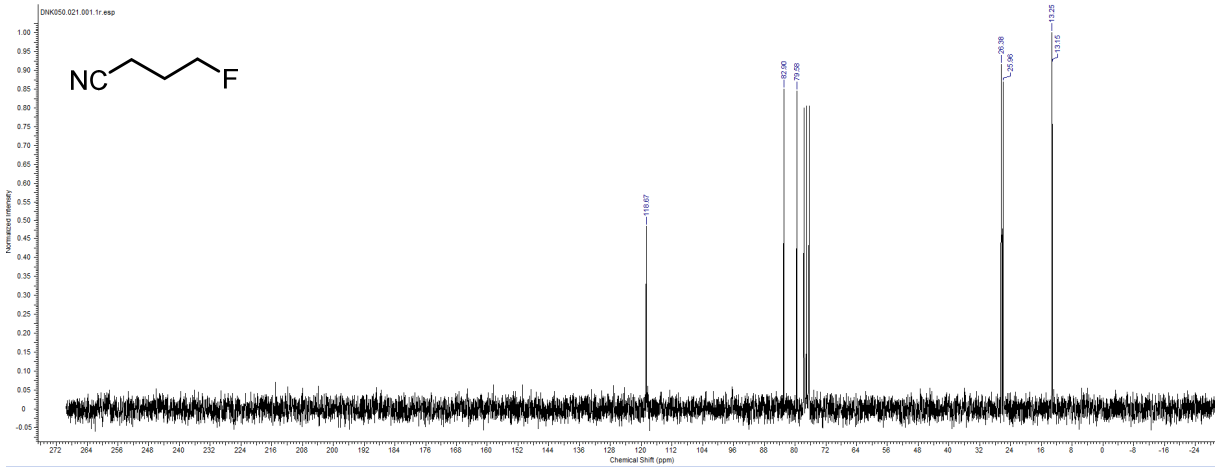
^{19}F Spectrum of compound **8**



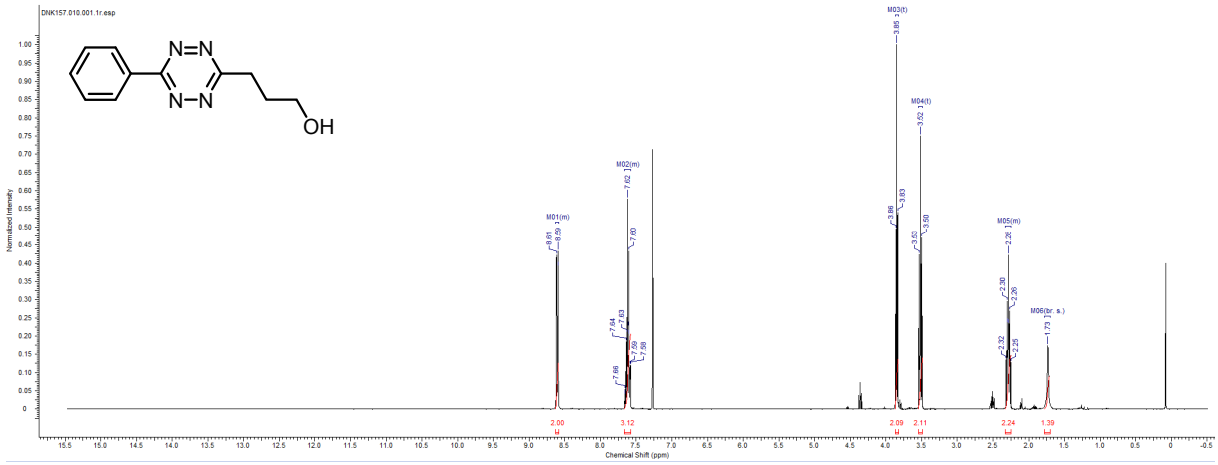
^{1}H Spectrum of compound **9**



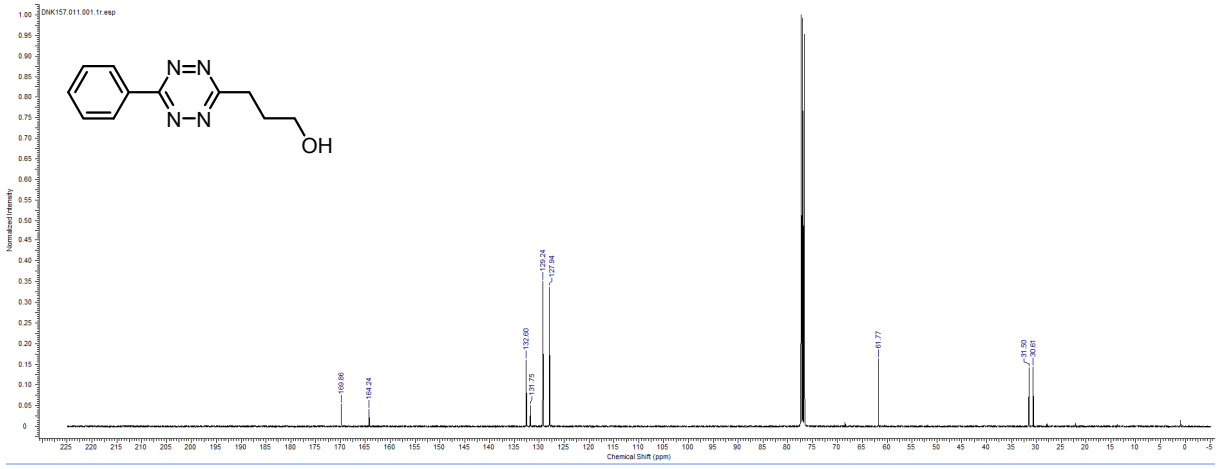
^{13}C Spectrum of compound **9**



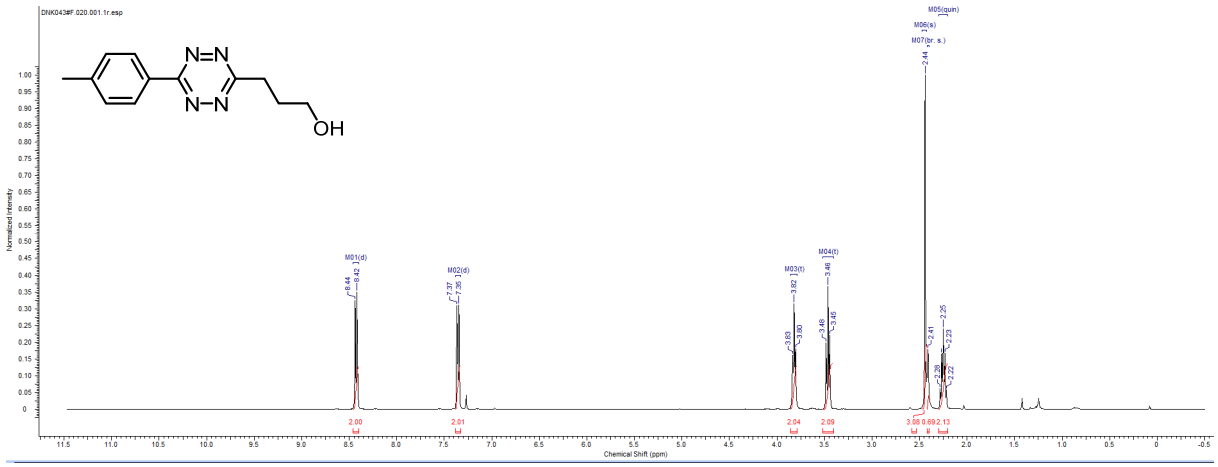
^{1}H Spectrum of compound **11**



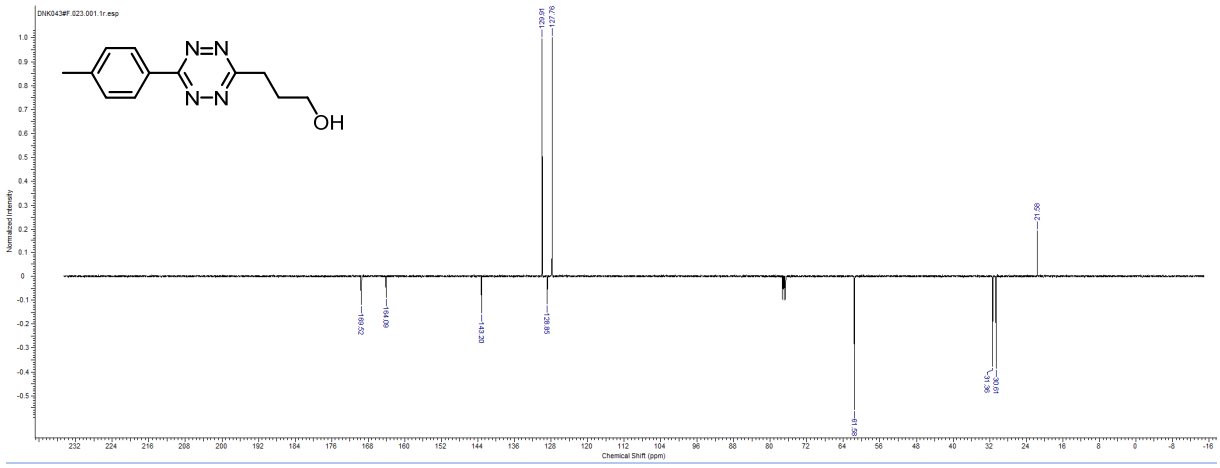
^{13}C Spectrum of compound **11**



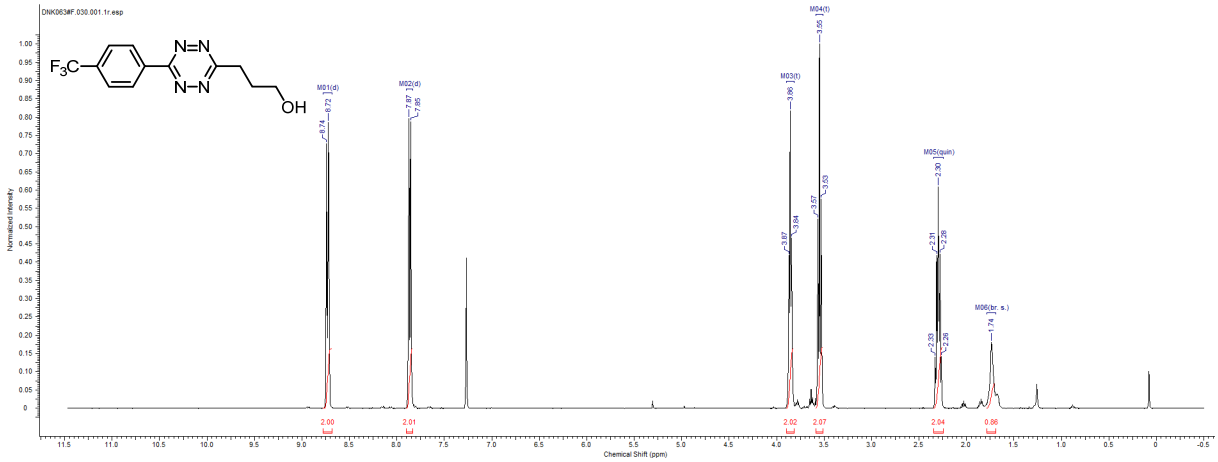
^{1}H Spectrum of compound **12**



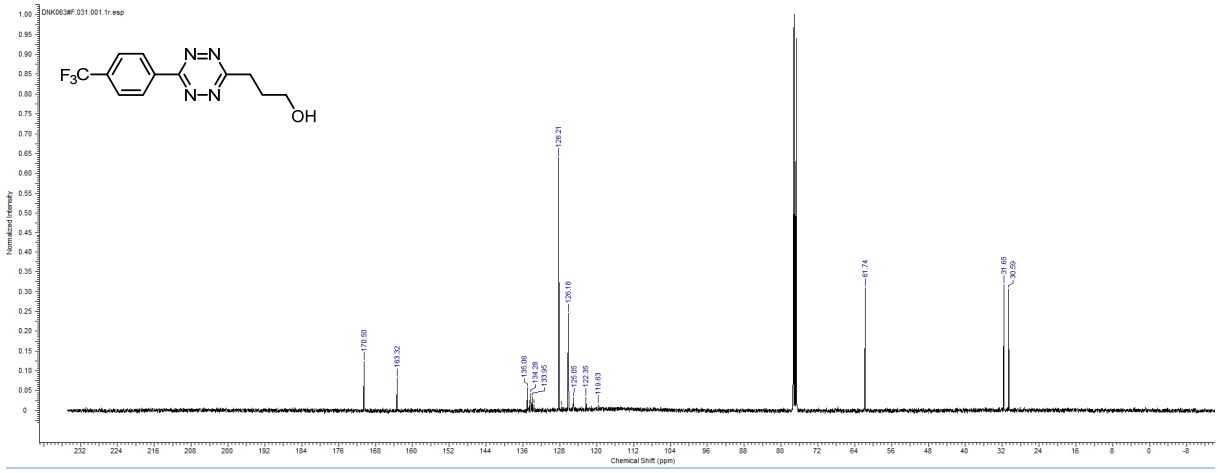
^{13}C Spectrum of compound **12**



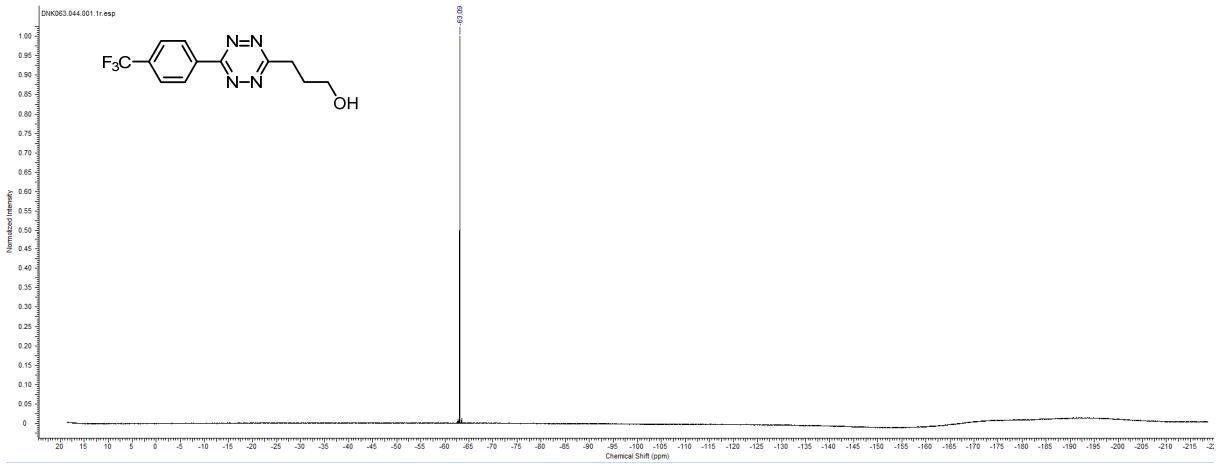
^{1}H Spectrum of compound **13**



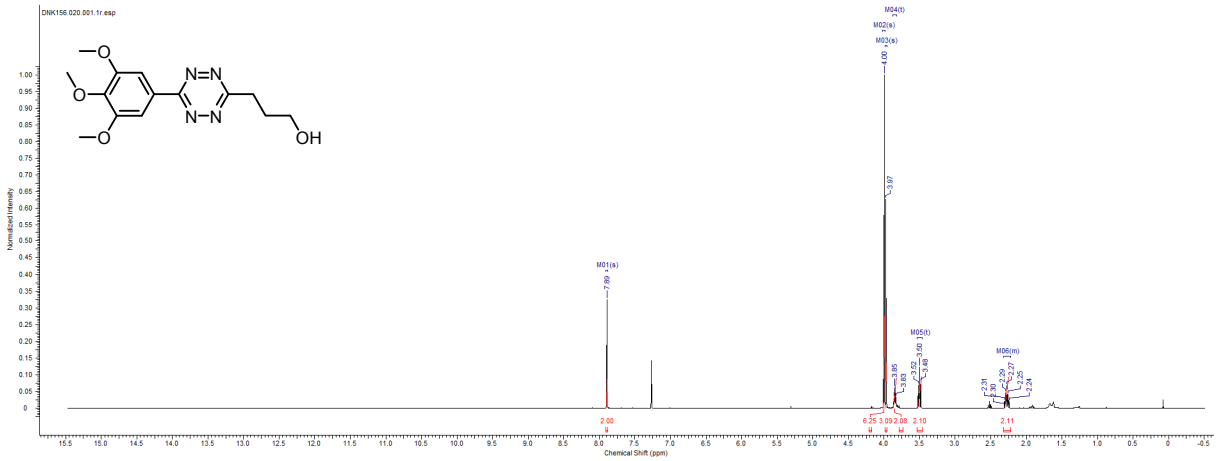
^{13}C Spectrum of compound **13**



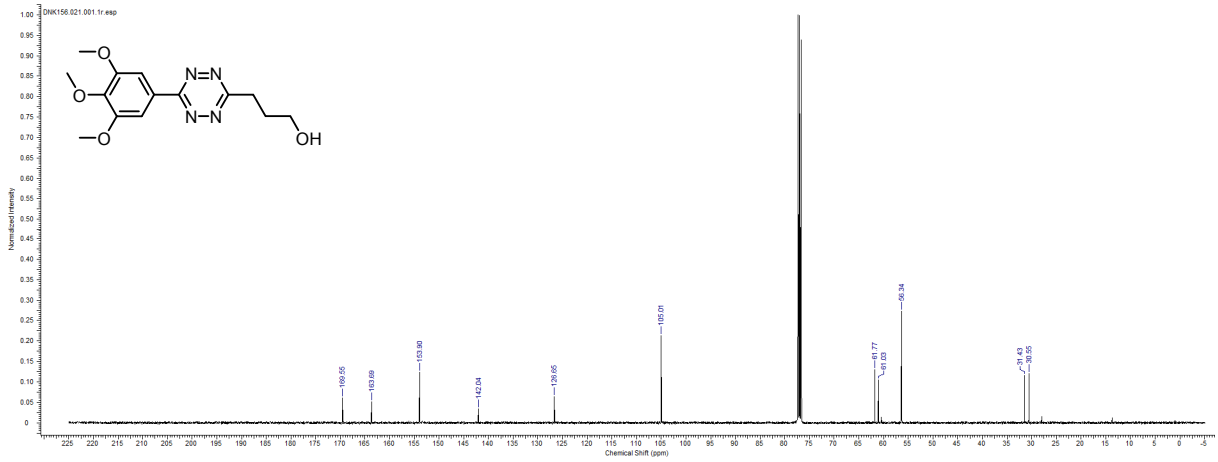
^{19}F Spectrum of compound **13**



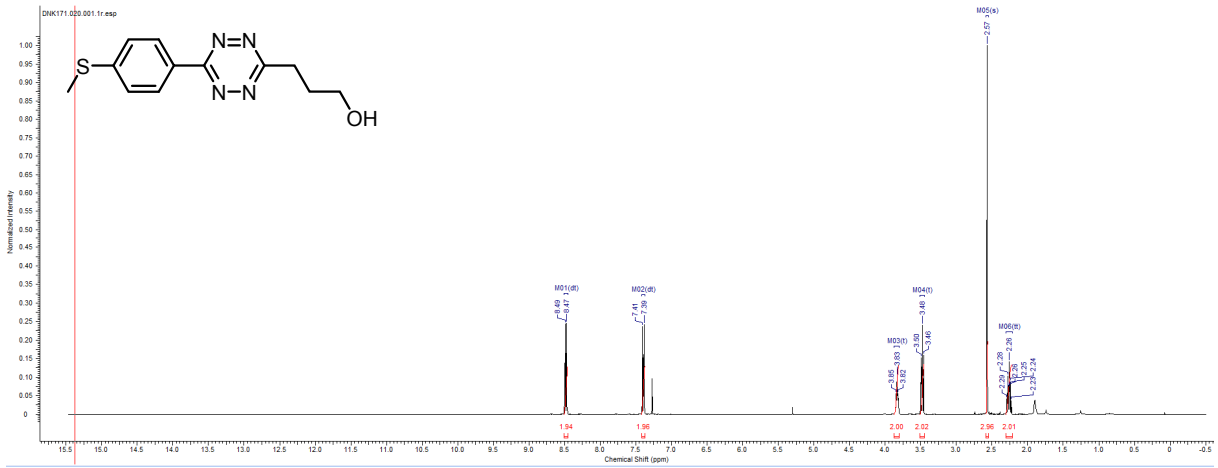
^{1}H Spectrum of compound **14**



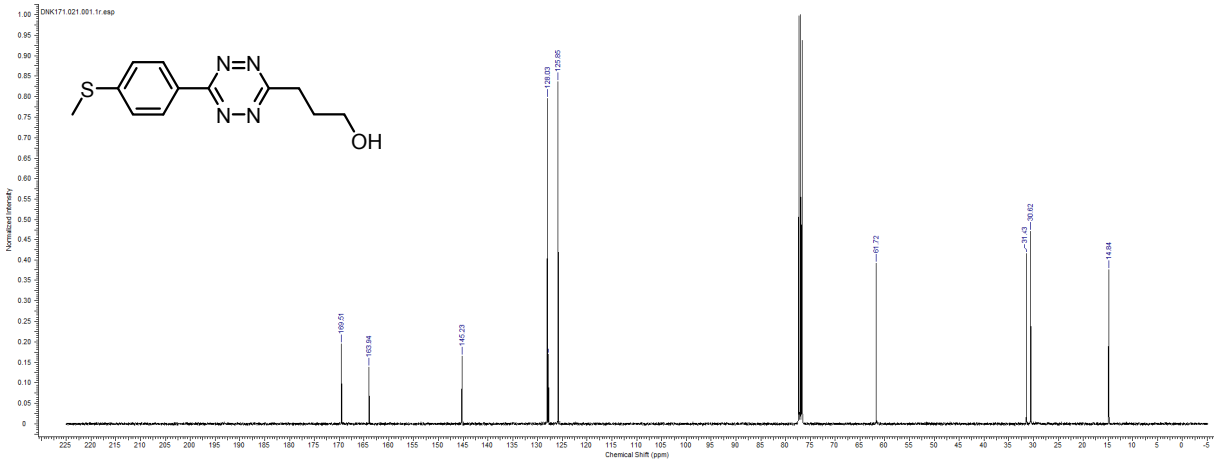
^{13}C Spectrum of compound **14**



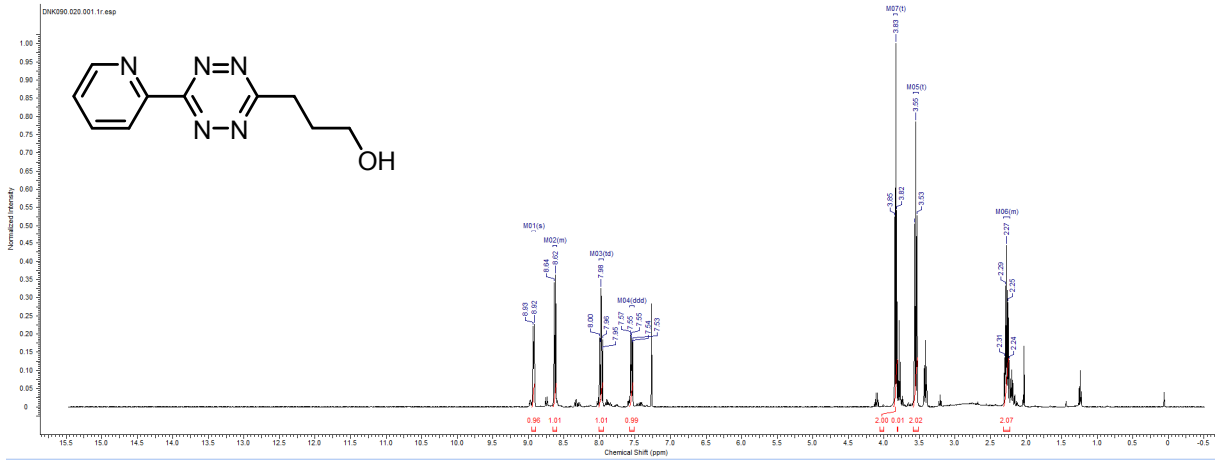
^{1}H Spectrum of compound **15**



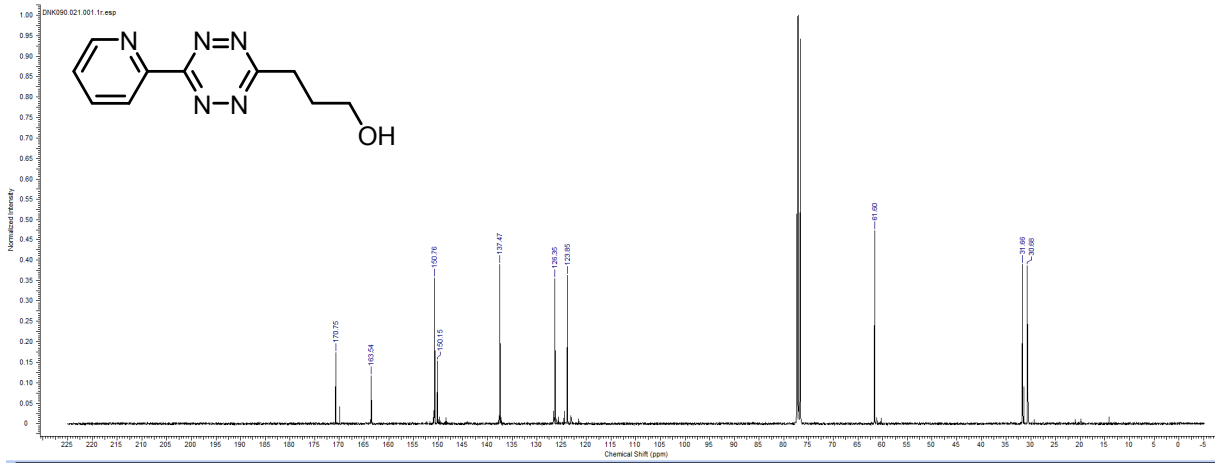
^{13}C Spectrum of compound **15**



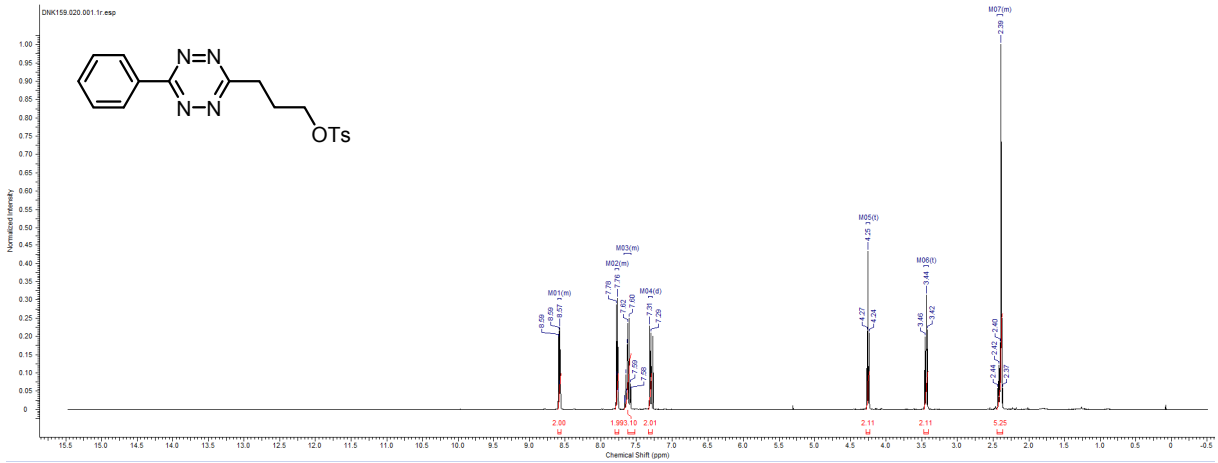
^{1}H Spectrum of compound **16**



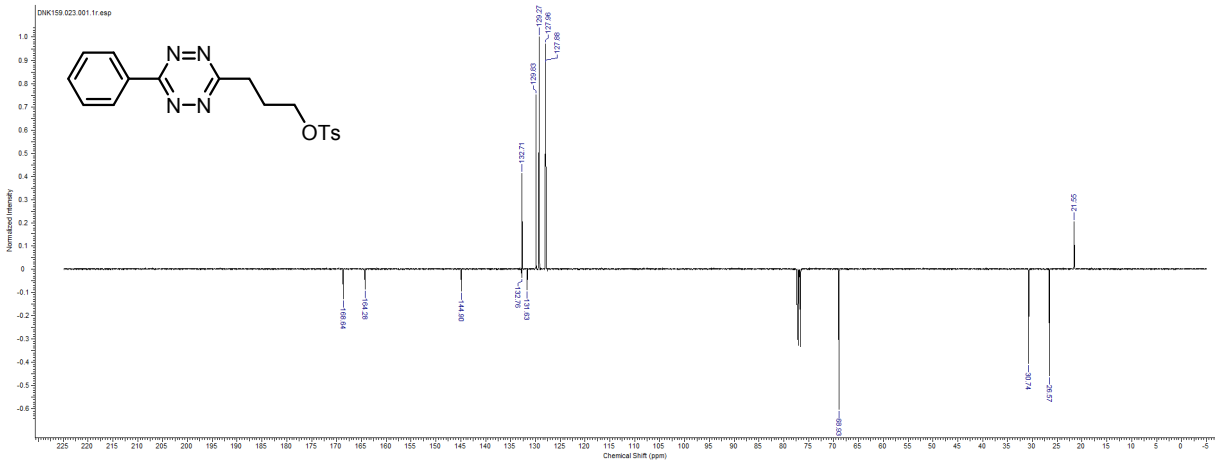
^{13}C Spectrum of compound **16**



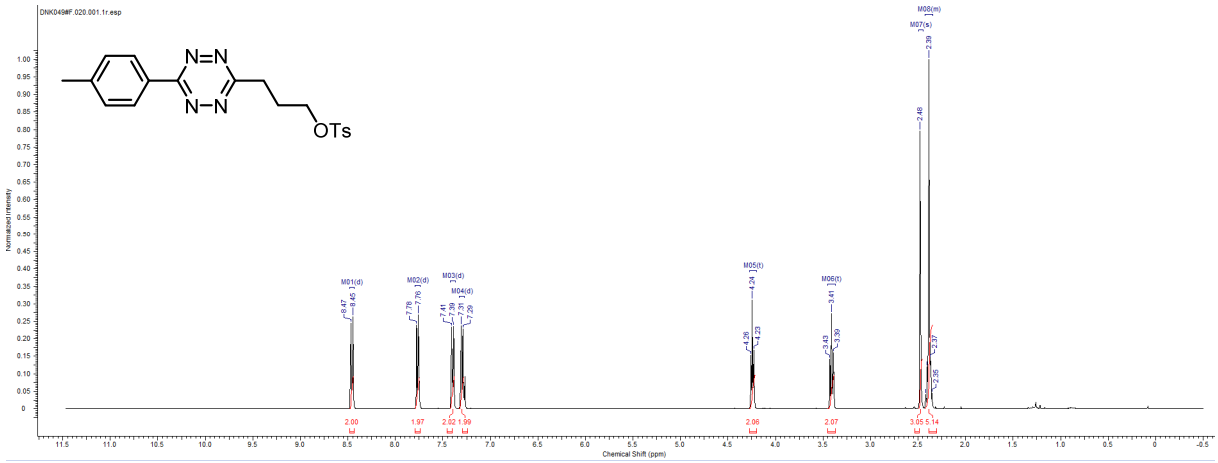
^{1}H Spectrum of compound **17**



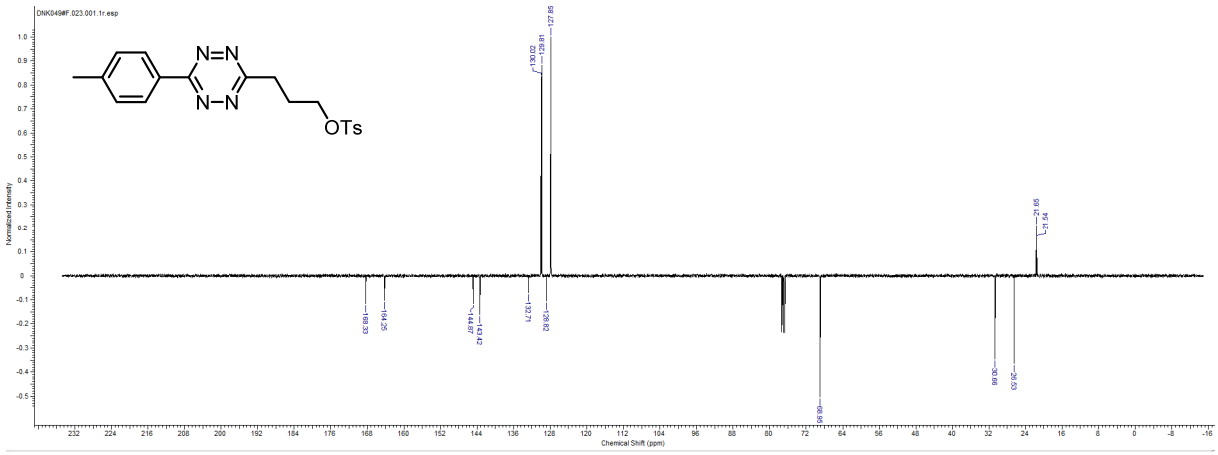
^{13}C Spectrum of compound **17**



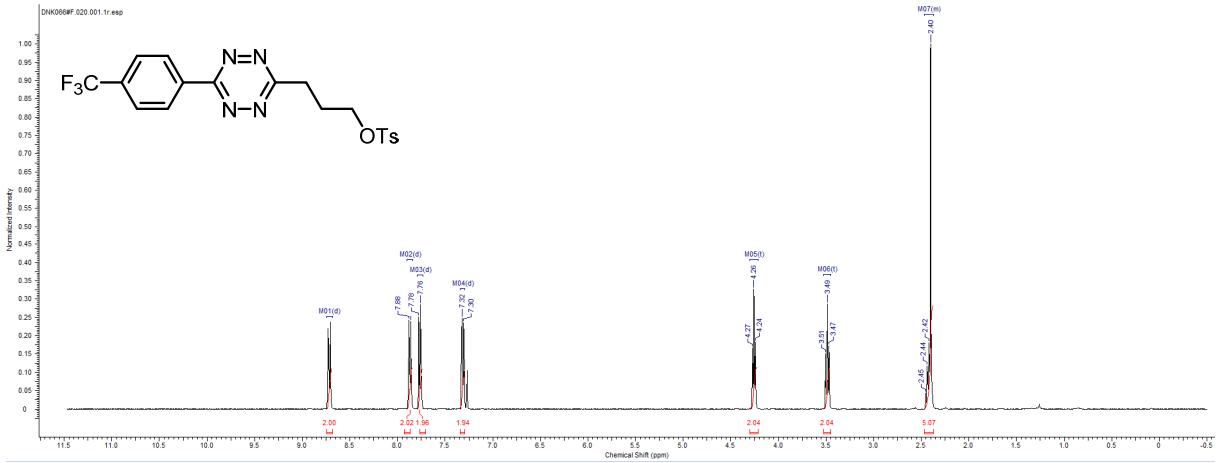
^{1}H Spectrum of compound **18**



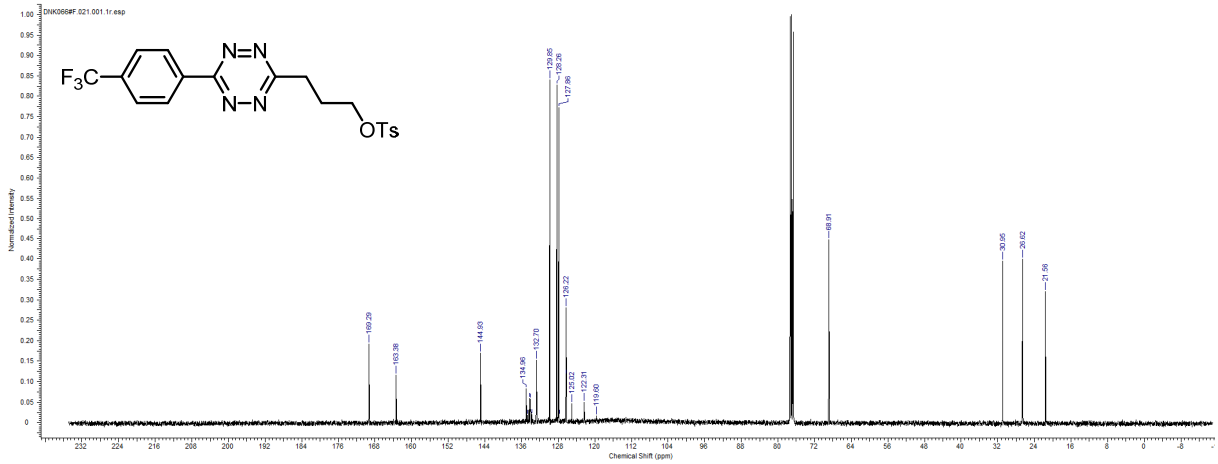
^{13}C Spectrum of compound **18**



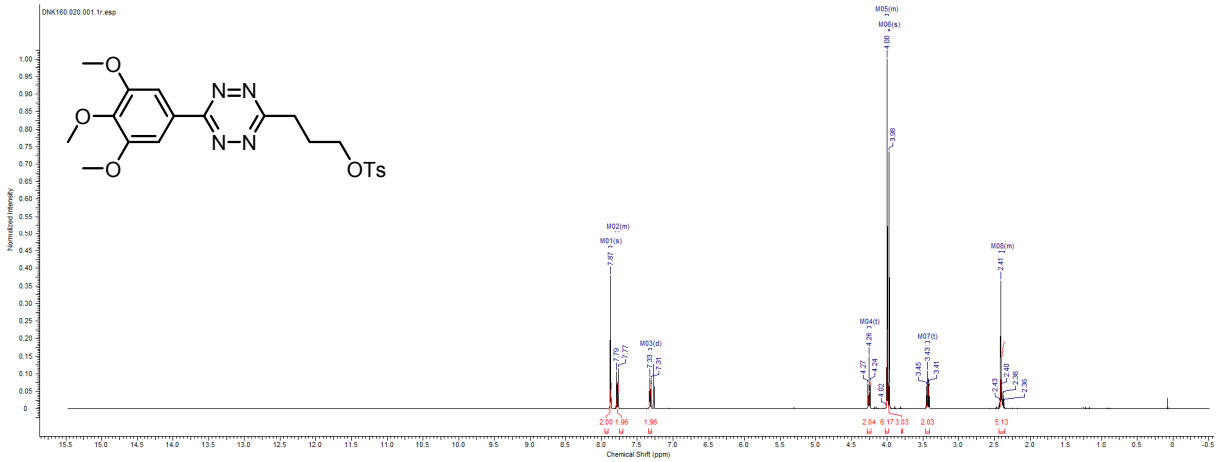
^{1}H Spectrum of compound **19**



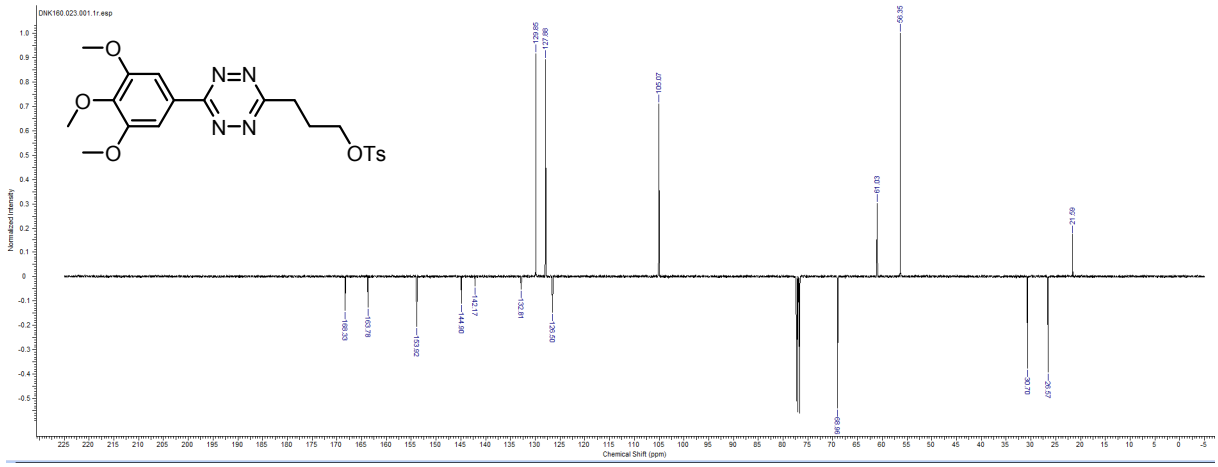
^{13}C Spectrum of compound **19**



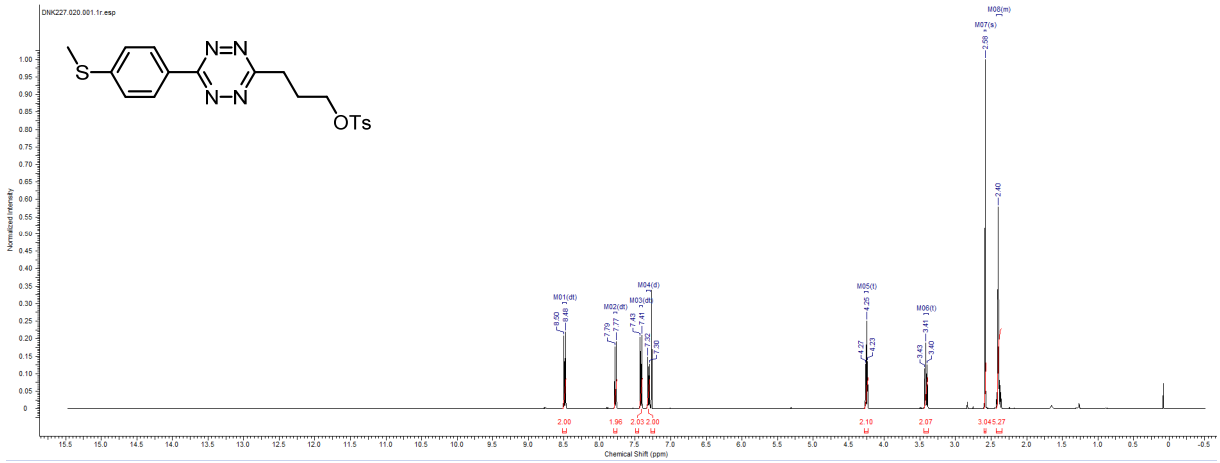
^{1}H Spectrum of compound **20**



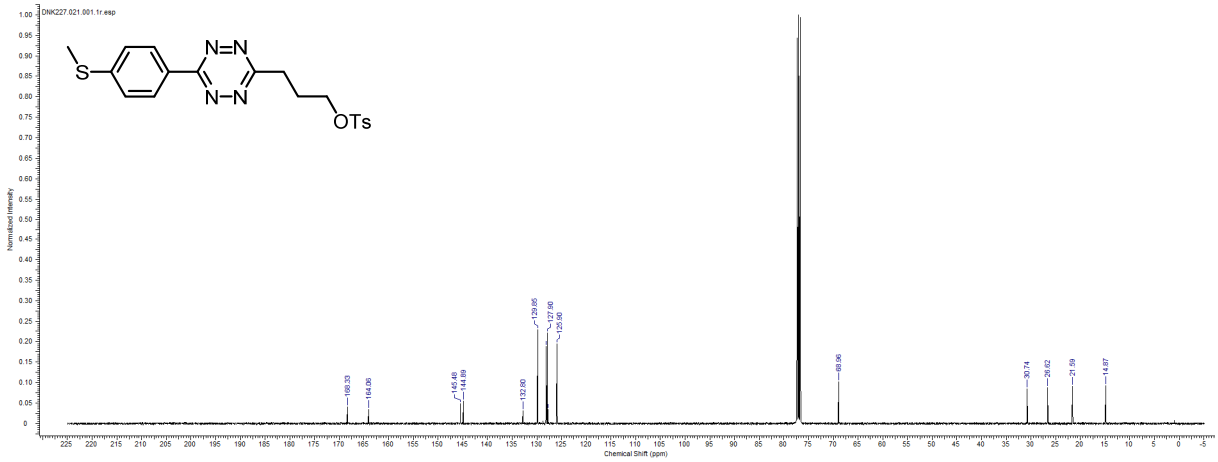
^{13}C Spectrum of compound **20**



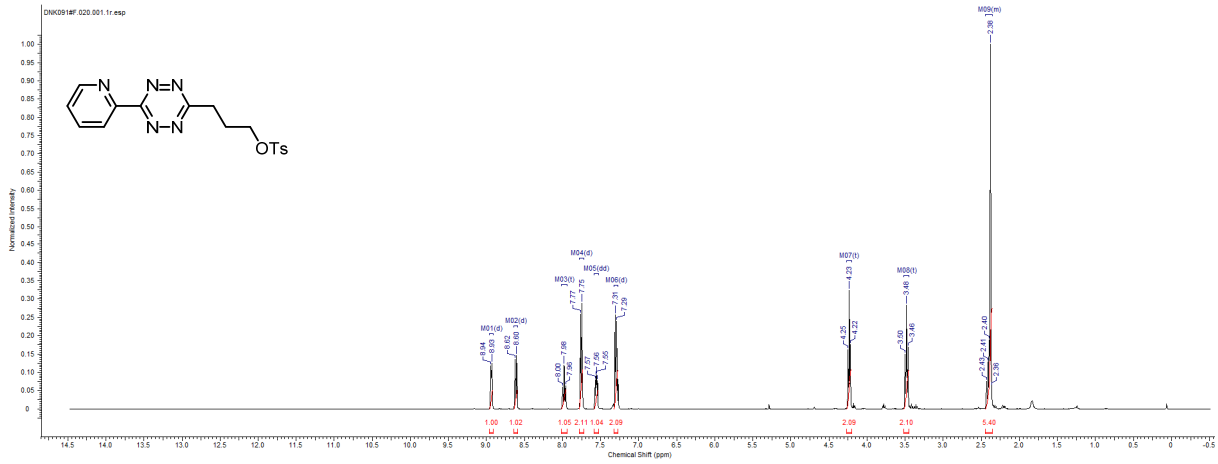
^{1}H Spectrum of compound **21**



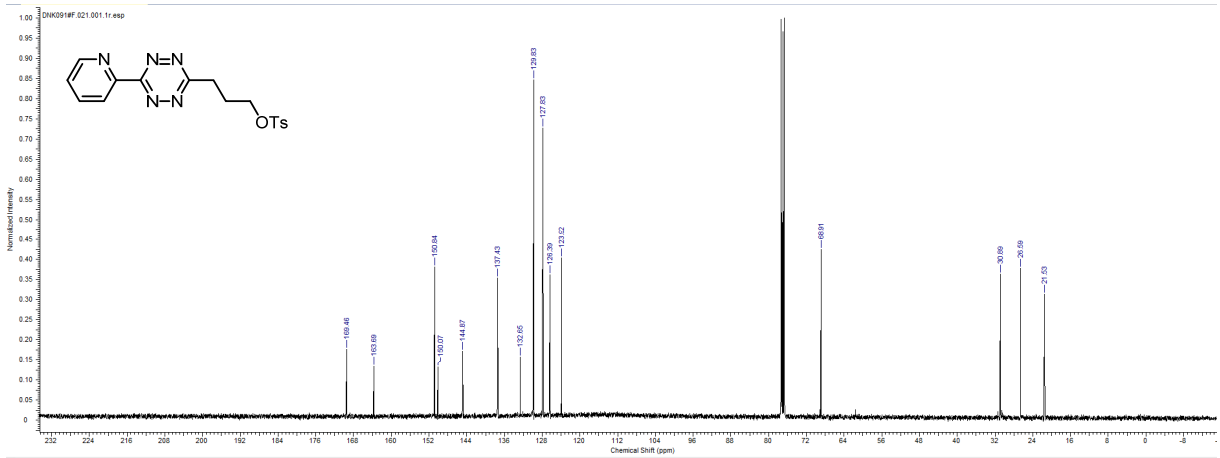
^{13}C Spectrum of compound **21**



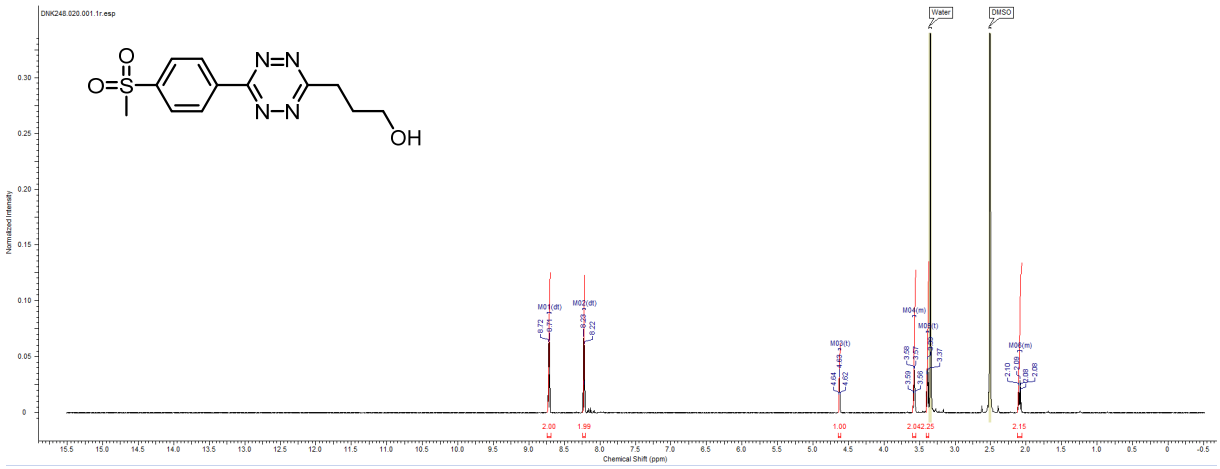
^{1}H Spectrum of compound **22**



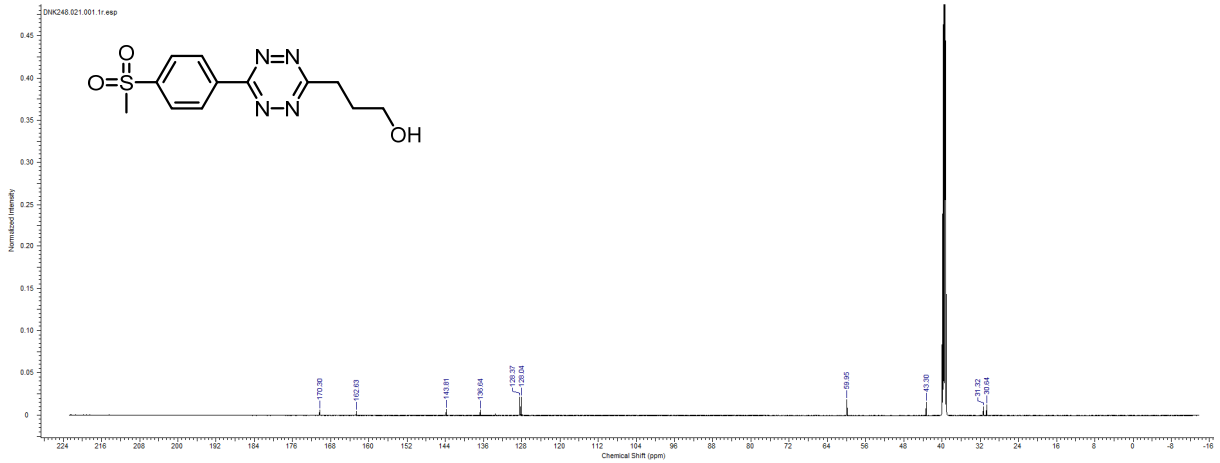
^{13}C Spectrum of compound **22**



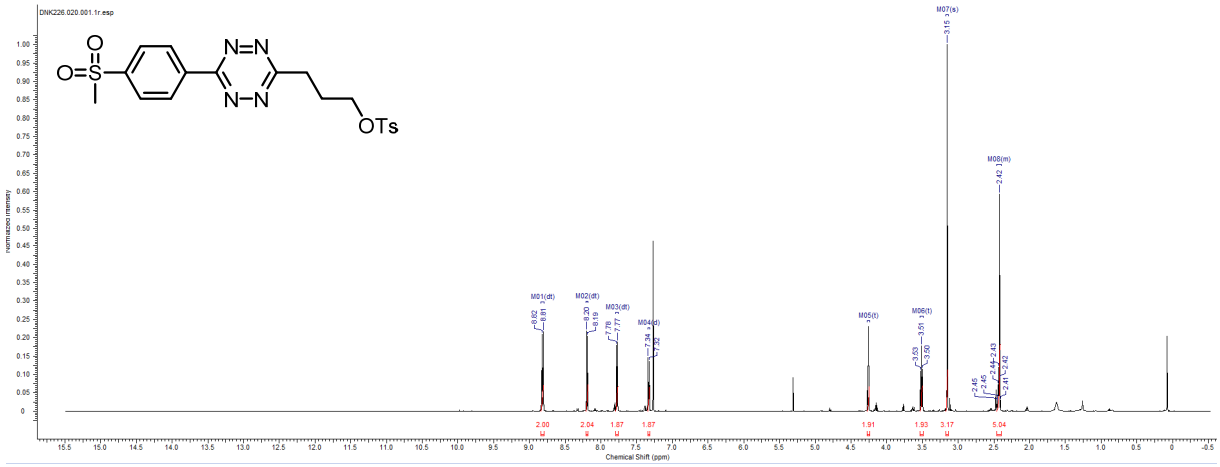
^{1}H Spectrum of compound **23**



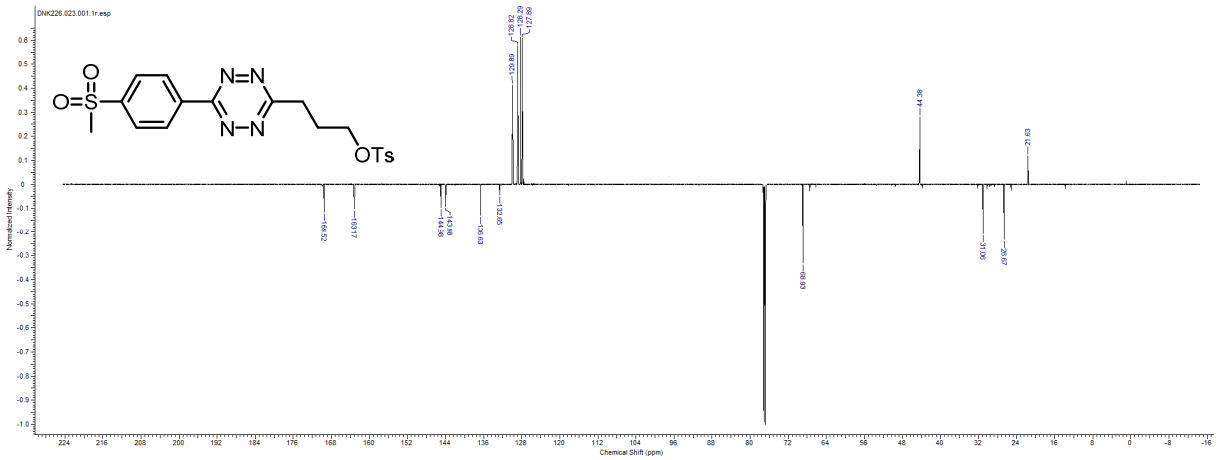
^{13}C Spectrum of compound **23**



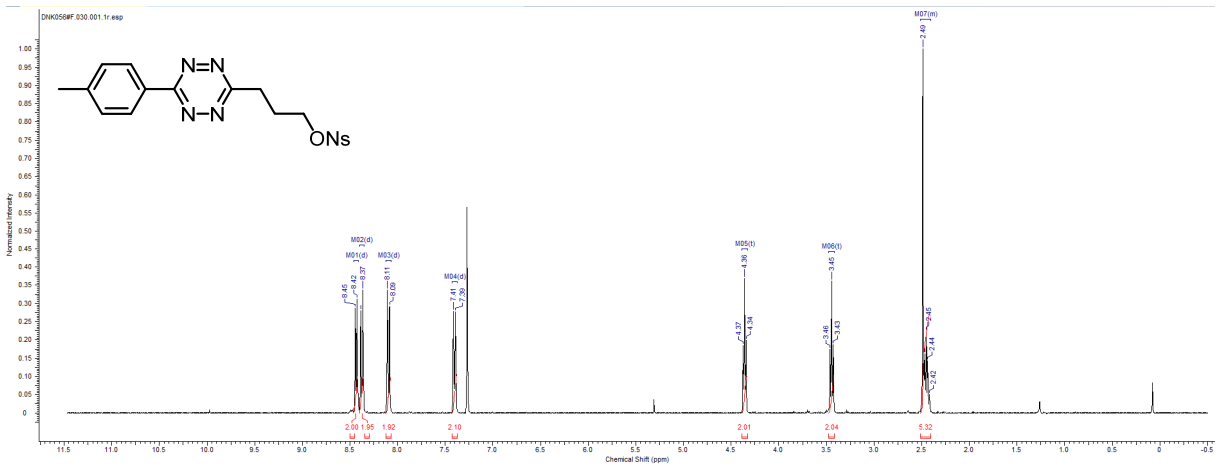
^{1}H Spectrum of compound **24**



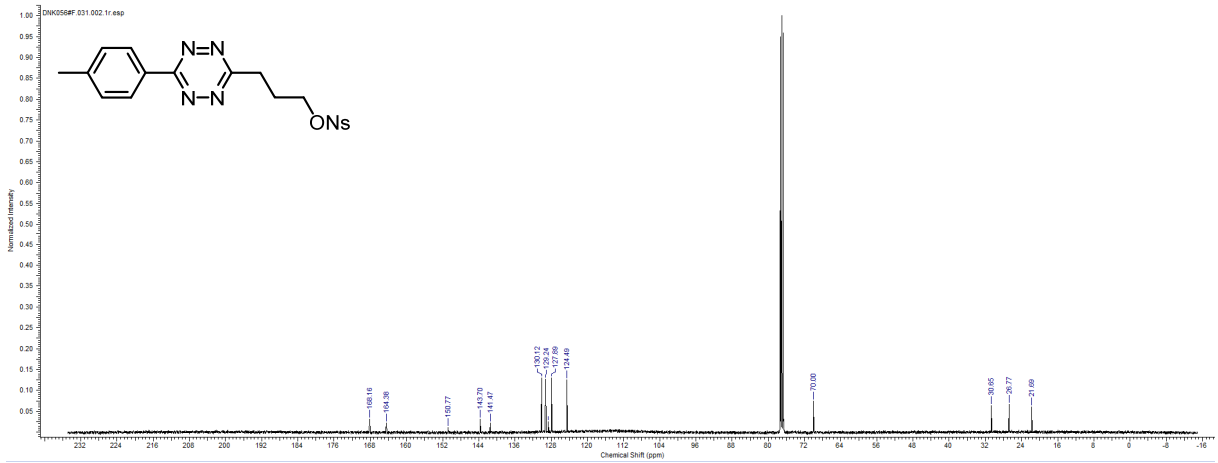
^{13}C Spectrum of compound **24**



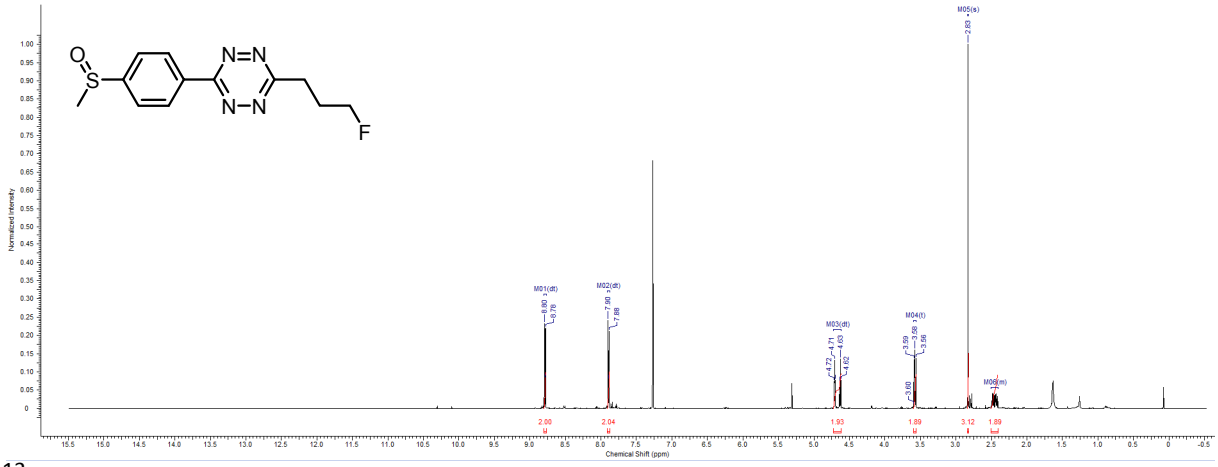
^{1}H Spectrum of compound **25**



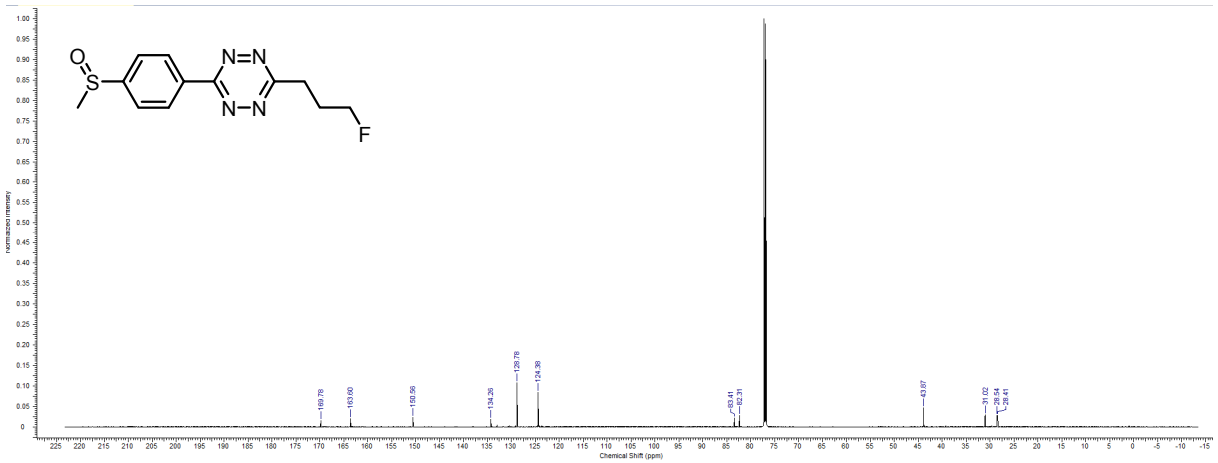
^{13}C Spectrum of compound **25**



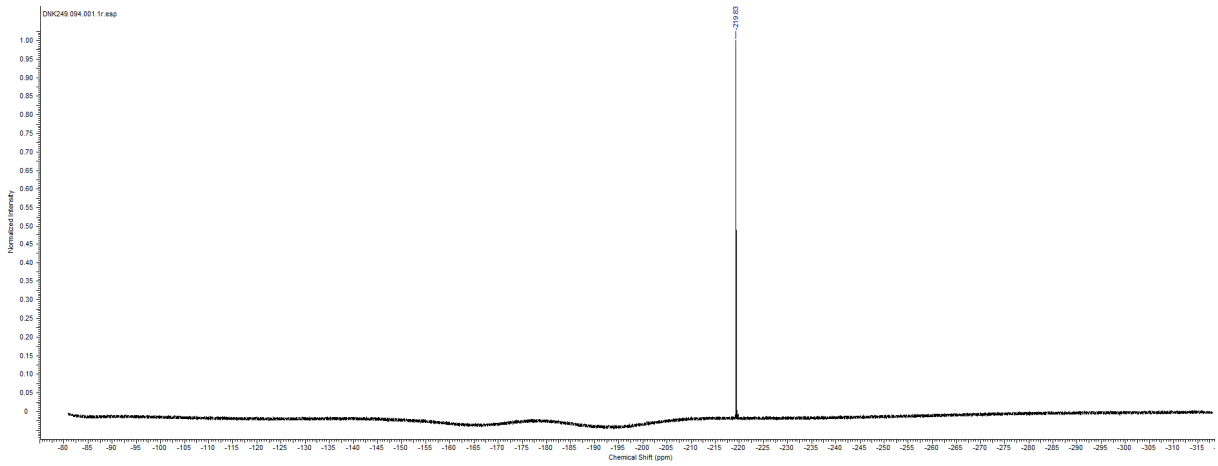
^{1}H Spectrum of compound **26**



^{13}C Spectrum of compound **26**

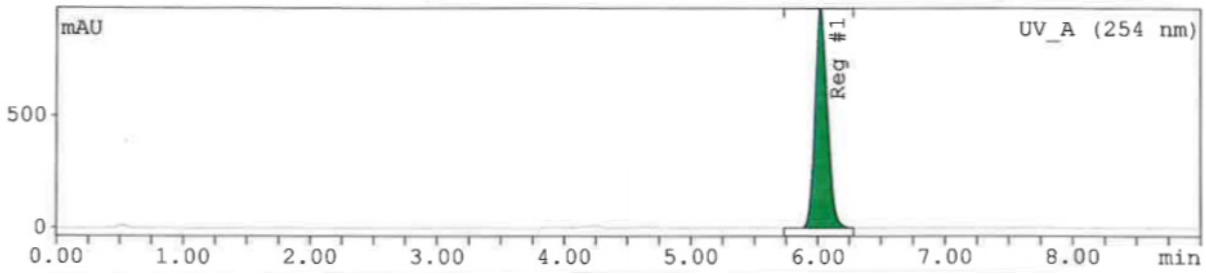


^{19}F Spectrum of compound **26**

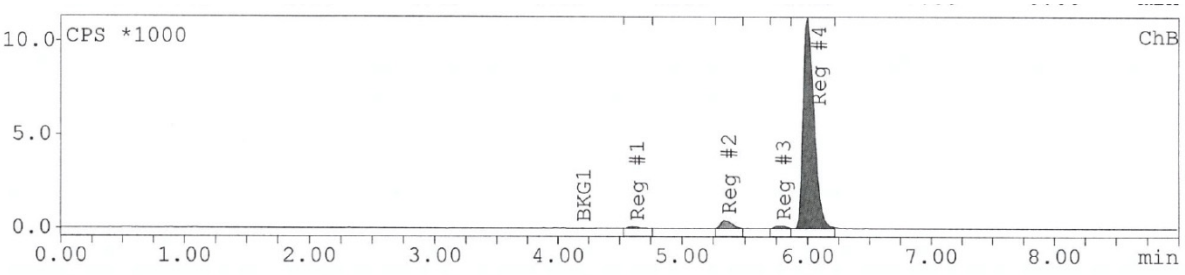


3. HPLC Data

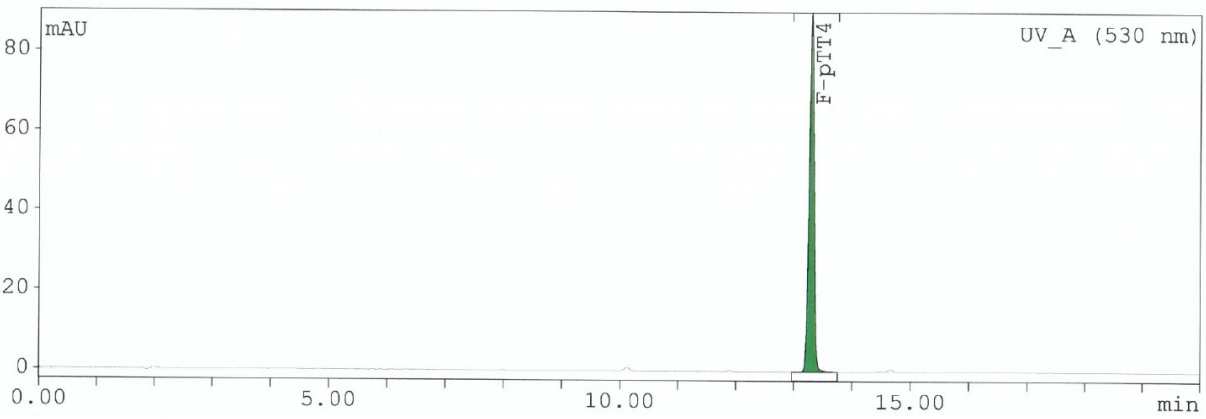
Chromatogram of **2** (254 nm, HPLC conditions A)



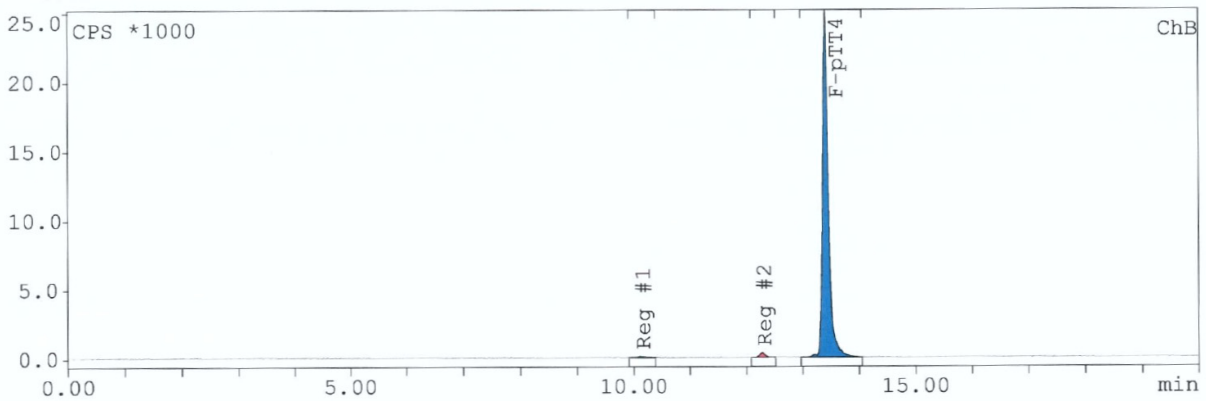
Radio-Chromatogram of [^{18}F]**2** (HPLC conditions A)



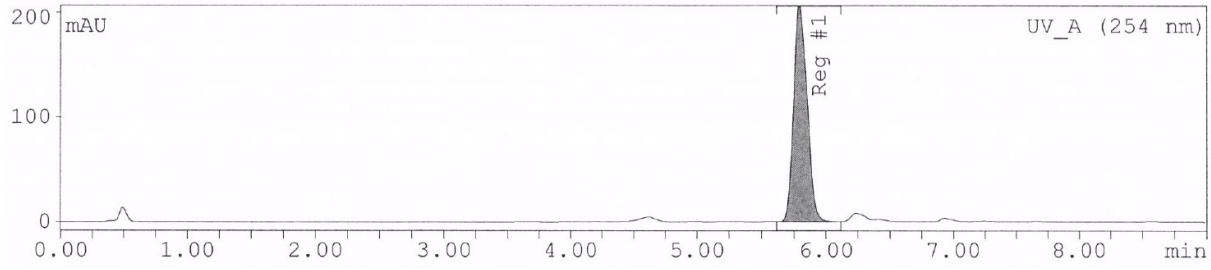
Chromatogram of **3** (540 nm, HPLC conditions B)



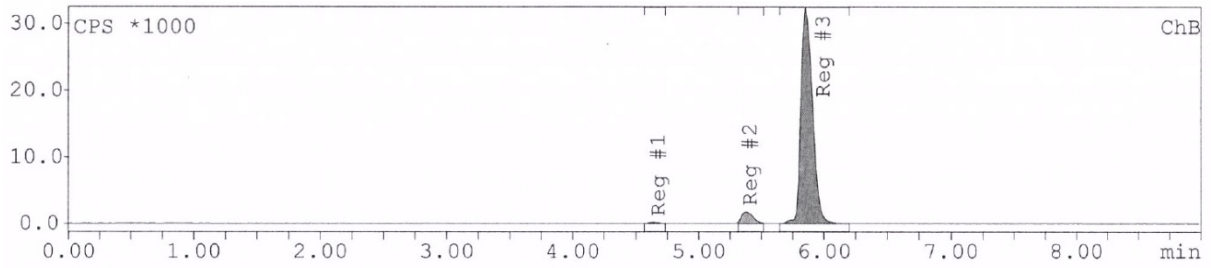
Radio-Chromatogram of [^{18}F]**3** (HPLC conditions B)



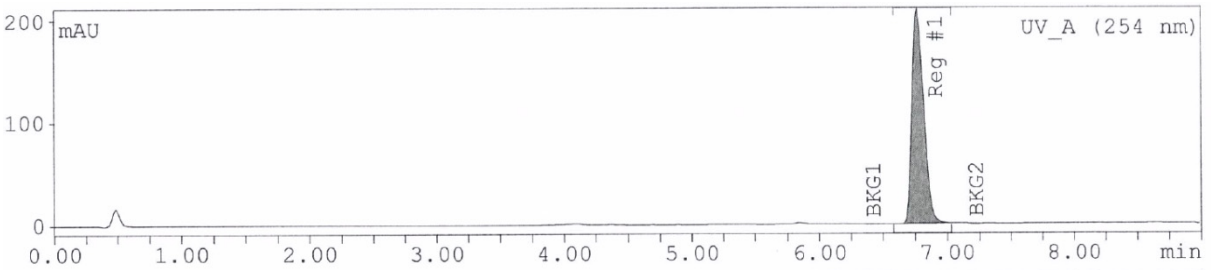
Chromatogram of **5** (254 nm, HPLC conditions A)



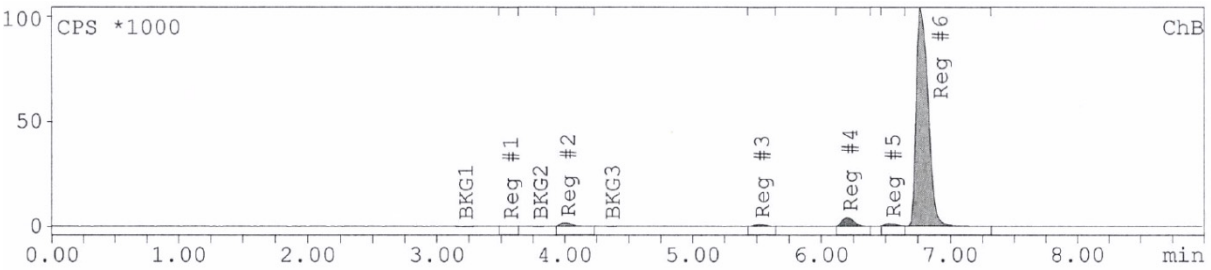
Radio-Chromatogram of [^{18}F]**5** (HPLC conditions A)



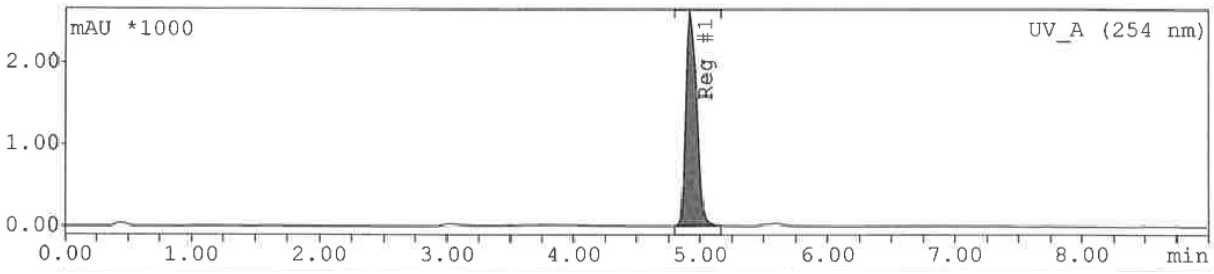
Chromatogram of **6** (254 nm, HPLC conditions A)



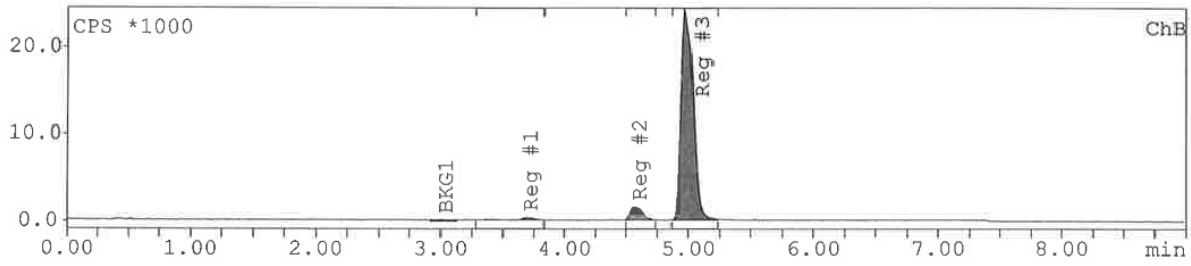
Radio-Chromatogram of [^{18}F]**6** (HPLC conditions A)



Chromatogram of **7** (254 nm, HPLC conditions A)



Radio-Chromatogram of [^{18}F]**7** (HPLC conditions A)

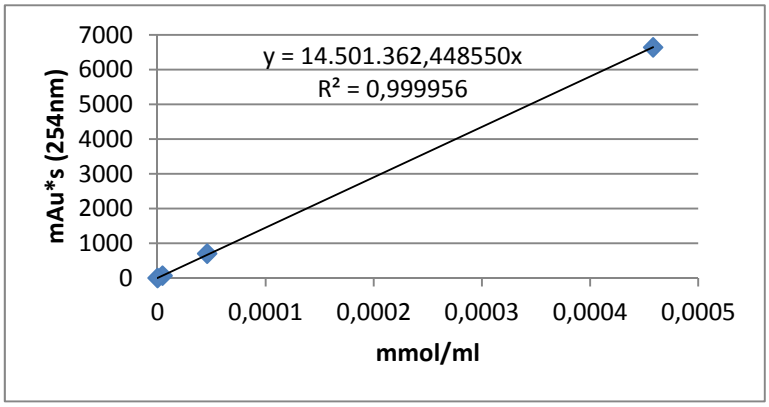


4. Determination of Specific Activity

The specific activity of [^{18}F]**2**, [^{18}F]**6** and [^{18}F]**7** was determined by injection of a dilution series of authentic standard materials into the analytical HPLC system in combination with UV-detection (254 nm). A sample of the radiotracer preparation was also injected into the same HPLC system. Linear regression was used, and the linear equation was furthermore employed to calculate the concentration of according tetrazine in the radiotracer preparation. Radioactivity in a aliquot (1 ml) of the radiotracer preparation was furthermore determined in a Capintec CRC-15 dose calibrator. The specific activity is expressed in GBq/µmol.

[^{18}F]**2**

Concentration	Response
[mmol/ml]	[mAu*s]
0,000458211	6641
4,58211E-05	701,3
4,58211E-06	66,72
0	0



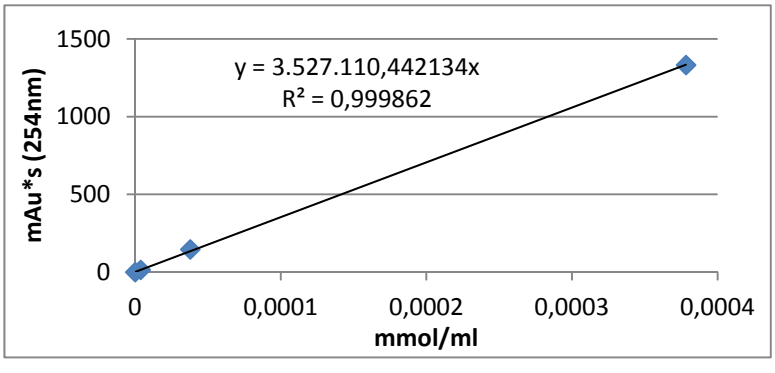
Detector response sample : 74.94 mAu*s

Activity Concentration : 511.7 MBq/ml

Specific activity : 99.0 GBq/µmol

[^{18}F]**6**

Concentration	Response
[mmol/ml]	[mAu*s]
0,000378329	1333,1
3,78329E-05	146,42
3,78329E-06	14,475
0	0



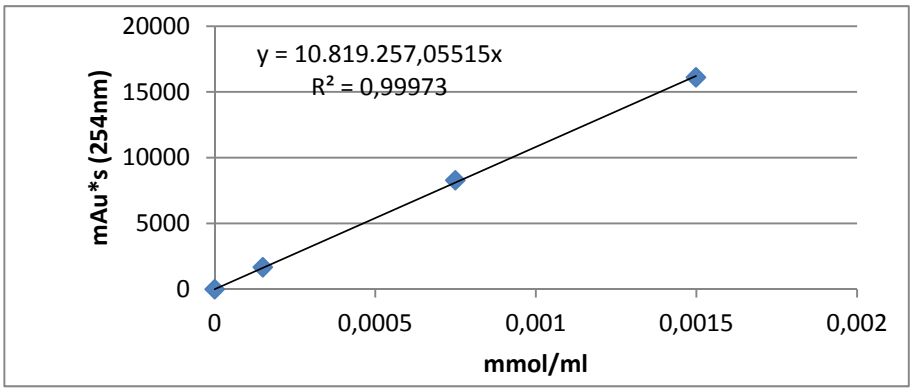
Detector response sample : 12.226 mAu*s

Activity Concentration : 795.5 MBq/ml

Specific activity : 229 GBq/µmol

[^{18}F]**7**

Concentration	Response
[mmol/ml]	[mAu*s]
0,00149838	16116,96667
0,00074919	8284,593333
0,000149838	1670,5
0	0



Detector response sample : 73.54 mAu*s

Activity Concentration : 381.8 MBq/ml

Specific activity : 56.2 GBq/µmol

5. Kinetic Measurements

Reaction rates of the Tetrazine ligation between *trans*-Cyclooctene (**10**) and tetrazines **1-8** and **26** in 1,4-dioxane were determined using a SX20 stopped flow spectrophotometer system (Applied Photophysics, Surrey, UK) equipped with a 535 nm LED light source. Pseudo first order conditions were used. An approximately 4 mM solution of **10** as well as an approx. 0.1 mM solution of the corresponding tetrazine were prepared in anhydrous 1,4-dioxane (Note: for correct measurements it is of utmost importance to use anhydrous 1,4-dioxane, since even small amounts of water will accelerate the reaction, leading to irreproducible data). These solutions were loaded into the driver syringes and equal volumes of both solutions were mixed, resulting in concentrations of approx. 2 mM and 0.05 mM respectively. The reaction progress was followed by measuring the absorption around 535 nm. Measurements were performed in sixtuplicates at 25 ± 0.16 °C, 37 ± 0.16 °C and 50 ± 0.16 °C. Observed reaction konstants (k_{obs}) were determined by non-linear regression (one-phase-decay) using Prism 6 (Graphpad) and second order rate constants were calculated from k_{obs}. Table S1shows k_{obs}, k as well as thermodynamic data for all observed reactions. Original data from stopped flow measurements is attached in the last part of this section.

Furthermore relative reaction values (RRVs) were assigned, which allows for easy comparison of reactivity of different tetrazines. We propose using reaction rates determined in anhydrous 1,4-dioxane at 25, 37 and 50 °C with TCO **10** and comparing them to the rates of tetrazine **1**. RRVs can be calculated as described in Formula S1.

$$RRV = \frac{\frac{k_{25°C}}{1.1077} + \frac{k_{37°C}}{1.5713} + \frac{k_{50°C}}{2.1962}}{3}$$

Formula S1

Using these RRVs and computational data described in chapter 6 (Supporting Information) we were able to find a good correlation between calculated $\Delta E^{\ddagger}$ (M06-2X/6-311+G(d,p), gas phase) and measured RRVs of alkly-aryl tetrazines **2-8**. This correlation can be used for prediction of RRVs of aryl-alkyl substituted tetrazines using Formula S2, whereas $\Delta E^{\ddagger}$ is the calculated value from M06-2X/6-311+G(d,p) gas phase calculation in kcal/mol.

$$RRV_{predicted} = e^{-0.8273 * \Delta E^{\ddagger} + 1.3728}$$

Formula S2

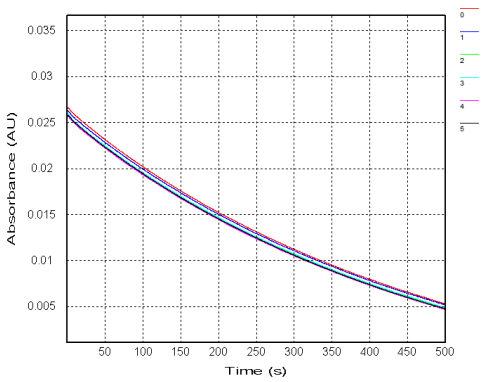
This was done for tetrazine **26**, where a $\Delta E^{\ddagger}$ value of 0.55 kcal/mol was calculated, which results in a $RRV_{predicted}$ of 2.50. This is in excellent agreement with observed RRV of 2.62.

reaction	k_{obs} [$M^{-1}s^{-1}$]			Initial concentration TCO [mM]	k [$M^{-1}s^{-1}$]			ΔS	ΔH	ΔG^a	RRV
	25°C	37°C	50°C		25°C	37°C	50°C	kcal/(mol*K)	kcal/mol	kcal/mol	
1+10	0.002141 ± 0.000003	0.003037 ± 0.000003	0.004245 ± 0.000021	3.87	1.108 ± 0.002	1.571 ± 0.001	2.196 ± 0.011	-0.0428	4.63	17.39	1.00
2+10	0.003280 ± 0.000002	0.004777 ± 0.000003	0.006627 ± 0.000034	4.16	1.576 ± 0.001	2.296 ± 0.002	3.185 ± 0.016	-0.0416	4.77	17.18	1.44
3+10	0.002646 ± 0.000002	0.003977 ± 0.000002	0.006107 ± 0.000003	4.19	1.262 ± 0.001	1.897 ± 0.001	2.913 ± 0.001	-0.0387	5.79	17.32	1.22
4+10	0.007797 ± 0.000011	0.011530 ± 0.000027	0.016210 ± 0.000006	4.03	3.870 ± 0.005	5.723 ± 0.014	8.047 ± 0.003	-0.0391	4.99	16.65	3.60
5+10	0.002046 ± 0.000002	0.002961 ± 0.000024	0.004027 ± 0.000015	4.10	0.998 ± 0.001	1.444 ± 0.012	1.964 ± 0.007	-0.0432	4.57	17.45	0.90
6+10	0.002697 ± 0.000001	0.004101 ± 0.000018	0.005269 ± 0.000004	4.16	1.296 ± 0.001	1.971 ± 0.009	2.532 ± 0.002	-0.0428	4.51	17.28	1.19
7+10	0.009852 ± 0.000004	0.014510 ± 0.000024	0.017080 ± 0.000003	3.87	5.097 ± 0.002	7.507 ± 0.012	8.837 ± 0.001	-0.0432	3.60	16.47	4.47
8+10	0.030670 ± 0.000004	0.043800 ± 0.000011	0.065150 ± 0.000139	4.19	14.631 ± 0.002	20.895 ± 0.005	31.080 ± 0.066	-0.0359	5.15	15.87	13.55
26+10	0.005805 ± 0.000004	0.0083 ± 0.000012	0.01066 ± 0.000034	3.92	2.962 ± 0.002	4.235 ± 0.006	5.439 ± 0.017	-0.0428	4.04	16.80	2.62

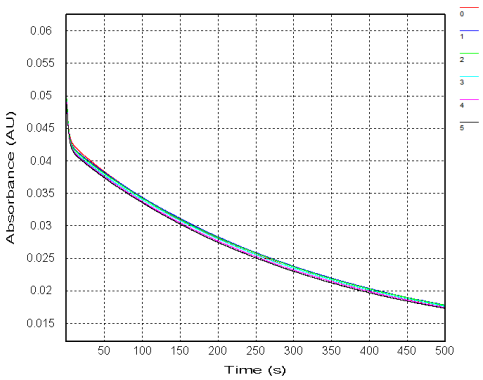
Table S1: *Kinetic data from stopped flow measurements of the reaction between **10** and tetrazines **1-8** and **26**. [a] ΔG was calculated for 298.15 K.*

Reactants 1+10

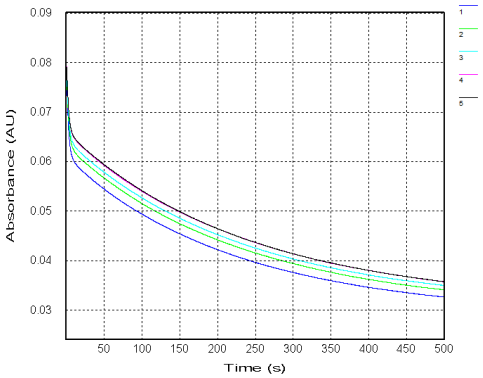
25°C



37°C

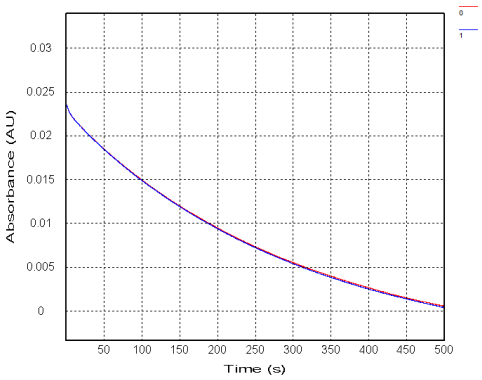


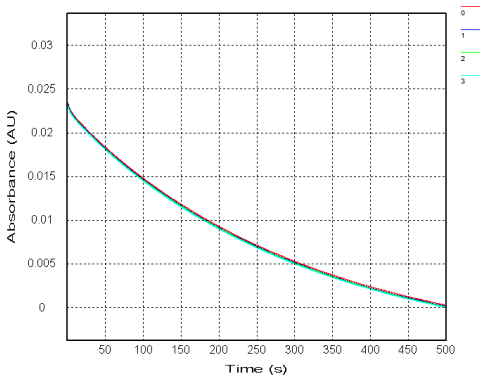
50°C



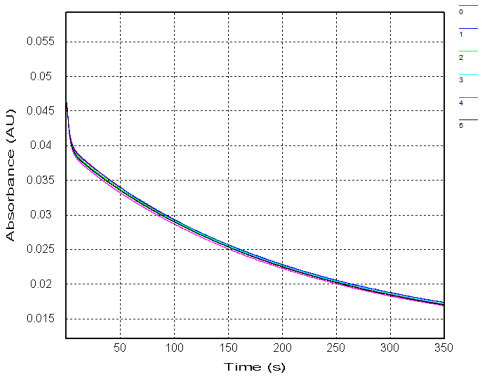
Reactants 2+10

25°C

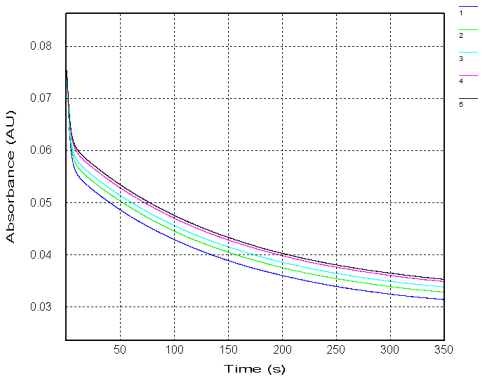


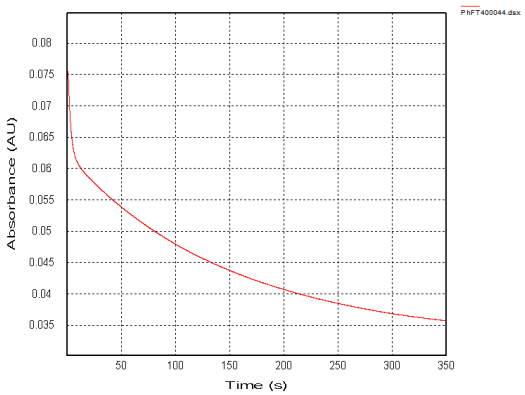


37°C



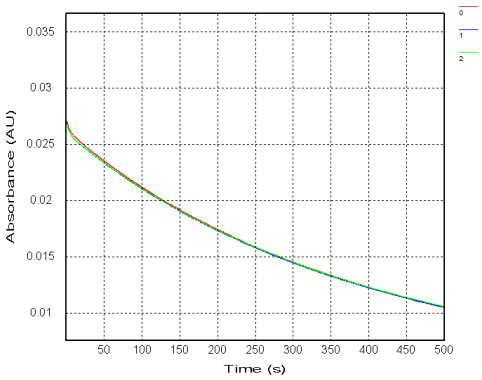
50°C

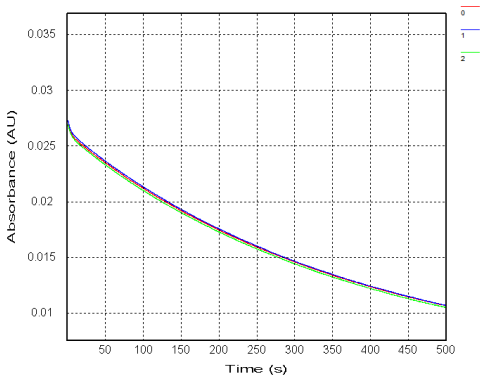




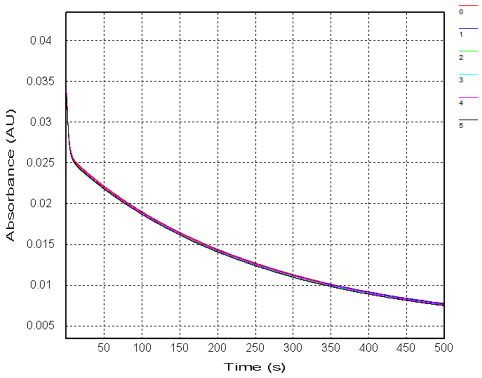
Reactants 3+10

25°C

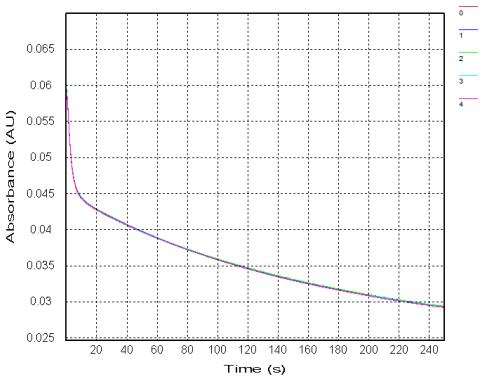


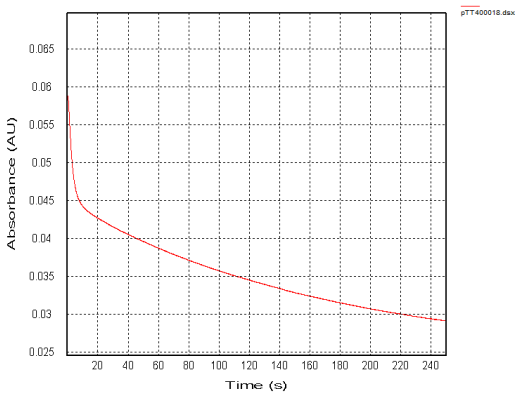


37°C



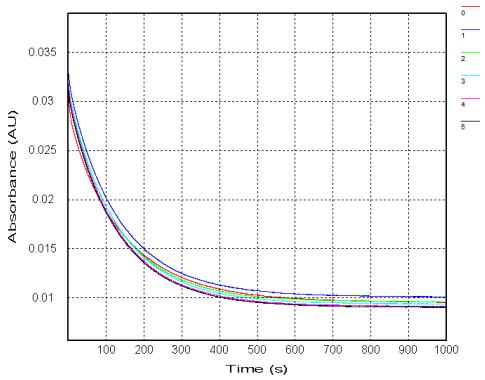
50°C



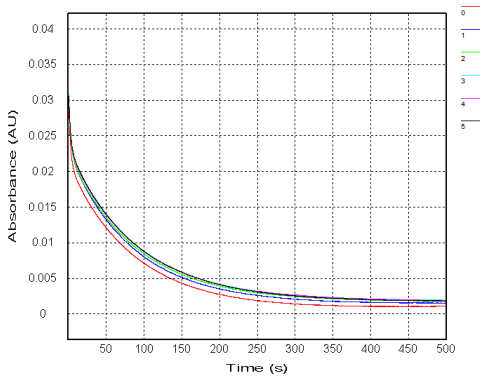


Reactants 4+10

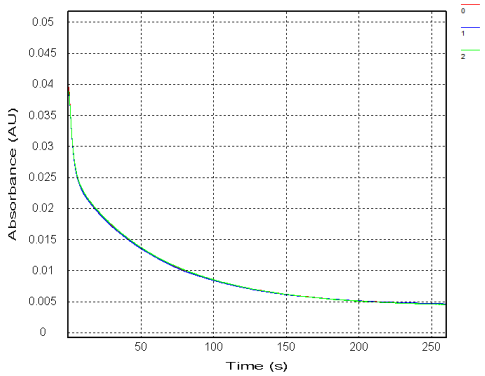
25°C

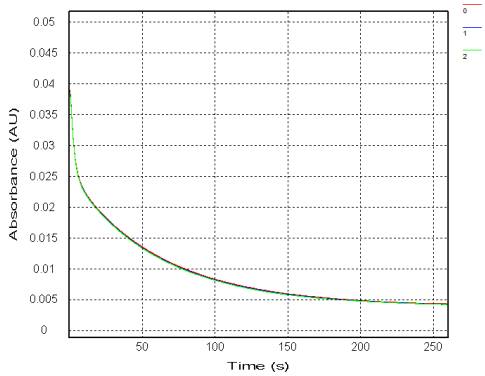


37°C



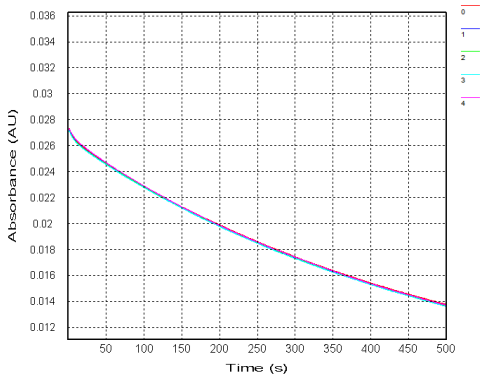
50°C

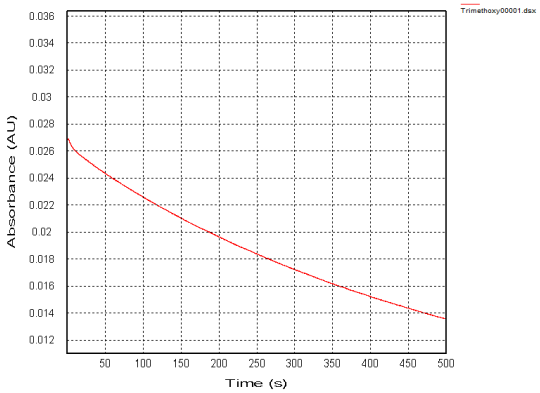




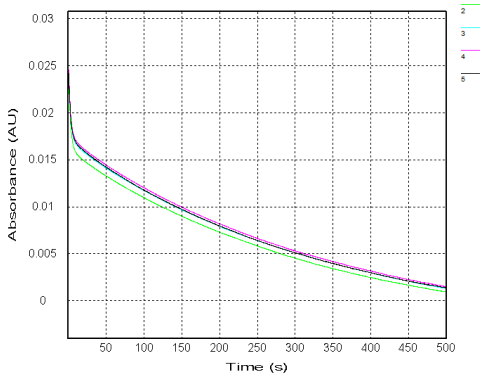
Reactants 5+10

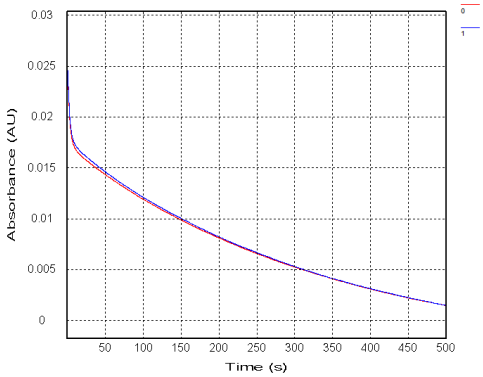
25°C



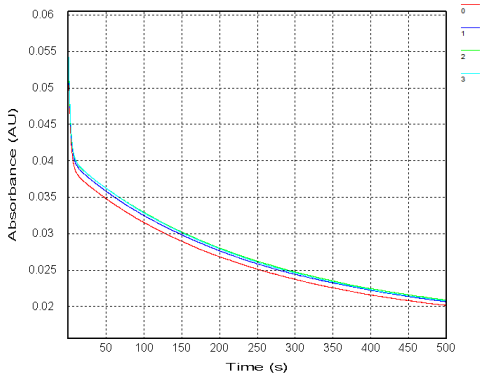


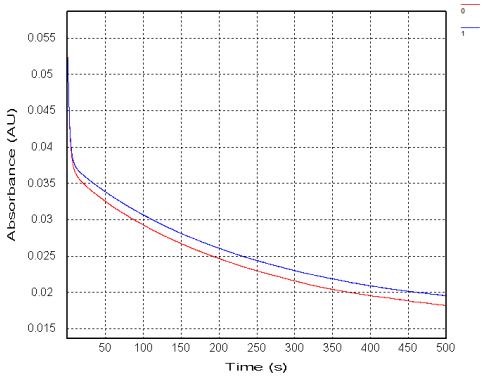
37°C





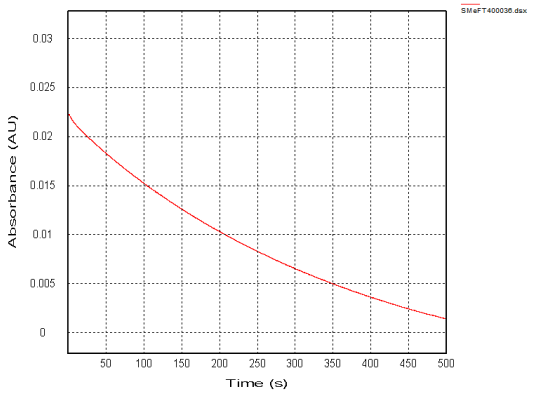
50°C

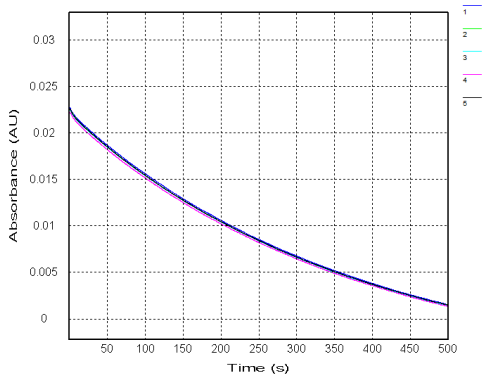




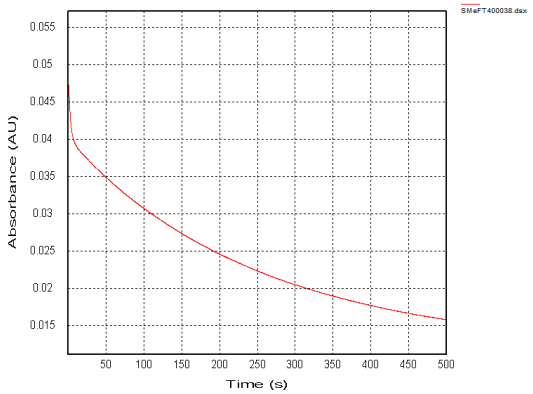
Reactants 6+10

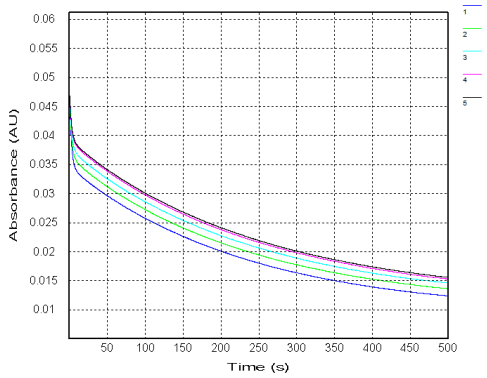
25°C



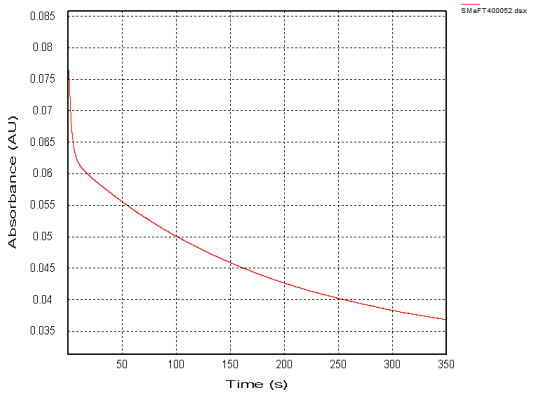


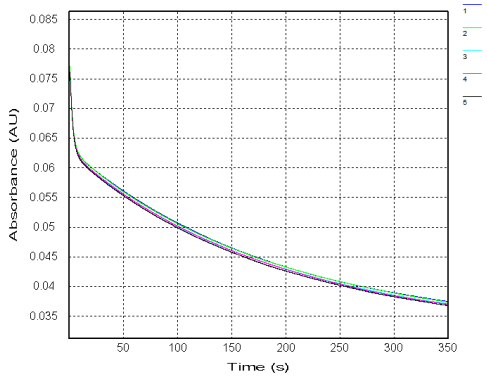
37°C





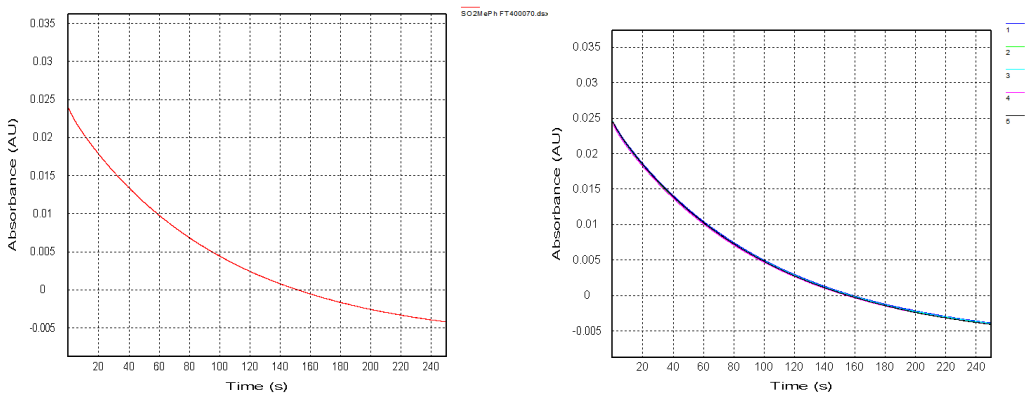
50°C



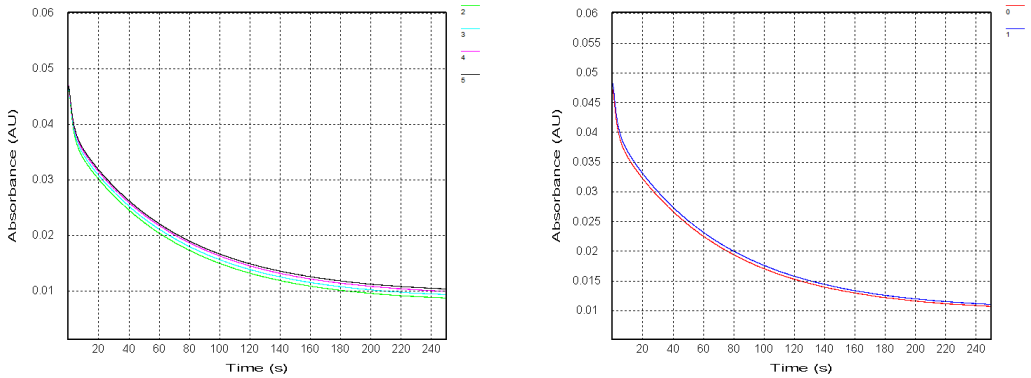


Reactants 7+10

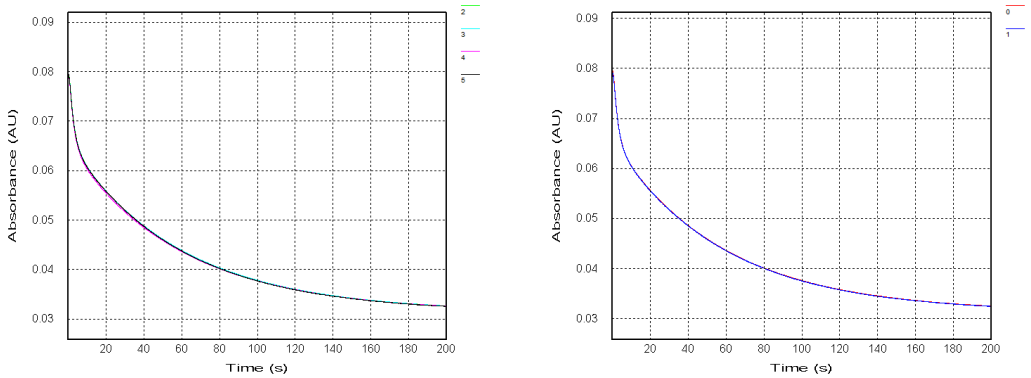
25°C



37°C

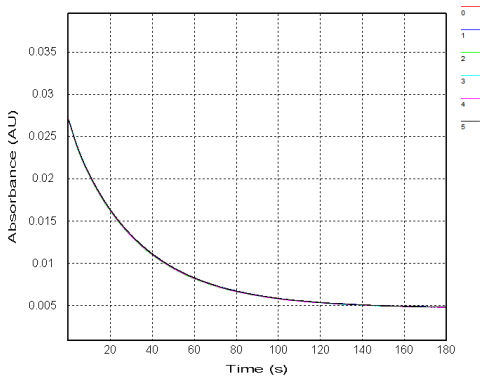


50°C

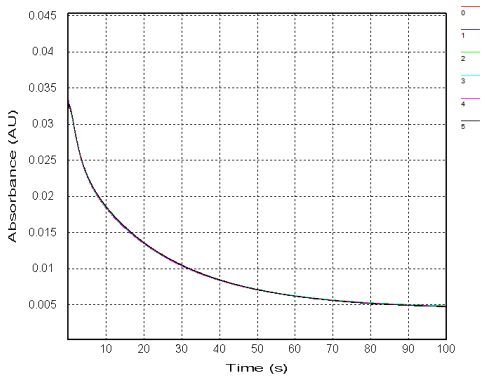


Reactants 8+10

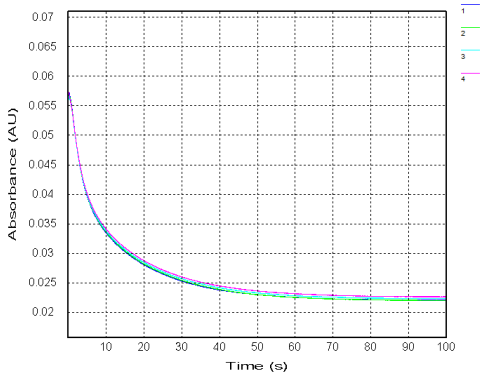
25°C

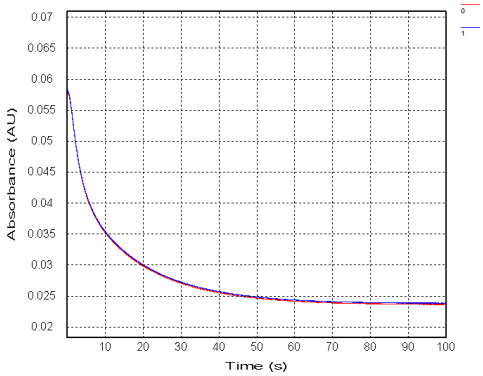


37°C



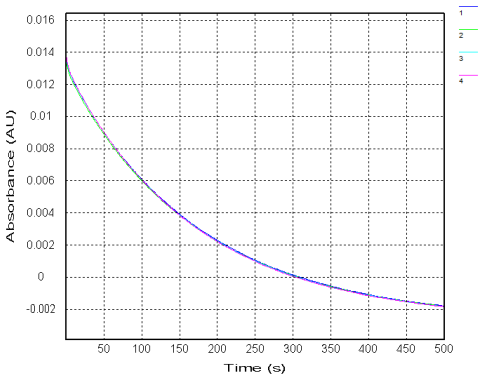
50°C

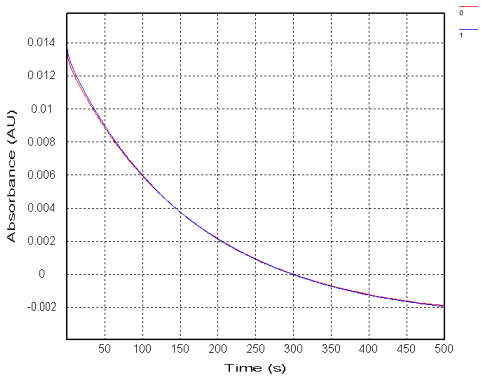




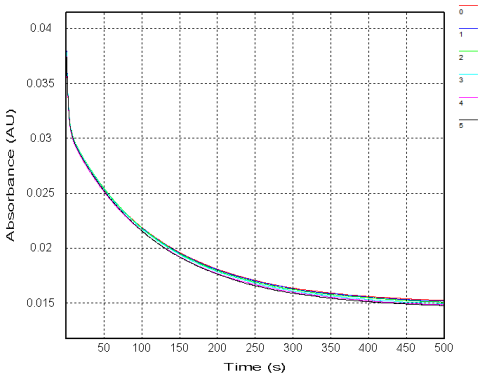
Reactants 26+10

25°C

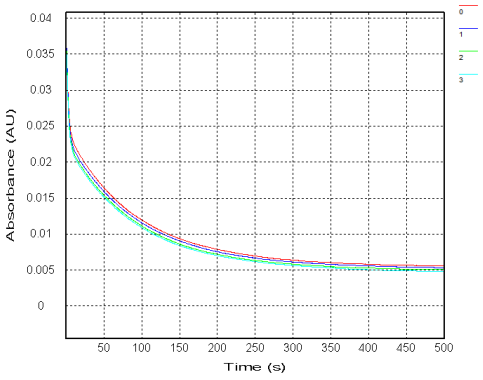


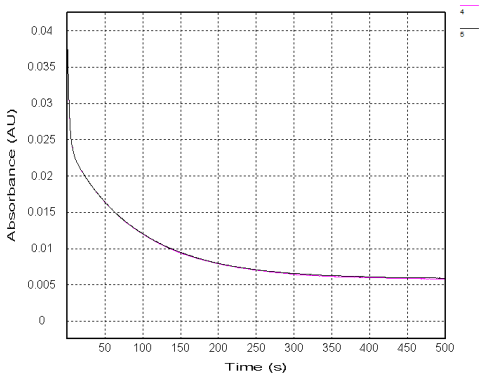


37°C



50°C

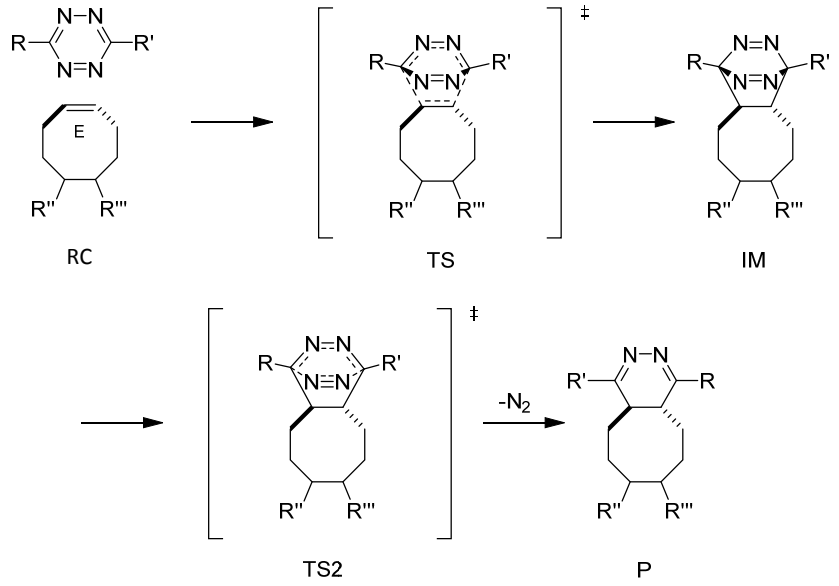




6. Quantum Chemical Calculations

All DFT calculations were performed on the Vienna Scientific Cluster 3 using the Gaussian 09 (Rev. D.01) program package.[1] Geometry optimizations to energy minima or transition states as well as subsequent frequency analyses at 298.15 K of all considered compounds and intermediates were achieved using the M06-2X density functional[2] in combination with the 6-311+G(d,p)[3] basis set as implemented in Gaussian 09, which has been found to give relatively accurate energy profiles for cycloadditions.[4,5] Imaginary frequencies corresponding to the desired reaction coordinates were obtained only in the case of transition state calculations. Data analysis was done using GaussView 5 (Gaussian, Inc.).

The reaction of tetrazines with strained dienophiles proceeds in two steps, the first being an inverse electron demand Diels-Alder (IEDDA)-initiated reaction leading to an intermediate that subsequently undergoes retro-Diels-Alder reaction with the loss of N_2 (Scheme S1).



Scheme S1: *General mechanism of the tetrazine ligation (RC = reactant complex, TS = transition state, IM = intermediate, P = product).*

The first step of this reaction (RC → TS), the inverse electron demand Diels-Alder reaction, is the rate-determining step and is therefore used for prediction of reaction rates.[19,20]

Original data is summarized in Tables S2 – S4 followed by listing of Cartesian coordinates of all relevant structures.

$\Delta G^{\ddagger}$ was used to predict relative rates, compared to the reaction between **1** and **10**, which are shown in table S5. However, correlation between these calculated values and experimental values was poor and M06-2X/6-311+G(d,p) calculated $\Delta G^{\ddagger}$ values should not be used for prediction of RRVs of alkyl-aryl tetrazines, instead above described method (See chapter "Kinetic Investigations" in the main manuscript) using M06-2X/6-311+G(d,p) calculated $\Delta E^{\ddagger}$ values provides very accurate results.

	TCO	Tetrazines								
	10	**1**	**2**	**3**	**4**	**5**	**6**	**7**	**8**	**26**
E (hartree)	-313.172677	-552.754462	-744.464487	-783.771996	-1081.51571	-1087.99437	-1181.95319	-1332.32808	-760.498963	-1257.12132
G (hartree)[a]	-312.999391	-552.634625	-744.295682	-783.579015	-1081.34784	-1087.73633	-1181.76109	-1332.12846	-760.342988	-1256.92684

Table S2: *M06-2X/6-311+G(d,p) calculated energies of TCO 10 and Tetrazines 1-8 and 26 (E: total electronic energy, [a] calculated for 298.15 K)*

	Transition States								
	1+10	**2+10**	**3+10**	**4+10**	**5+10**	**6+10**	**7+10**	**8+10**	**26+10**
E (hartree)	-865.924139	-1057.63536	-1096.94238	-1394.6878	-1401.16446	-1495.12347	-1645.50103	-1073.67414	-1570.293123
G (hartree)[a]	-865.604288	-1057.26854	-1096.55074	-1394.31978	-1400.70963	-1494.73171	-1645.1013	-1073.31944	-1569.898486

Table S3: *M06-2X/6-311+G(d,p) calculated energies of transition states between TCO 10 and Tetrazines 1-8 and 26 (E: total electronic energy, [a] calculated for 298.15 K)*

	Energies of activation								
	1+10	**2+10**	**3+10**	**4+10**	**5+10**	**6+10**	**7+10**	**8+10**	**26+10**
$\Delta E^{\ddagger}$ (kcal/mol)	1.88	1.13	1.44	0.36	1.62	1.51	-0.17	-1.57	0.55
$\Delta G^{\ddagger}$ (kcal/mol)[a]	18.65	16.65	17.36	17.22	16.37	18.05	16.66	14.40	17.41

Table S4: *Resulting energies of activation for the reaction between TCO 10 and Tetrazines 1-8 and 26 (E: total electronic energy, [a] calculated for 298.15 K)*

	Predicted RRV values using $\Delta G^{\ddagger}$							
	1+10	**2+10**	**3+10**	**4+10**	**5+10**	**6+10**	**7+10**	**8+10**
RRV	1.00	7.44	3.65	4.19	9.81	1.83	7.34	70.69

Table S5: *Predicted relative reactivity values based on $\Delta G^{\ddagger}$, calculated using M06-2X/6-311+G(d,p)*

Cartesian Coordinates

Tetrazines 1-8 and 26

1

C	2.6541930	0.0002870	-0.2232200
C	0.2201670	-0.0006280	0.5745190
C	-1.2178290	-0.0010960	0.9854390
H	-1.4060680	-0.8913470	1.5895580
H	-1.4061070	0.8878670	1.5914420
C	-2.1230580	0.0002210	-0.2533710
H	-1.9147170	0.8850880	-0.8612390
H	-1.9147810	-0.8833880	-0.8630860
C	-3.5828140	-0.0001300	0.1459580
H	-3.8375600	-0.8917360	0.7253640
H	-3.8375030	0.8903450	0.7271200
F	-4.3762250	0.0010110	-0.9909940
N	0.8145320	-1.1815150	0.3763060
N	2.0561370	-1.1814510	-0.0303980
N	2.0558240	1.1815710	-0.0286960
N	0.8142170	1.1806900	0.3780560
C	4.0818810	0.0007640	-0.6607650
H	4.2946430	0.8973360	-1.2405390
H	4.7337370	-0.0014270	0.2165170
H	4.2941590	-0.8934190	-1.2444350

2

C	-3.1521940	1.2090240	0.1404990
C	-4.5190400	1.2049210	0.3849500
C	-5.2046490	0.0000520	0.5077510
C	-4.5190490	-1.2048500	0.3851040
C	-3.1522160	-1.2090010	0.1406520
C	-2.4630470	0.0000040	0.0163490
H	-2.6109410	2.1412800	0.0432690
H	-5.0496500	2.1445310	0.4801930
H	-5.0496850	-2.1444330	0.4804720
H	-2.6109580	-2.1412670	0.0435370
C	-1.0079330	-0.0000290	-0.2468120
C	1.5140220	-0.0000660	-0.7211310
C	2.9912560	-0.0000730	-0.9519580
H	3.2502480	-0.8893680	-1.5309750
H	3.2502400	0.8891560	-1.5310810
C	3.7429490	0.0000130	0.3851970
H	3.4652680	0.8841140	0.9657830
H	3.4653050	-0.8840400	0.9658740
C	5.2397730	0.0000330	0.1607860
H	5.5604310	-0.8912350	-0.3856240
H	5.5603940	0.8912680	-0.3857010
F	5.8932640	0.0000990	1.3830140
N	0.8972530	-1.1808030	-0.6020580
N	-0.3842910	-1.1809240	-0.3622390
N	-0.3842460	1.1808620	-0.3622290
N	0.8972830	1.1807020	-0.6020450
H	-6.2712480	0.0000730	0.6988000

3

C	-2.7026230	1.2062180	0.0284130
C	-4.0734120	1.1985780	0.2435920
C	-4.7808230	0.0000290	0.3502500
C	-4.0721900	-1.1984910	0.2408390
C	-2.7022580	-1.2050210	0.0254940
C	-2.0058440	0.0012520	-0.0840000
H	-2.1635070	2.1415790	-0.0515770
H	-4.6040630	2.1405090	0.3325970
H	-4.6027480	-2.1408280	0.3277410
H	-2.1625100	-2.1397950	-0.0568590
C	-0.5473400	0.0016690	-0.3121950
C	1.9861470	0.0021230	-0.7255670
C	3.4685800	0.0022100	-0.9220460
H	3.7403890	-0.8857600	-1.4972760
H	3.7408980	0.8925620	-1.4933250
C	4.1900000	-0.0010640	0.4315110
H	3.9000810	0.8820560	1.0076040
H	3.8987920	-0.8860890	1.0040270
C	5.6914930	-0.0018280	0.2410090
H	6.0238060	-0.8923680	-0.2996340
H	6.0251840	0.8902800	-0.2961920
F	6.3174790	-0.0046890	1.4777450
N	1.3664050	-1.1785680	-0.6241810
N	0.0796490	-1.1793800	-0.4150590
N	0.0800790	1.1829660	-0.4097010
N	1.3668050	1.1826180	-0.6188540
C	-6.2725170	-0.0043320	0.5512460
H	-6.7863510	-0.0853490	-0.4108850
H	-6.5839480	-0.8509830	1.1650610
H	-6.6091650	0.9148590	1.0322880

4

C	-1.5884940	1.2097790	-0.1007950
C	-2.9648340	1.2090920	0.0720820
C	-3.6462980	-0.0001400	0.1563520
C	-2.9647830	-1.2091260	0.0691290
C	-1.5884340	-1.2093710	-0.1036970
C	-0.8962290	0.0003220	-0.1916220
H	-1.0429350	2.1420250	-0.1657500
H	-3.5076720	2.1431710	0.1477180
H	-3.5076340	-2.1433900	0.1424570
H	-1.0428770	-2.1414640	-0.1708470
C	0.5724420	0.0005530	-0.3805030
C	3.1116740	0.0010090	-0.7289640
C	4.5977370	0.0012060	-0.8890430
H	4.8837400	-0.8875720	-1.4558910
H	4.8837110	0.8911860	-1.4539910
C	5.2827210	-0.0003270	0.4835290
H	4.9779130	0.8833960	1.0509670
H	4.9774180	-0.8849940	1.0492250
C	6.7892070	-0.0006360	0.3332450
H	7.1361720	-0.8914980	-0.1975590
H	7.1368080	0.8912710	-0.1953750
F	7.3790050	-0.0023480	1.5866330
N	2.4900020	-1.1803940	-0.6400800
N	1.1982000	-1.1799830	-0.4635570
N	1.1978370	1.1813680	-0.4633510
N	2.4895830	1.1822500	-0.6398740
C	-5.1437330	-0.0004340	0.2796970
F	-5.5937270	-1.0809190	0.9311820
F	-5.7343990	-0.0003270	-0.9271820
F	-5.5941980	1.0795530	0.9316590

5

C	-1.4724740	1.2312030	-0.0025240
C	-2.8485250	1.2341470	0.2158810
C	-3.5447140	0.0252510	0.3410170
C	-2.8573860	-1.1891150	0.2197720
C	-1.4827300	-1.1999970	-0.0025220
C	-0.8027020	0.0128780	-0.1082760
H	-0.9120710	2.1494100	-0.0957410
H	-0.9303370	-2.1233350	-0.0930820
C	0.6556140	0.0065410	-0.3401360
C	3.1897640	-0.0047630	-0.7549980
C	4.6724200	-0.0109450	-0.9493870
H	4.9418480	-0.9008930	-1.5226380
H	4.9490210	0.8773250	-1.5219010
C	5.3917960	-0.0140830	0.4051930
H	5.1026440	0.8702030	0.9798980
H	5.0981250	-0.8978300	0.9784440
C	6.8936530	-0.0178320	0.2174020
H	7.2252170	-0.9091110	-0.3225150
H	7.2299270	0.8734460	-0.3196050
F	7.5170930	-0.0214860	1.4551980
N	2.5637490	-1.1824020	-0.6570490
N	1.2771000	-1.1771210	-0.4478120
N	1.2893520	1.1847040	-0.4372410
N	2.5757440	1.1784470	-0.6472940
O	-4.8737860	0.0377790	0.6148620
O	-3.6035840	2.3509060	0.3178260
O	-3.6231150	-2.2996320	0.3320870
C	-5.6969710	-0.1329560	-0.5345130
H	-5.4993600	-1.0987730	-1.0069690
H	-6.7267060	-0.0997800	-0.1837950
H	-5.5250070	0.6786600	-1.2474580
C	-2.9729280	-3.5534120	0.2531280
H	-2.2247060	-3.6591740	1.0440590
H	-3.7505270	-4.3018430	0.3860420

H	-2.4954170	-3.6896850	-0.7219880
C	-2.9422060	3.5975950	0.2286060
H	-2.4621280	3.7215120	-0.7470260
H	-3.7137300	4.3536450	0.3536250
H	-2.1940470	3.7047100	1.0195740

6

C	-1.8590560	1.3845800	0.0595180
C	-3.2281710	1.4008130	0.2465410
C	-3.9699580	0.2128850	0.1873920
C	-3.3066110	-0.9899720	-0.0633870
C	-1.9309730	-1.0029470	-0.2515310
C	-1.1936560	0.1791520	-0.1929100
H	-1.2917580	2.3053730	0.1061570
H	-3.7348830	2.3393740	0.4408350
H	-3.8487030	-1.9243430	-0.1151830
H	-1.4205660	-1.9378000	-0.4456940
C	0.2664170	0.1587420	-0.3908520
C	2.8106130	0.1211560	-0.7307540
C	4.2985370	0.0887230	-0.8743560
H	4.5607980	-0.7077460	-1.5744730
H	4.6281840	1.0458690	-1.2843680
C	4.9622330	-0.1630080	0.4858810
H	4.6863180	0.6317550	1.1844820
H	4.6086580	-1.1117460	0.8990630
C	6.4688180	-0.2074000	0.3494020
H	6.7848250	-1.0176360	-0.3134570
H	6.8629990	0.7399540	-0.0284430
F	7.0430000	-0.4346380	1.5907950
N	2.1475660	-1.0377220	-0.8169200
N	0.8560820	-1.0193930	-0.6454700
N	0.9350380	1.3186640	-0.3113550
N	2.2274360	1.2986160	-0.4833540
S	-5.7105570	0.3568620	0.4391630
C	-6.2773980	-1.3535760	0.3004270
H	-7.3545580	-1.3171100	0.4569990
H	-6.0779460	-1.7578780	-0.6917930
H	-5.8290690	-1.9821560	1.0695880

7

C	-1.2567830	1.2122850	-0.0826130
C	-2.6314930	1.2149090	0.1083940
C	-3.3000040	-0.0000510	0.1920610
C	-2.6313830	-1.2149120	0.1078140
C	-1.2566750	-1.2120780	-0.0832060
C	-0.5688740	0.0001590	-0.1835690
H	-0.7084350	2.1430310	-0.1468490
H	-3.1832430	2.1419510	0.2130190
H	-3.1830410	-2.1420580	0.2120070
H	-0.7082560	-2.1427500	-0.1478970
C	0.8986760	0.0002830	-0.3872050
C	3.4366310	0.0004410	-0.7420300
C	4.9230290	0.0004600	-0.8970650
H	5.2111490	-0.8887770	-1.4620690
H	5.2112250	0.8902230	-1.4611960
C	5.6021260	-0.0002510	0.4785930
H	5.2949170	0.8837340	1.0443230
H	5.2946230	-0.8846300	1.0435470
C	7.1093170	-0.0004090	0.3346350
H	7.4586720	-0.8917430	-0.1938080
H	7.4588810	0.8910830	-0.1934060
F	7.6934500	-0.0007650	1.5904250
N	2.8142010	-1.1810770	-0.6569120
N	1.5229310	-1.1802960	-0.4771880
N	1.5228720	1.1808840	-0.4763480
N	2.8142020	1.1818280	-0.6560960
S	-5.0780080	-0.0001800	0.3901790
O	-5.4573770	-1.2689480	0.9933070
O	-5.4575160	1.2684290	0.9935310
C	-5.6787240	-0.0000650	-1.2945900
H	-6.7662520	-0.0002430	-1.2205420
H	-5.3243940	0.9022250	-1.7899140
H	-5.3241270	-0.9021330	-1.7901300

8

C	4.4084840	-1.2021110	0.2704090
C	5.1636470	-0.0514040	0.4833620
C	4.5152010	1.1754160	0.4571360
C	3.1477890	1.2057880	0.2206510
C	2.4863800	-0.0074820	0.0245560
H	4.8801360	-2.1798850	0.2794480
H	5.0624740	2.0965590	0.6179130
H	2.5948690	2.1344560	0.1860080
C	1.0175010	-0.0198160	-0.2274670
C	-1.4956100	-0.0022670	-0.7050320
C	-2.9697570	-0.0022560	-0.9536280
H	-3.2202160	0.8798350	-1.5466610
H	-3.2233440	-0.8988940	-1.5242110
C	-3.7364270	0.0109660	0.3750630
H	-3.4571840	-0.8624240	0.9706470
H	-3.4733820	0.9057120	0.9461300
C	-5.2304720	-0.0047340	0.1332920
H	-5.5514560	0.8729830	-0.4344620
H	-5.5379840	-0.9091120	-0.3988740
F	-5.8981470	0.0146880	1.3476910
N	-0.8577890	1.1703040	-0.6871870
N	0.4262120	1.1578760	-0.4449670
N	0.3731540	-1.1944550	-0.2177950
N	-0.9066080	-1.1810740	-0.4622480
H	6.2287890	-0.1233740	0.6632790
N	3.0993460	-1.1898870	0.0466980

26

C	1.6016290	-1.1634990	0.0180620
C	2.9850510	-1.1061390	0.1381100
C	3.6335280	0.0890170	-0.1318540
C	2.9366580	1.2219790	-0.5392830
C	1.5566930	1.1621180	-0.6565970
C	0.8841650	-0.0318940	-0.3754670
H	1.0702300	-2.0834320	0.2256400
H	3.5747020	-1.9686220	0.4300610
H	3.4638450	2.1412370	-0.7735910
H	0.9916220	2.0306110	-0.9692980
C	-0.5884310	-0.0943560	-0.5020600
C	-3.1412400	-0.2007490	-0.7209570
C	-4.6334310	-0.2495200	-0.7951220
H	-4.9658490	0.4566240	-1.5592210
H	-4.9319510	-1.2585090	-1.0882140
C	-5.2454210	0.1120350	0.5644350
H	-4.8913300	-0.5873140	1.3269100
H	-4.9289550	1.1170630	0.8571200
C	-6.7572190	0.0628940	0.5057870
H	-7.1513990	0.7774940	-0.2218730
H	-7.1139320	-0.9396450	0.2544510
F	-7.2801160	0.3954880	1.7451640
N	-2.5366160	0.9625040	-0.9850170
N	-1.2383020	1.0160540	-0.8739390
N	-1.1973510	-1.2584650	-0.2401970
N	-2.4950830	-1.3123930	-0.3504240
C	5.4846340	1.0871920	1.5466080
H	6.5342200	1.1907180	1.8188750
H	5.0342680	2.0654540	1.3783240
H	4.9448980	0.5271780	2.3100390
S	5.4374590	0.1227530	0.0072310
O	5.8578880	-1.2725840	0.3782090

Trans-Cyclooctene **10**

C	0.5318520	-1.3589840	0.3996640
H	0.3744330	-1.3388160	1.4781560
C	-0.5318840	-1.3585380	-0.3995650
H	-0.3742230	-1.3368990	-1.4780190
C	-1.8690770	-0.9025640	0.0834010
H	-2.7109740	-1.3589110	-0.4431120
H	-1.9793480	-1.1138860	1.1513860
C	1.8688930	-0.9026020	-0.0836680
H	2.7109760	-1.3589910	0.4424710
H	1.9787600	-1.1140400	-1.1516990
C	-1.8811540	0.6346470	-0.1369480
H	-2.7888180	1.0457230	0.3159040
H	-1.9547410	0.8378520	-1.2114020
C	1.8812090	0.6344950	0.1367650
H	2.7887720	1.0455390	-0.3163480
H	1.9551820	0.8376990	1.2111940
C	0.6517960	1.3791870	-0.4284790
H	0.9536840	2.4199210	-0.5751010

H	0.4327970	0.9945680	-1.4305910
C	-0.6516990	1.3789050	0.4288570
H	-0.9534390	2.4195610	0.5763670
H	-0.4326710	0.9934100	1.4306360

Transition states

TS_{1+10}

C	-0.4598930	2.2404580	0.3446990
C	1.1972770	0.3836430	0.1175860
C	-0.7854570	-0.6163260	0.0087090
H	-0.5286230	-0.9843530	-0.9839530
C	-1.6880720	0.4221870	0.0713870
H	-2.1482380	0.6078670	1.0414010
N	1.0405830	0.9077220	1.3716170
N	0.1891350	1.8536100	1.4877050
N	1.0410400	1.2005900	-0.9688360
N	0.1979850	2.1541100	-0.8531000
C	-2.5356940	0.7422390	-1.1271580
H	-2.8589280	1.7849630	-1.1503770
H	-1.9611100	0.5534030	-2.0390390
C	-0.7566410	-1.6334830	1.1142560
H	0.2127220	-2.1253260	1.2129990
H	-0.9747400	-1.1396910	2.0662200
C	-3.7843400	-0.1659420	-1.0950830
H	-4.3388970	-0.0040260	-2.0240270
H	-4.4423080	0.1641310	-0.2831040
C	-1.8268060	-2.7074540	0.8190150
H	-1.8705430	-3.3797940	1.6809250
H	-1.4934410	-3.3174170	-0.0284050
C	-3.2395280	-2.1754820	0.5195030
H	-3.9377630	-2.9909010	0.7237870
H	-3.4918300	-1.3902720	1.2408280
C	-3.5042290	-1.6701120	-0.9273840
H	-4.3752420	-2.2034540	-1.3160430
H	-2.6720330	-1.9579560	-1.5797760
C	2.1887060	-0.7333330	-0.0300460
H	1.9088380	-1.3500350	-0.8895690
H	2.1518860	-1.3512450	0.8692640
C	3.6066850	-0.1812620	-0.2160880
H	3.6409660	0.4522930	-1.1051750
H	3.8750560	0.4336220	0.6471170
C	4.6041850	-1.3100800	-0.3573240
H	4.3857960	-1.9267090	-1.2339470
H	4.6182950	-1.9455740	0.5327590
F	5.8817180	-0.7936140	-0.5192230
C	-1.4759740	3.3321050	0.4939300
H	-1.0176350	4.1735120	1.0167010
H	-1.8094130	3.6679080	-0.4861620
H	-2.3308040	2.9963980	1.0828700

TS_{2+10}

C	0.7311520	-1.2454520	0.1233070
C	-1.6618810	-0.5248010	0.0806020
C	-0.5554150	1.3545970	-0.0064830
H	-1.0311280	1.5856570	-0.9591670
C	0.7724160	0.9830220	-0.0581610
H	1.3336740	1.0200930	0.8744720
N	-1.1790680	-0.9612620	1.2867610
N	0.0469450	-1.3148650	1.3101420
N	-1.1702080	-1.0924280	-1.0687350
N	0.0501080	-1.4615430	-1.0462900
C	1.5668860	1.2252480	-1.3067160
H	2.3983850	0.5251830	-1.4136560
H	0.9156820	1.1130200	-2.1795790
C	-1.0447240	2.1456290	1.1753080
H	-2.1154050	2.0281420	1.3507300
H	-0.5237880	1.8091680	2.0769810
C	2.1283050	2.6637560	-1.2517150
H	2.6111550	2.8691190	-2.2115740
H	2.9197070	2.7054160	-0.4949650
C	-0.7479730	3.6396040	0.9217890
H	-1.0137750	4.1909900	1.8285360
H	-1.4169000	4.0055770	0.1344910
C	0.7044110	3.9714380	0.5355400
H	0.8710520	5.0219850	0.7859750
H	1.3867230	3.4065300	1.1806750
C	1.0964000	3.7661230	-0.9557530
H	1.5128990	4.7056930	-1.3273260
H	0.1967010	3.5895730	-1.5564360
C	-3.1055630	-0.1125790	0.0460440
H	-3.2552750	0.6097980	-0.7621660
H	-3.3479100	0.3718990	0.9938510
C	-4.0168830	-1.3278130	-0.1568790
H	-3.7758060	-1.8164250	-1.1034530
H	-3.8490450	-2.0497660	0.6467920
C	-5.4708350	-0.9087240	-0.1589980
H	-5.6801950	-0.2004000	-0.9659110
H	-5.7600070	-0.4591070	0.7952910
F	-6.2803690	-2.0171840	-0.3581690
C	2.1743870	-1.5765140	0.1588270
C	2.8252280	-2.0485540	-0.9824600
C	2.8958650	-1.3923870	1.3395880
C	4.1853290	-2.3324390	-0.9383900
H	2.2570770	-2.1954090	-1.8926590
C	4.2556330	-1.6739940	1.3768890
H	2.3805740	-1.0413220	2.2259840
C	4.9035120	-2.1443820	0.2381630
H	4.6841460	-2.7047490	-1.8252800
H	4.8090440	-1.5301130	2.2971520
H	5.9637980	-2.3658620	0.2685960

TS_{3+10}

C	0.5660430	-1.0728470	0.0959220
C	-1.8927100	-0.6218930	0.0733100
C	-1.0098700	1.3665800	-0.0050320
H	-1.5167330	1.5512640	-0.9515690
C	0.3510160	1.1454790	-0.0698110
H	0.9117560	1.2370050	0.8594170
N	-1.3563740	-1.0103760	1.2735120
N	-0.0987610	-1.2258170	1.2867620
N	-1.3493460	-1.1261650	-1.0830210
N	-0.0956640	-1.3559480	-1.0713670
C	1.1049970	1.4809630	-1.3218080
H	2.0058340	0.8746960	-1.4386970
H	0.4626880	1.3052620	-2.1907520
C	-1.5710880	2.0902530	1.1884720
H	-2.6222660	1.8596170	1.3691180
H	-1.0112420	1.7995500	2.0828060
C	1.5073110	2.9713820	-1.2591490
H	1.9548040	3.2375370	-2.2211830
H	2.2963940	3.0932000	-0.5087140
C	-1.4348110	3.6109560	0.9529950
H	-1.7455290	4.1193750	1.8705120
H	-2.1477270	3.9154860	0.1781490
C	-0.0308690	4.0984170	0.5546050
H	0.0253270	5.1586240	0.8138880
H	0.7160930	3.6050460	1.1863800
C	0.3626710	3.9496590	-0.9426660
H	0.6672980	4.9326140	-1.3103980
H	-0.5187430	3.6776040	-1.5342420
C	-3.3757090	-0.3848870	0.0468160
H	-3.6155130	0.2974420	-0.7743190
H	-3.6709300	0.0838560	0.9874300
C	-4.1317970	-1.7070350	-0.1278970
H	-3.8271520	-2.1839490	-1.0620620
H	-3.8788910	-2.3824890	0.6936700
C	-5.6263260	-1.4722650	-0.1432140
H	-5.9187580	-0.8179770	-0.9695260
H	-5.9745000	-1.0378750	0.7982180
F	-6.2900050	-2.6788680	-0.3145920
C	2.0358400	-1.2420230	0.1194090
C	2.7321060	-1.6217740	-1.0284760
C	2.7449660	-1.0015050	1.2974750
C	4.1145020	-1.7565000	-0.9918760
H	2.1816710	-1.8198210	-1.9400680
C	4.1257820	-1.1360400	1.3216810
H	2.2041550	-0.7266870	2.1956260
C	4.8339250	-1.5125030	0.1780760
H	4.6444100	-2.0613030	-1.8883150
H	4.6645900	-0.9515300	2.2452860
C	6.3352320	-1.6292490	0.2051310
H	6.6839570	-2.0012860	1.1699530
H	6.6923130	-2.3049300	-0.5732130
H	6.8004870	-0.6533750	0.0389550

TS_{4+10}

C	0.1146240	-0.9075410	-0.0734930
C	2.6064060	-0.7485250	-0.0797570
C	1.9540780	1.3424440	0.0034160
H	2.4867060	1.4664620	0.9457210
C	0.5781420	1.2792140	0.0799810
H	0.0248010	1.4324850	-0.8457300
N	2.0137640	-1.0686440	-1.2733270
N	0.7392580	-1.1353640	-1.2716570
N	2.0204840	-1.1812890	1.0841960
N	0.7483700	-1.2638650	1.0866930
C	-0.1205230	1.7045450	1.3365830
H	-1.0863480	1.2114060	1.4671960
H	0.5044540	1.4590500	2.2010780
C	2.5877960	1.9883620	-1.1976280
H	3.6038040	1.6353450	-1.3814370
H	1.9928630	1.7601980	-2.0873590
C	-0.3476470	3.2314980	1.2672280
H	-0.7532450	3.5524810	2.2309140
H	-1.1247720	3.4385320	0.5230240
C	2.6319750	3.5155580	-0.9683400
H	2.9951790	3.9788950	-1.8903740
H	3.3811230	3.7364310	-0.1994590
C	1.2979990	4.1674630	-0.5642280
H	1.3676100	5.2260320	-0.8262240
H	0.4939950	3.7664020	-1.1915260
C	0.8985130	4.0709690	0.9360030
H	0.7084100	5.0838860	1.2992440
H	1.7482680	3.7071270	1.5250580
C	4.1059800	-0.6771280	-0.0692320
H	4.4279670	-0.0185190	0.7429770
H	4.4417710	-0.2531240	-1.0172600
C	4.7103180	-2.0744710	0.1120590
H	4.3570070	-2.5088300	1.0498090
H	4.3823810	-2.7226510	-0.7050030
C	6.2222760	-2.0086120	0.1215460
H	6.5902610	-1.3992280	0.9521510
H	6.6121980	-1.6068430	-0.8180050
F	6.7446540	-3.2840510	0.2771220
C	-1.3671080	-0.9091230	-0.0799890
C	-2.0814130	-1.2164950	1.0788970
C	-2.0518600	-0.5835340	-1.2524240
C	-3.4697090	-1.1952460	1.0662750
H	-1.5409980	-1.4783470	1.9796510
C	-3.4383420	-0.5580890	-1.2653970
H	-1.4903920	-0.3660290	-2.1529770
C	-4.1420620	-0.8644060	-0.1045690
H	-4.0289740	-1.4433160	1.9599040
H	-3.9745910	-0.3124180	-2.1739720
C	-5.6405400	-0.7769860	-0.1070870
F	-6.1627250	-1.1243350	-1.2915670
F	-6.0612210	0.4759820	0.1457670
F	-6.1947100	-1.5654520	0.8233670

TS_{5+10}

C	-0.2227370	-0.8475380	0.2432790
C	-2.7156860	-0.6500380	0.1766290
C	-2.0382330	1.3653060	-0.2717230
H	-2.5521880	1.3260760	-1.2318550
C	-0.6611080	1.2760290	-0.3082500
H	-0.1208320	1.5861610	0.5850390
N	-2.1458800	-0.7607710	1.4191130
N	-0.8732790	-0.8453740	1.4517000
N	-2.1211620	-1.2987080	-0.8781620
N	-0.8511430	-1.3991260	-0.8439060
C	0.0677790	1.4644370	-1.6049450
H	1.0264290	0.9414450	-1.6199740
H	-0.5440830	1.0771380	-2.4261230
C	-2.6820900	2.2306810	0.7770800
H	-3.7053850	1.9288240	1.0066890
H	-2.1035070	2.1661340	1.7037940
C	0.3167520	2.9754370	-1.8051820
H	0.7504640	3.1131140	-2.8000720
H	1.0787590	3.3061420	-1.0904560
C	-2.7033390	3.6895470	0.2706840
H	-3.0787880	4.3183940	1.0834330
H	-3.4338780	3.7724770	-0.5421880
C	-1.3540040	4.2461440	-0.2162830
H	-1.4168570	5.3354640	-0.1536280
H	-0.5674240	3.9598420	0.4910270
C	-0.9241990	3.8740400	-1.6640930
H	-0.7136220	4.8016540	-2.2019300
H	-1.7652450	3.4137030	-2.1950670
C	-4.2152050	-0.5707960	0.1343280
H	-4.5243100	-0.0575600	-0.7813500
H	-4.5544900	0.0129240	0.9920780
C	-4.8335320	-1.9720820	0.1909410
H	-4.4940310	-2.5604350	-0.6643270
H	-4.5032210	-2.4794570	1.1013360
C	-6.3446030	-1.8922610	0.1830150
H	-6.7144420	-1.4156380	-0.7294590
H	-6.7213360	-1.3443200	1.0515480
F	-6.8828920	-3.1699270	0.2319340
C	1.2574840	-0.8659180	0.2713260
C	1.9635420	-1.3604600	-0.8232890
C	1.9194600	-0.3524610	1.3846200
C	3.3572110	-1.3457120	-0.7961580
H	1.4145060	-1.7550770	-1.6659260
C	3.3133060	-0.3376620	1.4039120
H	1.3376350	0.0046070	2.2227380
C	4.0383340	-0.8435890	0.3183540
O	5.3962910	-0.8839920	0.3705130
O	4.0587260	0.1459120	2.4246210
O	4.1455810	-1.7926550	-1.8031740
C	3.3742770	0.6114430	3.5701530
H	4.1448130	0.9193920	4.2732120
H	2.7365740	1.4682300	3.3299400
H	2.7669420	-0.1815800	4.0162930
C	6.0245960	0.2067890	-0.2922620
H	5.7413790	1.1521170	0.1806460
H	7.0977480	0.0548590	-0.1904120
H	5.7534770	0.2184370	-1.3515500
C	3.5063540	-2.3497710	-2.9351060
H	2.8709870	-1.6114610	-3.4343470
H	4.3044230	-2.6573960	-3.6067980
H	2.9048430	-3.2205160	-2.6587840

TS_{6+10}

C	0.1000860	-0.9375810	-0.0037410
C	-2.3886690	-0.7174340	0.0926120
C	-1.7009040	1.3399550	0.0138870
H	-2.2614860	1.4927900	-0.9076690
C	-0.3285640	1.2503900	-0.1108020
H	0.2598430	1.3800160	0.7963840
N	-1.7630110	-1.0738380	1.2600190
N	-0.4920160	-1.1717140	1.2127200
N	-1.8550080	-1.1515170	-1.0967030
N	-0.5865920	-1.2631590	-1.1459240
C	0.3364400	1.6781510	-1.3848970
H	1.2859140	1.1649510	-1.5507590
H	-0.3216600	1.4558220	-2.2308870
C	-2.2784770	1.9864570	1.2434680
H	-3.2944920	1.6525070	1.4597800
H	-1.6574970	1.7353880	2.1087490
C	0.5967570	3.1990430	-1.3086180
H	0.9739840	3.5227700	-2.2828440
H	1.4029560	3.3840250	-0.5901070
C	-2.2971500	3.5165130	1.0347540
H	-2.6159370	3.9773460	1.9742510
H	-3.0670280	3.7645950	0.2953210
C	-0.9626250	4.1404650	0.5907170
H	-0.9935170	5.1963800	0.8703960
H	-0.1472110	3.7077220	1.1807240
C	-0.6221660	4.0553910	-0.9244080
H	-0.4317190	5.0692300	-1.2848630
H	-1.4979960	3.7076410	-1.4835760
C	-3.8871360	-0.6213350	0.1383350
H	-4.2279790	0.0609880	-0.6461980
H	-4.1791670	-0.2118930	1.1070260
C	-4.5257630	-2.0023370	-0.0486740
H	-4.2245300	-2.4198780	-1.0117240
H	-4.1728790	-2.6765250	0.7361870
C	-6.0346460	-1.9072450	0.0135960
H	-6.4270610	-1.2639280	-0.7790810
H	-6.3728920	-1.5285110	0.9821780
F	-6.5927180	-3.1657910	-0.1581350
C	1.5765850	-0.9752930	-0.0513600
C	2.2504600	-1.2549810	-1.2445350
C	2.3197690	-0.7078800	1.0957870
C	3.6337360	-1.2654930	-1.2821670
H	1.6780630	-1.4721030	-2.1378510

C	3.7093780	-0.7141450	1.0624740
H	1.8035170	-0.5054370	2.0269640
C	4.3804960	-0.9926440	-0.1292320
H	4.1459200	-1.4915510	-2.2107580
H	4.2552380	-0.5035630	1.9722650
S	6.1394080	-1.0288720	-0.2992500
C	6.7080160	-0.6928600	1.3824980
H	6.3621780	-1.4592070	2.0758810
H	7.7956770	-0.7230520	1.3352910
H	6.3963440	0.2963170	1.7171860

TS_{7+10}

C	0.3278320	-0.8534810	-0.0551720
C	2.8230410	-0.7988760	-0.0793820
C	2.2577990	1.3200370	-0.0063170
H	2.8025400	1.4274390	0.9311560
C	0.8811710	1.3169330	0.0812780
H	0.3277690	1.4877750	-0.8413940
N	2.2091500	-1.1014760	-1.2668340
N	0.9329470	-1.1145780	-1.2560960
N	2.2279050	-1.2002030	1.0910280
N	0.9535560	-1.2295600	1.1026210
C	0.2110940	1.7816320	1.3395470
H	-0.7738620	1.3313280	1.4819960
H	0.8318020	1.5177310	2.2016560
C	2.9092080	1.9291310	-1.2171640
H	3.9069500	1.5299340	-1.4067770
H	2.2968550	1.7219640	-2.1001780
C	0.0487040	3.3163860	1.2573030
H	-0.3383140	3.6620430	2.2199700
H	-0.7229020	3.5497390	0.5152990
C	3.0229550	3.4541610	-0.9984590
H	3.4003250	3.8945040	-1.9260680
H	3.7864970	3.6461340	-0.2360450
C	1.7222970	4.1677340	-0.5902090
H	1.8384580	5.2205140	-0.8587090
H	0.8966350	3.8006450	-1.2101980
C	1.3281520	4.0983050	0.9130720
H	1.1846400	5.1207720	1.2706360
H	2.1646920	3.7014760	1.4998660
C	4.3241340	-0.7871740	-0.0792940
H	4.6775980	-0.1331090	0.7234390
H	4.6695950	-0.3865650	-1.0339420
C	4.8752400	-2.2049440	0.1125540
H	4.5138740	-2.6156870	1.0578520
H	4.5157200	-2.8488230	-0.6945790
C	6.3885900	-2.1971520	0.1083810
H	6.7873640	-1.5954810	0.9303240
H	6.7850120	-1.8182570	-0.8379210
F	6.8627150	-3.4903390	0.2702240
C	-1.1524840	-0.7889050	-0.0508930
C	-1.8677000	-1.0552760	1.1188620
C	-1.8275530	-0.4261160	-1.2188920
C	-3.2535610	-0.9655360	1.1218830
H	-1.3292260	-1.3290760	2.0173070
C	-3.2117010	-0.3289940	-1.2221610
H	-1.2607800	-0.2242220	-2.1198500
C	-3.9062270	-0.6046610	-0.0500700
H	-3.8272010	-1.1502360	2.0228040
H	-3.7540160	-0.0249170	-2.1100980
S	-5.6901540	-0.5127210	-0.0576920
O	-6.1313980	-0.3033170	1.3138790
O	-6.0853280	0.3978380	-1.1229660
C	-6.1908800	-2.1603750	-0.5412690
H	-5.8194820	-2.8675470	0.1983630
H	-7.2807180	-2.1478440	-0.5540400
H	-5.7935550	-2.3661000	-1.5337280

TS_{8+10}

C	0.6919500	-1.2634430	0.1513560
C	-1.6838140	-0.5206690	0.0821400
C	-0.4988620	1.3761270	-0.0438210
H	-0.9710820	1.5949480	-1.0013730
C	0.8104710	0.9567870	-0.0783390
H	1.3699420	0.9675300	0.8557300
N	-1.2084850	-0.9288280	1.2993910
N	0.0138790	-1.2982080	1.3403980
N	-1.1984780	-1.1152670	-1.0493650
N	0.0196500	-1.5047560	-1.0102240
C	1.6182050	1.1403330	-1.3292200
H	2.4211690	0.4049930	-1.4253830
H	0.9680050	1.0422030	-2.2044600
C	-0.9737650	2.1890980	1.1266490
H	-2.0507640	2.1157460	1.2888990
H	-0.4752740	1.8400680	2.0359710
C	2.2359130	2.5567180	-1.2886050
H	2.7283990	2.7354720	-2.2490130
H	3.0251560	2.5745450	-0.5286840
C	-0.6134810	3.6690120	0.8632680
H	-0.8604300	4.2381170	1.7643860
H	-1.2620560	4.0565850	0.0692520
C	0.8541630	3.9342130	0.4824460
H	1.0647000	4.9788750	0.7249870
H	1.5074330	3.3453440	1.1357210
C	1.2444940	3.6998590	-1.0056360
H	1.6966530	4.6197540	-1.3847880
H	0.3410170	3.5504530	-1.6081010
C	-3.1091000	-0.0550690	0.0337560
H	-3.2307840	0.6451730	-0.7980700
H	-3.3318650	0.4687320	0.9651890
C	-4.0653070	-1.2420570	-0.1296600
H	-3.8422190	-1.7706340	-1.0590620
H	-3.9240680	-1.9419360	0.6982590
C	-5.5024200	-0.7691340	-0.1462960
H	-5.6887590	-0.0870770	-0.9809360
H	-5.7702020	-0.2703270	0.7895820
F	-6.3540970	-1.8536620	-0.2974780
C	2.1405060	-1.6042580	0.1870870
C	2.6961320	-2.4279080	-0.7915910
C	4.1444660	-1.3523210	1.2430310
C	4.0520720	-2.7145720	-0.7144820
H	2.0676860	-2.8248110	-1.5774560
C	4.7957840	-2.1697240	0.3239720
H	4.6926980	-0.9004030	2.0640050
H	4.5186020	-3.3560280	-1.4528830
H	5.8557200	-2.3659260	0.4240160
N	2.8466850	-1.0667110	1.1819690

TS_{26+10}

C	0.0854050	-0.8462950	-0.0125420
C	2.5810250	-0.7904700	-0.0899860
C	2.0215050	1.3199910	-0.0034180
H	2.5883590	1.4270170	0.9207240
C	0.6467750	1.3169200	0.1164840
H	0.0708510	1.4908150	-0.7913880
N	1.9420650	-1.0957040	-1.2640110
N	0.6666670	-1.1094850	-1.2262170
N	2.0116110	-1.1943500	1.0923970
N	0.7375400	-1.2238730	1.1312760
C	0.0060640	1.7741360	1.3927320
H	-0.9754400	1.3226990	1.5523540
H	0.6456310	1.5024580	2.2384990
C	2.6435580	1.9332030	-1.2277930
H	3.6368430	1.5362430	-1.4429530
H	2.0104610	1.7282520	-2.0963830
C	-0.1550120	3.3097050	1.3278680
H	-0.5122650	3.6492150	2.3041840
H	-0.9460760	3.5520730	0.6098130
C	2.7592190	3.4579810	-1.0083690
H	3.1079510	3.9033420	-1.9445370
H	3.5423060	3.6514140	-0.2665710
C	1.4661450	4.1621080	-0.5618840
H	1.5647290	5.2158380	-0.8335350
H	0.6260840	3.7873370	-1.1568940
C	1.1177760	4.0877530	0.9521090
H	0.9919920	5.1089120	1.3198510
H	1.9680610	3.6803420	1.5104890
C	4.0821780	-0.7827790	-0.1246790
H	4.4569260	-0.1314180	0.6704660
H	4.4051130	-0.3806980	-1.0865240
C	4.6349640	-2.2020110	0.0506290
H	4.3033510	-2.6108240	1.0074610
H	4.2473470	-2.8453730	-0.7436460
C	6.1474100	-2.1974080	-0.0019320
H	6.5726470	-1.5855690	0.7986800
H	6.5138460	-1.8316290	-0.9651730
F	6.6263180	-3.4887150	0.1621810
C	-1.3938560	-0.7839880	0.0228160
C	-2.0861410	-1.0541020	1.2069740
C	-2.0969340	-0.4215370	-1.1270290
C	-3.4708080	-0.9638760	1.2362060

H	-1.5308250	-1.3319420	2.0938940
C	-3.4834670	-0.3275790	-1.1027650
H	-1.5505790	-0.2226350	-2.0414430
C	-4.1537590	-0.6083620	0.0782990
H	-4.0099570	-1.1609380	2.1574810
H	-4.0581900	-0.0356790	-1.9751790
C	-6.2952930	-2.2390830	0.0699170
H	-5.8878410	-2.6963780	0.9714860
H	-7.3780770	-2.3530530	0.0379900
H	-5.8394130	-2.6570770	-0.8273620
S	-5.9558410	-0.4539380	0.0882240
O	-6.3441160	0.0558430	-1.2736200

7. References

(1) Frisch, M. J. G., Trucks, W., Schlegel, H. B., Scuseria, G. E., Robb, M. A., Cheeseman, J. R., Scalmani, G., Barone, V., Mennucci, B., Petersson, G. A., Nakatsuji, H., Caricato, M., Li, X., Hratchian, H. P., Izmaylov, A. F., Bloino, J., Zheng, G., and Sonnenberg, J. L. (2009) Gaussian 09, Revision D.01. *Inc. Wallingford, CT*.

(2) Zhao, Y., and Truhlar, D. G. (2008) The M06 suite of density functionals for main group thermochemistry, thermochemical kinetics, noncovalent interactions, excited states, and transition elements: Two new functionals and systematic testing of four M06-class functionals and 12 other function. *Theor. Chem. Acc. 120*, 215–241.

(3) Ditchfield, R., Hehre, W. J., and Pople, J. A. (1971) Self-Consistent Molecular-Orbital Methods. IX. An Extended Gaussian-Type Basis for Molecular-Orbital Studies of Organic Molecules. *J. Chem. Phys. 54*, 724.

(4) Lan, Y., Zou, L., Cao, Y., and Houk, K. N. (2011) Computational methods to calculate accurate activation and reaction energies of 1,3-dipolar cycloadditions of 24 1,3-dipoles. *J. Phys. Chem. A 115*, 13906–13920.

(5) Liu, F., Paton, R. S., Kim, S., Liang, Y., and Houk, K. N. (2013) Diels-Alder reactivities of strained and unstrained cycloalkenes with normal and inverse-electron-demand dienes: activation barriers and distortion/interaction analysis. *J. Am. Chem. Soc. 135*, 15642–9.

Manuscript #5 – Supporting Information

submitted manuscript

Denk, C.; Wilkovitsch, M.; Skrinjar, P.; Svatunek, D.; Mairinger, S.; Kuntner-Hannes, C.; Filip, T.; Fröhlich, J.; Wanek, T.; Mikula, H.:

Investigation of Small [^{18}F]-Fluoroalkylazides for Rapid Radiolabeling and *In Vivo* Click Chemistry

Investigation of Small [^{18}F]-Fluoroalkylazides for Rapid Radiolabeling and *In Vivo* Click Chemistry

Christoph Denk[a], Martin Wilkovitsch[a], Dennis Svatunek[a], Severin Mairinger[b], Philipp Skrinjar[a], Claudia Kuntner[b], Thomas Filip[b], Johannes Fröhlich[a], Thomas Wanek[b] and Hannes Mikula[a*]

a) Institut für Angewandte Synthesechemie, Technische Universität Wien (TUW) (Austria) E-mail: hannes.mikula@tuwien.ac.at b) Health and Environment Department, Biomedical Systems, Austrian Institute of Technology (AIT) Seibersdorf (Austria)

Supporting Information

Content

1. NMR Spectra 2

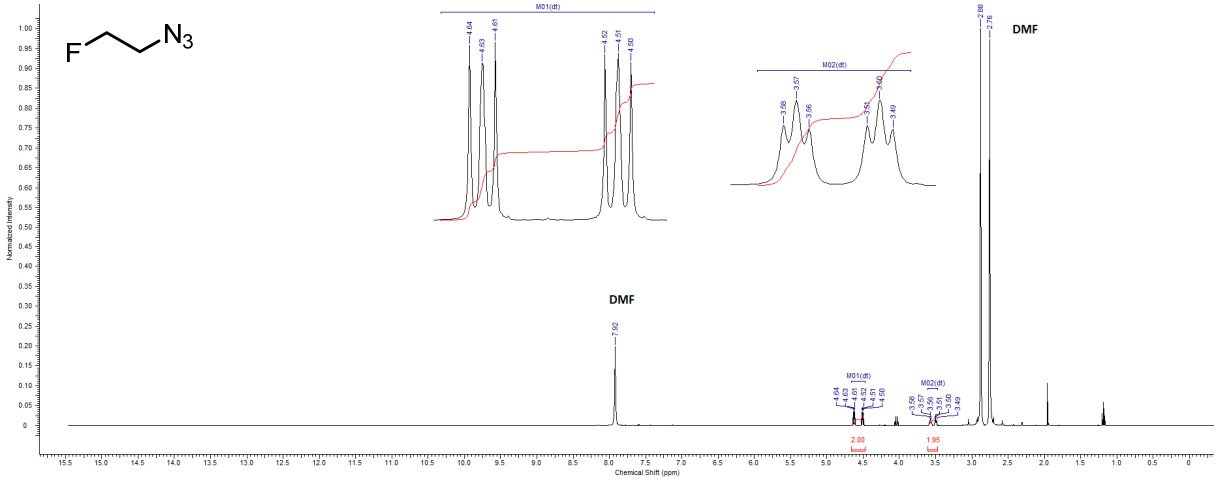
2. HPLC Data 14

3. LC/MS Data 19

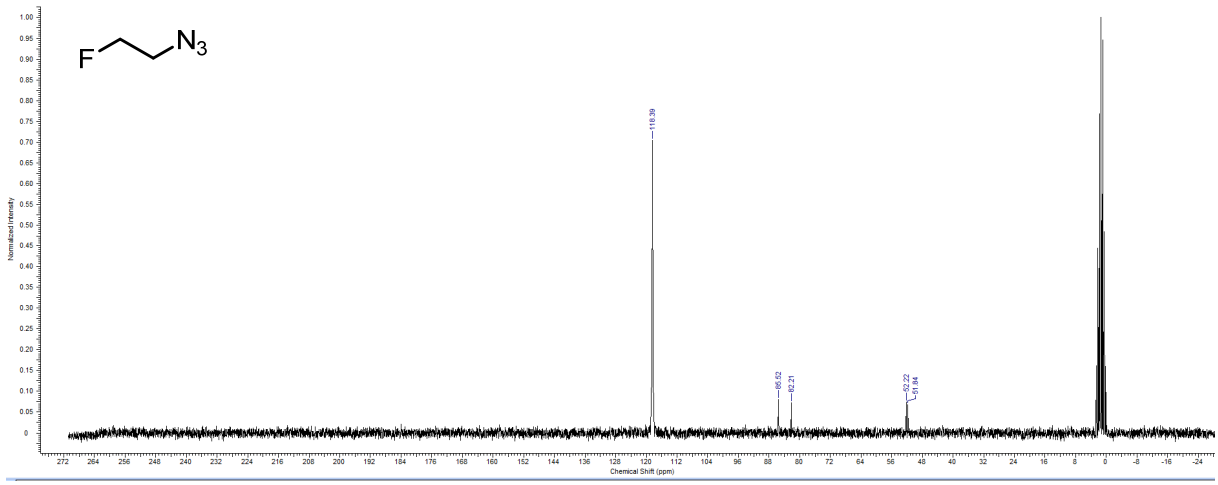
4. TLC Data 21

1. NMR Spectra

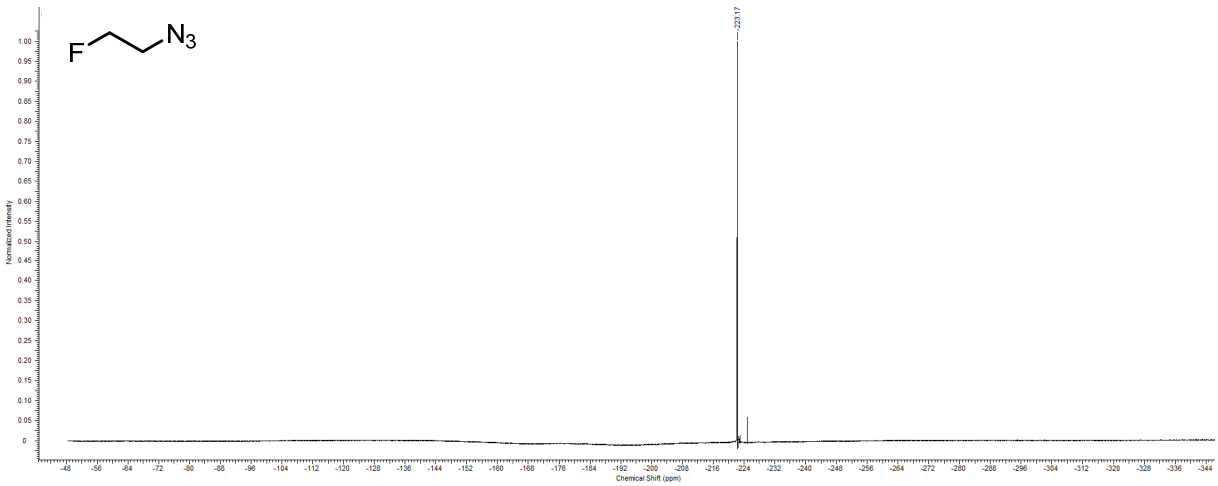
^{1}H-NMR spectrum of **1** (as solution in DMF)



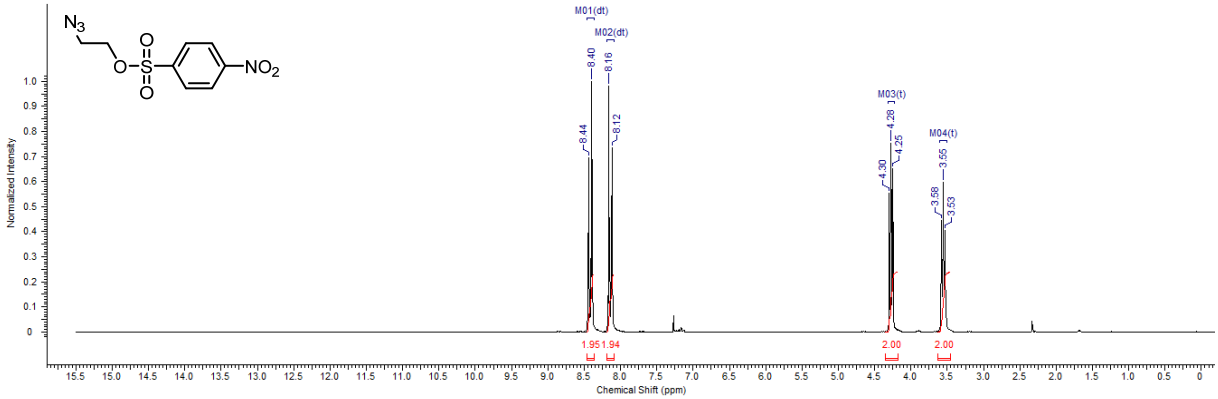
^{13}C-NMR spectrum of **1** (as solution in CD_3CN)



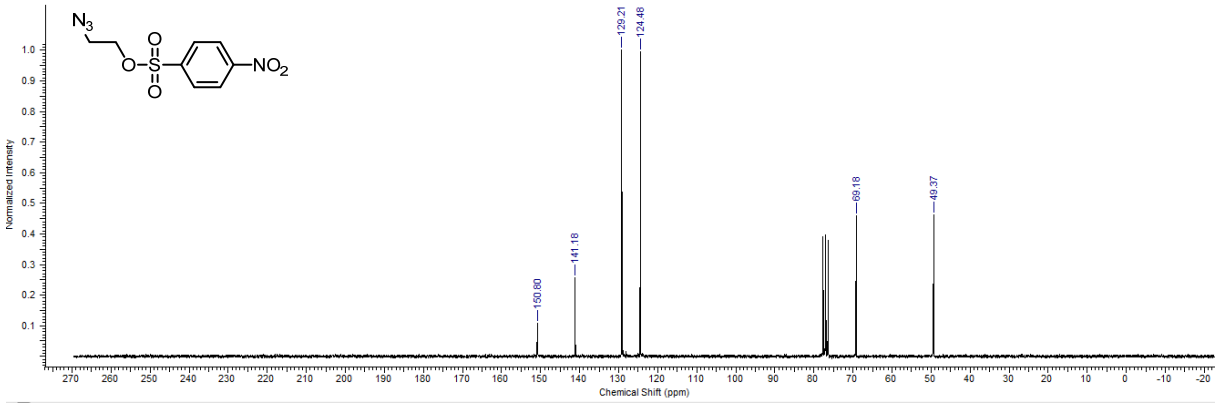
^{19}F-NMR spectrum of **1**



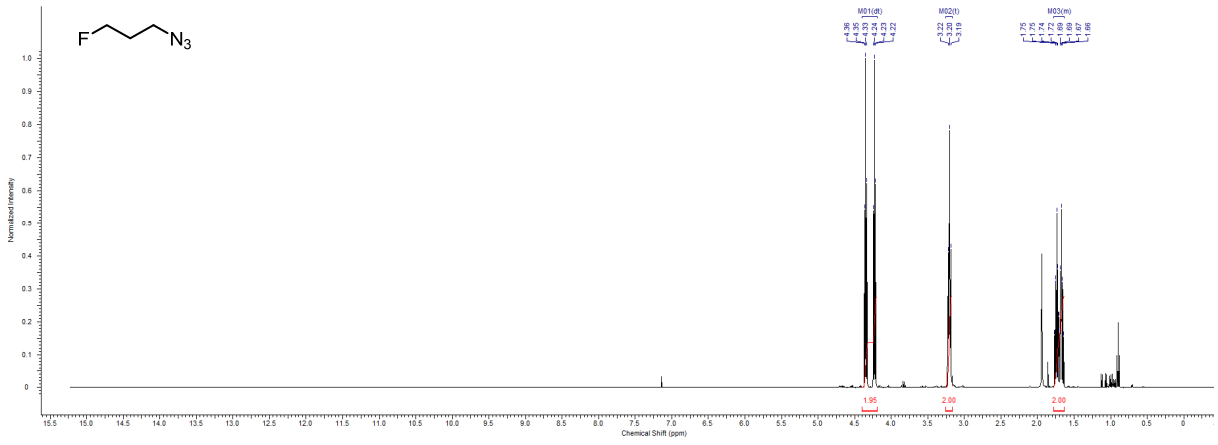
^{1}H-NMR spectrum of **2**



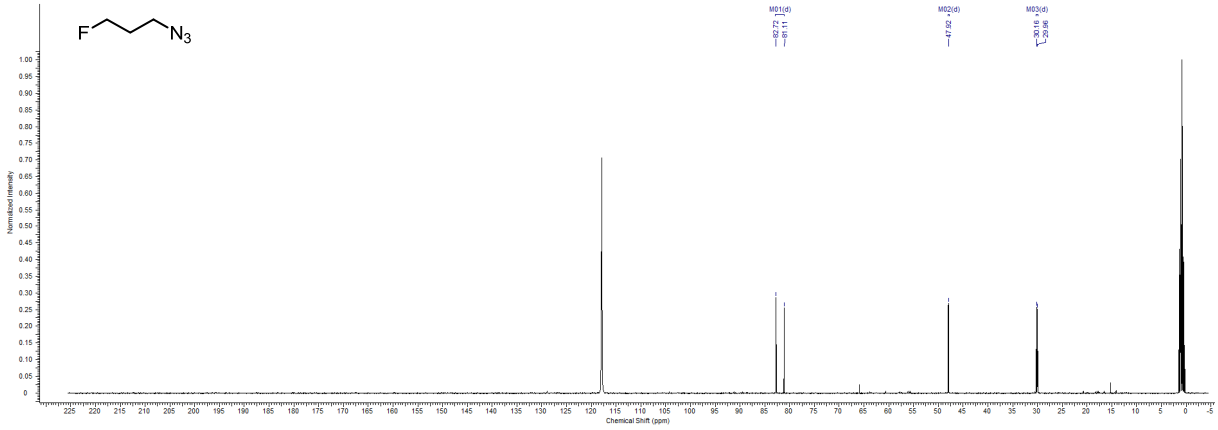
^{13}C-NMR spectrum of **2**



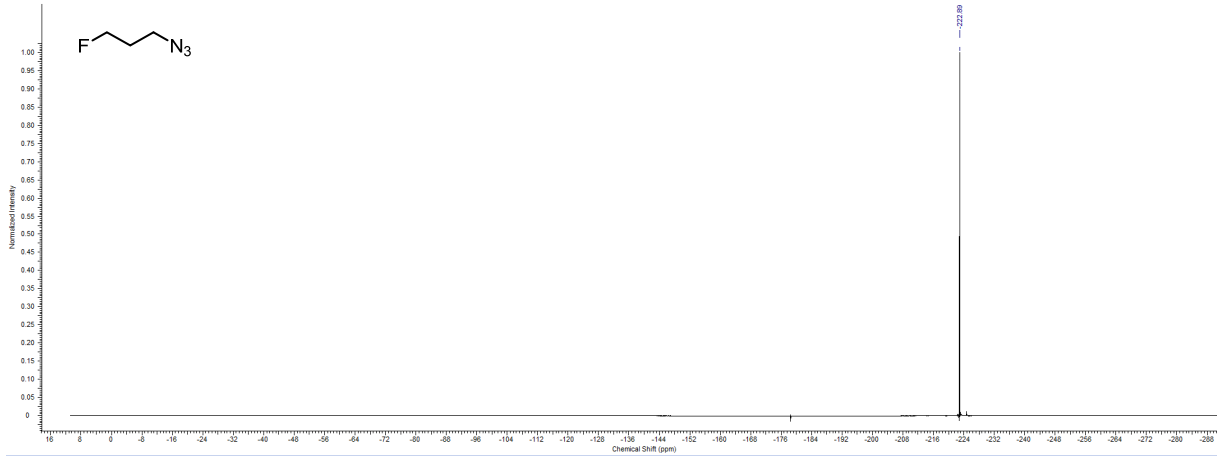
^{1}H-NMR spectrum of **3**



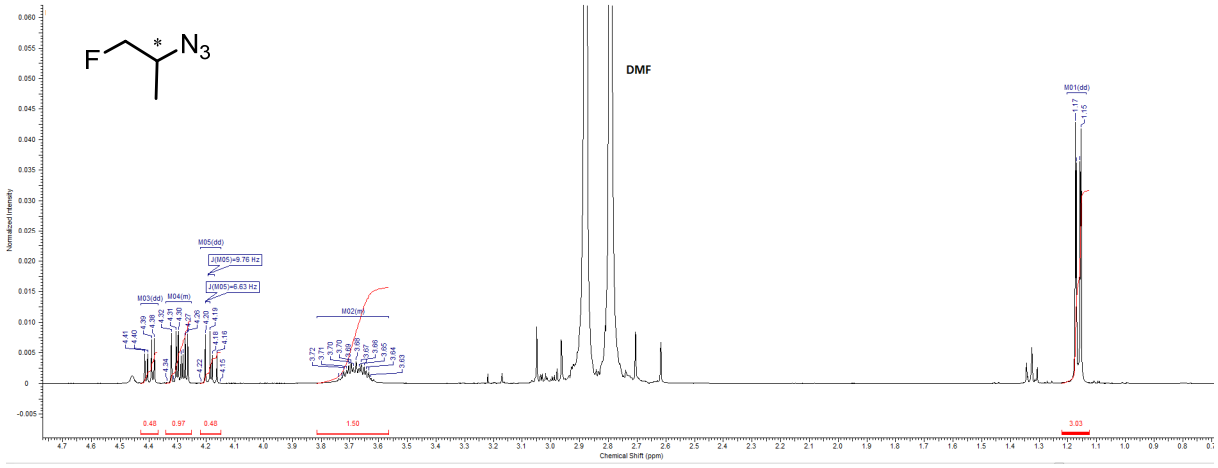
^{13}C-NMR spectrum of **3**



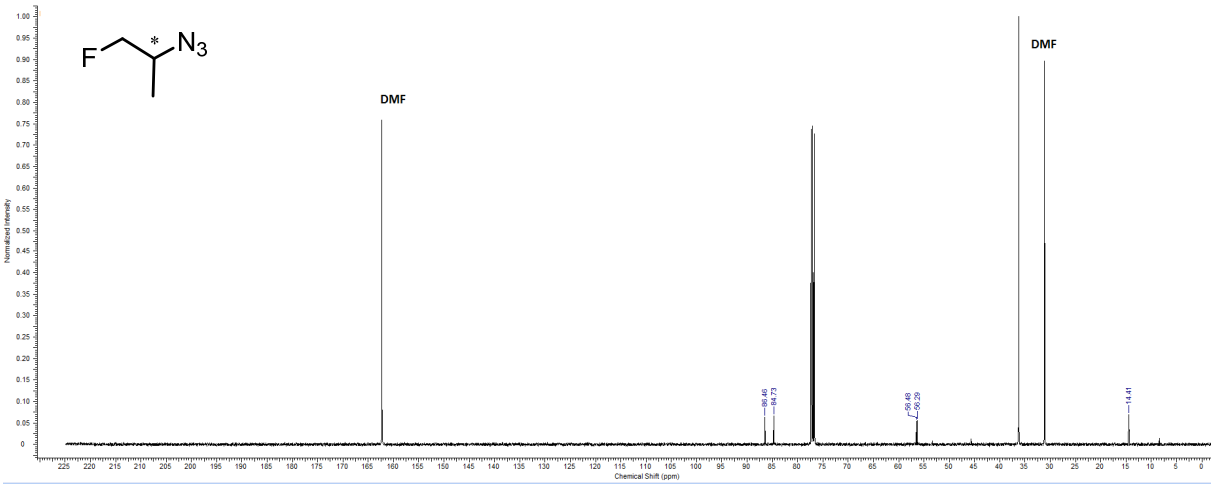
^{19}F-NMR spectrum of **3**



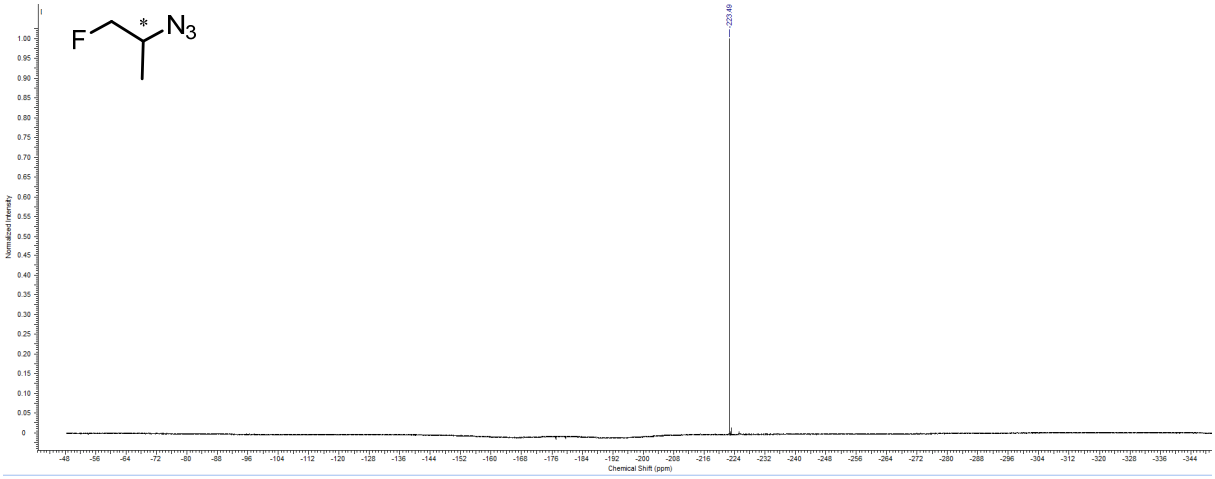
^{1}H-NMR spectrum of **4** (as solution in DMF)



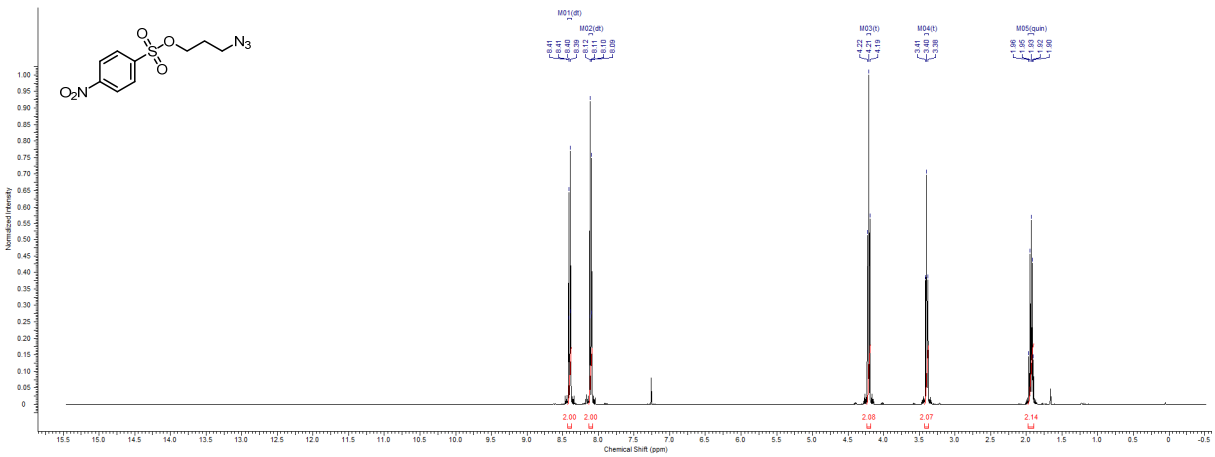
^{13}C-NMR spectrum of **4** (as solution in DMF)



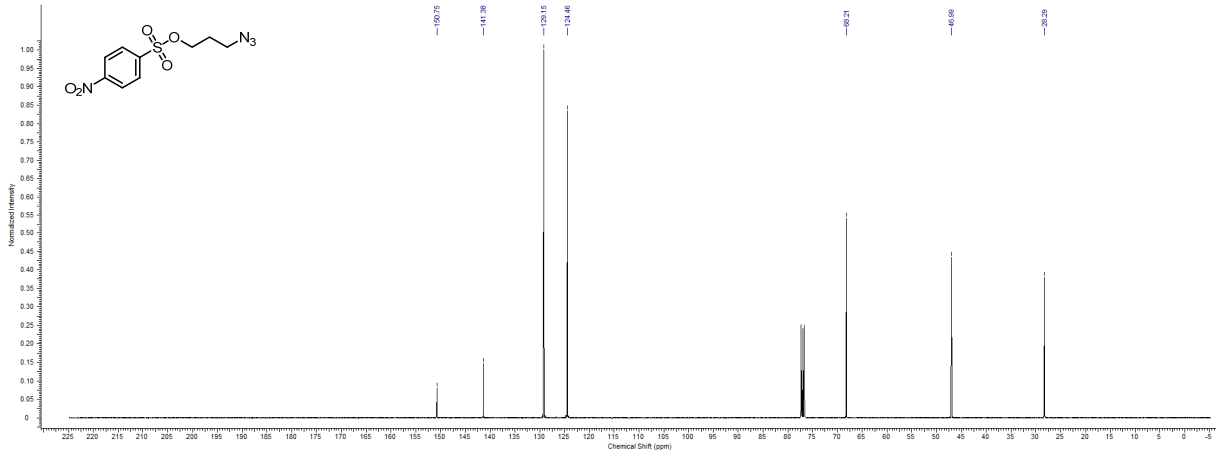
^{19}F-NMR spectrum of **4**



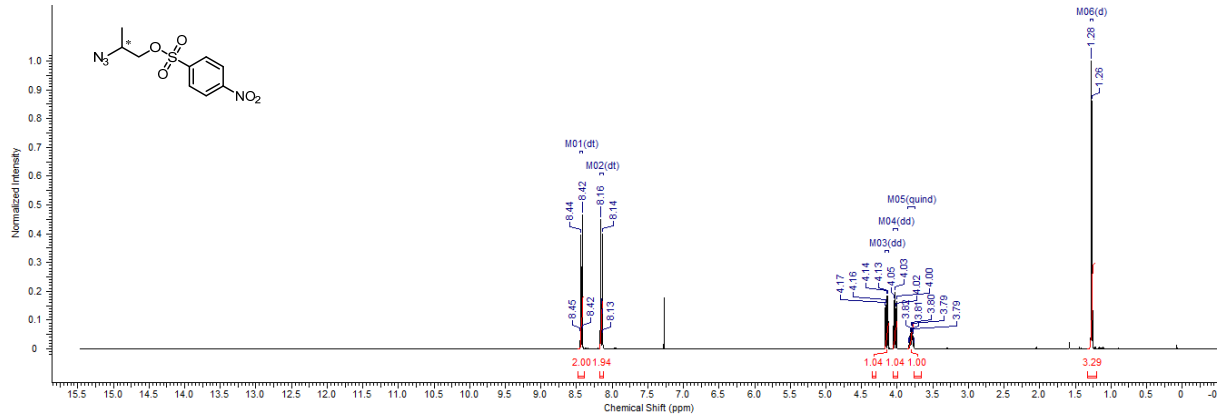
^{1}H-NMR spectrum of **6**



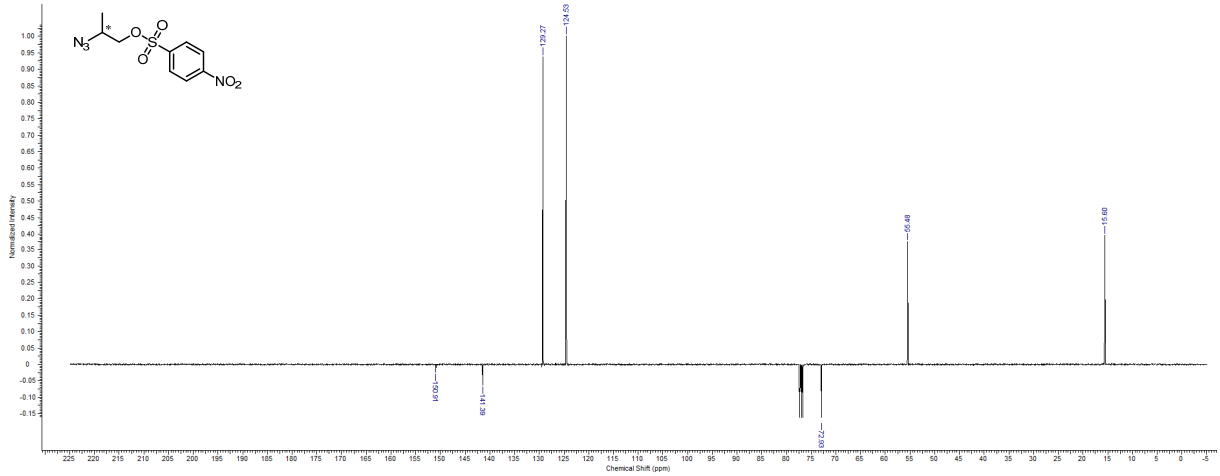
^{13}C-NMR spectrum of **6**



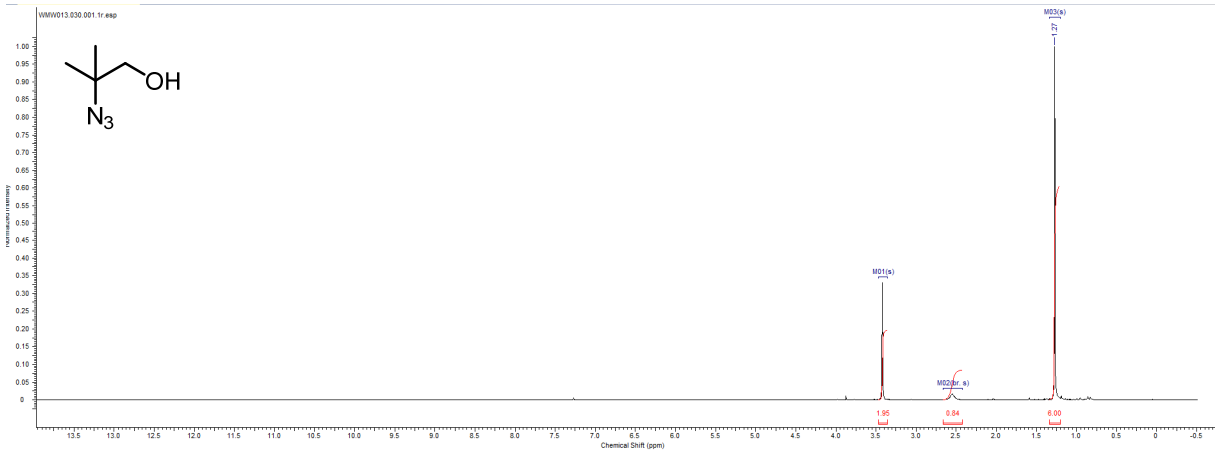
^{1}H-NMR spectrum of **8**



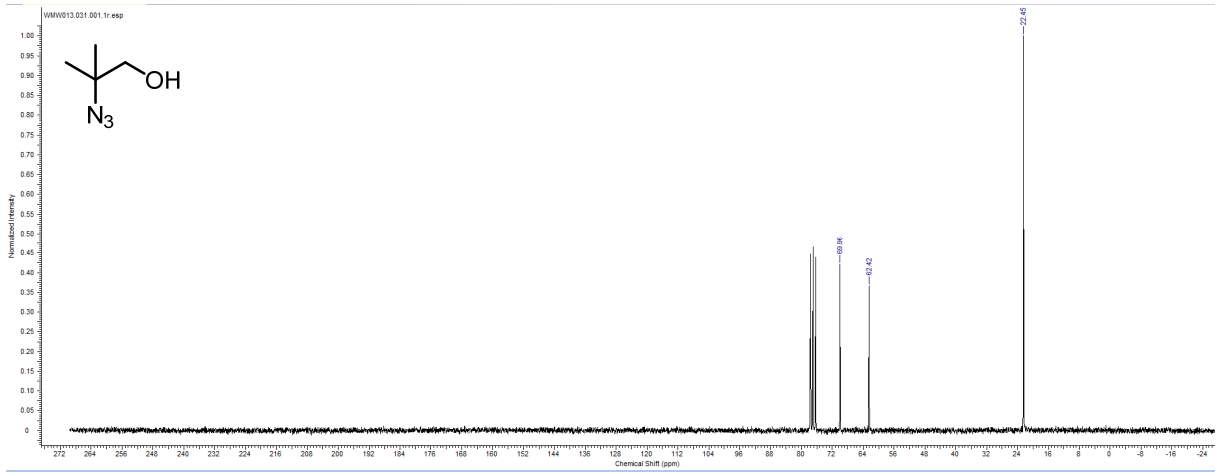
^{13}C-NMR spectrum of **8**



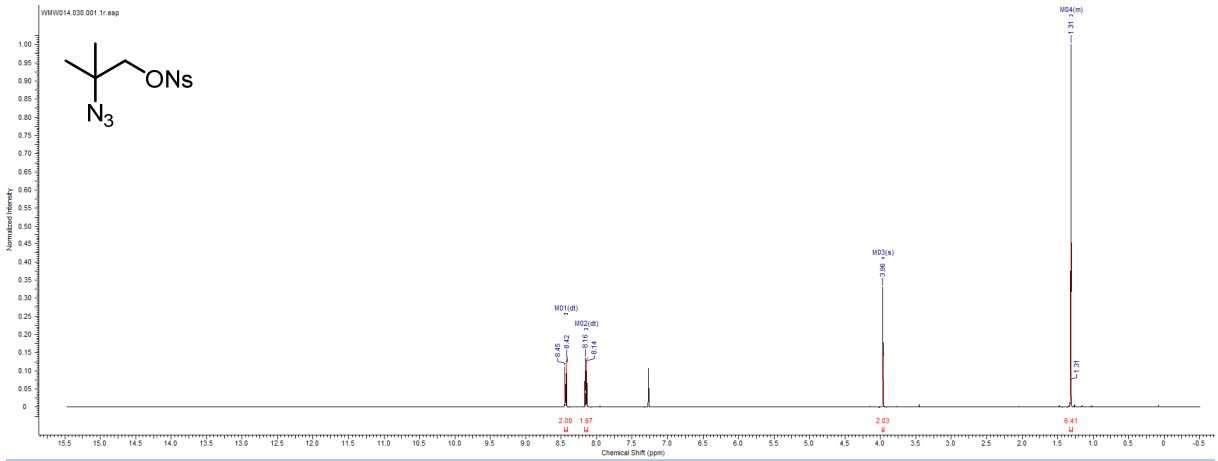
^{1}H-NMR spectrum of **9**



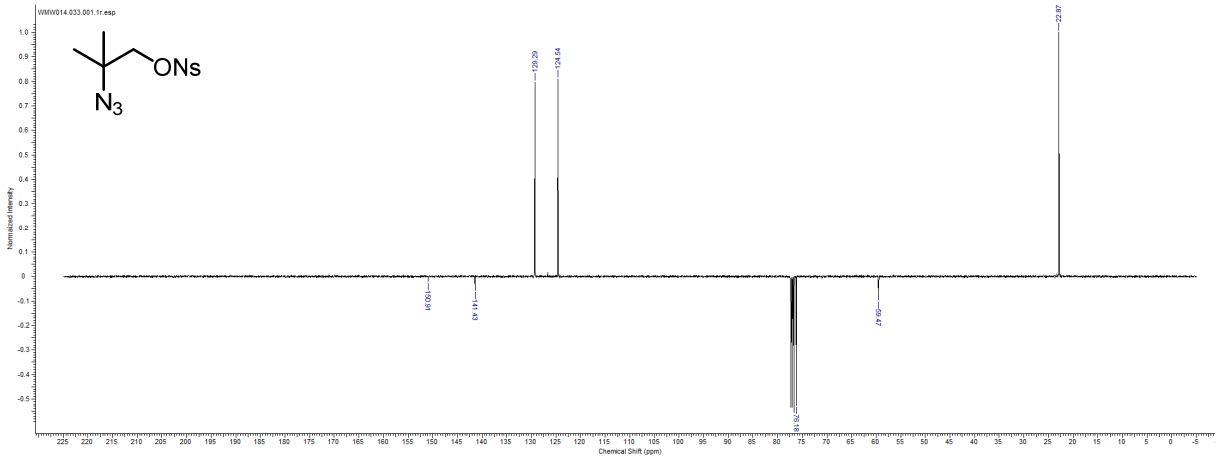
^{13}C-NMR spectrum of **9**



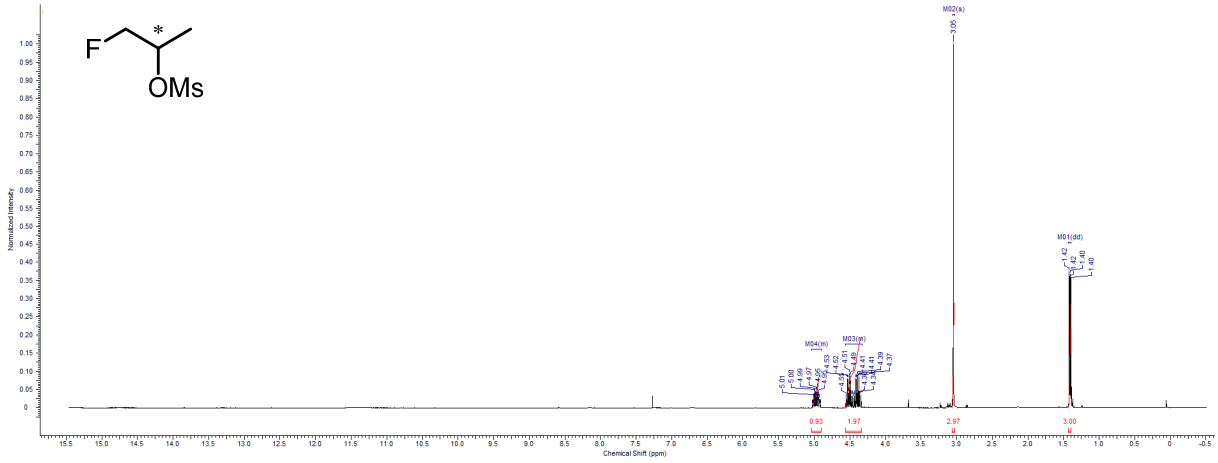
^{1}H-NMR spectrum of **10**



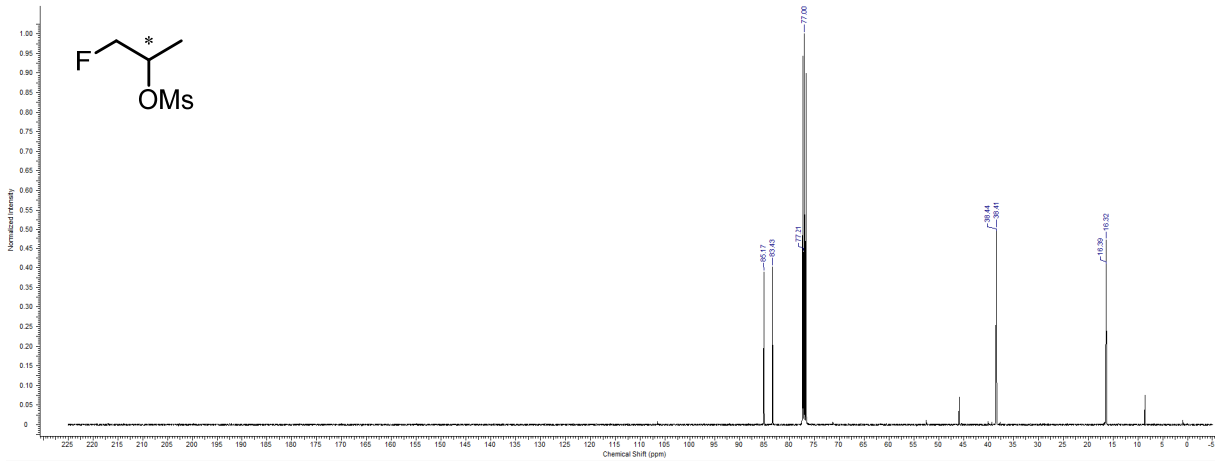
^{13}C-NMR spectrum of **10**



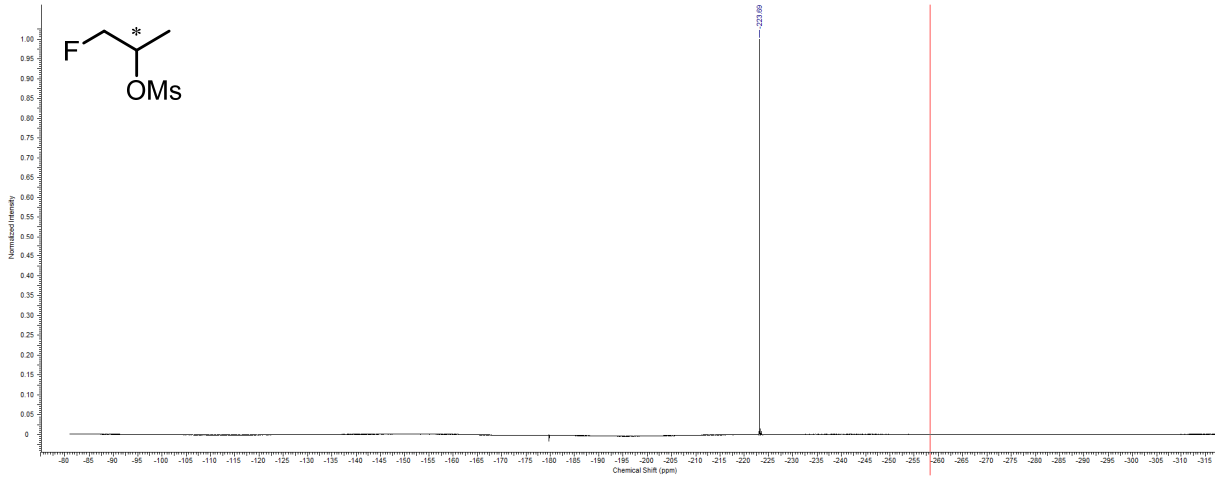
^{1}H-NMR spectrum of **13**



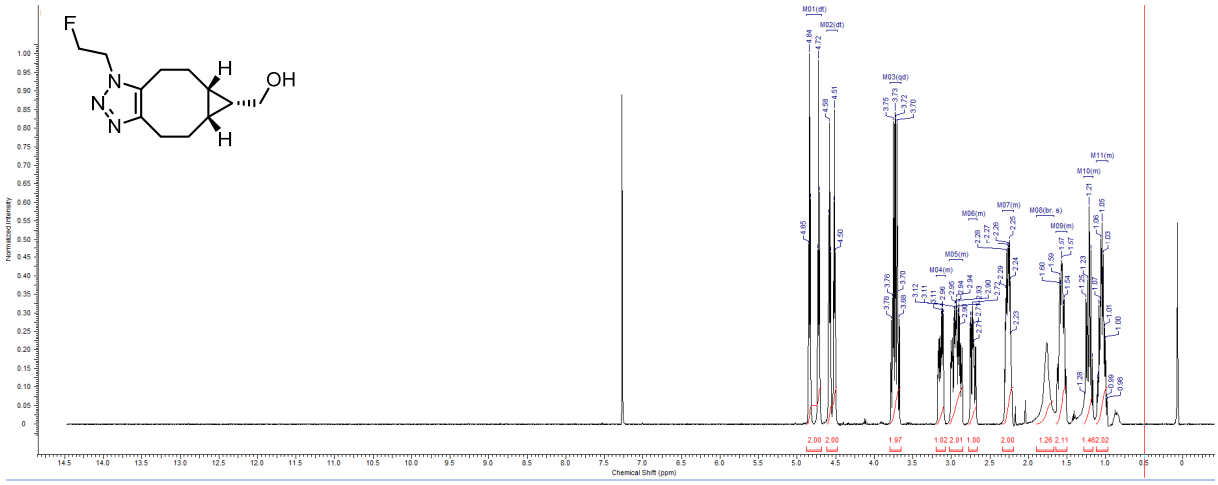
^{13}C-NMR spectrum of **13**



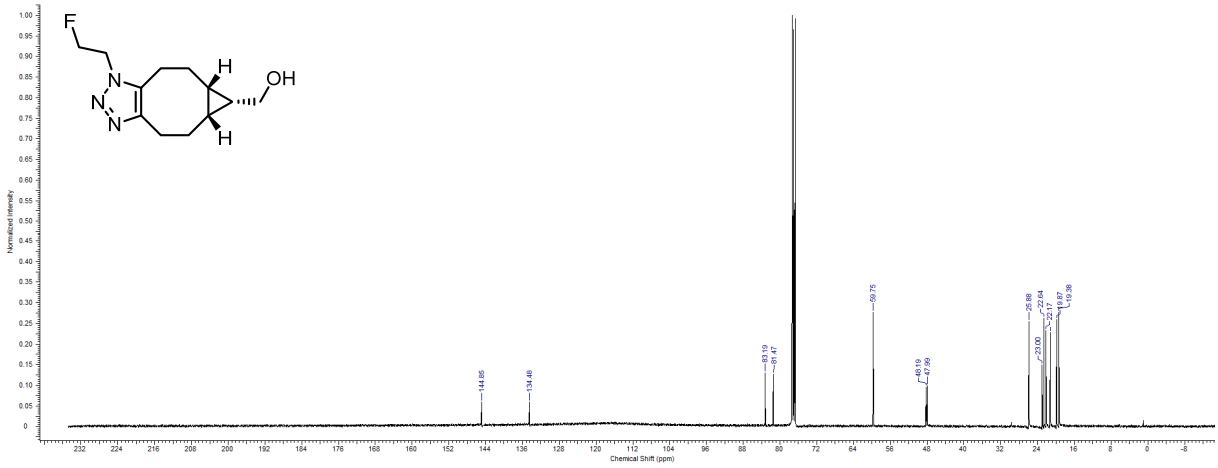
^{19}F-NMR spectrum of **13**



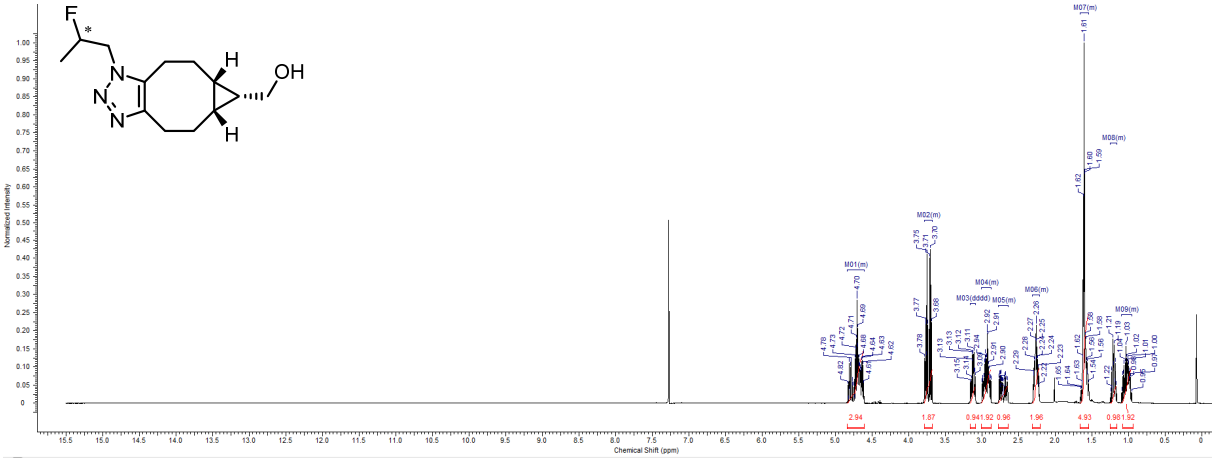
^{1}H-NMR spectrum of **15**



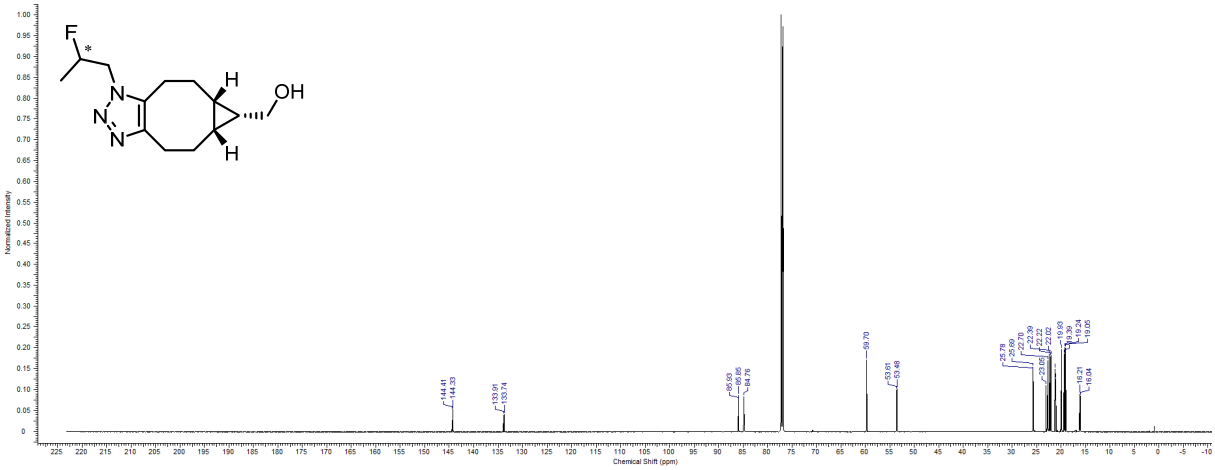
^{13}C-NMR spectrum of **15**



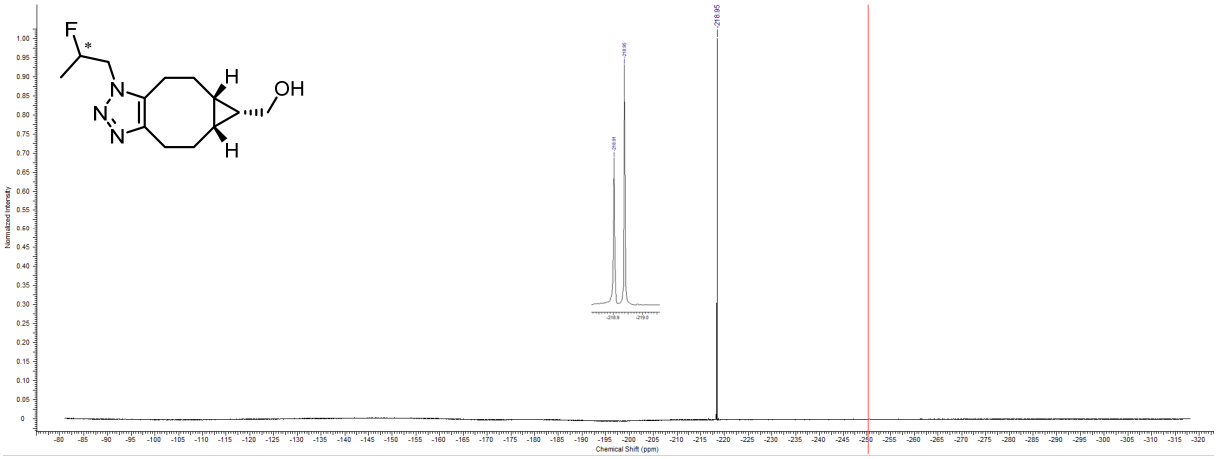
^{1}H-NMR spectrum of **16**



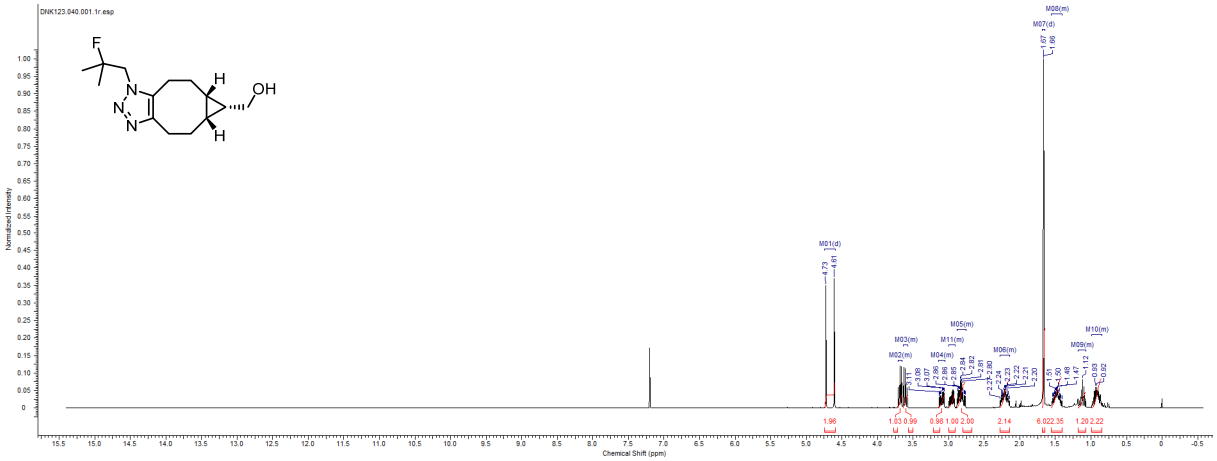
^{13}C-NMR spectrum of **16**



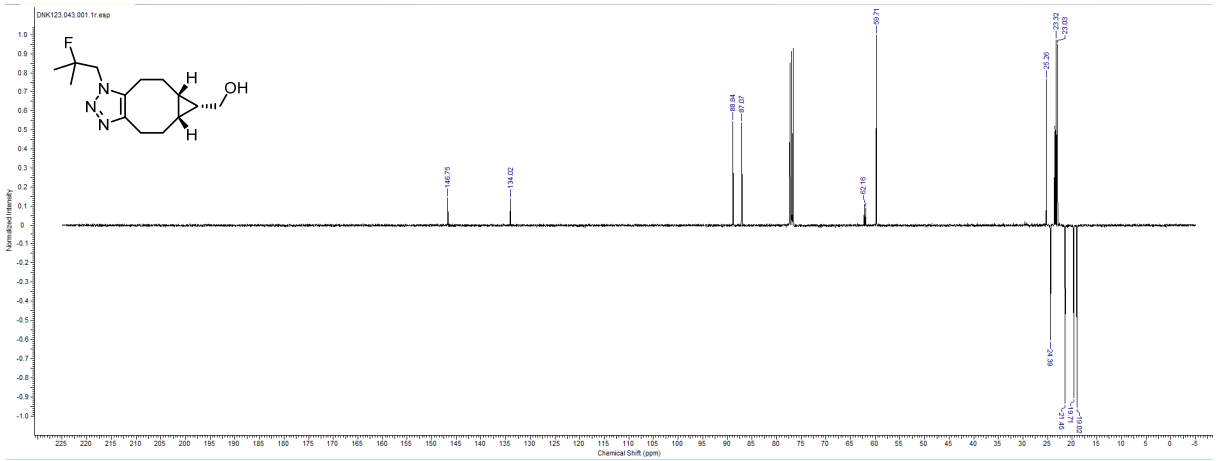
^{19}F-NMR spectrum of **16**



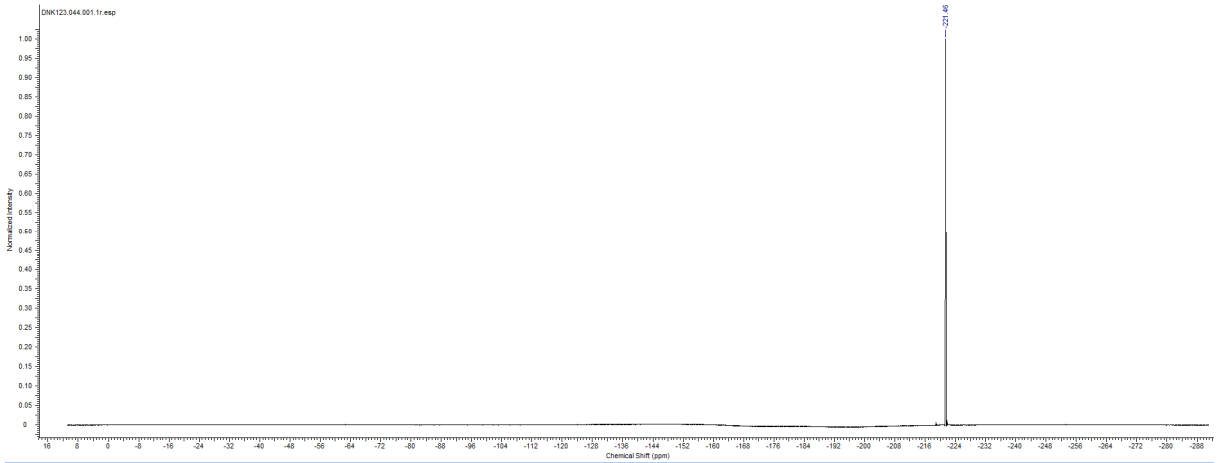
^{1}H-NMR spectrum of **17**



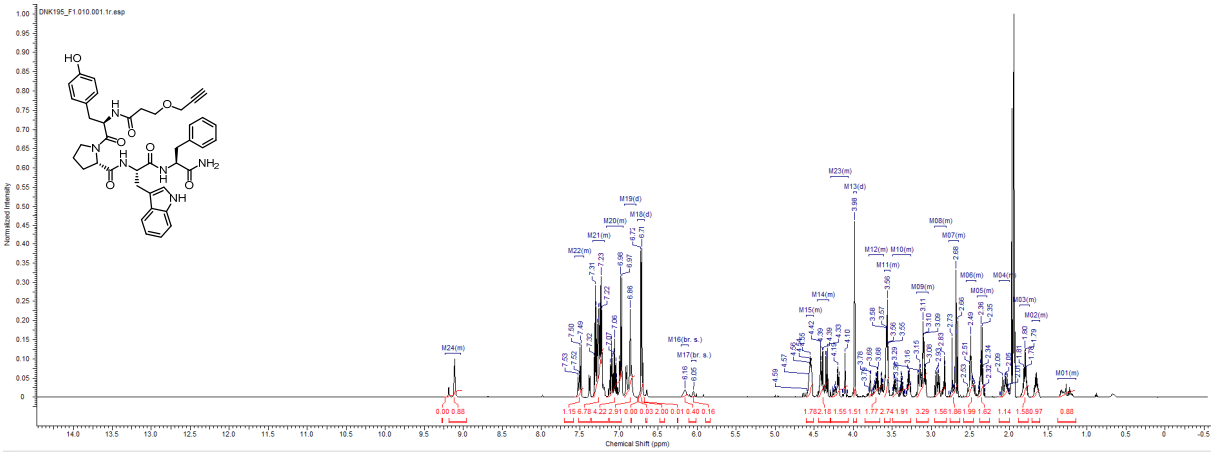
^{13}C-NMR spectrum of **17**



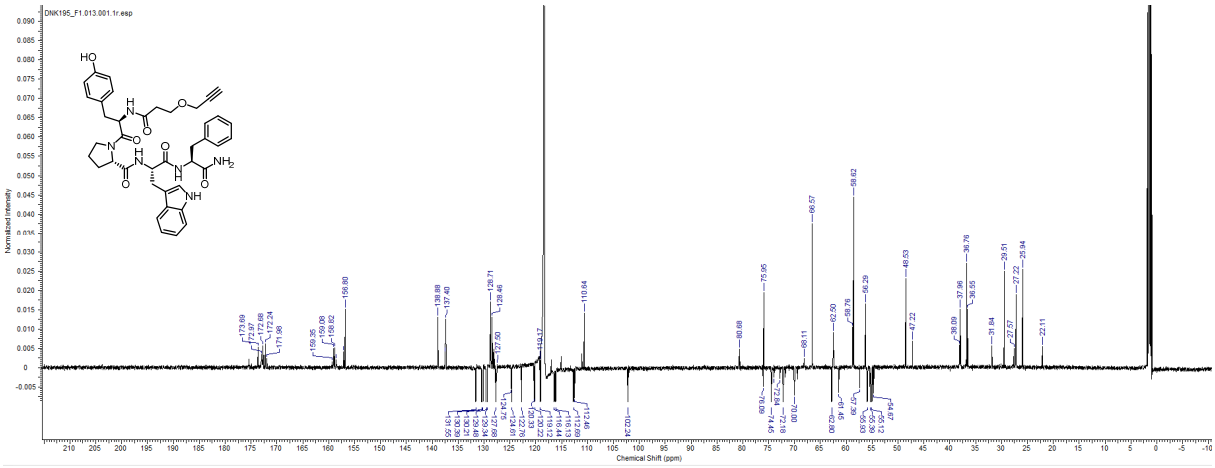
^{19}F-NMR spectrum of **17**



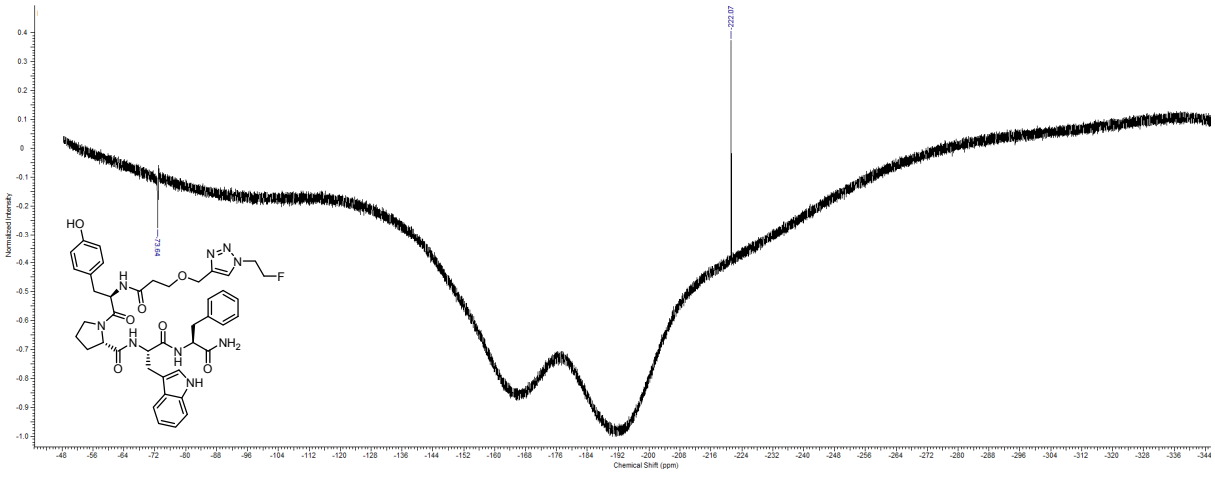
^{1}H-NMR spectrum of **18**



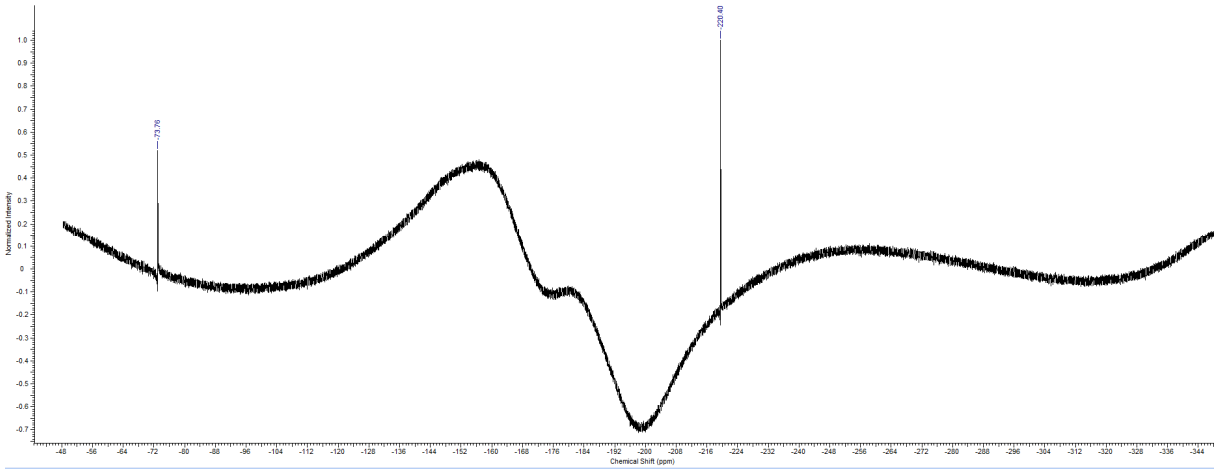
^{13}C-NMR spectrum of **18**



^{19}F-NMR spectrum of **19**

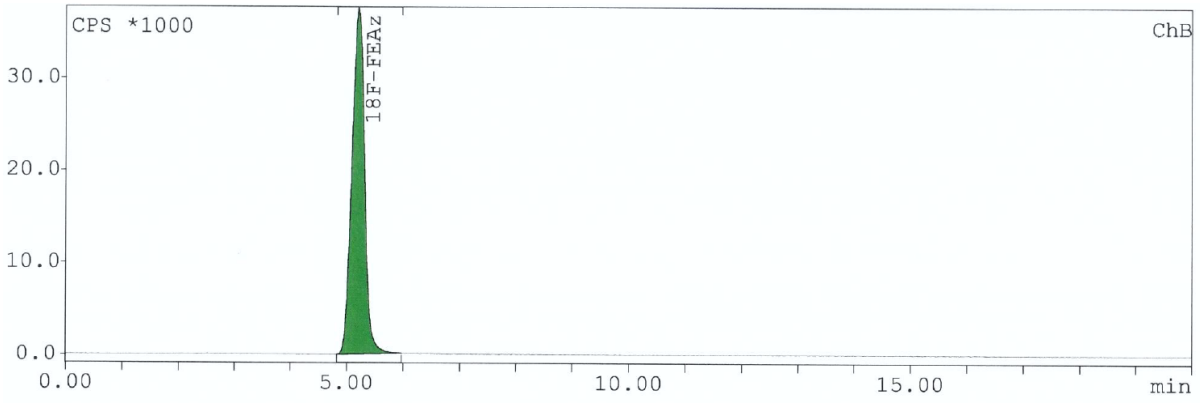


^{19}F-NMR spectrum of **20**

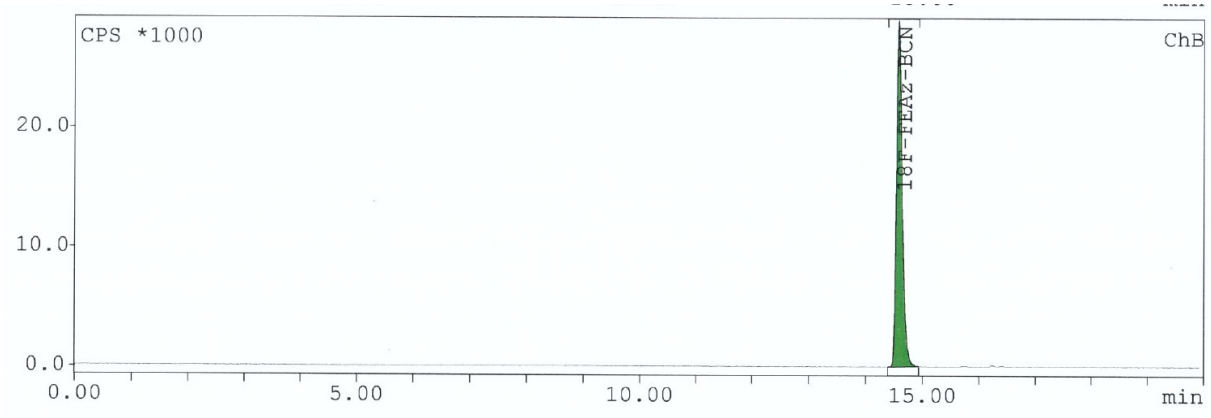


2. HPLC Data

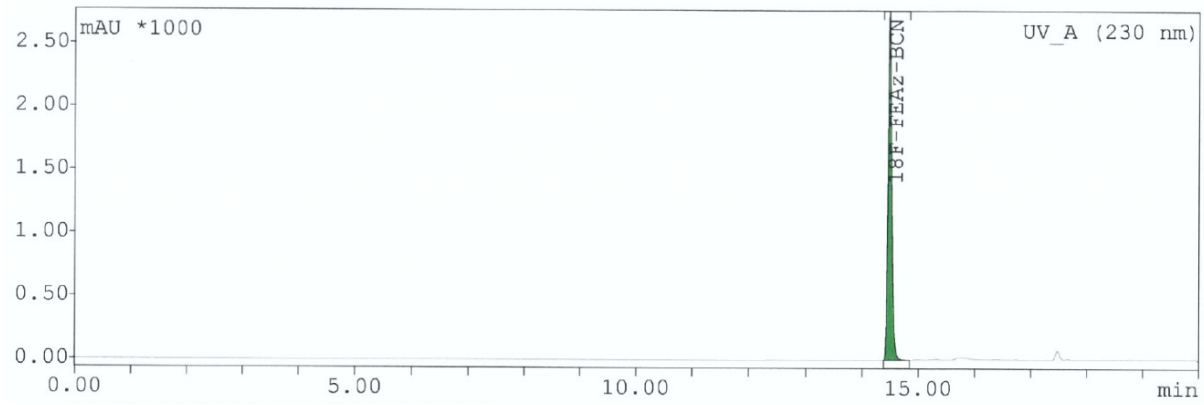
Radiochromatogram of [^{18}F]**1** (HPLC Conditions A)



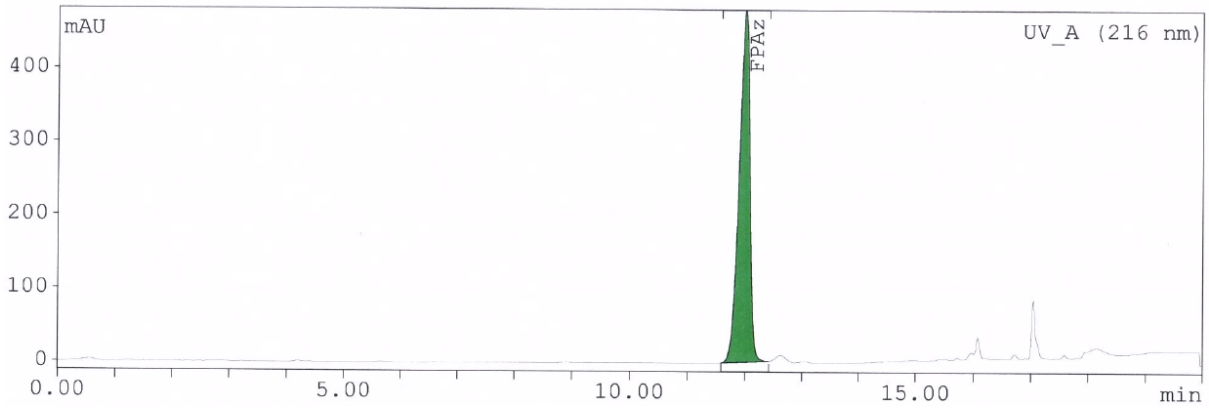
Radiochromatogram of [^{18}F]**15** (HPLC Conditions A)



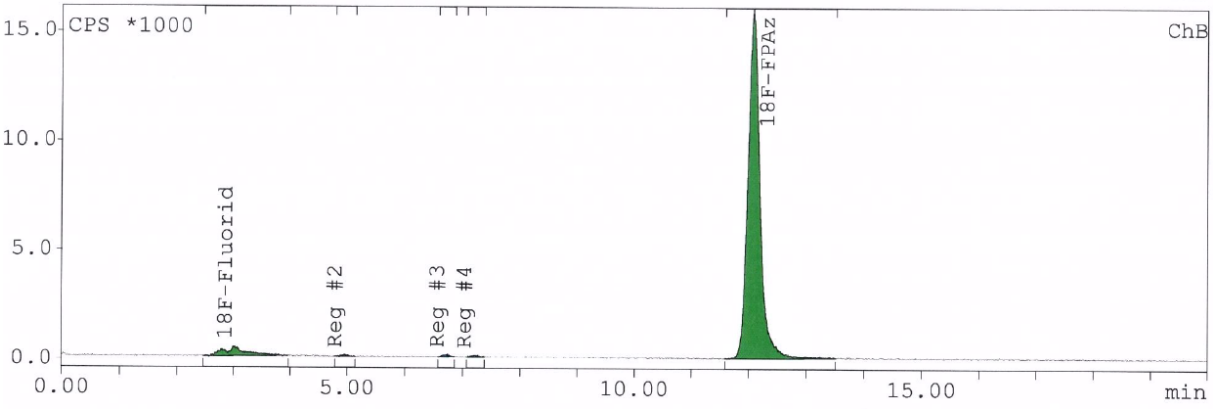
Chromatogram of **15** (230 nm, HPLC conditions A)



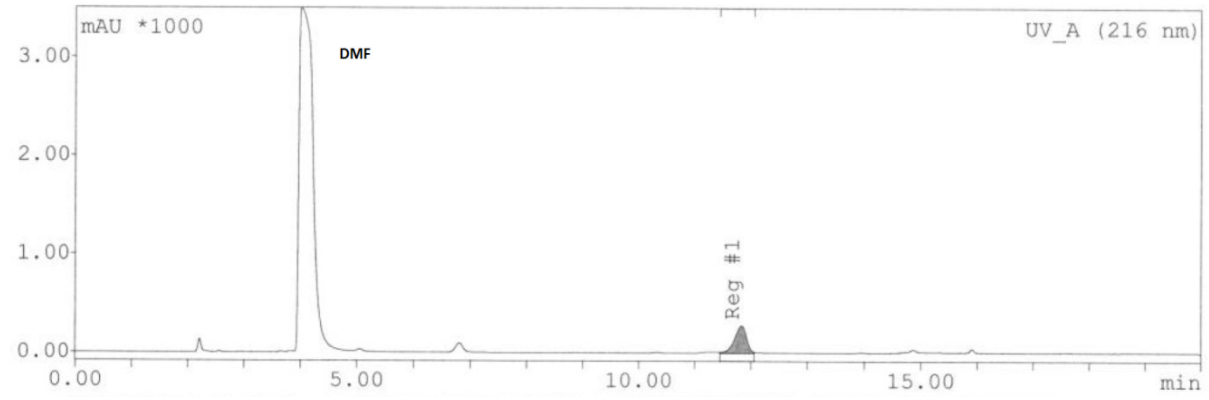
Chromatogram of **3** (216 nm, HPLC conditions A)



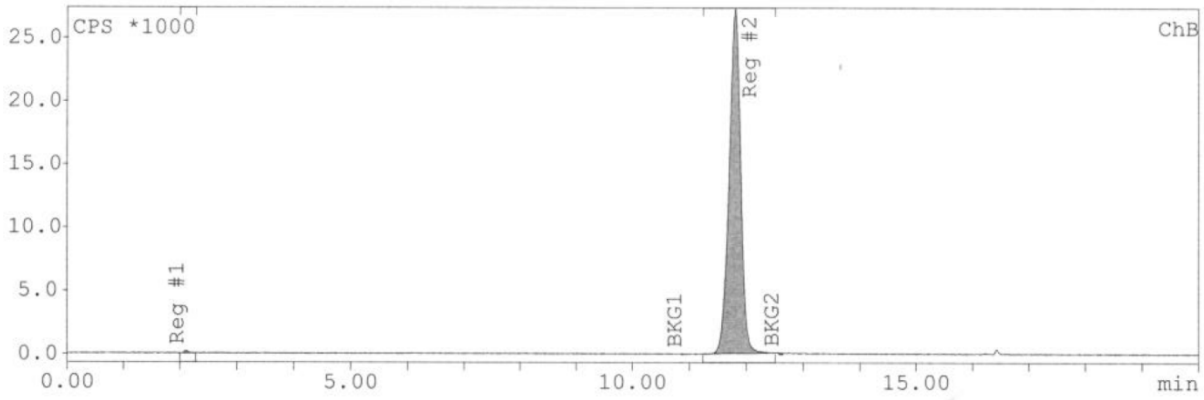
Radiochromatogram of [^{18}F]**3** (HPLC Conditions A)



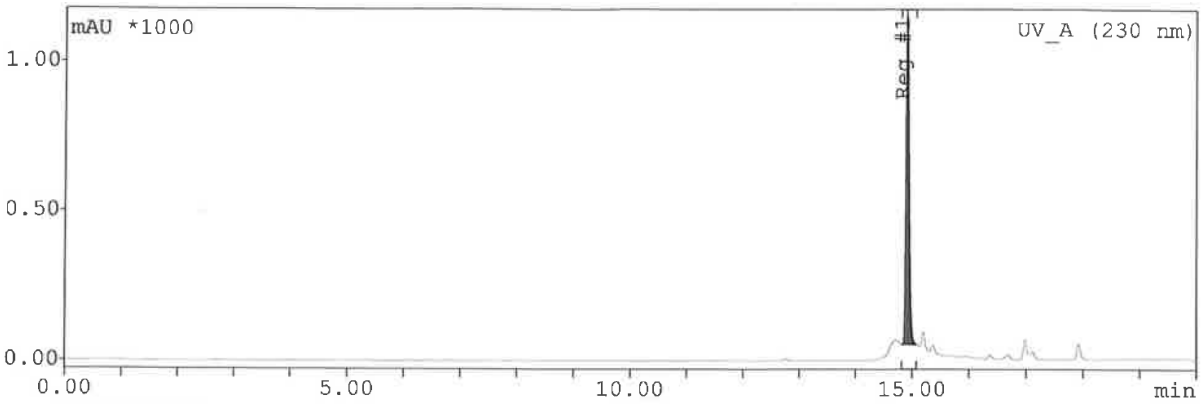
Chromatogram of **4** (solution in DMF, 216 nm, HPLC conditions A)



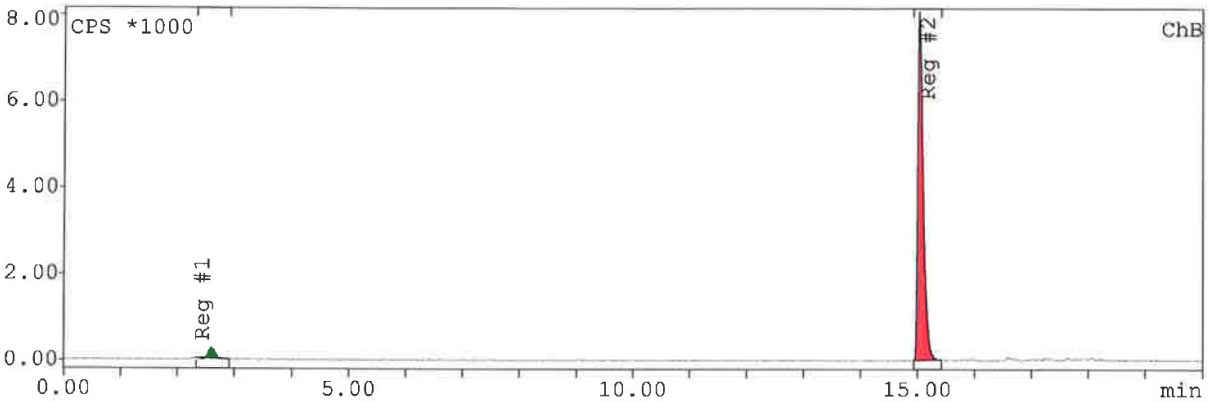
Radiochromatogram of [^{18}F]**4** (HPLC Conditions A)



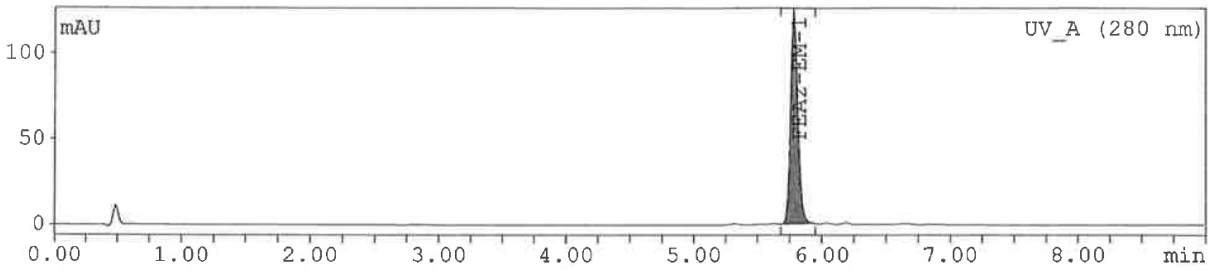
Chromatogram of **16** (230 nm, HPLC conditions A)



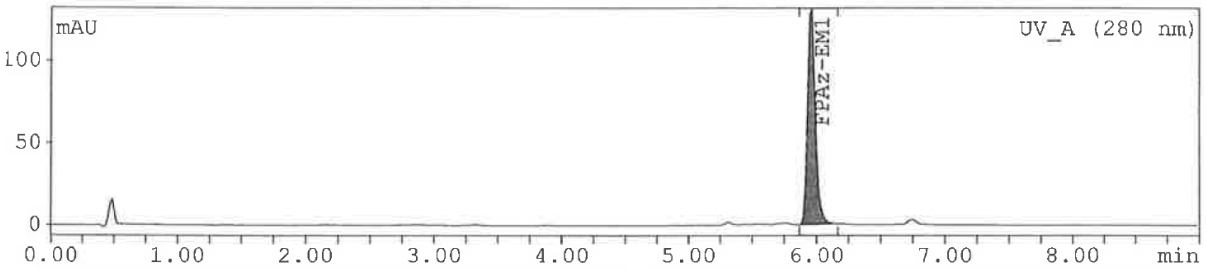
Radiochromatogram of [^{18}F]**16** (HPLC Conditions A)



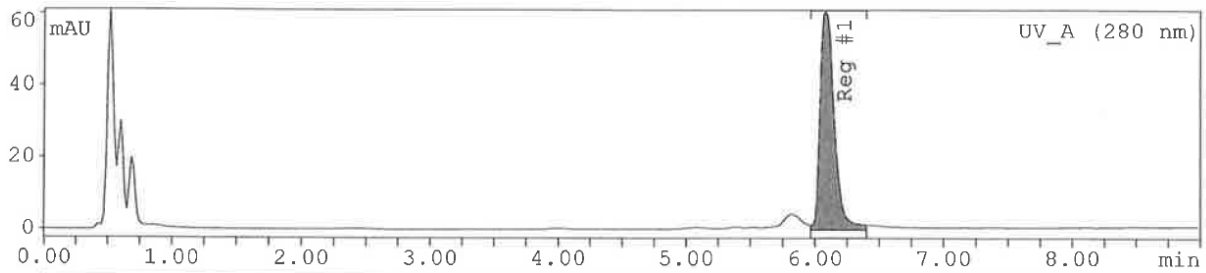
Chromatogram of **19** (280 nm, HPLC conditions B)



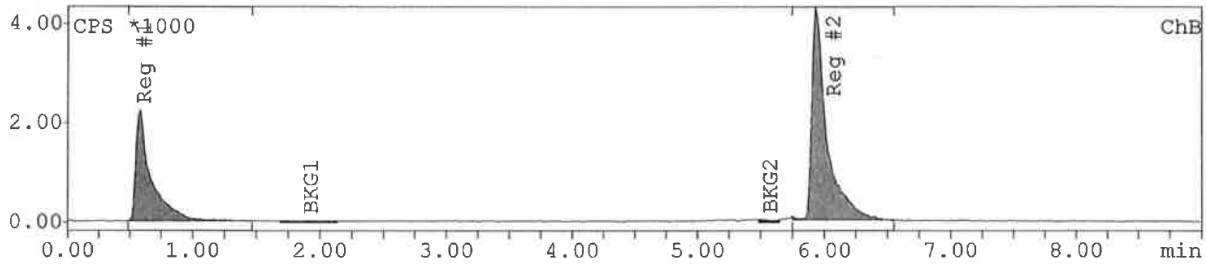
Chromatogram of **20** (280 nm, HPLC conditions B)



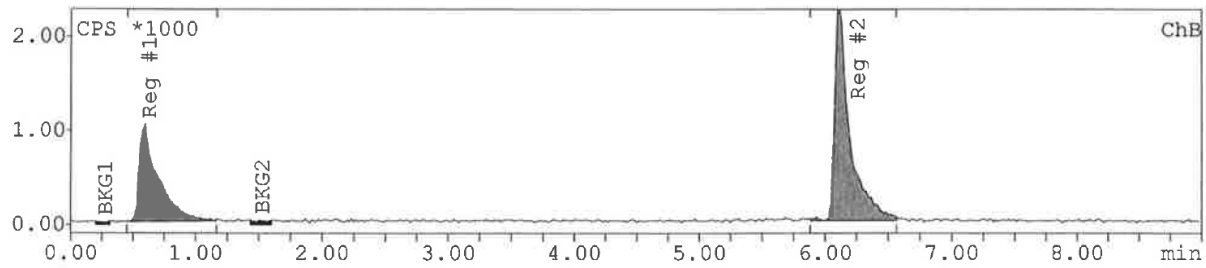
Chromatogram of **21** (280 nm, HPLC conditions B)



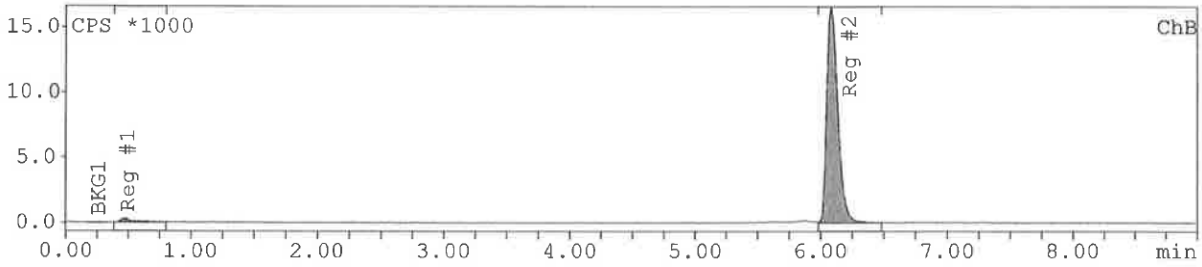
Radiochromatogram of [^{18}F]-**19** (quenched reaction mixture, HPLC conditions B)



Radiochromatogram of [^{18}F]-**20** (quenched reaction mixture, HPLC conditions B)

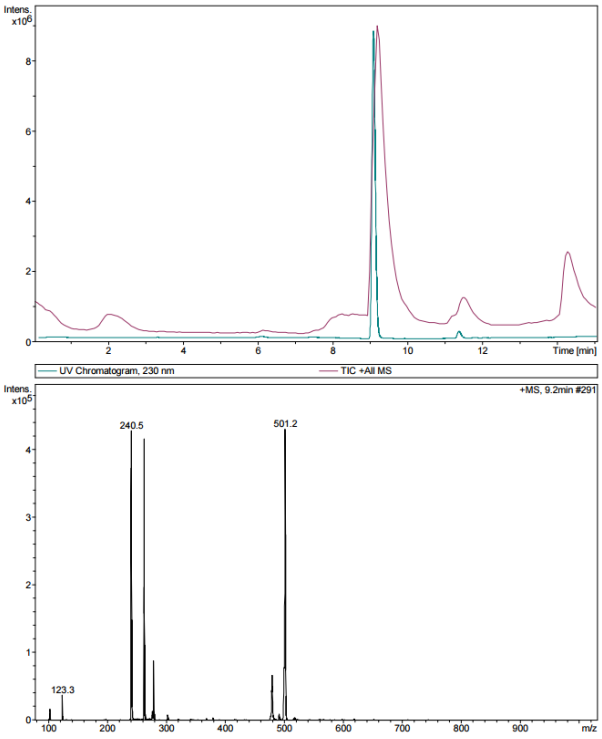


Radiochromatogram of [^{18}F]-**21** (quenched reaction mixture, HPLC conditions B)

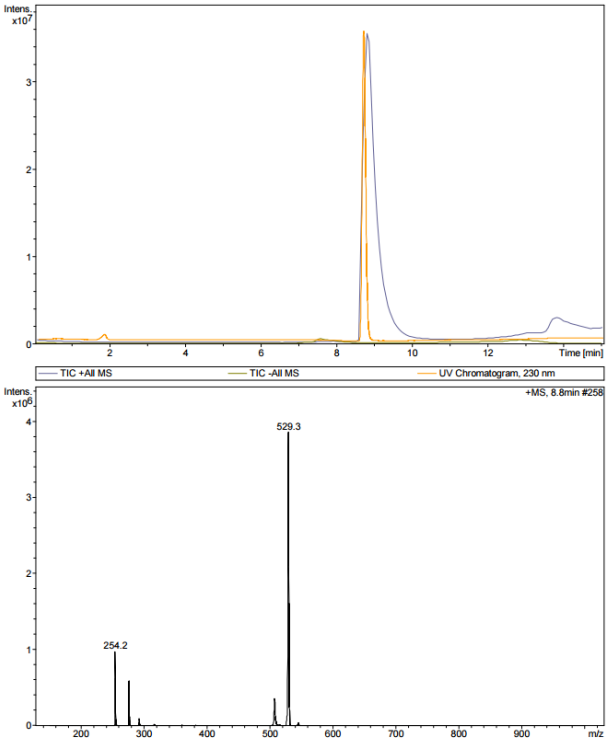


3. LC/MS Data

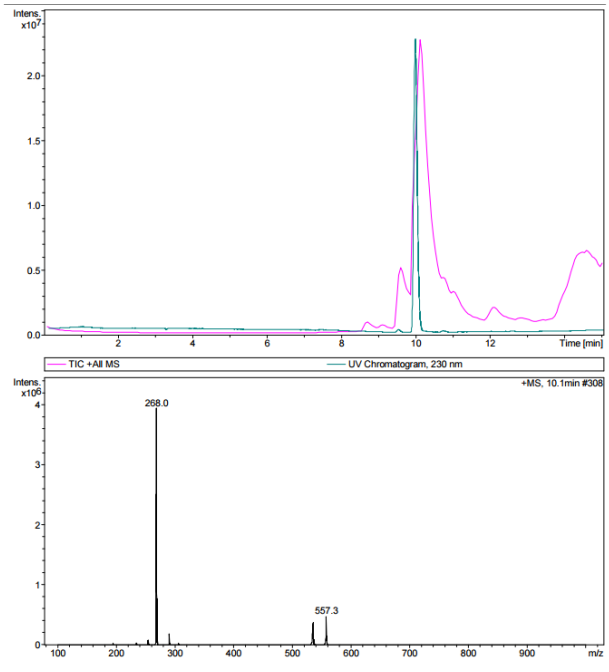
LC/ESI-MS of substance **15**
(green: DAD 230 nm, purple: TIC+)



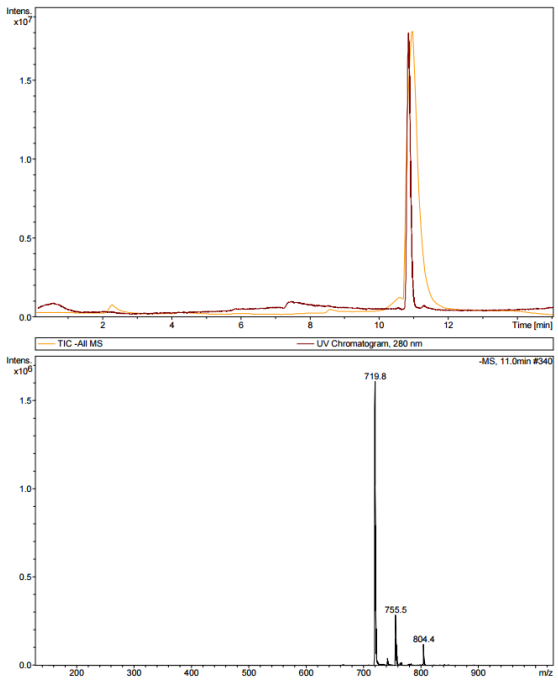
LC/ESI-MS of substance **16**
(yellow: DAD 230 nm, purple : TIC+)



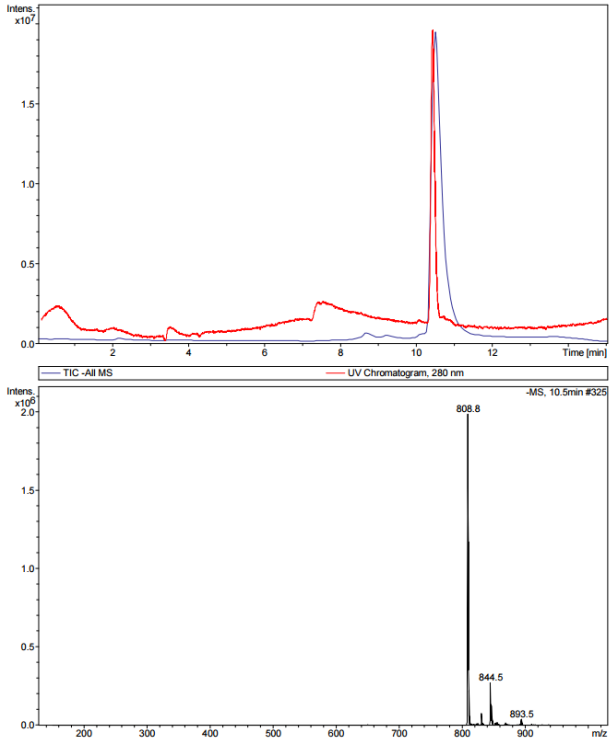
LC/ESI-MS of substance **17**
(green: DAD 230 nm, purple: TIC+)



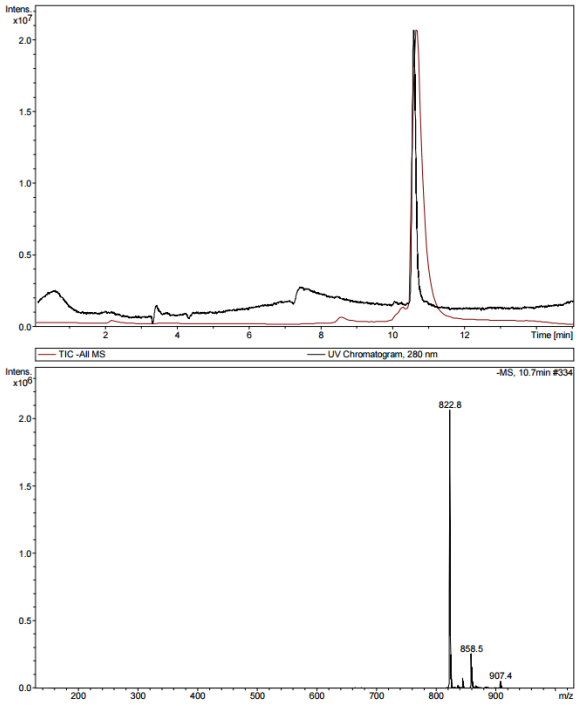
LC/ESI-MS of substance **18**
(red: DAD 280 nm, yellow: TIC-)



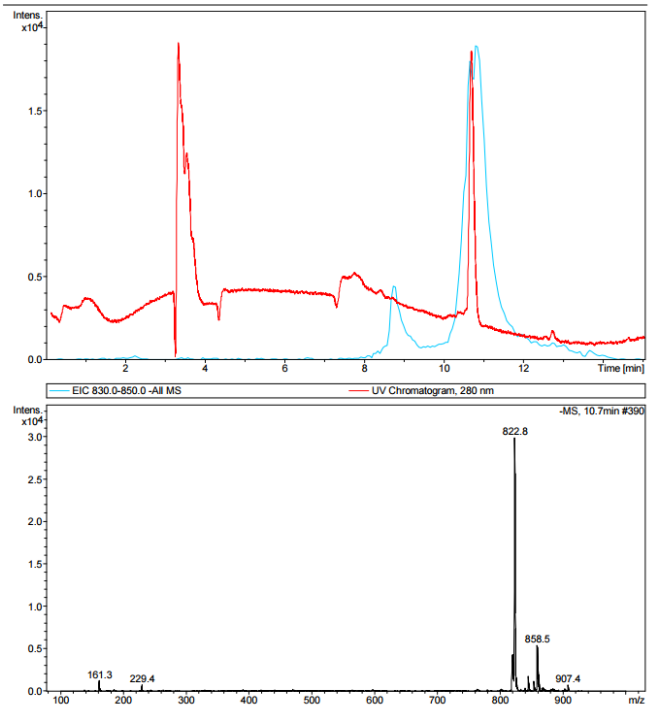
LC/ESI-MS of substance **19**
(red: DAD 280 nm, blue: TIC-)



LC/ESI-MS of substance **20**
(black: DAD 280 nm, purple: TIC-)



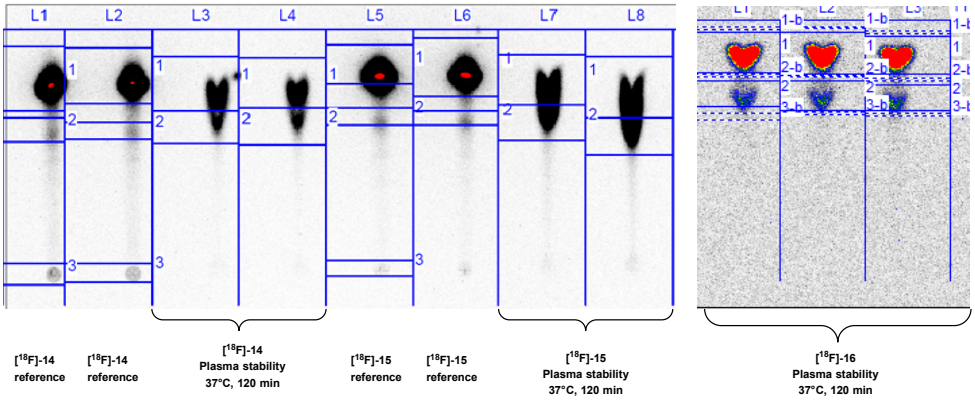
LC/ESI-MS of substance **21**
(red: DAD 280 nm, blue: TIC-)



4. TLC Data

Plasma stability of [^{18}F] endomorphin-1 conjugates [^{18}F]-**14**, [^{18}F]-**15** or [^{18}F]-**16**

TLC conditions: 50% MeCN in H_2O + 0.1% TFA, RP18-Silica



6. Curriculum Vitae

Christoph Denk, MSc.

Seitenberggasse 78/34, 1170 Wien

christoph.denk@tuwien.ac.at

+ 43 (0)650/220 93 29

Personal Details

Date of birth	27. September 1984
Place of birth	St.Pölten, Austria
Nationality	Austrian

Higher Education

11/2013 - 06/2016 **PhD programme at Vienna University of Technology, Institute of Applied Synthetic Chemistry**

- Visiting researcher at the European Institute of Molecular Imaging, Münster, Germany (03-04/2015)
- PhD Thesis „Development of Radiolabeled Bioorthogonal *In Vivo* Click Agents for Diagnostic Pretargeting„

04/2012 - 06/2013 **Master Programme Synthetic Chemistry at Vienna University of Technology, Karlsplatz 13, 1040 Vienna**

- Master thesis „Bioorthogonal Ligations in PET Imaging“, supervised by Prof. Johannes Fröhlich in cooperation with Seibersdorf Labor GmbH and Austrian Institute of Technology (AIT)
- Synthesis & radiolabeling of substances for a pretargeted PET strategy based on bioorthogonal ligations
- Graduation with distinction

10/2005 - 04/2012 **Bachelor programme Technical Chemistry at Vienna University of Technology, Karlsplatz 13, 1040 Vienna**

- Research internship at the Hebrew University of Jerusalem, Israel, supervised by Prof. Raphael Mechoulam

09/1999 - 06/2004 **Higher technical college for chemistry Rosensteingasse 79, 1170 Vienna**

Previous and current positions

11/2013 – ongoing	**Vienna University of Technology, Institute of Applied Synthetic Chemistry** **University research assistent**
05-06 /2013	**Vienna University of Technology, Institute of Applied Synthetic Chemistry** **Tutor in the synthesis lab**
02/2012 -08/2014	**Wirtschaftsförderungsinstitut Wien** **Trainer in adult education** - Training in physics & chemistry
06/2011 - ongoing	**Radiochemical Solutions Christoph Denk e.U.** **self employed** - Development of radiolabeling procedures - Quality control of radiopharmaceuticals - Radiation protection courses for task forces
10/2009 – 01/2010 10/2008 – 01/2009	**Vienna University of Technology, Institute of Chemical Technology and Analytics** **Tutor in the instrumental analysis lab** - Training of students in GC, IR, IC & AAS.
10/2008 - 08/2010	**Seibersdorf Labor GmbH – Radiopharmaceuticals** **Technical employee in production and quality control** - Synthesis & quality control of radiopharmaceuticals - Main operator of HPLC & GC systems - GMP process validation - Process development ^{68}Ga-radiopharmaceuticals
06/2006 - 06/2012	**Wirtschaftsförderungsinstitut Niederösterreich** **Trainer in adult education**

Grants and Awards

11/2015	Invitation to 2nd Göttingen SPIRIT Summer School: Multimodal Molecular Imaging: from high resolution in vitro towards in vivo imaging, Max Planck Institute, November 9th-13th 2015, Göttingen, Germany
09/2015	Grant fom the government of Lower Austria to support participation in the World of Molecular Imaging 2015 conference
09/2015	Student Travel Stipend, World of Molecular Imaging Conference 2014, Honolulu, USA

10/2014	Grant fom the government of Lower Austria to support participation in the World of Molecular Imaging 2014 conference
09/2014	Austrian Research Society, International Communication Stipend
09/2014	Student Travel Stipend, World of Molecular Imaging Conference 2014, Seoul, South Korea: Invitation to a scientific talk „Development and Evaluation of Radiolabeled 1,2,4,5-Tetrazines: Tools for Pretargeted PET Imaging“
11/2013	Merit grant, Vienna University of Technology
06/2013	Travel Grant, 5th European Congress on Chemistry for Life Sciences, Barcelona: Invitation to a scientific talk „Kinetics of Tetrazine Ligations: From Organic to Biological Media“

Further education

03/2014	**Radiation protection badge, silver**
07/2013	**Special education highly active sealed sources**
01/2009	**Radiation protection badge, bronze**
11/2008-12/2008	**Training as radiation protection officer, focused on work with open radioactive substances**

The listed educations were obtained at Seibersdorf Academy, Seibersdorf Labor GmbH, Forschungscenterstraße 1, 2444 Seibersdorf

Publications in Peer Reviewed Journals

Denk, C.; Svatunek, D.; Mairinger, S.; Stanek, J.; Filip, T.; Matscheko, D.; Kuntner-Hannes, C.; Wanek, T.; Mikula, H.:
"Design, Synthesis and Evaluation of a Low-Molecular-Weight ^{11}C-Labeled Tetrazine for Pretargeted PET Imaging applying Bioorthogonal *In Vivo* Click Chemistry"
Bioconjugate Chemistry, **2016**, accepted manuscript

D. Svatunek, C. Denk, V Rosecker, B. Sohr, C. Hametner, G. Allmaier, J. Fröhlich, H. Mikula:
"Efficient low-cost preparation of trans-cyclooctenes using a simplified flow setup for photoisomerization"
Monatshefte für Chemie **2016**, 147, 579 - 585.

C. Denk, D. Svatunek, T. Filip, T. Wanek, D. Lumpi, J. Fröhlich, C. Kuntner, H. Mikula:
“Development of a ^{18}F-labeled Tetrazine with Favorable Pharmacokinetics for Bioorthogonal PET Imaging”
Angew. Chem. Int. Ed. **2014**, *53*, 9655-9659. *Angew. Chem.* **2014**, *126*, 9810-9814
Cover picture, DOI: 10.1002/anie.201406154

Conference Contributions

C. Denk, D. Svatunek, B. Sohr, H. Mikula, J. Fröhlich, T. Wanek, C. Kuntner-Hannes, T. Filip:
"Investigation of Small [^{18}F]-Fluoroalkylazides for Rapid Radiolabeling and In Vivo Click Chemistry"
Poster: Austrian Society for Nuclear Medicine: 32nd Austrian Winter Symposium, January 20th-23rd 2016, Zell am See, Austria

C. Denk, D. Svatunek, T Wanek, S. Mairinger, J. Stanek, T. Filip, J. Fröhlich, H. Mikula and C. Kuntner-Hannes:
"Bioorthogonal Tools for PET Imaging: Development of Radiolabeled 1,2,4,5-Tetrazines"
Talk: Austrian Society for Nuclear Medicine: 32nd Austrian Winter Symposium, January 20th-23rd 2016, Zell am See, Austria

D. Svatunek, C. Denk, M. Wilkovitsch, T. Wanek, T. Filip, C. Kuntner-Hannes, J. Fröhlich, H. Mikula:
"^{18}F Labeled Azidoglucose Derivatives as "Click" Agents for Pretargeted PET Imaging"
Talk: Austrian Society for Nuclear Medicine: 32nd Austrian Winter Symposium, January 20th-23rd 2016, Zell am See, Austria

C. Denk:
„Radiolabeled 1,2,4,5-Tetrazines: Tools for Bioorthogonal PET Imaging"
Talk: Spirit Summer School: Multimodal Molecular Imaging: from high resolution in vitro towards in vivo imaging, Max Planck Institute, November 9th-13th 2015, Göttingen, Germany

C. Denk, S. Mairinger, J. Stanek, T. Wanek, T. Filip, D. Svatunek, J. Fröhlich, C. Kuntner-Hannes, H. Mikula:
„Development and Evaluation of a Small [11C]-Tetrazine as Bioorthogonal PET Probe"
Poster: World of Molecular Imaging Conference 2015, September 2nd-5th 2015, Honolulu, USA

C. Denk, M. Duffy, S. Hermann, A. Faust, D. Svatunek, J. Fröhlich, M. Schäfers, H. Mikula:
„Radioiodinated 1,2,4,5-Tetrazine : (Radio)Synthesis and in vivo Evaluation for Therapeutic Pretargeting"
Poster: World of Molecular Imaging Conference 2015, September 2nd-5th 2015, Honolulu, USA

C. Denk, D. Svatunek, T. Filip, T. Wanek, D. Lumpi, J. Fröhlich, C. Kuntner, H. Mikula:
„Development and Evaluation of Radiolabeled 1,2,4,5-Tetrazines: Tools for Pretargeted PET Imaging "
Talk: World of Molecular Imaging Conference 2014, September 17th-20th 2014, Seoul, South Korea

C. Denk, D. Svatunek, T. Filip, T. Wanek, D. Lumpi, J. Fröhlich, C. Kuntner, H. Mikula:
„Bioorthogonal Ligations in PET Imaging"
Talk: 6th Imaging in Life Sciences Workshop, April 29th 2014, Vienna, Austria

C. Denk, G. Eilenberger, W. Linert, D. Lumpi, H. Mikula, C. Hametner, J. Fröhlich:
„**Kinetics of Tetrazine Ligations: From Organic to Biological Media**“
Talk: 5th Congress Chemistry for Life Sciences, June 10th-12th 2013, Barcelona, Spain

G. Eilenberger, D. Lumpi, C. Denk, H. Mikula, C. Hametner, J. Fröhlich:
„ATR-IR Inline Monitoring of Strain Promoted Alkyne-Azide Cycloadditions in Biological Media“
Poster: 5th Congress Chemistry for Life Sciences, June 10th-12th 2013, Barcelona, Spain

H. Kvaternik, C. Denk, T. Wanek, J. Stanek, R. Müller, C. Kuntner, R. Aigner:
"Improved Synthesis of ^{131}I and ^{124}I labelled hyaluronic acid”
Poster : European Symposium on Radiopharmacy and Radiopharmaceuticals; April 26th-29th 2012, Nantes, France

Language skills

German:	mother tongue
English:	fluent